



18

ISBN 92-95003-26-8

trieste - italy

the
abdus salam
international
centre
for theoretical
physics


united nations
educational, scientific
and cultural
organization


international atomic
energy agency

ictp *lecture notes*

Invited Presentations College on Soil Physics 2003

2004

editors

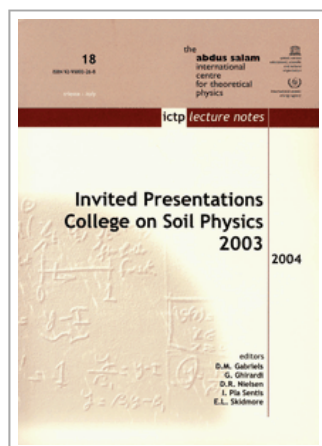
D.M. Gabriels
G. Ghirardi
D.R. Nielsen
I. Pla Sentis
E.L. Skidmore

ICTP Lecture Notes Series, Volume 18

(ISBN 92-95003-26-8) - May 2004

Invited Presentations, College on Soil Physics 2003

Editors: *D.M. Gabriels* (Univ. Ghent, Belgium), *G. Ghirardi* (Univ. Trieste, Italy), *D.R. Nielsen* (Univ. California, USA), *I. Pla Sentis* (Univ. Lleida, Spain), *E.L. Skidmore* (Kansas State Univ., USA)



Introduction

The beginning of ICTP College on Soil Physics - In 1980, Donald M. Gabriels, a soil physicist of Ghent University, Belgium and EdWARD L. Skidmore, a research leader at the USDA-ARS Wind Erosion Unit, Manhattan, Kansas, USA gave lectures at the ICTP Autumn Course on the *Physics of Flow in the Oceans, Atmosphere and Deserts*. Although they never met before, each knew about the work the other was doing.

At one of the lunches during the autumn course with the late Professor Abdus Salam, Nobel laureate in Physics and founder and director of ICTP, Trieste, Italy, Gabriels was asked about his main activities. Salam thought that Gabriels had said that his major field of interest was 'solar' - not 'soil' physics. In fact the two words 'solar' and 'soil' have something in common; just refer to 'el sol' (Spanish for 'sun') and 'le sol' (French for 'soil').

During the excursion in 'desertic' regions after the autumn course on the Physics of Flow in the Oceans, Atmosphere and Deserts, Skidmore was also asked his opinion about a soil physics course to be organised at ICTP. The encounter with some misunderstandings of terminology between Gabriels and Abdus Salam, which took place more than 20 years ago, and the enthusiasm of Skidmore, confirming the idea of organising a soil physics course was the start of one of ICTP's most successful activities: the *College on Soil Physics*.

After a first college in 1983, prepared and directed by Edward L. Skidmore and Donald M. Gabriels and co-directed by the local organiser Professor GianCarlo Ghirardi (ICTP consultant and University of Trieste), a number of colleges were organised every two or three years. Over time, more than 500 scientists, 80% of whom are from more than 50 developing countries, have participated in the College of Soil Physics, which in March 2003 celebrated its 20th anniversary.

In the course of these 20 years, Prof. Ildefonso Pla Sentis (previously at Universidad Central de Venezuela, at present with Universitat de Lleida, Spain), and Prof. Donald R. Nielsen, a former dean of the University of California, Davis, USA, joined the team of directors. Pla Sentis was long time coordinator of ELAFIS (Escuela Latinoamericana de Fisica de Suelos), sponsored by ICTP and organised for the first time in Peru (1986), and followed by courses in Brazil, Colombia, Argentina, Venezuela, Cuba and in 2003 in Chile.

Asked by 'News from ICTP' (see #104, Spring 2003) at the 20th anniversary College

on Soil Physics, 'what soil physics means', Skidmore defined it in simple terms as '*the study of the physical characteristics of soil*' or '*as the study of the physical laws of nature governing the behaviour of soil*'. The study and potential applications of soil physics involve an understanding not only of physics, but of biology, chemistry, hydrology, engineering and land use management.

And Nielsen added that soil physics is not just an academic exercise. It involves implications for understanding present critical issues as food security, drinking water, pollution of waters, contamination of soils, natural disasters as flooding and landslides. Soil physicists need to examine complex processes as water flow in soils, erosion and runoff, solute transport and oxygen diffusion.

Soil physicists belong to a big family and former participants of ICTP Colleges on Soil Physics take new initiatives to draw attention to the importance of soil physics for our environment. Reference is made to the symposia 'AgroEnviron' co-organized by former ICTP participants in Faisalabad, Pakistan (1998), Tekirdag, Turkey (2000), Cairo, Egypt (2002) and scheduled to be organised in 2004 in Udine, Italy.

The present book is a partial compilation of contributions from selected former participants of the College on Soil Physics invited to make presentations related to their achievements as a result of attending the College. It also serves as a testimony of the existing links between soil physicists throughout the world strengthened by the support and programs of the International Centre for Theoretical Physics originally envisioned by Abdus Salam to foster the growth of advanced studies and physics research in developing countries.

Donald M. Gabriels and Edward L. Skidmore
Founding Co-directors
ICTP College on Soil Physics
Ghent University, Belgium
May 2004

Table of Contents (PDF sources available)

All PDF sources of Volume 18: [lns018.tar.gz](#) (9019435 bytes)

(NB: This tar-compressed file contains the PDF versions of each lecture note)

ICTP
Publications & Printing
Strada Costiera, 11
Trieste, Italy
pub_off@ictp.it
© 2006

ICTP Lecture Notes Series, Volume 18

(ISBN 92-95003-26-8) - May 2004

Invited Presentations, College on Soil Physics 2003

Editors: *D.M. Gabriels* (Univ. Ghent, Belgium), *G. Ghirardi* (Univ. Trieste, Italy),
D.R. Nielsen (Univ. California, USA), *I. Pla Sentis* (Univ. Lleida, Spain), *E.L. Skidmore* (Kansas State Univ., USA)

Contents

1. **The Use of Wenner Configuration to Monitor Soil Water Content**
S.K. Agodzo, P.Y. Okyere and K. Kusi-Appiah
[Sources: pdf]
2. **Bulk Density, Cone Index and Water Content Relations for Some Ghanian Soils**
S.K. Agodzo and I. Adama
[Sources: pdf]
3. **Climatological Changing Effects on Wind, Precipitation and Erosion: Large, Meso and Small Scale Analysis**
Zafer Aslan
[Sources: pdf]
4. **Modelling of Environmental and Climatic Problems: Wind and Water Erosion**
Zafer Aslan
[Sources: pdf]
5. **In-Situ Determination of Directional Conductivities of Soil**
Gautam Barua
[Sources: pdf]
6. **Optimal Estimations of Random Fields Using Kriging**
Gautam Barua
[Sources: pdf]
7. **Rice Lands of South and South East Asia, Some Soil Physics Aspects**
R.M. Bhagat
[Sources: pdf]
8. **Management of Soil Physical Properties of Lowland Puddled Rice Soil For Sustainable Food Production**
R.M. Bhagat
[Sources: pdf]
9. **Hydrological Behaviour of Sealing Under Different Soil Management Conditions in the Center South Cordoba, Argentina**
Estela Bricchi
[Sources: pdf]
10. **Structure and Organic Matter Under Different Soil Management Conditions in the Center of Argentina**
Estela Bricchi
[Sources: pdf]
11. **Soil Physical Properties on Venezuelan Steeplands: Applications to Soil Conservation Planning**
Fernando Delgado
[Sources: pdf]
12. **A Soil Mechanics Approach to Study Soil Compaction and Traffic**

Effect On the Preconsolidation Pressure of Tropical Soils*Moacir de Souza Dias Junior*

[Sources: pdf]

13. Soil Physics and Agriculture*Durval Dourado Neto, Klaus Reichardt and Gerd Sparovek*

[Sources: pdf]

14. Agroclimatic Mapping of Maize Crop Based on Soil Physical Properties*Durval Dourado Neto, Gerd Sparovek, Klaus Reichardt, Luiz Carlos Timm and Donald R. Nielsen*

[Sources: pdf]

15. The Combined Effect of Wind and Rain on Interrill Erosion Processes*G. Erpul, D. Gabriels and L.D. Norton*

[Sources: pdf]

16. Physical Properties of Magnesium Affected Soils in Colombia*Alvaro Garcia-Ocampo*

[Sources: pdf]

17. Experimental and Modelling Studies of Infiltration*Mauro Giudici*

[Sources: pdf]

18. Inverse Modelling for Flow and Transport in Porous Media*Mauro Giudici*

[Sources: pdf]

19. Percolation Theory and its Application for Interpretation of Soil Water Retention Curves*Radka Kodesova*

[Sources: pdf]

20. Determination of Hydraulic Properties of Unsaturated Soil via Inverse Modeling*Radka Kodesova*

[Sources: pdf]

21. Soil Physical Properties Affecting Soil Erosion in Tropical Soils*Deyanira Lobo Lujan*

[Sources: pdf]

22. Aggregate Stability and Soil Degradation in the Tropics*Joe S.C. Mbagwu*

[Sources: pdf]

23. Environmental Control of Soil Structure in Mediterranean Soils*Joe S.C. Mbagwu*

[Sources: pdf]

24. Oxygen Transport in Waterlogged Soils, Part I.**Approaches to Modelling Soil and Crop Response to Oxygen Deficiency***Franco Humberto Obando Moncayo*

[Sources: pdf]

25. Oxygen Transport in Waterlogged Soils, Part II.**Diffusion Coefficient***Franco Humberto Obando Moncayo*

[Sources: pdf]

26. Influence of a Compacted Subsurface Layer on Soil Erosion*Svetla Rousseva*

[Sources: pdf]

27. Ideas for Physical Interpretation of the USLE*Svetla Rousseva*

[Sources: pdf]

28. Models for Predicting Water Use and Crop Yields - A Cuban

Experience*Maria Elena Ruiz and Angel Utset*

[Sources: pdf]

29. Soil Hydraulic Properties of Cuban Soils*Maria Elena Ruiz and Hanoi Medina*

[Sources: pdf]

30. Susceptibility of Coarse-textured Soils to Soil Erosion by Water in the Tropics*F.K. Salako*

[Sources: pdf]

31. Soil Physical Conditions in Nigerian Savanas and Biomass Production*F.K. Salako*

[Sources: pdf]

32. Boundary Layer Theory for Solute Transport in Soils*Mingan Shao*

[Sources: pdf]

33. General Similarity Theory and Integral Method for Water Flow in Soils*Mingan Shao*

[Sources: pdf]

34. State-Space Approach for Evaluating the Soil-Plant-Atmosphere System*L.C. Timm, K. Reichardt, J.C.M. Oliveira, F.A.M. Cassaro, T.T. Tominaga, O.O.S. Bacchi and D. Dourado-Neto*

[Sources: pdf]

35. Dimensional Analysis, Scaling and Fractals*Luis Carlos Timm, Klaus Reichardt and Osny Oliveira Santos Bacchi*

[Sources: pdf]

36. Use of a Combined Penetrometer-TDR Moisture Probe for Soil Compaction Studies*Carlos Manoel Pedro Vaz*

[Sources: pdf]

37. Automatic Gamma-Ray Equipment for Multiple Soil Physical Properties Measurements*Carlos Manoel Pedro Vaz*

[Sources: pdf]

38. Soil Shrinkage Characteristics in Swelling Soils*Miguel A. Taboada*

[Sources: pdf]

39. Soil Structural Behaviour of Flooded Soils*Miguel A. Taboada*

[Sources: pdf]

Back to LNS Volume 18 main page

ICTP

Publications & Printing

Strada Costiera, 11

Trieste, Italy

pub_off@ictp.it

© 2006

The Use of Wenner Configuration to Monitor Soil Water Content

S.K. Agodzo*, P.Y. Okyere and K. Kusi-Appiah

*School of Engineering, Kwame Nkrumah University of Science and Technology,
Kumasi (KNUST), Ghana*

*Lecture given at the
College on Soil Physics
Trieste, 3 – 21 March 2003*

LNS0418001

* agodzo@avuust.africaonline.com.gh

Abstract

A field investigation of the relationship between soil resistivity R_s and soil water content WC was conducted using the 4-probe Wenner Configuration Method WCM. The WCM is traditionally used by electrical engineers for earth testing but was adapted for use as a soil water monitor in this study. Calibration curves were established between R_s and WC, demonstrating that the earth tester can be used for such measurements. Power correlation ($R_s = k WC^n$) with r^2 values of 0.81, 0.83 and 0.97 were obtained for electrode spacing of 1400, 1300 and 1200 cm respectively. Linear correlation ($R_s = c WC + d$) yielded r^2 values 0.68, 0.87 and 0.99 for 1400, 1300 and 1200 cm, respectively. Generally, both the linear and power relationships get weaker with increasing spacing between electrodes. However, the power relationship holds better at higher electrode spacing while the linear relationship holds better at lower electrode spacing. The bulky nature of the equipment rendered the measurements cumbersome. It must be noted that electrode spacing of between 12 to 14 m will affect the spatial variability of the soil. This must have accounted for the weaker correlation as the electrode spacing increased, considering that the theory on which the earth tester is based assumes a homogeneous soil.

Introduction and Purpose

Engineers, agronomists and other professionals, at a stage in their professional work, need to know the amount of water in the soil and to be able to measure it quite accurately, easily and quickly. Water content determination of the soil is usually accomplished by direct and indirect methods. The purpose of this work is to adapt a method, traditionally used by electrical engineers for earthing landed properties against thunder, for soil water content determination. The method is known as the Wenner configuration method WCM.

Approach

The method is an indirect one, which measures soil water content WC as a function of soil resistivity R_s . Four metallic probes were driven into the ground with typical orientation (Figure 1). Soil resistivity at site was determined by sending electrical current through the ground via the electrodes. Resistance R was measured by the changes in voltage between horizontal electrode distances within the electrical field created by the current via the electrodes. With a homogeneous soil, Neidle (1975) computed soil resistivity as:

$$R_s = 4\pi aR = 12.6aV/I \quad (1)$$

where R_s is the soil resistivity (ohm-cm), R the soil resistance (ohm), V the voltage (V), I the Current (A), a the electrode spacing (cm) = $10b$, and b the electrode depth (cm).

Soil water contents (weight basis) were determined using the oven method for corresponding resistance measurements for electrode spacing of 1200, 1300 and 1400 cm.

Results and Discussion

Calibration curves (Table 1) were established between R_s and WC , demonstrating that the earth tester can be used for such measurements. Power correlation ($R_s = k WC^n$) with correlation coefficient r^2 values of 0.81, 0.83 and 0.97 were obtained for electrode spacing of 1400, 1300 and 1200 cm, respectively. Linear correlation ($R_s = c WC + d$) yielded r^2 values of 0.68, 0.87 and 0.99 for 1400, 1300 and 1200 cm, respectively. Generally, both the linear and power relationships get weaker with increasing spacing between electrodes. However, the power relationship holds better at higher electrode spacing while the linear relationship holds better at lower electrode spacing.

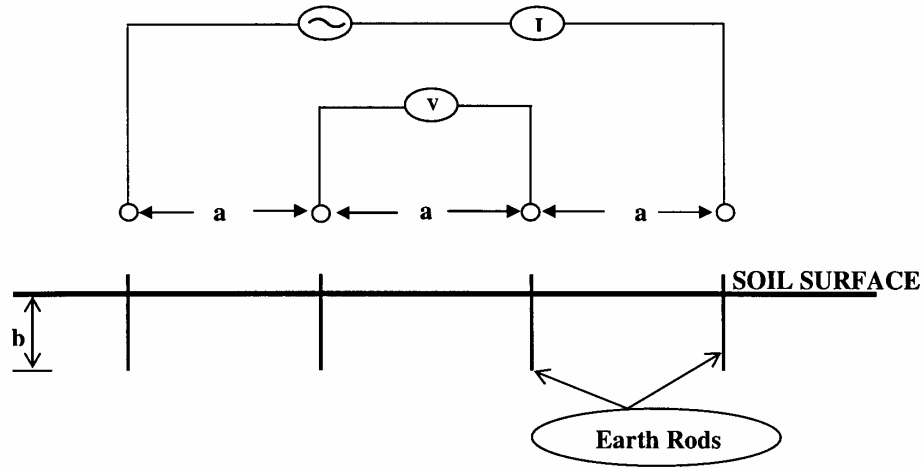


Figure 1. Experimental set-up.

Table 1. Wenner configuration results.

Electrode spacing, a (cm)	Power Function $R_s = k WC^n$			Linear Function $R_s = c WC + d$		
	k	n	r^2	c	d	r^2
1200	2×10^9	-4.75	0.97	-388.21	8772.8	0.99
1300	15409	-0.69	0.83	-45.67	2838.4	0.87
1400	8×10^7	-3.24	0.81	-258.47	8831.2	0.68

The bulky nature of the equipment rendered the measurements cumbersome. It must be noted that electrode spacing of between 12 to 14 m will affect the spatial variability of the soil. This must have accounted for the weaker correlation as the electrode spacing increased, considering that the theory on which the earth tester is based assumes a homogeneous soil. In fact this could even be an advantage with the method in that the measurement provides an integration of the effects of soil heterogeneity rather than homogeneity, which is in fact what pertains at the field level. Another advantage of the method is that a larger soil volume can be monitored to be representative of a wider area.

Conclusion

The oven method remains the standard method for the determination of soil water content but field sampling to be representative of a large area is still a problem. The other methods like tensiometry, neutron probing, gamma-ray attenuation and soil resistivity-based monitoring (Cassel and Klute, 1986) have become mainly research tools in understanding soil water behaviour but of limited practical field applicability. The Wenner configuration method, which is soil-resistivity based only adds to the existing procedures, but still with limited field applicability. The main advantage as already mentioned is that the method samples a larger soil volume and provides measurements for an integrated effect of soil heterogeneity rather than soil homogeneity at the field level. Further adaptations could be investigated to make the method more practicable.

References

- Niedle, M. (1970). Electrical installation technology. Butterworths, London. pp380.
Cassel, H. and A. Klute (1986). Methods of soil analysis: physical and mineralogical methods, American Society of Agronomy and Soil Science Society of America, Madison, Wisconsin, USA. pp1188.

Bulk Density, Cone Index and Water Content Relations for Some Ghanaian Soils

S.K. Agodzo* and I. Adama

*Agricultural Engineering Department,
Kwame Nkrumah University of Science and Technology, Kumasi, Ghana*

*Lecture given at the
College on Soil Physics
Trieste, 3 – 21 March 2003*

LNS0418002

* skagodzo7@usa.net

Abstract

Correlations were established between water content θ , bulk density ρ and cone index Δ for 4 Ghanaian soils, namely, *Kumasi*, *Akroso*, *Nta* and *Offin* series. The relationship between Δ and θ is in the form $\Delta = a \theta^2 + b \theta + c$, where the correlation coefficients r^2 for the various soils were found to be very high. Similarly, $\Delta - \rho$ relationships were linear but the correlations got weaker with increasing sand content of the soil, as expected. Soil sample sizes and compaction procedures did not conform to standard procedures, yet the results did not deviate from what pertains when standard procedures are used.

Introduction

The soil does not only serve as a medium for plant growth but also for engineering construction purposes. It is very weak in tension, very strong in compression and fails only by shearing. The behaviour of the soil under any form of loading and the interactions of the earth materials during and after any engineering construction work has a major influence on the success, economy and the safety of the work (Mitchell, 1976). Moreover, the soil also serves as a sink and recycling factory for numerous waste products which might otherwise accumulate and poison the environment. Soils and their management have therefore become a broad social concern. A limitless variety of soil materials are encountered in both agronomy and engineering problems, varying from hard, dense, large pieces of rock through gravel, sand, silt and clay to organic deposits of soft compressible peat. All these materials may occur over a range of physical properties, such as water contents, texture, bulk density and strength of soils. Therefore, to deal properly with soils and soil materials in any case requires knowledge and understanding of these physical properties.

The water content of the soil is an important property that controls its behaviour. As a quantitative measure of wetness of a soil mass, water content affects the level of compaction of soil, which is indicated by its bulk density. Soil bulk density is an indicator of the degree of compaction in engineering construction works. The desired value of bulk density varies with the degree of stability required in construction. Bulk density is also used as an indicator of problems of root penetration, soil aeration and also water infiltration. The cone index of a soil which is the degree of its strength has been shown to be affected by its water content and bulk density. This strength of soil has been widely used to predict the tractive capabilities of off-road vehicles, the draught forces in tillage operations and the compaction related to vehicle traffic. This property is also used in foundation engineering problems.

While not conforming to standard test procedures, this work attempts to add to the basic information on such important soil parameters as water content, bulk density and cone index for 4 Ghanaian soils namely, *Kumasi*, *Akroso*, *Nta* and *Offin* series.

Materials and Methods

Brief description of the test soils

The test soils are briefly described in Table 1.

Table 1. Brief description of the test soils.

Ghana Classification	FAO-UNESCO Classification	Soil Texture	Soil Depth (cm)	Soil Colour	Slope (%)	Drainage
Kumasi	Orthic-Ferric Acrisol	Gravelly and gritty/sandy clay loam and clay	Up to 70 cm	Very dark greyish brown to dark brown soil, underlain by reddish brown or red coarse sandy clay loam or clay	3-12	Well drained
Akroso	Dystric-Haplic Nitisol	Coarse sandy clay loam	Up to 90 cm	Dark brown to brown coarse sandy loam to coarse sandy clay, underlain by brownish yellow or yellowish red coarse sandy clay loam	2-5	Moderately to imperfectly drained, moderately slow permeability
Nta	Gleyic Arenosol	Coarse sand or loamy coarse sand	Up to 150 cm	Pale brown or yellowish brown loamy coarse sand, underlain by yellowish brown coarse sandy loam	2-5	Imperfectly drained, rapid permeability
Offin	Stagnic-Dystric Gleysol	Stratified sands and clays	> 30 cm to a few meters thick	Dark grey to dark brown loamy sand and sandy loam humus stained topsoil, underlain by grey to brownish grey coarse sand	Relatively flat	Slow internal drainage, rapid permeability

Source: Adapted and Modified from Adu (1992)

Experimental methods

Soils belonging to the various groups described in Table 1 were collected, air-dried and sieved with the 2 mm sieve. Texture classes were determined by the hydrometer method. Using core samplers (5 cm diameter x 5 cm length), moist soils were compacted into the cores at different levels of compaction. Both ends of the soil cores were trimmed and one end covered while exposing the other. This is to allow for progressive drying of the core under room conditions. Using a pocket penetrometer, cone indexes were determined progressively as the soils in the cores dried up. The core samplers plus the moist soils were weighed each day as the soil

dries up progressively. These took between 10 to 14 days to complete each set of data reading. At the last set of data reading, the samples were oven dried and the water contents and the wet bulk densities calculated. Dry bulk densities were also determined for each core sample. Correlations were established between water content, bulk density and cone index for the data generated.

Results and Discussion

Soil Texture

The textural classes of the soils used were determined as shown in Table 2.

Table 2. Texture class of test soils.

Soil Series	Percentage Soil Fraction			Soil Texture
	Sand	Silt	Clay	
Kumasi	63.6	9.8	26.6	Sandy clay loam
Akroso	71.6	11.8	16.6	Sandy loam
Nta	75.6	9.8	14.6	Loamy sand
Offin	83.6	9.8	6.6	Sand

Water content, bulk density and cone index

The data plotted for water content θ and cone index Δ generated polynomial equations of the form:

$$\Delta = a \theta^2 + b \theta + c \quad r^2 < 1 \quad (1)$$

where, a , b and c are soil constants.

Straight line relationships were obtained between dry bulk density ρ and cone index as:

$$\Delta = m \rho + n \quad r^2 < 1 \quad (2)$$

where m and n are soil constants. Detailed results are presented in Table 3.

Discussion

Being a sandy clay loam, *Kumasi* series has a clay content of 26.6 % and a sand content of 63.6 %. Its clay content is highest among the test soils and sand content, the least in the group. This suggests that it has the highest water holding capacity and at the same time the least dry bulk density values. Consequently, it recorded the least soil strength values at the same applied compactive efforts and as expected. For the

Kumasi series, the cone index - water content relationships obtained at different dry bulk densities showed some trend. The soil constants a , b and c for the *Kumasi* series increase with increasing dry bulk densities to a maximum and then begin to fall as the bulk densities continue to increase. No definite trends were observed for the *Akroso*, *Nta* and *Offin* series as shown in Table 3. As expected, dry bulk density increased linearly with increasing soil strength for all the soils. However, dry bulk density has smaller effect than water content for determining soil strength, partly due to cementation changes that occur with soil wetting and drying.

It must be noted that the samples used for the tests were small, that is, equivalent to the volume of the small core sampler. Even though the standard proctor test procedure was not used in soil compaction, the results obtained suggest that the procedure adopted in this study has produced results that conform to the standard test procedures. The hand penetrometer used is an improvement on the thumb-fingernail technique for estimating the engineering consistency of cohesive soils and designed to penetrate the soil up to 0.6 cm only and to give a direct reading of unconfined compressive strength.

Conclusion

The procedures used for determining relationships between water content, bulk density and cone index did not conform to standard test procedures. But results obtained did not deviate from what could have been obtained using the standard procedures. The data generated for the 4 Ghanaian soils could at best serve as a useful guide for basic soil data generation for development planning. This work is continuing to confirm the test procedures.

References

- Adu, S. V. (1992): *Soils of Kumasi, Ashanti Region, Ghana*. Soil Research Institute, Kumasi
- Mitchell, J. K. (1976): *Fundamental of soil behaviour*. Macmillan Press.

Table 3. Water content, bulk density and cone index relationship.

$\Delta = a \theta^2 + b \theta + c$					$\Delta = m \rho + n$
	<i>a</i>	<i>b</i>	<i>c</i>	<i>r</i> ²	
<i>Kumasi Series</i>					
1.010	0.0048	-0.2519	3.4960	0.9611	<i>m</i> = 2.7909
1.098	0.0038	-0.2110	3.1203	0.9946	<i>n</i> = -2.3545
1.112	0.0029	-0.1614	2.4918	0.9963	<i>r</i> ² = 0.8970
1.140	0.0029	-0.1664	2.6407	0.9944	
1.162	0.0032	-0.1799	2.7703	0.9815	
1.170	0.0041	-0.2394	3.6932	0.9918	
<i>Akroso Series</i>					
1.478	0.0155	-0.7087	8.3599	0.9824	<i>m</i> = 1.7793
1.542	0.0241	-1.0500	11.811	0.9900	<i>n</i> = -2.3820
1.641	0.0165	-0.7728	9.3165	0.9491	<i>r</i> ² = 0.7943
1.645	0.0520	-2.0248	20.3130	0.9851	
1.649	0.0629	-2.3866	23.2490	0.9157	
1.700	0.0108	-0.5827	7.8100	0.9245	
<i>Nta Series</i>					
1.330	0.0037	-0.1743	2.2811	0.9319	<i>m</i> = 2.0891
1.364	0.0036	-0.1737	2.3336	0.8963	<i>n</i> = -2.4764
1.367	0.0034	-0.1625	2.1869	0.9347	<i>r</i> ² = 0.8719
1.414	0.0098	-0.4044	4.3829	0.8480	
1.420	0.0067	-0.3026	3.6499	0.9440	
1.432	0.0073	-0.3216	3.7969	0.9224	
<i>Offin Series</i>					
1.257	0.0062	-0.3036	3.9371	0.7049	<i>m</i> = 1.9466
1.278	0.0025	-0.1189	1.6875	0.9477	<i>n</i> = -2.0434
1.313	0.0051	-0.2430	3.1615	0.9795	<i>r</i> ² = 0.3727
1.347	0.0021	-0.1073	1.6234	0.9638	
1.354	0.0014	-0.0904	1.6834	0.9712	
1.372	0.0037	-0.1744	2.3475	0.9537	

Climatological Changing Effects on Wind, Precipitation and Erosion: Large, Meso and Small Scale Analysis

Zafer Aslan*

*Beykent University, Faculty of Science and Literature,
Beykent, Istanbul, Turkey*

*Lecture given at the
College on Soil Physics
Trieste, 3 – 21 March 2003*

LNS0418003

* zaslan@beykent.edu.tr

Abstract

The Fourier transformation analysis for monthly average values of meteorological parameters has been considered, and amplitudes, phase angles have been calculated by using ground measurements in Turkey. The first order harmonics of meteorological parameters show large scale effects, while higher order harmonics show the effects of small scale fluctuations. The variations of first through sixth order harmonic amplitudes and phases provide a useful means of understanding the large and local scale effects on meteorological parameters. The phase angle can be used to determine the time of year the maximum or minimum of a given harmonic occurs. The analysis helps us to distinguish different pressure, relative humidity, temperature, precipitation and wind speed regimes and transition regions. Local and large scale phenomenon and some unusual seasonal patterns are also defined near Keban Dam and the irrigation area. Analysis of precipitation based on long term data shows that semi-annual fluctuations are predominant in the study area. Similarly, pressure variations are mostly influenced by semi-annual fluctuations. Temperature and humidity variations are mostly influenced by meso and micro scale fluctuations. Many large and meso scale climate change simulations for the 21st century are based on concentration of green house gasses. A better understanding of these effects on soil erosion is necessary to determine social, economic and other impacts of erosion. The second part of this study covers the time series analysis of precipitation, rainfall erosivity and wind erosion at the Marmara Region. Rainfall and runoff erosivity factors are defined by considering the results of field measurements at 10 stations. Climatological changing effects on rainfall erosion have been determined by monitoring meteorological variables. In the previous studies, Fournier Index is defined to estimate the rainfall erosivity for the study area. The Fournier Index or in other words a climatic index is defined by Odura-Afriye (1996). New, Hulme and Jones (1999, 2000) describe the construction of a 0.5 latitude by 0.5 longitude surface climatology of global land areas excluding Antarctica between 1901 and 1998. The climate surfaces have been constructed from a new data-set of station 1961-1990 climatological normals. The station data were interpolated as a function of latitude, longitude and elevation using thin plate splines. Analysis of Fournier Index values with the additional data between 1901-2002 shows that the study area is under the moderate and serve erosion risk especially in winter and spring.

INTRODUCTION

Harmonic analysis has emerged as a useful tool in studying annual patterns of some meteorological parameters, (Aslan and Topçu, 1994). The spatial distributions of temperature, precipitation and pressure have been examined by Krikyla and Hameed (1989), and Currie and Hameed (1990). The first and higher order harmonics show the local and large scale effects on meteorological parameters in this study. The amplitude and phase values are calculated and analyzed for each harmonics by using the long and short-term temperature, precipitation, pressure, humidity and wind speed data observed in the vicinity of a dam area over Eastern Anatolia and other geographical regions in Turkey (Aslan and Okçu, 1997; Aslan, Okçu and Kartal, 1997).

In order to evaluate climate change impacts, climate information is usually needed at the regional scale (i.e. up to 10^7) or the country level. Seasonally and averaged precipitation and surface air temperature for the future period (2070-2099) as compared to the period of 1961-1990 are examined by Giorgi and Francisco (2000). The dominant source of uncertainty in the simulation of average regional climate change is due to inter-model variability with inter-scenario and internal model variability playing secondary roles. The range of predicted climate changes by different realizations of the same ensemble is small, and simulated changes exhibit a high level of coherency among different forcing scenarios.

METHOD

Harmonic analysis is based on the series of trigonometric functions (Krikyla and Hameed, 1989)

$$X = X_0 + \sum_{i=1}^{N/2} A_i \cos(360it/p + \Phi_i) \quad (1)$$

where X is the value at time t , X_0 the arithmetic mean, A_i the amplitude of harmonics, Φ_i the phase angles, N the number of observations, t the time, and p the period of observation ($p = 12$ months).

Harmonic analyses of pressure, air temperature, relative humidity, wind speed, pressure and precipitation based on ground measurements over 14 stations have been presented. Environmental effects of Keban Dam and irrigation systems have been analyzed in the Northern part of Elazig. There are large irrigation systems in the near vicinity of Urfa, Mus, Bitlis and Van. Long (between 1940 - 1990) and short term data (between 1990 and 1994) for all Turkey are individually analyzed. Time series analysis based on half gridded data between 1900 and 2002 are presented.

ANALYSIS

Analysis of Pressure: Annual mean values of pressure based on short term observations decrease in the range of 1.1hPa to 1.8hPa in Gümüşhane, Erzurum, Erzincan and Elazig. Increasing of pressure observed over other stations is lower than these values. First order harmonics decreased in Bitlis, Diyarbakir, Elazig and Gaziantep between 1990-1994. By comparing the long term data with the short term observations, it is concluded that large scale effects on annual pressure variation increases over Diyarbakir, Elazig, Erzurum and Gaziantep in the short period. The role of large scale fluctuations increase in the first half and decrease in the second half of the short term observation period

Analysis of Temperature: Annual mean temperature values showed 2 to 3.6°C increase over all stations between 1990 and 1994. The highest values of temperature increase have been observed in Erzincan (3.6°C), Elazig (3.5 °C), Malatya (3.1°C) and Diyarbakir (3.0°C). Lower values are observed in Erzurum (1.4°C) and in Kars (2.0°C). First order amplitudes of temperature data shows increasing and decreasing trend in short term. Effects of meso scale fluctuation play an important role on temperature fluctuations over Elazig, Gaziantep, Malatya, Tokat, Urfa and Van during short term period. Small scale fluctuations play an important role on temperature variation over the stations (Bayburt, No-1 to Malatya, No-9).

Analysis of Relative Humidity: Annual mean humidity values based on short term data increase in Diyarbakir, Elazig, Gaziantep, Gümüşhane, Tokat, Urfa and Van. These values slightly decrease in Erzincan and Erzurum between 1990 and 1995. Minimum relative humidity differences of annual average value were observed in Mardin (2.1%), Gümüşhane (39%) and Erzurum (4%) in recent years.

Analysis of Wind Speed: Annual wind speed values decrease in Bayburt, Bitlis, Diyarbakir, Gaziantep and Urfa. They show some increasing and decreasing trends over other stations during the short term period. Meso and small scale fluctuations played an important role over Bitlis and Diyarbakir in recent years. The wind speed fluctuations showed similar behavior over Erzincan and Malatya. The largest dam area is between these two stations.

Analysis of Wind Speed and Precipitation: Annual mean rainfall rate increases over Bayburt, Erzincan, Gümüşhane, Kars, Tokat and Van. Large, meso and small scale fluctuations show some decreasing and increasing fluctuations during the short-term observation period. Large and meso scale fluctuations played an important role over Van in recent years. The annual oscillation of rainfall data is observed in the Southwest and Central Anatolia. Oscillations of six months are dominant in the East of Turkey. The first three harmonics play an important role on the rainfall data in the East and West of Turkey. Amplitudes and phase values of six harmonics of precipitation and wind speeds shows that large (1st harmonics) and meso-scale (4th

harmonics) phenomena play an important role on wind speed variation in January. These fluctuations have a great importance on wind erosion risk in the pilot area in January.

Time Series Analysis: Descriptive analyses have been presented in this lecture notes (2002) between 1901 and 1998, Aslan, Okçu and Sogut, (2002), Türkes, Sümer and Kılıç, (2002), Türkes, Sümer and Demir, (2002) and Gocer et al., (2002). Analyses of Aridity Index (Fig. 1) and Fournier Index (Fig. 2) values between 1901-2002 show that the study area is under the moderate and serve erosion risk. Fig. 3 shows a decreasing trend of wind speed values in Istanbul.

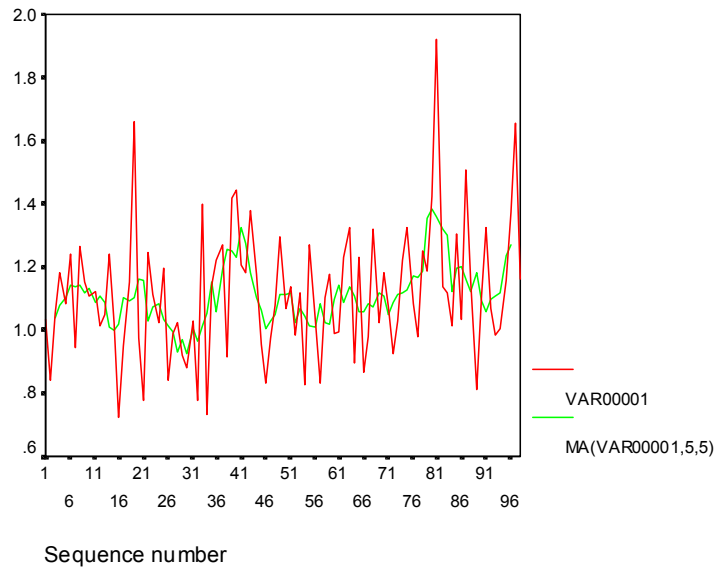


Figure 1- Time variation of aridity index values in Istanbul (1901-1998) for moving average.

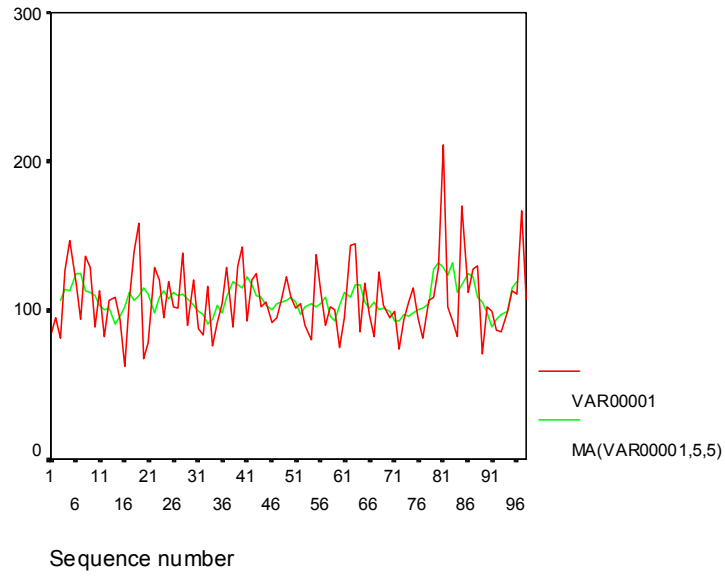


Figure 2- Time variation of FI values in Istanbul (1901-1998) for moving average.

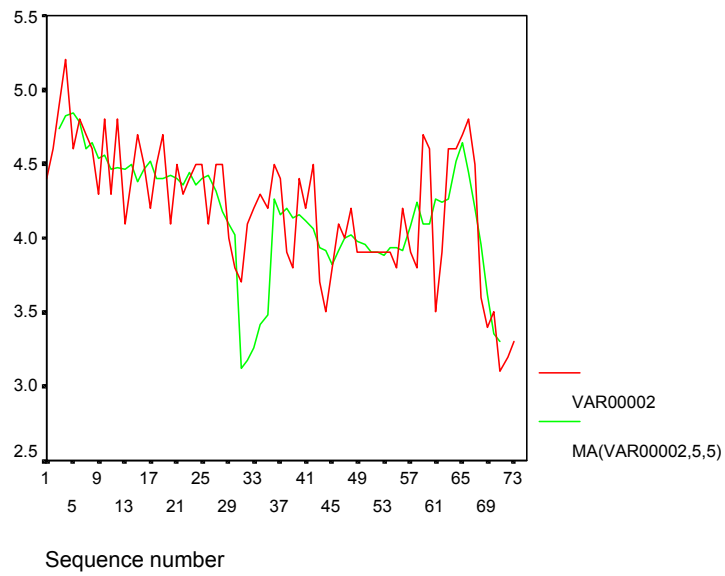


Figure 3- Time variation of wind speed values in Istanbul for moving average.
Note the decreasing trend of wind speed values.

CONCLUSION

Topographic structure, land and sea interactions cause complexity of meteorological parameters such as air temperature, relative humidity, and wind velocity, pressure and precipitation variations. A harmonic analysis of monthly average values of these parameters shows annual, semi-annual, and short term variations. Harmonic analysis determines effects of seasonal variations. This study shows some local effects on meteorological parameters, caused by large dam area and irrigation systems over The Eastern part of Anatolia. Temperature, relative humidity, wind speed, pressure and precipitation variations have mostly been effected by meso scale fluctuations. Large scale phenomenon has also played an important role on the precipitation regime of the study area. Because of water-land temperature differences, wind speeds increase over Elazig and Malatya. The Increase of the relative humidity value over the study area coincides with the increasing evaporating rate from water surface of the dam. Other irrigation systems over The Southern part of the study area contribute to the evaporation rate and relative humidity variations. Because of the chemical ingredients of Van Lake water, evaporation rate over it's surface is generally less than The Keban Dam. Large scale effects on precipitation, annual average of precipitation increases over Van. Meso scale circulation decreases wind speed. They increase relative humidity values over Van. In conclusion evaporation rate decreased and lake-water level increased in recent years. When the effect of large, meso, and small scale fluctuations on meteorological parameters in recent years are compared with the effects observed in previous years, the results present some details on climatological changing effects. The results of harmonic analysis and time series related with precipitation and wind data show the climatological changing effects on water and wind erosion problems.

ACKNOWLEDGEMENTS

This study has been supported by The Turkish Scientific and Research Council (TÜBİTAK, Project No: TOGTAĞ- 2846). The authors also wish to thank the Abdus Salam International Centre for Theoretical Physics, Prof. F. Giorgi, the Climate Impacts LINK project members for gridded data supporting; and Mr. O. Kardes for data processing.

REFERENCES

- Aslan, Z., and S. Topçu, (1994) Seasonal Variation of Surface Fluxes and Atmospheric Interaction in Istanbul, September, 22 - 27, Lisbon, Portugal.
- Aslan, Z., and D. Okçu, (1997) Analysis of Large, Meso and Small Scale Effects on Pressure, Relative Humidity, Temperature, Precipitation and Wind Speed Variations, ICTP Pre-print, Trieste.
- Aslan, Z., D. Okçu, S. Kartal, (1997) Harmonic Analysis of Precipitation, Pressure and Temperature over Turkey, *Il Nuovo Cimento*, Vol. 20, p. 595-605.
- Aslan, Z., D. Okçu and A. S. Sogut, (2002) Climatological Changing Effects on Erosion in Turkey, 3rd. AGROENVIRON Symposium, 25-29 October, Cairo.
- Currie, R.G., and S. Hameed, (1990) Atmospheric Signals at High Latitudes in a Coupled Ocean-Atmosphere General Circulation Model, *Geophysical Research Letters*, Vol. 17, No. 7, 945-948.
- Giorgi, F., and R. Francisco; (2000) Evaluating Uncertainties in the Prediction of Regional Climate Change, *Geophysical, Research Letters*, Vol. 27, No. 9, pages, 1295-1298.
- Göçer, K., D. Okçu, Z. Aslan and I. Sanlı, (2002) Remote Sensing of Vegetation Urbanisation and Industrial Development, 3rd International Symposium of Remote Sensing of Urban Areas, Vol:II, İstanbul, Turkey, pp. 545-551.
- Krikyla, K., and S. Hameed, (1989) Harmonic Analysis of the Seasonal Cycle in Precipitation over the United States: A Comparison between Observations and a General Circulation Model, *Journal of Climate*, Vol. 2, Dec., p.1463-1475.
- New, M. G., M. Hulme and P. D. Jones, (1999) Representing 20th century space-time climate variability. I: Development of a 1961-1990 mean monthly terrestrial climatology. *J. Climate*. Vol. 12, pp. 829-856.
- New, M. G., M. Hulme and P. D. Jones, (2000) Representing 20th. Century space-time climate variability. II: Development of 1901-1996 monthly terrestrial climate fields. *J. Climate*. Vol. 13, pp. 2217-2238.
- Odoro-Afriye, K., (1996) Rainfall Erosivity Map for Ghana, *Geoderma*, Elsevier Science B.V., 1125, pp.6.
- Türkes, M., U. M. Sümer and S. Demir, (2002) Re-Evaluation of Trends and Changes in Mean, Maximum and Minimum Temperatures of Turkey for the Period 1929-1999, *Int. Journal of Climatolog*, Vol. 22, p. 947-977.
- Türkes, M., U. M. Sümer, G. Kılıç, (2002) Persistence and Periodicity in the Precipitation Series of Turkey and Associations with 500hPa Geopotential Heights, *Climate Reseach*, Vol. 21, p. 59-81.

Modelling of Environmental and Climatic Problems: Wind and Water Erosion

Zafer Aslan*

*Beykent University, Faculty of Science and Literature,
Beykent, Istanbul, Turkey*

*Lecture given at the
College on Soil Physics
Trieste, 3 – 21 March 2003*

LNS0418004

* zaslan@beykent.edu.tr

Abstract

Magnitude of wind and water erosion mainly depend on wind velocity, rainfall rate, slope and soil characteristics. The main purpose of this lecture is to define the role of small, meso and large scale phenomena (local and synoptic fluctuations) on water and wind erosion. These lecture notes presents some results on wind speed simulation and seasonal fluctuations of water deficit for the selected station in different erosion risk and transition regions of Turkey.

INTRODUCTION

In order to simulate the process of soil erosion by wind, wind speed and its characteristics are considered, (Skidmore, 1986, 1995, 2000a, 2000b). Prediction of wind speed and direction is extremely difficult. Raindrops, water and soil type play an important role on soil erosion, flood, landslides etc. The reason of soil erosion is mainly caused by the impact of raindrops on the soil surface and its flow between rills and in channels down slope. It also causes landslides on steep slopes. The erosivity effect of raindrops depends on the energy of a rainstorm, Pla Sentis (1998), Flanagan and Livingston (1995) and Gabriels (1993). Monthly rainfall data were used to compute rainfall erosivity indices for various stations in Ghana, (Oduro-Afriye, 1996). Temporal and spatial variation of rainfall erosivity and climatic factor of wind erosion are investigated in Turkey, Aslan, (1997), Tulunay et al., (2002), Aslan et al., (2002). Higher values of Fournier Index are observed in the North-eastern Black Sea, the Southern Aegean Sea and Mediterranean Sea Regions. This manuscript also presents some results on wind and water erosion characteristics at the Northwestern part of Turkey (Gökçeada).

METHODOLOGY

Rainfall Erosivity Factor and Water Erosion

Rainfall and runoff erosivity factors are defined by considering the results of field measurements. The Fournier Index described as a climatic index is defined by Oduro-Afriye (1996) as

$$C_p = P_{\max}^2 / P \quad (1)$$

where C_p is the Fournier Index (mm), P_{\max} the rainfall amount in the wettest month and P the annual precipitation (mm).

Table 1 shows classes of rainfall erosion risk based on the Rainfall Erosivity Index. C_p values above 60 show severe to extremely severe erosion risk in average climatic conditions, Oduro-Afriye (1996).

Table 1. Classes of rainfall erosion risk, indexes and soil losses.

Class No	Erosion Risk Class	Fournier Index C_p	Soil Loss (T/ha year)
1	Very Low	<20	<5
2	Low	21-40	5-12
3	Moderate	41-60	12-50
4	Severe	61-80	50-100
5	Very Severe	81-100	100-200
6	Extremely Severe	>100	>200

Soil Moisture Prediction

Soil moisture over the western Turkey (in Istanbul) basin has been evaluated for long-term data by using De Martonne's Index I (Piervitali et al., 1999). The index is given by the following equation:

$$I = P / (T + 10) \quad (2)$$

where P is the total yearly precipitation (mm) and t the mean yearly temperature (°C). Index values more than 30 correspond to the humid areas where time adjusted irrigation was necessary.

Wind Erosion (Climatic Factor)

Wind erosion index is also defined as climatic factor C_w . It is a function of horizontal wind speed as given below:

$$C_w = V^3 \quad (3)$$

Erosion risk classes based on mean wind speed values have been studied by Aslan (1997) and Aslan et al., (2002).

Determination of Daily Wind Speed

The cumulative Weibull distribution function $F(u)$ and probability density function $f(u)$ are defined by Skidmore (1986) and (1995) as below:

$$F(u) = 1 - \exp [-(u/c)^k] \quad (4)$$

where u is wind speed, k the shape parameter (dimensionless) and c the scale parameter (m/s).

$$F(u) = dF(u)/du = (k/c)(u/c)^{k-1} \exp [-(u/c)^k] \quad (5)$$

$$F_1(u) = [(F(u) - F_o) / (1 - F_o)] = 1 - \exp [-(u/c)^k] \quad (6)$$

where $F_1(u)$ is the cumulative distribution with the calm periods eliminated, and F_o the frequency of the calm periods. The dependent variable is wind speed u given by

$$u = c \{ -\ln[1 - (F(u) - F_o) / (1 - F_o)] \}^{1/k} \quad (7)$$

The program draws a random number, $0.0 < RN < 1.0$ which is assigned to $F(u)$, and subtracted from it the frequency of calm periods F_o .

Determination of Sub-daily Wind Speed

Program reads from the wind data-base the ratio of maximum to minimum mean hourly wind speed and the hour of maximum wind speed for the location and month under consideration. Calculate the maximum and minimum wind speed for the day based on the representative wind speed as calculated above and given the ratio of maximum to minimum wind speed:

$$u_{rep} = (u_{max} + u_{min}) / 2 \quad (8)$$

$$u_{ratio} = u_{max} / u_{min} \quad (9)$$

where u_{rep} is the daily mean representative wind speed as calculated from Eq. (8) and u_{ratio} the ratio of daily maximum u_{max} to daily minimum u_{min} wind speed. Wind speed for any hour of the day $u(I)$ can be simulated from

$$u(I) = u_{rep} + 0.5 (u_{max} - u_{min}) \cos [2\pi(24 - hr_{max} + I)/24] \quad (10)$$

where hr_{max} is the hour of the day when wind speed is maximum and I the index for hour of day.

Aridity Index

Aridity index AI is given by the following equation (Türkes. 1999; Aslan and Tokgözlü, 2000).

$$AI = P/PE \quad (11)$$

where P is the annual total precipitation (mm) and PE the potential evaporation (mm). Aridity Index values for arid and dry sub-humid areas have been ranged between 0.05 and 0.65.

ANALYSIS

Analysis of Rain-Erosivity

Time variation of regional average annual total precipitation values in Turkey shows a increasing trend between 1900-1998. Erosivity values determined for overall over Turkey (average value) show severe erosion risk in winter. Table 2 gives some statistical characteristics of annual regional total precipitation and FI values based on the "Climate, Impacts LINK Project" (Giorgi and Francisco, 2000; New et al., 1999, 2000); Aslan et al., (2002).

Table 2. Seasonal variation of erosivity (Fournier Index) and erosion risk class in Turkey.

Year	Spring	Erosion Class	Summer	Erosion Risk Class	Autumn	Erosion Class	Winter	Erosion Class	Mean	Erosion Class
1900-1930	20.9	Very Low	10.4	Very Low	54.2	Moderate	78.2	Severe	40.9	Low
1931-1960	30.7	Low	28.5	Low	47.5	Moderate	59.8	Moderate	41.6	Moderate
1961-1998	36.3	Low	24.5	Low	47.0	Moderate	60.7	Severe	42.1	Moderate
1900-1998	33.9	Low	27.1	Low	48.2	Moderate	59.6	Moderate	42.2	Moderate

Analysis of Wind Speed and Erosion

Data used in this study is hourly wind speed measurements from an automatic wind recording system mounted in Gökçeada (Tuzburnu, Altitude: 34m msl, Latitude: 40° 11' N, Longitude: 25° 54' E) between 1997 and 1998, and Ugurlu, Çınaralti and National Station between 1992-1993, 1997-1998). To define water erosion at the study area, monthly and annual rainfall rate values based on long term observations are analysed.

When the other wind speed values are considered at Ugurlu, Çınaralti and National Station between 1992-1993, the linear regression coefficient r between wind speed observations u and theoretical values is 0.97 with the significant level 1 (confidence limits 0.99). The linear regression coefficient r between wind speed observations u^3 and theoretical values at all stations in Gökçeada (Tuzla, Ugurlu, Çınaralti and National Station) between 1992-1993, and 1997-1998) is 0.94 with the significant level 1 (confidence limits 0.99) (Figure 1).

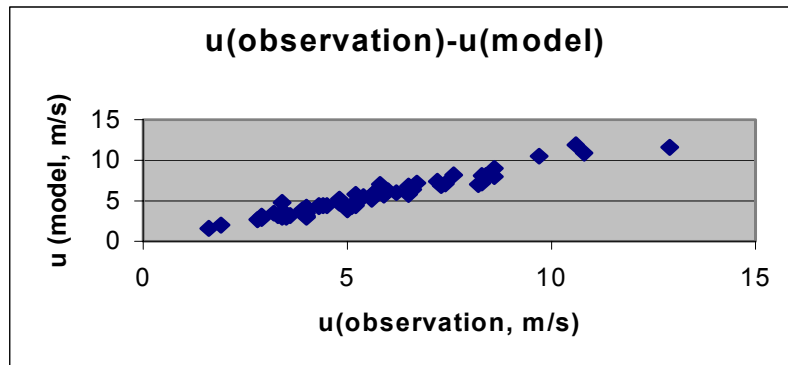


Figure 1. Linear relation between average wind speed values at Gökçeada (Tuzla, Ugurlu, Çınaralti, National Station) between 1992-1993 and 1997-1998.

ACKNOWLEDGEMENTS

This study has been supported by The Turkish Scientific and Research Council (TÜBİTAK, Project No: TOGTAĞ- 2846). The authors also wish to thank the Abdus Salam International Centre for Theoretical Physics and Prof. F. Giorgi and the Climate Impacts LINK project members for gridded data supporting.

REFERENCES

- Aslan, Z., (1997) Analysis of Rainfall Erosivity and Climatic Factor of Wind Erosion. ICTP Pre-print, IC/97/135, Trieste, Italy.
- Aslan, Z., and A. Tokgözlü, (2000) Climatological Changing Effects on rainfall Erosivity and Wind Erosion”, AGROENVIRON2000: 2nd. International Symposium on New Technologies for Environmental Monitoring and Agro-Applications, Tekirdag, Turkey, pp.265-273.
- Aslan, Z., E. Skidmore, E. Feoli, D. Maktav, H. Erol, F. S. Erbek, D. Okçu, A. S. Sogut, P. Giacomich, S. Mauro, K. Mighozzi, (2002) “The Use of Conventional Data and Remote Sensing for Classification of Erosion and Land Degradation”, 3rd. AGROENVIRON Symposium, 26-28 October, Cairo.
- Flanagan, D.C and J. Livingston, (1995) USDA-Water Erosion Prediction Project (WEPP), Soil and Water Conservation Society, Iowa, USA, pp.131.
- Gabriels, D., (1993) The USLE for Predicting Rainfall Erosion Losses. ICTP-SMR. 705-3. Trieste, Italy.
- Giorgi, F., and R. Francisco, 2000- Evaluating uncertainties in prediction of regional climate changing. Geophysical letters, Vol. 27, No. 9, pp. 1295-1298.
- New, M. G., M. Hulme and P. D. Jones, (1999) Representing 20th century space-time climate variability. I: Development of a 1961-1990 mean monthly terrestrial climatology. J. Climate. Vol. 12, pp. 829-856.
- New, M. G., M. Hulme and P. D. Jones, (2000) Representing 20th. Century space-time climate variability. II: Development of 1901-1996 monthly terrestrial climate fields. J. Climate. Vol. 13, pp. 2217-2238.
- Odoro-Afriye, K., (1996) Rainfall Erosivity Map for Ghana”, Geoderma, Elsevier Science B.V., 1125, pp.6.
- Piervitali, E., M. Conte and M. Colacino. (1999) Rainfall Over the Central-Western Mediterranean Basin in the Period, 1951- 1995.II. Precipitation Scenarios. Nuovo Cimento C. 22C. 5. pp. 649 - 661.
- Pla Sentis, I., (1998) Modeling the Influence of Soil Sealing and Soil Compaction on Soil Erosion Processes, College on Soil Physics, ICTP/SMR.1065-9, Trieste, Italy.
- Skidmore, E. L., (1986) Wind Erosion Climatic Erosivity, Climate Change, 9, pp. 195-208.
- Skidmore, E.L., (1995) Wind Erosion Climatic Erosivity, ICTP College on Soil Physics, SMR., 873-19, Trieste, Italy.

- Skidmore, E., L., (2000a) Air, Soil, and Water Quality as Influenced by Wind Erosion and Strategies for Mitigation, AGROENVIRON2000: 2nd. International Symposium on New Technologies for Environmental Monitoring and Agro-Applications”, Tekirdag, pp.216-221.
- Skidmore, E., L., (2000b) Sustainable Agriculture: Actions and Strategies, AGROENVIRON2000: 2nd. International Symposium on New Technologies for Environmental Monitoring and Agro-Applications”, Proceedings (Workshops), Tekirdag, Turkey, pp. 1-3.
- Tulunay, E., E. T. Senalp, Y. Tulunay and Z. Aslan, (2002) “Development of Neural Net Based Models for Non-Linear Agro-Environmental systems”, 3rd. AGROENVIRON Symposium, 26-28 October, Cairo.
- Turkes, M., (1999) Vulnerability of Turkey to Desertification With Respect to Precipitation and Aridity Conditions. Tr. J. of Engineering and Environmental Science. 23. pp. 363-380.

In-Situ Determination of Directional Conductivities of Soil

Gautam Barua*

*Department of Civil Engineering, Indian Institute of Technology,
Guwahati, India*

*Lecture given at the
College on Soil Physics
Trieste, 3 – 21 March 2003*

LNS0418005

* barua@nerist.ernet.in

Darcy's law mostly governs the flow of fluid in a porous medium. For an anisotropic medium, Darcy's law at a point P in a porous continuum (Bear, 1972) may be expressed as

$$\begin{bmatrix} v_1 \\ v_2 \\ v_3 \end{bmatrix} = \begin{bmatrix} K_{11} & K_{12} & K_{13} \\ K_{21} & K_{22} & K_{23} \\ K_{31} & K_{32} & K_{33} \end{bmatrix} \begin{bmatrix} -\frac{\partial \phi}{\partial x_1} \\ -\frac{\partial \phi}{\partial x_2} \\ -\frac{\partial \phi}{\partial x_3} \end{bmatrix} \quad (1)$$

where v_1, v_2 and v_3 are the components of Darcy velocity \mathbf{v} and ϕ is the average hydraulic head over a representative elemental volume REV at the point P . The second rank symmetric tensor

$$\mathbf{K} = \begin{bmatrix} K_{11} & K_{12} & K_{13} \\ K_{21} & K_{22} & K_{23} \\ K_{31} & K_{32} & K_{33} \end{bmatrix} \quad (2)$$

is called the hydraulic conductivity of the porous medium. Thus,

$$v_i = -K_{ij} \frac{\partial \phi}{\partial x_j} = -K_{ji} \frac{\partial \phi}{\partial x_j} = -K_{ji} \frac{\partial}{\partial x_j} \left(-\frac{p}{\rho g} + z \right); \quad (i = 1, 2, 3) \quad (3)$$

Hydraulic conductivity \mathbf{K} is a macroscopic parameter which depends on the properties of both the fluid as well as the porous matrix. At a point P in a porous medium, it may be expressed as

$$\mathbf{K} = \frac{\mathbf{k} \rho g}{\mu} \quad (4)$$

where ρ and μ are the macroscopic averages of density and viscosity of the fluid over an REV at the point P , g is the acceleration due to gravity, and \mathbf{k} is the intrinsic permeability of the medium. It should be noted that \mathbf{k} is independent of the properties of the fluid and has the dimensions of L^2 . From equations (3) and (4), we obtain

$$v_i = -\frac{k_{ij}}{\mu} \left(\frac{\partial p}{\partial x_j} + \rho g \frac{\partial z}{\partial x_j} \right) \quad (5)$$

Stratified soils are usually anisotropic in nature. In most soils, the water transmitting capacity in the horizontal direction is observed to be higher than the vertical conductivity. However, in many soils (e.g., loess), vertical joints, root holes

and animal burrows make the vertical conductivity higher than the horizontal. Accurate estimations of the horizontal and the vertical conductivities of a soil medium in its natural water-saturated state is of considerable importance in obtaining rational solutions to drainage and other groundwater flow problems.

One of the most commonly used and reliable methods for in-situ determination of saturated hydraulic conductivity of soil below a water table is the auger hole method (Dorsey et al., 1990). The method was described in detail, among others, by Van Bavel and Kirkham (1948), Luthin (1957), Bouwer and Jackson (1974), Oosterbaan and Nijland (1994). Barua and Tiwari (1995) gave an extensive review of the various theories and procedures associated with the method. The method essentially consists of pumping a cylindrical hole dug below a water table and noting the rate of rise of water in the pumped hole. The rate of rise is then translated into saturated hydraulic conductivity of the soil by applying a suitable theory obtained from the classical works of Kirkham and Van Bavel (1948), Kirkham (1958) and Boast and Kirkham (1971). For an auger hole dug into a water table aquifer and underlain by an impervious stratum, the theories proposed by Barua and Tiwari (1995) may also be employed to get the directional conductivities values; however, if the hole pierces a confined aquifer, none of the above theories can be safely applied and in that case the theories proposed by Barua and Hoffmann (2002) may be used. This lecture will be mainly concerned with the development of a suitable auger hole seepage theory for the confined situation.

Figure 1 shows pumping from an auger hole of radius a dug into a homogeneous and anisotropic confined aquifer of infinite radial extent. An impervious layer at a finite distance from the confining stratum underlies the aquifer. The depth to the impervious layer, partial penetration of the auger hole, level of water in the auger hole, and confining pressure of the aquifer are taken as h_i , H_3 , H_1 and t , respectively, all distances being measured from the confining stratum as shown in the figure. The saturated hydraulic conductivities of the soil in the horizontal and vertical directions are taken as K_r and K_z , respectively. Because of axial symmetry, we consider only one half of the flow domain for analysis located towards the right of the vertical axis passing through the origin O . For convenience, we take the z axis to be positive vertically downward and r axis to be positive towards the right. Further, in the analysis to follow, we assume the flow to be steady, the drawdown near the vicinity of the hole during one experimental cycle to be negligible the aquifer material and water to be incompressible and the principal directions of anisotropy of the aquifer to coincide with the horizontal and vertical directions, respectively. Following a similar approach like that of Barua and Tiwari (1995), we solve the boundary value problem by dividing each flow domain into two sub-domains: (1) the region between the bottom of the hole and the impervious layer and (2) the rest of the flow domain. The hydraulic head function for region (1) is designated as $\phi_{1(i)}$ and for region (2) $\phi_{2(i)}$.

The boundary conditions of the flow problem can now be expressed as

$$\begin{aligned}
\frac{\partial \phi_{1(i)}}{\partial r} &= 0; & r &= 0; & H_3 \leq z \leq h_i & \quad (\text{B.C. I}) \\
\phi_{1(i)} &= -H_1; & z &= H_3; & 0 \leq r \leq a & \quad (\text{B.C. II}) \\
\phi_{1(i)} &= \phi_{2(i)}; & r &= a; & H_3 \leq z \leq h_i & \quad (\text{B.C. IIIa}) \\
K_r \frac{\partial \phi_{1(i)}}{\partial r} &= K_r \frac{\partial \phi_{2(i)}}{\partial r}; & r &= a; & H_3 \leq z \leq h_i & \quad (\text{B.C. IIIb}) \\
\frac{\partial \phi_{1(i)}}{\partial z} &= 0; & z &= h_i; & 0 \leq r \leq a & \quad (\text{B.C. IV}) \\
\phi_{2(i)} &= -z; & r &= a; & 0 \leq z \leq H_1 & \quad (\text{B.C. Va}) \\
\phi_{2(i)} &= -H_1; & r &= a; & H_1 \leq z \leq H_3 & \quad (\text{B.C. Vb}) \\
\phi_{2(i)} &= t; & z &= 0; & a < r \leq \infty & \quad (\text{B.C. VI}) \\
\frac{\partial \phi_{2(i)}}{\partial r} &= 0; & r &= \infty; & 0 \leq z \leq h_i & \quad (\text{B.C. VII}) \\
\frac{\partial \phi_{2(i)}}{\partial z} &= 0; & z &= h_i; & a \leq r \leq \infty & \quad (\text{B.C. VIII})
\end{aligned}$$

In order to obtain solution to the problem as shown Fig. 1, the hydraulic head functions $\phi_{1(i)}$ and $\phi_{2(i)}$, must be determined such that the governing equations

$$K_r \frac{\partial^2 \phi_{1(i)}}{\partial r^2} + \frac{K_r}{r} \frac{\partial \phi_{1(i)}}{\partial r} + K_z \frac{\partial^2 \phi_{1(i)}}{\partial z^2} = 0 \quad (6)$$

in region (1) and

$$K_r \frac{\partial^2 \phi_{2(i)}}{\partial r^2} + \frac{K_r}{r} \frac{\partial \phi_{2(i)}}{\partial r} + K_z \frac{\partial^2 \phi_{2(i)}}{\partial z^2} = 0 \quad (7)$$

in region (2) must be satisfied together with the boundary conditions as listed above.

The quantity of water, $Q_{(i)}$, entering the auger hole is given by

$$Q_{(i)} = 2\pi a \sum_{n=1}^N B_{n(i)} \sqrt{(K_r K_z)} k_{1(i)} \left[\frac{-N_{n(i)} a}{K_0'} \right] \quad (8)$$

where (for $N_{n(i)} \neq N_{m(i)}$)

$$\begin{aligned}
B_{n(i)} = & \frac{-2}{h_i(N_{n(i)})^2} \sin(N_{n(i)}H_1) - \frac{2t}{h_i(N_{n(i)})} \\
& + \sum_{m=1}^M \frac{A_{m(i)}}{h_i} \left\{ \frac{1}{(N_{n(i)} - N_{m(i)})} \sin[N_{m(i)}H_3 + (N_{n(i)} - N_{m(i)})h_i] \right. \\
& \quad - \frac{1}{(N_{n(i)} - N_{m(i)})} \sin[N_{m(i)}H_3 + (N_{n(i)} - N_{m(i)})H_3] \\
& \quad + \frac{1}{(N_{n(i)} + N_{m(i)})} \sin[N_{m(i)}H_3 - (N_{n(i)} + N_{m(i)})h_i] \\
& \quad \left. - \frac{1}{(N_{n(i)} + N_{m(i)})} \sin[N_{m(i)}H_3 - (N_{n(i)} + N_{m(i)})H_3] \right\}
\end{aligned} \tag{9}$$

$$\begin{aligned}
A_{m(i)} = & \sum_{n=1}^N \frac{P_{nm(i)}B_{n(i)}}{(h_i - H_3)} \left\{ \frac{1}{(N_{n(i)} - N_{m(i)})} \sin[N_{m(i)}H_3 + (N_{n(i)} - N_{m(i)})h_i] \right. \\
& \quad - \frac{1}{(N_{n(i)} - N_{m(i)})} \sin[N_{m(i)}H_3 + (N_{n(i)} - N_{m(i)})H_3] \\
& \quad + \frac{1}{(N_{n(i)} + N_{m(i)})} \sin[N_{m(i)}H_3 - (N_{n(i)} + N_{m(i)})h_i] \\
& \quad \left. - \frac{1}{(N_{n(i)} + N_{m(i)})} \sin[N_{m(i)}H_3 - (N_{n(i)} + N_{m(i)})H_3] \right\}
\end{aligned} \tag{10}$$

$$P_{nm(i)} = \frac{(-N_{n(i)})}{(N_{m(i)})} \frac{k_{1(i)} \left(\frac{-N_{n(i)}a}{K_0^a} \right)}{i_{1(i)} \left(\frac{-N_{m(i)}a}{K_0^a} \right)} \tag{11}$$

$$N_{m(i)} = \left\lceil \frac{(1-2m)\pi}{2(h_i - H_3)} \right\rceil \tag{12}$$

$$N_{n(i)} = \left[\frac{(1-2n)\pi}{2h_i} \right] \quad (13)$$

$$i_{0(i)} \left(\frac{-N_{m(i)}r}{K_0^a} \right) = \frac{I_0 \left(\frac{-N_{m(i)}r}{K_0^a} \right)}{I_0 \left(\frac{-N_{m(i)}a}{K_0^a} \right)} \quad (14)$$

$$i_{1(i)} \left(\frac{-N_{m(i)}r}{K_0^a} \right) = \frac{I_1 \left(\frac{-N_{m(i)}r}{K_0^a} \right)}{I_0 \left(\frac{-N_{m(i)}a}{K_0^a} \right)} \quad (15)$$

$$k_{0(i)} \left(\frac{-N_{n(i)}r}{K_0^a} \right) = \frac{K_0 \left(\frac{-N_{n(i)}r}{K_0^a} \right)}{K_0 \left(\frac{-N_{n(i)}a}{K_0^a} \right)} \quad (16)$$

$$k_{1(i)} \left(\frac{-N_{n(i)}r}{K_0^a} \right) = \frac{K_1 \left(\frac{-N_{n(i)}r}{K_0^a} \right)}{K_0 \left(\frac{-N_{n(i)}a}{K_0^a} \right)} \quad (17)$$

$$K_0^a = (K_r / K_z)^{1/2}; \quad (18)$$

$I_0(\cdot)$, $I_1(\cdot)$, $K_0(\cdot)$ and $K_1(\cdot)$ are zero order and first order modified Bessel functions of first and second kinds, respectively, m and n are summation indices 1, 2, 3, $M = N \rightarrow \infty$.

Let us now apply the developed theory to the auger hole experimental data obtained from a real field situation. An auger hole experiment was performed near “De Nieuwelanden” at Wageningen University (The Netherlands) in 2001, where the following data were observed: soil isotropic, i.e. $K_0^a = 1$, confining pressure, $t = 42$ cm, $h_i = 300$ cm, $H_l = 30.5$ cm, $H_3 = 82$ cm, $a = 5$ cm, and rate of rise of water in the auger hole = 0.2680 cm/sec; therefore, $Q_{(i)} = \pi(5)^2 0.2680 = 21.049 \text{ cm}^3/\text{sec}$.

Substituting the above values in equation (8), we obtain

$$21.049 = 2\pi \times 5 \times \sum_{n=1}^N B_{n(i)} \frac{K}{1} k_{1(i)} \left[\frac{-N_{n(i)} \times 5}{1} \right] \quad (19)$$

where

$$N_{m(i)} = \left[\frac{(1-2m)\pi}{2(300-82)} \right] \quad \text{and} \quad N_{n(i)} = \left[\frac{(1-2n)\pi}{2 \times 300} \right]$$

The constants $B_{n(i)}$ of equation (19) can now be determined by means of equations (9), (10) and (11). By expanding up to 100 terms ($M = N = 100$) of the infinite series, we find K to be 0.96 m/day.

If the entire computation is repeated (again by taking $M = N = 100$) by neglecting the confining pressure, i.e. $t = 0$, the K value now turns out to be 2.90 m/day. It can be observed that this value differs considerably from that of 0.96 m/day obtained by considering the confining pressure of the aquifer. As can be seen, an error of about 200% $[(2.90 - 0.96) \times 100/0.96]$ occurs for this flow situation due to neglect of this confining water head.

References

- Barua, G. and Hoffmann, M.R., 2002. Auger hole seepage theories for confined aquifers. A paper submitted to the Editorial Office, Journal of Hydrology, Elsevier Science, Amsterdam, the Netherlands, for review and possible publication in December, 2002.
- Barua, G. and Tiwari, K.N., 1995. Theory of seepage into auger holes in homogeneous anisotropic soil. *J. Hydrol.*, 167: 1-22.
- Bear, J., 1972. *Dynamics of Fluids in Porous Media*. American Elsevier Publishing Company, New York, pp. 119-157.
- Boast, C.W. and Kirkham, D., 1971. Auger hole seepage theory. *Soil Sci. Soc. Am. Proc.*, 35: 365-373.
- Bouwer, H. and Jackson, R.D., 1974. Determining Soil Properties. In: Jan Van Schilfgaarde (Editor), *Drainage for Agriculture*. Am. Soc. Agron. No. 17, Madison, WI, pp. 611-672.
- Dorsey, J.D., Ward, A.D., Fausey, N.D. and Bair, E.S., 1990. A comparison of four field methods for measuring saturated hydraulic conductivity. *Transactions of ASAE*, 33: 1925-1931.
- Kirkham, D., 1958. Theory of seepage into an auger hole above an impermeable layer. *Soil Sci. Soc. Am. Proc.*, 22: 204-208.
- Kirkham, D. and Van Bavel, C.H.M., 1948. Theory of seepage into auger holes. *Soil Sci. Soc. Am. Proc.*, 13: 75-82.

- Luthin, J.N., 1957. Drainage of Agricultural Lands. Am. Soc. Agron., Vol. 7, Madison, WI, pp. 420-432.
- Oosterbaan, R.J. and Nijland, H.J., 1994. Determining the Saturated Hydraulic Conductivity. In: Drainage Principles and Applications, 2nd edn., ILRI Publ. 16, Wageningen, the Netherlands, pp. 435-476.
- Van Bavel, C.H.M. and Kirkham, D., 1948. Field measurement of permeability using auger holes. Soil Sci. Soc. Am. Proc., 13: 90-96.

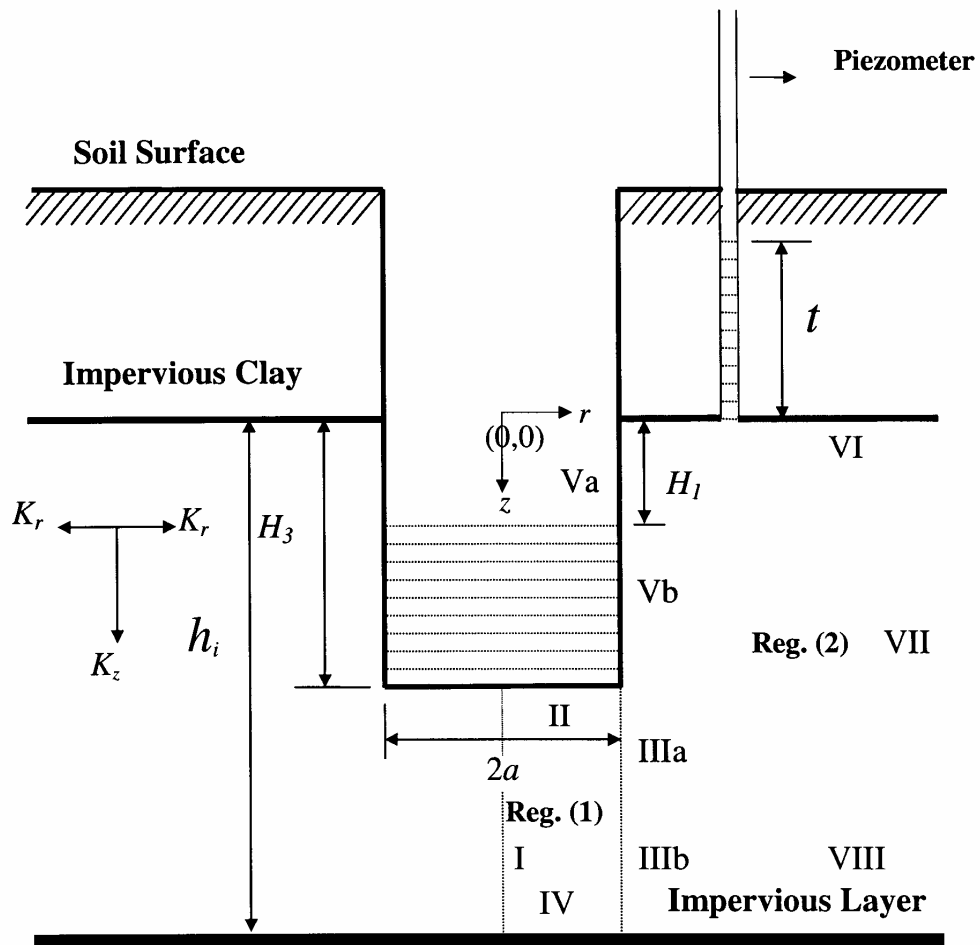


Fig. 1. Geometry of the flow system of a partially penetrating auger hole in a confined aquifer underlain by an impervious layer – water level of the pumped hole lying below the confining clay layer.

Optimal Estimations of Random Fields Using Kriging

Gautam Barua*

*Department of Civil Engineering, Indian Institute of Technology,
Guwahati, India*

*Lecture given at the
College on Soil Physics
Trieste, 3 – 21 March 2003*

LNS04180006

* barua@nerist.ernet.in

Kriging is a statistical procedure of estimating the ‘best weights’ of a linear estimator. Suppose there is a point or an area or a volume of ground over which we do not know a hydrological variable and wish to estimate it. In order to produce an estimator, we need some information to work on, usually available in the form of samples. Let there be a set S of n samples with values $g_1, g_2, g_3, \dots, g_n$. The estimator, T^* , can then be calculated as

$$T^* = w_1 g_1 + w_2 g_2 + w_3 g_3 + \dots + w_n g_n \quad (1)$$

where $w_1, w_2, w_3 \dots w_n$ are the weights assigned to each sample. If all the weights are equal and sum up to one, T^* is just the arithmetic mean of the sample values.

The estimation variance for the general ‘unbiased linear’ estimator can be determined as

$$\sigma_\epsilon^2 = 2 \sum_{i=1}^n w_i \bar{\gamma}(S_i, A) - \sum_{i=1}^n \sum_{j=1}^n w_i w_j \bar{\gamma}(S_i, S_j) - \bar{\gamma}(A, A) \quad (2)$$

where $w_i \bar{\gamma}(S_i, A)$ is the weighted average semi-variogram value between each point in the ‘sample set’ S and each point in the panel A , $w_i w_j \bar{\gamma}(S_i, S_j)$ is the weighted average semi-variogram value between each point in the sample set and each point in the sample set, and $\bar{\gamma}(A, A)$ is the average semi-variogram value between each point in the panel and each point in the panel.

Now for the linear estimator to be unbiased, we require that

$$E(T^*) = E(T) = m \quad (3)$$

$$E\left[\sum_{i=1}^n w_i g_i\right] = E[g_i] \sum_{i=1}^n w_i = m \sum_{i=1}^n w_i = m \quad (4)$$

Thus

$$\sum_{i=1}^n w_i = 1 \quad (5)$$

There can, however, be an infinite number of linear unbiased estimators for which the weights sum up to one. The problem is how to determine the ‘best’ weights for which the estimation variance is the least? This can be done by minimizing σ_ϵ^2 subject to equation (5). This calls for the introduction of a Langrange’s multiplier λ in the minimizing function $F(w_1, w_2, w_3, \dots, w_n, \lambda)$, such that

$$F(w_1, w_2, w_3, \dots, w_n, \lambda) = 2 \sum_{i=1}^n w_i \bar{\gamma}(S_i, A) - \sum_{i=1}^n \sum_{j=1}^n w_i w_j \bar{\gamma}(S_i, S_j) - \bar{\gamma}(A, A) - \lambda \left(\sum_{i=1}^n w_i - 1 \right) \quad (6)$$

Minimizing (6) with respect to $w_1, w_2, w_3, \dots, w_n$ and λ , we obtain the following set of $n+1$ equations

$$\begin{aligned}
 w_1 \bar{\gamma}(S_1, S_1) + w_2 \bar{\gamma}(S_1, S_2) + \dots + w_n \bar{\gamma}(S_1, S_n) + \lambda &= \bar{\gamma}(S_1, A) \\
 w_1 \bar{\gamma}(S_2, S_1) + w_2 \bar{\gamma}(S_2, S_2) + \dots + w_n \bar{\gamma}(S_2, S_n) + \lambda &= \bar{\gamma}(S_2, A) \\
 \dots & \dots \dots + \lambda \dots \\
 w_1 \bar{\gamma}(S_n, S_1) + w_2 \bar{\gamma}(S_n, S_2) + \dots + w_n \bar{\gamma}(S_n, S_n) + \lambda &= \bar{\gamma}(S_n, A) \\
 w_1 + w_2 + \dots + w_n &= 1
 \end{aligned} \tag{7}$$

The system of equations as shown above is generally known as the kriging system and the estimator produced is the kriging estimator. The variance of the kriging estimator can be found by substitution of the weights in the general estimation variance equation (2). However, it can be shown that the kriging variance σ_ϵ^2 can be expressed as

$$\sigma_k^2 = \sum_{i=1}^n w_i \bar{\gamma}(S_i, A) + \lambda - \bar{\gamma}(A, A) \tag{8}$$

These lecture notes have been compiled from the following texts (Clark, 2001; Gelhar, 1993).

Example

Let us now show an application of the kriging equations to a one-dimension problem. Let there be a line segment of length l and let it contain three samples, S_1, S_2, S_3 , one at the beginning, the other at the middle, and the last at the end of the line as shown in the figure below

We assume here a linear model for the semi-variogram of the form $\gamma(h) = ph$ where h is the separation and p is the slope of the semi-variogram. For the model considered, $\lambda(A, A)$ works out to be $pl/3$ and $\lambda(S, A)$ becomes equal to $pl/2$. Applying the model to equation (7), we obtain the following set of kriging equations

$$\begin{aligned}
 w_2 pl/2 + w_3 pl + \lambda &= pl/2 \\
 w_1 pl/2 + w_3 pl/2 + \lambda &= pl/4 \\
 w_2 pl/2 + w_3 pl + \lambda &= pl/2 \\
 w_1 + w_2 + w_3 &= 1
 \end{aligned}$$

By solving these equations, we obtain $\lambda = 0, w_1 = w_3 = 1/4$ and $w_2 = 1/2$. Substituting these values in (8), we obtain the kriging variance σ_k^2 to be $pl/24$. If we evaluate the estimation variance by treating all the weights to be same (arithmetic mean), we

find σ_{ϵ}^2 to be $pl/18$. Thus, for the one-dimensional problem considered, kriging definitely gives a better estimation variance than the extension variance.

References

- Clark, I., 2001. Practical Geostatistics. Geostokos Limited, Alloa Business Centre, Whins Road, Alloa, Scotland. This text is freely available in the net.
- Gelhar, LW, 1993. Stochastic Subsurface Hydrology, Prentice Hall, Englewood Cliffs, New Jersey.

Rice Lands of South and South East Asia, Some Soil Physical Aspects

R.M. Bhagat*

Department of Soil Science, CSKHPAU, Palampur, H.P., India

*Lecture given at the
College on Soil Physics
Trieste, 3 – 21 March 2003*

LNS0418007

* rmbhagat@glide.net.in

Worldwide about 148 million ha are planted to rice (*Oryza sativa* L.) each year, taking into account double and triple cropping. About 90 percent of this area is in Asia and two thirds in South and South-East Asia, where rice is the most dominant crop grown during the wet season. When wetland rice is included in a cropping system, the soils undergo unique changes in physical properties (Bhagat et al., 1996). Wet tillage or puddling has become synonymous with wetland rice culture and it refers to the destruction of aggregated condition of the soil by mechanical manipulation within a narrow range of moisture contents above and below field capacity (0.03 MPa), so that soil aggregates lose their identity and the soil is converted into a structurally more or less homogenous mass of ultimate particles. During puddling, soils are subjected to two kinds of deforming stresses: (a) the normal stress (load) associated with compression and (b) tangential stress causing shear. The compression is more effective below the upper plastic limit (moisture content at which the soil-water system can flow as a sticky fluid paste); shearing effects dominate above the upper plastic limit. The work done in puddling can be represented by the following relation:

$$W = -\int_{V_i(c)}^{V_f(c)} P dv - \int_{V_f(c)}^{V_z} P dv / M_s + \int_{\eta_0}^{\eta_z} T d\eta$$

Total work done in puddling	=	Work done by normal stress before shear	-	Work done by normal stress during shear	+	Work done by tangential stress during shear
-----------------------------------	---	---	---	---	---	---

where P is the normal stress, M_s the mass of dry soil, T the torque, η the angular rotation of a piston, v the apparent specific volume, $V_i(c)$ the initial specific volume at the beginning of normal stress, $V_f(c)$ the final specific volume due to normal stress, V_z the terminal value due to shear, η_0 the zero angular displacement of a piston, and η_z the final displacement of a piston.

Puddling or wet tillage coupled with submerged conditions are responsible for making drastic effects on soil physical characteristics of rice soils. These effects can be continued either for short time or long time. During rice-rice or rice-wheat cropping sequence the system undergoes transition from saturated to unsaturated conditions. While this happens, the soil physical properties again undergo changes. The following discussion shows how the physical characteristics of the whole soil system behave:

Soil structure

Puddling destroys and coverts aggregates and peds into plastic mud. When an initially dry soil is wetted, there is uneven swelling of aggregates, which subsequently explode due to entrapped air resulting in aggregates slaking. Continuous wet tillage (repeated plowings and harrowings) converts the soil into a plastic mud with massive

structure. While the puddled layer is not uniform, a drop in mean weight diameter has been observed. In the puddle layer, clay particles are oriented in parallel rows and are surrounded by water saturated capillary pores. The soil matrix therefore exhibits a two phase system i.e. solid and liquid, the gaseous phase is either missing or some air is entrapped in storage and residual pores. The practice of lowland rice-rice system in some parts of South and South East Asia has made the soils excessively soft due to puddling season after season resulting in a progressive deterioration in soil structure. In fact these soils do not get time to rejuvenate by way of renewal of soil aeration.

In a long term study on lowland rice carried out in north-western India (Table 1), it was observed that, immediately after lowland rice harvest water stable aggregates WSA > 0.25 mm as well as the mean weight diameter MWD were lower in puddled plots compared to the non puddle plots (Bhagat et al., 1994). Long term addition of residue at 30 t ha^{-1} , although increased both the WSA and MWD of puddled plots, but the trend remained the same. In a six years study of a lowland- rice and upland-wheat system (Table 3), WSA > 0.25 and MWD determined after six rice crops were significantly lower in a continuously puddled silty clay loam soil (Sharma et al., 1995). Addition of residues although improve aggregation status of this soil.

Bulk density and soil strength

Puddling effects on bulk density are dependent on the aggregation status of the soil before puddling. If a parallel oriented, closely packed structure is produced from a well aggregated open structure, bulk density would increase. The strong inter-particle forces favor well oriented structure, while weak inter-particle forces favor an open gel structure. Initial submergence before tillage (a practice in many parts of Asia) also decreases bulk density. Bulk density increases when the puddled soils undergo desiccation in a lowland-upland (e.g. rice-wheat) situation because of soil shrinkage.

During lowland rice growth (Table 2), bulk density significantly decreased under puddled plots compared to non puddled plots (Bhagat et al. 1999a). However, when the lowland system made a transition to upland system, significant increase in bulk density was observed (Table 1) when no residues were added (Bhagat et al., 1994).

The puddle soils become very hard upon drying and progressively develop polygonal cracks, whose width and depth increases with time, depending upon the nature and type of clay and the moisture regime. The crack spacing depends on the ability of the soil to deform under tensile stresses, which are generated parallel to the soil surface, when the puddled soil dries and shrinks. The cracked soils dry very quickly, because of development of the secondary planes of evaporation at the exposed edges. The open cracked hard soils are difficult to till and upon tillage brings out large clods (big lumps of soil weighing from few grams to few kilograms). These clods have high clod breaking strength CBS and require large amount of energy to break them to prepare a fine seed bed (for a proper seed-soil contact for germination). Sharma et al. (1995) have found out that a puddle soil without residues had the highest CBS compared to the puddle soils with residues (Table 3). In the same study

the non puddled soil (data not shown) had lower CBS compared to the puddle soil. On the other hand, when a hard desiccated soil is puddle under wet condition, it brings the soil particles back into the suspension and lowers the bulk density. The bulk density, however, may increase when the soil is still submerged, due to settling of particles. The particles may settle and consolidate because of self flocculation of dispersed clay, depending possibly on soil texture and type of clay. Settling is faster in sandy soils with kaolinitic mineralogy.

The soil strength is a measure of resistance that must be overcome to cause penetration/deformation in soil. This resistance is to both volumetric compression and linear deformation, which depends on moisture content, texture, type and amount of clay and the arrangements of particles in the soil matrix. The soil strength falls rapidly with increase in moisture content and increases with an increase in bulk density. The very high moisture content and a fairly loose arrangement of soil particles in the puddle layer may bring the soil strength to near zero. However when the puddle soils dry out soil penetration resistance increases rapidly, as bulk density increases. Figure 1 shows lower penetration resistance in non puddled plots compared to puddled plots in a desiccating soil of northern India (Bhagat et al., 1994). Although the soil penetration can be rapidly measured with a penetrometer, the readings need careful interpretation because a wide combination of soil properties may give rise to the same values.

The pore space

Change in the orientation of soil particles in puddled layer brings about changes in soil porosity. The parallel oriented structure produced following puddling from an initially open gel structure, total porosity will decrease. Total pore volume may, however, temporarily increase upon puddling. But an ultimate decline in total porosity is noticed upon puddling in many studies (Bhagat, 1990; Sharma and Bhagat, 1993; Bhagat et al., 1994). Bhagat et al. (1999a), in study on tillage effects on lowland rice observed that puddling decreased drainage pores and increased water retention pores. The pore size distribution also undergoes major changes upon puddling. Sharma and Bhagat (1993) have found out that puddling decreased water transmission pores from 14.6 to 10.9 per cent in loamy sand, 10.2 to 6.8 per cent in silt loam, 23.2 to 7.3 percent in loam and 17.6 to 4.9 percent in clay loam. The depth of puddling further influences the total porosity in the soil to deeper depths, thereby affecting the water flux through the soil. The results of the studies carried out by Sharma and Bhagat (1993) indicated that flux was a negative power function of puddling depth. About 95 percent reduction in water flux due to per unit increase in puddling depth was explained by the linear function of clay content, whereas the relative water flux was an exponential function of clay content (Fig. 2). The measurement of porosity of puddled soils should be carefully made, because the capillary rise equation normally used for rigid porous system is difficult to apply in non-rigid, swollen system, which deflates (shrinks) when the moisture loss occurs.

Changes in pore space (pore size distribution) upon puddling effects other soil physical properties like the aeration status, the retention-transmission characteristics and evaporation losses of soils.

Water retention and transmission characteristics

Depending upon the soil texture and the initial aggregation status at low soil water potential (more negative), water retention in puddled soils is always higher than the non puddle soil. In a long term study on rice straw management in lowland rice - upland wheat system, Bhagat and Verma (1991) observed that water retention was always higher in plots which were puddle in a previous rice compared to the non puddle plots, even if these were supplied with straw mulch or farm yard manure in the following upland wheat crop (Fig 3). Normally the available water capacity [defined as per the classical concept to be $(\eta_{0.01\text{MPa}} - \eta_{1.5\text{MPa}})$] of puddled soil is higher than the non puddle soil. However, when the submerged puddle soils revert back to upland non puddle condition, its water retention falls. Resaturation of such soils may not necessarily restore the soils original water retention capacity. Close packing of soil particles in parallel orientation in puddle soils reduces their saturated hydraulic conductivity and percolation losses in submerged puddled rice fields. Continuous inclusion of lowland puddled rice in a cropping sequence year after year results in the development of hard subsurface layers, which act as a hydraulic barrier and impede water movement. However, the puddling effects on water transmission characteristics vary widely with soil type, intensity of puddling, and the type of the implement used. Percolation rates have been found to fall rapidly with the increase in intensity of puddling in several soils. In a study carried out in Central Luzon, Philippines (Table 4), it was observed that increased tillage intensity (repeated puddling) in lowland rice significantly decreased percolation +seepage compared to less intensive tillage (Bhagat et al., 1999b).

The thermal regime

Wet tillage (puddling) in rice soils affects the thermal regime by changing soil properties, such as bulk density, moisture regime and the transmission characteristics. Thermal conductivity (k) and the volumetric heat capacity (c) increase with bulk density and moisture content, because the k and c of soil particles and water are much higher than those of air. Thermal diffusivity (k/c), which denotes the temperature changes in any part of soil, also increases with increasing moisture content to about -0.1 MPa water potential and then it falls, because above -0.1 MPa water potential, c increases much faster than k . Increase in percolation rates may increase or decrease soil temperature depending on irrigation water temperature and solar radiation received.

Thermal regimes of air, flood water and soil monitored for diurnal variations in temperature, shown in Fig. 4, indicate that for flood water as well as soil, the puddled plots always maintained a higher temperature compared to non puddle plots.

(Bhagat et al., 1994). Increase in temperature following puddling is attributed to a decrease in percolation rates. In puddled plots water continue to pond on the surface for longer periods compared to non puddled plots resulting in an increase in temperature.

References

- Bhagat, R.M. 1990. Effect of tillage and residue management on hydro-thermal regime, nutrient uptake and yield of wheat in a river deposit. *Soil Tillage Res.* 17: 315-326.
- Bhagat, R.M. and Verma, T.S. 1991. Impact of rice straw management on soil physical properties and wheat yield. *Soil Sci.* 152: 108-115.
- Bhagat, R.M., Sharma, P.K. and Verma, T.S. 1994. Tillage and residue management effects on soil physical properties and rice yield in north- western Himalayan soils. *Soil Tillage Res.* 29: 323-334.
- Bhagat, R.M., Bhuiyan, S.I. and Moody, K. 1996. Water, tillage and weed interactions in lowland tropical rice: A review. *Agril Water Mgt.* 31: 165-184.
- Bhagat, R.M., Mangotra, M. and Sharma, Pradeep K (1999a). Tillage effects on soil physical properties and yield of rainfed rice (*Oryza sativa* L.). *J. Indian Soc. Soil Sci.* 47: 415-421
- Bhagat, R.M., Bhuiyan, S.I. and Moody, K. 1999b. Water, tillage and weed management options for wet seeded rice in the Philippines. *Soil and Tillage Res.*, 52: 51-58
- Sharma, P.K. and Bhagat, R.M. 1993. Puddling and compaction effects on water permeability of texturally different soils. *J. Indian soc. Soil Sci.* 41: 1-6.
- Sharma, Pradeep K., Verma, T.S. and Bhagat, R.M. 1995. Soil structural improvements with addition of Lantana camara biomass in rice-wheat cropping. *Soil Use and Management*, 11: 199-203.

Table 1. Mean values of water - stable aggregates (WSA) greater than 0.25 mm, mean weight diameter (MWD), bulk density, total porosity and saturated hydraulic conductivity for 0-0.15 m depth under various treatments.

(Bhagat, R.M., Sharma, P.K. and Verma, T.S., 1994)

Structural indices	Treatment*						L.S.D. (0.05)
	PM ₃	CM ₃	NPM ₃	PM ₀	CM ₀	NPM ₀	
WSA>0.25mm (g(100 g) ⁻¹)	40.6	39.7	42.7	37.5	38.2	39.0	3.5
MWD (mm)	2.38	2.24	3.01	2.10	2.30	2.27	0.34
Bulk density (Mg m ⁻³)	1.37	1.44	1.28	1.55	1.52	1.29	0.14
Total porosity (m ³ (100 m) ⁻³)	46.8	44.2	50.3	39.9	41.0	50.0	3.7
Saturated Hydraulic conductivity (m s ⁻¹)	8.33x10 ⁻⁷	7.77x10 ⁻⁷	1.37x10 ⁻⁶	3.88x10 ⁻⁷	3.33x10 ⁻⁷	4.72x10 ⁻⁷	-

*P = Puddling; C = Compaction; NP = Non puddled dry tillage; M₀ = No residue; M₃ = 30t ha⁻¹ residue

Table 2. Soil physical properties at 60 days after seeding for the surface (0-0.15 m) depth in a wet season.
(Bhagat, R.M, Mangotra, M., and Sharma, P.K., 1999)

Treatment*	Bulk density (Mg m ⁻³)	Soil penetration resistance (MPa)	Pore size distribution			Hydraulic conductivity (m s ⁻¹)
			% of total porosity			
			Drainage pores (>50 λm)	Water retention pores (0.5 -50 λm)	Residual pores (<0.5 λm)	
DS	1.01	0.80	14	40	46	4.70x10 ⁻⁶
DS+H	0.89	0.58	6	50	44	1.00x10 ⁻⁶
DS+FYM	0.98	0.69	17	40	43	3.30x10 ⁻⁶
C	1.24	1.05	9	42	49	0.90x10 ⁻⁶
RF	1.10	0.95	14	42	44	3.25x10 ⁻⁶
P+TP	0.95	0.63	4	51	45	1.10x10 ⁻⁶
CD (<i>p</i> = 0.05)	0.06	0.18	-	-	-	1.18x10 ⁻⁶

*DS = Dry conventionally tilled plots; DS+H = Dry conventionally tilled plots followed by wet tillage (*Halod*) at 3-4 leaf stage of rice; DS+FYM = Dry conventionally tilled plots supplied with 10 t ha⁻¹ farm yard manure; C = Soil compaction; RF = Ridge furrow system; P+TP = Puddling and transplanting

Table 3. Effect of six annual applications of *Lantana camara* on bulk density of soil, aggregates and clods, water stability of aggregates and clod-breaking strength in a silty clay loam soil under rice-wheat cropping. (Sharma, P.K., Verma, T.S. and Bhagat, R.M., 1995).

Lantana application (t ha ⁻¹)	Bulk density (t m ⁻³)				Water Stable aggregates >0.25 mm (%)	Aggregate porosity (%)	Mean weight diameter (mm)	Clod breaking strength (kPa)
	Soil		Aggregates	Clods				
	0-7.5 cm	7.5-15 cm	(2-8 mm)	4-6 cm				
0	1.42	1.48	1.54	1.49	72.9	38.2	2.66	419.9
10	1.39	1.48	1.50	1.45	79.0	39.8	3.89	377.2
20	1.34	1.46	1.49	1.44	81.9	40.2	4.18	220.8
30	1.31	1.38	1.48	1.40	82.8	40.6	4.09	215.6
L.S.D. (p ≤ 0.05)	0.05	0.07	0.04	0.03	3.3	1.04	0.67	87.0

Table 4. Changes in Percolation plus seepage during Wet season of 1995 (WS-95) and Dry season of 1996 (DS-96)
(Bhagat, R.M., Bhuiyan, S.I., and Moody, K. 1999).

Season	Weeks after planting	Treatments						LSD ^f		ET ^g
		W1 ^a T1 ^b	W1 ^a T2 ^d	W2 ^c T1 ^b	W2 ^c T2 ^d	W3 ^c T1 ^b	W3 ^c T2 ^d	Tillage	Water	
WS-95	2	17.7	17.1	16.9	17.0	10.1	9.4	ns ^h	3.1	4.5
	4	24.0	21.9	18.1	16.4	7.5	6.2	ns ^h	7.8	4.7
	6	20.3	16.7	15.9	16.4	7.7	8.2	1.2	6.1	4.3
	8	16.1	16.9	6.9	9.7	8.4	6.7	1.3	5.9	5.3
	10	11.9	11.4	5.3	5.6	5.1	6.0	ns ^h	5.5	4.4
	12	6.6	4.8	4.5	3.7	2.1	1.7	ns ^h	ns ^h	4.2
	14	1.4	1.1	0.0	0.4	0.1	0.0	ns ^h	ns ^h	5.3
DS-96	2	22.1	21.5	22.0	20.5	16.5	14.2	ns ^h	2.5	5.2
	4	19.7	22.5	22.5	17.6	13.5	12.0	ns ^h	3.2	5.8
	6	21.7	20.4	18.6	16.5	12.4	10.4	1.5	3.1	5.8
	8	17.4	14.6	13.5	12.0	10.6	9.0	1.3	2.1	5.28
	10	12.3	11.4	8.4	7.2	6.2	6.0	ns ^h	ns ^h	4.6
	12	11.5	11.6	5.6	4.5	4.0	2.5	ns ^h	ns ^h	5.1
	14	7.8	5.5	4.6	3.1	3.0	1.8	ns ^h	ns ^h	5.8

^a Shallow flooding throughout the crop growth; ^b One plowing+two harrowings; ^c Shallow flooding until panicle initiation then saturation; ^d Two plowings+two harrowings; ^e Saturated soil; ^f Least significant difference; ^g Daily transpiration rate; ^h Not significant

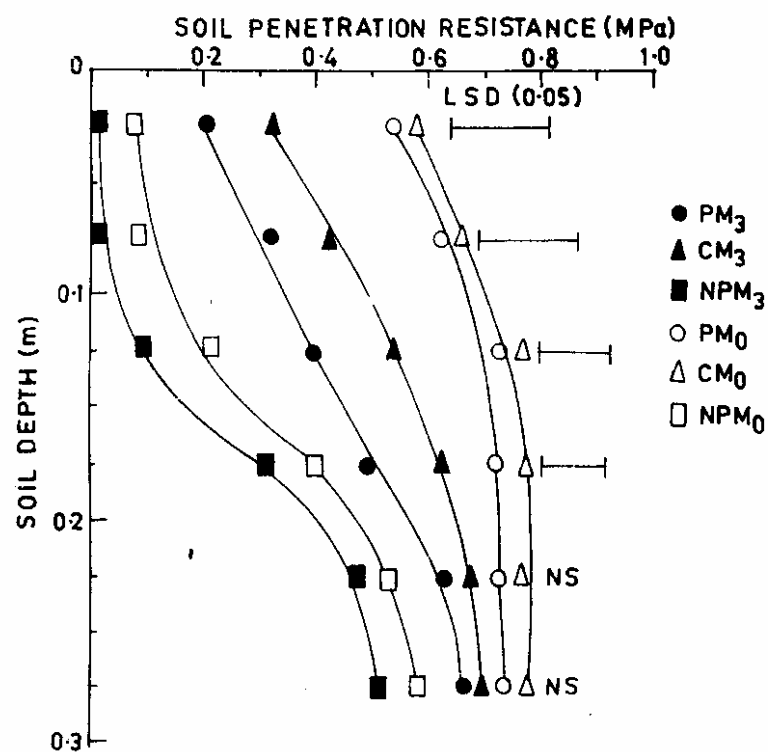


Fig.1. Soil penetration resistance one month after rice harvest for the 0-0.30 m depth under various treatments. P = Puddled; NP = Non puddle; C = Compaction; M0 = No residue; M3 = 30 t ha⁻¹ residue addition. (Bhagat et al., 1994)

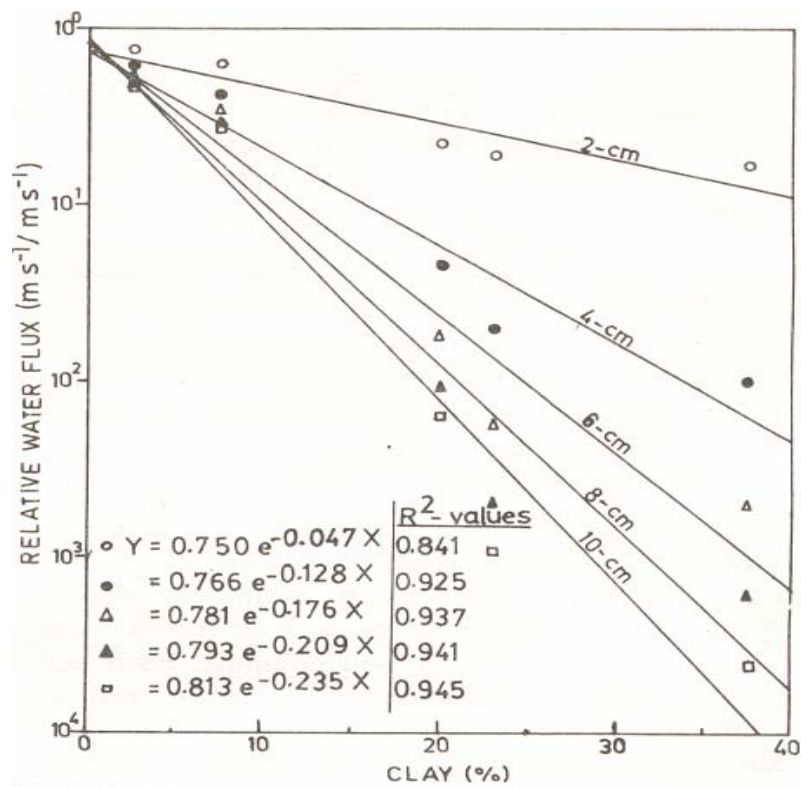


Fig 2. Relative water flux (the ratio of water flux in puddle to the one in non puddle soil) in relation to the clay content of soils. (Sharma and Bhagat, 1993)

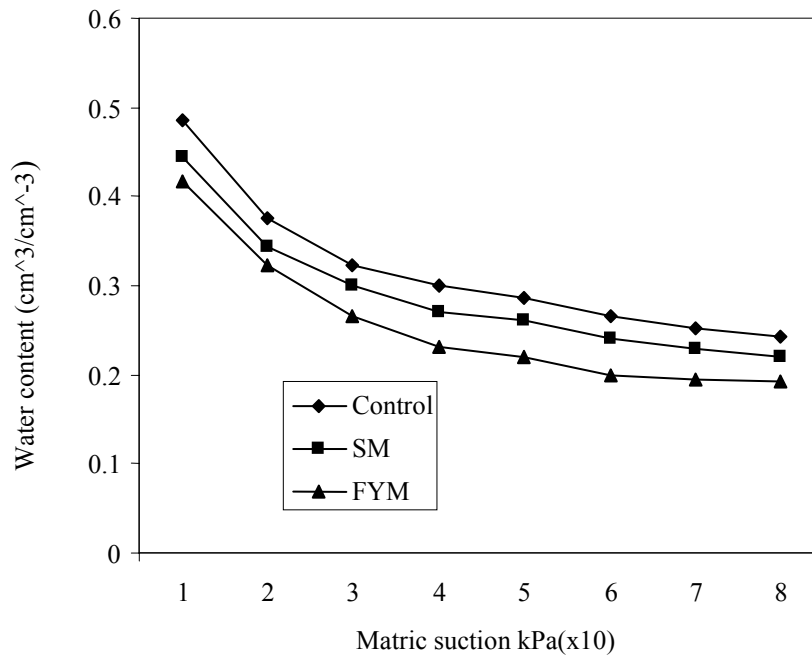


Fig. 3. Soil water release curves under different treatments. Control=Puddling with no residue; SM= Straw mulching; Farm yard Manure. (Bhagat and Verma, 1991)

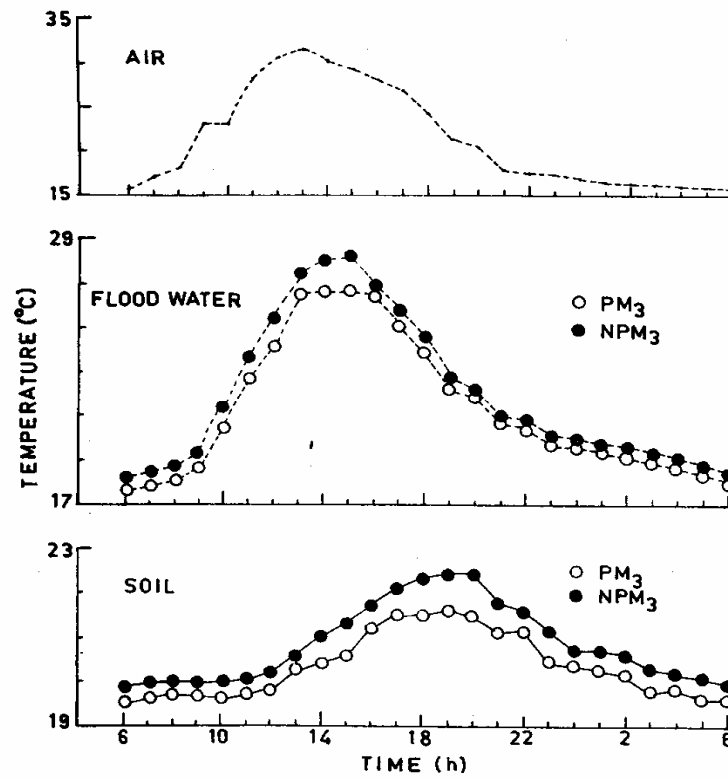


Fig 4. Diurnal temperature fluctuations in air, soil and flood water as affected by puddling and residue incorporation. P = Puddled; NP = Non puddle; M3 = 30 t ha⁻¹ residue addition. (Bhagat et al., 1994)

Management of Soil Physical Properties of Lowland Puddled Rice Soil for Sustainable Food Production

R.M. Bhagat*

Department of Soil Science, CSKHPAU, Plaampur, H.P., India

*Lecture given at the
College on Soil Physics
Trieste, 3 – 21 March 2003*

LNS0418008

* rmbhagat@glide.net.in

About 3 billion people who rely on rice as their staple food today will have multiplied to some 4.4 billion by the middle of this century. With rice demand growing at an average rate of about 3 percent annually, 70 percent more rice has to be produced in next 30 years compared to present day production levels. More rice has to come from less favorable environments, with less water and nutrients. Agricultural population densities on Asia's rice producing lands are among the highest in the world and continue to increase at a remarkable rate. Rice has widely adapted itself: to the hot Australian and Egyptian deserts, to the cool Himalayan foothills of Nepal. Hill tribes in Southeast Asia plant it on slash-and-burned forest slopes; that's upland rice. However, low lying areas in Asia, which are subject to uncontrolled flooding, are home to more than 100 million poor farmers.

Enormous amounts of water are generally used in rice production. On average, more than 5000 liters of water are used to produce one kg of rice (Bhagat et al., 1996). A significant portion of the total water requirement for rice production is used in land preparation. Large amounts of water are required during the land soaking phase as huge water losses occur through cracks before the soil saturation is actually reached; surface drainage also contributes to this loss. This causes delays in completing land preparation, low water use efficiency, and a strained irrigation system.

Puddling or wet tillage in rice, decreases total soil porosity only slightly, but markedly changes porosity distribution with both storage and residual porosity increasing at the expense of transmission porosity. Soil texture plays an important role in soil water retention following soil disturbance. Besides, the textural response, tillage may further influence water retention if it incorporates crop residues or if it alters the distribution of sand silt and clay in soil by mixing particles from different soil horizons (Bhagat, 1990). Tillage operations markedly affect soil hydraulic properties including saturated and unsaturated hydraulic conductivity, soil water content, soil water retention and soil water diffusivity. These properties in turn affect hydraulic processes such as infiltration, water flow through soils, drainage and evaporation.

Surface as well as subsurface soil conditions influence water infiltration. Tillage alters both through the shearing action of tillage tool and may determine the amount of water required for land preparation. Puddling causes destruction of soil structure in rice, which results in a decrease in soil water transmission – a condition often desired for rice. Consequently, puddling decreases percolation and therefore better retains standing water in the field, which may also decrease the irrigation requirement.

Tillage exposes the subsoil to the atmosphere, which increases the rate of water loss from the soil through evaporation. By loosening the soil near the surface, tillage may reduce capillary water rise to the surface and thereby decrease evaporative losses of deeply stored soil water. However, the prevention or the substantive reduction of evaporative losses of water is mostly not cost effective in flooded lowland rice fields.

Rice response to tillage varies with soil texture and climatic water balance. Depending on the soil texture, tillage may induce a gain or loss in soil permeability which may affect rice yield through better retention of surface water. Wet tillage (puddling) and compaction in rice soils decreases water permeability by decreasing the volume of transmission pores. Sharma and Bhagat (1993) have found out that in soils with less than 70 percent sand, puddling as well as compaction are equally effective in decreasing water percolation to satisfactory levels for growing a good crop of rice. The choice between the two methods depends upon factors like susceptibility of rice to compaction levels, residual effects of puddling and compaction on upland crops grown after rice, and regeneration of soil structure after puddled crop. However, in soils having greater than 70 percent sand, compaction rather than puddling is effective in decreasing water permeability.

One of the requirements of an efficient rice based production system is to decrease energy inputs. Puddled soils shrink on drying, become compact and hard and produce surface fissures of varying size and shape. After rice, preparation of seed beds with fine tilth for wheat is difficult. Plowing of puddled soil after rice results in the formation of large clods, having high breaking strength (Sharma and Bhagat, 1993) and very large amounts of energy and time are consumed in producing fine seed beds. Tillage, irrigation and fertilizer constitute the major energy inputs in a crop production system. As energy costs continue to increase, it becomes imperative to develop energy efficient crop production system. At low yield levels, water and nutrients can substitute for each other and tillage increases efficiency of water and fertilizer use. Interactions among energy intensive inputs of tillage, irrigation and nutrients can be gainfully exploited to combat soil and management related stresses for improved crop performances. Bhagat et al. (2003) have indicated that energy inputs in a conventional tillage was about 276 kwh more than that in a no-till system; however the former system produced more grains per unit of energy consumed.

The foregoing discussion indicated that strategic management of physical properties of rice soils is of utmost importance to have successful production of rice and post rice crops. Major initiatives taken so far in this direction are summarized below:

Incorporation of plant residues coupled with appropriate tillage build up organic carbon status of soil (Bhagat and Verma, 1991). Also use of residue as a mulch has been shown to modify hydro-thermal regime of soils (Bhagat and Acharya, 1988). Field experiments conducted on rice straw management and farm yard manure for five years in humid temperate climate (Bhagat and Verma, 1991; Verma and Bhagat, 1992), have indicated the superiority of addition of rice straw in combination with farm yard manure to wheat in rice/wheat cropping sequence, in improving the soil structure and available soil moisture content (Table 1).

Further studies conducted on long term addition of residue and tillage combinations to typical rice soils in north-western India have shown favorable modifications in soil physical properties (Bhagat et al., 1994, Sharma et al., 1995). These studies have specifically shown that residue incorporation (in the form of lantana (*Lantana camara* L.) leaves and twigs addition) increased water retention in

post soils (Fig. 1). Further the drying characteristics of these soils (Fig.2) indicated that residue addition irrespective of the tillage treatments invariably delayed surface drying. In post rice soils, the higher unsaturated hydraulic conductivity of the puddled soils keep the surface soil moist, longer by transferring more profile water upward to the surface. In one of these studies, Bhagat et al. (1994) have observed that residue addition increased infiltration rate of puddled and compacted soil by about $2.5 \times 10^{-7} \text{ m sec}^{-1}$ compared to puddled and compacted soils without residue addition (Fig.3).

Further investigations of long term effects of residue addition indicated that although there is build up of organic carbon in soil (although slow), however, much of the organic carbon applied through plant residue (lantana in the present case) remained in soil as discrete particles and only a part of it entered into close association with soil particles/aggregates (Sharma et al., 1995). Consequently, the percentage of organic carbon of the whole soil, especially at 20-30 t ha⁻¹ residue application rates was higher than the organic carbon in water stable aggregates. Thus it may take several years of regular additions of plant residues for the added carbon to enter and stabilize micro-aggregates.

Cracking pattern of the soils studied after six years of different levels of regular addition of residue is shown in plate 1. Cracking pattern at a soil surface affects the hydrodynamic properties of soil. Cracking extends the soil-air interface into the soil profile and thereby may increase the moisture loss through evaporation. Besides, it has direct bearing on the extent and size-distribution of clods formed during plowing of land. Deep and wide cracks, arranged in hexagonal pattern, typical of the control plots, are expected to produce large clods, compared to the network of fine and shallow cracks typical of the residue (lantana) treated plots. Further the clods formed in residue treated plots were much weaker than the clods formed in control plots (Table 2). This difference would be reflected in much less energy input in the preparation of seedbed for wheat following rice. Measurements made in the same experiment, revealed that plowing energy after rice harvest was 3.4 GJ ha⁻¹ in lantana treated plots as against 5.4 GJ ha⁻¹ in control plots (Bhagat et al., 1994).

Some more studies carried out on long term tillage and residue management in rice soils have also indicated improvement in various soil physical parameters (Bhagat et al. 2003; Bhagat et al., 2002; Sharma and Bhushan, 2001). In a long term residue management study, the non limiting water range (NLWR) was determined in the root zone (15-18 cm soil layer) by using data on air filled porosity and soil penetration resistance (SPR). NLWR, which is the difference between moisture contents at 10 % air-filled porosity and 2 MPa SPR, increased with the residue addition. NLWR appeared more sensitive to changes in soil organic carbon and plant available water capacity (PAWC) as shown in table 3. Further since NLWR integrates three important soil physical properties directly influencing plant growth, viz. soil moisture, soil-air and soil mechanical impedance, it correlated linearly, positively and significantly with grain yield of post rice crop (winter wheat). The correlation was better with NLWR compared with PAWC-the classical concept of soil water availability.

References

- Bhagat, R.M. and Acharya, C.L. 1988. Soil water dynamics during wheat growth under different soil management practices. *J.Indian Soc. Soil Sci.* 36: 389-396.
- Bhagat, R.M. 1990. Effect of tillage and residue management on hydrothermal regime, nutrient uptake and yield of wheat in a river deposit. *Soil Tillage Res.* 17: 315-326
- Bhagat, R.M. and Verma, T.S. 1991. Impact of rice straw management on soil physical properties and wheat yield. *Soil Sci.* 152: 108-115
- Bhagat, R.M., Sharma, P.K. and Verma, T.S. 1994. Tillage and residue management effects on soil physical properties and rice yields in north western Himalayan soils. *Soil Tillage Res.* 29: 323-334
- Bhagat, R.M., Bhuiyan, S.I. and Moody, K. 1996. Water, tillage and weed interactions in lowland tropical soils. *Agril. Water Mgt.* 31: 165-184
- Bhagat, R.M., Sharma, Pradeep K. and Verma, T.S. 2002. System productivity and wheat yield trends in a long term lantana amended alfisol. Paper presented at the International Conference on Challenges and options for sustainable development of the Himalayas – beyond 2002 held at Palampur, Himachal Pradesh India from October 1-4, 2002.
- Bhagat, R.M., Bhardwaj, A.K. and Sharma, Pradeep K. 2003 Long term effect of residue management on soil physical properties, water use and yield of rice in north-western India. *J Indian Soc. Soil Sci.* 51: 111-117.
- Sharma, P.K. and Bhagat, R.M. 1993. Puddling and compaction effects on water permeability of texturally different soils. *J.Indian Soc. Soil Sci.* 41:1-6
- Sharma, P.K. and Bhagat, R.M. 1993. A simple apparatus to measure clod breaking strength. *J. Indian soc, Soil Sci.* 42: 112-114.
- Sharma, Pradeep K., Verma, T.S. and Bhagat, R.M. 1995. Soil structural improvements with addition of Lantana camara biomass in rice-wheat cropping. *Soil Use and Mgt.* 11: 199-203.
- Verma, T.S. and Bhagat, R.M. 1992. Impact of rice straw management practices on yield, nitrogen uptake and soil properties in a wheat-rice rotation in Northern India. *Fert. Res.* 33: 97-106.

Table 1. Mean values of water stable aggregates, mean weight diameter, bulk density and total porosity to 0-0.15 m depth
(*Bhagat and Verma, 1991*)

Structural indices	Treatment*						LSD (0.05)
	Contro	SI	SM	SB	FYM	SI+FYM	
WSA>0.25 mm (%)	69.7±5.7	77.3±6.7	76.9±6.1	67.3±6.1	80.7±8.5	81.2±9.0	3.1
MWD (mm)	0.61±0.19	0.74±0.24	0.72±0.22	0.59±0.21	0.81±0.32	0.83±0.28	0.11
Bulk density (Mg m ⁻³)	1.32±0.04	1.25±0.04	1.33±0.04	1.32±0.04	1.20±0.05	1.18±0.04	0.11
Total porosity (%)	49.4±2.8	51.9±2.9	48.8±2.7	49.2±2.9	53.8±3.4	54.6±3.9	2.9

*SI = Straw incorporation; SM = Straw mulch; SB = Straw burning; FYM = Farm yard manure,

WSA = Water stable aggregates; MWD = Mean weight diameter

Table 2. Effect of six annual applications of Lantana camara on bulk density of soil, aggregates and clods, water stability of aggregates and clod –breaking strength in a silty clay loam soil under rice-wheat cropping (Sharma, P.K., Verma, T.S. and Bhagat, R.M., 1995)

Lantana application (t ha ⁻¹)	Bulk density (t m ⁻³)				Water Stable aggregates >0.25 mm (%)	Aggregate porosity (%)	Mean weight diameter (mm)	Clod breaking strength (kPa)
	Soil	7.5-15 cm	Aggregates (2-8 mm)	Clods				
0	1.42	1.48	1.54	1.49	72.9	38.2	2.66	419.9
10	1.39	1.48	1.50	1.45	79.0	39.8	3.89	377.2
20	1.34	1.46	1.49	1.44	81.9	40.2	4.18	220.8
30	1.31	1.38	1.48	1.40	82.8	40.6	4.09	215.6
L.S.D. (p≤0.05)	0.05	0.07	0.04	0.03	3.3	1.04	0.67	87.0

Table 3. Effect of ten annual applications of lantana biomass on bulk density, moisture contents at 10 % air filled porosity and 2 MPa SPR, NLWR and PAWC determined during wheat cropping season (Sharma and Bhushan, 2001)

Lantana (t ha ⁻¹)	Bulk density (Mg ha ⁻¹)		Soil moisture content (vol %) at 15-18 cm depth			Water retention (vol%) at water potentials (kPa)		PAWC	NLWR:PAWC ratio
	7.5-10.5 cm	15-18 cm	10% air-filled porosity	2 MPa SPR	NLWR	-33.3	-1500		
0	1.26	1.43	31.2	26.9	4.3	33.5	20.6	12.9	0.33
10	1.22	1.41	32.2	24.8	7.4	33.6	20.2	13.4	0.55
20	1.11	1.37	33.9	23.0	10.9	33.7	20.0	13.7	0.80
30	1.08	1.35	34.7	19.6	15.1	34.8	19.9	14.9	1.01
LSD (0.05)	0.04	0.05	1.0	1.2	1.0	0.9	0.4	1.1	0.17

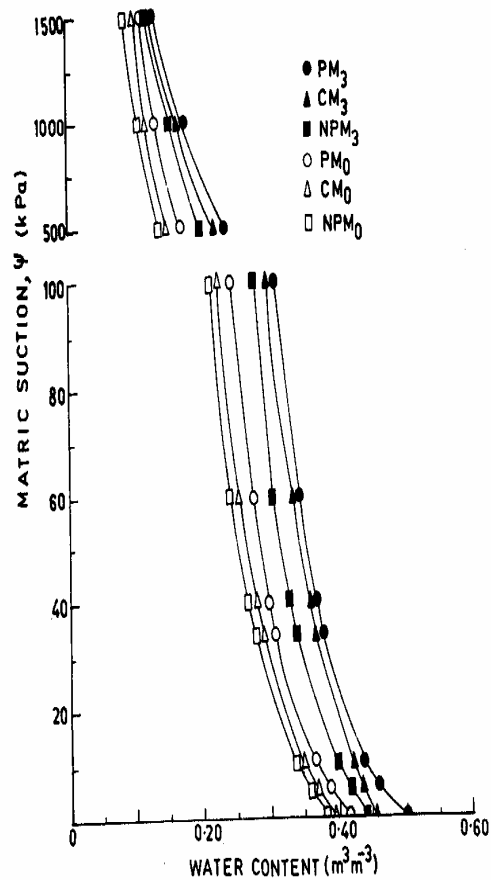


Fig 1. Soil Moisture characteristics after rice harvest at 0-0.15 m depth, under various treatments. P=Puddling; C = Compaction; NP = Non puddle; M0 = No residue; M3 = 30 Mg ha⁻¹ residue addition. (Bhagat *et al*, 1994)

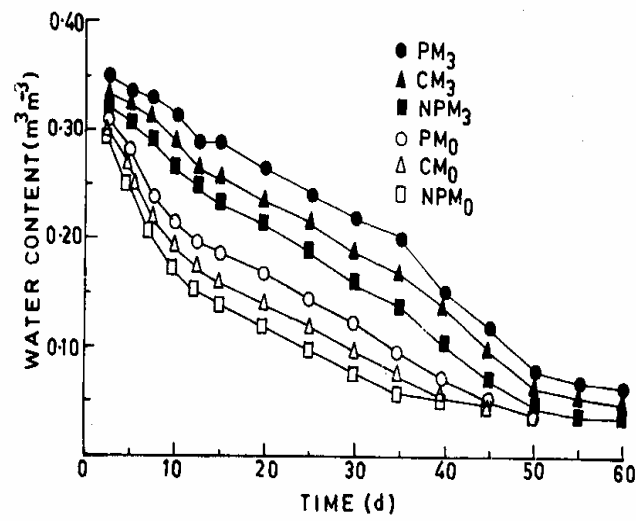


Fig. 2 Drying characteristics after rice harvest at 0 - 0.05m depth, under various treatments. P = Puddling; C = Compaction; NP = Non puddle; M₀ = No residue; M₃ = 30 Mg ha⁻¹ residue addition. (Bhagat *et al*, 1994)

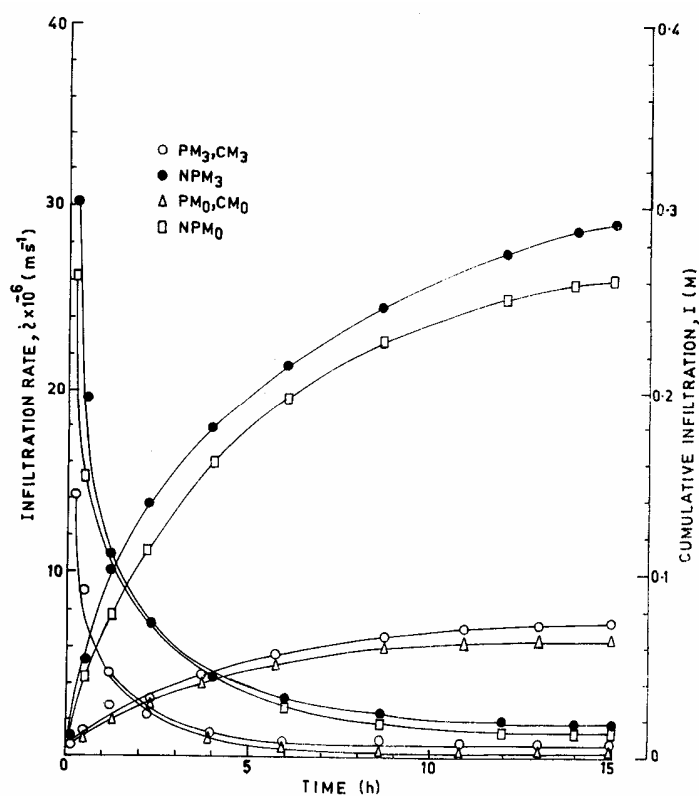


Fig. 3. Infiltration rate and cumulative infiltration vs. time at rice harvest, under various treatments. P = Puddling; C = Compaction; NP = Non puddle; M0 = No residue; M3 = 30 Mg ha⁻¹ residue addition. (Bhagat *et al*, 1994)



No residue



30 Mg ha⁻¹ residue

Effect of Lantana residue on soil cracking
Plate 1. Sharma et al. (1995)

Hydrological Behaviour of Sealing Under Different Soil Management Conditions in the Center South Cordoba, Argentina

Estela Bricchi*

National University of Río Cuarto, Argentina

*Lecture given at the
College on Soil Physics
Trieste, 3 – 21 March 2003*

LNS0418009

* ebricchi@ayv.unrc.edu.ar

The susceptibility of soils to form seals induced by rain depends on a combination of physical, chemical and biological processes, which are, indeed, affected by climatic characteristics and the type of soil.

If we consider the weather factors, the energy of rain, as a function of quantity and intensity, is the most important one. The soil properties that favor the formation of sealing are texture, organic matter content, structural stability and sodium adsorption relationship. Regarding texture, silt is the particle, which is most highly involved.

In central Argentina, specifically in the central southern region of Cordoba Province, the most representative soils show a low content of clays and a high content of silt and fine sand. This land has undergone different production systems, not only agricultural ones but also combined systems, as summer crops, with intense laboring and scarce, even lacking, stubble supply. Therefore these soils have had important loss in organic matter, degradation of the structure of the superficial horizons. This degradation is observed by the high quantity of aggregates presenting a little diameter as well as the important amount of dust. So that, the impact of rain drop showing certain intensity causes a break of those less stable aggregates which along with the free particles fit together in order to fill the inter-aggregate pore spaces and they also reduce the hydraulic conductivity as well as infiltration in a noticeable way. On the other hand, it is well known that seals have a high dynamism, that is to say that their porosity, thickness and hydraulic properties change as they develop.

It also has to be noticed that in the sub-humid areas, as the one we have studied, the rainfall distribution is related to the weather seasons. Rains begin once the seedling bed is prepared. A rain start when crops show low height, which favor, the sealing processes.

It became necessary, then, to look for a combination of technologies leading to an energy input throughout conservation tillage systems, soil covering and agro-chemicals which tend to improve soil quality in order to obtain a sustainable production.

One of the research efforts has as a main objective to conduct a temporal analysis about the influence of some technological factors on hydraulic conductivity on the surface of a Typical Hapludoll having a very fine sandy loam texture. We have worked in a region located at 32° 57' South latitude and 64° 50' West longitude. The mean annual temperatures range from 8-23°C and the mean annual rainfall value is up to 850 mm. Eighty percent of the rainfall take place during spring and summer. The natural vegetation belongs to an open forest, presenting caducous leaves trees, with inner grasslands. The relief is normally wavy, showing slopes of 3 to 4% gradient. The original material is a loessic sediment.

The trial was conducted on a production system. It began in August 1994. The production sequence that the production system followed was corn-corn-sunflower- corn-sunflower, they were planted according to the following factors: a) Two different topographic positions: medium high slope (I) and medium low slope (II). b) Under three different tillage systems: Conventional with moldboard plow (CT), minimum with chisel plow (MT) and non-tillage (NT). c) The after harvest the

stubble were grassed by cattle (G) on the other hand, in 50 % of the plot no grassing was allowed during the trial years (NG) d) Two different fertilizer doses were studied: zero fertilization (NF) and fertilization of crops at the beginning of planting every years (F).

The trial was conducted by using a simple at-random design with two repetitions for each treatment. Only in F the initial saturated hydraulic conductivity (K_{sj}) (non-sealing condition) and the final hydraulic conductivity (K_{sf}) (sealing conditions) were determined in the superficial of soil in 2000, by means of a rain simulator using an intensity up to 50 mm/h for 60 minutes (kinetic energy of $0.1336 \text{ J}\cdot\text{cm}^{-2}$). The K_s values obtained by applying Darcy's equation were used to fit the Horton type exponential decay function which describes K_s as a function of the time of exposure to a simulated rain, this is:

$$K_s = K_{sf} + (K_{sj} - K_{sf}) \exp^{-at}$$

where t is time expressed as minutes. The value of a was obtained for each of the treatments by regression analysis until a regression coefficient higher than 70% was obtained.

In order to include the kinetic energy of rain, the exponential term was considered as the product of stability factor S ($\text{cm}^2 \cdot \text{J}^{-1}$) for the kinetic energy of rain E ($\text{J}\cdot\text{cm}^{-2}$). The crusting hazard (or risk of sealing) R was used to relate the K_{sf} values with susceptibility indicators of sealing depending on soil characteristics (Pieri, 1989, cited by Van der Watt and Valentin, 1992). $R(\%)$ is calculated as a relation among the following:

$$R = \frac{OM \cdot 100}{(clay + silt)}$$

where OM is the organic matter content, clay and silt are the clay and silt contents (%), respectively. The above mentioned author considered an R value of 5% to be a high crusting hazard or sealing risk, while a value over 9% represents a low crusting hazard or sealing risk. They considered 7% to be the threshold value.

The quantity of superficial residues was estimated every year after grassing for each treatment. Results were statistically processed by using the general linear model and Kruskal-Wallis' non-parametric test, for a significance level of 95% with the SPSS software. The studied variables were also evaluated on a site showing a minimum disturbance level at a relict area, which has natural vegetation, presents a relief condition similar to the trial sites and it shows a low use of soil (MD, MDI and MDII). The following results were obtained:

Table 1. Hydraulic parameters of seals for the studied factors.

Factor	Level	K_{si} (cm/h)	K_{sf} (cm/h)	S (cm ² ·J ⁻¹)
Position	I	1.72	0.78 a	83.63 a
	II	1.72	0.72 a	127.97 a
Grassing	NG	2.03	0.83 a	115.05 a
	G	1.46	0.66 a	96.55 a
Tillage	NT	2.32	0.87 a	157.49 a
	MT	2.28	0.75 ab	99.48 ab
	CT	0.64	0.62 b	60.42 b
Minimum Disturbance	MD	5.02	1.84 c	14.97 c

Interaction grassing * tillage ** at the 5% C.V. 17%

Differing letters are significantly different at the 5 % level

Table 1 shows significant differences between MD and the treatments for the three studied parameters. K_{si} and K_{sf} are the highest values, and S value is lower. This would mean a high stability and permeability of soils under natural condition. There is also a significant difference between NT and CT regarding K_{sf} and S .

Table 2. Analysis of grassing*tillage interaction for K_{si}

Treatments	K_{si} (cm·h ⁻¹)
NT NG	3.24 a
MT G	2.35 b
MT NG	2.21 b
NT G	1.40 c
CT NG	0.66 d
CT G	0.62 d

Differing letters are significantly different at the 5 % level.

The interaction effect between tillage and grassing (Table 2) was shown in NT, because this system shows a decay of K_{Si} when stubble is removed. This could be caused by a lower input of organic matter and the cattle trampling which produce a higher sealing of the superficial soil. This interaction does not show in MT because the minimum laboring would balance the beneficial effects of stubble, that is to say, that the effect of cattle grassing would be compensate by the minimum laboring on this site. On the other hand, the intense laboring as in CT, with the total stubble buried presents a marked decrease of K_{Si} .

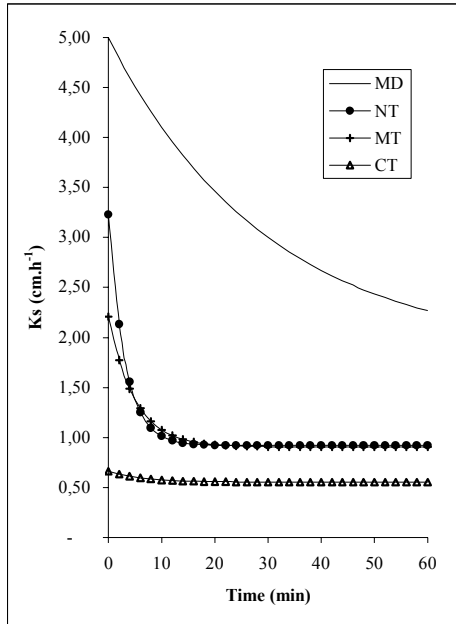


Figure 1. Saturated Hydraulic Conductivity in non grassing

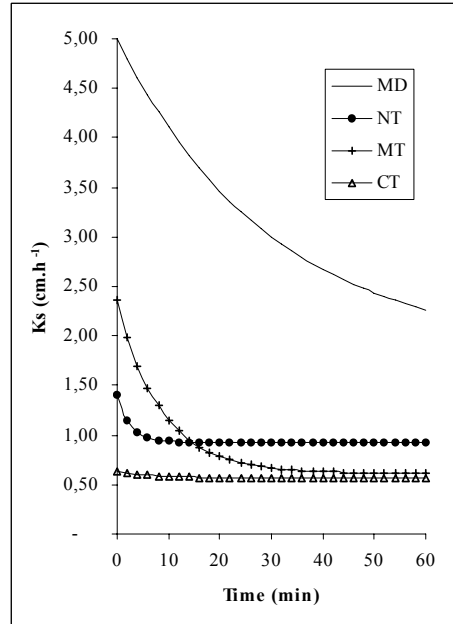


Figure 2. Saturated Hydraulic Conductivity in grassing

It can be observed in both figures that K_s from MD is higher than that for the other treatments. Moreover, its S coefficient is the lowest (See Table 1). Hence, this treatment yields the highest stability. By comparing the remaining treatments it can be seen that the NT and MT non-grassing condition (Fig 1) keep values of initial and final conductivity higher than those of CT, indicating that even though a seal is formed, the K_{sf} is higher in the first two treatments. Considering that the S parameter explains the curve shape, and has been considered as a stability factor, those treatments which are likely to be the less stable (NT and MT) due to their high S value are those showing higher values of both K_{Si} and K_{sf} . On the other hand, the lowest S value is obtained in treatment CT, where K_s does not change by the effect of simulated rain. This condition could be attributed to a permanent sealing of soils. For this reason, we consider S to be nonappropriate for the studied condition. It can be

seen in Fig 2 that even MT having the highest K_{si} is sealed at a K_{sf} value lower than NT - meaning a less permeable seal, similar to that of CT.

After analyzing different indicators of stability, the risk of sealing (R) was selected as the one that best expresses soil susceptibility to sealing, contributed to a higher adjustment ($R^2=0.69$) between K_{sf} and R (Fig. 3). It should also be noticed that MD obtained a 13.5% value which indicates an extremely small sealing susceptibility caused by the high organic matter content being up to 7%. The remaining treatments had a crusting hazard of 5%.

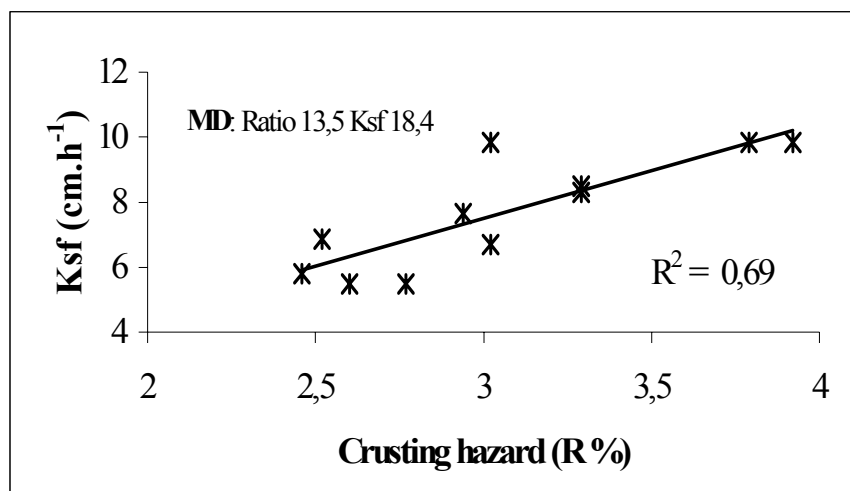


Figure 3. Relation between K_{sf} and Crusting hazard R.

It can be concluded that the removal of natural vegetation and crop systems have produced a decrease of K_{si} and K_{sf} on soil surface by 87% and 66%, respectively. Hence, there is a significant amount of water not available for crop production as well as the occurrence of erosion processes associated with run-off. In the soils that we have studied, which show a high content of skeleton particles, a little increase of organic matter could lead to a re-arrangement of those soil particles with higher porosity. Therefore, a more permeable seal will be formed.

Commentary: There are other variables being analyzed in this production system along the time: Organic matter fraction, Compactibility, Pore distribution according to size and characteristic wetness curve, Simulation on non saturated hydrologic conductivity, and Calculations of the continuity index by pore classes. We hope to be able to estimate change rates through the evolution of the studied indicators. These change rates will help us to obtain a monitoring of soil quality versus time.

Structure and Organic Matter Under Different Soil Management Conditions in the Center of Argentina

Estela Bricchi*

National University of Río Cuarto, Argentina

*Lecture given at the
College on Soil Physics
Trieste, 3 -21 March 2003*

LNS0418010

* ebricchi@ayv.unrc.edu.ar

In Central Argentina, Córdoba Province, as in different parts of the world, the equilibrium state of soil under natural condition has been modified by both the replacement of natural vegetation and by tillage. With time, these two disturbing factors have led to a new soil state whose main characteristic is an important decrease of chemical, physical and biological soil functions. The degree of these changes is directly related to soil resistance according to soil genesis.

The soil organic matter and the structure of the superficial profile of soil are suitable indicators mainly for physical functions. As it has been demonstrated in temperate areas, the changes of soil use have meant loss of organic carbon. These changes happened very quickly at the beginning (10 to 20 first years). Then, they subsequently happened at a slower rate. Finally, after 50 to 70 years, soils reach a new equilibrium state where the organic carbon quantities are lower and the quality differs from the original organic matter. This loss means a lower plasma quantity among skeleton particles, and therefore, disturbance of soil structure due to the mineralization of those compounds which are more easily degraded and are responsible of soil structure. This phenomenon is common in soils having very fine sandy loam texture.

The great subdivision of land took place in 1920, when the agricultural activity began with winter crops (wheat, oats and rye). Soon after, these crops were substituted by summer crops (corn, peanut, sunflower and soybean). Intense mechanization using heavy equipment occurred from 1960 to 1990. We consider this period of time to be the cause of the most important deterioration of physical conditions of soil profile, resulting in an important loss of organic matter, the breakdown of superficial aggregates that later on will form a seal under heavy rainfall. Moreover, the broken-down subsuperficial aggregates, can be turned into compact horizons. All these processes not only affect the infiltration, distribution and storage of water, but they also favor erosion.

Recently, it became necessary to look for a combination of technologies leading to an energy input throughout conservation tillage systems, soil covering and agro-chemicals which tend to improve soil quality in order to obtain a sustainable production. One research project had as a main objective to conduct a temporal analysis about the influence of some technological factors on two quality indicators: organic matter and superficial structure of a Typical Hapludoll showing a very fine sandy loam texture. We have worked in a region located at 32° 57' South latitude and 64° 50' West longitude. The mean annual temperatures range from 8-23° C and the mean annual rainfall value is up to 850 mm. Eighty per cent of the rainfall takes place during spring and summer. The natural vegetation belongs to an open forest, presenting caducous leaves trees, with inner grasslands. The relief is normally wavy, showing slopes of 3 to 4% gradient. The original material is a loessic sediment.

The experiment was conducted on an agricultural production system beginning in August 1994. The production sequence followed in the production system was corn-corn-sunflower-corn-sunflower, planted according to the following factors: a) Two different topographic positions: medium high slope (I) and medium low slope (II). b) Under three different tillage systems: Conventional with moldboard

plow (CT), minimum with chisel (MT) and non-tillage (NT). c) After harvest the stubble were grassed by cattle (G) on the other hand, in 50 % of the plot no grassing was allowed during the trial years (NG) d) Two different fertilizer doses were studied: zero fertilization (NF) and fertilization of crops at the beginning of planting every year (F). The experiment was conducted by using a simple at-random design with two repetitions for each treatment. Soil organic matter content (CO) and the distribution of sizes of water stable aggregates were determined in 2000. The quantities of superficial residues were estimated every year after grassing for each treatment. Results were statistically processed using the general linear model and Kruskal-Wallis' non-parametric test, for a significance level of 95% with the SPSS software. The studied variables were also evaluated on a site showing a minimum disturbance level a relict area, which has natural vegetation, presents a relief condition similar to the trial sites and it shows a low use of soil (MD, MDI and MDII).

Results

Soil organic carbon content

Table 1. Organic carbon content ($\text{gr} \cdot \text{kg}^{-1}$) for studied factors.

Factor	Level	OC ($\text{gr} \cdot \text{kg}^{-1}$)	
Position	I	8.72	a
	II	10.17	b
Grassing	NG	10.06	a
	G	8.83	b
Tillage	NT	9.76	a
	MT	9.76	a
	CT	8.60	b
Fertilization	F	9.36	a
	NF	9.47	a

Different letter mean significant differences at the 5% level

Table 1 shows the significant differences between positions (about 14%). On the other hand, the OC is significantly higher when stubble is left on surface. The conservation tillages (MT and NT) show similar values of OC and they are significantly higher than that of CT. With the OC for conservation tillages being observed 11% higher for 5 years, this indicates that an improvement function has been initiated. Note that fertilization did not bring about any differences in OC content of soil.

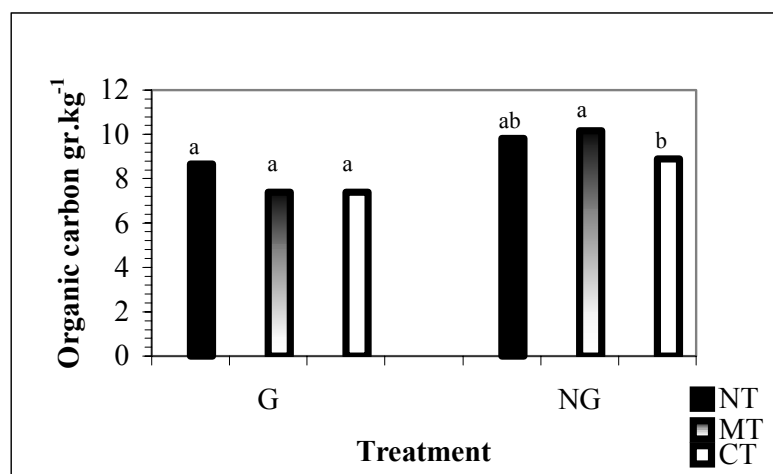


Fig. 1.- Effect of tillage system and stubble quantity on the organic carbon at topographic positions: medium high slope (I). Different letter means significant differences at the 5% level.

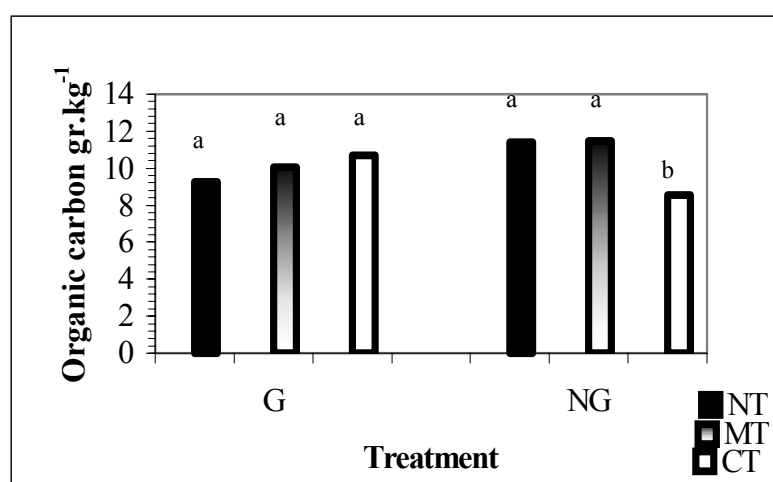


Fig. 2.- Effect of tillage system and stubble quantity on the organic carbon at topographic positions: medium low slope (II). Different letter means significant differences at the 5% level.

Both figures (1 and 2) show no significant differences among tillage systems in the two studied positions under cattle grassing. On the other hand, minimum tillage

differs from CT tillage in position I without grassing, while in position II the CT system differs from the other two systems.

Table 2. Differences in Organic Carbon (%) among treatments and MD situation.

Treatments	OC (gr·kg ⁻¹)	Differences (%)
I	8.72	-77.98
II	10.17	-78.19
NG	10.06	-76.66
G	8.83	-79.52
NT	9.76	-77.36
MT	9.76	-77.36
CT	8.60	-80.05
F	9.36	-78.29
NF	9.47	-78.03
MD I	39.60	
MD II	46.63	

Table 2 shows a higher loss of OC in CT under grassing. The values obtained for conservation tillage are a little lower for NG.

Aggregate Stability

Table 3 shows a significant different MD for all treatments no matter sizes. On the other hand, in MD the highest percentage belong to the larger aggregates while the treatments present a bimodal distribution (very large and very small). The only significant differences that can be observed are produced by tillage except for 1-2 mm diameter. NT produces the highest percentage in larger sizes. Fine aggregates show a lower percentage, obtaining the same results for 0.5–1 mm where tillage systems are different.

Table 3. Distribution of sizes of water stable aggregates in treatments and MD.

Factor	Level	Stable Aggregates in water (%)			
		Diameters			
		0.1-0.5 mm	0.5-1 mm.	1-2 mm	2-4 mm
Position	I	17.85 a	7.72 a	10.56 a	19.85 a
	II	16.87 a	8.08 a	11.89 a	20.78 a
Grassing	NG	16.92 a	7.78 a	11.39 a	23.92 a
	G	17.79 a	8.01 a	11.06 a	16.71 a
Tillage	NT	11.64 a	4.90 a	12.6 a	33.06 a
	MT	18.25 b	8.03 b	10.20 a	15.69 b
	CT	22.19 b	10.69 b	10.87 a	12.20 b
Fertilization	F	17.46 a	7.83 a	12.09 a	21.74 a
	NF	17.26 a	7.96 a	10.37 a	18.89 a
Situation					
Min. Dist.	MD	5.19 c	1.91 c	15.09 c	52.50 c

Different letter means significant differences at the 5% level

Organic matter and structure relation

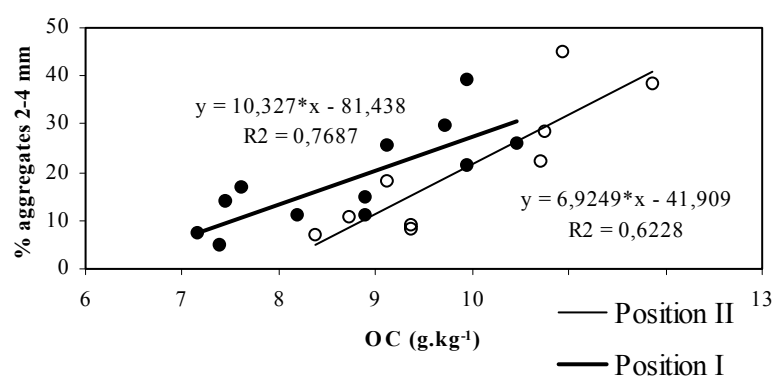


Fig. 3. Relation between OC and 2-4 mm aggregates % for the two topographic positions.

Increasing of organic matter content yields a linear relation with macroaggregate proportion for both relief positions, with the slope being higher in position II. See Fig. 3.

Conclusions

The removal of natural vegetation and tillage systems have caused the following effects on the first centimeters of soils: A 77 to 80% loss of organic matter during a period of about 80 years. Changes in the water stable aggregates distribution. A 77% loss of large aggregates and a 55% gain of fine aggregates. Our results would indicate that the disturbance level was higher to the natural resistance of soil.

The organic carbon content in the first centimeters of soil is increased when all crop stubble remains on the field and conservationist tillage is applied. Conservation tillages are more efficient in the lower position of relief, meaning the beginning of a change of organic matter tendency that would possibly tend to new equilibrium state. On the other hand, the percentage of water stable aggregates would also be increased as consequence of a higher organic carbon content.

Commentary

There are other variables being analyzed in this production system along the time: Organic matter fraction, Compactibility, Pore distribution according to size and characteristic wetness curve, Simulation on non saturated hydrologic conductivity, and Calculations of the continuity index by pore classes. We hope to be able to estimate change rates through the evolution of the studied indicators. These change rates will help us to obtain a monitoring of soil quality versus time.

Soil Physical Properties on Venezuelan Steeplands: Applications to Soil Conservation Planning

Fernando Delgado*

CIDIAT, University of Los Andes, Mérida, Venezuela

*Lecture given at the
College on Soil Physics
Trieste, 3 – 21 March 2003*

LNS0418011

* delgado@cidiat.ing.ula.ve

Abstract

This paper presents a framework to support decision making for soil conservation on Venezuelan steeplands. The general approach is based on the evaluation of two important land qualities: soil productivity and soil erosion risk, both closely related to soil physical properties. Soil productivity can be estimated from soil characteristics such as soil air-water relationships, soil impedances and soil fertility. On the other hand, soil erosion risk depends basically on soil hydrologic properties, rainfall aggressiveness and terrain slope. Two indexes are obtained from soil and land characteristics: soil productivity index (PI) and erosion risk index (ERI), each one evaluates the respective land quality. Subsequently, a matrix with these two qualities shows different land classes as well as soil conservation priorities, conservation requirements and proposed land uses. The paper shows also some applications of the soil productivity index as an approach to evaluate soil loss tolerance for soil conservation programs on tropical steeplands.

INTRODUCTION

Agriculture on Venezuelan Andes is affected by two very important biophysical land qualities: soil productivity and soil erosion risk. The notorious scarcity of complex data in these tropical mountains hinders conservation planning for land use.

Thus, the need to count on analytical tools that permit estimating soil productivity in terms of easily obtainable soil variables, or simple methods that permit forecasting the water erosion risk on steepplands with scarce data.

In this sense and in order to direct sustainable agriculture on Venezuelan steepplands, a methodological approach for soil conservation planning has been developed at CIDIAT, University of Los Andes, Mérida-Venezuela, over the last decade. This approach is sustained mainly on the evaluation of soil physical properties related to these two important land qualities: soil productivity and soil erosion risk.

SOIL PRODUCTIVITY

As a central concept, soil productivity is the capacity of a soil, in its normal environment, to support plant growth under a specific management system. In this sense, soil productivity is a function of the soil's physical, chemical and biological properties as well as climate, management and other non-inherent factors used to produce crops. Crop yields are usually used as a measure of soil productivity.

To quantify soil productivity on Venezuelan steepplands, during the last decade we have been modifying and validating a numerical approach (Soil Productivity Index) initially developed by Pierce *et al.*, (1983).

The Productivity Index (PI) model is a derived measure of soil productivity. The PI model is an algorithm based on the assumption that crop yield is a function of root development, which in turn is controlled by the soil environment.

The Productivity Index is calculated with the following multi-factorial model:

$$PI = \sum_{i=1}^n (A_i \cdot B_i \cdot C_i \cdot K_i)$$

where PI is the Soil Productivity Index ranging from 0 to 1. Value 1 corresponds to a soil without any kind of limitation for root development.

In the present approach factor A_i evaluates conditions that regulate the air-water relations of horizon i ; factor B_i evaluates the conditions that determine mechanical resistances (impedances) to the crop root exploration in horizon i ; and factor C_i evaluates the conditions that regulate the potential fertility of horizon i . Finally, K_i evaluates the relative importance of horizon i in the soil profile (weighting factor of the respective horizon) and also the importance of soil depth. All these factors are evaluated in each soil horizon n , up to a depth of 100 cm if the soil has a depth equal to or greater than this value, or up to the effective soil depth, if it is less than 100 cm, as shown in Figure 3.

In this approach, as a difference with former models, each factor of the Soil Productivity Index PI represents a specific soil quality that has to be evaluated and quantified through specific sub-factors, represented by direct or indirect measurable soil characteristics.

Evaluation of the Soil Productivity Index PI factors

Each one of the factors of the Soil Productivity Index PI is evaluated in terms of the respective most relevant sub-factor. The selection of the specific sub-factor depends on local conditions, generally the local climate, so the interaction between soils and climate is an important issue in this approach. In this sense, the following relations must be taken into account:

Factor A: conditions that regulate the air-water relations of horizon i

- In dry climate ($P/ETP < 0.50$): Factor A = subfactor A_1
- In humid climate ($P/ETP > 2.00$): Factor A = subfactor A_2
- In subhumid to dry climate ($0.50 \leq P/ETP \leq 2.00$): Factor A = most limiting value (the lowest numerical value) between subfactors A_1 and A_2

Factor B: conditions that determine mechanical resistances (impedances) to the crop root exploration in horizon i

- If the volumetric content of coarse fragments in the soil is less than or equal to 30%, then Factor B = subfactor B_1
- If the volumetric content of coarse fragments in the soil is greater than 30%, then Factor B = subfactor B_2

Factor C: conditions that regulate the potential fertility of horizon i

- In humid climate ($P/ETP > 2.00$): Factor C = subfactor C_1
- In dry climate ($P/ETP < 0.50$): Factor C = subfactor C_2
- In subhumid to dry climate ($0.50 \leq P/ETP \leq 2.00$): Factor C = most limiting value (lowest numerical value) between factors C_1 and C_2

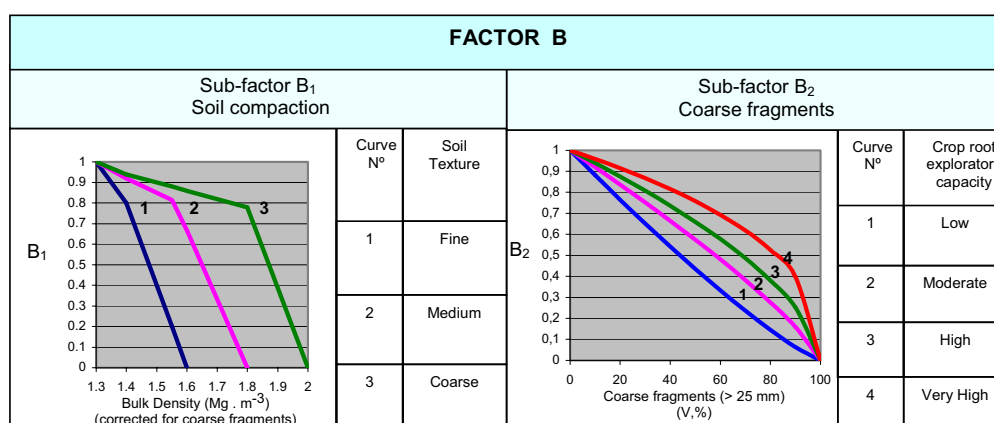
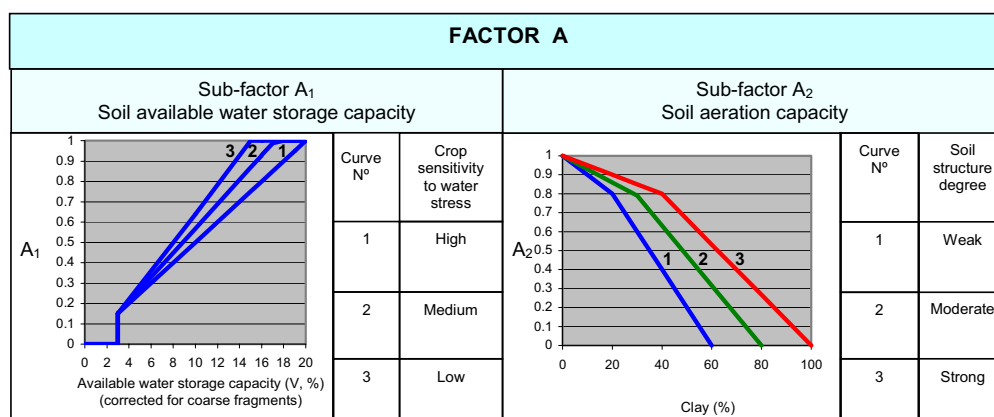
Factor K: This factor evaluates the relative importance of horizon i in the soil profile (weighting factor of the respective horizon). It is important to consider that Factor K, as shown in Figure 2, is the cumulative weighting factor of the soil profile up to the lower limit of horizon i , so the K value for the respective horizon i must be calculated as follows:

$$K_{(i)} = K_{cum(i)} - K_{cum(i-1)}$$

Figures 1 and 2 show the relations to calculate sub-factors of the Soil Productivity Index in conjunction with the above-mentioned relations. Relative values of soil productivity, estimated with the soil productivity index PI may be qualified as indicated in Table 1.

Table 1. Ranking soil productivity in terms the Soil Productivity Index PI

PI	Soil productivity
≤ 0.10	Low
0.11- 0.30	Moderate
0.31-0.50	High
> 0.50	Very high



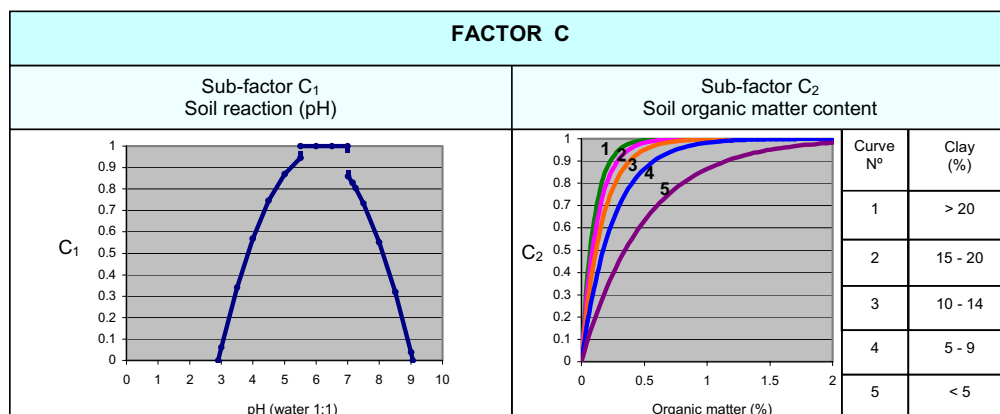


Figure 1. Factors A, B, C and respective sub-factors to evaluate the soil productivity index PI.

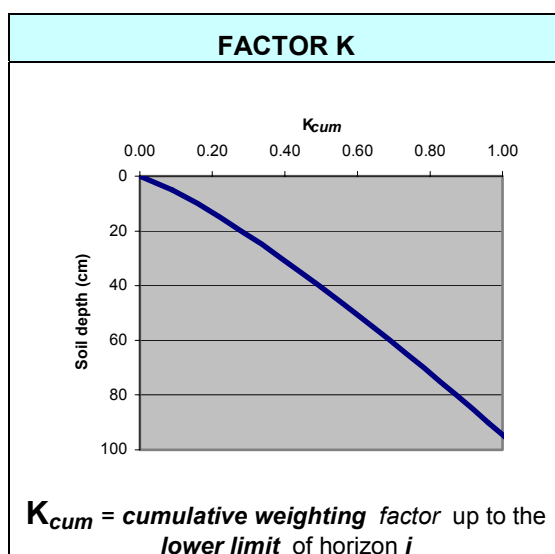


Figure 2. Factor K of the soil productivity index (weighting factor).

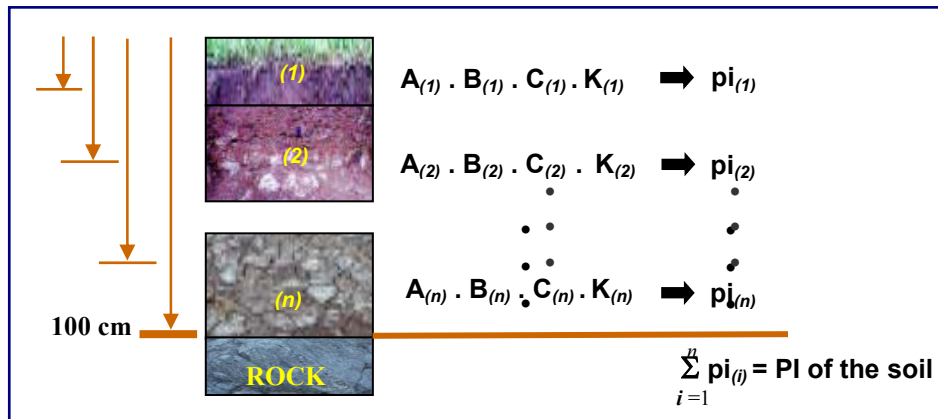


Figure 3. General procedure to calculate the soil productivity index (PI) of the soil.

SOIL LOSS TOLERANCE

Soil Loss Tolerance T is the maximum rate of annual soil erosion that may occur and still permit a high level of crop productivity to be obtained economically and indefinitely (Bergsma *et al.*, 1996). Values of Soil Loss Tolerance T have been based on: 1.

Soil renewal rates, and 2.

Arbitrarily determined from published tables taking into account soil depth as other soil properties affecting root development. Currently used rates for tolerable soil loss of $10\text{-}12 \text{ Mg}\cdot\text{ha}^{-1}\cdot\text{year}^{-1}$ are far too high for most fragile tropical soils.

The (δ - H) Approach to Evaluate Soil Loss Tolerance (Delgado and López, 1998)

In this approach soil loss tolerance T is defined in terms of the following socio-economic variables: 1. The soil productivity permissible loss rate: δ (%) and 2. The planning horizon for sustainable land use: H (years). The method starts with the soil erosion vulnerability curve relating PI values and soil losses, as the example shown in Figure 4. Vulnerability is defined as the rate of change in productivity, measured by changes in PI values, per unit of soil removed by erosion.

To estimate soil loss tolerance (T) we apply the following equation:

$$PI_f = PI_i (1 - \delta)$$

where PI_f is the final soil productivity index after soil removal, PI_i the initial soil productivity index and δ the soil productivity permissible loss rate (%).

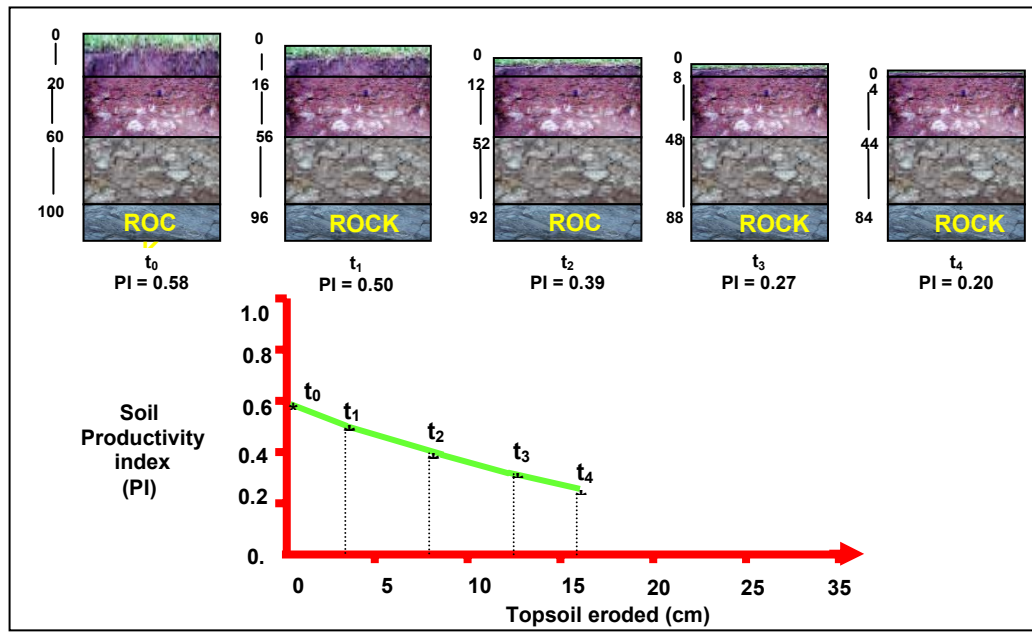


Figure 4. Soil vulnerability curve.

With the value of PI_f on the respective vulnerability curve, the correspondence amount of soil loss (cm) is obtained, which, when divided by a previously selected planning horizon (H , years) allows the calculation of soil loss tolerance (T , $\text{cm}\cdot\text{year}^{-1}$). Knowing the values for bulk density ($\text{Mg}\cdot\text{m}^{-3}$), soil loss tolerance can be expressed in $\text{Mg}\cdot\text{ha}^{-1}$. The values δ and H are assumed as related to the needs and socio-economics premises adopted by land use planners and soil conservationists. Normally, δ varies between 0.05 to 0.10 (5-10%), and H could be assumed to be 100 to 200 years.

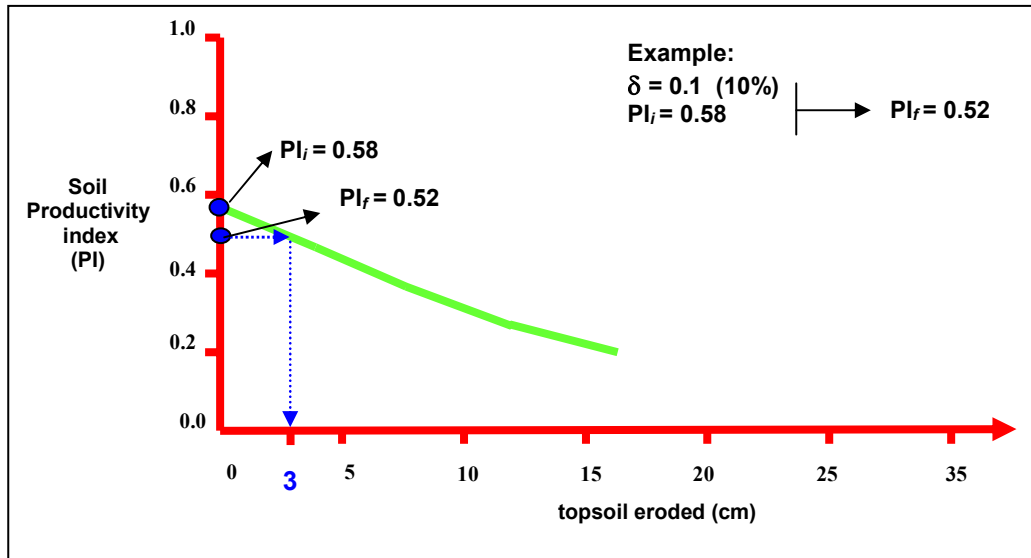


Figure 5. Soil erosion vulnerability curve showing the topsoil removed corresponding to a final productivity index PI_f .

Soil loss tolerance can be calculated from Figure 5 as follows: assume 3 cm of topsoil is eroded which is equivalent to a 10% soil productivity loss (3 cm = 0.03 m x 10,000 m².ha⁻¹ = 300 m³.ha⁻¹). If the bulk density equals 1.40 Mg.m⁻³, then (300 m³.ha⁻¹ x 1.40 Mg.m⁻³) equals a soil loss of 420 Mg.ha⁻¹.

This procedure allows to obtain a family of T values:

Planning horizon (H):

Soil loss tolerance (T_H):

$$\begin{array}{l} 50 \text{ years} \\ (T_{50}) \end{array} \Rightarrow 420 \text{ Mg. ha}^{-1} / 50 \text{ years} = 8.4 \text{ Mg.ha}^{-1} \cdot \text{year}^{-1}$$

$$\begin{array}{l} 100 \text{ years} \\ (T_{100}) \end{array} \Rightarrow 420 \text{ Mg. ha}^{-1} / 100 \text{ years} = 4.2 \text{ Mg.ha}^{-1} \cdot \text{year}^{-1}$$

$$\begin{matrix} 200 \text{ years} \\ (T_{200}) \end{matrix} \Rightarrow 420 \text{ Mg. ha}^{-1} / 200 \text{ years} = 2.1 \text{ Mg.ha}^{-1} \cdot \text{year}^{-1}$$

$$\begin{matrix} \vdots \\ \vdots \\ \infty \\ (T_{\infty}) \end{matrix} \Rightarrow 420 \text{ Mg. ha}^{-1} / \infty \text{ years} = 0 \text{ Mg.ha}^{-1} \cdot \text{year}^{-1}$$

Table 2 shows the results of soil loss tolerance calculations from the application of the (δ - H) method to three sectors of “Las Playitas” watershed at the Venezuelan Andes.

Table 2. Soil loss tolerance T (Mg.ha⁻¹.year⁻¹) for two productivity permissible loss rate δ and two planning horizons H, on “Las Playitas”, Mérida, Venezuela. (Delgado, Terrazas and López, 1998).

Sector 1				Sector 2				Sector 3			
PI _i = 0.227				PI _i = 0.304				PI _i = 0.365			
$\delta = 5\%$		$\delta = 10\%$		$\delta = 5\%$		$\delta = 10\%$		$\delta = 5\%$		$\delta = 10\%$	
T ₁₀₀	T ₂₀₀	T ₁₀₀	T ₂₀₀	T ₁₀₀	T ₂₀₀	T ₁₀₀	T ₂₀₀	T ₁₀₀	T ₂₀₀	T ₁₀₀	T ₂₀₀
3.8	1.9	7.5	3.7	2.7	1.3	5.3	2.6	3.7	1.9	7.4	3.7

SOIL EROSION RISK

Soil

erosion risk (or soil potential erosion), is the maximum soil loss in the absence of soil cover and conservation practices, that is to say, taking into account the interactions between the physical factors of the land: soil, climate and topography (Paez, 1994).

The proposed model to evaluate this land quality is based on a modification from Delgado (1997). The approach takes into consideration three basic factors for

estimating the susceptibility of a soil to water erosion: soil hydrological characteristics (infiltration-runoff ratio), rainfall aggressiveness and terrain slope. The Erosion Risk Index ERI is calculated with the following equation:

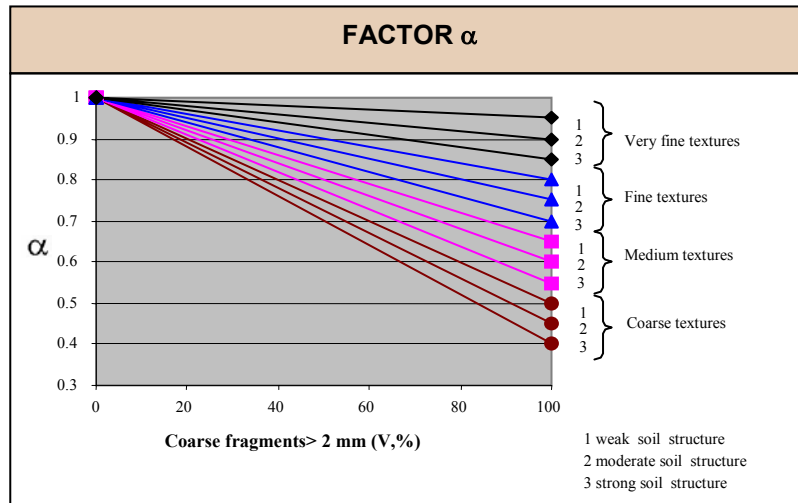
$$ERI = \frac{\eta}{10(1 - \alpha)}$$

ERI is the Erosion Risk Index and has a value between 0 and 1, corresponding 1 to a land unit that presents the highest potential conditions for inducing water erosion processes; factor α evaluates the soil runoff potential; and factor η evaluates the impact of the terrain slope on erosion risk under different rainfall aggressiveness patterns. Each factor is evaluated ranging from 0 to 1, corresponding 1 to the condition that potentially promotes the highest occurrence of water erosion processes.

Evaluation of the Erosion Risk Index ERI factors

Factor α

This factor evaluates the soil runoff potential beginning with granulometry and the soil structure degree of topsoil. The soil structure mainly includes the qualitative appraisal of its degree of development (weak, moderate or strong). Value α is obtained from Figure 6.

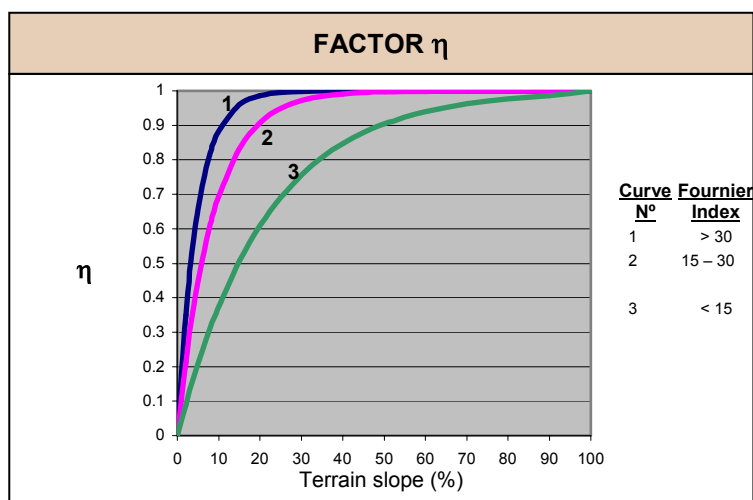
Figure 6. Factor α of the erosion risk index.

Factor η

This factor evaluates the impact of the topography and rainfall aggressiveness on erosion risk. The value of the factor is determined by the interaction between terrain slope (modal slope gradient) and the Fournier index (Fournier, 1960; quoted by FAO-PNUMA, 1980), which calculates the annual relative concentration of rain. This index has been correlated satisfactorily with annual discharges of sediment in tropical watersheds in several parts of the world (Morgan, 1986). It is determined with the following equation:

$$F = p^2 / P$$

where F is the Fournier Index, p the highest monthly precipitation (mm) and P the annual precipitation (mm). With it, Factor η value is obtained from Figure 7.

Figure 7. Factor η of the *erosion risk index*.

Relative values for the water erosion risk of a land unit, estimated by means of the Erosion Risk Index ERI, can be classified as indicated in Table 3.

Table 3. Ranking erosion risk in terms of values of the ERI.

ERI	Erosion risk
≤ 0.10	Low
0.11-0.30	Moderate
0.31-0.50	High
> 0.50	Very high

Land Classification System for tropical steplands

Soil Productivity Index PI and Erosion Risk Index ERI have finally permitted establishing a classification system for agricultural lands in tropical mountains based on these two fundamental qualities. This system is similar to those developed by Sheng (1972) and Larson et al. (1988), and it is shown in Figure 8.

<i>Erosion Risk Index (ERI)</i>					<i>General land use</i>
<i>Soil Productivity Index (PI)</i>	≤ 0.10 (low)	0.11-0.30 (moderate)	> 0.31-0.50 (high)	>0.50 (very high)	
≤ 0.10 (low)	Reserve lands (R) (4th priority conservation treatment)		Critical lands (C) (2nd priority conservation treatment)		Permanent vegetation Agroforestry
0.11-0.30 (moderate)					Special crops/ Agroforestry
0.31-0.50 (high)	Sub-critical lands (S) (3rd priority conservation treatment)		Super-critical lands (P) (1st priority conservation treatment)		Semi-intensive agriculture
>0.50 (very high)					Intensive agriculture
	low	moderate	high	very high	
<i>Soil conservation requirements</i>					

Figure 8. Land Classification System for soil conservation on tropical steep lands.

CLASSIFICATION OF SOIL MANAGEMENT AND CONSERVATION PRACTICES

The different conservation practices are grouped in three main categories indicated in Tables 4, 5 and 6.

Table 4 Category I : Practices for improving the soil productivity and soil resistance to erosion, as well as to reduce impacts from rainfall erosivity (“green practices”).

Group I-A Soil improvement (MS)	Group I-B Ground covers and plant management (MC)
MS - 1 reduced-tillage MS - 2 vertical-tillage MS - 3 mulch- tillage MS - 4 zero-tillage MS - 5 ridge-tillage MS - 6 ripping-tillage MS - 7 sub-soiling MS - 8 deep ploughing MS - 9 soil fertilization MS-10 residue incorporation MS-11 organic manures MS-12 green manures MS-13 acid soil amendments MS-14 sodic soil amendments MS-15 synthetic conditioners	MC - 1 cover crops MC - 2 mulching MC - 3 high density planting MC - 4 multiple-cropping MC - 5 crop rotations MC - 6 intercropping MC - 7 tolerant crops MC - 8 perennial crops MC - 9 under shadow cropping MC-10 pastures MC-11 agroforestry MC-12 tree replanting and afforestation MC-13 natural re-vegetation

Table 5. Category II: Practices for reducing runoff impacts on hillsides (“blue practices”).

Group II-A Slowing down runoff speed (AE)	Group II-B runoff catchment and/or transport (CE)
AE - 1 contour cropping AE - 2 hedgerows AE - 3 brush barriers AE - 4 strip cropping AE - 5 alley cropping	CE - 1 diversion channels CE - 2 hillside ditches CE - 3 retention ditches CE - 4 filtering ditches CE - 5 trench ditches CE - 6 diversion terraces CE - 7 retention terraces CE - 8 narrow-ridge terraces CE - 9 contour furrows
Group II-C slope length modification (LP)	Group II-D slope gradient modification (GP)
LP-1 wattlings LP-2 stone barriers LP-3 contour bunds LP-4 dams for gully control	GP-1 stone walls GP-2 continuous bench terraces GP-3 alternating bench terraces GP-4 individual terraces

Table 6. Category III: Complementary practices (“brown practices”).

Complementary practices	
PC-1 stones removal PC-2 land levelling PC-3 trickle irrigation PC-4 sprinkler irrigation PC-5 surface drainage	PC-6 subsurface drainage PC-7 firebreaks PC-8 protective fences PC-9 windbreaks PC-10 animal paths

Selection of soil conservation practices

In terms of the main limitations detected in the analysis of factors corresponding to soil productivity, in Table 7 there are some management and conservation practices that could be used to improve it.

Table 7. Identification of some soil management and conservation practices for reducing soil productivity limitations.

limiting soil condition	limiting factor	Limiting sub-factor	soil management and conservation practices (*)
air-water ratios	A	A ₁ (available water capacity)	MS-3, MS-4, MS-11, MS-12, MS-15, CE-3, CE-4, CE-5, CE-7, PC-3, PC-4
		A ₂ (aeration capacity)	MS-1, MS-5, MS-8, MS-10, MS-15, MC-7, CE-1, CE-2, CE-6, PC-2, PC-5, PC-6
mechanical resistances for root exploration	B	B ₁ (bulk density)	MS-2, MS-6, MS-7, MS-8, MS-10, MS-11, MS-12, MS-15
		B ₂ (coarse fragments)	PC-1, MS-1, MS-2, MC-4, MC-6, MC-7, MC-8, MC-10, MC-11, MC-12
potential fertility	C	C ₁ (pH)	MS-9, MS-10, MS-11, MS-12, MS-13, MC-5, MC-7, MC-10, MC-11
		C ₂ (organic matter)	MS-10, MS-11, MS-12, MS-14, MC-7, MC-10, PC-7

(*) codes are explained in Tables 4, 5 and 6

In terms of the main limitations detected in the analysis of factors corresponding to erosion risk, in Table 8 some management and conservation practices are mentioned that could be used to reduce such risks or to improve land conditions.

Table 8. Identification of some soil management and conservation practices for reducing limitations.

Limiting land condition	Limiting factor	Soil management and conservation practices (*)
soil runoff potential	α	MS-1, MS-2, MS-3, MS-4, MS-6, MS-7, MS-8, MS-10, MS-11, MS-12, MS-15, AE-1, AE-2, AE-3, AE-4, CE-1, CE-2, CE-6, CE-9, PC-5
rainfall aggressiveness & terrain slope	η	for rainfall aggressiveness : MS-3, MS-4, MS-5, MS-12, MC-1, MC-2, MC-3, MC-4, MC-5, MC-6, MC-8, MC-9, MC-10, MC-11, MC-12, MC-13
		for terrain slope : CE-8, LP-1, LP-2, LP-3, LP-4, GP-1, GP-2, GP-3, GP-4, PC-3, PC-4, PC-8, PC-10

(*) codes are explained in Tables 4, 5, and 6

CONCLUSIONS

This paper underlines the role, importance and applications of soil physics on land use planning and soil conservation on tropical steepplands.

The relevance of soil productivity and erosion risk are emphasized as important qualities that allow integrating several relevant physical characteristics of these lands, as well as to adequately formulate a system adapted to the particular conditions of tropical mountains for the identification and selection of the most appropriate alternatives for soil conservation programs.

REFERENCES

- BERGSMA, E. 1996. Terminology for soil erosion and conservation. International Society of Soil Science (ISSS). Wageningen, the Netherlands.
- DELGADO, F. 1997. Sistema para la evaluación y clasificación de tierras agrícolas y prioridades de conservación de suelos en áreas montañosas tropicales. Un enfoque metodológico. Serie Suelos y Clima N° SC-73. Cidiat. Mérida, Venezuela.
- DELGADO, F. and R. LOPEZ. 1998. Evaluation of soil degradation impact on the productivity of Venezuelan soils. *Advances in GeoEcology* 31: 133-142.
- DELGADO, F., R. TERRAZAS and R. LOPEZ. 1998. Planificación de la conservación de suelos en cuencas altas, utilizando relaciones erosión-productividad. *Agronomía Tropical*, 48 (4): 395-411.
- FAO-PNUMA. 1980. Metodología provisional para la evaluación de la degradación de suelos. Rome, Italy.
- LARSON, G. G. ROLOFF and W. LARSON. 1988. A new approach to marginal agriculture land classification. *Journal of Soil and Water Conservation*. 43 (1):103-106.
- MORGAN, R.P.C. 1986. Soil erosion & conservation. Editorial Longman. Essex, Inglaterra.
- PAEZ, M.L. 1994. Clasificación de suelos por riesgos de erosión hídrica con fines de planificación agrícola. *Revista de la Facultad de Agronomía. UCV. Maracay*. 20:83-100.

- PIERCE, F.J., W.E. LARSON, R.H. DOWDY and W.A. GRAHAM, 1983. Productivity of soils: assessing long-term changes due to erosion. *Journal of Soil and Water Conservation*. 38 (1): 39-44.
- SHENG, 1972. A treatment-oriented land capability classification scheme for hilly marginal lands in the humid tropics. *Journal of Scientific Research Council*. Kingston, Jamaica. 3: 93-112.

A Soil Mechanics Approach to Study Soil Compaction and Traffic Effect on the Preconsolidation Pressure of Tropical Soils

Moacir de Souza Dias Junior*

Soil Science Department, Federal University of Lavras, Brazil

*Lectures given at the
College on Soil Physics
Trieste, 3 – 21 March 2003*

LNS0418012

* msouzadj@ufla.br

A SOIL MECHANICS APPROACH TO STUDY SOIL COMPACTION

Introduction

The intensive use of the soil without moisture control has been causing dissemination of the soil compaction (Pedrotti and Dias Junior, 1996), due to the increase of the traffic of agricultural machines through the year (Hill and Meza-Montalvo, 1990; Muller et al., 1990), causing in consequence, a reduction of the productivity in the areas of intense traffic (Stone, 1987).

Soil compaction has been identified as one of the leading problem causing soil degradation (Canillas and Salokhe, 2002). Different soil uses has been altering the physical and mechanical soil properties (Barnes et al., 1971; Gupta et al., 1985; Larson et al., 1989; Soane and van Ouwerkerk, 1994; Dias Junior and Pierce, 1996ab, Dias Junior and Miranda, 2000, Horn et al., 2000; Dias Junior, 2000), causing soil compaction and restricting root penetration due to the insufficient root turgor pressure to overcome the mechanical resistance of the soil (Gysi, 2001). Soil compaction increase bulk density and soil strength (Taylor, 1971; Lebert et al., 1989; Hill and Meza-Montalvo, 1990; Lebert and Horn, 1991; Dias Junior et al., 1999, Arvidsson, 2001; Ishaq et al., 2001); decrease total porosity, size and continuity of the pores (Hillel, 1982; Smucker and Erickson, 1989; Servadio et al., 2001) and limit nutrient uptake, water infiltration and redistribution, gas exchange, seedling emergency and root development (Tardieu, 1988; Smucker and Erickson, 1989; Bicki and Siemens, 1991; Dürr and Aubertot, 2000, Arvidsson, 2001; Ishaq et al., 2001) resulting in decreased yields (Arvidsson, 2001; Radford et al., 2001; Dauda and Samari, 2002), increased erosion and increased power requirement for tillage (Stone, 1987, Canillas and Salokhe, 2002).

In tropical conditions, the soil compaction process has been occurring in annual crops due to tillage and harvest operation is carried out when the soil surface is wetter than optimal for wheel traffic (Silva et al., 1986, Dias Junior, 1997); in pasture, due to the excessive trampling of the cattle (Kondo and Dias Junior, 1999) and in forest areas due to the traffic of the harvest operations and wood transport under inadequate soil water conditions (Dias Junior et al., 1999; Dias Junior, 2000).

On the other hand, with the standardization of specific legislation regarding the use of natural resources, the companies involved in this activity type, should adapt their activities in a way to match sustainable development, avoiding therefore, the degradation of their areas. Thus, a consensus of which soil physics or mechanics property should be used as a universal indicator of soil structure sustainability is needed. Gupta and Raper (1994), suggested that there is a scarcity of reliable information concerning soil compaction that can be widely used to develop guidelines to determine: a) the maximum pressure a specific soil can withstand over a range of water content and b) the range of applied stresses and moisture contents that are conducive to excessive soil compaction.

In spite of this, there are evidences in literature indicating that preconsolidation pressure or precompression stress (σ_p) is an indication of soil strength (Arvidsson, 2001) and of the maximum previously applied stress sustained by a soil and defines the limit of elastic deformation in the soil compression curves (Holtz and Kovacs, 1981, Dias Junior and Pierce, 1995; Defosseze and Richard, 2002), and may be used as a quantitative indicator of soil structure sustainability (Dias Junior et al., 1999) and to estimate, root growth (Römken and Miller, 1971). Thus, in agriculture, application of stress greater than the precompression stress should be avoid (Gupta et al., 1989; Lebert and Horn, 1991; Defosseze and Richard, 2002). Therefore, changes in σ_p as a function of moisture content is important for root growth and also to assess the load support capacity of the soil.

Although, several researchers (Barnes et al., 1971; Gupta et al., 1985; Larson et al., 1989; Soane and van Ouwerkerk, 1994; Dias Junior and Pierce, 1996ab, Dias Junior and Miranda, 2000; Horn et al., 2000) had already quantified the soil management effect in the soil physics properties, there is a need for a methodology that predicts the maximum stress that a soil can withstand over a range of water contents without causing soil structure degradation.

Inside of this context, Dias Junior (1994) seeking for a property that might be used as an indicator of soil management sustainability, developed a methodology that may be used to predict: a) the maximum pressure that a specific soil can withstand over a range of water content without additional soil compaction occurs and b) the range of applied stresses and water content that are conducive to additional soil compaction. Therefore, in this notes it will be present the development of this methodology and its application in studies of structure sustainability of some tropical soils.

Methodology Development

The soil compression curves obtained from laboratory compressibility test are frequently used in compaction studies (Larson et al., 1980; Larson and Gupta, 1980; Bingner and Wells, 1992; O'Sullivan, 1992; MacNabb and Boersma, 1993; Dias Junior, 1994; Dias Junior and Pierce, 1996ab; Canarache et al., 2000). These curves describe the relationship between the logarithm of the applied pressure and bulk density or void ratio (Casagrande, 1936; Leonards, 1962; Holtz and Kovacs, 1981). The precompression stress divides the soil compression curves into a region of small, elastic and recoverable deformation (secondary compression curve) that defines soil management history and a region of plastic and unrecoverable deformation (virgin compression curve) (Holtz and Kovacs, 1981; Jamiolkowski et al., 1985; Gupta et al, 1989; Lebert and Horn, 1991; Dias Junior and Pierce, 1995; Canarache et al., 2000) (Figure 1). Thus the development of this methodology was based on the soil compression curve.

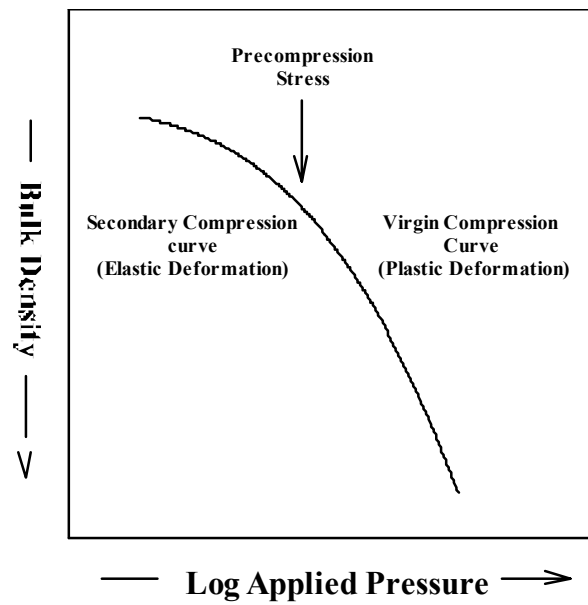


Figure 1. Soil compression curve. Source: Dias Junior (1994).

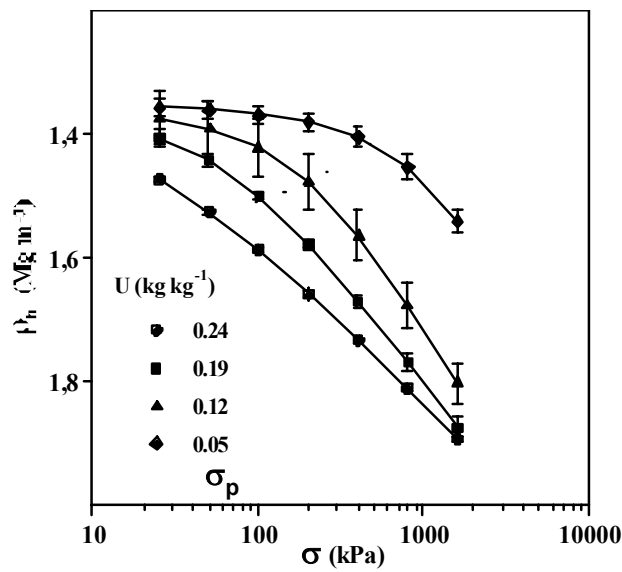


Figure 2. Soil compression curves at different moisture content (U). The dotted line indicates the precompression stress. Source: Dias Junior (1994).

The shape of the soil compression curves varies with moisture content (Figure 2) and therefore, affecting the secondary and the virgin compression curves (Dias Junior, 1994; Dias Junior and Pierce, 1995) and the precompression stress (figure 2).

Considering the changes in the shape of the soil compression curves, Dias Junior (1994) suggested a soil compressibility model based on the soil compression curves, obtained for different moisture conditions. This model consists of two parts (Figure 3):

a) Soil management model (Figure 3a) that may be used to estimate the maximum pressure that can be applied to the soil in order to avoid structure degradation and also may be used to estimate the pressure that roots may need to do in order to overcome soil strength. This model takes the general form: $\sigma_p = 10^{(a + b U)}$, where: σ_p = precompression stress (kPa), U = moisture content (kg kg^{-1}), and “a” and “b” are fitted parameters.

b) Virgin compression model (Figure 3b) that may be used to estimate the deformations that could occur when pressure greater than the precompression stress is applied to the soil. This model takes the general form: $\rho_{b\text{final}} = \rho_{b\text{ocp}} + m \log (\sigma_{\text{final}} / \sigma_p)$ where $\rho_{b\text{final}}$ = final bulk density (Mg m^{-3}), $\rho_{b\text{ocp}}$ = bulk density at the precompression stress (Mg m^{-3}), m = compression index (Mg m^{-3}), σ = applied pressure (kPa) and σ_p = precompression stress (kPa).

The next step of the development of this methodology was based on how to determine precompression stress in a fast a simple way. In order to do that it was found in the literature that some of the methods used to estimate precompression stress are graphical procedure (Casagrande, 1936; Burmister, 1951; Schmertmann, 1955). Additional methods have been used to estimate precompression stress, primarily involving regression (Sällfors, 1975; Culley and Larson, 1987; Jose et al., 1989; Lebert and Horn, 1991) and prediction from undrained shear strength and effective vertical overburden pressure (Anderson and Lukas, 1981). None of these estimation techniques is considered a standard technique. Although the method suggested by Casagrande (1936) is one of the most used in civil engineering, this method is based on the choice of the point in the compression curve with minimum radius of curvature. It has been shown that as soil sample disturbance increases, the selection of this point is increasingly more difficult and the precompression stress will be lower than those obtained for undisturbed soil samples (Schmertmann, 1955; Brumund et al., 1976; Holtz and Kovacs, 1981). Also, when using undisturbed soil samples at high moisture content, the selection of the point of minimum radius also can be difficult because the compression curve is nearly linear (Dias Junior, 1994).

Therefore, Dias Junior and Pierce (1995) evaluated a number of procedures for estimation of the precompression stress from uniaxial compression test. The procedures were evaluated against the Casagrande graphical estimation procedure and published values of precompression stress. The procedure that best met the performance criteria for prediction of precompression stress was programmed into standard computer spreadsheet software (Table 1 and Figure 4).

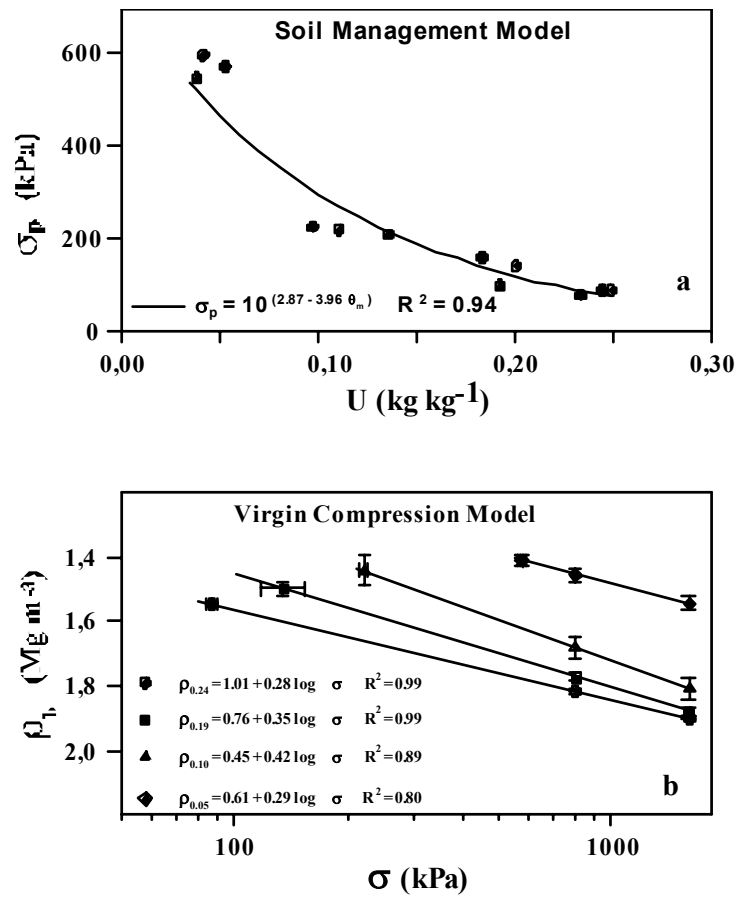


Figure 3. The soil management model (a) expressing precompression stress (σ_p) as a function of moisture content (U); and the virgin compression model (b) expressing bulk density (ρ_b) as a function of applied stress (σ). Source: Dias Junior (1994) and Dias Junior and Pierce (1996).

Table 1. Spreadsheet for determination of the precompression stress (σ_p) from soil compression curves. Source: Dias Junior and Pierce (1995).

Stress	Log Stress	ρ_b	ρ_b vcc	ρ_b reg
25	1.3979	1.3905	1.2897	1.3845
50	1.6960	1.4444	1.3825	1.4502
100	2.0000	1.5097	1.5160	1.5160
200	2.3010	1.5878	1.5681	1.5847
400	2.6021	1.6712	1.6609	1.6474
800	2.9031	1.7537	1.7537	1.7131
1600	3.2041	1.8465	1.8465	
Method 1 (Suction < 100 kPa)			Method 3 (Suction > 100 kPa)	
$\sigma_p = 151$ kPa			$\sigma_p = 238$ kPa	
$\rho_b = 1,53$ Mg m ⁻³			$\rho_b = 1,61$ Mg m ⁻³	

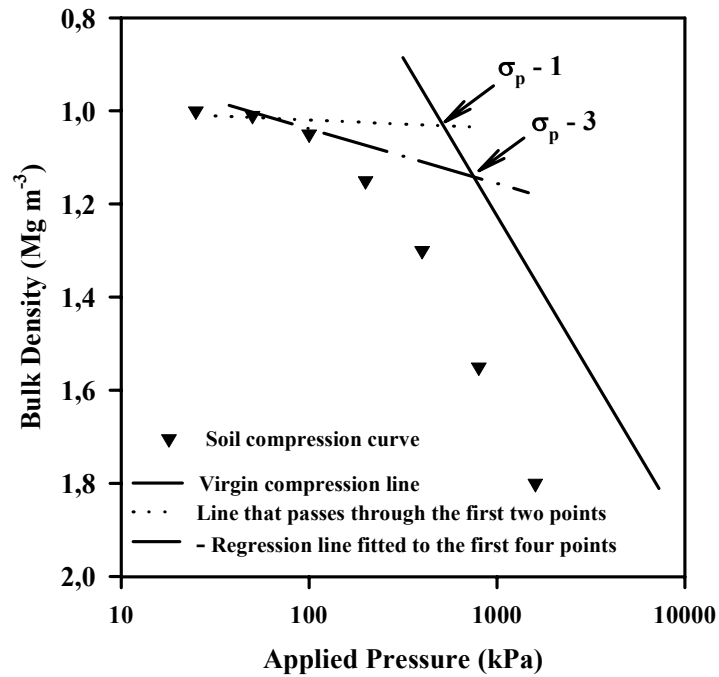


Figure 4. Computer screen of the soil compression curve showing the precompression stress (σ_p) obtained using method 1 and method 3. Source: Dias Junior (1994).

TRAFFIC EFFECT ON THE PRECONSOLIDATION PRESSURE OF TROPICAL SOILS

Evaluation of the susceptibility of soil management systems to compaction

Kondo and Dias Junior (1997 and 1999) evaluated the changes in the precompression stress as a function of the moisture content of a Red-Yellow Latosol (Oxisol) under annual crop, cultivated pasture and native forest. The undisturbed soil samples were taken randomly at 0-3 cm depth. According to figure 5, it was observed a shifting for the region of lower pressure of the curve of precompression stress as a function of moisture content for the annual crop in relation of the curve of native forest, which is due to the destruction of soil structure by the tillage tools, suggesting therefore, greater soil susceptibility to compaction of the soil under annual crop. For the cultivated pasture, the precompression stress was greater than for the annual crop and the native forest, evidencing the influence of the trampling of the cattle on the compaction of the soil surface.

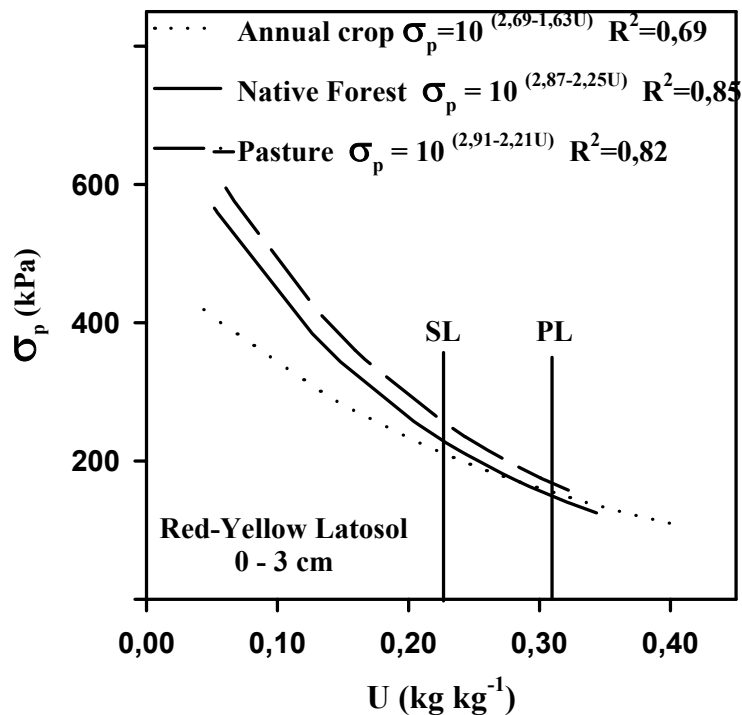


Figure 5. Relationship between precompression stress (σ_p) and moisture content (U) for a Red-Yellow Latosol at 0-3 cm depth, for annual crop, native forest and cultivated pasture. SL = Shrinkage limit, PL = Plastic limit. Source: Kondo and Dias Junior (1997 and 1999).

In order to verify the possible alteration of the soil structure caused by the *Eucalyptus* plantation at 0-3 cm and 35-38 cm depth of a Yellow Podzolic (Acridoxic Kandudult), Dias Junior et al., (1999), compared the curves of precompression stress as a function of moisture content for the conditions of native forest and eucalyptus plantation (Figure 6). The curves of precompression stress as a function of moisture content at 0-3 cm depth were statistically different and showed smaller precompression stress than the native forest for any moisture condition. This fact evidenced an alleviation of the natural soil strength by the tillage operations. There were no statistically differences in the precompression stress at 35-38 cm depth for these two conditions, showing that the soil tillage operations did not alter the soil structure at this depth.

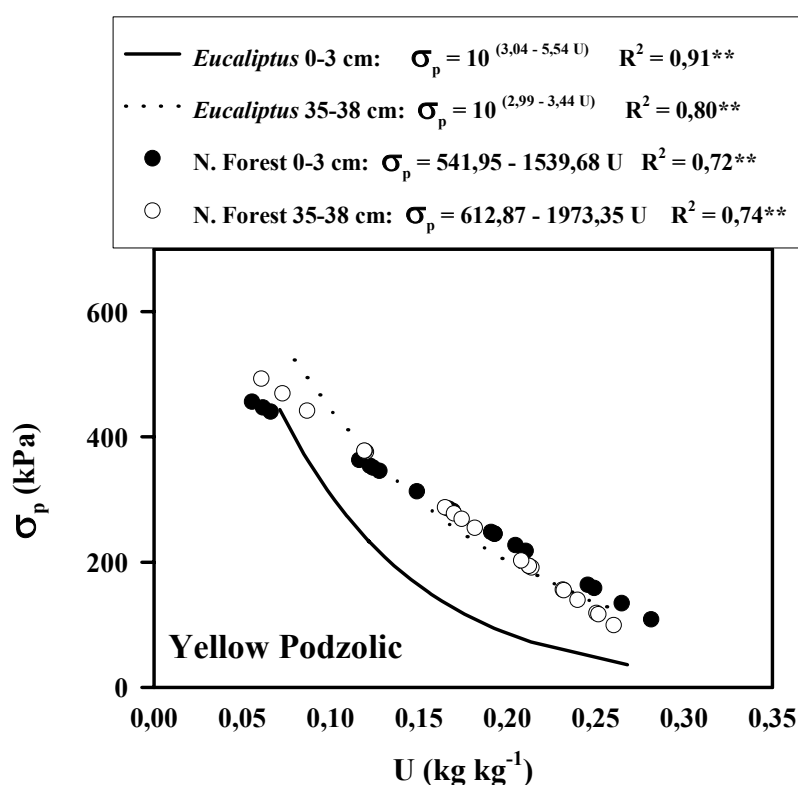


Figure 6. Relationship between the precompression stress (σ_p) and moisture content (U) for the Yellow Podzolic for the 0-3 and 35-38 cm depth for native forest and *Eucalyptus* plantation. Source: Dias Junior et al. (1999).

Evaluation of the susceptibility of soil classes/horizons to compaction

The figures 7 and 8 show the curves of precompression stress as a function of moisture content for a Yellow Podzolic (Acrudoxic Kandiuult) and for a Plinthosol (Acrudoxic Plintic Kandiuult) at 0-3 and 35-38 cm depth. For the 0-3 cm depth (Figure 7), the curves of the two soils were statistically different and the Plinthosol showed values of precompression stress significantly greater than the Yellow Podzolic, for any value of moisture content. It is expect, therefore, that at 0-3 cm depth, the Yellow Podzolic should be more susceptible to soil compaction than Plinthosol. For the 35-38 cm depth, the curves of precompression stress as a function of moisture content were not statistically different (Dias Junior et al., 1999).

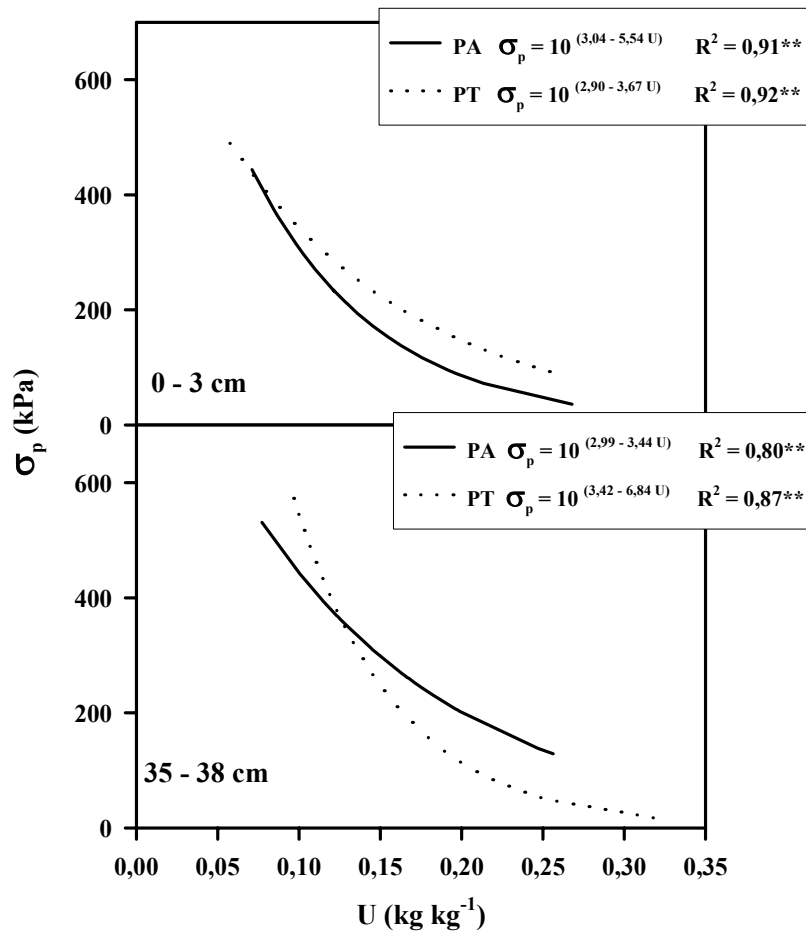


Figure 7. Relationship between precompression stress (σ_p) and moisture content (U), for the Yellow Podzolic (PA) and Plinthosol (PT) for the 0-3 and 35-38 cm depth. Source: Dias Junior et al. (1999).

The curves of precompression stress as a function of moisture content at 0-3 cm depth were statistically different from those at 35-38 cm for the Yellow Podzolic and for the Plinthosol (Figure 8). The depth 35-38 for a Yellow Podzolic, showed greater value of precompression stress than at 0-3 cm depth, and for the Plinthosol it was observed only when the moisture content was smaller than 0,14 kg kg⁻¹. These differences might be related with the soil formation processes. Considering those results, it is expected that at 0-3 cm depth of these soils should be more susceptible to soil compaction than at 35-38 cm depth, except for the Plinthosol at moisture content greater than 0,14 kg kg⁻¹. (Dias Junior et al., 1999).

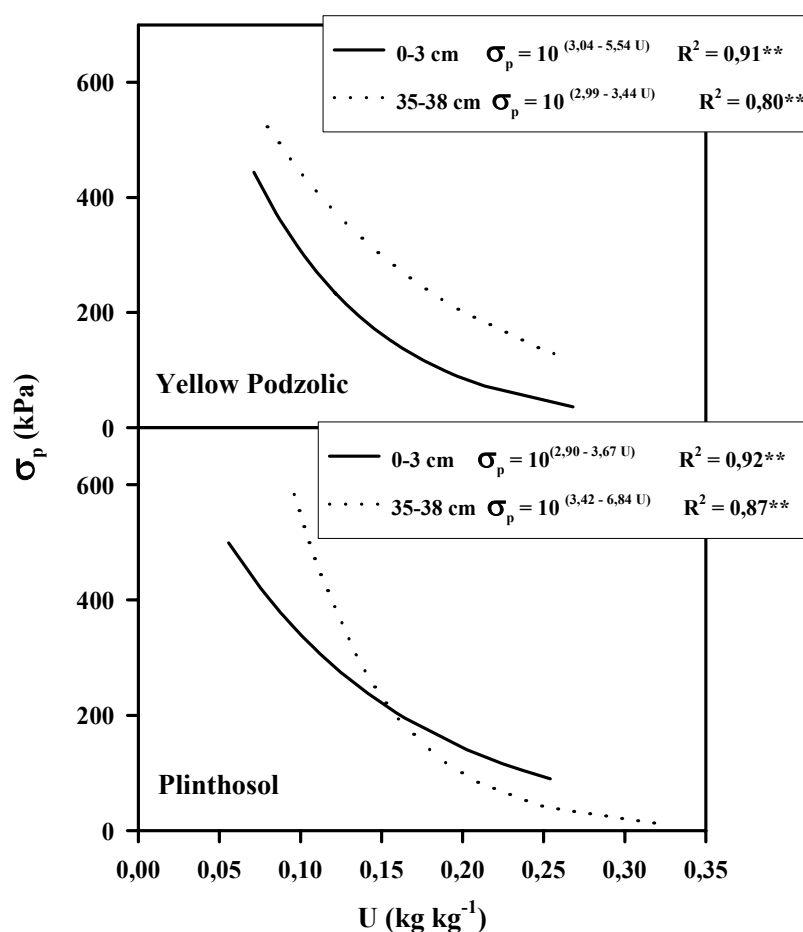


Figure 8. Relationship between precompression stress (σ_p) and moisture content (U) at 0-3 and 35-38 cm depth of the Yellow Podzolic and Plinthosol. Source: Dias Junior et al. (1999).

For a Yellow Latosol (Oxisol), it was observed that at 15-18 cm depth, was statistically different from the 0-3 cm depth (Figure 9), showing greater values of precompression stress than this depth and therefore higher resistance to soil compaction.

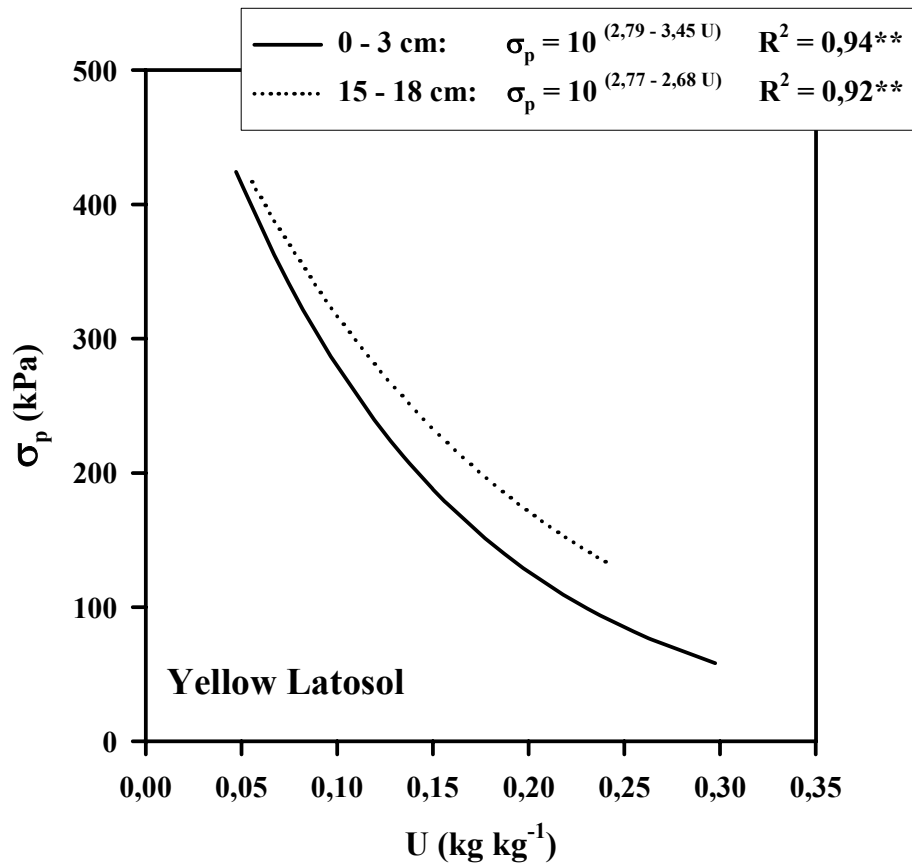


Figure 9. Relationship between the precompression stress (σ_p) and moisture content (U) for the 0-3 and 15-18 cm depth of Yellow Latosol. Source: Dias Junior (2000).

In summary, one might expect that soil with larger values of precompression stress should have large values of load support capacity and therefore, and larger resistance to soil compaction. However, one might consider that root system developing in a place with large precompression stress, should experiment higher soil mechanics resistance than those that are growing in place of lower precompression stress. Thus, the understanding of changes in precompression stress with the soil management is important.

Evaluation of the susceptibility of soil under *Eucalyptus* plantation

Considering that in agriculture, the application of pressures larger than the largest pressure applied previously to the soil should be avoided in order to avoid additional soil compaction (Gupta et al., 1989; Lebert and Horn, 1991) and that the precompression stress is an indicative of the maximum applied pressure to the soil in the past (Holtz and Kovacs, 1981; Dias Junior, 1994) figure 10, was then divided into three regions to evaluate the traffic effects and the natural alleviation of the precompression stress. The considered regions (Figure 10) are: a) the region where the precompression stress determined after the traffic (σ_{pt}) are larger than the maximum precompression stress estimated with the equation of the Confidence Interval at 95% (σ_p maximum estimated), being considered as the region where the soil structure degradation had already happened; b) the region where precompression stress determined after the traffic (σ_{pt}) are larger than the precompression stress estimated with the equation of the relationship between σ_p and $U(\sigma_p)$ and smaller than the maximum precompression stress estimated with the equation of the Confidence Interval at 95% (σ_p maximum estimated), being considered as the region where there is a tendency of soil structure degradation to happen and c) a region where the precompression stress determined after the traffic (σ_{pt}) are smaller than the precompression stress estimated with the equation of the relationship between σ_p and $U(\sigma_p)$, being considered as the region where there is no soil structure degradation.

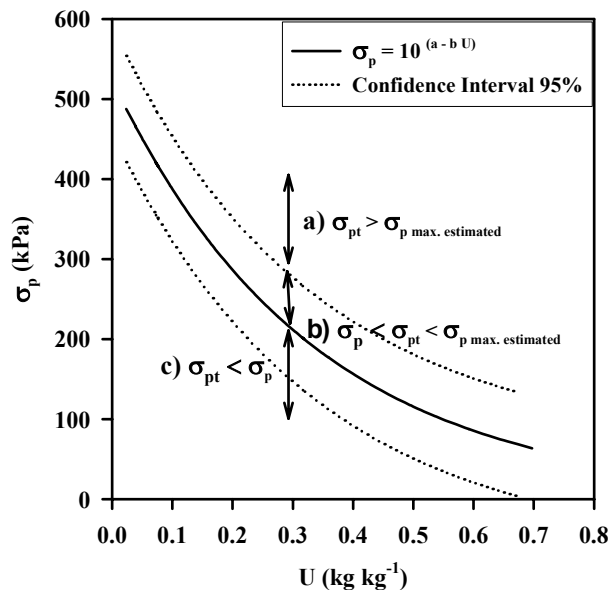


Figure 10. Relationship between precompression stress (σ_p) and moisture content (U). (Source: Dias Junior, 2002).

With the standardization of specific legislation regarding the exploration of natural resources, the companies involved in this type of activity are alert about the problems that their mechanical activities can cause to the soil structure. Therefore, they are interested in obtain answer to questions such as: a) Any increase in soil bulk density values means additional soil compaction? b) Which soil class is more susceptible to soil compaction? c) Which harvest machinery can cause more soil compaction? d) What is the influence of harvest operations in A and B-horizons? Thus, the studies conducted in this area should consider as an attempt to find some answer for those question, in a way to contribute with the sustainability of the areas of *Eucalyptus* exploration.

One of the studies conducted, as an attempting to answer those questions was done by Dias Junior et al., (1999). The objectives of this study were: a) to suggest and monitor precompression stress as a quantitative indicator of the structure sustainability of the soils cultivated with *Eucalyptus*; b) to propose a model of structure sustainability of the soils cultivated with *Eucalyptus*, based on precompression stress and moisture content; c) to determine the effect of harvest machinery on soil structure, through these models; d) to monitor precompression stress every two years in order to verify if some alleviation of the structure degradation is occurring, due to the biological activity or due to drying and wetting cycles. This study was conducted in a Yellow Podzolic (Acrudoxic Kandiodult) and in a Plinthosol (Acrudoxic Plintic Kandiodult), under native forest and *Eucalyptus*. In each soil class, sampling consisted of two stages: before and after the mechanized harvest operations. In each stage, nine undisturbed soil samples were collected at 0-3 cm and at 35-38 cm depth, using 3 replications, with a total of 54 undisturbed soil samples. The undisturbed soil samples were used in the uniaxial compression tests. The soils samples taken before the crop operations were used to obtain the relationship between precompression stress and moisture content and the confidence interval at 95%. The relationship between precompression stress and moisture content will be called from now on, structure sustainability model. The soils samples taken after the mechanized harvest were done after the operation with Feller-Büncher, Harvester and Forwarder. From these soil samples precompression stress were obtained at the natural moisture content and these values were plotted in the structure sustainability model as an attempt to find a methodology that may be became used to quantify the effect of harvest operations in the soil structure (Figures 11 to 14).

In figures 11 to 14, it is observed that the Feller-Büncher did not cause structure degradation in both depth and soil classes. In figures 11 to 14 it is observed that only for the Yellow Podzolic at 0-3 cm depth, the Harvester caused some structure degradation (Figure 11). The Forwarder, however, caused structure degradation in both soil classes at 0-3 cm depth, as showing in figures 11 and 13. For the 35-38 cm depth, the Forwarder also did not caused structure degradation.

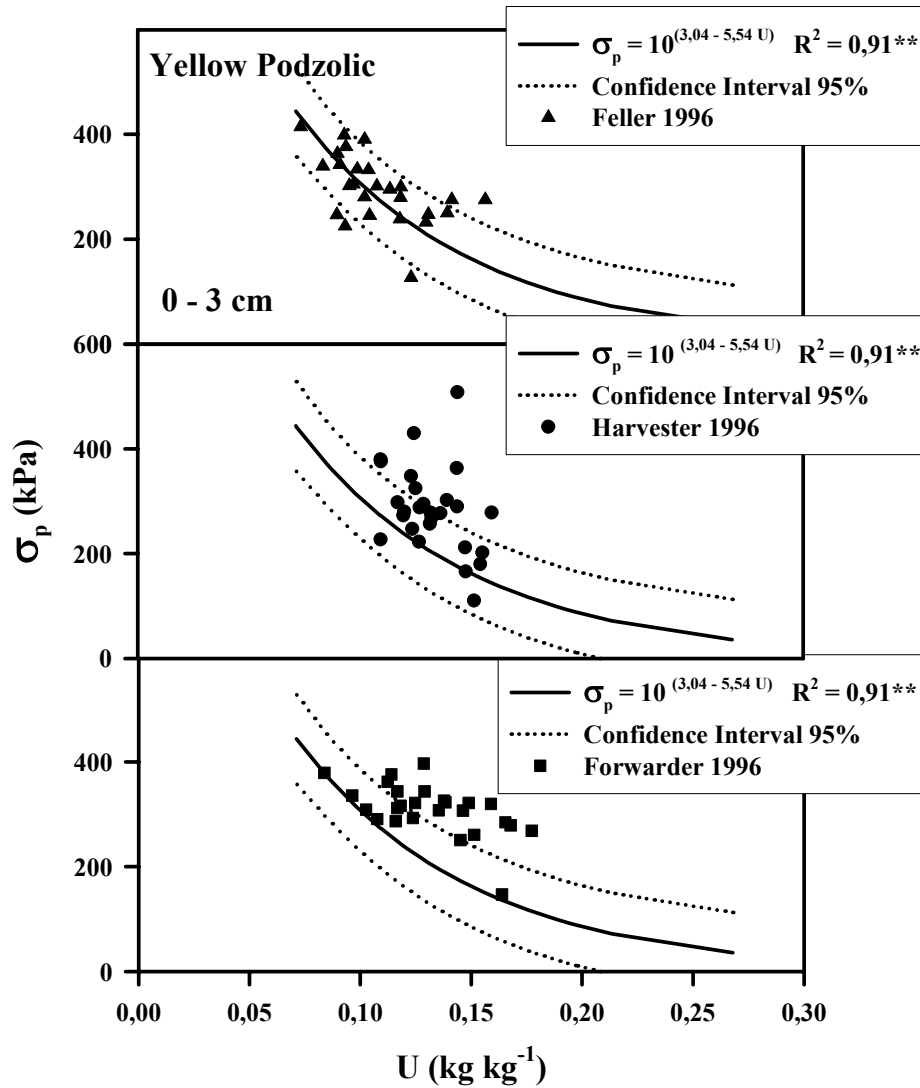


Figure 11. Relationship between the precompression stress (σ_p) and moisture content (U) for Yellow Podzolic after Feller-Büncher, Harvester and Forwarder operations, on the 0-3 cm depth. Source: Dias Junior et al. (1999).

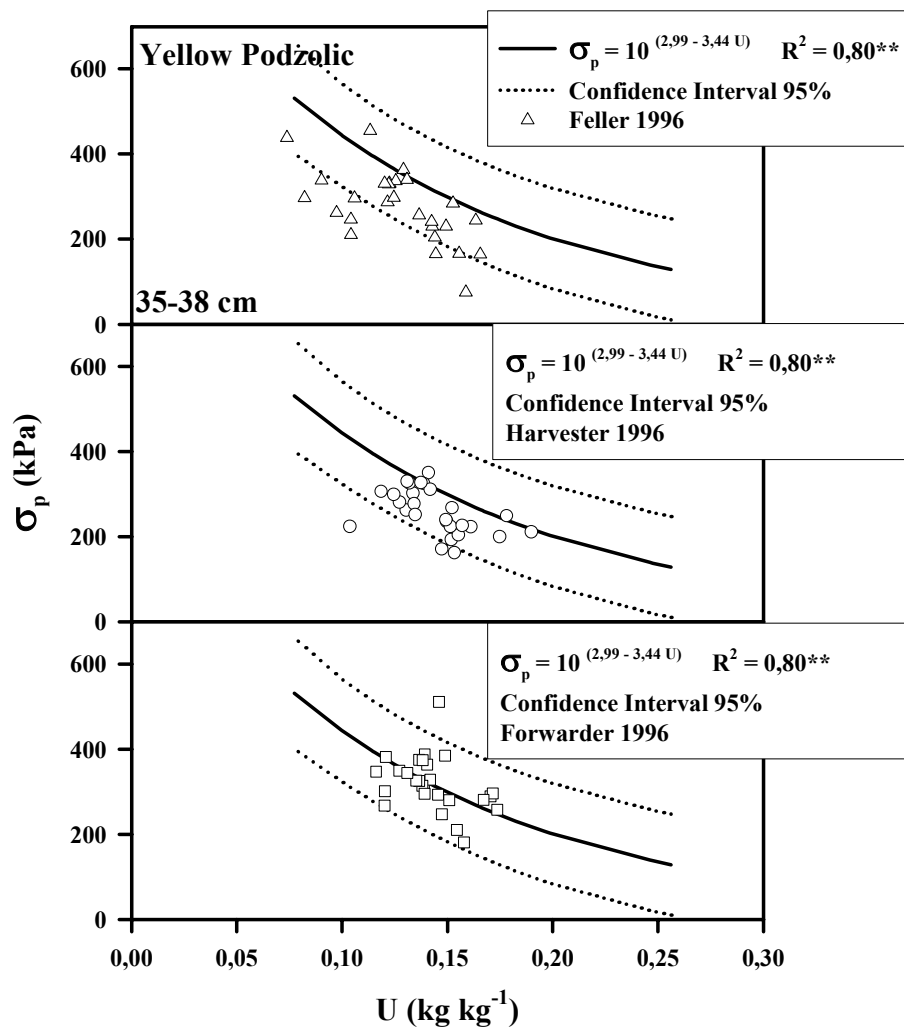


Figure 12. Relationship between the precompression stress (σ_p) and moisture content (U) for Yellow Podzolic after Feller-Büncher, Harvester and Forwarder operations, on the 35-38 cm depth. Source: Dias Junior et al. (1999).

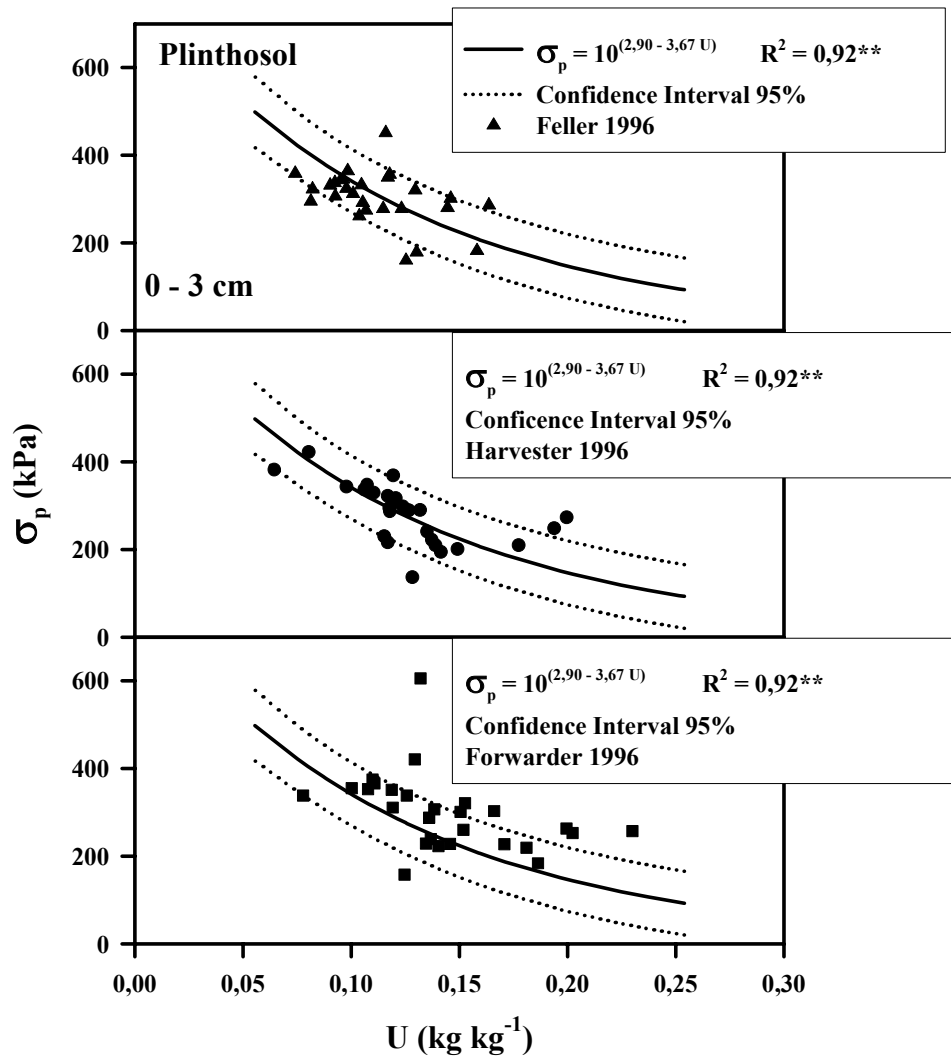


Figure 13. Relationship between the precompression stress (σ_p) and moisture content (U) for Plinthosol after Feller-Büncher, Harvester and Forwarder operations, on the 0-3 cm depth. Source: Dias Junior et al. (1999).

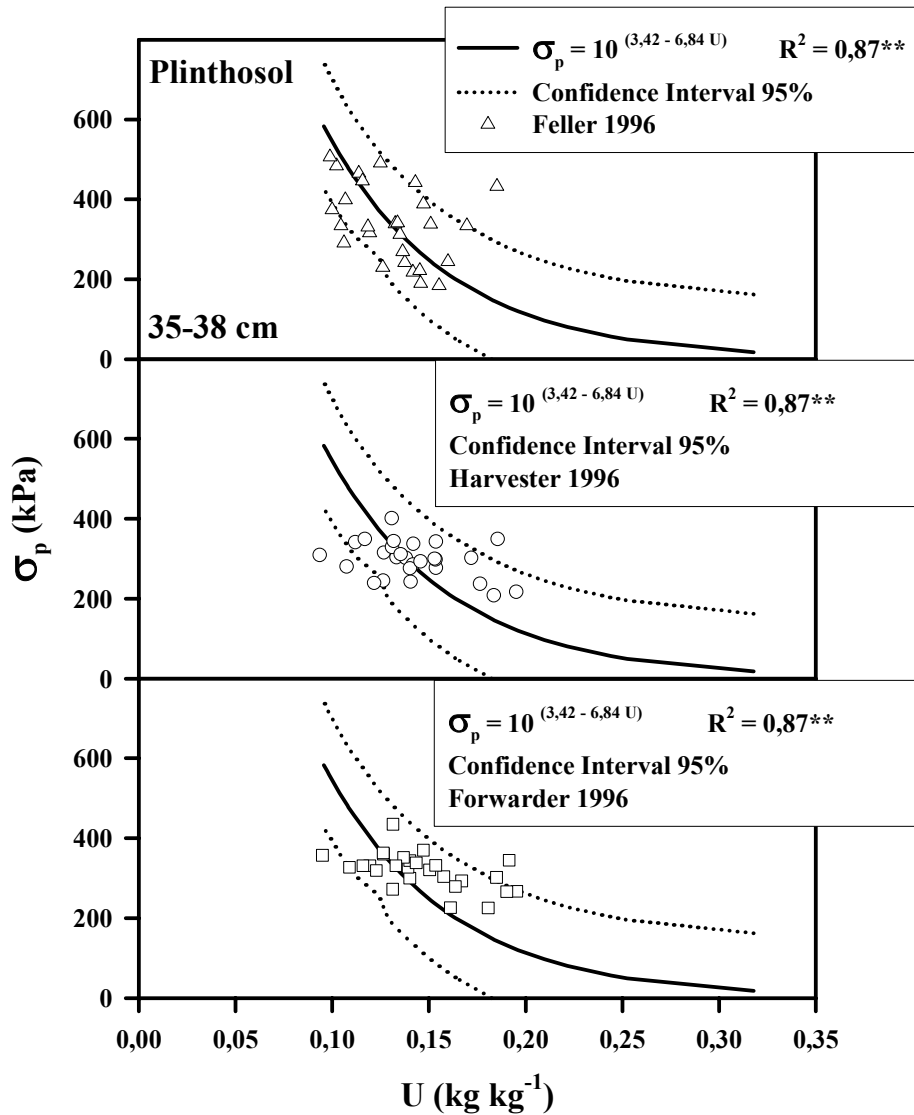


Figure 14. Relationship between the precompression stress (σ_p) and moisture content (U) for Plinthosol after Feller-Büncher, Harvester and Forwarder operations, on the 35-38 cm depth. Source: Dias Junior et al. (1999).

To quantify the impact on the soil structure caused by the harvest operations of the eucalyptus plantation, done by two sets of machines, one Feller Büncher (2618 crawler) and Skidder (460 with tires 30.5L.32) and the other Harvester (1270 with tires 700 x 26.5) and Forwarder (1710 with tires 750 x 26.5) in the dry and rainy

seasons, a experiment was conducted in a Red Yellow Latosol (Oxisol) at 0.10-0.125 m depth. The results of this experiment are showed in table 2.

Table 2. Precompression stress induced by Feller Büncher (2618 de crawler) and Skidder (460 with tires 30.5L.32), and Harvester (1270 tires 700x26.5) and Forwarder (1710 with tires 750x26.5) in a Red Yellow Latosol, at 0.10-0.125 m depth. (Source: Dias Junior, 2002b)

Harvest machines	$\sigma_{pt}^1 > \sigma_{p \max est}^2$		Δ (%)
	Dry season	Rainy season	
Feller Büncher and Skidder	5	15	200
Harvester and Forwarder	8	31	287
Δ (%)	60	106	

1 – Pressure applied by the harvest machines, 2 – Precompression stress estimated with the equation of the confidence interval at 95%.

Table 2, shows that the harvest operations performed with Harvester and Forwarder in the dry season, increased the precompression stress values in 60% in relation to the precompression stress induced by Feller Büncher and Skidder and in the rainy season this increase was 106%. In addition, the precompression stress induced by Feller Büncher and Skidder, and Harvester and Forwarder increased in 200% and 287%, respectively, when the harvest operations were performed in the rainy season. Although, the operations performed with Harvester and Forwarder caused more soil structure degradation, one might consider that the traffic done with Harvester and Forwarder is located, while the traffic done with Feller Büncher and Skidder is random and could consequently, disseminate the compaction in the whole area.

Assessment of the natural alleviation of the precompression stress

To access the natural alleviation of the precompression stress due to the drying and wetting cycle, as well as, due to the biological activity, the criteria suggested in figure 10, was considered and the precompression stress as a function of moisture content were determined in 1996, 1998 and 2000 in the traffic line of the Forwarder, and plotted in figures 15 and 16 for the Yellow Podzolic at 0-3 cm depth and for the Phinthosol at 35- 38 cm depth, respectively. Figure 15 shows that at 0-3 cm depth, is occurring a decreasing in the percentage of soil samples in the region where soil structure degradation had already happened (44, 22 and 11%) and an increase in the percentage of soil samples in the region where there is no soil structure degradation (4, 26 and 56%). In figure 16, it was observed only an increase in the percentage of soil samples in the region where there is no soil structure degradation (30, 33 and 52%). Thus, it was concluded that: a) the soil compaction

occurred only in the topsoil layer and it was restricted to the Harvester traffic line; b) at the end of four years, even without soil tillage, it was observed that there was a natural alleviation of the topsoil compaction due to the biological activity proportionate by the eucalyptus plantation and c) there were no indications of irreversible alterations in the soil structure at 35-38 cm depth.

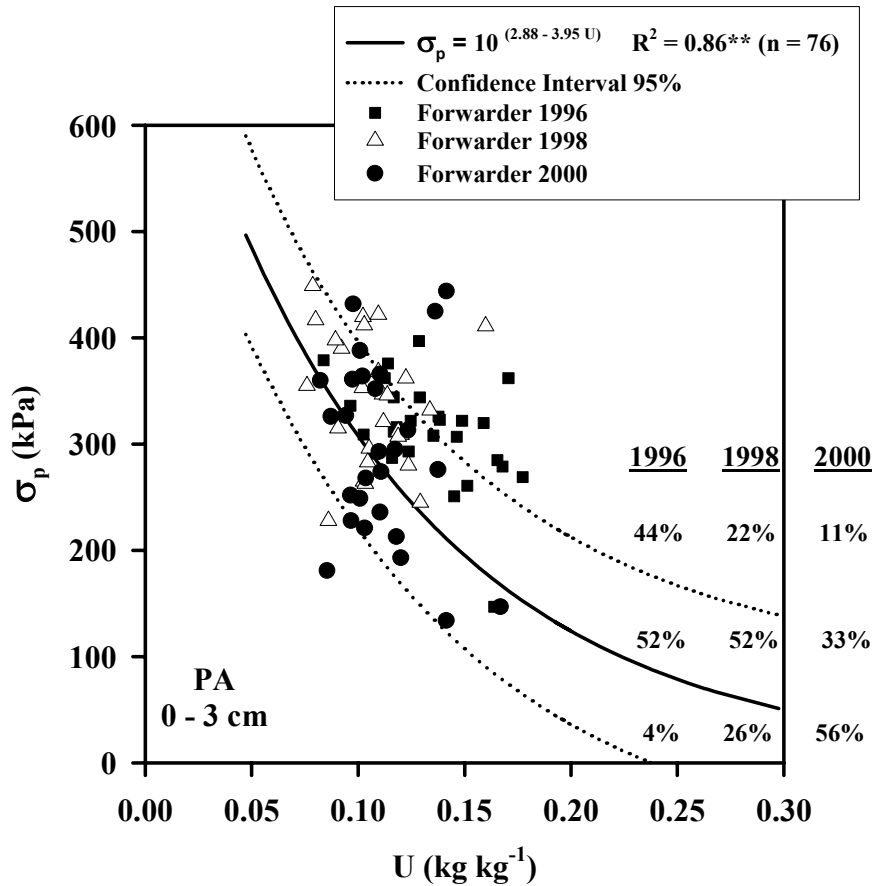


Figure 15. Relationship between precompression stress (σ_p) and moisture content (U) for a Yellow Podzolic at 0-0,03 m depth. The symbols represent the values of the precompression stress determined in soil samples collected in 1996, 1998 and 2000, in the area where the Forwarder operations occurred. (Source: Dias Junior, 2002a).

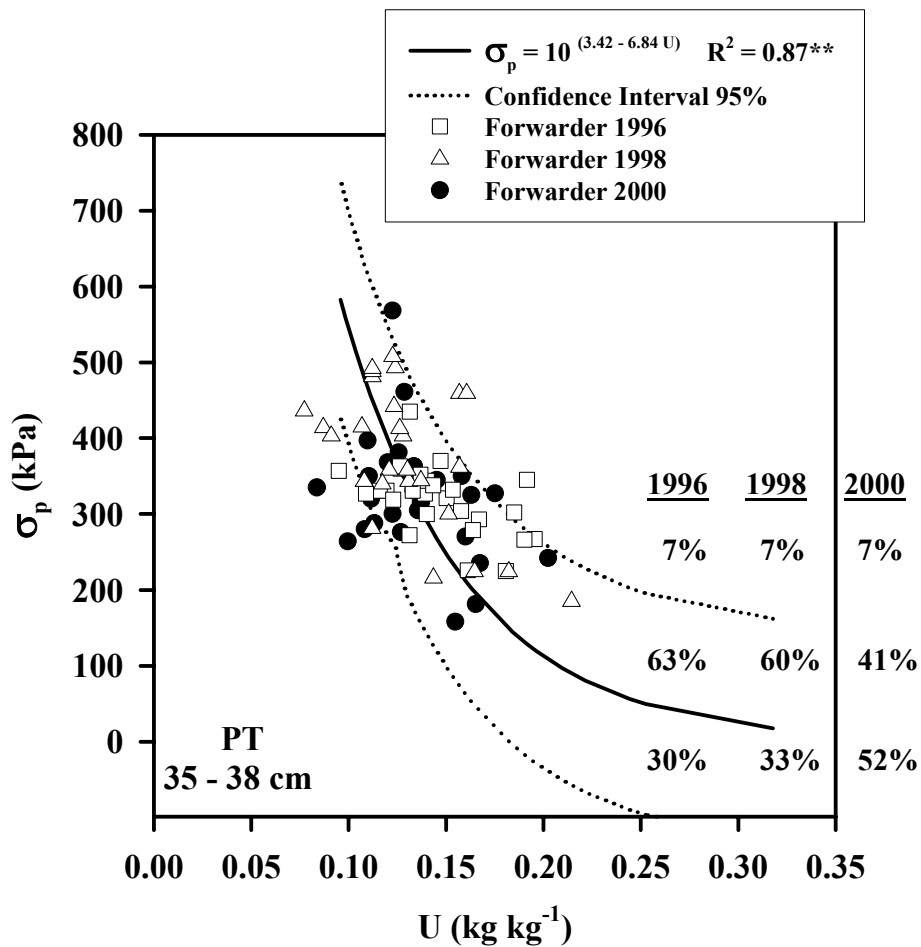


Figure 16. Relationship between precompression stress (σ_p) and moisture content (U) for a Plinthosol, at 0,35-0,38 m depth. The symbols represent the values of the precompression stress determined in soil samples collected in 1996, 1998 and 2000, in the area where the Forwarder operations occurred. (Source: Dias Junior, 2002a).

General Considerations

Several researchers have already demonstrated the causes and the effects of soil compaction. These studies showed that the soil compaction is a limiting factor in the agricultural production. The attributes of the soil conventionally monitored has not been capable to quantify the load support capacity of the soil, not allowing to foresee the levels of pressures that can be applied to the soils at different moisture conditions without additional soil compaction (structure degradation) happens. The

researches done in the soil compressive behavior of some tropical soils indicate that the precompression stress may be used as an alternative measure of the load support capacity and as a quantitative indicator of the structure sustainability of the tropical soils.

References

- Anderson, T.C. and Lukas, R.G. Precompression stress predicted using S_u/p' ratio. 1981. In: Yong, R.N. and Townsend, F.C., eds. Laboratory shear strength of soil. Symposium of the ASTM. p.502-515. (Spec. Tech. Pub., 740).
- Arvidsson, J., 2001. Subsoil compaction caused by heavy sugarbeet harvesters in southern Sweden I. Soil physical properties and crop yield in six field experiments. *Soil Till. Res.* 60, 67-78.
- Barnes, K.K.; Carleton, W.M.; Taylor, H.M.; Throckmorton, R.I. and Vanden Berg, G.E. 1971. Compaction of agricultural soils. *Am. Soc. Agric. Eng. Monogr.*, St. Joseph, 471p.
- Bicki, T.J., and Siemens, J.C., 1991. Crop response to wheel traffic soil compaction. *Trans. Am. Soc. Agric. Eng.*, 34, 909-913.
- Bingner, R.L.; and Wells, L.G., 1992. Compact - a reclamation soil compaction model part I. model development. *Trans. Am. Soc. Agric. Eng.*, 35: 405-413.
- Brumund, W.F.; Jonas, E. and Ladd, C.C., 1976. Estimating in situ maximum past (preconsolidation) pressure of saturated clays from results of laboratory consolidometer test. In: Transportation Research Board, National Research Council. Estimation of Consolidation Settlement. Special Report 163. National Academy of Science. Washington, DC, pp. 4-12.
- Burmister, D., 1951. The application of controlled test methods in consolidation testing. In: Fifty -Four Annual Meeting of the ASTM. Symposium on Consolidation Testing of Soils. Special Technical Publication 126. Atlantic City, NJ. 18 June 1951, Philadelphia, PA, pp. 83-98.
- Canarache, A.; Horn, R. and Colibas, I., 2000. Compressibility of soils in a long term field experiment with intensive deep ripping in Romania. *Soil Till. Res.* 56, 185-196.
- Canillas, E. C. and Salokhe, V. M., 2002. A decision support system for compaction assessment in agricultural soils. *Soil Till. Res.* 65, 221-230.
- Casagrande, A., 1936. The determination of the pre-consolidation load and its practical significance. In: Int. Conf. on Soil Mech. and Found. Eng., Proc. of the ICSMFE. Cambridge, MA, 22-26 June 1936. Col. 3. Cambridge, MA, pp. 60-64.
- Culley, J.L.B. and Larson, W.E., 1987. Susceptibility to compression of a clay loam Haplaquoll. *Soil Sci. Soc. Am. J.*, 51, 562-567.

- Dauda, A. and Samari, A., 2002. Cowpea yield response to soil compaction under tractor on a sandy loam soil in the semi-arid region of northern Nigeria. *Soil Till. Res.* 68, 17-22.
- Defossez, P. and Richard, G., 2002. Models of soil compaction due to traffic and their evaluation. *Soil Till. Res.* 67, 41-64.
- Dias Junior, M. S., 1994. Compression of three soils under long-term tillage and wheel traffic. Ph.D Thesis, Michigan State University.
- Dias Junior, M. S., 2000. Compactação do solo. In R.F. Novais; V.H. Alvarez V and C.E.G.R. Schaefer (Editors). *Topics in Soil Science. Soc. Bras. Ci. Solo.* pp. 55-94.
- Dias Junior, M. S., 2002a. Compactação do solo. Relatório de Pesquisa. Aracruz Celulose S.A. 72pp.
- Dias Junior, M. S., 2002b. Avaliação de impactos de sistemas de colheita nas características físicas dos solos. Relatório de Pesquisa. Celulose Nipo-Brasileira S.A. 113 pp.
- Dias Junior, M.S. 1997. Uso da história de tensão e da variação da umidade como instrumento para evitar a compactação adicional do solo. In: IVO, W.M.P.M.; SILVA, A.A.G.; MOTA, D.M. and FERNANDES, M.F., eds. *Workshop sobre avaliação e manejo dos recursos naturais em áreas de exploração de cana-de-açúcar.* EMBRAPA, p.67-81.
- Dias Junior, M.S. 2000. Compactação do solo. Relatório Técnico. 46p.
- Dias Junior, M.S., Ferreira, M.M., Fonseca, S., Silva, A.R., Ferreira, D.F., 1999. Avaliação quantitativa da sustentabilidade estrutural dos solos em sistemas florestais na região de Aracruz – ES. *R. Árv.*, 23, 371-380.
- Dias Junior, M. S. and Miranda, E.E.V., 2000. Comportamento da curva de compactação de cinco solos da região de Lavras (MG). *Ci. Agrot.* 24, 337-346.
- Dias Junior, M. S. and Pierce, F.J., 1995. A simple procedure for estimating preconsolidation pressure from soil compression curves. *Soil Tech.*, 8, 139-151.
- Dias Junior, M. S. and Pierce, F.J., 1996a. Influência da história de tensão e da umidade na modelagem da compactação do solo. In: V.H. ALVAREZ V; L.E.F. FONTES and M.P.F., FONTES (editors). *O solo nos grandes domínios morfoclimáticos do Brasil e o desenvolvimento sustentado.* Soc. Bras. Ci. Solo, Viçosa, MG. pp.445-452.
- Dias Junior, M. S. and Pierce, F.J., 1996b. Revisão de literatura: O processo de compactação do solo e sua modelagem. *R. Bras. Ci. Solo*, 20, 175-182.
- Dürr, C. and Aubertot, J. N., 2000. Emergence of seedling of sugar beet (*Beta vulgaris* L.) as affected by aggregate size, roughness and position of aggregates in the seedbed. *Plant Soil*, 219, 211-220.
- Gupta, S.C.; Hadas, A. and Schafer, R.L., 1989. Modeling soil mechanical behavior during compaction. In W.E. Larson; G.R. Blake; R.R. Allmaras; W.B. Voorhees and S.C. Gupta (editors). *Mechanics and related process in*

- structured agricultural soils. NATO Applied Sciences 172. Kluwer Academic Publishers, The Netherlands. pp.137-152.
- Gupta, S.C.; Hadas, A.; Voorhees, W.B.; Wolf, D.; Larson, W.E. and Schneider, E.C., 1985. Development of quids for estimating the ease of compaction of world soils. Bet Dagan, Israel. Research Report, Binational Agric. Res. Development, University of Minnesota, 178 pp.
- Gupta, S.C. and Raper, R.L. Prediction of soil compaction under vehicles. In: Soane, B.D. and van Ouwerkerk, C., eds. Soil compaction in crop production. Amsterdam, Elsevier, 1994. p.71-90.
- Gysi, M., 2001. Compaction of a Eutric Cambisol under heavy wheel traffic in Switzerland: Field data and a critical state soil mechanics model approach. Soil Till. Res. 61, 133-142.
- Hill, R.L. and Meza-Montalvo, M., 1990. Long- term wheel traffic effects on soil physical properties under different tillage systems. Soil Sci. Soc. Am. J., 54, 865-870.
- Hillel, D., 1982. Introduction to Soil Physics. San Diego, Academic Press, 1982. 364pp.
- Holtz, R.D. and Kovacs, W.D., 1981. An introduction to Geotechnical Engineering. Prentice-Hall, Inc., Englewood Cliffs, NJ, 733pp.
- Horn, R.; van den Akker, J. J. H. And Arvidsson. J., 2000. Subsoil compaction. Sistribution, processes and consequences. Advances in Geocology, 32, 462p.
- Jamiolkowski, M., Ladd, C. C., Germaine, J. T. and Lancellota, R., 1985. New development in field and laboratory testing of soils. In: Publications Committee of XI ICSMFE (editor). Proc. of the Eleventh Int. Conf. on Soil Mech. and Found. Eng. San Francisco, Ca 12-16 August 1985. Netherlands, pp. 57-153.
- Ishaq, M; Ibrahim, M.; Hassan, A.; Saeed, M. and Lal, R., 2001. Subsoil compaction effects on crop in Punjab, Pakistan: II. Root growth and nutrient uptake of wheat and sorghum. Soil Till. Res. 60, 153-161.
- Jose, B.T.; Sridharan, A. and Abraham, B.M., 1989. Log-log method for determination of preconsolidation pressure. Geotech. Testing J., 12, 230-237.
- Kondo, M.K. and Dias Junior, M.S., 1997. Compressibilidade de um Latossolo Vermelho amarelo sob diferentes usos. Anais do Congresso Brasileiro de Ciência do Solo, 26, Rio de Janeiro, RJ, pp. 26.
- Kondo, M.K. and Dias Junior, M.S., 1999. Compressibilidade de três latossolos em função da umidade e uso. R. Bras. Ci. Solo, 23:211-218.
- Larson, W.E.; Blake, G.R.; Allmaras, R.R.; Voorhees, W.B. and Gupta, S.C., 1989. Mechanics and related processes in structured agricultural soils. The Netherlands, Kluwer Academic Publishers. 273p. (NATO Applied Science, 172).

- Larson, W.E. and Gupta, S.C., 1980. Estimating critical stress in unsaturated soils from changes in pore water pressure during confined compression. *Soil Sci. Soc. Am. J.* 44, 1127-1132.
- Larson, W.E.; Gupta, S.C. and Useche, R. A., 1980. Compression of agricultural soils from eight soil orders. *Soil Sci. Soc. Am. J.* 44, 450-457.
- Lebert, M.; Burger, N. and Horn, R., 1989. Effects of dynamic and static loading on compaction of structured soils. In: W.E. Larson; G.R. Blake; R.R. Allmaras; W.B. Voorhees and S.C. Gupta (editors). *Mechanics and related process in structured agricultural soils*. NATO Applied Sciences 172. Kluwer Academic Publishers, The Netherlands. pp.73-80.
- Lebert, M. and Horn, R., 1991. A method to predict the mechanical strength of agricultural soils. *Soil Till. Res.*, 19, 275-286.
- Leonards, G.A., 1962. *Foundation Engineering*. New York, McGraw-Hill Book Company, 1136p.
- MacNabb, D.H. and Boersma, L., 1993. Evaluation of the relationship between compressibility and shear strength of Andisols. *Soil Sci. Soc. Am. J.*, 57:923-929.
- Muller, L.; Tille, P. and Kretschmer, H., 1990. Trafficability and workability of alluvial clay soils in response to drainage status. *Soil Till. Res.* 16, 273- 287.
- O'Sullivan, M.F., 1992. Uniaxial compaction effects on soil physical properties in relation to soil type and cultivation. *Soil Till. Res.*, 24:275-286.
- Pedrotti, A. and Dias Junior, M.S., 1996. Compactação do solo: como evitá-la. *Agrop. Catarinense*, 9, 50-52.
- Radford, B. J.; Yule, D. F.; McGarry, D. and Playford, C., 2001. Crop response to applied soil compaction and to compaction repair treatment. *Soil Till. Res.* 61, 155-170.
- Römkens, M.J.M. and Miller, R.D. 1971. Predicting root size and frequency from one-dimensional consolidation data – A mathematical model. *Plant and Soil*, 35:237-248.
- Sällfors, G., 1975. Preconsolidation pressure of soft high plastic clays. Thesis. Department of Geotechnical Engineering, Gothenburg.
- Schmertmann, J.H., 1955. The undisturbed consolidation behavior of clay. *Trans. ASCE*, 120, 1201-1233.
- Servadio, P.; Marsili, A.; Pagliai, M.; Pellegrini, S. and Vignozzi, 2001. Effect on some clay soil qualities following the passage of rubber-tracked and wheeled tractors in central Italy. *Soil Till. Res.* 61, 143-155.
- Silva, A.P. da; Libardi, P.L. and Camargo, O.A. 1986. Influência da compactação nas propriedades físicas de dois latossolos. *R. Bras. Ci. Solo*, 10:91-95.
- Smucker, A.J.M. and Erickson, A.E., 1989. Tillage and compactive modifications of gaseous flow and soil aeration. In: W.E. Larson; G.R. Blake; R.R. Allmaras; W.B. Voorhees and S.C. Gupta (editors). *Mechanics and related process in structured agricultural soils*. NATO Applied Sciences 172. Kluwer Academic Publishers, The Netherlands. pp. 205-221.

- Soane, B.D. and van Ouwerkerk, C., 1994. Soil compaction in crop production. Amsterdam, Elsevier, 660pp.
- Stone, J.A., 1987. Compaction and the surface structure of a poorly drained soil. Transaction of the American Society of Agricultural Engineering. St. Joseph, 30, 1370-1373.
- Tardieu, F. 1988. Analysis of the spatial variability of maize root density: I. Effect of wheels compaction on the spatial arrangement of roots. Plant Soil, 107,259-266.
- Taylor, H.M., 1971. Effects of soil strength on seedling emergence, root growth and crop yield. In: Barnes, K.K.; Carleton, W.M.; Taylor, H.M.; Throckmorton, R.I. and Vanden berg, G.E. eds. Compaction of agricultural soils. St. Joseph. pp. 292-305.(ASAE. Monogr.)

Soil Physics and Agriculture

Durval Dourado Neto¹, Klaus Reichardt² and Gerd Sparovek³

¹*Crop Science Department, ESALQ, University of São Paulo, Piracicaba, Brazil*

²*Department of Exact Sciences, ESALQ, University of São Paulo,
Piracicaba, Brazil*

³*Soil Science Department, ESALQ, University of São Paulo, Piracicaba, Brazil*

*Lecture given at the
College on Soil Physics
Trieste, 3 – 21 March 2003*

LNS0418013

¹ dourado@esalq.usp.br

² klaus@cena.usp.br

³ gerd@esalq.usp.br

INTRODUCTION

The approach that integrates knowledge is very important in Agriculture, including farmers, extensionists, researchers and professors. The specialists, including the soil physicists, must have a global view of the crop production system. Therefore, their expertise can be useful for the society. The Essence of scientific knowledge is its practical application.

The soil physics is a subarea of Agronomy. There are many examples of this specific subject related to Agriculture. This paper will focus, in general, the following cases: (i) erosion, environmental pollution and human health, (ii) plant population and distribution, soil fertility, evapotranspiration and soil water flux density, and (iii) productivity, effective root depth, water deficit and yield.

EROSION, ENVIRONMENTAL POLLUTION AND HUMAN HEALTH

Normally, at dry season, from May to August, the air temperature and rainfall are limitations for economical Agriculture under Brazilian politic (no subsidies to Agriculture). For these reasons, the cover crop is not common to all farmers. Therefore, the soils present high erodibility.

The exploration of almost all Brazilian annual crops (without irrigation) occurs on wet season, where the main criteria is based on the maximum probability of rainfall to be equal or superior to evapotranspiration at flowering period. Therefore, the majority of sowing dates is done between September and December, where there is tropical precipitation with high intensity (high erosivity) when the leaf area has low value.

The combination of high rainfall erosivity and high soil erodibility is responsible for about 10,000 to 15,000 kg.ha⁻¹.year⁻¹ of erosion on maize, for example. This first millimeter of the soil, in Agriculture, represents chemical products (herbicides and fertilizers, mainly) in the rivers and less soil fertility (less organic matter and nutrients).

The human water consumption in Brazil is around 100 to 500 liters per day per person, where the water capture from the river is common. The environmental pollution caused by erosion prejudices water quality and human health. Therefore, the water and diseases treatments in the cities are necessary.

The alternative crop system and agricultural politic to minimize the soil losses problem is a challenge for the soil physicists (under economical, social and environmental view). The no tillage system could be an option, because the cover crop can protect the rainfall drop impact on the soil, responsible for about 95% (energy balance) of the erosion process. Some changes in the sowing dates and agricultural politic (subsidies) must be done to make mulching. It will be benefic for the environment, farmer and the whole society.

PLANT POPULATION AND DISTRIBUTION, EVAPOTRANSPIRATION, SOIL FERTILITY, AND SOIL WATER FLUX DENSITY

The understanding of relationship of plant population and distribution, soil fertility, evapotranspiration and soil water flux density is fundamental to optimize the soil resources. This implies that soil physicists, with agricultural system global vision, could develop techniques to make the crop production system more adequate for each specific environment.

Increasing of plant population demands more water and better plant distribution. Increasing evapotranspiration requires more soil water flux density. The soil fertility depends on the soil volume per plant (plant population and distribution), evapotranspiration (leaf area, species, wind, air temperature and relative humidity, mainly) and soil water flux density.

The maximum water requirement occurs at flowering. The correct plant population is defined as function of the probability of soil water flux density to be equal or superior to maximum evapotranspiration any day in the whole crop cycle.

For high population, the plant distribution becomes more important. The soil physicist must minimize intra specific competition for water and nutrients. The better plant distribution maximizes the soil volume per plant, and the critical content values for all nutrients (soil fertility) are lower. Consequently, the fertilizer requirement decreases.

The corn grain production per plant is constant when there is no intra specific competition for water and nutrients, and the grain production per area has linear increment with the increasing of plant population (phase A – Figure 1).

The corn grain production per plant decreases when there is intra specific competition for water and nutrients, and the grain production per area has potential (less than linear) increment with the increasing of plant population (phase B – Figure 1). The grain production per plant decrement rate is lower than the plant population increment rate, then the grain production per area increases.

The corn grain production per plant decreases when there is intra specific competition for water, nutrients and light, and the grain production per area decreases with the increasing of plant population (phase C – Figure 1). The grain production per plant decrement rate is higher than the plant population increment rate, then the grain production per area decreases.

The point AB (Figure 1) shows when the intra specific competition for water and nutrients starts. The correspondent plant population can be larger in better plant distribution, and the maximum grain production per area also can be larger in higher plant population (point BC – Figure 1), when the intra specific competition for light starts.

The soil resources (physical and chemical attributes) optimization (plant distribution) is a subject of soil physicists (see Plant population below). Soil physicists should start with a dynamic focus and replace the traditional static emphasis. An example is the critical value for potassium (soil fertility) (see Plant distribution still further below).

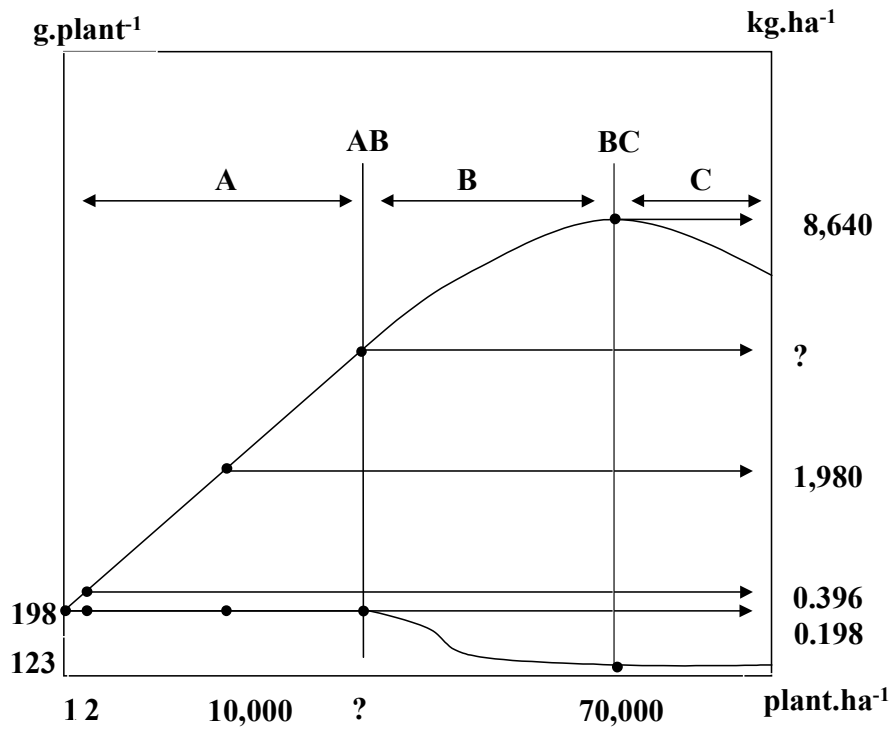


Figure 1. Corn grain production per plant (g.plant^{-1}) and per area (kg.ha^{-1}) as function of plant population (plant.ha^{-1}).

Plant population

To better define maize plant population (P , pl.ha^{-1}), the following assumptions were made in conjunction with the optimization given in Table 1:

- (i) there is a critical population (P_c , plant.ha^{-1}) where the production per plant (Y , g.pl^{-1}) is constant and production per area has linear increasing (R , kg.ha^{-1})

$$Y = Y_m \quad (1 \leq P \leq P_c) \quad (1)$$

$$Y_m = Pr_M \cdot Fe_M \cdot Gf_M \cdot Mg_M \quad (2)$$

where Y_m (g.plant^{-1}) is the maximum production per plant, Pr_M the maximum prolificity (ear.plant^{-1}), Fe_M the number of grain rows per ear (row.ear^{-1}), Gf_M the

maximum number of grains per row (grain.row⁻¹) and Mg_M the maximum grain mass (g.grain⁻¹).

- (ii) the production per plant (Y , g.plant⁻¹) and the production per area (R , kg.ha⁻¹), when plant population is larger than critical population (P_c , plant.ha⁻¹), follows the next equations:

$$Y = \frac{Ym}{\left\{1 + [\alpha(P - P_c)]^m\right\}^n}, (P > P_c) \quad (3)$$

$$R = \frac{Y.P}{1000}, (P > P_c) \quad (4)$$

where α , m and n are the empirical parameters.

Therefore:

$$R = \frac{Ym.P}{1000\left\{1 + [\alpha(P - P_c)]^m\right\}^n}, (P > P_c) \quad (5)$$

Table 1. Maize plant population optimization.

Case	Restriction	Mathematical expression
1	$l \leq P \leq Pc$	$Y = Ym$
2	$P > Pc$	$Y = \frac{Ym}{\left\{1 + [\alpha(P - Pc)]^m\right\}^n} Y$
3	$P > Pc$	$\lim_{P \rightarrow \infty} Y = 0$
4	$l \leq P \leq Pc$	$\frac{dY}{dP} = 0$
5	$P > Pc$	$\frac{dY}{dP} < 0$
6	$l \leq P \leq Pc$	$\frac{d^2 Y}{dP^2} = 0$
7	$Pc < P < Pi$	$\frac{d^2 Y}{dP^2} < 0$
8	$P = Pi$	$\frac{d^2 Y}{dP^2} = 0$
9	$P > Pi$	$\frac{d^2 Y}{dP^2} > 0$
10	$l \leq P \leq Pc$	$R = \frac{Ym.P}{1000}$
11	$P > Pc$	$R = \frac{Ym.P}{1000 \left\{1 + [\alpha(P - Pc)]^m\right\}^n}$
12	$P = Pm$	$R = Rm$
13	$P > Pm$	$\lim_{P \rightarrow \infty} R = 0$
14	$l \leq P \leq Pc$	$\frac{dR}{dP} = \frac{Ym}{1000}$
15	$Pc < P < Pm$	$\frac{dR}{dP} > 0$
16	$P = Pm$	$\frac{dR}{dP} = 0$
17	$P > Pm$	$\frac{dR}{dP} < 0$
18	$l \leq P \leq Pc$	$\frac{d^2 R}{dP^2} = 0$
19	$P > Pc$	$\frac{d^2 R}{dP^2} < 0$

The first derivation of (5):

$$\frac{dR}{dP} = \frac{Ym}{1000} \left\langle \frac{\left\{1 + [\alpha(P - Pc)]^m\right\}^n - Pn \left\{1 + [\alpha(P - Pc)]^m\right\}^{n-1} m [\alpha(P - Pc)]^{m-1} \alpha}{\left\{1 + [\alpha(P - Pc)]^m\right\}^{2n}} \right\rangle \quad (6)$$

If $\frac{dR}{dP} = 0$, then:

$$\left\{1 + [\alpha(Pm - Pc)]^m\right\}^n = m.n.Pm.\alpha^m (Pm - Pc)^{m-1} \left\{1 + [\alpha(Pm - Pc)]^m\right\}^{n-1} \quad (7)$$

$$m.n.Pm.(Pm - Pc)^{m-1} - (Pm - Pc)^m - \frac{1}{\alpha^m} = 0 \quad (8)$$

To obtain the solution, the general iterative Newton-Raphson procedure can be used, creating the following function $f(Pm)$:

$$f(Pm) = m.n.Pm.(Pm - Pc)^{m-1} - (Pm - Pc)^m - \frac{1}{\alpha^m} \quad (9)$$

and:

$$f'(Pm) = m.(Pm - Pc)^{m-1} \left[n + \frac{Pm.(m-1)}{Pm - Pc} - 1 \right] \quad (10)$$

Therefore:

$$Pm_{k+1} = Pm_k - \frac{f(Pm_k)}{f'(Pm_k)} \quad (11)$$

To verify the modeled conditions of maize plant population optimization, the second derivation of (5) is given by the following equation:

$$\frac{d^2 R}{dP^2} = \frac{Ym}{1000} \left\langle \frac{g'(P) \left\{1 + [\alpha(P - Pc)]^m\right\}^{2n} - g(P) 2.m.n.\alpha^m \left\{1 + [\alpha(P - Pc)]^m\right\}^{2n-1} (P - Pc)^{m-1}}{\left\{1 + [\alpha(P - Pc)]^m\right\}^{4n}} \right\rangle \quad (12)$$

where:

$$g(P) = \left\{1 + [\alpha(P - Pc)]^m\right\}^n - m.n.\alpha^m h(P) \quad (13)$$

and

$$g'(P) = m.n.\alpha^m (P - Pc)^{m-1} \left\{1 + [\alpha(P - Pc)]^m\right\}^{n-1} - h'(P) \quad (14)$$

where

$$h(P) = P(P - Pc)^{m-1} \left\{1 + [\alpha(P - Pc)]^m\right\}^{n-1} \quad (15)$$

$$h'(P) = (P - Pc)^{m-1} \left\{1 + [\alpha(P - Pc)]^m\right\}^{n-1} + P.s'(P) \quad (16)$$

$$s(P) = (P - Pc)^{m-1} \left\{1 + [\alpha(P - Pc)]^m\right\}^{n-1} \quad (17)$$

$$s'(P) = (m-1)(P-Pc)^{m-2} \left\{ 1 + [\alpha(P-Pc)]^m \right\}^{n-1} + (P-Pc)^{m-1} (n-1) \left\{ 1 + [\alpha(P-Pc)]^m \right\}^{n-2} m [\alpha(P-Pc)]^m \quad (18)$$

Plant distribution

Assumptions

To define the better maize plant distribution, the following assumptions were made:

- (i) in the nature, there are only three regular polygons that can stay side by side without empty space (see Fig. 2): triangle, square and hexagon (a fourth possibility is the rectangle)

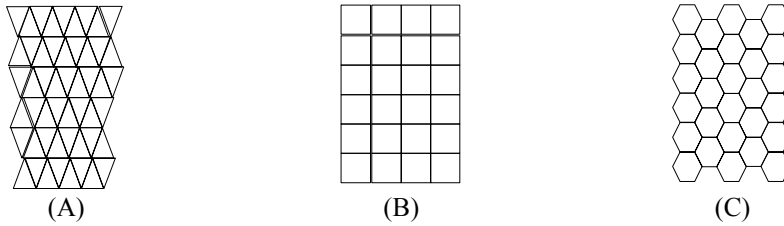


Figure 2. (A) Triangular, (B) square and (C) hexagonal plant distribution.

- (ii) the maize plant explores circular area
 (iii) the better plant distribution, for a fixed plant population, maximizes explored soil area per plant
 (iv) higher soil area per maize plant minimizes stress
 (v) the gross soil area explored by plant (Ap , $m^2 \cdot \text{plant}^{-1}$) is calculated as function of plant population (P , $\text{plant} \cdot \text{ha}^{-1}$):

$$Ap = \frac{10000}{P} \quad (19)$$

Triangular plant distribution

For the triangular distribution (Figure 3), the space between rows (e_1 , m) can be calculated as follows:

$$e_1 = \frac{x}{2} \quad (20)$$

By triangle ABC (Figure 3):

$$x = 2r\sqrt{3} \quad (21)$$

$$e_1 = \frac{100}{\frac{1}{3^4} \frac{1}{P^2}} \quad (27)$$

$$e_2 = \frac{200}{\frac{3}{3^4} \frac{1}{P^2}} \quad (28)$$

Square plant distribution

For the square distribution (Figure 4), the space between rows (e_1 , m) and between plants (e_2 , m) can be calculated as follows:

$$e_1 = 2r \quad (29)$$

$$e_2 = 2r \quad (30)$$

The explored gross area per plant (A_p , m².plant⁻¹) (Figure 4):

$$A_p = x^2 \quad (31)$$

Therefore:

$$x = \frac{100}{\frac{1}{P^2}} \quad (32)$$

and

$$x = 2r \quad (33)$$

The explored useful area per plant (A_u , m².plant⁻¹) is calculated as function of the inscribed circle radius r (Figure 4):

$$A_u = \pi r^2 \quad (34)$$

Substituting (32) and (33) in (34):

$$A_u = \frac{2500\pi}{P} \quad (35)$$

Substituting (32) and (33) in (29) and (30):

$$e_1 = \frac{100}{\frac{1}{P^2}} \quad (36)$$

$$e_2 = \frac{100}{\frac{1}{P^2}} \quad (37)$$

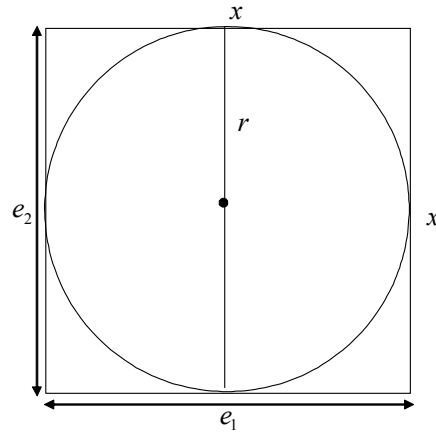


Figure 4. Square plant distribution.

Hexagonal plant distribution

For the hexagonal distribution (Figure 5), the space between rows (e_1 , m) can be calculated as follows:

$$e_1 = \frac{3x}{2} \quad (38)$$

By triangle CDE:

$$\alpha = \frac{\pi}{3} \quad (39)$$

By triangle ABC:

$$\operatorname{tg}\left(\frac{\pi}{3}\right) = \frac{2r}{x} \quad (40)$$

Therefore:

$$x = \frac{2r}{3} \sqrt{3} \quad (41)$$

Substituting (41) in (38):

$$e_1 = r\sqrt{3} \quad (42)$$

The space between plants (e_2 , m) (Figure 5):

$$e_2 = 2r \quad (43)$$

The gross explored area per plant (A_p , $\text{m}^2 \cdot \text{plant}^{-1}$) can be computed as 12 times the triangle ABC area (Figure 5):

$$A_p = 3xr \quad (44)$$

Substituting (41) and (19) in (44):

$$r^2 = \frac{5000}{P\sqrt{3}} \quad (45)$$

or:

$$r = \frac{10.}{3^{\frac{1}{4}}} \left(\frac{50}{P} \right)^{\frac{1}{2}} \quad (46)$$

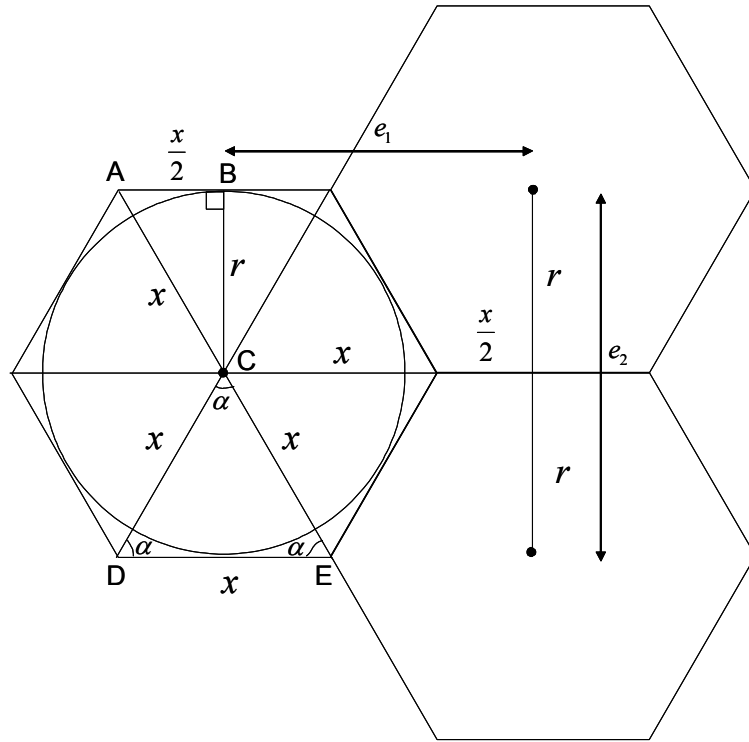


Figure 5. Hexagonal plant distribution.

The useful explored area per plant (A_u , $m^2 \cdot \text{plant}^{-1}$) (Figure 5):

$$A_u = \pi r^2 \quad (47)$$

Substituting (45) in (47):

$$A_u = \frac{5000\pi\sqrt{3}}{3P} \quad (48)$$

Substituting (46) in (42) and (43):

$$e_1 = 10.3^{\frac{1}{4}} \left(\frac{50}{P} \right)^{\frac{1}{2}} \quad (49)$$

$$e_2 = \frac{20.}{3^{\frac{1}{4}}} \left(\frac{50}{P} \right)^{\frac{1}{2}} \quad (50)$$

Other solutions can be obtained positioning circles minimizing empty spaces (Figure 6A). For this particular case (Figure 7), the height (h, m) and the area of triangle ABC (A_t , m^2) can be calculated as follows:

$$h = r\sqrt{3} \quad (51)$$

$$A_t = r^2 \sqrt{3} \quad (52)$$

Therefore, there are $2.P$ triangles ABC per hectare ($10.000m^2$):

$$2.P.r^2 \sqrt{3} = 10000 \quad (53)$$

Then:

$$r = \frac{10.}{3^{\frac{1}{4}}} \left(\frac{50}{P} \right)^{\frac{1}{2}} \quad (54)$$

The equations (46) and (54) are similar.

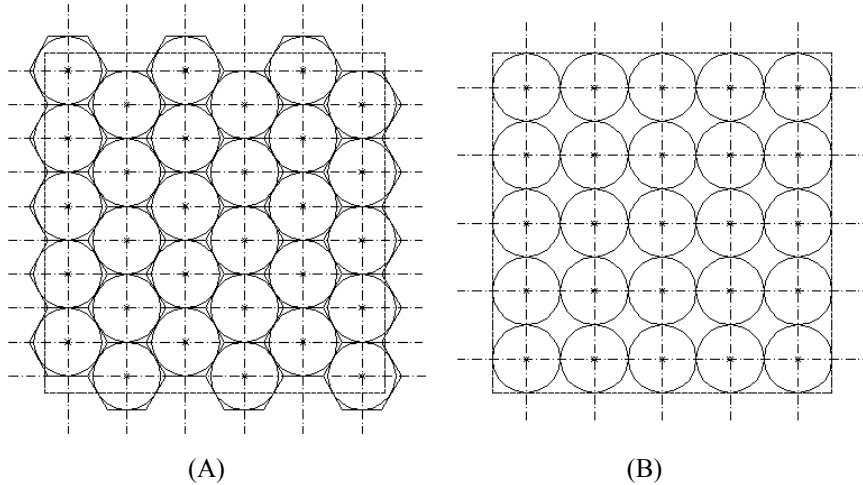


Figure 6. Circles (A) minimizing and (B) maximizing empty spaces.

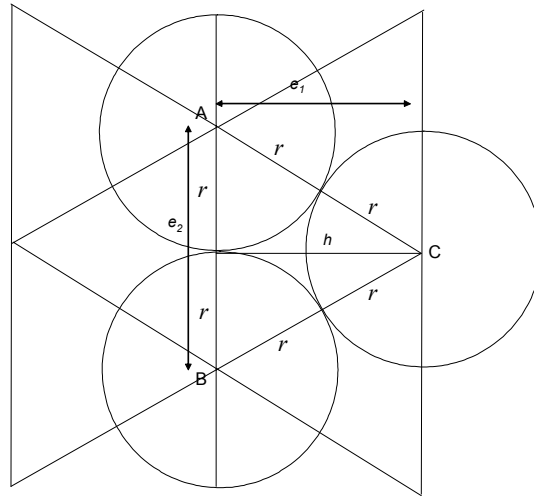


Figure 7. Circles maximizing explored area per plant.

Potassium availability

The potassium availability in the soil could be express in terms of offer rate ($\text{kg K} \cdot \text{ha}^{-1} \cdot \text{day}^{-1}$) to compare with the crop potassium requirement rate ($\text{kg K} \cdot \text{ha}^{-1} \cdot \text{day}^{-1}$) (*dynamic focus* – soil physics contribution) (Figure 8) instead critical values for soil potassium content (*static emphasis*) (Figure 9).

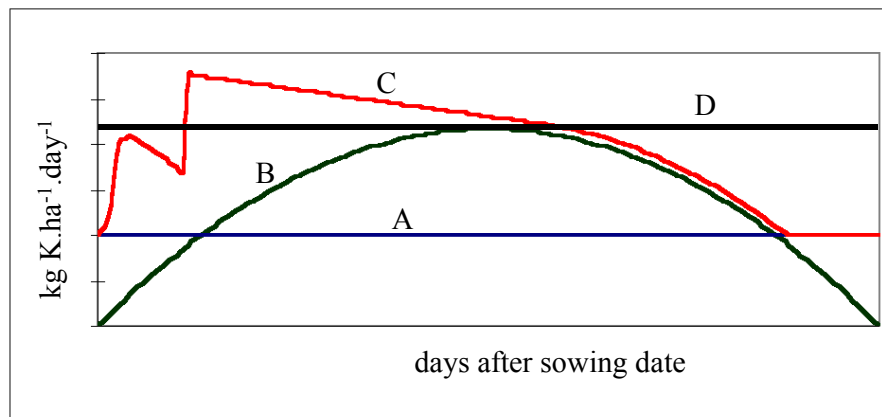


Figure 8. The potassium availability in the soil express in terms of offer rate: (A) deficient soil fertility, (C) deficient soil fertility with two fertilizations, (D) sufficient soil fertility, and (B) the crop potassium requirement rate ($\text{kg K} \cdot \text{ha}^{-1} \cdot \text{day}^{-1}$).

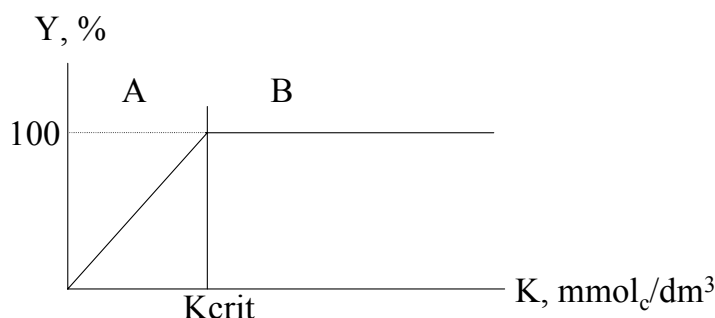


Figure 9. The relative grain yield (Y , %) as function of soil potassium content (K , $\text{mmol}_c.\text{dm}^3$): (A) deficient soil fertility, (B) sufficient soil fertility, and the critical soil potassium content (K_{crit} , $\text{mmol}_c.\text{dm}^3$).

Actually, there is a unique value for the critical soil potassium content (K_{crit} , $\text{mmol}_c.\text{dm}^3$) independently of the soil type, specie and weather conditions. This *static emphasis* was important in the past, but must be replaced per *dynamic focus* by the soil physicists. It will be an important contribution (it optimizes the fertilizer utilization) for Agriculture.

PRODUCTIVITY, EFFECTIVE ROOT DEPTH, WATER DEFICIT AND YIELD

Yield means the grain (or other part of the plant) production per area ($\text{kg}.\text{ha}^{-1}$), and the productivity will be defined as the potential yield. Then, the productivity depends only of the genotype and weather (soil water content in the *field capacity*), and yield depends on the genotype, weather and biotic (weeds, diseases and pests, mainly) and abiotic interference.

For practical purposes, the first step is the definition of target yield and price that defines technology level. Then, the first components for agricultural planning at farm scale are: genotype, weather condition (depends on the sowing date), water availability, plant population and nitrogen fertilization.

The water deficit occurs when the soil water flux density is lower than the maximum evapotranspiration (Figure 10). The decreasing of evapotranspiration causes stress. The plant stress reduces yield and increases cost with weeds, diseases and pests control, and decreases profit.

For practical purposes, the soil water holding capacity per unit of effective root depth defines the plant population support with no irrigation agricultural system. When the soil water content is lower than the critical value (θ_{crit}), the soil water flux density (q) is lower than maximum evapotranspiration (ET_m) and real evapotranspiration (ET_r) decreases (Zone A – Figure 10).

If the soil water content is larger than θ_{crit} , the soil water flux density (q) is larger than maximum evapotranspiration (ET_m) and real evapotranspiration (ET_r) is equal to ET_m (Zone B – Figure 10).

The water deficit reduces effective root depth (Z_e), because there is no sufficient water to make more roots (the consumption of new cells require more water than old cells). The water excess also reduces Z_e , because the oxygen diffusion is limiting (the oxygen diffusion in the air is larger than in the water) (Figure 11). The agricultural management must improve effective root depth to optimize natural resources. Each 1 cm soil depth holds around 12,500 L.ha⁻¹ of water (see the modal soil in the nature Figure 10).

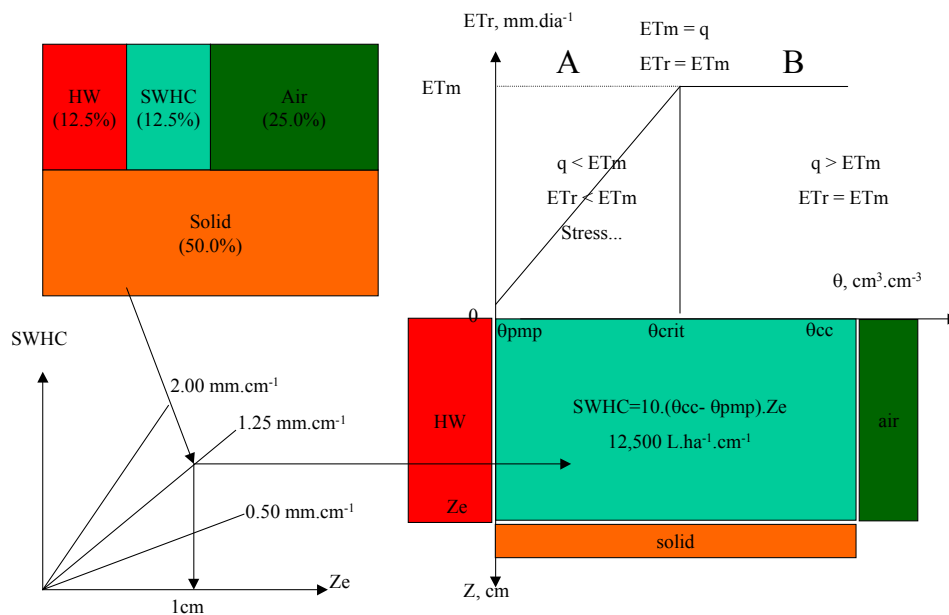


Figure 10. The modal soil physics properties in the nature. HW: hygroscopic water, SWHC: soil water holding capacity, θ : soil water content, ET_r : real evapotranspiration, ET_m : maximum evapotranspiration, Z_e : effective root depth and q : soil water flux density.

For more details related to grain productivity, effective root depth, water deficit and grain yield, refer to the lecture “Agroclimatic Mapping of Maize Crop Based on Soil Physical Properties” starting on page 159.

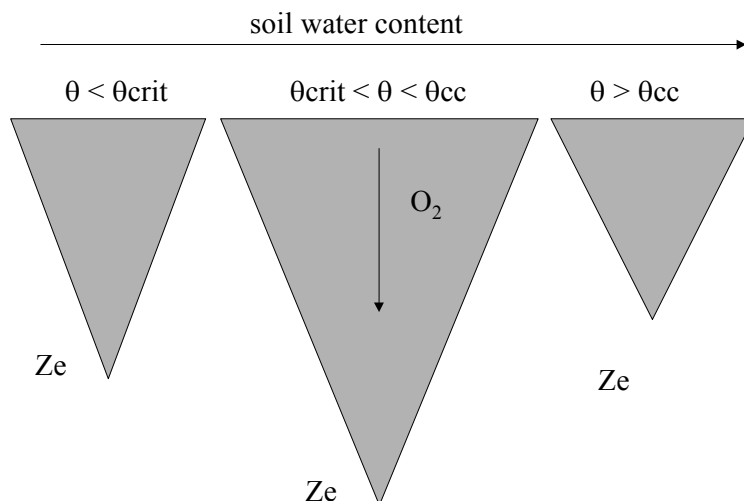


Figure 11. Relationship between oxygen diffusion (O_2), soil water content (θ) and effective root depth (Ze).

REFERENCES

- ASSIS, F.N.; MENDEZ, M.E.G. Relação entre radiação fotossinteticamente ativa e radiação global. *Pesquisa Agropecuária Brasileira*, v.2, n.7, p.797-800, 1989.
- CASTRO, P.T. Evapotranspiração atual e potencial de uma cultura de milho (*Zea mays* L.). Piracicaba, 1979. 61p. Dissertação (Mestrado) – Escola Superior de Agricultura “Luiz de Queiroz”, Universidade de São Paulo.
- COSTA, A.F.S. Influência das condições climáticas no crescimento e desenvolvimento de plantas de milho (*Zea mays* L), avaliada em diferentes épocas de plantio. Viçosa, 1994. 109p. Dissertação (Doutorado) – Universidade Federal de Viçosa.
- DAKER, A. A água na agricultura: manual de hidráulica agrícola. 3.ed. Rio de Janeiro: Freitas Bastos, 1969. v.3 (irrigação e drenagem), 453p.
- DOURADO-NETO, D. Modelos fitotécnicos referentes à cultura do milho. Piracicaba, 1999. 229p.: il. Tese (Livre-Docência) – Escola Superior de Agricultura “Luiz de Queiroz”, Universidade de São Paulo.
- DOURADO-NETO, D.; SAAD, A.M.; JONG van LIER, Q. Curso de agricultura irrigada. Piracicaba: ESALQ, Depto de Agricultura, 1991. 190p.
- FANCELLI, A.L.; DOURADO-NETO, D. Produção de milho. Guaíba: Agropecuária, 2000. 360p.
- FANCELLI, A.L.; LIMA, U.A. Milho: Produção, pré-processamento e transformação agroindustrial. São Paulo: FEALQ, 1982. 112p.

- GADIOLI, J.L. Estimativa de rendimento de grãos e caracterização fitotécnica da cultura de milho (*Zea mays* L). Piracicaba, 1999. 86p.: il. Dissertação (Mestrado.) – Escola Superior de Agricultura “Luiz de Queiroz”, Universidade de São Paulo.
- LOZARDA, B.I.; ANGELOCI, L.R. Efeito da temperatura do ar e da disponibilidade hídrica do solo na duração de subperíodos e na produtividade de um híbrido de milho (*Zea mays*, L.). Revista Brasileira de Agrometeorologia, v.7, n.1, p.37-43, 1999.
- MONDRAGÓN, V.E.C. Estimativa da produtividade da cultura do milho em minas gerais, baseada em variáveis climáticas e em tendência tecnológica. Viçosa, 1990. 68p. Dissertação (Mestrado) – Universidade Federal de Viçosa.
- OMETTO, J.C. Bioclimatologia vegetal. São Paulo: Ceres, 1981. 440p.
- REICHARDT, K. A água em sistemas agrícolas. São Paulo: Manole, 1987. 188p.
- REICHARDT, K. Processos de transferência no sistema solo-planta-atmosfera. 4.ed. Campinas: Fundação Cargill, 1985. 466p.
- SALISBURY, F.B. Plant Physiology. Belmont: Wadsworth, 1992. 682p.
- SAUNDERS, L.C.U.; CASTRO, P.T.; MATIAS FILHO, J.; BEZERRA, F.M.L. Uso consutivo da cultura do milho sob condições naturais de precipitação na microrregião homogênea de Quixeramobim. In: CONGRESSO BRASILEIRO DE ENGENHARIA AGRÍCOLA, 14., Fortaleza, 1984. Anais. Fortaleza: UFC/SBEA, 1984. p.142-151.
- SPITTERS, C.J.T.; TOUSSAINT, H.A.J.; GOUDRIAAN, J. Separating the diffuse and direct component of global radiation and its implications for modelling canopy photosynthesis. I: Components of incoming solar radiation. Agricultural and Forest Meteorology, n.38, p.217-229, 1986a.
- SPITTERS, C.J.T.; TOUSSAINT, H.A.J.; GOUDRIAAN, J. Separating the diffuse and direct component of global radiation and its implications for modelling canopy photosynthesis. II: Calculation of canopy photosynthesis. Agricultural and Forest Meteorology, n.38, p.231-242, 1986b.
- THORNLEY, J.H.M. Mathematical models in plant physiology: a quantitative approach to problems in plant crop physiology. London: Academic Press, 1976. 318p.
- VANCLOOSTER, M.; VIAENE, J.; DIELS, J.; CHRISTIAENS, K. Wave: a mathematical model for simulating water and agrochemicals in the soil and vadose environment. Leuven: Katholieke Universiteit Leuven Press, 1994. 1v.
- VILLA NOVA, N.A.; PEDRO Jr, M.; PEREIRA, A.R.; OMETTO, J.C. Estimativa de graus-dia acumulados acima de qualquer temperatura base, em função das temperaturas máxima e mínima. Cadernos de Ciências da Terra, São Paulo: Instituto de Geografia/USP, n.30, 1972. 8p.
- VILLA NOVA, N.A.; SANTIAGO, A.V.; RESENDE, F.C. Energia solar: aspectos físicos e de captura pela biomassa. Piracicaba: ESALQ/USP, 2001. 20p.
- VILLANUEVA, J.G. Estudo do coeficiente de transferência do vapor d’água sobre a cultura do feijão. Piracicaba, 1987. 58p. Dissertação (Mestrado) – Escola Superior de Agricultura “Luiz de Queiroz”, Universidade de São Paulo.

Agroclimatic Mapping of Maize Crop Based on Soil Physical Properties

Durval Dourado Neto¹, Gerd Sparovek², Klaus Reichardt³
Luiz Carlos Timm⁴ and Donald R. Nielsen⁵

¹*Crop Science Department, ESALQ, University of São Paulo, Piracicaba, Brazil*

²*Soil Science Department, ESALQ, University of São Paulo, Piracicaba, Brazil*

³*Department of Exact Sciences, ESALQ, University of São Paulo,
Piracicaba, Brazil*

⁴*CENA, University of São Paulo, Piracicaba, Brazil*

⁵*Department of Land, Air and Water Resources, University of California, Davis, USA*

*Lecture given at the
College on Soil Physics
Trieste, 3 – 21 March 2003*

LNS0418014

¹ dourado@esalq.usp.br

² gerd@esalq.usp.br

³ klaus@cena.usp.br

⁴ lctimm@cena.usp.br

⁵ drnielsen@ucdavis.edu

INTRODUCTION

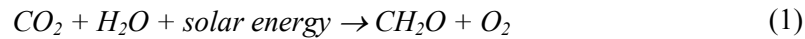
With the purpose of estimating water deficit to forecast yield knowing productivity (potential yield), the water balance is useful tool to recommend maize exploration and to define the sowing date. The computation can be done for each region with the objective of mapping maize grain yield based on agroclimatic data and soil physical properties.

AGRICULTURE: THE PROPOSED MODEL TO ESTIMATE YIELD

Based on agroclimatic data, air temperature and solar radiation, a model was built to estimate the corn grain productivity (the energy conversion results in dry mass production). The proposed model is presented in the Figure 2.

Conversion of CO₂ in CH₂O

The carbon dioxide (CO₂) fixation by plants is related to gross carbohydrate (CH₂O) production and solar radiation, according with the following equation:



The CO₂ assimilation by C₄ plants depends on the photosynthetic active radiation (PAR) and temperature (T) Figure 1. According to the experimental data (Heemst, 1986):

$$A_{dc} = \frac{a + b.q + c.q^2 + d.q^3 + e.\ln(T)}{1 + f.q + g.q^2 + h.\ln(T) + i.[\ln(T)]^2} \quad (2)$$

where A_{dc} is the carbon dioxide assimilation ($\mu\text{L}.\text{cm}^{-2}.\text{h}^{-1}$), q the photosynthetic active radiation (PAR, $\text{cal}.\text{cm}^{-2}.\text{min}^{-1}$), T the air temperature ($^{\circ}\text{C}$), and a, b, c, d, e, f, g, h and i are the empirical parameters obtained by multiple regression analysis ($a = 1.732748682$; $b = 61.81088751$; $c = -254.72111$; $d = 333.7473141$; $e = -0.54180211$; $f = -0.19106242$; $g = 0.29248608$; $h = -0.5521966$; $i = 0.080139046$).

Knowing the specific mass of CO₂ ($44\text{g}.\text{mol}^{-1}$) and CH₂O ($30\text{g}.\text{mol}^{-1}$), the carbon dioxide assimilation (A_{dc} , $\mu\text{L}.\text{cm}^{-2}.\text{h}^{-1}$) is converted to carbohydrate mass produced (MP_{CH_2O} , $\text{g}.\text{h}^{-1}.\text{cm}^{-2}$ of leaf) as function of leaf area index (IAF), climatic data, air temperature (T , $^{\circ}\text{C}$) and PAR (q , $\text{cal}.\text{cm}^{-2}.\text{min}^{-1}$).

For the whole crop cycle (C , days), knowing the degrees-day to flowering (GD_f , $^{\circ}\text{C}.\text{day}$), the reproductive phase duration (D_{FR} , days), theoretical photoperiod (H , $\text{h}.\text{day}^{-1}$) and mean leaf area index (IAF_m), the total carbohydrate production (M_{CH_2O} , $\text{kg}.\text{ha}^{-1}.\text{cycle}^{-1}$) can be estimated using the following equation:

$$M_{CH_2O} = \frac{36,585.P.A_{dc}.IAF_m.C.H}{T + 273} \quad (3)$$

where P is the local atmospheric pressure (atm). Solar radiation and theoretical photoperiod values are given in Tables 1 and 3, respectively.

Grain productivity, maintenance and growth respiration and solar radiation

To convert the final gross carbohydrate mass (M_{CH_2O}) in dry mass of different corn organs (grain, stem, root and seeds), to estimate grain yield (P_{gr} , $kg \cdot ha^{-1}$), is necessary some corrections. The first correction refers to carbohydrate mass consumption by respiration process (FAO, 1979):

$$CR_{MC} = 0.6 \quad (T < 20^\circ C) \quad (4) \quad CR_{MC} = 0.5 \quad (T \geq 20^\circ C) \quad (5)$$

where CR_{MC} is the maintenance and growth respiration coefficient and T the air temperature ($^\circ C$). The second correction refers to intercepted solar radiation as function of maximum leaf area index (IAF_{max}):

$$CR_s = \frac{1 - e^{-0.75 IAF_{max}}}{2} \quad (6)$$

where CR_s is the solar radiation extinction coefficient.

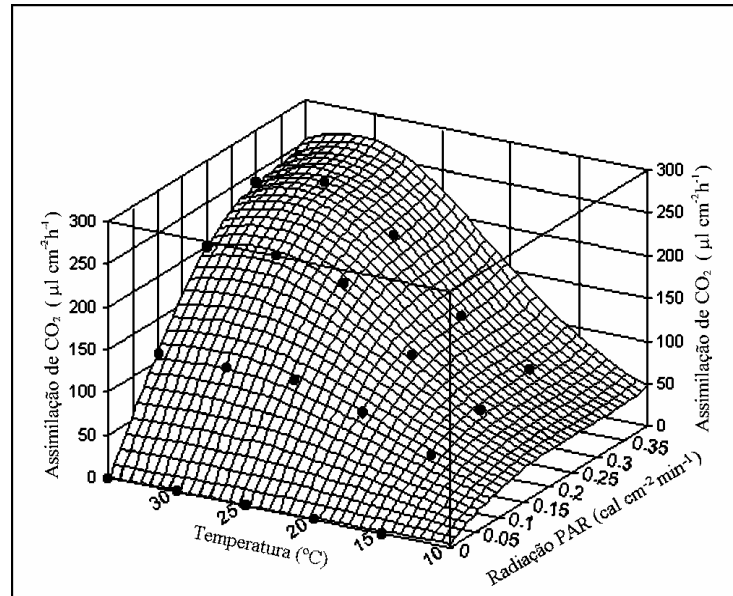


Figure 1. CO_2 assimilation by C_4 plants as function of PAR and air temperature (Heemst, 1986).

The dry mass of maize grain is a fraction of the total dry mass harvested. According to experimental data (Dourado-Neto, 1999) for maize (grain), the harvest index is around 40% ($IC = 0.4$). Then, the final grain productivity (P_{gr}) can be estimated as follows:

$$P_{gr} = M_{CH_2O} \cdot CR_{mc} \cdot CR_s \cdot IC \quad (7)$$

Table 1. Solar radiation at horizontal surface in the atmosphere (15th day of each month).

Lat	Jan	Feb	Mar	Apr	May	Jun	Jul	Aug	Sep	Oct	Nov	Dec
S	Solar radiation ($MJ\ m^{-2}\ dia^{-1}$)											
0°	35.59	36.80	37.05	35.84	33.83	32.87	33.37	34.83	36.30	36.55	35.84	34.83
2°	36.05	37.05	37.05	35.59	33.12	32.11	32.62	34.33	36.30	36.80	36.55	35.59
4°	36.80	37.56	37.05	35.09	32.62	31.36	31.61	33.83	36.05	37.05	37.05	36.55
6°	37.56	37.81	37.05	34.58	31.61	30.65	31.11	33.37	36.05	37.56	37.56	37.26
8°	38.06	38.06	36.80	34.08	30.90	29.64	30.15	32.62	35.84	37.56	38.06	37.81
10°	38.06	38.52	36.55	33.58	30.15	28.64	29.39	32.11	35.59	37.56	38.31	38.52
12°	39.27	38.52	36.30	33.12	29.18	27.68	28.64	31.61	35.09	37.56	38.77	39.02
14°	39.77	38.77	36.05	32.36	28.43	26.67	27.68	30.90	35.09	37.81	39.27	39.52
16°	40.03	39.02	35.84	31.61	27.68	25.71	26.67	30.15	34.58	37.81	39.52	40.03
18°	40.53	39.02	35.59	31.11	26.67	24.70	25.96	29.39	34.08	37.81	40.03	40.78
20°	40.99	39.02	35.09	30.15	25.71	23.70	24.95	28.64	33.58	37.56	40.28	41.24
22°	41.49	39.02	34.58	29.39	24.70	22.73	23.95	27.68	33.12	37.56	40.53	41.49
24°	41.49	39.02	34.08	28.64	23.70	21.73	22.99	26.92	32.62	37.56	40.53	41.99
26°	41.74	38.77	33.58	27.68	22.73	20.77	21.73	26.17	31.86	37.30	40.78	42.50
28°	41.99	38.52	33.12	26.92	21.73	19.26	20.77	22.21	31.11	37.05	40.99	42.75
30°	41.99	38.52	32.62	25.96	20.77	18.30	19.76	24.20	30.65	36.55	40.99	43.00
32°	42.25	38.06	32.20	24.95	19.76	17.04	18.76	23.24	29.90	36.30	40.99	43.25
34°	42.25	37.81	31.11	24.20	18.76	15.83	17.52	22.23	29.14	36.05	40.99	43.46
36°	42.25	37.56	30.65	23.24	17.54	14.82	16.29	21.23	28.18	35.59	40.99	43.46
38°	42.25	37.05	29.89	22.23	16.29	13.82	15.32	20.26	27.17	35.09	40.78	43.71
40°	41.99	36.80	28.89	21.23	15.07	12.35	14.07	19.26	26.42	34.58	40.53	43.71

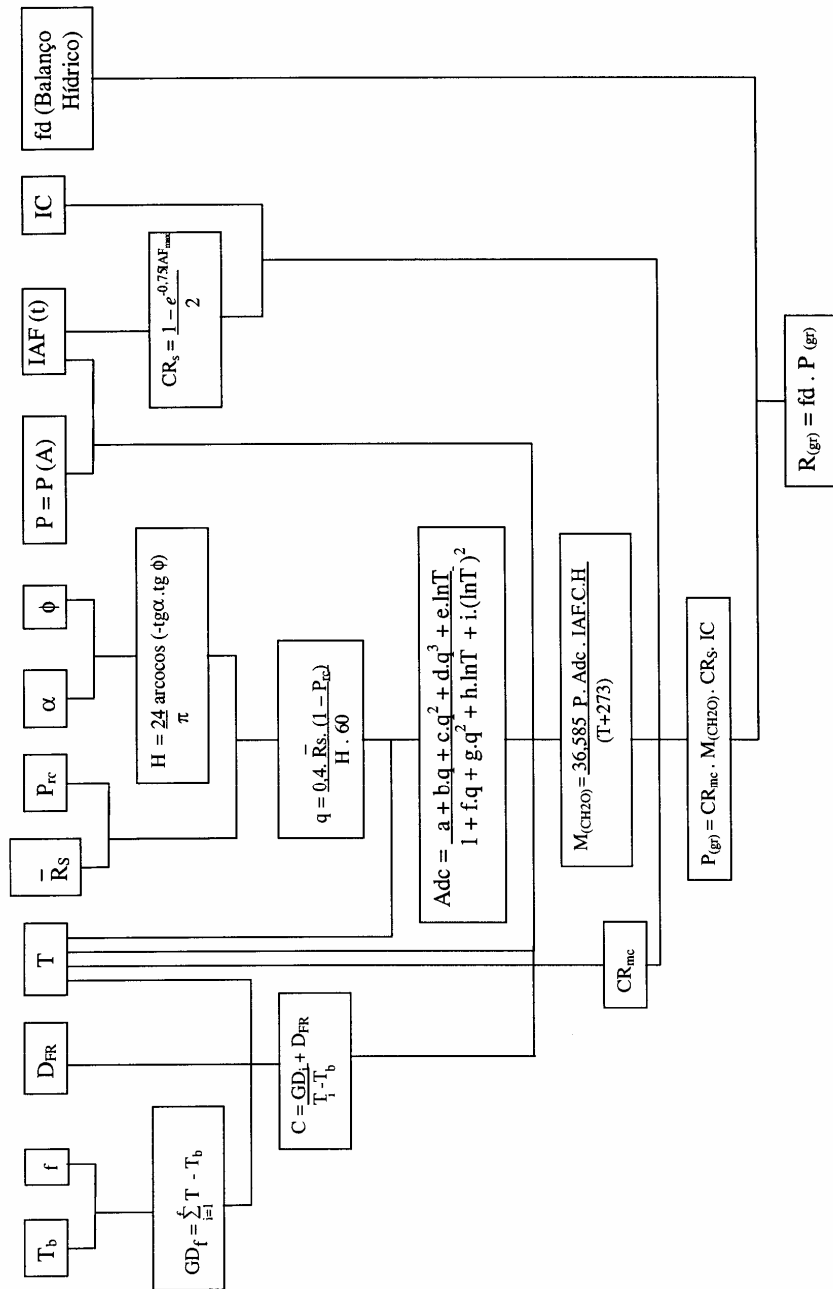


Figure 2. Schematic representation of the model

AGROMETEOROLOGY AND SOIL PHYSICS

Water balance

The water balance can be done with the following variables (Thornthwaite & Mather, 1955; Dourado-Neto, 1999): crop coefficient (K_c) and root effective depth (Z_e) for any weather data distribution.

Potential and maximum evapotranspiration

The potential evapotranspiration (ET_0 , mm.period⁻¹) by the Thornthwaite method (Dourado-Neto, 1999) can be estimated as follows:

$$ET_0 = 0.53 N_i \left(\frac{H_i}{12} \right) \left(10 \frac{T_i}{I} \right)^a \quad (8)$$

$$a = a_0 + a_1 I + a_2 I^2 + a_3 I^3 \quad (9)$$

where T_i is the air temperature (°C), I the termic index, a the empirical coefficient, N_i the number of days per period and H_i the theoretical photoperiod in the median day of the period i , and a the empirical coefficient ($a_0 = 0.49239$, $a_1 = 0.01792$, $a_2 = -0.0000771$ and $a_3 = 0.000000675$).

The thermic index (I) and the theoretical photoperiod (H) can be calculated as follows:

$$I = 0.08745 \sum_{j=1}^{12} T_j^{1.514} \quad (10)$$

$$H = \frac{24}{\pi} \cos^{-1} [-\operatorname{tg}(\alpha) \operatorname{tg}(\phi)] \quad (11)$$

$$\alpha = C_0 + \sum_{i=1}^3 [C_i \sin(2i\pi d / 365) - D_i \cos(2i\pi d / 365)] \quad (12)$$

where T_j is the air temperature (°C) of the month j , α the solar declination (rad) in the median day of the period, d the Julian day ($1 \leq d \leq 365$), C_0 , C_i and D_i are the empirical parameters ($C_0 = 0.006918$, $C_1 = 0.070257$, $C_2 = 0.000907$, $C_3 = 0.00148$, $D_1 = 0.399912$, $D_2 = 0.006758$ and $D_3 = 0.002697$) and ϕ the latitude (rad).

The maximum evapotranspiration (ET_{m_i}) corresponds the maximum crop yield:

$$ET_{m_i} = ET_{0_i} \cdot K_{c_i} \quad (13)$$

where K_{c_i} is the crop coefficient (Table 2 and Figure 3).

Table 2. Maize crop coefficient (Kc) for Brazilian weather condition.

Phenological stage ¹	up to	Kc ²
I	10% of vegetative phase	0.20 to 0.40
II	80% of vegetative phase	Figure 3
III	Flowering	0.95 to 1.20
IV	physiological maturity point	Figure 3
V	harvest	0.3 to 0.5

¹ Food and Agricultural Organization (1979)

² Low values of Kc for relative humidity larger than 70% and wind speed lower than 5 m.s⁻¹

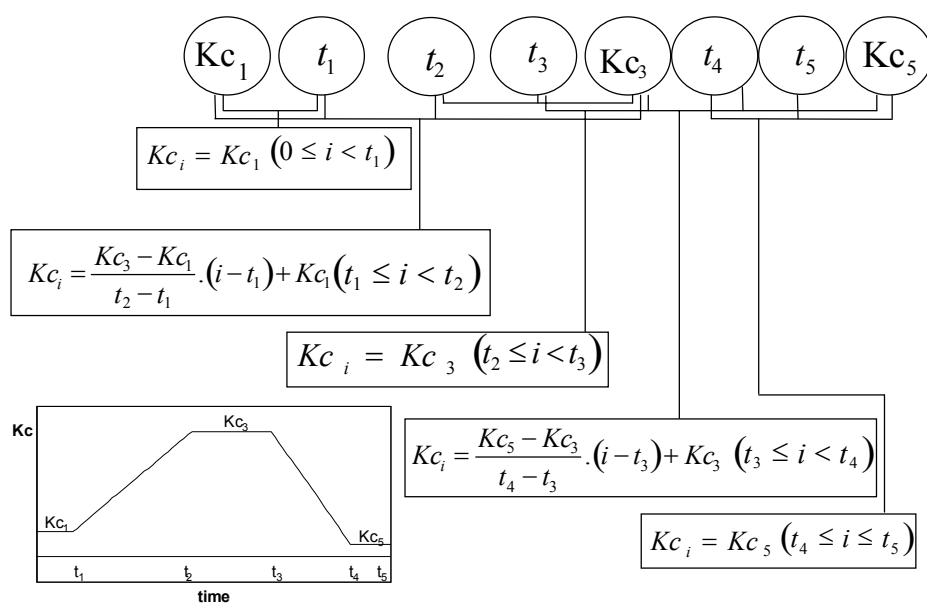


Figure 3. Temporal variation (t_1 , t_2 , t_3 , t_4 , and t_5 : phenological stages duration) of crop coefficient (K_{c1} , K_{c3} and K_{c5}) (FAO, 1979).

Table 3. Theoretical photoperiod (H, hour.day⁻¹) for different latitudes corresponding to 15th day of each month.

Lat	Jan	Feb	Mar	Apr	May	Jun	Jul	Aug	Sep	Oct	Nov	Dec
S	Theoretical photoperiod											
0	12.1	12.1	12.1	12.1	12.1	12.1	12.1	12.1	12.1	12.1	12.1	12.1
2	12.2	12.2	12.1	12.1	12.0	12.0	12.0	12.0	12.1	12.1	12.2	12.2
4	12.3	12.2	12.1	12.0	11.9	11.8	11.9	12.0	12.1	12.2	12.3	12.4
6	12.4	12.3	12.1	12.0	11.9	11.7	11.8	11.9	12.1	12.2	12.4	12.5
8	12.5	12.4	12.1	11.9	11.7	11.6	11.7	11.9	12.1	12.3	12.5	12.6
10	12.6	12.4	12.1	11.9	11.7	11.5	11.6	11.8	12.0	12.3	12.6	12.7
12	12.7	12.5	12.2	11.8	11.6	11.4	11.5	11.7	12.0	12.4	12.7	12.8
14	12.8	12.6	12.2	11.8	11.5	11.3	11.4	11.6	12.0	12.4	12.8	12.9
16	13.0	12.7	12.2	11.7	11.4	11.2	11.2	11.6	12.0	12.4	12.9	13.1
18	13.1	12.7	12.2	11.7	11.3	11.1	11.1	11.5	12.0	12.5	13.0	13.2
20	13.2	12.8	12.2	11.6	11.2	10.9	11.0	11.4	12.0	12.5	13.2	13.3
22	13.4	12.8	12.2	11.6	11.1	10.8	10.9	11.3	12.0	12.6	13.2	13.5
24	13.5	12.9	12.3	11.5	10.9	10.7	10.8	11.2	11.9	12.6	13.3	13.6
26	13.6	12.9	12.3	11.5	10.8	10.5	10.7	11.2	11.9	12.7	13.4	13.8
28	13.7	13.0	12.3	11.4	10.7	10.4	10.6	11.1	11.9	12.8	13.5	13.9
30	13.9	13.1	12.3	11.4	10.6	10.2	10.4	11.0	11.9	12.8	13.6	14.1
32	14.0	13.2	12.3	11.3	10.5	10.0	10.3	10.9	11.9	12.9	13.7	14.2
34	14.2	13.3	12.3	11.3	10.3	9.8	10.1	10.9	11.9	12.9	13.9	14.4
36	14.3	13.4	12.4	11.2	10.2	9.7	10.1	10.7	11.9	13.0	14.0	14.6
38	14.5	13.5	12.4	11.1	10.1	9.5	9.8	10.6	11.8	13.1	14.2	14.8
40	14.7	13.6	12.4	11.1	9.9	9.3	9.6	10.5	11.8	13.1	14.3	15.0

Water deficit and grain yield

To estimate water deficit, the rainfall (C_i , mm) and the maximum crop evapotranspiration (ET_{m_i} , mm) must be computed:

$$S_i = C_i - ET_{m_i} \quad (14)$$

$$\text{If } S_i < 0: L_i = L_{i-1} + |S_i| \quad (15) \quad Arm_i = CAD_i \cdot e^{\left(\frac{L_i}{CAD_i}\right)} \quad (16)$$

$$\text{If } S_i \geq 0: L_i = -CAD \cdot \ln\left(\frac{Arm_i}{CAD_i}\right) \quad (17) \quad Arm_i = Arm_{i-1} + S_i \quad (18)$$

where S_i and L_i are auxiliary variables (mm), CAD_i the soil water holding capacity (mm), and Arm_i the soil water holding available (mm) in the period i .

Thornthwaite & Mather (1955) suggested the following criterion to begin the water balance: $L = 0$ and $Arm = CAD$ in the last period of wet season.

The soil water holding capacity (CAD , mm), the soil water holding available (Arm , mm), the real evapotranspiration (ETr , mm) and water deficit (WD , mm) are calculated as follows:

$$CAD_i = 10.(\theta_{cc} - \theta_{pmp}).Ze_i \quad (19)$$

$$Arm_i = 10.(\theta_i - \theta_{pmp}).Ze_i \quad (20)$$

$$ETr_i = ETm_i \quad (C_i \geq ETm_i) \quad (21) \quad ETr_i = C_i + \sqrt{Va_i} \quad (C_i < ETm_i) \quad (22)$$

$$Va_i = Arm_i - Arm_{i-1} \quad (23)$$

$$WD_i = 0 \quad (C_i \geq ETm_i) \quad (24) \quad WD_i = ETm_i - ETr_i \quad (C_i < ETm_i) \quad (25)$$

where Ze_i is the effective root depth (cm) in the period i , θ_{cc} and θ_{pmp} are soil water content corresponding to *field capacity* and *wilting point* ($\text{cm}^3.\text{cm}^{-3}$), θ_i the actual soil water content, C_i the rainfall, and Va_i the soil water holding variation in the period i .

The corn grain yield (R_{gr}) is calculated as function of grain productivity (P_{gr}) and depletion factor (fd):

$$fd = \frac{\prod_{i=1}^n (ETr_i)^{Kc_i}}{\prod_{i=1}^n (ETm_i)^{Kc_i}} \quad (26)$$

$$R_{gr} = fd.P_{gr} \quad (27)$$

AGROCLIMATIC MAPPING OF MAIZE CROP BASED ON SOIL PHYSICAL PROPERTIES

From agroclimatic data and soil physical properties, a map with region identification can be built for solar radiation (Figure 4), air temperature, rainfall, maize grain productivity and yield, potential and real evapotranspiration and water deficit.

The map allows to identify the agroclimatic and the soil physical restrictions. This procedure can be used in different spatial (farm to State) and temporal (daily to monthly data) scales.

The statistical analysis allows to compare estimated and observed values in different situations to validate the model and to verify which scale is more appropriate.

A software was developed (Visual BASIC for Microsoft Windows environment) to forecast corn productivity.

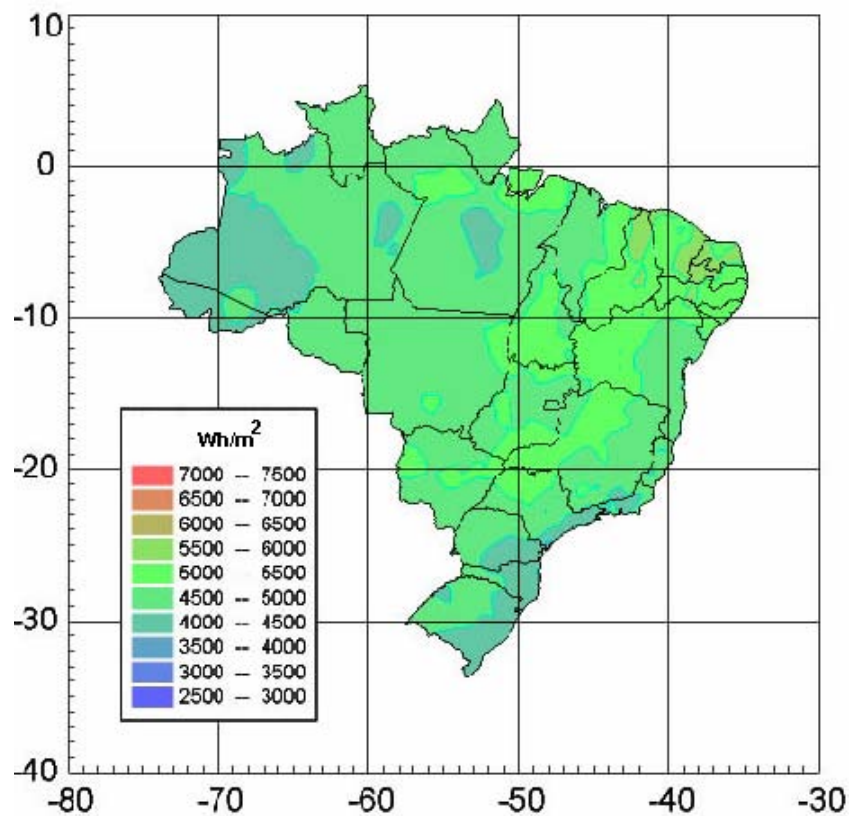


Figure 4. Annual solar radiation in Brazil.

REFERENCES

- DOORENBOS, J.; KASSAM, A.H. Efeito da água no rendimento das culturas. Campina Grande: UFPB, 1994. 306p.
- DOURADO-NETO, D. Modelos fitotécnicos referentes à cultura do milho. Piracicaba, 1999. 229p.: il. Tese (Livre-Docência) – Escola Superior de Agricultura “Luiz de Queiroz”, Universidade de São Paulo.
- FAO. Irrigation and drainage paper, Roma, n.33, 1979. 193p.
- GOUDIAAN, J.; LAAR, H.H. van. Modelling potential crop growth processes: the textbook with exercises. Dordrecht: Kluwer, 1994. 239p.
- HEEMST, H.D.J. van. Physiological principles. In: KEULEN, H. van.; WOLF, J. Modeling of agricultural production: Weather, soils and crops. Wageningen: Pudoc, 1986. p.13-26.

- HOOGENBOOM, G. Contribution of Agrometeorology to the simulation of crop production and its applications. *Agricultural and Forest Meteorology*, n.103, p.137-157, 2000.
- KEULEN, H. van.; PENNING DE VRIES, F.W.T.; DRESS, E.M. A summary model for crop growth. In: PENNING DE VRIES, F.W.T.; VAN LAAR, H. H. (Ed). *Simulation of plant growth and crop production*. Wageningen: Pudoc, 1982. p.87-97.
- KEULEN, H. van.; WOLF, J. Modeling of agricultural production: Weather, soils and crops. Wageningen: Pudoc, 1986. 463p.
- LIMA, M.G. Calibração e validação do modelo cerez-maize em condições tropicais do Brasil. Piracicaba, 1995. 119p. Tese (Doutorado) – Escola Superior de Agricultura “Luiz de Queiroz”, Universidade de São Paulo.
- MUCHOV, R.C.; HAMMER, G.L.; CARBERRY, P.S. Optimizing crop and cultivar selection in response to climatic risk. In: MUCHOV, R.C.; BELLAMY, J.A. (Ed.) *Climatic risk in crop production models and management for the semiarid Tropics and Subtropics*. Wallingford: CAB International, 1991. p.235-262.
- PANDOLFO, C. Parâmetros básicos para uso na modelagem do rendimento de matéria seca em alfafa (*Medicago sativa* L.). Porto Alegre, 1995. 128p. Dissertação (Mestrado) – Faculdade de Agronomia, Universidade do Rio Grande do Sul.
- RAMALHO FILHO, A.; BEEK, K.J. Sistema de avaliação da aptidão agrícola das terras. Rio de Janeiro: EMBRAPA-CNPS, 1995. 65p.
- REYNOLDS, J.F. Some misconceptions of mathematical modeling. *What's New Plant Physiology*, v.10, n.11, p.41-44, 1979.
- ROSENBERG, N.J.; BLAD, B.L.; VERMA, S.B. *Microclimate: The biological environment*. New York: John Wiley and Sons, 1983. 495p.
- SALISBURY, F.B. *Plant Physiology*. Belmont: Wadsworth, 1992. 682p.
- SPITTERS, C.J.T.; TOUSSAINT, H.A.J.; GOUDRIAAN, J. Separating the diffuse and direct component of global radiation and its implications for modelling canopy photosynthesis. I: Components of incoming solar radiation. *Agricultural and Forest Meteorology*, n.38, p.217-229, 1986a.
- SPITTERS, C.J.T.; TOUSSAINT, H.A.J.; GOUDRIAAN, J. Separating the diffuse and direct component of global radiation and its implications for modelling canopy photosynthesis. II: Calculation of canopy photosynthesis. *Agricultural and Forest Meteorology*, n.38, p.231-242, 1986b.
- THORNLEY, J.H.M. *Mathematical models in plant physiology: a quantitative approach to problems in plant crop physiology*. London: Academic Press, 1976. 318p.
- THORNTHWAITE, C.W.; MATHER, J.R. The water balance. *Drexel Institute of Technology*, v.8, n.1, p.1-14, 1955.
- VANCLOOSTER, M.; VIAENE, J.; DIELS, J.; CHRISTIAENS, K. Wave: a mathematical model for simulating water and agrochemical in the soil and vadose environment. Leuven: Katholieke Universiteit Leuven Press, 1994. 1v.

WIT, C.T. Simulation of living systems. In: PENNING DE VRIES, F.W.T.; LAAR, H.H. van (Ed.) Simulation of plant growth and crops production. Wageningen: Pudoc, 1982. p.3-8.

The Combined Effect of Wind and Rain on Interrill Erosion Processes

G. Erpul¹, D. Gabriels² and L.D. Norton³

¹*Faculty of Agriculture, Department of Soil Science, Ankara University,
Diskapi, Ankara, Turkey*

²*Department of Soil Management and Soil Care, Ghent University,
Ghent, Belgium*

³*USDA – ARS National Soil Erosion Research Laboratory,
Purdue University, West Lafayette, USA*

*Lecture given at the
College on Soil Physics
Trieste, 3 – 21 March 2003*

LNS0418015

¹ erpul@agri.ankara.edu.tr

Introduction

Wind-driven rain is described as raindrops falling through a wind field at an angle from vertical under the effects of both gravitational and drag forces. Wind-driven raindrops gain some degree of horizontal velocity and strike the soil surface with an angle deviated from vertical. Additionally, the distribution and intensity of rainfall on sloping surfaces differs depending on wind direction and velocity. Schematic representation of wind-driven rain incidental on a sloping soil surface is given in Figure 1.

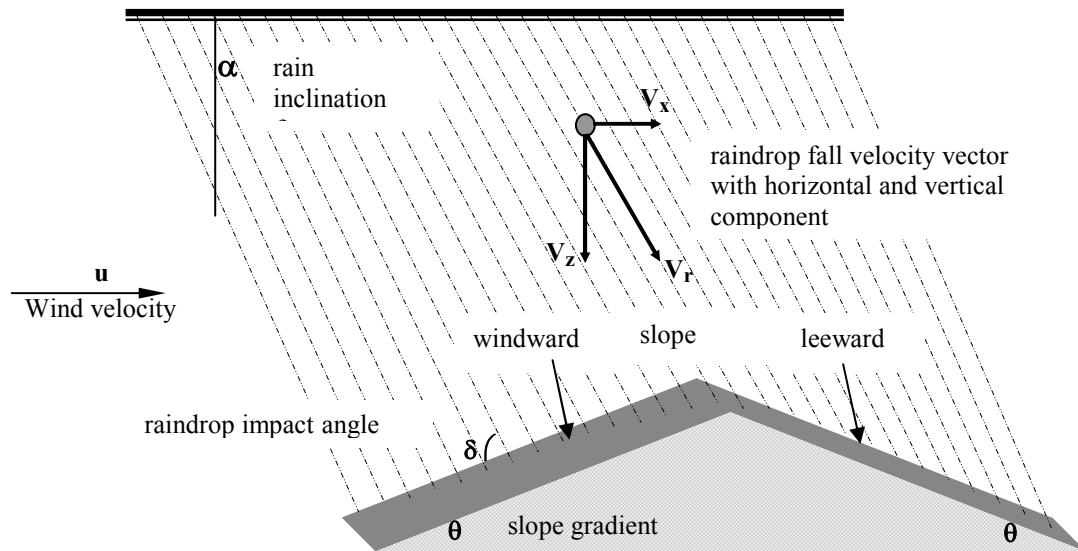


Figure 1. Schematic representation of wind-driven rain with an angle from vertical and incident on sloping surface.

The changes in raindrop trajectory and frequency with wind velocity and direction can have significant effects on rainsplash detachment process. The resultant impact velocity, impact angle, and impact frequency of raindrops determine the magnitude of rainsplash detachment by wind-driven rain. This differs from the detachment process by windless rain, in which a straight-line trajectory of raindrops and accordingly greatest rainfall intensity for a given rain are implicitly assumed. Wind, as well as slope and overland flow, is another possible factor capable of transporting detached particles by raindrop impact. Once soil particles are entrained in the splash droplets that have risen into the air by raindrop impact, wind velocity gradient will transport these particles. Obviously, in addition to its role in the rainsplash detachment process, the wind accompanying rain is an important consideration in the rainsplash transport process, which can cause a net transportation

in wind direction. In wind-driven rains, wind velocity and direction is expected to affect not only rainsplash detachment and transport processes but also shallow flow sediment transport induced by raindrop impacts with an angle on flow and the rainsplash trajectories of soil particles within flow.

Under wind-driven rain, the interrill transport process is a combined work of both rainsplash sediment transport and raindrop-impacted shallow flow sediment transport. The rainsplash process acts alone until runoff occurs, and net soil transport is caused by wind. As soon as runoff starts, the flow-driven process begins to transport the detached soil particles. This is different from the approach of recent interrill erosion models that soil detached by the rainsplash will be subsequently transported by overland flow.

The Effect of Wind on Raindrop Impact and Rainsplash Detachment

Raindrop impact frequency

The raindrop fall trajectories influenced by the horizontal wind velocity and the geometry of the surface, slope gradient and aspect, leads to differences in the amounts of raindrops hitting the soil surface.

$$\phi = \frac{I_a}{I} = \cos(\alpha \mp \theta) \quad [1]$$

where ϕ is the impact efficiency, I the rainfall intensity in respect to a plane normal to the rain vector, I_a the actual intensity, α the raindrop inclination from vertical, and θ the slope gradient. In the Eq. [1], the positive sign indicates the windward facing slope and the negative sign corresponds to the leeward facing slope, implying raindrop deficit with the same values of the slope gradient and the raindrop inclination. Eq. [1] points in fact to that the actual rate of wind-driven raindrop impact per unit area varies with the rain inclination induced by the horizontal wind velocity and the slope gradient and aspect (De Lima, 1990). Theoretically, in the situations where wind direction from which rain is falling z_α and the plane of surface on which raingauges are placed z_θ are on the same plane, rain interception will be the greatest in the windward slopes as α is approaching θ , and no raindrops will be intercepted by the surface as the sum of α and θ is approaching 90 degrees.

Angle of rain incidence

The mean angle of rain incidence between wind vector and the plane of the surface is calculated as a function of the rain inclination, slope gradient and aspect and given by the cosine law of spherical trigonometry (Sellers, 1965):

$$\cos(\alpha \mp \theta) = \cos \alpha \cos \theta \pm \sin \alpha \sin \theta \cos(z_\alpha \mp z_\theta) \quad [2]$$

where z_α and z_θ are the azimuth from which rain is falling and the azimuth towards which the plane of surface is inclined, respectively. Since wind-driven raindrop

strikes the soil surface with an angle deviated from the vertical because of its horizontal and vertical velocities, its vertical impact pressure differs from that of the vertically falling raindrop. No impact pressure acts on a soil surface by a raindrop with a velocity 'v' regardless of its magnitude that is parallel to the surface, and the soil surface experiences a maximum impact pressure when raindrop fall perpendicular to the soil surface (Ellison, 1947). In general, if a raindrop falls at an angle of incidence ($\alpha \mp \theta$), only the component of velocity $v \cos(\alpha \mp \theta)$ normal to the surface gives rise to an impact pressure (Heymann, 1967; Springer, 1976).

Figure 2 shows calculated average rain inclination (a) from vertical and average angle of incidence (b) between the wind vector and the plane of surface as a function of horizontal wind velocity. These results were obtained in a wind tunnel rainfall simulator facility at Ghent University in Belgium (Gabriels et al., 1997) with the rains driven by wind velocities of 6, 10 and 14 m s⁻¹ and incidental on both windward and leeward slopes of 7, 15 and 20% (Erpul et al., 2003a). Median drop sizes were 1.63, 1.53, and 1.55 mm for the rains driven by 6, 10 and 14 m s⁻¹ winds, respectively.

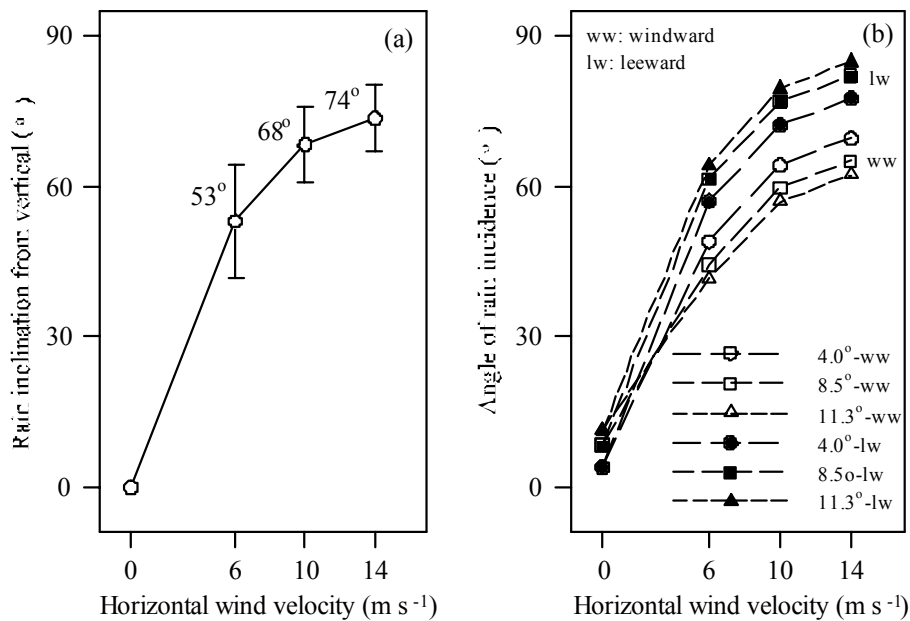


Figure 2. Calculated average rain inclination from vertical (a), and average angle of incidence between the wind vector and the plane of surface (b) as a function of horizontal wind velocity.

Raindrop impact velocity

For an understanding of dynamics of wind-driven raindrop, one needs to know the full spectrum of forces acting on the raindrops entering a wind field. For a two dimensional analytical model to estimate raindrop trajectories, the equations for vertical z and horizontal along wind x are as follows:

$$m \frac{\partial^2 z}{\partial t^2} = mg - \rho_a g \nabla - \frac{1}{2} C_d \rho_a \left(\frac{\partial z}{\partial t} \right)^2 A \quad [3]$$

$$m \frac{\partial^2 x}{\partial t^2} = -\frac{1}{2} C_d \rho_a \left(\frac{\partial x}{\partial t} \right)^2 A \quad [4]$$

If raindrops are considered spherical of diameter d (m) and density ρ_w (kg m^{-3}), then the mass of the raindrop is $m = (\rho_w/6)\pi d^3$ (kg) with the projected frontal area of $A = \pi d^2/4$ (m^2), and the raindrop volume $\nabla = \pi d^3/6$ (m^3); g is the gravitational acceleration (m s^{-2}); ρ_a is the air density (kg m^{-3}); C_d is the drag coefficient on the raindrop and calculated as a function of Reynolds number R_e :

$$R_e = \frac{\rho_a u d}{\mu} \quad [5]$$

where u is free stream wind velocity (m s^{-1}) and μ the viscosity of air (N s m^{-2}). Eq. [3] and Eq. [4] show that the forces acting on the raindrop are due to gravity, buoyancy, and drag. It is here assumed that raindrops reach their terminal velocities in the z -direction and satisfy $m(\partial^2 z/\partial t^2) = 0$ and the x -component of the raindrop velocity is a function of horizontal wind velocity profile, $m(\partial^2 x/\partial t^2) = f(u_z)$. An expression for the horizontal raindrop velocity with respect to the fall height $[\partial V_x/\partial z]$ is derived using Eq. [3] and Eq. [4] (Pedersen and Hasholt, 1995):

$$\frac{\partial V_x}{\partial z} = \frac{3C_d \tilde{n}_a}{4d\tilde{n}_w} (V_x - u) \quad [6]$$

Rainsplash detachment

When raindrops impact a soil surface, the pressure builds up at the raindrop-soil interface. Pressure acting on the contact area leads to a force normal to the soil surface and forces the splash droplets to escape laterally, entraining soil particles. Rainsplash detachment results from these splashes (Huang et al., 1982; Moss and Green, 1983). In the wind-driven rains, velocity, angle, and frequency of raindrop impact determine the magnitude of rainsplash detachment. If we assume that the effect of wind shear stress on the detachment is insignificant when compared to the

effects of the impacting raindrops, the rainsplash detachment rate (D) at which soil particles are supplied into the air is a linear function of the raindrop kinetic energy (E_r) (Erpul et al., 2003a):

$$D = K(E_r) = K \left\{ \frac{1}{2} m [V_r^2 \cos^2(\alpha \mp \theta)] \right\} \quad [7]$$

where, K is the soil detachment factor, and $V_r^2 = V_z^2 + V_x^2$ with $V_z = \partial z / \partial t$ and $V_x = \partial x / \partial t$. Since raindrops with Ξ_a (#) strike a soil surface under wind-driven rain, the total kinetic energy flux E_m ($W m^{-2}$) is described by $E_m = \hat{I}_a E_r = \hat{I} E_r \cos(\alpha \mp \theta)$, and Eq. [7] becomes:

$$D = K \Xi \left\{ \frac{1}{2} m [V_r^2 \cos^3(\alpha \mp \theta)] \right\} \quad [8]$$

The maximum soil detachment rate for the case of the rainsplash transport occurs when there is no water running on the soil surface. Therefore, considering the effect of shallow overland flow depth on the detachment, the contribution of impacts of wind-driven raindrops in interrill flow-driven sediment transport process can be given by:

$$D_\Phi = K \Xi \left\{ \frac{1}{2} m [V_r^2 \cos^3(\alpha \mp \theta)] \right\} \Phi \quad [9]$$

where, D_Φ is the soil detachment term for overland flow-driven transport, and Φ is the parameter introduced to distinguish the raindrop impact on a bare soil surface from the impact on a surface with a shallow water depth.

Sediment Transport from Interrill Areas under Wind-Driven Rain

Unlike recent erosion prediction technologies, a technology considering the combined effect of wind and rain on the erosion processes hypothesizes that when raindrops first impact bare soil, wind-driven rainsplash process operates alone, and by the time that runoff occurs, produces net transport and provides the first stage of transport sequence of interrill soil erosion. This reasoning implies that sediment transport by rain-impacted shallow flow shows a complementary relationship to the rainsplash, which rapidly becomes less effective as flow depth increases from zero. Therefore, total interrill erosion under wind-driven rain is defined by:

$$q_i = Q_s + q_s \quad [10]$$

where, q_i is the total interrill sediment transport, Q_s is the wind-driven rainsplash transport, and q_s is the sediment transport by raindrop-impacted shallow flow.

Wind-driven rainsplash transport

The approach to the rainsplash transport process under wind-driven rain is based on the concept that once lifted off by the raindrop impact, the soil particles entrained into the splash droplets travel some distance, which varies directly with the wind shear velocity (Erpul et al., 2002). The raindrop impacts induce the process that wind would otherwise be incapable of transporting wet and cohesive soil particles. Erpul et al. (2003b) adequately described the process by relating transport rate to the flux of rain energy (E_m , $W m^{-2}$) and the wind shear velocity (u_* , $m s^{-1}$):

$$Q_s = K_1 E_m^{a_1} u_*^{b_1} \quad [11]$$

where K_1 is the relative soil transport parameter for the wind-driven rainsplash process, and a_1 and b_1 are the regression coefficients.

Sediment transport by raindrop impacted shallow flow

The essential processes of sediment transport by rain impacted thin flow are rainsplash detachment and flow-driven transport. In other words, shallow flow-driven sediment transport from the interrill areas is determined by the interaction of rain and flow parameters. Julien and Simons (1985) investigated the applicability of several sediment transport equations under different hydraulic conditions. The transport capacity of rain-impacted thin flow was characterized by rainfall intensity (I), unit discharge (q), and channel bottom slope (S) by:

$$q_s = KI^a q^b S^c \quad [12]$$

where, q_s is the sediment transport rate by rain-impacted thin flow, and K , a , b , and c are the experimental coefficients. Under wind-driven rains, Erpul et al. (2003b) developed a simplified model equation similar to Eq. [12]. Flux of rain energy provided much better result than the intensity since it accounted for the variations in the velocity and angle of raindrop impacts as well as that in the frequency of raindrop impacts:

$$q_s = K_2 E_m^{a_2} q^{b_2} S^{c_2} \quad [13]$$

where, q_s is in $g m^{-1} min^{-1}$ and q is in $m^2 min^{-1}$, and S in mm^{-1} . K_2 is the relative soil transport parameter for shallow flow-driven process, and a_2 , b_2 , and c_2 are the regression coefficients.

Total sediment transport

Using Eq. [10], Erpul et al. (2003b) defined the total interrill erosion by:

$$q_i = K_1 E_m^{a_1} u_*^b + K_2 E_m^{a_2} q^{b_2} S^{c_2} \quad [14]$$

The results of their study showed that, when compared to the contribution of the flow-driven transport, the contribution of the rainsplash transport was significant to the extent that it should not be neglected in accurately predicting water erosion from interrill areas under wind-driven rains (Figure 3).

References

- De Lima, J. L. M. P., 1990. The effect of oblique rain on inclined surfaces: A nomograph for the rain-gauge correction factor. *Journal of Hydrology*, 115: 407-412.
- Ellison, W. D. 1947 (7 parts). Soil erosion studies. *Agric. Eng.*, 28: 145-146; 197-201; 245-248; 297-300; 349-351; 407-408; 447-450.
- Erpul, G., L. D., Norton, and D. Gabriels. 2002. Raindrop-induced and wind-driven soil particle transport. *Catena*, 47: 227-243.
- Erpul, G., L. D., Norton, and D. Gabriels. 2003a. The effect of wind on raindrop impact and rainsplash detachment. *Trans. of ASAE* (in press).
- Erpul, G., L. D., Norton, and D. Gabriels. 2003b. Sediment transport from interrill areas under wind-driven rain. *Journal of Hydrology* (in press).
- Gabriels, D., W. Cornelis, I. Pollet, T. Van Coillie and M. Quessar. 1997. The I.C.E. wind tunnel for wind and water erosion studies. *Soil Technology*, 10: 1-8.
- Heymann, F. J., 1967. A survey of clues to the relation between erosion rate and impact parameters, Second Rain Erosion Conference, 2: 683-760.
- Huang, C., J. M. Bradford, and J. H. Cushman. 1982. A numerical study of raindrop impact phenomena: the rigid case. *Soil Sci. Soc. Amer. J.* 46: 14-19.
- Julien, P. Y. and D. B. Simons. 1985. Sediment transport capacity of overland flow. *Transactions of the ASAE* 28: 755-762.
- Moss, A. J. and P. Green. 1983. Movement of solids in air and water by raindrop impact. Effects of drop-size and water-depth variations. *Aust. J. Soil Res.*, 21: 373-382.
- Pedersen, H. S. and B. Hasholt. 1995. Influence of wind speed on rainsplash erosion. *Catena*, 24: 39-54.
- Sellers, W. D. 1965. *Physical Climatology*. University of Chicago Press, Chicago, Ill. pp. 33-35.
- Springer, G. S., 1976. *Erosion by liquid impact*. John Wiley and Sons, Inc., New York.

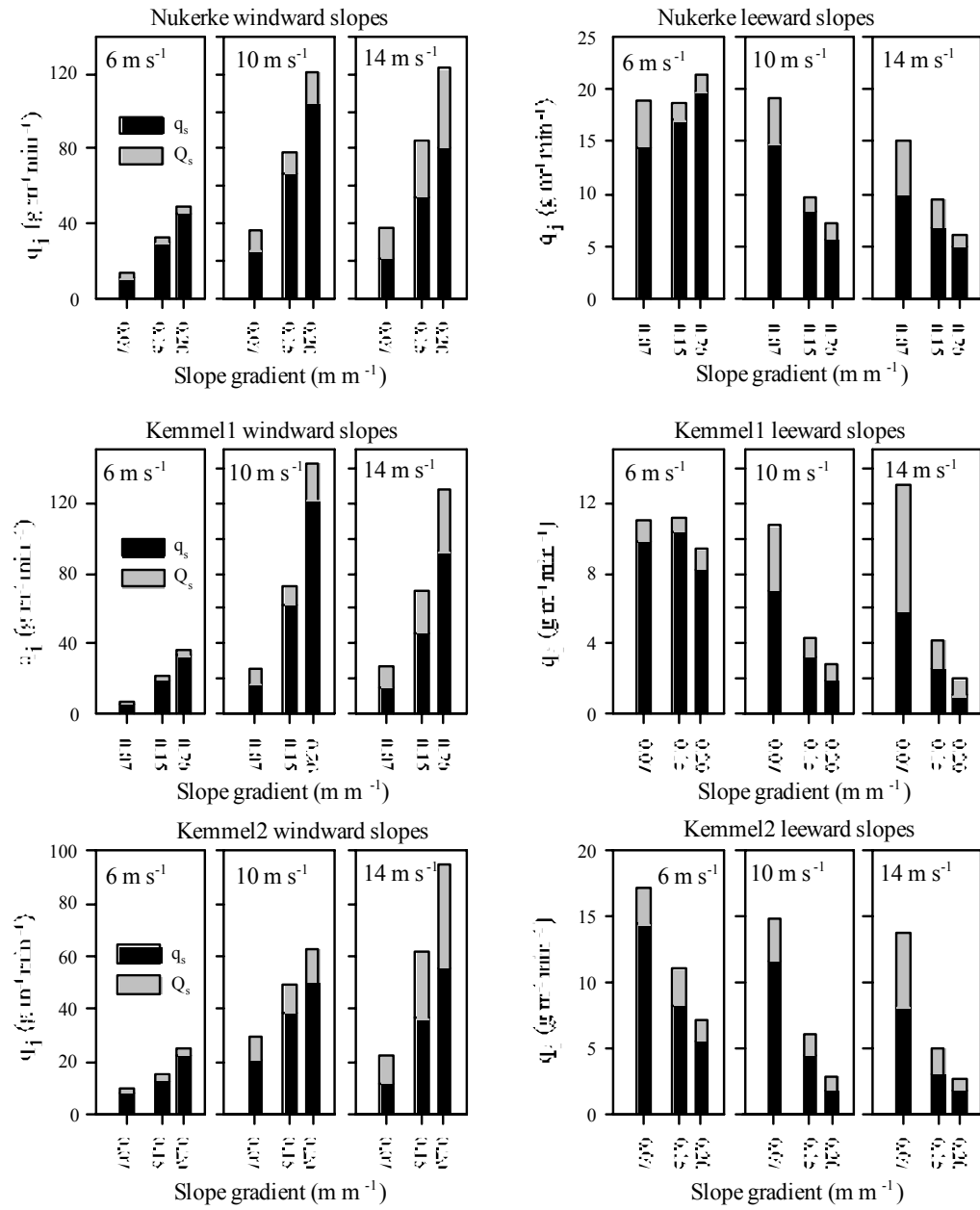


Figure 3. Total sediment transport from interrill areas based on the wind-driven rainsplash and the sediment transport by the rain-impacted shallow flow for three soils.

Physical Properties of Magnesium Affected Soils in Colombia

Alvaro Garcia-Ocampo¹

National University of Colombia, Palmira, Colombia

*Lecture given at the
College on Soil Physics
Trieste, 3-21 March 2003*

LNS0418016

¹ sccsueloagarcia@uniweb.net.co

Introduction

Magnesium has some capacity to develop higher exchangeable sodium levels in clays and soil materials. The Mg^{+2} accumulation on the exchange complex of soils to a very high saturation levels affect their physical, chemical and biological properties. Colombia has a large area of these soils, located mainly in the main rivers valleys and in the Caribbean Region. In the Cauca River Valley there are about 117,000 hectares affected. There is a lack of information about the soil forming processes, the Mg^{+2} effects on soils, the type and source of compounds responsible for the magnesium enrichment, their relationship with the landscape and the way this accumulation occurs.

Materials and Methods

To identify and quantify soil Mg^{+2} enriched areas over 2500 soil profiles from different landscape positions of the Cauca River Valley were studied. The information was processed to generate Mg-saturation maps, to identify the different soil profile types and to estimate the affected area. A topographic sequence from the alluvial inundation plain to the hills was used to explore the presence of diagnostic horizons and to determine the main soil characteristics and genetic, mineralogical or chemical evidences of soil forming processes. Two 180 kilometer transects parallel to the river were used to: a) study the type and source of Mg-compounds responsible for the Mg-enrichment and the way this accumulation occurs. b) the soil hydraulic properties like infiltration, saturated hydraulic conductivity and matric potential at different depths were also measured. Samples of nine profiles were collected and the porosity and soil volume changes at different water content were examined. The program RETC was used for prediction of the hydraulic properties of non saturated soils. These properties involved the retention curve, the function of hydraulic conductivity and the diffusivity of the water in the soil.

Results

By grouping together the soil profiles, five main type of Mg-affected soils were identified as being predominant in the different landscape units. Their distribution in the landscape units showed two different origins: soils developed under hydromorphic conditions and soils related to igneous Mg-materials.

The toposequence studied showed the presence of natric or gypsic horizons on the basin soil profiles and evidence of Ca^{+2} and Mg^{+2} precipitation as calcite and/or aragonite. As the hydromorphic conditions changed from the basin to the hills the vertic characteristics disappeared but calcium accumulation and precipitation still occurred. Light alkalinity is ordinary in all the strata but in the upper horizons. Sulphate and bicarbonate ions were found in all profiles but the later was not found in the soil parent materials of the lower plains. As the soil becomes deeper, sulphate ions become predominant and gypsum accumulation appears due to reductive

environment. The mineralogical composition of the clay fraction showed the presence of vermiculite and smectite in all profiles but predominant in the basin and lower plains.

Calcium and Mg bicarbonates were also the predominant salts in the surface (0 to 20 cm) of the soils located in the transect parallel to the river. In the deeper layers (20 to 40 cm and 40 to 60 cm) Mg-sulphate acquired predominance. The presence and activity of the Ca and Mg ions in the deeper layers of the profiles played a decisive role in the physical-chemical relationships of these soils.

Wetting and drying periods facilitate calcite concentration and precipitation out of the soil solution, affecting soil capacity to water and gas flow and making it easy to SO_4^{+2} and Mg^{+2} ions to predominate into the profile. The Ca^{+2} decrement allows a relative accumulation of Mg and, later on, of Na. In this way Mg^{+2} determines the soil chemical and physical properties depending on its saturation in the exchange complex and high hydration energy. It was considered CaCO_3 precipitation as the main chemical process affecting soil physical properties.

High bicarbonate and sulphate waters used to perform laboratory experiments showed the effect of irrigation on these soils causing soil sealing and crusting, decrease of aggregate stability, hydraulic conductivity and soil permeability associated to ESP and EMgP increments (Tables 1 and 2). The presence of illite on the clay fraction was related to low soil tolerance to chemical and physical degradation.

Table 1. Changes in the Exchangeable Magnesium Percentage (EMgP) and Exchangeable Sodium Percentage (ESP) of three Colombian soils treated with high bicarbonate and sulphate waters.

	EMgP		ESP	
Soil	%			
	Initial	Final	Initial	Final
Alfisol	26.7	31.5	4.2	4.5
Mollisol	24.8	45.1	0.7	7.8
Vertisol	28.5	33.8	2.2	3.7

Table 2. Saturated Hydraulic Conductivity of three Colombian soils treated with high bicarbonate and sulphate saline water (40 cmol (+) L^{-1})

Hydraulic Conductivity (Ksat) mm/h					
Alfisol		Mollisol		Vertisol	
Before	After	Before	After	Before	After
95.1	86.0	60.1	5.0	46.4	27.5

After several days representative 5 cm core samples of selected soils (Udic Pellustert, Typic Pellustert, Typic Haplustalf, Fluvaquentic Haplustoll and Vertic Ustropept), did not reach the saturation point when they were left in water to capillarity rise. The levels of relative saturation showed small changes at different hydraulic heads, but it was observed the water film formed on the soil surface was expelled to low suction (0.1 bar).

The nonsaturation of magnesian soils by hydrophobic forces is possible. The water content under different suctions (0.1 up to 15 bar) showed small differences due to the low hydraulic conductivity limiting the effective saturation and the residual water capacity of the soil, being the hydraulic adjustments strongly restricted by the high matrix energies that govern the water-soil relationships associated to the microporosity of the soils.

In the magnesian vertisols, porosity is limited by the lack of spaces for the water and air movement the total porosity is very low (15-30%), with micropores prevalence and high water retention capacity.. Soils don't have any structural arrangement to form macropores due to dispersion of the clays caused by the magnesium saturation and the reorientation of their layers by the attraction forces. The content of clays is high (45-75%), The drainage is slow to imperfect which it is associated to the dominance of vertic conditions (Cole>0.09), high plasticity (PI>20%), high residual humidity, structural uncertainty, rigidity in dry and impediment to reach the total saturation (Tables 3 and 4).

Table 3. Physical characterization of the three Mg-enriched soils of the Valley of the Cauca River (Colombia)

Texture		O.M. (%)	Bulk density (g/cm ³)	Dr (g/cm ³)	PI (%)	CD (%)	H.W (%)	SI	Porosity (%)	WR ₁₅ bar
Typic Haplustalf	ArL	2.79	1.37	2.63	35.9	1.81	1.93	0.97	42.96	31.01
Pachic Haplustoll	FL	2.50	1.17	2.73	20.7	11.53	1.47	0.51	57.14	14.28
Typic Haplustert	Ar	2.37	1.43	2.56	34.7	48.69	2.71	1.38	40.41	31.39

O.M=Organic Matter, Dr=density, PI=plasticity Index, DC=Dispersion coefficient, HW=hygroscopic water, SI= stability Index, WR₁₅ bar=Water retention at 15 bar.

Soil volume changes from saturation to dryness with a measured mean value of 30%. When the water retained in pores is extracted the soil mass contraction give place to cracks of different size which explain the volume reduction. The function change of volume was: $\Delta V = 3.65h^{0.203}$.

Precipitations of CaCO₃ and other salts are observed on the flat court surfaces, sealing of pores and high removal potential when they are exposed to watering or rain. The nature of clays and the mineral solubility processes have favored the Mg enrichment of the soils of the valley, causing clay peptization and dispersion and affecting the porosity and the hydraulic conductivity of the soil.

Additional Index words: salinity, soil Mg-enrichment, soil hydraulic properties porosity, soil volume changes.

References

- Amezquita E. 1997. The physical properties and the productive soil. Soil fertility: diagnose and control. Colombian Soil Science Society. . Santafé of Bogotá. p 137-154.
- Borrero, J.; García-Ocampo, A. and Gómez, C. A. 1998. Magnesium affected soils in the Valley of the Cauca River. *Suelos Ecuatoriales* Vol. 28. SCCS. Colombia.
- García-Ocampo, A. 1997. Magnesic Soils in the Valley of the the Cauca River Colombia. In: International Symposium on Sustainable Management of Salt Affected Soils in the Arid Ecosystem, Cairo, Egypt.
- García-Ocampo, A. and Torrente, A. 2000. Water Relationships in a High Magnesium Saturation in a Vertisol of the Cauca River Valley (Colombia). *Remade Lands 2000*. Fremantle. Australia.
- Madero, E.; García-Ocampo, A.; Borrero, J.; and Yamil, L.E. L.999. Distribution of High Magnesium Saturated soils the Valley of the Cauca River. CD Proceedings of the 14 Latin American Congress of Soils Science. Temuco, Chile. Nov. of 1.999. 10 p
- Torrente, A. 2001. Study of the porosity and the pore distribution of some magnesics argillaceous soils of the Valley of the Cauca, Colombia. Public Seminary. National University of Colombia from Palmira.

Table 4. Some physical properties of Mg enriched soils from the Cauca river Valley (Colombia).

Soil	Depth (cm)	Bulk density Mg m ⁻³	Density Mg m ⁻³	Porosity (%)	Compaction susceptibility (%)	Cut resistance (Kgcm ⁻³)	Hydraulic Conductivity (cm hr ⁻¹)
Berginie	0-20	1.95	2.79	27.41	91.93	4.08	1.17
	20-40	1.79	2.67	27.69	93.87	5.00	2.15
	40-60	1.59	2.70	32.83	86.53	5.58	3.14
Cabaña 1	0-20	1.80	2.57	30.57	97.20	3.17	1.16
	20-40	1.84	2.71	32.09	97.86	2.67	0.17
	40-60	1.74	2.74	28.24	95.20	2.08	2.21
Cabaña 2	0-20	1.41	2.54	29.2	96.98	2.83	0.80
	20-40	1.41	2.64	28.85	98.52	4.00	0.00
	40-60	1.41	2.69	33.58	97.45	3.50	0.80
Cabaña 3	0-20	1.61	2.61	15.15	95.85	4.03	0.27
	20-40	1.20	2.87	15.15	95.36	3.92	0.00
	40-60	1.20	2.67	15.15	91.28	4.33	0.00
Cabaña 4	0-20	1.51	2.73	32.16	94.70	3.38	1.17
	20-40	1.45	2.75	31.37	95.46	3.22	0.27
	40-60	1.22	2.73	36.19	97.68	2.33	1.41
Argelia	0-20	1.23	2.62	24.63	91.85	5.00	0.87
	20-40	1.20	2.67	22.85	94.33	4.50	0.00
	40-60	1.19	2.66	22.85	95.52	4.50	0.00
Trinidad	0-20	1.09	2.67	16.10	92.24	5.50	25.45
	20-40	1.18	2.42	20.45	97.23	5.70	0.40
	40-60	1.18	2.47	20.45	100.00	6.00	0.67
Esperanza	0-20	1.15	2.58	26.13	97.20	5.18	2.01
	20-40	1.26	2.73	20.82	97.86	5.18	0.00
	40-60	1.16	2.67	20.82	95.20	5.18	0.00
Cabaña Rozo	0-20	1.24	2.72	24.44	92.33	3.50	0.00
	20-40	1.89	2.71	26.04	93.41	3.50	0.13
	40-60	1.09	2.71	26.04	95.36	2.83	0.00
Ceniuva	0-20	1.85	2.64	29.57	91.93	5.75	0.00
	20-40	1.47	2.60	24.71	93.80	6.50	0.00
	40-60	1.84	2.56	24.71	86.53	5.83	0.06
Paso Ancho	0-20	1.57	2.78	39.56	98.49	3.33	4.63
	20-40	1.50	2.66	45.39	99.20	3.58	1.88
	40-60	1.46	2.66	45.39	98.72	4.33	30.49
Villa Clara	0-20	1.83	2.63	29.15	97.92	3.33	21.76
	20-40	1.91	2.57	24.33	97.68	3.58	9.84
	40-60	1.88	2.66	24.33	95.68	4.33	26.25

Experimental and Modelling Studies of Infiltration

Mauro Giudici¹

*Dipartimento di Scienze della Terra, Sezione di Geofisica,
Università degli Studi di Milano, Milano, Italy*

*Lecture given at the
College on Soil Physics
Trieste, 3-21 March 2003*

LNS0418017

¹ Mauro.Giudici@unimi.it

Introduction and motivation

This presentation describes a study of infiltration in the unsaturated soil with the objective of estimating the recharge to a phreatic aquifer. The study area is at the border of the city of Milano (Northern Italy), which draws water for both domestic and industrial purposes from ground water resources located beneath the urban area. The rate of water pumping from the aquifer system has been varying during the XX century, depending upon the number of inhabitants and the development of industrial activities. This caused variations with time of the depth of the water table below the ground surface and in turn some emergencies: the two most prominent episodes correspond to the middle '70s, when the water table in the city centre was about 30 m below the undisturbed natural conditions, and to the last decade, when the water table has raised at a rate of approximately 1 m/year and caused infiltrations in deep constructions (garages and building foundations, the underground railways, etc.).

We have developed four ground water flow models at different scales, which share some characteristics: they are based on quasi-3D approximation (horizontal flow in the aquifers and vertical flow in the aquitards), conservative finite-differences schemes for regular grid with square cells in the horizontal plane and are implemented with proprietary computer codes. The four models are:

- 1) *Espin* (Ponzini et al., 1989), which models ground water flow at a well field of the municipal Water Works, considers the traditional aquifer (100 m thickness) and has a grid spacing equal to 50 m.
- 2) *ModMil* (Giudici et al., 2000), which models ground water flow in an area of about 400 km² and includes the municipality of Milan; in the area more than 600 public wells and more than 400 private wells are drilled. The model considers the traditional aquifer and has a grid spacing equal to 500 m.
- 3) *modLambro* (Romano et al., 2002), which models an area of about 20 km², at the margin of the city area, includes a park area and is crossed by the Lambro river and includes four pumping stations of the municipal Water Works. It considers both the traditional and the deep aquifers (thickness of almost 200 m) and has a grid spacing equal to 100 m. Since the physical boundaries of the aquifer system are far from the modelled area, the results of *ModMil* are used to fix the boundary conditions of *modLambro*.
- 4) *ProvMI*, which is the extension of *ModMil* toward North, up to the hills formed by the moraines deposited by alpine glaciers. It models the traditional aquifer and has a grid spacing is equal to 1500 m.

Among the problems that were studied for the development of these models, I recall some numerical problems, related to the behaviour of the phreatic aquifer under conditions of strong exploitation (Valota et al., 2002). Model calibration and validation for *ModMil* has been performed with a two-stage process, i.e., using some of the available data for model calibration and the remaining data for model validation.

It is of paramount importance the estimation of the source terms, which can be summarized in the following list (Giudici et al., 2001):

1. abstraction from public wells for domestic use and from private wells for industrial or agricultural use,
2. abstraction from topographic sources;
3. drainage/recharge from rivers and natural or artificial channels;
4. recharge from rain infiltration;
5. recharge from losses from the aqueduct and sewage networks;
6. recharge from infiltration of water used for irrigation.

The location of the abstraction wells is in general well known, and estimates of the water abstraction rates at point 1 are available; some data for point 2 are also available, whereas estimates of location and strength of points from 3 to 6 of the previous list are very uncertain and depend on water infiltration through unsaturated soil.

Research description

The following sections summarize some of the results obtained with the research program “The contribution of geophysics to hydrogeological risk assessment: exploration, monitoring and modelling”, which involved the Universities of Milano, Modena e Reggio Emilia and Padova. Figure 1 shows the study area and the location of the three sites where experimental studies have been performed.

In particular at site B we have acquired a high-resolution seismic profile and geoelectrical tomography. The results are in good agreement with those obtained from stratigraphic logs of the wells drilled in the area and showed some further heterogeneous features. Instead, a magnetotelluric sounding has not provided good results, because, as expected, anthropogenic noise was too strong.

The electrical tomography performed in area C has provided interesting results, showing that the lake and the phreatic aquifer have a good hydraulic contact. This is very important information for ground water model development.

In the following section some of the monitoring data are resumed.

Monitoring

At site C, we performed a statistical analysis of piezometric head and rainfall rates. In particular we have shown that the piezometric head sampled with an approximately monthly rate are correlated with the cumulated rainfall for a period of time longer than 90 days before the date of measurement of the piezometric head, whereas it is not correlated with the cumulated rainfall for a period shorter than 30 days. In other words, the monthly sampling of piezometric head does not allow us to study the effect of a rain event on the piezometric head, whereas it is correlated with the seasonal behaviour of rainfall.

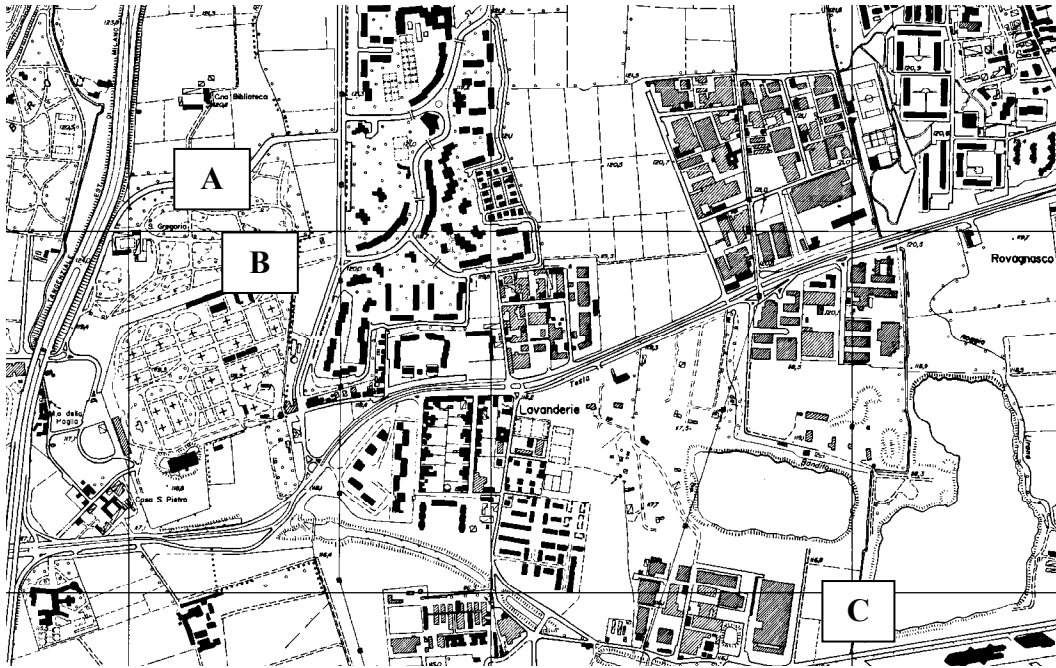


Figure 1 – Map of the study area, with represented the three sites where experiments have been conducted (site A – Lambro pumping station; site B – Lambro Park; site C – artificial mining lake)

At site A, a hydrometeorological station has been installed, which collected meteorological and soil data from 20 June 2001 to 5 November 2002. In particular the meteorological data were collected with instruments installed on a 12-meters-high telescopic pole to measure the following quantities: atmospheric pressure (at an height of 2 m), air temperature and moisture (0.1, 2 and 6 m), wind velocity and direction (10 m), short wavelength incident radiation (2 m), net radiation at short and long wavelength (2 m), rainfall and evaporation at soil. Horizontally buried TDR probes to measure soil water content were installed at depths of 5.5, 17, 33, 52 and 76 cm; soil temperature was monitored with PT100 thermometers at four different depths (6, 15, 32, 50 cm). Finally from 28 June to 27 July 2002 capillary pressure was monitored with four tensiometers (2 at a depth of 32 cm, 1 at 80 cm, and 1 at 90 cm).

The studied soil consists of a natural soil, which has been altered during building works and mixed with building residuals. Therefore, this is a very common soil in urban areas where natural soils are modified during building or civil engineering works.

Figure 2 shows the data collected by the TDR probes at 5.5 and 76 cm and by the rainfall gauge. The sampling period was 30 minutes. We stress a couple of features apparent from the time series.

The decrease of soil water content observed for the shallow probe during December 2001-January 2002 is not due to a real decrease of this physical quantity,

but is due to partial frozen of soil water in a period when soil temperature was close to 0°C for quite a long period.

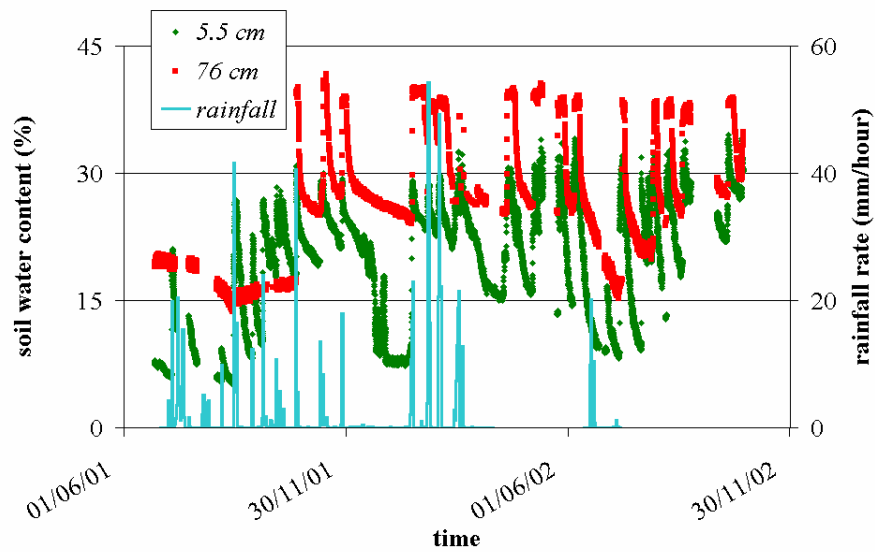


Figure 2 – Soil water content and rainfall rate monitored at site A.

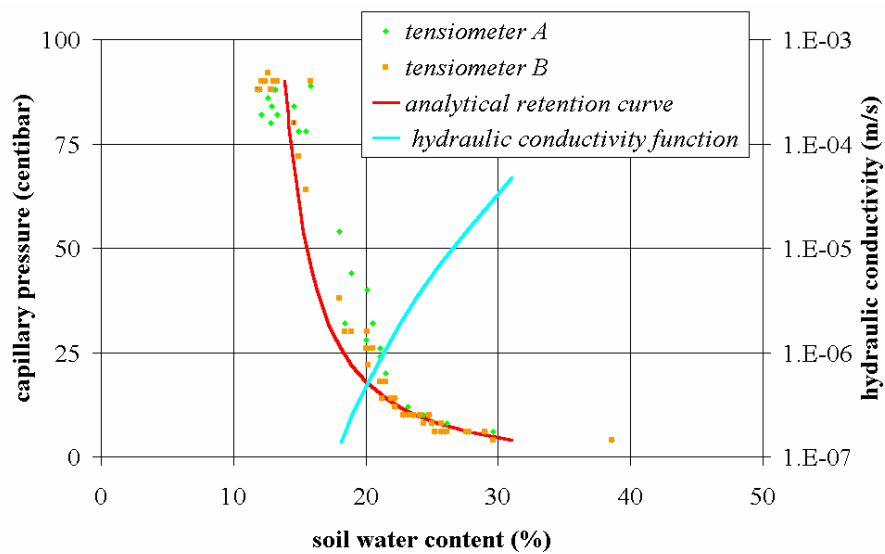


Figure 3 – Characteristic curve of the soil.

Modelling

An unsaturated flow model has been developed with the following characteristics:

- 1-D vertical single phase flow;
- finite-differences conservative scheme with a Crank-Nicholson scheme for the time discretisation;
- discretisation grid step 0.1 m;
- time step 60 s;
- Dirichlet boundary conditions at the upper boundary at a depth of 0.35 m, where water content is fixed from experimental data, and at the lower boundary at a depth of 13.95 m, which approximately corresponds to the depth of the water table at the site;
- retention and conductivity curves from observations shown in Fig. 3;
- initial condition as solution of stationary unsaturated flow.

The response of the model to variations of the top boundary condition strongly depends on the initial condition and, as a consequence, infiltration strongly depends not only on rainfall, but also on soil condition before the rain event.

Synthetic models show that if we have a periodic boundary condition at the top boundary, the behaviour is periodic after few cycles; this result is not trivial for a non linear model. It offers a possible suggestion to impose initial conditions, e.g. obtaining them from the response to periodical (annual, seasonal or daily) boundary conditions.

Summary and perspectives

The application of geophysical exploration techniques, in particular seismic and geoelectrical prospecting, has been very useful to complete the data and information on the hydrogeological structure obtained from stratigraphic logs.

Meteorological and soil data collected at site A are a time series which is very interesting and promising for further processing, which is going to provide important information on water infiltration in the soil found at site A of the study area. For this we are improving modelling of unsaturated media, not only with numerical models, but also with analytical models, and taking into account not only the water mass balance, but also the energy budget and exchanges between water, soil, atmosphere and vegetation.

Another important perspective comes from measurements of the soil characteristic curve which are going to be performed on soil samples with the Richard's apparatus.

Acknowledgement

The work described in this communication was partly supported by the Italian Ministry for University and Scientific and technological research (Progetto di Ricerca

di Interesse Nazionale “The contribution of geophysics to hydrogeological risk assessment: exploration, monitoring and modelling”).

The research program was developed with the participation of the University of Milano (M. Giudici, E. Romano, M. Manera, C. Sisti, G. Ponzini), the University of Modena and Reggio Emilia (S. Pugnaghi, M. Menziani, M. De Leva, L. Lombroso, R. Santangelo, S. Vincenzi - ISDGM CNR) and the University of Padova (A. Zaja, R. Francese, G. Fardin, G. Girardi, N. Praticelli).

Some of the data were provided by or collected with the cooperation of the following companies or institutions: Comune di Milano (R. Airolti), INERTI Holding spa (M. Noris, M. Carini), Provincia di Milano (C. Arduini, F. Di Palma), Università di Milano - Istituto di Fisica Generale Applicata (M. Maugeri, L. Buffoni), University of Alberta, Edmonton, CA (D. Schmitt, M. Lazorek).

References

- Giudici, M., Foglia, L., Parravicini, G., Ponzini, G. and Sincich, B. 2000. A quasi three dimensional model of water flow in the subsurface of Milano (Italy): the stationary flow, *Hydrology and Earth System Sciences* 4: 113-124.
- Giudici, M., Colpo, F., Ponzini, G., Romano, E. and Parravicini, G. 2001. Calibration of ground water recharge and hydraulic conductivity for the aquifer system beneath the city of Milan (Italy), in *Impact of Human Activity on Ground water Dynamics*, 43-50, IAHS Publ. no. 269.
- Ponzini, G., Crosta, G. and Giudici, M. 1989. The hydrogeological role of an aquitard in preventing drinkable water well contamination: a case study. *Environmental Health Perspectives*, 83, 77-95.
- Romano, E., Giudici, M., and Ponzini, G. 2002. Simulation of interactions between well fields with nested models: a case study, *Acta Universitatis Carolinae – Geologica* 46: 637-640.
- Valota, G., Giudici, M., Parravicini, G., Ponzini, G. and Romano, E. 2002. Is the forward problem of ground water hydrology always well posed? *Ground water* 40: 500-508.

Inverse Modelling for Flow and Transport in Porous Media

Mauro Giudici¹

*Dipartimento di Scienze della Terra, Sezione di Geofisica,
Università degli Studi di Milano, Milano, Italy*

*Lecture given at the
College on Soil Physics
Trieste, 3-21 March 2003*

LNS0418018

¹ Mauro.Giudici@unimi.it

Introduction

The problem of parameter identification for flow and transport model in porous media is discussed in this communication. First, a general framework for the development and application of environmental models is discussed, following the review by Giudici (2001). Then the forward and inverse problems for discrete models are described in detail, introducing fundamental concepts (uniqueness, identifiability, stability, conditioning). The importance of model scales is reviewed and is shown its link with the stability and conditioning issues. Finally some remarks are given to the use of several independent sets of data in inverse modelling.

The general framework for the development and application of environmental models

The process of the development and application of an environmental model is sketched in figure 1. The complete description of this scheme can be found in Giudici (2001). Here I recall some issues.

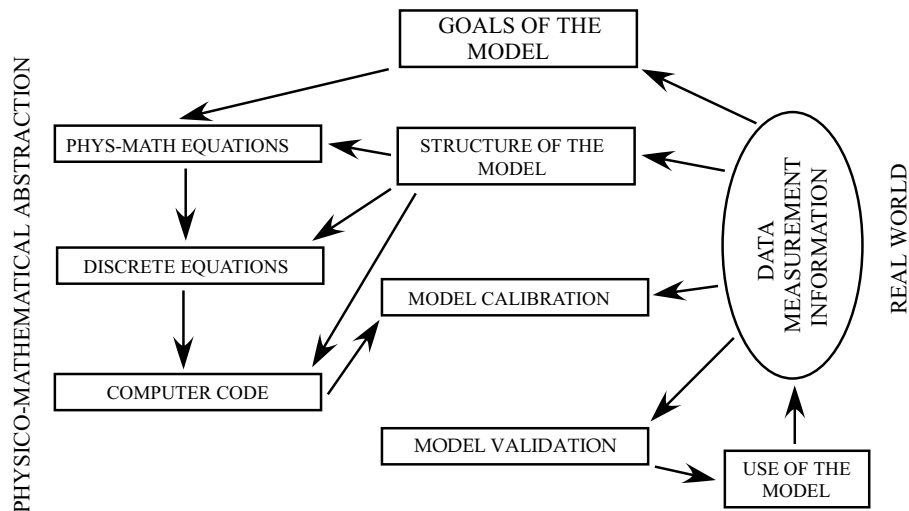


Figure 1 – Scheme of the process of development and application of an environmental model.

Data on the physical system are fundamental at every step of model development and application. In fact they guide the definition of the goals of the model and of several other steps. They are obviously very important for model calibration and validation, as well. Model calibration is the process of fixing the values of the model parameters, e.g., hydraulic conductivity or diffusivity, so that model predictions honour data (measurements and information). This is usually done with inverse modelling, i.e. solving an inverse problem.

In several applications, e.g. for geophysical exploration or medical imaging, the goal of the inverse problem is to obtain a map which shows the spatial and, in some cases, temporal distribution of some physical parameters. Among the parameters of interest, we recall seismic velocity for the seismic tomography (Nolet, 1987) and electrical resistivity for the electrical tomography (Griffiths and Barker, 1993; Loke and Barker, 1996).

Instead in environmental applications, this is only one part of the problem, because the results of the inverse problem must be used to solve forward problems that answer the specific questions of the final users. This implies that the whole process of model development and application must take into account the goals of the model and this is a must also for the model calibration.

We mentioned the importance of data. In environmental modelling we have to take care of some problems:

- Data include not only measurements of physical quantities (hard and soft data, see below), but also qualitative or descriptive information. We differentiate between hard and soft data: if we consider water contamination, the measurements of the concentration of chemical species in water samples are “hard data”, since they are measurements of physical quantities strictly related with the process under study. The measurements of water conductivity are related to the presence of dissolved salts and are “soft data” since they are related to the process under study, but the relationship with pollutant concentration is the result of an interpretation. Furthermore we could have qualitative information on the presence of industrial or agricultural activities which produce or handle toxic species: this is qualitative information, which is nevertheless very important for the development and application of a transport model, mainly for risk analysis. Other data and information come from the geological studies and are sometimes available as quantitative “soft” data, e.g. from the results of field and laboratory tests, or qualitative information on the characteristics of geological formations.
- The environmental data are often affected by strong errors. In fact, it is very difficult to perform experiments under controlled conditions in the field and the acquisition of specific data for model development could be very expensive. As a consequence one is often forced to work only with already available data, which are often sparse or irregularly spaced, are lacking in a check of the measurement procedures and in the accuracy of measurement devices. Therefore the model calibration in environmental sciences has often to do with large uncertainties on the data.

A general abstract description of the forward and inverse problem for discrete models

This section is devoted to the introduction of a formalism that allows us to describe a general discrete model and is based on Giudici (2003).

We consider the 1-D stationary balance equation for single-phase flow in porous media as an example:

$$K_{i-1/2} (H_{i-1} - H_i) + K_{i+1/2} (H_{i+1} - H_i) = F_i, \quad i = 1, \dots, N-1 \quad (1)$$

In particular we have assumed that the 1-D domain has been discretised with $N+1$ nodes, where the values of piezometric head (H_i , $i = 0, \dots, N$) are computed or assigned as Dirichlet boundary conditions. The physical parameters appearing in (1) are the so-called internode conductivities ($K_{i-1/2}$, $i = 0, \dots, N-1$) and the source terms (F_i , $i = 1, \dots, N-1$) include all the sources and sinks in a cell.

We introduce the following notation:

- \mathbf{u} is a N -dimensional array of parameters that describe the state of the system; it consists, e.g., of the values of pressure head or solute concentration in pore water at the nodes of a finite difference grid.
- \mathbf{m} is a M -dimensional array of model parameters; it consists, e.g., of the values of internode conductivity or diffusion coefficient; among these parameters we include also those used to fix the boundary and initial conditions and the forcing terms, e.g. sources and sinks.
- $\mathbf{f}(\mathbf{m}, \mathbf{u}) = 0$ are L state equations, e.g., the continuity equation (mass balance equation) for each cell or element of the discrete grid, like (1).

Definition (Forward problem)

Given \mathbf{m} , find \mathbf{u} such that $\mathbf{f}(\mathbf{m}, \mathbf{u}) = 0$. In explicit form $\mathbf{u} = \mathbf{g}(\mathbf{m})$.

Some further notation

\mathbf{d} is a D -dimensional array of measurements, e.g., pressure head or solute concentration in pore water at some points of the domain

$\mathbf{r}(\mathbf{m}, \mathbf{u}, \mathbf{d})$ is a residual function, which links the model and the state parameters to measured data. Simple examples of residual functions are $\mathbf{r}(\mathbf{m}, \mathbf{u}, \mathbf{d}) = \sum_j \mathbf{c}_j \mathbf{u}_{uj} - \sum_i \mathbf{c}_i \mathbf{d}_{di}$, which describes the interpolation process or $\mathbf{r}(\mathbf{m}, \mathbf{u}, \mathbf{d}) = \mathbf{f}(\mathbf{m}, \mathbf{d})$, which is called equation error.

Definition (Inverse problem – direct formulation)

Given \mathbf{d} , find \mathbf{m}^{dir} such that $\mathbf{r}[\mathbf{m}^{\text{dir}}, \mathbf{g}(\mathbf{m}^{\text{dir}}), \mathbf{d}] = 0$.

This definition implicitly assumes that we neglect:

1. the modelling errors, including discretization and parameterization errors, are negligible, i.e., we assume that (1) describes perfectly the physical phenomenon under study;

2. the forward problem is exactly solved, e.g. no numerical approximation is introduced;
3. the measurement errors are negligible.

When some of these three conditions fail, we cannot guarantee that a solution to the inverse problem exists, in particular this is the case for over-determined problems. Therefore, we are led to the following new definition.

Definition (Inverse problem – indirect formulation)

Given \mathbf{d} and a norm $||\cdot||$, find \mathbf{m}^{ind} such that $|r(\mathbf{m}, \mathbf{g}(\mathbf{m}), \mathbf{d})| \geq |r[\mathbf{m}^{\text{ind}}, \mathbf{g}(\mathbf{m}^{\text{ind}}), \mathbf{d}]| \forall \mathbf{m}$. Typical examples of norms used in practice are the l2 norm, which leads to the least-squares problem, and the l1 norm, which correspond to finding the minimum average absolute error. See, e.g., Menke (1989) for a description of the maximum-likelihood method; in the framework of that method, it is proven that the l2 norm corresponds to the assumption that errors (measurement and modeling errors) follow a gaussian distribution and that the l1 norm is more robust and can account for some outliers in the data set, i.e. few data with a great error.

With the formalism introduced above we can give some important definitions.

Definition (Uniqueness)

Let \mathbf{m} and \mathbf{m}' be two solutions of the inverse problem corresponding to the same data \mathbf{d} ; we say that the solution to the inverse problem is unique if $\mathbf{m} = \mathbf{m}'$.

Definition (Identifiability)

Let \mathbf{m} and \mathbf{m}' be two arrays of model parameters; the problem is identifiable if $\mathbf{g}(\mathbf{m}) = \mathbf{g}(\mathbf{m}')$ implies $\mathbf{m} = \mathbf{m}'$.

Definition (Stability)

Let \mathbf{m} and \mathbf{m}' be two solutions of the inverse problem corresponding to the data \mathbf{d} and \mathbf{d}' , respectively; the solution to the inverse problem is stable if $|\mathbf{d} - \mathbf{d}'| \rightarrow 0$ implies $|\mathbf{m} - \mathbf{m}'| \rightarrow 0$.

Definition (Conditioning)

Let \mathbf{m} and \mathbf{m}' be two solutions of the inverse problem corresponding to data \mathbf{d} and \mathbf{d}' , respectively, such that $|\mathbf{m} - \mathbf{m}'| < C|\mathbf{d} - \mathbf{d}'|$ (Lipschitz condition). We say that the inverse problem is well conditioned if C is small.

In the literature one can find several results for identifiability and uniqueness: for a review see Giudici (2001). Here I spend a few words for stability and conditioning.

Most of the methods applied for computing solutions to the inverse problems consists of applications of continuous operations, so that the stability of the inverse technique is guaranteed. Unfortunately many of the practical inverse problems are often ill-conditioned, so that small errors in the data prevent the effective computation of the inverse solution: this effect is often misinterpreted as an instability of the discrete inverse problem.

Space and time scales and their relation with the stability problem

The space and time scales at which a given process is modelled control the ability of the model to reproduce real features and the discretization of the domain for the numerical model. A necessary condition to be confident on model forecast is that the model scales are consistent with the space and time distribution of the field measurements.

Decreasing the grid spacing can improve the ability of the model to reproduce fine-scale features. However modelling physical processes with a fine grid requires a detailed knowledge of the physical system, which is a difficult task if the natural system is heterogeneous or anisotropic, as is often the case for geological formations or turbulent flows.

Therefore the modeller of the physical system must work with numerical techniques that provide “good solutions” even for grids with “large spacing”.

“Large spacing” means that (1) the grid elements or cells could be larger than the optimal value obtained from the purely mathematical theory, but nevertheless consistent with the distribution of the available measurements and (2) the grid elements could be larger than the volume over which phenomenological laws are validated with laboratory or field experiments. For instance we validate Darcy’s law with samples whose size is of the order of 1 m, whereas typical grid elements for the study of regional ground water flow could have side length of hundreds of meters.

“Good solutions” are those solutions which satisfy the physical principles that are at the base of the model, i.e. the conservation principles.

These remarks have important consequences for model calibration and therefore for the solution to the inverse problem, in particular for the inverse problem in the discrete case, which is the most important for applications. From the above remarks, the following questions arise.

1. Can we use field tests to infer the values of model parameters, even if the relevant scales are often different?
2. Stability is usually an overwhelming problem for continuous domains. Is it a problem also for discrete models? Or does numerical instability arise from ill conditioning? How does ill conditioning depend upon the grid size?

The first question is related to scaling problems, which are discussed in a comprehensive review by Renard and de Marsily (1997) for the study of dynamics of fluids in porous media. Scaling of physical parameters is discussed in relation with measurement scales by Cushman (1986) and Beckie (1996). Some discussions on this topic, connected with the inverse problem, can be found also in Giudici et al. (1995) and Ginn and Cushman (1992), whereas a real case study is presented by Bersezio et al. (1999).

A simple example shows why space and time scales are important for the stability and ill-conditioning problems. The example refers to modelling ground water flow, when typical values of hydraulic gradient are of the order of 10^{-3} .

The accuracy of measuring devices is of the order of 10^{-2} m if measurements are taken manually, whereas it is smaller by one order of magnitude (10^{-3} m) if automatic devices are used (e.g. pressure transducers). However measurement errors are due also to other sources, for instance the presence of pumping wells nearby the piezometers: these errors might be rather great, of the order of 1 m.

The spacing of the discrete grid can vary from 10 m (for applications to small areas, e.g. for site remediation) to 10^2 or even 10^3 m (for regional studies, e.g. ground water management). If we take into account these values of spacing, the head difference between adjacent nodes varies between 10^{-2} m (for local applications) and 1 m (for regional studies).

A direct comparison shows that measurement errors could strongly affect the results of inversion for a local application, whereas they could be less severe for large scale models.

The role of multiple data sets

Several works, dealing with both statistical and deterministic inverse techniques, have shown the importance of using several independent data sets (for both stationary and transient conditions) to reduce uncertainty in the model calibration and validation (Sagar et al., 1975; Carrera and Neuman, 1986; Ginn et al., 1990; Snodgrass and Kitanidis, 1998; Parravicini et al., 1995; Giudici et al., 1995; Vázquez González et al., 1997) for ground water hydrology. This is very important because, in principle, the parameters of the discrete models are non local quantities, in the sense that they depend upon the space distribution in a region wider than the area to which the parameters refers to and on the flow direction. The cartoon in figure 2 shows the distribution of hydraulic conductivity of a real porous medium, estimated by a detailed facies analysis and assigning a single value of hydraulic conductivity to each sedimentary facies.

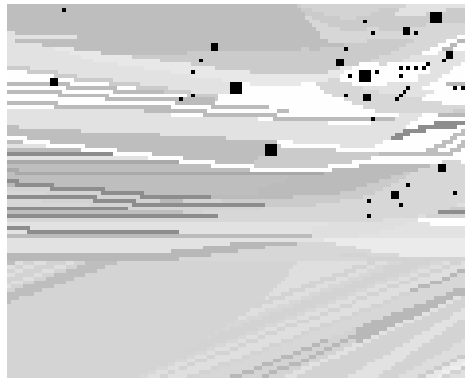


Figure 2 – Hydraulic conductivity distribution of an aquifer analog (Bersezio et al., 1999); hydraulic conductivity is represented with the grey logarithmic scale ranging from 10^{-20} (black) to 10^{-2} (white) m/s.

When the domain is discretised with a grid of cell, several cells will be characterized by non-isotropic physical properties, in general with lower conductivity in the vertical direction. The complete tensor characteristics cannot be obtained from a single flow situation, which will not give information on the direction perpendicular to the actual flow direction. Therefore, parameters obtained from data sets corresponding to different flow situations are more confident and, as a consequence, the use of several independent sets of data improves the reliability of model forecasting.

References

- Beckie R. 1996. Measurement scale, network sampling scale, and groundwater model parameters, *Water Resour. Res.* 32: 65-76.
- Bersezio R., Bini A. and Giudici M. 1999. Effects of sedimentary heterogeneity on groundwater flow in a quaternary pro-glacial delta environment: joining facies analysis and numerical modeling, *Sedimentary Geology* 129: 327-344.
- Carrera J. and Neuman S. P. 1986. Estimation of aquifer parameters under transient and steady-state conditions: 3. application to synthetic and field data, *Water Resour. Res.* 22: 228-242.
- Cushman, J. H. 1986. On measurement, scale, and scaling, *Water Resour. Res.* 22: 129-134.
- Ginn T. R. and Cushman J. H. 1992. A continuous-time inverse operator for groundwater and contaminant transport modeling: model identifiability, *Water Resour. Res.* 28: 539-549.
- Ginn T. R., Cushman J. H. and Houch M. H. 1990. A continuous-time inverse operator for groundwater and contaminant transport modeling: deterministic case, *Water Resour. Res.* 26: 241-252.
- Giudici M. 2001. Development, calibration and validation of physical models, in *Geographic Information Systems and Environmental Modeling* (K. C. Clarke, B. O. Parks and M. C. Krane, Eds.), 100-121, Prentice-Hall, Upper Saddle River (NJ).
- Giudici, M. 2003. Some problems for the application of inverse techniques to environmental modeling, in *Inverse Problems: Theory and Applications* (G. Alessandrini and G. Uhlman, Eds.), vol. 333 *Contemporary Mathematics*, American Mathematical Society.
- Giudici M., Morossi G., Parravicini G. and Ponzini G. 1995. A new method for the identification of distributed transmissivities, *Water Resour. Res.* 31: 1969-1988.
- Griffiths D.H. and Barker R.D. 1993. Two-dimensional resistivity imaging and modeling in areas of complex geology, *Journal of Applied Geophysics*, 29: 211-226.
- Loke M.H. and Barker R.D. 1996. Practical techniques for 3D resistivity surveys and data inversion, *Geophysical Prospecting*, 44: 499-524.

- Menke W. 1987. Geophysical data analysis: discrete inverse theory, Academic Press, San Diego, 1989.
- Nolet G. (ed.) 1987. Seismic tomography: with applications in global seismology and exploration geophysics, D. Reidel Pub Co.
- Parravicini G., Giudici M., Morossi G. and Ponzini G. 1995. Minimal a priori assignment in a direct method for determining phenomenological coefficients uniquely, *Inverse Problems* 11: 611-629.
- Renard P. and Marsily G. de 1997. Calculating equivalent permeability: A review, *Adv. Water Res.* 20: 253-278.
- Sagar B., Yakowitz S. and Duckstein L. 1975. A direct method for the identification of the parameters of dynamic non-homogeneous aquifers, *Water Resour. Res.* 11: 563-570.
- Snodgrass M. F. and Kitanidis P. K. 1998. Transmissivity identification through multi-directional aquifer stimulation, *Stochastic Hydrology and Hydraulics* 12: 299-316.
- Vázquez González R., Giudici M., Parravicini G. and Ponzini G. 1997. The differential system method for the identification of transmissivity and storativity, *Transport in Porous Media* 26: 339-371.

Percolation Theory and its Application for Interpretation of Soil Water Retention Curves

Radka Kodesová (Rösslerová)¹

*Department of Soil Science and Geology, Czech University of Agriculture,
Prague, Czech Republic*

*Lecture given at the
College on Soil Physics
Trieste, 3-21 March 2003*

LNS0418019

¹ kodesova@af.czu.cz

Abstract

The soil porous system has traditionally been deduced from the soil-water retention curve with the assumption of homogeneity and free accessibility of pores, defined as capillary tubes, from the sink/source of water. But real soil fabric is mostly characterized by aggregates. In this case, the soil porous system cannot be modeled as a homogeneous one. To examine the differences between homogeneous and heterogeneous soil porous systems, we studied two types of soils: sandy soil and coarse sandy soil. We applied image processing filters and the ARC/INFO Grid module to analyze pore sizes in both soils from their electron microscope images taken at two different magnifications. We used the resulting pore-size distribution data to generate 3-D porous media consisting of pores and throats. The homogeneous pore structure was created as a mono-modal pore-throat network with one pore-size distribution. The heterogeneous pore structure was designed as a bi-modal pore-throat network with two pore-size distributions, where the pore sizes were hierarchically arranged in the nodes of the network. We applied the percolation model to simulate water and air displacement in these networks. The distribution of water in the nodes of the networks was studied for several increasing/decreasing steps of pressure head and the drainage and wetting branches of the retention curves were evaluated. The soil-water retention curves modeled for the mono-modal and bi-modal porous systems had different characters. The simulated shape of the retention curve in the mono-modal case was close to the step-like form of a retention curve characteristic of unstructured soil. The shape of the simulated retention curve in the bi-modal case was smoother, more gradual, and closer to the shape of the retention curve of a real, structured soil.

Introduction

The retention curve (i.e., relationship of soil water content θ to pressure head h [L]) is one of the hydraulic characteristics of soil. To understand hydraulic processes in porous media it is necessary to physically explain this relationship. Several models of porous media have been designed for this purpose. These models are based on the capillary behavior of porous materials. The simplest model consists of parallel capillary tubes, but the real geometry of porous systems plays a key role, especially in the case of hysteresis of the retention curve. A porous medium can be considered as a system of directly connected capillary tubes or as a system of pores connected by throats. To study the displacement of two immiscible phases in such a system and find the capillary pressure curve, the mathematical percolation theory developed in statistical physics [Stauffer, 1985] was applied by Chatzis and Dullien [1985], Diaz *et al.* [1987], Li *et al.* [1986], Jerauld and Latter [1990], Ferrand and Celia [1992] and Rösslerová [1992a; 1992b; 1992c]. The porous media have been mostly modeled as regular, rectangular, 2-D or 3-D networks of pores and throats. Lowry and Miller [1995] developed a random network approach, which provided a 3-D network with stochastic geometry and variable connectivity.

To test percolation theory, two-phase displacement processes were originally examined on micromodels [McKellar and Wardlaw, 1982; Wardlaw and Li, 1988] and in a pore system created by glass particles [Wardlaw and McKellar, 1985]. A three-fluid porous media system was designed by Soll *et al.* [1993]. In a real soil porous system, a two-phase distribution at a given level of wetting and nonwetting saturation is only possible to study on thin sections of soil using the Wood's metal method [Yadav *et al.*, 1987; Dullien, 1991].

To simulate capillary pressure curves for a real porous material with a percolation model, the pore-size distribution and arrangement of pore sizes in space (i.e., in the nodes of the network) must be defined. The pore volume can be studied directly using Wood's metal porosimetry with an optical microscope or with an electron microscope [Dullien, 1981; Dullien and Dhawan, 1975; Wardlaw *et al.*, 1987; 1988]. Rösslerová and Kodes [1996] analyzed electron microscope images of soil fracture planes.

Percolation studies have shown that it is necessary to investigate the correlation between neighboring pores and throats. Pore bodies have been usually described as spheres and throat bodies as tubes. The relationship between sizes of pores and throats, commonly expressed as diameters or radii, has been studied by Mohanty and Salter [1982], who used a 3-D model in which 50% of pores had uncorrelated pore throats and 50% had directly connected throats of identical size. Chatzis and Dullien [1985] developed a network model in which the size of a throat connecting two neighboring pores was correlated with the size of the smaller pore. Li *et al.* [1986] proposed a model with throat sizes which were correlated to the size of both adjoining pores. Reeves and Celia [1996] defined pore bodies as spheres and throats as biconical tubes with constrictions located at the midpoint between pore

body centers, and studied the influence of fluid-fluid interfacial area. *Ioannidis et al.* [1993] used the bond-correlated site-percolation model proposed by *Chatzis and Dullien* [1985] and applied spectral methods to generate networks in which the sites were spatially correlated according to exponential or Gaussian autocovariance functions. *Rösslerová* [1992a; 1992b; 1992c] presented a network with randomly generated pore and throat sizes that were correlated to the sizes of adjoining pores as proposed by *Li et al.* [1986]. The percolation model for simulation of soil-water retention curves was tested for an unstructured material defined as homogenous mono-modal porous systems and for normal and log-normal pore-size distributions. The model was then applied for a hypothetical structured material, characterized as a heterogeneous bi-modal porous system. This system included pores with two pore-size distributions. The pore sizes were arranged hierarchically in the nodes of the network. The importance of the introduction of bi-modality to the simulation of the retention curve was also discussed by *Kutílek et al.* [1992].

Rösslerová-Kodesová and Kodes [1999] presented application of percolation model [*Rösslerová*, 1992a] with consideration of mono-modal and bi-modal soil-porous system theory for real soil-porous media. For this purpose we studied two types of real soils: a homogeneous soil - sandy soil, and a heterogeneous one - coarse sandy soil. We presented a simple procedure to obtain pore-size distribution data from a given electron microscope image of an investigated soil using image processing filters and the ARC/INFO Grid module. On images of these two soils we demonstrated the difference between mono-modal and bi-modal soil-porous systems. We explained the construction of mono-modal and bi-modal porous 3-D networks consisting of pores and throats. We then used pore-size distribution data resulting from soil-porous system analysis to generate pore sizes for the nodes of the designed networks. Finally we presented some simulation results of the percolation model. Selected results of our work are presented here.

Methods

Percolation Model

The system of void spaces of a porous medium is described as a network of pores and throats. Pores are situated in nodes of a rectangular, regular, 3-D network. Bonds of the network are defined as throats (constrictions) between pores. Pores and throats are described as spherical and capillary elements, respectively. The volume of each element is specified by the equivalent radius of the pore, R_p [L], or throat, R_t [L]. The pore radii are generated independently of the throat radii at the nodes of the network. The throat radii can also be independently generated, or evaluated according to the following equation [*Li et al.*, 1986]:

$$R_t = C R_{p1} R_{p2} / R_{pmax} \quad (1)$$

where R_{p1} [L] and R_{p2} [L] are the radii of neighboring pores, R_{pmax} [L] is the largest pore radius in the network and C is an empirical factor. In the version of the simulation program presented here, (1) is used to obtain the throat radii with $C = 1$.

The definitions of boundaries in the 3-D network arise from the common drainage and wetting experiment used for determination of the soil-water retention curve, when a core sample is placed in a Tempe pressure cell. The sides of the network are impermeable to water and air. The top is the source (sink) of air and the bottom is the sink (source) of water.

Drainage and imbibition processes are simulated in sequential steps of increasing/decreasing pressure heads, h_i [L]. The water and air displacement process is controlled by the following equation:

$$h_i = (2 \sigma \cos \gamma) / (\rho_w g R_{Mi}) \quad (2)$$

where γ [MT⁻²] is the interfacial tension, σ the contact angle, g [LT⁻²] the gravitational constant, ρ_w [ML⁻³] the density of water, and R_{Mi} [L] the equivalent radius of the capillary tube, i.e., throat or pore.

The pressure head steps h_i or radius steps R_{Mi} can be defined by the user directly, or automatically determined by the simulation program from pore-size distribution data with the assumption of a uniform frequency distribution of throats or pores [Li *et al.*, 1986]. In this case, the throat/pore radii are ordered sequentially and divided into intervals of uniform frequency. The radius steps, R_{Mi} , for the drainage/imbibition process are then defined as the smallest/largest radii of the throats/pores in these intervals.

During the drainage process, water in an element with a radius larger than R_{Mi} is displaced by air if it is connected by a continuous path of water and a continuous path of air to the boundaries defined as the sink of water and the source of air, respectively. Similarly, during the imbibition process, air in an element with a radius smaller than R_{Mi} is displaced by water if it is connected by a continuous path of water and a continuous path of air to the boundaries defined as the source of water and the sink of air, respectively.

An element is accessible from boundaries of both phases (i.e., there are paths to the boundaries) if it is situated at the border between an infinite domain of air and an infinite domain of water. The simulation process is based on displacement of these two infinite domains. A domain is a region of pores and throats, which is occupied by a continuous cluster of air or water. A domain is infinite if it is connected to its own source (sink) boundary. A phase in a finite domain, which is disconnected from its source, cannot be extended into the other elements connected to this domain. A phase in a finite domain, which is disconnected from its sink, cannot be removed from the system.

In the case of a real soil porous material, thin layers of water maintain a connection of water in the system. The percolation model accounts for this during

drainage. Thus, a pore can be empty, but the neighboring throats containing water maintain a connection, due to the thin layer of water on the sides of the pore.

The distribution of phases during drainage or imbibition is found by an iterative process for each pressure head step. To obtain a point of the retention curve, the relative water content Θ is evaluated at the end of each iteration. The relative water content Θ is the sum of the volumes of elements containing water divided by the sum of the volumes of all elements in the network. The volumes of the throats S_T [L³] and pores S_P [L³] are calculated according to the following equations [Diaz *et al.*, 1987]:

$$S_T = l_T (R_T)^2 \quad (3a)$$

$$S_P = l_P (R_T)^2 \quad (3b)$$

where l_T [L] and l_P [L] are empirical parameters ($l_T = l_P = 1$).

Pore-Size Analysis

Two types of soils were investigated: a homogeneous porous system - a sandy soil (Sample A) and a heterogeneous porous system - a coarse sandy soil (Sample B). Sample A was taken at the Hupselse Beek experimental area in the Netherlands. Sample B was taken at an experimental area in the Šumava Mountains in the Czech Republic. Information about these soils and their hydraulic properties were presented by Císlarová *et al.* (1990) and Císlarová *et al.* (1988), respectively.

The composition of pores of these soils was studied with an electron microscope. Fracture planes of the soil samples were prepared according to the technique described by Werner *et al.* [1991]. Images of the fracture planes were taken at several magnifications. Two images for each soil, A1, A2 and B1, B2, were found to be sufficient to describe the structure of these soils. The images were scanned and saved as grayscale TIFF images at a resolution of 200x200 dpi. To detect pores, image-processing filters were used. In the first step, the darkest pixels in a particular range of grayscale (from black to a certain threshold level of gray) were considered as possible pores. A sensitivity analysis was done and finally the threshold for each image was determined subjectively. The resulting images were converted to black and white images. Potential disturbances were partially eliminated by proper image filters, which removed black and white regions smaller than two pixels in size. The processed black and white TIFF images were converted into ARC/INFO grids. To analyze pore sizes, the ARC/INFO GRID Region group function was applied. The areas of pores, given by the number of cells multiplied by cell-size, were then used as inputs to calculate the equivalent pore radii. The equivalent pore radii were evaluated with the assumption that existing regions could be substituted by circles of the same area. A log-normal probability density function was used to describe the pore-size distribution curves pertaining to images A1, A2, B1, and B2:

$$f(x) = \frac{1}{\sqrt{2\pi}\sigma} e^{-\frac{[\ln(x)-\mu]^2}{2\sigma^2}} \quad (4)$$

where μ is the mean and σ the standard deviation.

Model Application

The percolation model was then applied for the two soil porous systems to simulate soil-water retention curves. The network dimensions in both cases were 50 nodes in the X- and Y-axis directions, and 55 nodes in the Z-axis direction, where X and Y were horizontal axes and Z was the vertical axis of the coordinate system. The homogeneous porous system was created for Sample A - sandy soil. The pore sizes were randomly generated into the nodes of the network using pore-size distribution A1. The heterogeneous porous system was designed for Sample B - coarse sandy soil. The pore sizes were hierarchically located in the nodes of the network using two pore-size distributions, B1 and B2. The bi-modal pore-size matrices used in the earlier studies (Rösslerová, 1992a; 1992c) were composed as regular systems of cube aggregates (peds) and the spaces between them. Inside the entire network region, subregions designed as identical cubes were defined. Subregions of spaces of the same width were set between the cubic subregions. A random number generator was used to input the pore sizes into the nodes of each subregion. Smaller pores were situated in the nodes of the cubic subregions and larger pores were placed in nodes of subregions of spaces. Sensitivity studies showed that the simulated slope of the retention curve and relative residual water content increased with a decrease in space size and an increase in cube size. To reduce the influence of a preconditioned regular cubic structure in this study, the porous medium was created by variably-sized blocks and porous spaces between the blocks. The pore sizes were again randomly generated inside the blocks and between blocks using pore-size distribution B2, and pore-size distribution B1, respectively. Throat sizes were correlated to pore sizes according to (1) in both cases.

The first and second drainage branches and the first wetting branch of the retention curves were simulated with the percolation model for each pore-throat network. At the beginning of the simulation the systems of pores and throats were fully saturated. Then sequential steps of increasing/decreasing pressure heads, h_i , were applied. The h_i values were automatically calculated by the simulation program from determined pore and throat-size data, respectively. In (2) the contact angle γ was set equal 0, and values for the interfacial tension, σ , and the density of water, ρ_w , were taken for a temperature of 20°C. The distributions of water and air in the system were exactly defined by the percolation model for each pressure head step.

Results and Discussion

Pore-Size Analysis

Images of the investigated soils (presented in *Rösslerová-Kodesová and Kodes, 1999*) were taken at four different magnifications. One image was taken for the sandy soil and two images were taken for the coarse sandy soil at each magnification. The images of the sandy soil demonstrate that the soil porous material is mainly made up of single, almost spherical, different size particles. Images further show the presence of some organic material. Images at two scales (labeled as A1 and A2) were chosen to analyze the porous structure of this soil. The evaluated pore-size distribution functions, A1 and A2, (Table 1) for both scales are very similar. Results for Sample A indicate homogeneity of the porous system typical of unstructured soils. In addition, it is obvious that the image scale did not have a significant influence on the evaluated pore-size distribution describing this porous system. Images of the coarse sandy soil demonstrate the presence of different types of soil particles and organic material. The soil porous material is composed of peds (aggregates). Interpedal pores exist between peds, and intrapedal pores are present inside the peds. The soil porous system was designed as bi-modal, and again, only two images (labeled as B1 and B2) were analyzed. The sizes of the interpedal pores were examined on B1 and the sizes of intrapedal pores were studied on B2 (Table 1). The pore sizes inside the peds are considerably smaller than the pore sizes between the peds.

Table 1. The parameters of the log-normal pore-size distributions A1, A2, B1, and B2 evaluated for images A1 and A2 of Sample A - sandy soil, and images B1 and B2 of Sample B - coarse sandy soil.

Sample Image	Pore Radius Mean [cm]	Std. Deviation [cm]
Sandy Soil - A1	9.93×10^{-4}	12.15×10^{-4}
Sandy Soil - A2	5.64×10^{-4}	6.53×10^{-4}
Coarse Sandy Soil - B1	15.09×10^{-4}	12.84×10^{-4}
Coarse Sandy Soil - B2	0.211×10^{-4}	0.261×10^{-4}

Results for Sample B prove heterogeneity of this porous system characteristic of structured soils. The images and the evaluated pore-size distributions A1, A2, B1 and B2 clearly demonstrate the differences between the porous systems of the examined soil samples. The mean of the larger pore sizes (B1) of the coarse sandy soil is higher than the mean of the pore sizes of the sandy soil (A1, A2), but the standard deviations are almost the same as A1. The mean of pore sizes (B2) inside the aggregates is approximately 50 times lower than the mean of pore sizes (B1) between the aggregates.

Simulation Results

Results of the percolation model are discussed in *Rösslerová-Kodesová and Kodes [1999]*. Only the fractions of pores and throats occupied by water and relative water content at the end of drainage process and at the end of wetting process are presented here in Table 2. After drainage, water was trapped randomly in the few smallest pores (nodes) of the network for the mono-modal porous system. The fraction of pores occupied by water was 0.7 %. In the case of the bi-modal soil porous system, water was isolated in the pores of the block aggregates. The fraction of pores occupied by water was considerably higher (33.9%). On the other hand, after imbibition, water filled 73.9 % of pores for the mono-modal case and air was again trapped randomly in the largest network pores. In the bi-modal case, water filled 88.9 % of pores, and air was trapped in the spaces between the aggregates. This shows the relative continuity of the phases during the displacement process in the mono-modal case, and discontinuity of phases in the bi-modal case.

Table 2. Fraction of throats occupied by water residual, $f(R_{Twp})_r$, and resaturated, $f(R_{Twp})_s$, fraction of pores occupied by water residual, $f(R_{Pwp})_r$, and resaturated, $f(R_{Pwp})_s$, residual, Θ_r , and resaturated, Θ_s , water content.

	Sample A Sandy Soil	Sample B Coarse Sandy Soil
$f(R_{Twp})_r$ [%]	11.65	37.10
$f(R_{Twp})_s$ [%]	93.61	96.96
$f(R_{Pwp})_r$ [%]	0.74	33.90
$f(R_{Pwp})_s$ [%]	73.91	88.90
Θ_r [%]	0.21	0.34
Θ_s [%]	46.60	48.00

The shape of the retention curve [Rösslerová-Kodesová and Kodes, 1999] simulated for the mono-modal porous system is similar to the step-like form characteristic of unstructured soils, while that of the bi-modal porous system is closer to the retention curve of a real structured soil. In the case of the bi-modal system, the slope of the retention curve and the relative residual water content did not increase as much as was found in previous studies (Rösslerová, 1992a; 1992c), due to the considerable difference between the pore-size distributions B1 and B2 and the irregularity of the block system. The retention curves for the mono-modal and bi-modal networks are shifted according to the mean radius size of the A1 and B1 pore-size distributions. The slopes interior parts of the curves are similar due to the similarity of the standard deviations of the A1 and B1 pore-size distributions. As shown previously, (Rösslerová, 1992a; 1992c), a log-normal distribution of pore sizes increases the size of the hysteresis loops with respect to that of a normal pore-size distribution, due to the relationship of R_T to R_p . In addition, the log-normal distribution causes a low relative water content at the end of imbibition because of air trapped in the largest pores at the last step of the simulation. These effects become even more significant when the standard deviation for the pore-size distribution increases. Despite the fact that the larger pores have a dominant influence on the shape of the Sample B retention curve, and that some similarities to the Sample A retention curve were found, the resulting retention curves have different characters. The Sample B retention curve is smoother and slightly more gradual than the Sample A retention curve. The relative residual water content of Sample B is higher than that of Sample A, due to trapped water in the pores inside of the block aggregates. The relative resaturated water content of Sample B is higher than that of Sample A, because air was trapped in few pores inside of the regions between the aggregates.

Conclusions

The percolation model briefly described here was tested for real soil-porous media. For this purpose, two soil porous systems were examined: an unstructured soil - sandy soil and a structured soil - coarse sandy soil. The evaluated pore-size distributions were considerably different. The necessity of two approaches for describing soil-porous systems was confirmed. Two pore-size networks were generated to represent the two types of soil-porous systems. One mono-modal porous system and one bi-modal porous system with hierarchically composed pore-sizes were introduced. The different courses of displacement of water and air simulated for these two porous systems were documented. Water distributions at two limiting states for the bi-modal porous system clarified the discontinuity effect of these phases in structured soils. The drainage and wetting branches of the soil water-retention curves modeled for the mono-modal and bi-modal porous systems had different characters. The shapes of the simulated retention curves for the mono-modal and bi-modal porous systems were similar to the retention curve shapes of the real unstructured and structured soils, respectively.

Remark

Overview of different percolation models is presented for instance in *Characterization and Measurement of the Hydraulic Properties of Unsaturated Porous Media*, eds. van Genuchten, M. Th., and F. J. Leij, University of California, Riverside, 1999.

References

- Cislerová, M., J. Šimůnek, and T. Vogel, Changes of steady-state infiltration rates in recurrent ponding infiltration experiments, *J. of Hydrology*, 104, 1-16, 1988.
- Cislerová, M., T. Vogel, and J. Šimůnek, The infiltration-ouflow experiment used to detect flow deviations, *Proc. Field-Scale Solute and Water Transport Through Soils* eds. K. Roth, H. Fluhler, W. A. Jury and J. C. Parker, Birkhauser Verlag, Basel, 109-117, 1990.
- Chatzis, I., and F. A. L. Dullien, Modelling pore structure by 2-D and 3-D networks with application to sandstones, *J. Can. Pet. Technol.*, 16(1), 97-108, 1977.
- Chatzis, I., and F. A. L. Dullien, The modelling of mercury porosimetry and relative permeability of mercury in sandstones using percolation theory, *Int. Chem. Eng.*, 25(1), 47-66, 1985.
- Diaz, C. E., I. Chatzis, and F. A. L. Dullien, Simulation of capillary pressure curves using bond correlated site percolation on simple cubic network, *Transp. Porous Media*, 2, 245-240, 1987.
- Dullien, F. A. L., and G.K. Dhawan, Bivariate pore-size distribution of some sandstones, *J. Coll. Interface Sci.*, 52, 129-135, 1975.
- Dullien, F. A. L., Wood's metal porosimetry and its relation to mercury porosimetry, *Powder Tech.*, 29, 109-116, 1981.

- Dullien, F. A. L., Characterization of porous media - pore level, *Transp. Porous Media*, 6, 581-606, 1991.
- Ferrand, L. A. and M. A. Celia, The effects of heterogeneity on the drainage capillary pressure: Saturation relations, *Water Resour. Res.*, 28(3), 859-870, 1992.
- Ioannidis, M.A., I. Chatzis, and E. A. Sudicky, The effect of spatial correlations on the accessibility characteristics of three-dimensional cubic network as related to drainage displacements in porous media, *Water Resour. Res.*, 29(6), 1777-1785, 1993.
- Jerauld, G. R., and S. J. Latter, The effect of pore-structure on hysteresis in relative permeability and capillary pressure: pore-level modelling, *Transp. Porous Media*, 5, 103-151, 1990.
- Kutílek, M., R. Rösslerová, and H. Othmer, Models of soil porous systems for unsaturated flow, *Proc. Colloquium Porous or Fractured Unsaturated Media: Transport and Behavior*. Swiss Federal Institute of Technology of Lausanne (EPFL) and University of Neuchatel, 71-86, 1992.
- Li, Y., W. G. Laidlaw, and N. C. Wardlaw, Sensitivity of drainage and imbibition to pore structures as revealed by computer simulation of displacement process, *Adv. Colloid Interface Sci.*, 26, 1-68, 1986.
- Lowry, M. I. and C. T. Miller, Pore-scale modeling of nonwetting-phase residual in porous media, *Water Resour. Res.*, 31(3), 455-473, 1995.
- McKellar, M., and N. C. Wardlaw, A method of making two-dimensional glass micromodel of pore systems, *J. Can. Petrol. Technol.*, 21(4), 39-41, 1982.
- Mohanty, K. K., and S. J. Salter, Multiphase flow in porous media: II. Pore-level modeling, S.P.E. 11018, *57th Annual Technical Conference*, Dallas, 1-21, 1982.
- Reeves, P. C. and M. A. Celia, A functional relationship between capillary pressure, saturation, and interfacial area as revealed by pore-scale network model, *Water Resour. Res.*, 32(8), 2345-2358, 1996.
- Rösslerová, R., Percolation models - Application for interpretation of soil water retention curves (in Czech), PhD Thesis, Czech Technical University, Prague, 1992a.
- Rösslerová, R., Percolation theory - Application for determination of retention curves of soil moisture content: 1. Model. (in Czech) *Vodohosp. Čas.*, 40, 425-434, 1992b.
- Rösslerová, R., Percolation theory - Application for determination of retention curves of soil moisture content: 2. Description of homogeneous and heterogeneous porous systems. (in Czech) *Vodohosp. Čas.*, 40, 435-445, 1992c.
- Rösslerová, R., and V. Kodes, The use of GIS in percolation study of soil porous system, *Proc. HydroGIS 96, Application of geographic information systems in hydrology and water resources management*, eds. K. Kovar and H. P. Nachtnebel, IAHS, Vienna, pp. 259-265, 1996.
- Rösslerová-Kodesová R. and V. Kodes, Percolation model for interpretation of moisture retention curves for mono-modal and bimodal soil porous system,

- In: *Characterization and Measurement of the Hydraulic Properties of Unsaturated Porous Media*, eds. van Genuchten, M. Th., and F. J. Leij, University of California, Riverside, 527-539, 1999.
- Soll, W. E., M. A. Celia, and J. L. Wilson, Micromodel studies of three-fluid porous media system: Pore-scale processes relating to capillary pressure-saturation relationship, *Water Resour. Res.*, 29(9), 2963-2974, 1993.
- Stauffer, D., *Introduction to Percolation Theory*, Taylor & Francis, London and Philadelphia, 1985.
- Wardlaw, N. C., and M. McKellar, Oil blob population and mobilization of trapped oil in unconsolidated packs, *Can. J. Chem. Eng.*, 63, 525-532, 1985.
- Wardlaw, N. C., Y. Li, and D. Forbes, Pore-throat size correlation from capillary pressure curves, *Transp. Porous Media*, 2, 597-614, 1987.
- Wardlaw, N. C., and Y. Li, Fluid topology, pore size and aspect ratio during imbibition, *Transp. Porous Media*, 3, 17-34, 1988.
- Wardlaw, N. C., M. McKellar, and Y. Li, Pore and throat size distributions determined by mercury porosimetry and by direct observation, *Carbonates and Evaporites*, 3(1), 1-15, 1988.
- Werner, D., P. Paris, and A. Rudiger, The influence of electron beams on soil structure (Zum Einfluss des Radschlupfes auf das Bodengefüge), *Mitt. D. Dtschl. Bodenkundl. Gesellsch.*, 66, 249-253, 1991.
- Yadav, G. D., F. A. L. Dullien, I. Chatzis, and I. F. MacDonald, Microscopic distribution of wetting and nonwetting phases during immiscible displacement, *SPE Reservoir Eng.* 2, 137-145, 1987.

Determination of Hydraulic Properties of Unsaturated Soil via Inverse Modeling

Radka Kodesová¹

*Department of Soil Science and Geology, Czech University of Agriculture,
Prague, Czech Republic*

*Lecture given at the
College on Soil Physics
Trieste, 3-21 March 2003*

LNS0418020

¹ kodesova@af.czu.cz

Abstract

The method for determining the hydraulic properties of unsaturated soil with inverse modeling is presented. A modified cone penetrometer has been designed to inject water into the soil through a screen, and measure the progress of the wetting front with two tensiometer rings positioned above the screen. Cumulative inflow and pressure head readings are analyzed to obtain estimates of the hydraulic parameters describing $K(h)$ and $\theta(h)$. Optimization results for tests at one side are used to demonstrate the possibility to evaluate either the wetting branches of the soil hydraulic properties, or the wetting and drying curves simultaneously, via analysis of different parts of the experiment. The optimization results are compared to the results of standard laboratory and field methods.

Introduction

The soil-moisture characteristic $\theta(h)$ and hydraulic conductivity $K(h)$ curves are two basic hydraulic properties of soils. Current direct laboratory and in-situ methods for their determination are often time consuming and costly. Parameter optimization is an indirect approach that makes it possible to obtain $K(h)$ and $\theta(h)$ simultaneously from transient flow data [Kool *et al.*, 1987]. In this case, a flow event is modeled with an appropriate governing equation and analytical expressions of $K(h)$ and $\theta(h)$. The unknown parameters of $K(h)$ and $\theta(h)$ are obtained by minimization of an objective function describing the differences between some measured flow variables and those simulated with a numerical flow code. This methodology was originally applied to laboratory one-step column outflow data [Kool *et al.*, 1985; Parker *et al.*, 1985; van Dam *et al.*, 1992] and multi-step column outflow data [van Dam *et al.*, 1994; Echling and Hopmans, 1993; Echling *et al.*, 1994]. Parameter estimation has also been used with data obtained with the evaporation method (see for example, Santini *et al.*, [1995]; Ciollaro and Romano [1995]; Simunek *et al.* [1998a]). All of these laboratory methods provide information about the drying branches of the soil-moisture characteristics.

For field determination of the wetting branches of soil hydraulic properties, parameter estimation methods were applied to ponded infiltration flow data [Russo *et al.*, 1991; Bohne *et al.*, 1992], and tension disc infiltrometer flow data [Simunek and van Genuchten, 1996; 1997; Simunek *et al.*, 1998b]. Another technique for gaining information about the drying branches of the soil hydraulic properties via multi-step soil water extraction and parameter optimization was developed by Inoue *et al.* [1998]. The field methods described above are applicable only in the near surface. Gribb [1996] proposed a new cone penetrometer tool (e.g., cone permeameter) and use of parameter optimization to estimate soil hydraulic properties at depth. A prototype was further developed by Leonard [1997]. A detailed description of the prototype, and its use under saturated and unsaturated conditions were previously presented by Gribb *et al.* [1997]. The cone permeameter is placed in the soil, and a constant head of water is then supplied to the 5-cm long screen. Cumulative inflow volume is determined from scale readings of the mass of water removed from the source. Progress of the wetting front is measured with tensiometer rings 5 and 9 cm above the screen. After the water supply valve is closed, the tensiometers monitor the redistribution of water in the soil profile. Kodesová *et al.* [1998] discussed results of the numerical analysis of data from the wetting parts of cone experiments which were performed for one type of soil but under different initial and boundary conditions. Simunek *et al.* [1999] finally examined both the wetting and redistribution parts of cone permeameter experiments to find the wetting and drying branches of the soil hydraulic properties. Kodesová *et al.* [1999] presented results of field testing in two types of sandy soil. Test procedure and results from one side are briefly discussed here.

Theory

Flow Equation

The governing flow equation for radially symmetric, isothermal Darcian flow in an isotropic, rigid porous medium, assuming that the air phase plays an insignificant role in the liquid flow process is (Richards, 1931):

$$\frac{1}{r} \frac{\partial}{\partial r} \left[r K \frac{\partial h}{\partial r} \right] + \frac{\partial}{\partial z} \left[K \left(\frac{\partial h}{\partial z} + I \right) \right] = \frac{\partial \theta}{\partial t}$$

where r is the radial coordinate [L], z the vertical coordinate positive upward [L], t the time, h the pore water pressure head [L], K the unsaturated hydraulic conductivity [LT^{-1}], and θ the volumetric moisture content [L^3L^{-3}].

Soil Hydraulic Properties Functions

The *van Genuchten* (1980) expressions for moisture content and hydraulic conductivity, $\theta(h)$ and $K(\theta)$, are used in this work:

$$\theta_e = \frac{\theta(h) - \theta_r}{\theta_s - \theta_r} = \frac{1}{\left(1 + |\alpha h|^n\right)^m}, \quad h < 0$$

$$\theta_e = 1, \quad h \geq 0$$

$$K(\theta) = K_s \theta_e^{0.5} \left[1 - \left(1 - \theta_e^{1/m} \right)^m \right]^2, \quad h < 0$$

$$K(\theta) = K_s, \quad h \geq 0$$

where θ_e is the effective moisture content [L^3L^{-3}], K_s is the saturated hydraulic conductivity, θ_r and θ_s are the residual and saturated moisture contents [L^3L^{-3}], respectively, and α [L^{-1}], n and m ($= 1 - 1/n$) are empirical parameters. The equations contain 5 unknown parameters: K_s , θ_r , θ_s , α and n .

Objective Function

To derive estimates of the hydraulic parameters using parameter optimization, an objective function Φ expressing the differences between flow responses measured

with the permeameter and those predicted by a numerical model with hydraulic

$$\Phi(b, q, p) = \sum_{j=1}^{m_q} v_j \sum_{i=1}^{n_{qj}} w_{i,j} [q_j^*(x, t_i) - q_j(x, t_i, b)]^2 + \sum_{j=1}^{m_p} v_j \sum_{i=1}^{n_{pj}} w_{i,j} [p_j^*(\theta_i) - p_j(\theta_i, b)]^2$$

parameter inputs, is minimized:

where the first term on the right-hand side represents deviations between measured and predicted space-time variables (e.g., observed pressure heads or moisture contents at different locations and/or times, or the cumulative infiltration rate versus time). In this term, m_q is the number of different sets of measurements, and n_{qj} is the number of measurements in a particular measurement set. Specific measurements at time t_i for the j th measurement set at location $x(r, z)$ are represented by $q_j^*(x, t_i)$, $q_j(x, t_i, b)$ are the corresponding model predictions for the vector of optimized parameters b (e.g., θ_r , θ_s , α , n , K_s), and v_j and $w_{i,j}$ are weights associated with a particular measurement set or point, respectively. The weighting factor v_j is given by the inverse of the number of measurements multiplied by the variance of those observations, and $w_{i,j}$ is equal to 1 in this work. The second term represents differences between independently measured and predicted soil hydraulic properties (e.g., $\theta(h)$, $K(\theta)$ or $K(h)$ data), while the terms m_p , n_{pj} , $p_j^*(\theta_i)$, $p_j(\theta_i, b)$, v_j and $w_{i,j}$ have similar meanings as for the first term, but are now for the soil hydraulic properties.

Field Testing of the Cone Permeameter (Poinsett State Park, South Carolina)

Test Procedure

- ◆ 4 Guelph permeameter tests for determining field saturated hydraulic conductivities were performed.
- ◆ Soil anchors were placed into the Guelph test holes and the insertion frame was secured.
- ◆ The soil core sampler was then inserted. Soil samples of known volume were removed from the barrel of the core sampler. Measured volumetric moisture contents were paired with initial cone permeameter tensiometer readings and used in the inversion process as known points of the retention curve, $\theta(h)$.
- ◆ The cone permeameter was inserted into the core sampler hole.
- ◆ A constant head (in one or two steps) was then applied to the 5-cm long screen to inject water into the soil. 5 Tests were performed:
 - A, B, C with applied pressure heads of 30 and 50 cm
 - D with applied pressure heads of 21 and 108 cm
 - E with applied pressure heads of 21 and 80 cm
- ◆ Cumulative inflow volume was measured.
- ◆ The advance of the wetting front was detected as pore water pressure increases were measured with tensiometer rings 5 and 10 cm above the screened section.

- ◆ The redistribution of water in the soil profile was monitored with tensiometers after the source of water was shut off.
- ◆ Undisturbed soil samples were taken near the permeameter for pressure plate, hanging column, and falling head permeability tests to determine the drying soil-moisture characteristic curves and saturated hydraulic conductivities.
- ◆ An inverse solution method was used to predict the soil hydraulic properties.
- ◆ Independent measurements were carried out:
 - Retention curve:
 - Pressure plate test
 - Capillary rise test
 - Hanging column test
 - Saturated hydraulic conductivity:
 - Guelph permeameter test (mentioned before)
 - Falling head permeability tests

Inverse Simulations

- ◆ Inverse simulation was performed to obtain parameters of *van Genuchten* (1980) expressions for $K(h)$ and $\theta(h)$. The unknown parameters of $K(h)$ and $\theta(h)$ were obtained by minimization of an objective function describing the differences between some measured flow variables and those simulated with a numerical flow code HYDRUS-2D (*Simunek et al.*, 1996)
- ◆ Inputs were:
 - cumulative inflow
 - pressure heads at two locations
 - point of the retention curve given by initial moisture content and initial tensiometer reading at the corresponding depth
- ◆ Performed inverse solutions:
 - one-step test, applied pressure head of 30 (or 21) cm
 - two-step test, applied pressure heads of 30 and 50 (or 21 and 108, 21 and 80) cm
 - three-step test, two applied pressure heads and redistribution
- ◆ Obtained results:
 - wetting soil hydraulic properties
 - wetting soil hydraulic properties
 - wetting and drying soil hydraulic properties

Results

Measured data and resulting hydraulic parameters are discussed in detail in *Kodesová et al.* [1999]. Therefore only resulting soil hydraulic parameters are presented here in Table 1.

Table 1. Hydraulic parameters obtained from different tests for sandy soil, Bulk density: $1.45 \div 1.68 \text{ g/cm}^3$, Porosity: $0.350 \div 0.452$

Test Method	Hydraulic Parameters				
	α^w / α^d [10^{-2} cm^{-1}]	n	θ_r	θ_s	K_s [10^{-3} cm/s]
Pressure Plate (9 Samples)	6.8	1.54	0.000	0.423	-
Capillary Rise (1 Column)	6.8	3.57	0.000	0.446	-
Hanging Column (1 Sample)	3.4	3.29	0.113	0.420	-
Guelph Permeameter (4 Test Holes)	-	-	-	-	2.4 □ □ 3.8
Laboratory Falling Head (9 Tests)	-	-	-	-	1.3 □ □ 4.4
Permeameter A, $h_0 = 30 \text{ cm}$	3.7	3.97	0.088	0.379	2.2
Permeameter A, $h_0 = 30, 50 \text{ cm}$	3.5	4.81	0.089	0.377	2.0
Permeameter B, $h_0 = 30 \text{ cm}$	3.7	3.95	0.088	0.400	1.8
Permeameter B, $h_0 = 30, 50 \text{ cm}$	3.5	4.79	0.089	0.393	1.6
Permeameter B, $h_0 = 30, 50, 0 \text{ cm}$	2.6 □ □ 3.5	4.46	0.088	0.390	1.6
Permeameter C, $h_0 = 30 \text{ cm}$	3.4	3.65	0.082	0.433	1.1
Permeameter C, $h_0 = 30, 50 \text{ cm}$	3.3	4.04	0.083	0.449	1.1
Permeameter D, $h_0 = 21 \text{ cm}$	4.7	2.53	0.055	0.443	4.0
Permeameter D, $h_0 = 21, 108 \text{ cm}$	4.4	3.11	0.069	0.447	3.6
Permeameter E, $h_0 = 21 \text{ cm}$	3.5	3.19	0.087	0.333	1.1
Permeameter E, $h_0 = 21, 80 \text{ cm}$	3.1	4.09	0.089	0.350	1.0
Permeameter E, $h_0 = 21, 80, 0 \text{ cm}$	2.6 to 3.1	4.02	0.089	0.349	1.0

The soil was very homogeneous, without obvious layering or anisotropy, so optimization of parameters K_s , α , n , θ_r and θ_s was sufficient for describing observed flow responses. Initial moisture content paired with the initial tensiometer reading allowed for realistic estimation of θ_r and θ_s . Analysis of one- and two-step tests yielded similar parameters, due to the influence of the first step on the inverse solution. However, addition of the second step stabilized the solution for Test A of Site 2. The wetting hydraulic parameters obtained from analysis of the wetting and redistribution parts of the experiment were consistent with those obtained from analysis of the wetting parts of the two-step experiments. The drying α parameter was lower, as expected. The different α values clearly described the effects of hysteresis.

It is obvious that the optimized parameters are in the range of the independently measured data.

Conclusions

The inverse modeling technique has proved many times to be an efficient tool for determination of soil hydraulic properties. For more details about this method see for instance Hopmans *et al.* (2002), Simunek *et al.* (2002a, 2002b).

References

- Bohne, K., C. Roth, F. J. Leij and M. Th. van Genuchten, Rapid method for estimating the unsaturated hydraulic conductivity from infiltration measurement, *Soil Science*, 155(4), 237-244, 1992.
- Ciollaro, G., and N. Romano, Spatial variability of the soil hydraulic properties of a volcanic soil, *Geoderma*, 65, 263-282, 1995.
- Eching, S. O., and J. W. Hopmans, Optimization of hydraulic functions from transient outflow and soil water pressure data, *Soil Sci. Soc. Amer. J.*, 57(5), 1167-1175, 1993.
- Eching, S.O., J. W. Hopmans, and O. Wendroth, Unsaturated hydraulic conductivity from transient multi-step outflow and soil water pressure data, *Soil. Sci. Soc. Amer. J.*, 58, 687-695, 1994.
- Gribb, M. M., Parameter estimation for determining hydraulic properties of a fine sand from transient flow measurements, *Water Resour. Res.*, 32(7), 1965-1974, 1996.
- Gribb, M. M., J. Simunek, and M. F. Leonard, Use of a cone penetrometer method to determine soil hydraulic properties., *J. Geotech. Geoenviron.*, 124, 820-829, 1997.
- Hopmans J.W., J. Simunek, N. Romano and W. Durner. Inverse methods, in *Methods of Soil Analysis*, SSSA, Madison, Wisconsin, 963-1008, 2002.
- Inoue, M., J. Simunek, J. W. Hopmans, and V. Clausnitzer, In-situ estimation of soil hydraulic functions using a multi-step soil-water extraction technique, *Water Resour. Res.* 34, 1035-1050, 1998.
- Kodesová, R., M. M. Gribb, and J. Simunek, Estimating soil hydraulic properties from transient cone permeameter data, *Soil Sci.* 163, 436-453, 1998.
- Kodesová, R., S.E. Ordway, M. M. Gribb, and J. Simunek, Estimating soil hydraulic properties with the cone permeameter: Field studies, *Soil Sci.* 164, 527-541, 1999.
- Kool, J. B., J. C. Parker, and M. Th. Van Genuchten, Parameter estimation for unsaturated flow and transport models – A review, *J. of Hydrol.*, 91, 255-293, 1987.
- Kool, J. B., Parker, J. C., and M. Th. van Genuchten, Determining soil hydraulic properties from one step outflow experiments by parameter estimation: I. Theory and numerical studies, *Soils Sci. Soc. Am. J.*, 49, 1348-1354, 1985.

- Leonard, M. F., Design and laboratory evaluation of a cone permeameter for unsaturated soil hydraulic parameter determination, MS thesis, Univ. of S. Carolina, Columbia, SC, 1997.
- Parker, J. C., J. B. Kool, and M. Th. van Genuchten, Determining soil properties from one-step outflow experiments by parameter estimation, II. Experimental studies, *Soil Sci. Soc. Am. J.*, 49, 1354-1359, 1985.
- Richards, L. A., Capillary conduction of liquids through porous mediums, *Physics*, 1, 318-333, 1931.
- Russo, D., E. Bresler, U. Shani, and J. C. Parker, Analyses of infiltration events in relation to determining soil hydraulic properties by inverse-problems methodology, *Water Resour. Res.*, 27(6), 1361-1373, 1991.
- Santini, A., N. Romano, G. Ciollaro, and V. Comegna, Evaluation of a laboratory inverse method for determining unsaturated hydraulic properties of a soil under different tillage practices, *Soil Sci.*, 160, 340-351, 1995.
- Simunek, J., H. Othmer, and M. Th. van Genuchten, *HYDRUS-2D, Simulation Water Flow and Solute Transport in Two-Dimensional Variably Saturated Media*, TPS 53, International Groundwater Modeling Center, Colo. School of Mines, Golden, CO, 1996.
- Simunek, J., and M. Th. van Genuchten, Estimating unsaturated soil hydraulic properties from tension disk infiltrometer data by numerical inversion, *Water Resour. Res.* 32(9), 2683-2696, 1996.
- Simunek, J. and M. Th. van Genuchten, Estimating unsaturated soil parameters from multiple tension disc infiltrometer data, *Soil Sci.*, 162(6), 383-398, 1997.
- Simunek, J., O. Wendroth, and M. Th. van Genuchten. A parameter estimation analysis of the evaporation method for determining soil hydraulic properties, *Soil Sci. Soc. Am. J.* 62, 894-905, 1998a.
- Simunek, J., D. Wang, P. J. Shouse, and M. Th. van Genuchten, Analysis of a field tension disc infiltrometer experiment by parameter estimation, submitted to *Int. Agrophysic.* 12, 167-180, 1998b.
- Simunek, J., R. Kodesová, and M. M. Gribb, Estimating hysteresis in the soil water retention function from modified cone penetrometer test, *Water Resour. Res.*, 35, 1329-1345, 1999.
- Simunek, J. and J.W Hopmans. Parameter optimization and nonlinear fitting, in *Methods of Soil Analysis*, SSSA, Madison, Wisconsin, 139158, 2002a.
- Simunek, J., M.T.van Genuchten, D. Jacques, J.W Hopmans, M. Inoue and M. Flury. Solute transport during variably saturated flow – inverse modeling, in *Methods of Soil Analysis*, SSSA, Madison, Wisconsin, 139158, 2002a.
- van Dam, J. C., N. M. Stricker, and P. Droogers, Inverse method for determining soil hydraulic functions from one-step outflow experiments, *Soil Sci. Soc. Am. J.*, 56, 1042-1050, 1992.
- van Dam, J. C., N. M. Stricker, and P. Droogers, Inverse method to determine soil hydraulic functions from multi-step outflow experiments, *Soil Sci. Soc. Am. J.*, 58, 647-652, 1994.

van Genuchten, M. Th., A closed-form equation for predicting the hydraulic conductivity of unsaturated soils, *Soil Sci. Soc. Am. J.*, 892-898, 1980.

Soil Physical Properties Affecting Soil Erosion in Tropical Soils

Deyanira Lobo Lujan¹

*Facultad de Agronomía, Instituto de Edafología,
Universidad Central de Venezuela, Maracay, Venezuela*

*Lecture given at the
College on Soil Physics
Trieste, 3-21 March 2003*

LNS0418021

¹ lobod@agr.ucv.ve

INTRODUCTION

The total vegetated land area of the earth is about 11,500 hectare. Of this, about 12% is in South America. Of this, about 14% is degraded area. Water erosion, chemical degradation, wind erosion, and physical degradation have been reported as main types of degradation. In South America water erosion is a major process for soil degradation.

Nevertheless, water erosion can be a consequence of degradation of the soil structure, especially the functional attributes of soil pores to transmit and retain water, and to facilitate root growth. Climate, soil and topographic characteristics determine runoff and erosion potential from agricultural lands. The main factors causing soil erosion can be divided into three groups

- Energy factors: rainfall erosivity, runoff volume, wind strength, relief, slope angle, slope length.
- Protection factors: population density, plant cover, amenity value (pressure for use) and land management.
- Resistance factors: soil erodibility, infiltration capacity and soil management.

The degree of soil erosion in a particular climatic zone, with particular soils, land use and socioeconomic conditions, will always result from a combination of the above mentioned factors. It is not easy to isolate a single factor. However, the soil physical properties that determine the soil erosion process, because the deterioration of soil physical properties is manifested through interrelated problems of surface sealing, crusting, soil compaction, poor drainage, impeded root growth, excessive runoff and accelerated erosion.

When an unprotected soil surface is exposed to the direct impact of raindrops it can produce different responses: Production of smaller aggregates, dispersed particles, particles in suspension and translocation and deposition of particles. When this has occurred, the material is reorganized at the location into a surface seal. Aggregate breakdown under rainfall depends on soil strength and a certain threshold kinetic energy is needed to start detachment.

Studies on necessary kinetic energy to detach one kilogram of sediments by raindrop impact have shown that the minimum energy is required for particles of 0.125 mm. Particles between 0.063 to 0.250 mm are the most vulnerable to detachment. This means that soils with high content of particles into vulnerable range, for example silty loam, loamy, fine sandy, and sandy loam are the most susceptible soils to detachment.

Many aspects of soil behavior in the field such as hydraulic conductivity water retention, soil crusting, soil compaction, and workability are influenced strongly by the primary particles. In tropical soils also a negative relation between structure stability and particles of silt, fine sand and very fine sand has been found, this is attributed to low cohesiveness of these particles.

The ability of a structure to persist is known as its stability. There are two principal types of stability: the ability of the soil to retain its structure under the action

of water, and the ability of the soil to retain its structure under the action of external mechanical stresses. (e.g. by wheels). Both types of stability are related with susceptibility to erosion.

The soil susceptibility to sealing and crusting has been related to different indices:

- Consistency index C_{5-10}
Consistency Index $C_{5-10} = (w_5 - w_{10})$ where w_5 and w_{10} are the water contents, in percentage of dry weight for which the two sections of a part of the soil in the Casagrande cup touch each other over a distance of 1 cm, after 5 and 10 blows, respectively. It has been found that stable topsoils have values of $C_{5-10} > 3$, whereas unstable soils have values less than 2.5.
- Wet-sieving
The distribution of water stable aggregates is determined by wet-sieving. During wet-sieving, soil aggregates are submerged and gently sieved under water to characterize the aggregate resistance to breakdown.
- Absolute Sealing Index ASI
ASI is the minimum value of the hydraulic conductivity in the seal formed by impact of water drops. The test measures the changes of saturated hydraulic conductivity of the seal formed by raindrop impact obtained from a layer of soil aggregates of approximately 1.5 cm thick and 2 to 4 mm in diameter that receive a simulated rainfall during 60 minutes with an intensity around 90 mm/hour.
- Infiltrability of wet and more or less sealed topsoils
A non-destructive method whereby small amounts of water is supplied by drip sources placed close to the soil surface without dissipation of kinetic energy and the area of saturated flux is measured when gravitational flow begins to prevail. Once a steady flow is apparently obtained, lateral flow as well as evaporative flux are neglected, with the relation between the source discharge rate Q and the equivalent radius r of the saturated patch written as

$$Q = \pi r^2 q_i$$

where q_i is the infiltration rate through the crusted topsoil.

One of the processes that determine water erosion is infiltration. Hydrologically the infiltration process separates rain into two parts. One part stored within the soil supplies water to the roots of vegetation and recharges ground water, while the other part which does not penetrate the soil surface is responsible for surface runoff.

On stable soils without gradual deterioration of the soil structure, the decrease of infiltration rate results from the inevitable decrease in the gradient of matric

potential, one of the forces drawing water into the soil, which occurs as the infiltration process proceeds. In unstable soils, a second cause for the decrease in the infiltration rate with time is the deterioration of soil structure on the surface occurring during the infiltration process. This deterioration may cause the formation of a dense crust, and a partial sealing of the profile.

Runoff and soil loss prediction has been widely used as a tool to guide conservation planning. The prediction technology can be characterized as empirically based, process-based or a combination of the two.

There are numerous process-based models. In a hydrologic simulation model to compute runoff and soil loss, relationships for fundamental runoff and soil loss processes should be combined with relationships for fundamental hydrologic processes. One of these models, SOMORE, accounts for infiltration of rainfall into the soil as limited by surface sealing effects and limited layers close to the soil surface, and by internal drainage or subsurface runoff as affected by rainfall infiltration, effective root depth and saturated hydraulic conductivity of the limiting soil layer.

The SOMORE model uses as inputs: daily rainfall, daily evapotranspiration, infiltration rate, and rainfall intensity and soil conditions at the rooting depth, such as soil moisture at saturation, soil moisture at liquid limit, soil moisture at plastic limit, soil moisture at field capacity, soil moisture at -0.15 MPa, soil moisture at -1.5 MPa, soil moisture at the first day, and saturated hydraulic conductivity of the subsoil.

Some outputs of model are: water losses by runoff or surface drainage (mm), waterlogging (mm), duration of waterlogging (hours), water losses by internal drainage (mm) and soil moisture at rooting depth (mm). The model also provides additional outputs, e.g. days with waterlogging, days with excessive soil moisture for tillage, days with excessive soil moisture for the crop, days with appropriate soil moisture for tillage for the crop, etc.

CASE STUDIES

Two case studies in Venezuela will be used to illustrate the role of soil physical properties in the erosion process. Two soils of gently rolling topography (5 – 10 % slopes) representating large rainfed agricultural areas were selected. The Barinas soil is located in the Western Plains. The Chaguaramas soil is located in the Central Plains.

Thirty years ago, the land use changed from pasture and livestock to crops like maize and sorghum in the Western Plains, and to sorghum in the Central Plains, highly mechanized and livestock. Tillage operations previous to seeding, generally include two or three disc harrowing, oftentimes leaving a bare surface soil exposed to the rainfall impact during the first days of the crop.

A modification of Fournier's Index was used to assess the climatic aggressiveness

$$FI = \frac{1}{p} \sum p_i$$

where p_i is monthly precipitation and P the annual precipitation. Correlations between monthly FI values and R factor values (Wishmeier's method) are highly significant.

Figure 1 shows the monthly Fournier Index distribution. For the Barinas soil the high values of Fournier Index (>7.5) occur from April to October, whereas for the Chaguaramas soil high values occur from May to August.

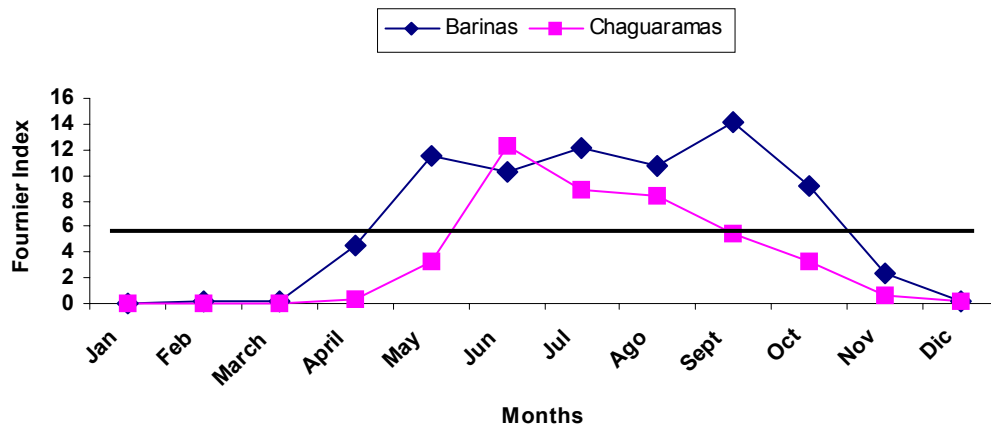


Figure 1. Fournier Index distribution

In Barinas most of the rainfall occurs from April through November (Figure 2). In Chaguaramas most of the rainfall (about 750 mm) occurs from May through October (Figure 3). In both regions, 50% of the rainfalls have intensities greater than 25mm/h.

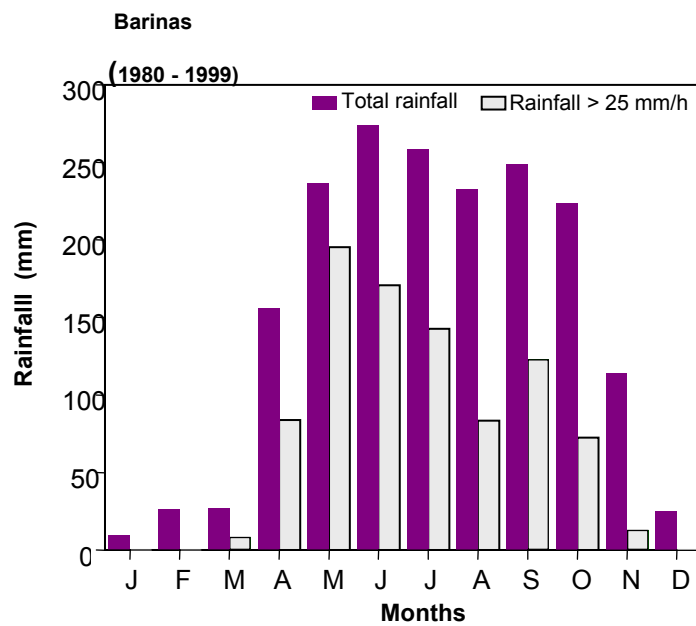


Figure 2. Total rainfall and rainfall with intensities higher than $25 \text{ mm} \cdot \text{h}^{-1}$ in Barinas

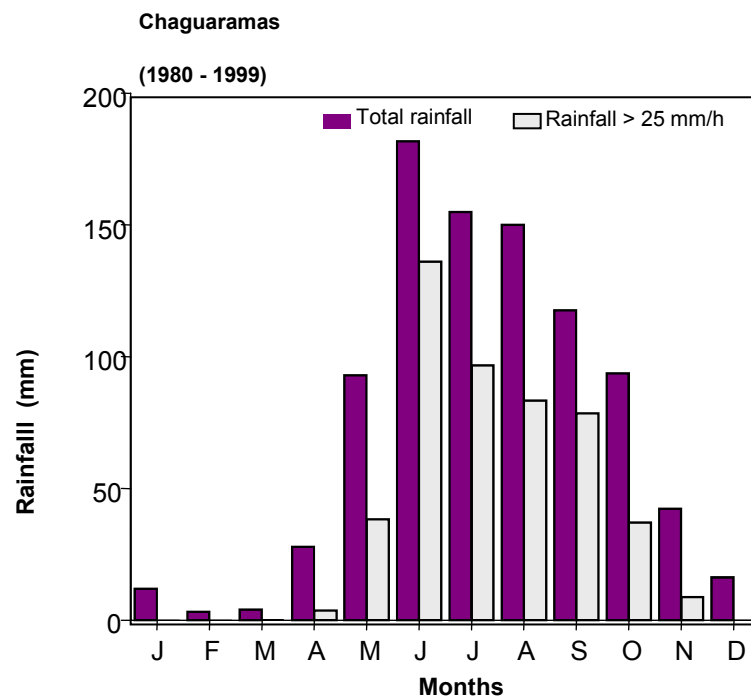


Figure 3. Total rainfall and rainfall with intensities higher than $25 \text{ mm} \cdot \text{h}^{-1}$ in Chaguaramas

Table 1 shows the particle size distribution of two Venezuelan Alfisols. Both soils are sandy loam in the soil surface, but they differ in the proportion of silt and different sand sizes.

Table 1. Particle size distribution

Soil	Depth	Particle diameter (μm)							Textural Class
		< 2	2 – 50	50 – 100	100 – 250	250 – 500	500 – 1000	1000 – 2000	
Barinas	0-15	15	12.0	21.0	28.0	16.5	3.5	1.0	SL
	15-35	18	10.5	19.5	25.0	22.0	6.5	1.5	SL
	35-55	24	12.0	22.0	24.0	13.5	3.5	1.0	CSL
	55-70	27	14.5	22.0	21.5	11.0	3.0	1.0	CSL
Chaguaramas	0-10	10	34.0	21.0	25.5	8.5	1	0	SL
	10-18	14	37.5	23.5	18.5	4.5	1	1	L
	18-35	17	47.0	16.0	12.0	4.0	2	2	L
	35-45	24	44.0	13.5	9.5	5.0	2	2	L
	45-70	20	40.0	20.0	13.5	4.5	2	0	L

In the Chaguaramas soil particles between 2 and 250 μm prevail. In the Barinas soil particles between 50 and 500 μm prevail.

Figure 4 shows the structure stability of Barinas and Chaguaramas soils assessed by means of wet-sieving (Yoder's method). The Chaguaramas soil shows a low proportion of larger water stable aggregates and a high proportion of smaller water stable aggregates. The Barinas soil shows a higher proportion of large water stable aggregates. The maintenance of large aggregates stable in water on the surface soil is important to maintain high water intake rates and to reduce evaporation losses of the water stored in the soil.

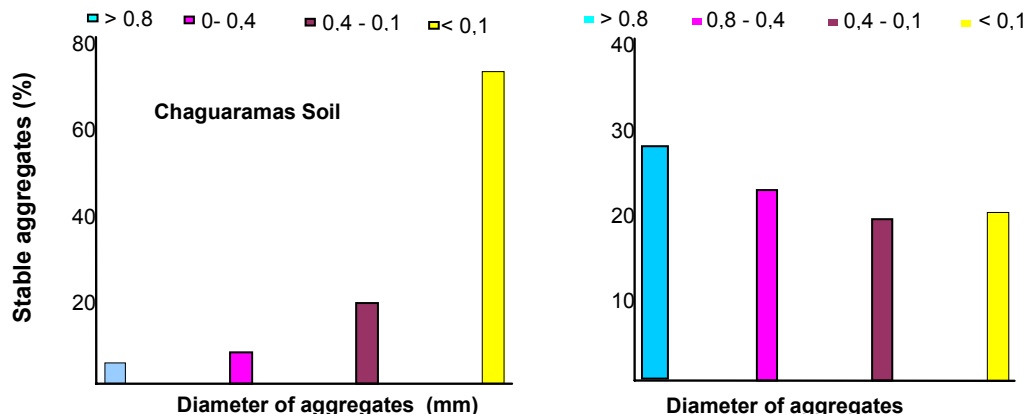


Figure 4. Stable aggregates distribution

Figure 5 shows the behavior of saturated hydraulic conductivity obtained from a layer of soil aggregates of approximately 1.5 cm thick and 2 to 4 mm in diameter that received a simulated rainfall during 60 minutes with an intensity around 90 mm/hour. ASI is the Absolute Sealing Index which is equal to the minimum value of hydraulic conductivity in the seal formed by impact of water drops, K_{ws} the hydraulic conductivity value with seal, K_{ns} the hydraulic conductivity value without the seal and RSI the Relative Sealing Index which is the ratio K_{ns}/K_{ws} .

The effect of raindrop impact on the hydraulic properties of the layer of soil aggregates is more evident in the Chaguaramas soil. This can be explained because the Chaguaramas soil shows a relatively high percentage of silt, fine sand and very fine sand. The Absolute Sealing Index in the Chaguaramas soil is very low - about 2.9 mm/h, and that in the Barinas soil is higher - about 8 mm/h.

The amount of surface soil removed by runoff water depends to a large extent on the resistance of soil aggregates to be disrupted by the energy of raindrop impact. The ability of a surface soil to accept a continuous heavy rainfall is a critical factor in the prevention of accelerated erosion of soils, and is related to the stability of aggregates to raindrop impact and to the resistance to the shearing force of running water. Moreover, any dispersed clay may effectively block the pores between the micro-aggregates and give an extremely low infiltration rate. Dispersion and swelling of clay results in the elimination of the larger soil pores with a consequent reduction in soil hydraulic conductivity. Soil compaction, a process resulting in an increase in soil bulk density and a decrease in total pore space, significantly influences soil hydraulic properties (pore size distribution, water retention and hydraulic conductivity) as well as soil strength and mechanical impedance to root growth. The pore size distribution and continuity is related to water transmission, especially to the relative proportion of drainage pores.

Figure 6 shows that a compacted layer is evident at 15 cm in the Barinas soil and at 10 cm in the Chaguaramas soil. Figure 7 shows the relative importance that changes in physical conditions on the surface or inside the profile could affect the infiltration process. In the Chaguaramas soil, the infiltration and water movement are more limited by a compacted layer close to the surface. In Barinas soil the surface seal is more limiting.

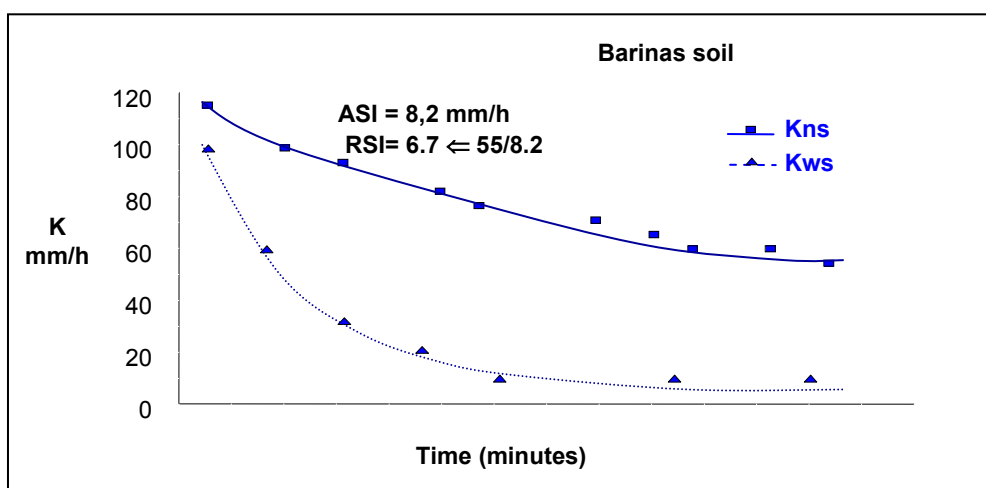
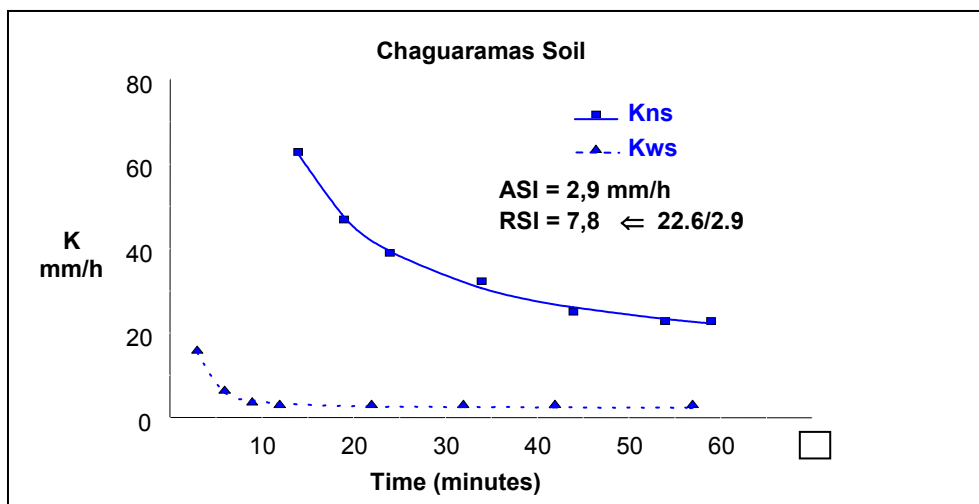


Figure 5. Absolute and Relative Sealing Indices in Chaguaramas and Barinas soils

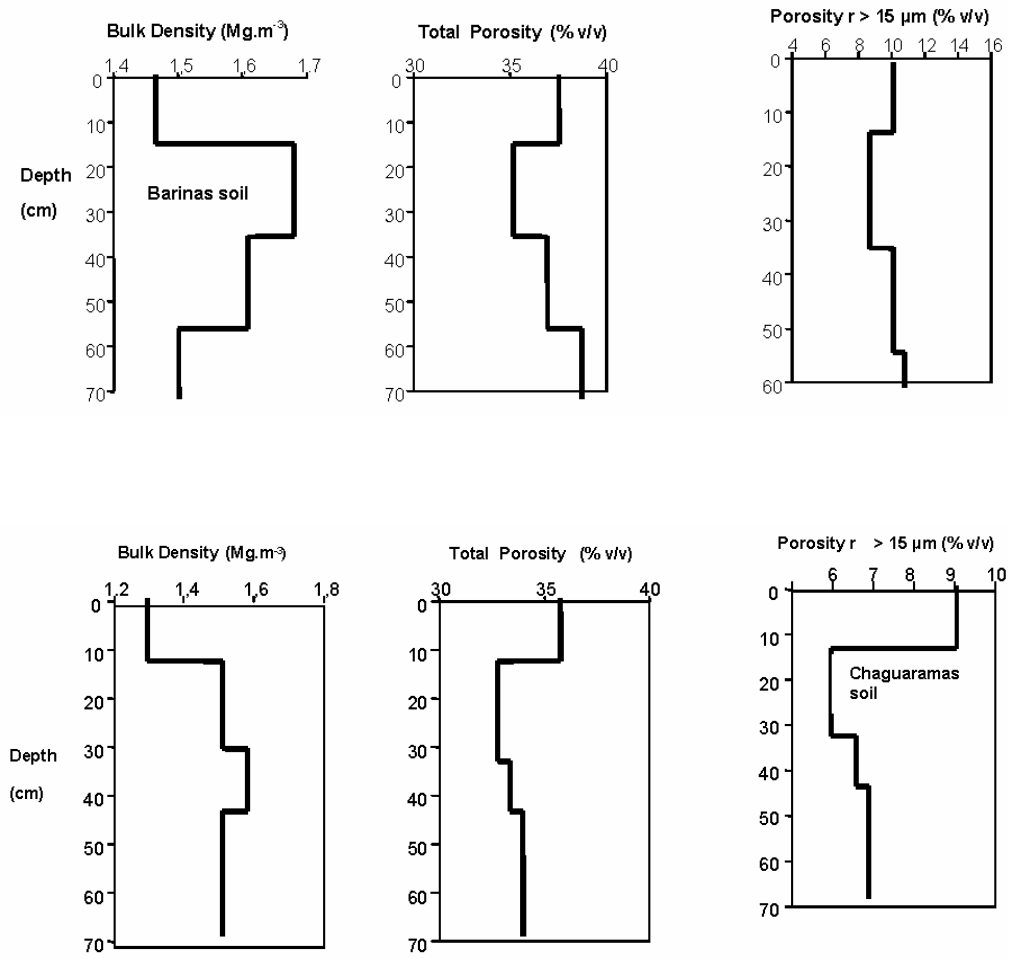


Figure 6. Structural Indices

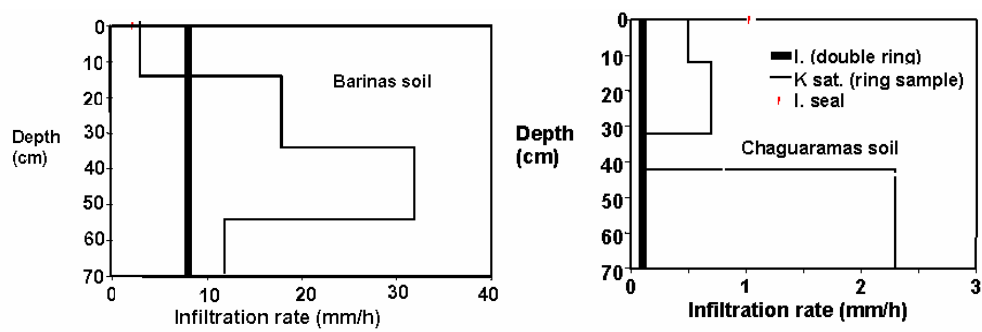


Figure 7. Infiltration rate and saturated hydraulic conductivity in the profile

The most important effect of soil sealing is the reduction in infiltration rate shown in Fig. 8. However, infiltration may be also severely impeded by compacted layers, because they become limiting barriers for deep percolation and drainage of excess infiltrated rainfall, thus increasing the risks of waterlogging, water runoff losses and soil erosion.

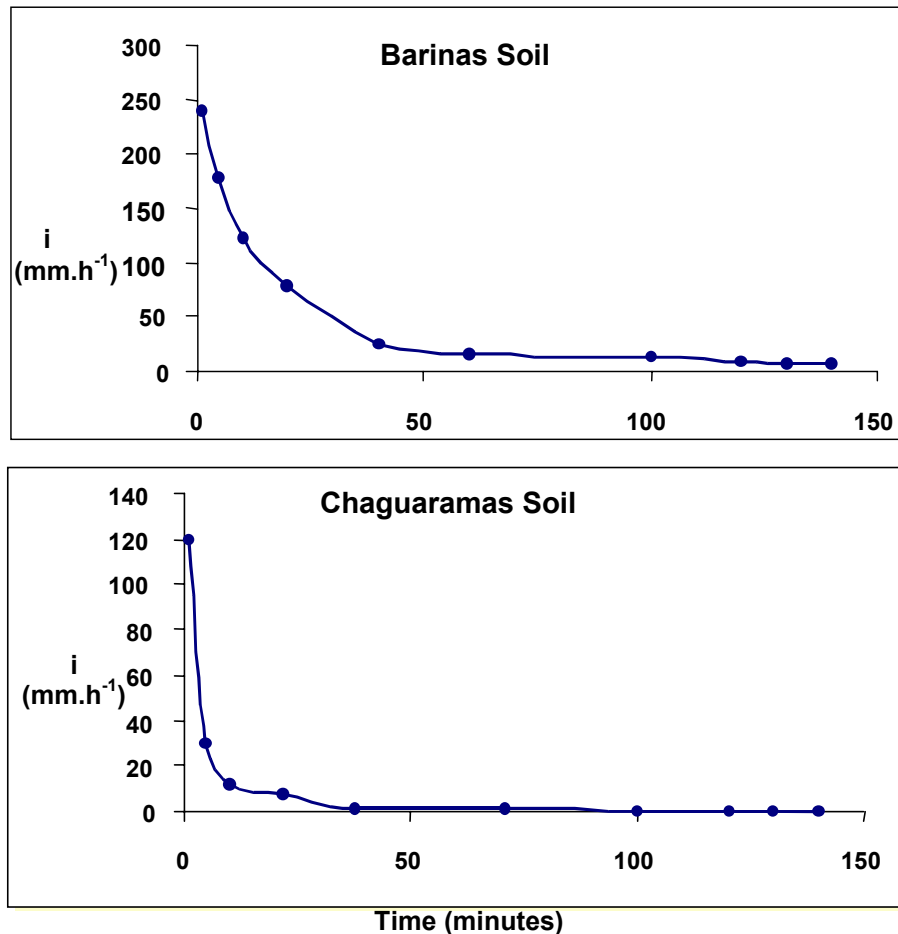


Figure 8. Infiltration rate (double ring method)

Estimates of water runoff losses during the growing period of sorghum was obtained using the hydrological process-based model SOMORE for the two conditions: 1) bare soil, and 2) rainy seasons of years with annual rainfall close to the average (return period of two years).

Figure 9 shows the accumulated rainfall and runoff in the Barinas soil. The runoff after saturation is insignificant, because the compacted layer does not limit water movement. The total runoff is about 30%. In the Chaguaramas soil (Figure 10),

the compacted layer close to the soil surface and soil sealing affects the runoff. The total runoff is greater than 50%.

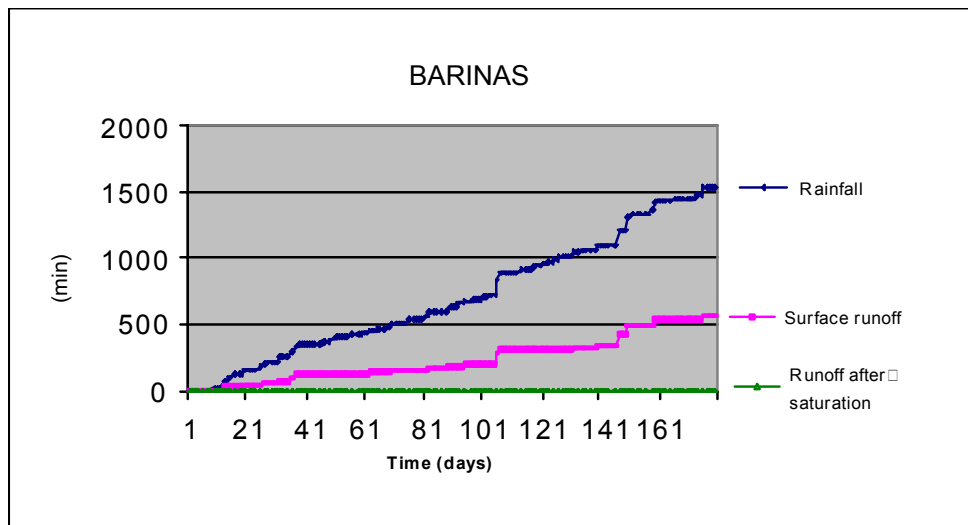


Figure 9. Accumulated rainfall and runoff in the Barinas soil

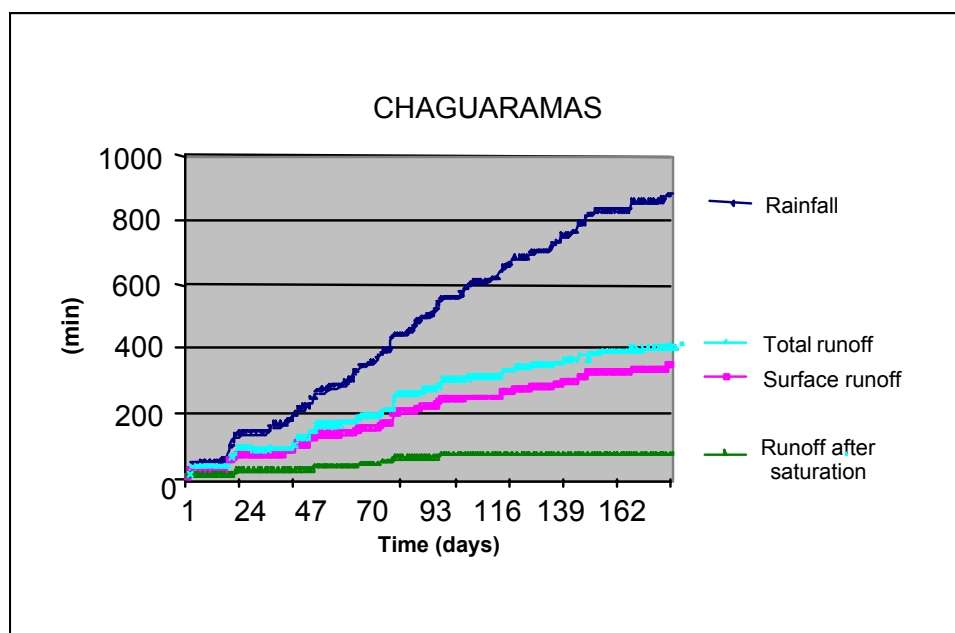


Figure 10. Accumulated rainfall and runoff in the Chaguaramas soil

Aggregate Stability and Soil Degradation in the Tropics

Joe S.C. Mbagwu¹

*Department of Soil Science, University of Nigeria
Nsukka, Nigeria*

*Lecture given at the
College on Soil Physics
Trieste, 3-21 March 2003*

LNS0418022

¹ joembagwu2003@yahoo.com

INTRODUCTION

Aggregate stability is a measure of the structural stability of soils. Factors that influence aggregate stability are important in evaluating the ease with which soils erode by water and/or wind, the potential of soils to crust and/or seal, soil permeability, quasi-steady state infiltration rates and seedling emergence and in predicting the capacity of soils to sustain long-term crop production. Aggregate stability of soils can be measured by the wet-sieving or raindrop techniques. A reduction in soil aggregate stability implies an increase in soil degradation. Hence aggregate stability and soil degradation are interwoven.

EXTENT OF STUDIES COVERED

The factors that influence aggregate stability of tropical soils depend on the soil environment, the type and dominance of the stabilizing substances and land use. On some tropical soils in Nigeria decreased aggregate stability was observed in unmulched than mulched plots. Also it was shown that the more frequent the irrigation, the more was the disintegration of water-stable aggregates on the unmulched than mulched plots. The type of surface active agents (surfactants) which enter into the soil is important in maintaining aggregate stability, with the anionic surfactants degrading and the nonionic surfactants aggrading aggregate stability.

Using simple step-wise regression analysis, the relative importance of organic carbon, iron and aluminum oxides on aggregate stability of tropical soils in Indonesia was compared. It was found using the raindrop technique for determining aggregate stability, that the oxides of Fe and Al and CaCO_3 were more important stabilizing substances than organic carbon. In subtropical soils in China it was observed that the mechanisms of aggregate breakdown were slaking > mechanical breakdown > micro-cracking. The normalized mean-weight diameter, which is a measure of aggregate stability, correlated with soil properties than clay and soil organic carbon.

In Nigeria and Ethiopia it was observed that as aggregate stability of soils increased with time, soil carbohydrates decreased which implies that aggregate stability did not depend on the content of carbohydrates in the soils. Some authors who reviewed the physical, chemical and mineralogical soil properties that influence aggregate stability in alluvial and upland soils in Nigeria pointed out that organic carbon was less important as an aggregating agent than other intrinsic stabilizing substances. They also showed the importance of some aggregate stability indices in predicting the potential of soils to erode and the possibility of using humic substances to improve the stability of degraded tropical soils.

SOIL DEGRADATION

Soil degradation is the temporary or permanent lowering of the productive capacity of soil caused by overgrazing, deforestation, inappropriate agricultural practices, over exploitation of fuel wood leading to desertification and other man-induced activities.

All processes of soil degradation are grouped into six classes: water erosion, wind erosion, soil fertility decline, salinization, water logging and lowering of the water table.

- (i) Soil erosion by water includes inter-rill and rill erosion, gullying, and land sliding caused by clearing of vegetation and road construction. Soil erosion by wind produces sand dunes.
- (ii) Soil fertility decline refers to deterioration in soil physical, chemical and biological properties caused by (a) reduction in soil organic matter status, leading to decline in soil biological activity; (b) degradation in soil physical properties (structure, aeration, water holding capacity) caused by reduced OM; (c) adverse changes in soil nutrient status, including reduction in availability of the major nutrients (N, P, K), initiation of micronutrient deficiencies and development of nutrient imbalances; and (iv) build up of toxicities (by heavy metals, xenobiotics, and acidification through incorrect use of fertilizers).
- (iii) Water logging is caused by over irrigation, and restricted infiltration of water into the soil. This lowers land productivity through rise in ground water close to the soil surface.
- (iv) Salinization refers to all types of land degradation brought about by increased concentration of salts in the soil. It occurs by planning mistakes and mismanagement of irrigation schemes (salinization in the strictest sense), and sodification (also called alkalization), which refers to the dominance of the exchange complex by Na^+ .
- (v) Lowering of the water table is brought about by pumping of ground water for irrigation which exceeds the natural recharge capacity. Pumping of water for urban and industrial use also causes this form of land degradation.

Other types of land degradation include (i) deforestation, (ii) forest degradation (reduction in biotic resources and lowering of the productive capacity of forests), (iii) range land degradation (lowering of the productive capacity of range lands), (iv) acid sulphate formation, (v) soil pollution, (vi) soil destruction through mining and quarrying activities, (vii) urban and industrial encroachment on to agricultural land, (viii) destruction of irrigation schemes, and (ix) potential effects of global climatic change (including global warming which may lead to modifications in the general atmospheric circulation, causing changes in rainfall pattern)

In Nigeria, some workers summarized the causes of as (i) fire and burning of vegetation, (ii) deforestation, (iii) increasing intensity of farming and cultivation (including irrigation practices in the north) and tillage-related practices, (iv) low input agriculture, (v) accelerated erosion by water and wind, and (vi) road building and other construction works.

About 85% of the causes of land degradation worldwide are due to soil erosion by wind and water. Hence soil and land degradation are often used interchangeably. In Fig. 1 we show the casual nexus between land, population, poverty and degradation. In this figure it is argued that increase in rural population and decrease in usable land resources enhance land degradation.

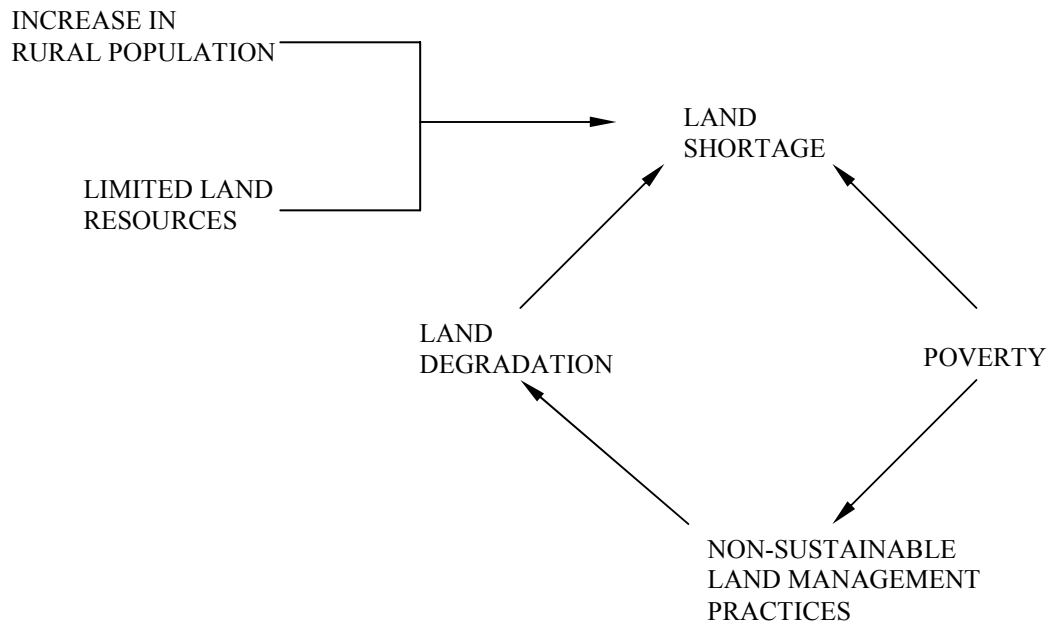


Figure 1. Casual nexus between land, population, poverty and degradation

Processes, Factors and Causes of Soil Degradation

As already defined, soil degradation is the loss in the productive potential of soil induced by human activities. The processes of soil degradation are the mechanisms responsible for the decline in soil quality (Fig. 2) and they are grouped into three types: physical, chemical and biological types, each of which has different processes affecting it (Fig. 3). In Fig. 4 it is shown that soil degradation is governed by environmental agents and catalysts which propel their actions.

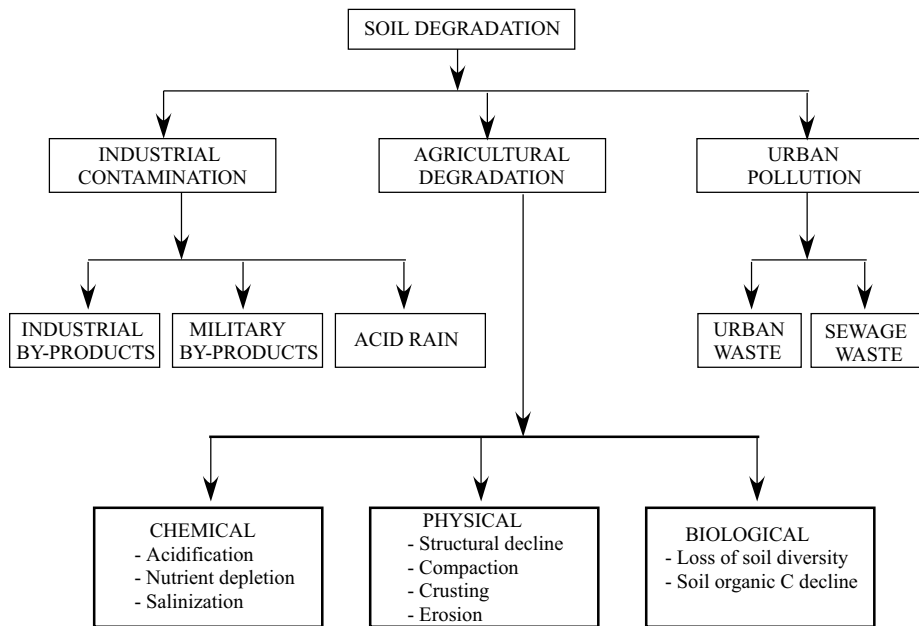


Figure 2. Principal types of soil degradation mechanisms

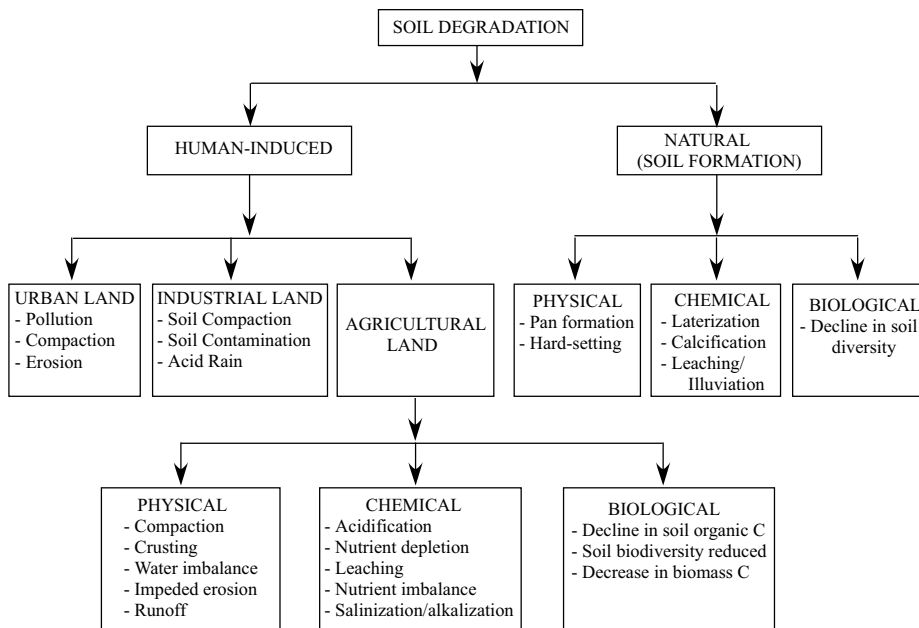


Figure 3. Principal types of soil degradation: (i) natural and (ii) anthropogenic

Measures Used to Prevent or Combat Soil Degradation

The measures used can either be preventive or remedial. Preventive practices minimize the chances of soil degradation occurring or the magnitude or severity of the damage when the degradation manifests. These include in Nigeria, (i) manuring and mulching, (ii) planted fallows and cover crops, (iii) sustainable farming systems, (iv) adequate rotations, (v) home gardens or compound farms, (vi) alley cropping and related agro forestry systems, and (vii) chemical fertilizers which are mainly remedial measures.

Because of alterations in soil properties that affect particular land uses, soils may degrade for one crop (maize rather sorghum). As long as some land use is possible soil degradation is not always an absolute concept.

Decline in agricultural productivity should be evaluated in terms of inputs such as fertilizer use, water management and tillage methods. We can alleviate some types of soil degradation by use of micronutrients, inorganic fertilizers and organic residues. Soil that responds to management practices cannot be said to be degraded.

Since crop growth depends on weather, degraded soils may be more sensitive to harsh weather (e.g. drought, temperature) than undegraded soils. A soil is degraded if its productivity falls below the economic threshold even under favourable weather conditions or with judicious inputs. All human-induced changes in soil properties are not always degrading to all soil's functions. Therefore, soil degradation has to be referenced to the initial soil properties. We need to know if reduction in agricultural productivity due to soil erosion is reversible or not. A soil is degraded if its present or potential utility cannot be restored by improved management for the intended or other uses. A soil is degraded if the loss of intrinsic qualities, which manifest in reduced crop yields, is permanent.

SUGGESTIONS FOR FURTHER READING

- Lal, R. 1989. Conservation tillage and sustainable agriculture: tropics vs. temperate environment. *Adv. Agron.* 42: 85-197.
- Lal, R., Hall, G.F. and Miller, F.P. 1989. Soil degradation. I. Basic processes. *Land Degradation & Rehabilitation*. 1: 51-69.
- Mbagwu, J.S.C. 1989. Effects of organic amendments on some physical properties of a tropical Ultisol. *Biol. Wastes* 28: 1-13.
- Mbagwu, J.S.C. 1992. Improving the productivity of a degraded Ultisol using organic and inorganic amendments. 1. Chemical properties and maize yield. *Biores. Technol.* 42: 149-154.

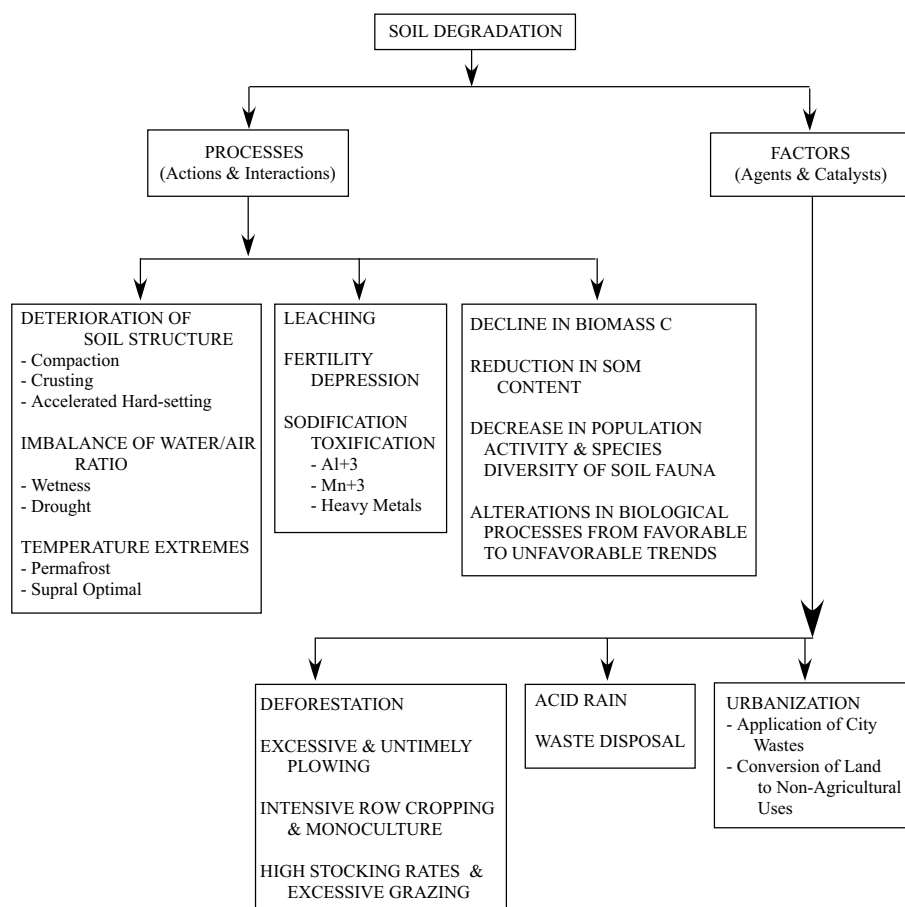


Figure 4. Factors and processes of soil degradation

Oxygen Transport in Waterlogged Soils, Part I. Approaches to Modelling Soil and Crop Response to Oxygen Deficiency

Franco Humberto Obando Moncayo¹

*Faculty of Agricultural Sciences, Department of Natural Resources and Environment,
University of Caldas, Manizales, Colombia*

*Lecture given at the
College on Soil Physics
Trieste, 3-21 March 2003*

LNS0418024

¹ fobando@yahoo.com

INTRODUCTION

Many authors have emphasized the complex nature of anaerobiosis in soils produced by water logging. Poor aeration may cause the accumulation of various gases and toxic products, but depletion of oxygen below critical levels can be considered as a major effect on plant growth and crop production. From practical, point of view, the questions is “what level of oxygen is critical”. The amount of oxygen in soil is determined by the supply of oxygen from the atmosphere and its consumption in the soil. These aspects are highly dynamic and very difficult to quantify. So, a convenient way to develop quantitative theory on soil aeration has been to split the diffusion process in macro and micro diffusion. In fact, there is abundant literature on mathematical models to describe these two processes. This lecture outlines in a simple way the mathematics of various cases of diffusion which have been widely used in modeling soil aeration. Simplifications of the general equation of diffusion (Fick’s law) giving two possible forms of the problem: planar or one-dimensional diffusion and radial diffusion are given. Furthermore, the solution of diffusion equation is obtained by the analogy to the problem of electrical flow (Ohm’s law). Taking into consideration the soil respiration process, the continuity equation which accounts for the law of conservation of mass is solved. The purpose of this paper has been to review the interrelation soil structure-air movement in waterlogged clay soils, and its consequences on plant growth and crop production. Thus, the mathematics of diffusion is presented, and then its application to specific cases of soil aeration such as diffusion in the soil profile, soil aggregates and roots is given. The following assumptions are taken into consideration.

Gas flow in soils is basically diffusion-dependent. Gas-phase diffusion is the major mechanism for vertical or longitudinal transport (long distance transport); this means, with depth Z in the soil profile (macro diffusion).

For horizontal transport (short distance transport or micro diffusion) which is assumed to be in X direction; in this case, the geometry of aggregates and the liquid phase are the major components of resistance for diffusion. Soil aggregates and roots are considered to be spherical and cylindrical in shape respectively.

Soil oxygen consumption, S_r , is taken to be independent of the oxygen concentration and considered to proceed at the same rate until oxygen supply drops to critical levels. Thus, aeration problems are assumed to begin when at any time, in the root zone, the oxygen diffusion rate, ODR, becomes less than $30 \times 10^{-8} \text{ g.cm}^{-2} \cdot \text{sec}^{-1}$, or the value of redox potential E_h is less than +525 mv (Obando, 1990).

Planar Diffusion

The first stages in the soil aeration process in the short term can be described by assuming simple steady-state one-dimensional diffusion system in which there is no net lateral movement and where a linear gradient of oxygen concentration is developed between the atmosphere and an adjacent or more remote sink in the soil profile. As indicated in figure 1 the soil profile is considered bounded by two parallel

planes, e.g. the layers at $z = 0$ and $z = L$. Obviously, these will apply in practice to diffusion into the soil profile where effectively all oxygen enters through the surface layer. An equation describing the steady-state linear diffusion from planar source to planar sink of equal area, through an isotropic medium in which there is no lateral loss or gain of molecules of the gas can be derived from the differential equation for planar diffusion (first Fick's law), which for vertical transport (in z direction) becomes:

$$\frac{\partial C}{\partial t} = D_e \frac{\partial^2 C}{\partial z^2} \quad (1)$$

The steady state

Let us consider the case of diffusion through a soil profile of depth L and coefficient diffusion D_e , whose layers at $z = 0$ and $z = L$, are maintained at constant concentrations C_0 and C_z , respectively. After a time, a steady state is reached in which the concentration remains constant at all points of the profile and provided that D_e is constant, equation (1) reduces to: (Crank, 1975)

$$\frac{d^2 C}{dz^2} = 0 \quad (2)$$

on integrating with respect to z we have

$$\frac{dC}{dz} = \text{constant} = K_1 \quad (3)$$

where K_1 is a constant > 0 confirming that the concentration must change linearly through the soil profile from C_0 to C_z . Introducing the conditions at $z = 0$, $z = L$, and integrating a second time we obtain

$$C = K_1 z + K_2 \quad (4)$$

where K_2 is a second constant of integration.

Applying the boundary conditions $C = C_0$ on $z = 0$ and $C = C_z$ on $z = L$ then $C_0 = K_2$ and $C_z = K_1 L + C_0$ and hence,

$$K_1 = \frac{dC}{dz} = \frac{(C_z - C_0)}{L} \quad (5)$$

both equations (3) and (5) show that the concentration changes linearly from C_0 to C_z through the soil profile. Also, the rate of transfer of diffusing substance is the same across the whole profile and is given by

$$F_\varepsilon = -D_\varepsilon \frac{dC}{dz} = -D_\varepsilon \frac{(C_z - C_0)}{L} \quad (6)$$

where F_ε , the one-dimensional flux of oxygen is constant through the length of diffusion path from $z = 0$ to $z = L$.

If the depth L and the surface concentration C_0 and C_z are known, D_ε can be deduced from an observed value of F_ε by using equation (6). Graphically the plot of C against depth z for this system has the form illustrated in fig. 1.

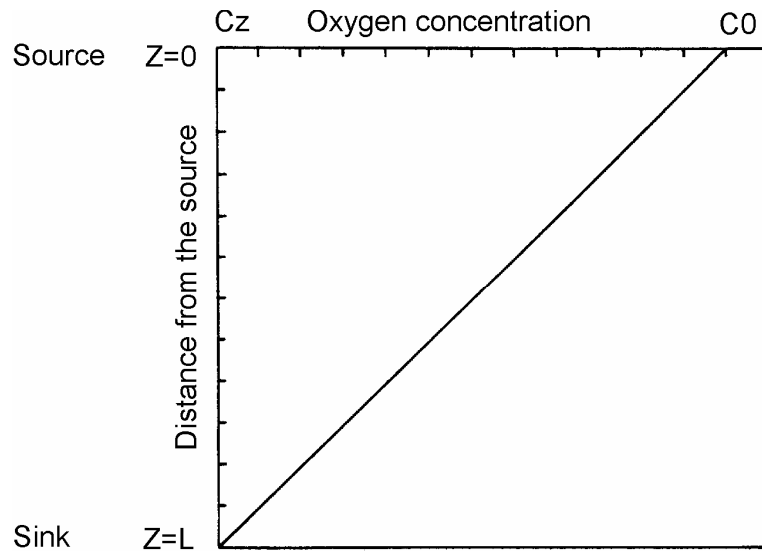


Fig. 1. Linear diffusion gradient in simple planar source-sink system. Oxygen source, C_0 , on $z = 0$ and sink, C_z , on $z = L$ (Armstrong, 1979).

In equation (6) dC can be likened to a “force” analogous in part to the potential difference in an electric circuit while the term D/dz is a measure of the conductance (reciprocal to resistance).

In equation (6) there is no restricting area term and the conductance D/L is simply a measure of the linear conductance between planar layers or compartments. Providing that the areas of these surfaces are equal the units of D/L are (m/s) . The oxygen flux, which has dimensions of quantity, area and time may also be written as

$$F_{\varepsilon} = \frac{Q}{At} = -D_{\varepsilon} \frac{(C_z - C_o)}{L} \quad (7)$$

where Q is in grams, A in m² and t in seconds. Hence the equation can be rearranged as

$$\frac{Q}{t} = -A \cdot D_{\varepsilon} \frac{(C_z - C_o)}{L} \quad (8)$$

where the term Q/t is referred to as the diffusion rate (g·s⁻¹) for the finite system of planar sectional area A (cm²). Under steady conditions the flux of gas Q/t, across any surface is constant, though the flux density may change if the area available for flow changes. In fact, equation (7) specifies the area through which diffusion takes place and the conductance K becomes D_ε·A/L and has units of m³/s. Thus, conductance K is better expressed as a function of area by

$$K = D_{\varepsilon} \frac{A}{L} \quad (9)$$

then equation (8) becomes

$$\frac{Q}{t} = K(C_o - C_z) \quad (10)$$

From equations (6) and (7) we obtain

$$F_{\varepsilon} = -D_{\varepsilon} \frac{dC}{dz} = \frac{Q}{At} \quad (11)$$

Integrating equation (11) yields

$$\frac{Q}{t} \int_0^z \frac{1}{A(z)} dz = -D_{\varepsilon} \int_0^z dC = D_{\varepsilon} (C_z - C_o) \quad (12)$$

By using equations (8) and (10)

$$\frac{Q}{t} = \frac{A \cdot D_{\varepsilon}}{L(C_o - C_z)} = K(C_o - C_z) \quad (13)$$

and combining equations (12) and (13), yields

$$K(C_o - C_z) \int_0^z [1/A(z)] dz = D_\varepsilon (C_z - C_o) \quad (14)$$

or

$$K = \frac{D_\varepsilon}{\int_0^z [1/A(z)] dz} \quad (15)$$

For simple geometries the integration is straightforward and the conductances determined. When diffusion is purely one-dimensional, the area available for flow remains constant with distance. The conductance is therefore planar diffusion: $K = D_\varepsilon / (z_1 - z_0)$ where the subscript following the distance z indicates a location of measurement.

Radial diffusion

Radial diffusion is an interesting case for modeling gas transport in soils. It forms the foundation for the development of the so-called micro models. In fact, the theory of the micro site concept for diffusion in soil crumbs, microorganism colonies and roots are based on radial diffusion. In particular, it constitutes the basis for the assessment of data obtained using the platinum electrode technique. The mathematics of the process is outlined below.

Diffusion in a cylinder: steady state

Considering a long circular cylinder in which diffusion is everywhere radial, concentration is then a function of radius r and time only. If the medium is formed by a system of coaxial cylinders whose radii are r_a and r_b as indicated in fig. 2, the differential equation describing the steady-state condition is: (Crank, 1975)

$$\frac{1}{r} \frac{d}{dr} \left[r \cdot D \frac{dC}{dr} \right] = 0 \quad (16)$$

If the diffusion coefficient D is constant, equation (16) becomes:

$$\frac{1}{r} \frac{d}{dr} \left[r \frac{dC}{dr} \right] = 0 \quad a \leq r \leq b \quad (17)$$

the general solution of equation (16) is

$$C = K_1 + K_2 \ln r \quad (18)$$

where K_1 and K_2 are constants to be determined for the boundary conditions: $C = C_1$ on $r = a$, $C = C_0$ on $r = b$ and $a \leq r \leq b$. Hence,

$$C = \frac{C_1 \ln(b/a) + C_0 \ln(r/a)}{\ln(b/a)} \quad (19)$$

the quantity of diffusing substance Q which diffuses through unit area of the cylinder A in time t is equal to the diffusion coefficient times the concentration gradient (Letey and Stolzy, 1964; 1967):

$$\frac{Q}{At} = \frac{D_\varepsilon (C_0 - C_1)}{\ln(b/a)} \quad (20)$$

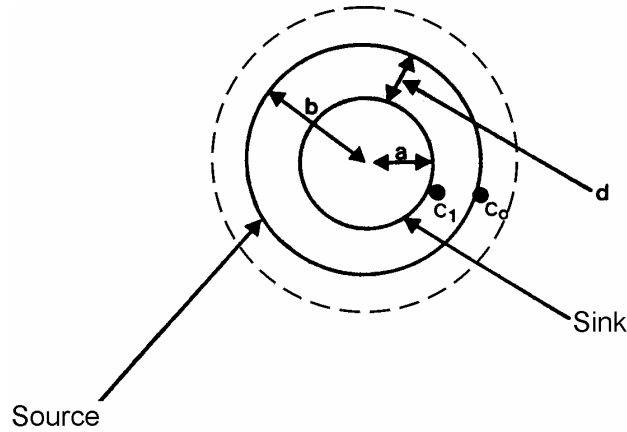


Fig. 2 The model which is applied in order to explain cylindrical diffusion (After Phene, 1986)

The oxygen flux for such a coaxial cylindrical model is given by

$$\frac{Q}{t} = 2\pi r h D_\varepsilon \frac{C_0 - C_1}{r \ln(b/a)} \quad (21)$$

By analogy with equation (8) it may be noted that the conductance K is given by the term $D_\varepsilon 2\pi r h / [r \ln(b/a)]$ where $2\pi r h$ is the surface area of a cylinder of radius r , length h .

If our observation concerns the diffusion incident upon the inner cylinder of $r = a$, the conductance term becomes $D_e 2\pi a h / [a \cdot \ln(b/a)]$. We may also note that the terms $a \cdot \ln(b/a)$ and $b \cdot \ln(b/a)$ are analogous with L in equations (7) and (8). It may be thought of as the effective path length for diffusion.

As indicated in fig. 3 for equal increments of the path $(b - a)$, the conductance component of $D_e A / [r \cdot \ln(b/a)]$ is distributed in a curvilinear manner and hence at equilibrium the concentration profile between b and a is also curvilinear (Crank, 1975). This contrasts with the linear profile in the corresponding planar system. Application of these equations to modeling soil aeration is presented by Letey and Stolzy (1967), and Kowalk, (1985).

By analogy with equation (13) for x direction

$$K = \frac{D_e}{\int_0^x [1/A(x)] dx} \quad (22)$$

when diffusion is cylindrical $A(x) = 2\pi r h = 2\pi x h$ and $A(x)\pi = 2x$ per meter of root, where x is the distance from the centre. Using equation (18) gives

$$K = \frac{D_e}{\int_0^x [1/(2\pi x)] dx} \quad (23)$$

Assuming the boundary conditions $x = a$ (root or platinum electrode radius) and $x = b$ (radial distance from the root axis to the outer boundary of the liquid phase of the soil matrix surrounding the root) the solution for equation (19) yields

$$K = \frac{2\pi h D_e}{\ln(b/a)} \quad (24)$$

for cylindrical systems, the flux per unit length is constant, so K has units of m^2/sec and the flux is per meter of length.

Diffusion in a sphere

Spherical diffusion, as it may be from soil aggregates or fungal masses, has been widely used in soil aeration studies. Its derivation is also presented by Crank (1975). Mathematically it is similar to the linear case which can be derived by simple transformation.

The differential equation for radial diffusion coefficient is expressed by equation (11) for steady-state it becomes

$$\frac{d}{dr} \left[r^2 \cdot D \frac{dC}{dr} \right] = 0 \quad (25)$$

for which the general solution is

$$C = K_2 + K_1/r \quad (26)$$

where K_1 and K_2 are constants to be determined from the boundary conditions. If in the hollow sphere, $a \leq r \leq b$, the surface $r = a$ is kept at a constant concentration C_1 , and $r = b$ on C_2 , then

$$C = \frac{aC_1(b-r) + bC_2(r-a)}{r(b-a)} \quad (27)$$

The final solution is:

$$\frac{Q}{t} = -D_\varepsilon \cdot A \frac{ab(C_1 - C_2)}{r(b-a)} \quad (28)$$

where $a \leq r \leq b$.

The quantity of diffusing substance Q which passes through the spherical wall in time t is given by

$$\frac{Q}{t} = 4\pi D_\varepsilon \frac{ab(C_2 - C_1)}{(b-a)} \quad (29)$$

where $a \leq r \leq b$.

The conductance in the radial direction measured in $\text{cm}^3 \cdot \text{sec}^{-1}$ will be

$$K = 4\pi D_\varepsilon \frac{ab}{(b-a)} \quad (30)$$

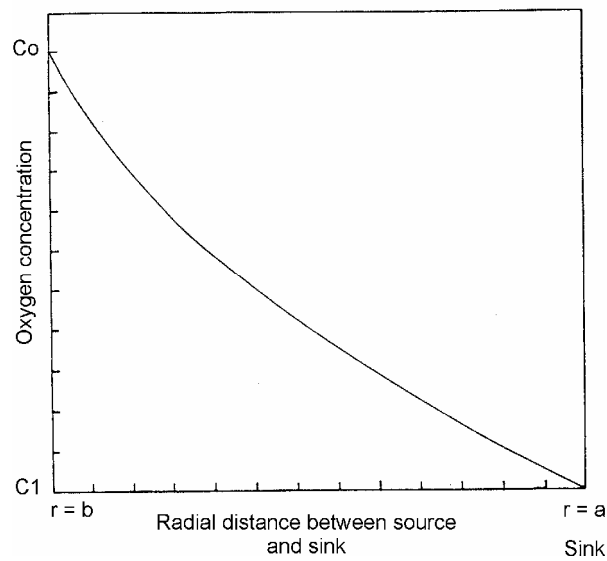


Fig. 3 A curvilinear concentration profile characteristic of a diffusive system in which source and sink lie on concentric cylinders (After Crank, 1975).

Equation (30) may be obtained by analogy with equation (15). For spherical diffusion $A(x) = 4x^2$, where x is the radial distance from the centre of the sphere. Integration of equation (15) for the boundary conditions $x = a$ and $x = b$ gives the solution for K as expressed by equation (30).

It is interesting to note that, for a spherical aggregate, the conductance becomes independent of b when b is large compared to the radius of the aggregate. In other words when $b \gg a$ equation (30) becomes (Campbell, 1985):

$$K = 4\pi D \cdot a \quad (31)$$

Continuity equation including sink terms

Fick's law describes the flux of oxygen but it does not account for oxygen consumption. According to the law of conservation of mass the change of the amount of oxygen in the volumetric unit of soil and in the unit of time for one-dimensional flow is equal to the change of flux dF_x in this elemental volume of soil dx minus the volumetric oxygen consumption of soil S_r , according to the equation:

$$\frac{\partial Q}{\partial t} = -\frac{\partial F_x}{\partial x} - S_r \quad (32)$$

As the amount of oxygen in the soil Q is taken equal to the amount of oxygen in the gas phase of the soil ($C_\varepsilon \cdot \varepsilon$) when we neglect the oxygen in the liquid phase and solid phase, equation (32) becomes:

$$\frac{\partial(C_\varepsilon \cdot \varepsilon)}{\partial t} = -\frac{\partial F_x}{\partial x} - S_r \quad (33)$$

Substituting $F_x = -D_\varepsilon \partial C / \partial x$ (first Fick's law) into equation (33) yields:

$$\frac{\partial(C_\varepsilon \cdot \varepsilon)}{\partial t} = \frac{\partial}{\partial x} \left(D_\varepsilon \frac{\partial C}{\partial x} \right) - S_r \quad (34)$$

In the three-dimensional space it is written as:

$$\frac{\partial Q}{\partial t} = \nabla \cdot (D_\varepsilon \nabla C) - S_r \quad (35)$$

where ∇ is the nabla operator indicating three-dimensional flux.

If we consider only longitudinal transport in the z direction, that means with depth z , the one-dimensional equation (34) becomes.

$$\frac{\partial(C_\varepsilon \cdot \varepsilon)}{\partial t} = \frac{\partial}{\partial z} \left(D_\varepsilon \frac{\partial C}{\partial z} \right) - S_r \quad (36)$$

and for this equation the initial and boundary conditions are:

$$\begin{aligned} \text{for } t = 0 \text{ and } z > 0, \quad C &= C_0; \\ \text{for } t > 0 \text{ and } z = 0, \quad C &= C_0; \\ \text{for } t > 0 \text{ and } z = L \quad \partial C / \partial z &= 0 \end{aligned}$$

Additional assumptions are related to the values of ε_g , D_ε and S_r . It is known, for example, that the oxygen diffusion coefficient D_ε is not dependent upon oxygen concentration C . It is assumed that the oxygen respiration S_r is zero if oxygen concentration C is lower than or equal to a certain critical value. In fact, oxygen uptake S_r is not greatly dependent upon oxygen concentration when C is higher than few percent ($S_r > 0$ for $C > 0$).

Additional solutions of diffusion equation (36) can give the values of C as a function of z , t , ε_g , D_ε and S_r .

After assuming that ε_g and D_ε are constant (case of a homogeneous soil profile) from Fick's second law the continuity equation for z direction can be expressed: (Currie, 1961).

$$\varepsilon \frac{\partial \mathcal{C}_\varepsilon}{\partial t} = D_\varepsilon \frac{\partial^2 C}{\partial z^2} - S_r \quad (37)$$

Equation (37) can also be expressed as follows

$$\frac{\partial \mathcal{C}_\varepsilon}{\partial t} = \frac{D_\varepsilon}{\varepsilon} \frac{\partial^2 C}{\partial z^2} - \frac{S_r}{\varepsilon} \quad (38)$$

The respiration rate S_r may be increased in several ways: by increasing the amount of readily degradable organic matter, by increasing root activity, by watering in so far this encourages microbial and root activity, and by warming the soil (Currie, 1984).

Ohm's law and diffusion analogy

If we have a multilayered soil composed of n layers or elements of thicknesses z_1, z_2, \dots, z_n and diffusion coefficients $D_{\varepsilon_1}, D_{\varepsilon_2}, \dots, D_{\varepsilon_n}$, the fall in concentration through the whole soil profile is the sum of the falls through the elements. Since the rate of transfer F is the same across each element, the total drop in concentration can be expressed by

$$\frac{F_{z_1}}{D_{\varepsilon_1}} + \frac{F_{z_2}}{D_{\varepsilon_2}} + \dots + \frac{F_{z_n}}{D_{\varepsilon_n}} = (R_1 + R_2 + \dots + R_n)J \quad (39)$$

where $R_1 = z_1/D_{\varepsilon_1}$, etc. may be termed formally the resistance to diffusion of each layer (reciprocal of conductance). Thus, the resistance to diffusion of the whole profile is simply the sum of the resistances of the separate layers; assuming that there are not barriers to diffusion between them.

There are close similarities between equations (7) and (8) and the expression of Ohm's law for the conduction of electricity through a homogeneous conductor and it is often helpful to consider diffusion problems using such electrical analogues; it has also proved helpful to develop functional model of diffusion using electrical system (Campbell, 1985). In its expanded form Ohm's law may be written (Armstrong, 1979):

$$\frac{e}{t} = f \cdot (V_0 - V_1) \frac{A}{L} \quad (40)$$

where e is the quantity of electricity (coulombs) flowing through a conductor in t (seconds), L the length of the conductor (cm), A its sectional area (cm²), V_0 and V_1 the electrical potential (volts) at the beginning and end of the conductor, and f the conductivity constant, the value of which depends on the quality of the conducting material and on temperature. Comparing equations (8) and (40) it will be apparent that Q/t is analogous with e/t , D_g with f , $(C_0 - C_z)$ with $(V_0 - V_1)$, and that diffusive resistance $L/(D_g A)$ is an analogue of electrical resistance L/f . In the condensed version of Ohm's law e/t is reduced to the term I (amperes), $(V_0 - V_1)$ reduces to V , and L/fA becomes R , the resistance of the conductor which is measured in ohms (Ω). Ohm's law is then written as

$$I = \frac{V}{R} \quad (41)$$

and is equivalent to a condensed form of equation (8), i.e. $Q/t = \Delta C/R$, where ΔC represents $(C_0 - C_z)$ and R represents $L/(D_g A)$.

At this stage it may be useful to note that just as in an electrical circuit one may calculate the voltage drop V' along any section of conductor by applying the relationship $V' = IR'$ where I is the current flowing through the whole conductor and R' is the resistance in the segment; in a diffusion system one may calculate a localized concentration drop. For homogeneous conductors $R' = R/L$ where R is the length of the segment, L the length of conductor and R its total resistance.

For a number of conductors in series Ohm's law reads:

$$I = \frac{V}{R' + R'' + R''' + \dots} = \frac{V}{R} \quad (42)$$

Similarly, diffusive resistances in series become additive and, as with the flow of electricity where only R approaches zero, so too with diffusion: Q/t remains finite at all values of $R < \infty$. Therefore $R \rightarrow \infty$ as $J \rightarrow 0$; for instance when depth z approaches the water table position at depth L . This important principle is illustrated in fig. 4 where the change in diffusion rate consequent upon extending the distance between source and sink across an isotropic medium is plotted against the change in diffusive resistance. While diffusive resistance increases linearly with increasing path length (depth z) the diffusion rate decreases in a curvilinear fashion, certainly, conductors in series are additive in their resistance to flow in both electrical and diffusion systems.

Models on soil aeration following this direction are presented by Campbell (1985) and Kowalik (1985).

Diffusion in soil aggregates

As declared earlier First Fick's law is fairly realistic for longitudinal transport within the soil profile as a whole. However, if the gas phase is discontinuous somewhere within the soil profile, the assumption of constant S_r/D_g will not hold for a soil profile. Thus, the microconcept is applied for aggregates. Oxygen supply and oxygen flow into the soil aggregates take place in the radial direction from outside to the centre of aggregates, with oxygen consumption in the way.

Mathematical description and solution of oxygen diffusion process in spherical aggregates was given by Currie (1961) and Kowalik (1985). Assuming for simplicity a spherical crumb having an isotropic concentric shell of radius r , the diffusion equation may be written:

$$\frac{\partial(\epsilon C)}{\partial t} = \frac{D_\epsilon}{r^2} \left[\frac{\partial}{\partial r} \left(r^2 \frac{\partial C}{\partial r} \right) \right] - S_r \quad (43)$$

where the symbols are as before but are referring to the properties exclusive to the crumbs as opposed to those of the soil as a whole. Thus, C_r is the concentration of the gas in the pore space ϵ_g .

In a soil in equilibrium, the term $\delta\epsilon \cdot C_r / \delta t$ is zero (steady-state) and the equation (43) rewritten in the form.

$$\frac{\partial}{\partial r} \left(r^2 D_\epsilon \frac{\partial C}{\partial r} \right) = S_r r^2 \quad (44)$$

Further development of equation (44) is presented by Currie (1961) and Kowalik (1985). By assuming $C_r = C_x$ for $r = R$ at the surface of the aggregate the final solution is:

$$C_r = C_x - \frac{S_r}{6D_\epsilon} (R^2 - r^2) \quad (45)$$

Equation (45) allows to calculate the oxygen concentration distribution inside the soil aggregate as a function of radius of the aggregate R , diffusion coefficient D_ϵ , biological respiration S_r and oxygen concentration in the gas phase of the soil profile C_x (it is equal to C_z in the equations dealing with oxygen diffusion in the soil profile). Currie (1984) proposed that the difference $(C_x - C_r)$ could be called an oxygen deficit in the soil aggregate. Taking $(C_x - C_r) = \Delta$ we have:

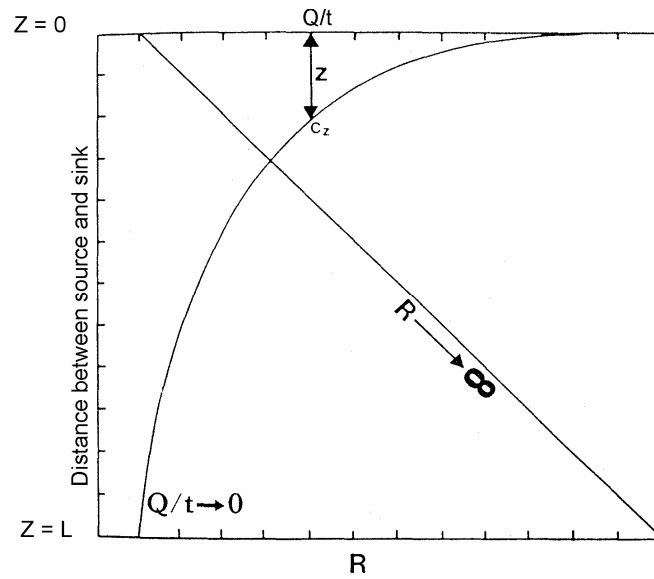


Fig. 4 Showing how a linear increase in diffusive resistance between source and sink in a simple diffusive system is accompanied by a curvilinear decrease in flux (After Armstrong, 1979).

$$\Delta = C_x - C_r = \frac{S_r}{6D_\varepsilon} (R^2 - r^2) \quad (46)$$

And for the maximum deficit at the centre of the aggregate, for $r = 0$:

$$\Delta = \frac{S_r R^2}{6D_\varepsilon} \quad (47)$$

Thus, oxygen deficit Δ is directly proportional to the square of the radius of the aggregate R^2 . This means, the oxygen deficit is quadrupled when the crumb radius is doubled.

For the soil profile, if we want to avoid creating anaerobic conditions inside soil aggregates, then the maximal radius of the soil aggregate is determined by: (Smith, 1977, 1980; Currie, 1984; Kowalik, 1985).

$$R \leq \sqrt{6D_\varepsilon C_x / S_r} \quad (48)$$

Diffusion through the water films

The final segment of the diffusion path to roots takes place through the water films or shell surrounding the roots. The geometry of water-films is depicted in fig. 5, where the cylindrical coordinates can be applied. For steady-state diffusion in cylindrical coordinates, we have: (Letey and Stolzy, 1964)

$$F_x = D' \frac{C_p}{R_r \ln(R_w / R_r)} \quad \text{mg} \cdot \text{cm}^{-2} \cdot \text{s}^{-1} \quad (49)$$

where D' is the coefficient of oxygen diffusion through the water films. The rest of the symbols are indicated in fig. 5. Instead of F_x the symbol ODR (oxygen diffusion rate) has been proposed (Letey and Stolzy, 1964); then

$$ODR = 60 \cdot 10^{-3} D' \frac{C_p}{R_r \ln(R_w / R_r)} \quad \text{g} \cdot \text{cm}^{-2} \cdot \text{min}^{-1} \quad (50)$$

or

$$ODR = 60 \cdot 10^{-3} D' \frac{C_p / R_r}{\ln(1 + d / R_r)} \quad (51)$$

If we consider not only the situation of oxygen respiration at the surface of the root, but also take a cylindrical sample of soil with supply of oxygen from outside and oxygen diffusion and consumption inside the medium the situation from fig. 6 is described by the cylindrical form of the diffusion equation:

$$\frac{\partial(\varepsilon_g \cdot C)}{\partial t} = \frac{1}{r} \frac{\partial}{\partial r} \left(r D_\varepsilon \frac{\partial C}{\partial r} \right) - S_r \quad (52)$$

and for steady state and appropriate boundary conditions, (Lemon, 1962; Kowalik, 1985) derived the following equation:

$$C_r = C_p - \frac{S_r}{4D_\varepsilon} (R_r^2 - r^2) \quad (53)$$

From equation (46) it is possible to calculate for which conditions the middle part of the root can be anaerobic, having S_r , D_ε , C_p and R_r .

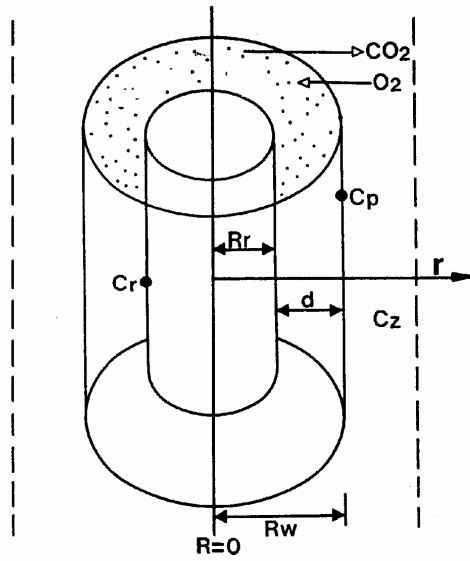


Fig. 5 Plant root surrounded by water-film (After Hillel, 1980; Kowalik, 1985). R_r : radius of plant root or platinum electrode; R_w : radius of outside surface of water film on the plant root or on the platinum electrode; C_p : oxygen concentration in the soil liquid phase on the border with the gas phase.

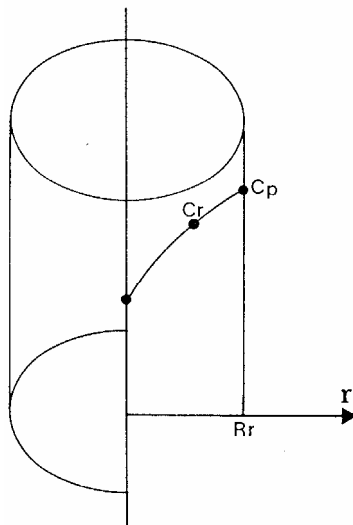


Fig. 6 cylindrical part of the soil body with oxygen consumption inside and oxygen supply from outside (simplified, after Kowalik, 1985).

References

- Armstrong, A.C. 1979. Aeration in higher plants. *Advances in Botanical Res.* 7, 225-332.
- Campbell, G.S. 1985. *Soil physics with basic, developments in soil science* 14, Elsevier, Amsterdam: 12-25.
- Crank, J. 1975. *The mathematics of diffusion*. Oxford University Press.
- Currie, J.A. 1984. Gas diffusion through soil crumbs: the effects of compaction and wetting. *J. of Soil Sci.* 35, 1-10.
- Currie, J.A. 1961. Gaseous diffusion in porous media. III. Wet granular materials. *Brit. J. Appl. Phys.* 12, 275-281.
- Hillel, D. 1980. *Fundamentals of soil physics*. Academic Press, London.
- Kowalik, P.J. 1985. Influence of land improvement on soil oxidation. Swedish University of Agricultural Sciences, Department of Ecology and Environmental Research, Energy Forestry project, Report 42, Uppsala.
- Letey, J. and Stolzy, L.H. 1964. Measurements of oxygen diffusion rates with the platinum microelectrode. III. correlation of plant response to oxygen diffusion rates. *Hilgardia* 35, 567-576.
- Obando, F.H. 1990. Oxygen transport in tilled clay soils, Ph.D. Thesis, Cranfield Institute of Technology, Silsoe College, U.K. Unpublished.
- Phene, C.J., Campbell, R.B. and Doty, C.W. 1976. Characterization of soil aeration in situ with automated oxygen diffusion measurements. *Soil Sci.* 122,5:271-281.
- Smith, K.A. 1980. A model of the extent of anaerobic zones in aggregated soils, and its potential application to estimates of denitrification. *Journal of Soil Sci.* 31, 263-277.
- Smith, K.A. 1977. Soil aeration. *Soil Sci.* 123(5), 284-291.
- Stolzy, L.H. and Letey, J. (1964). Characterizing soil oxygen conditions with a platinum microelectrode. *Advances in Agronomy*, 16, 249-279.

Oxygen Transport in Waterlogged Soils, Part II. Diffusion Coefficients

Franco Humberto Obando Moncayo¹

*Faculty of Agricultural Sciences, Department of Natural Resources and Environment,
University of Caldas, Manizales, Colombia*

*Lecture given at the
College on Soil Physics
Trieste, 3-21 March 2003*

LNS0418025

¹ fobando@yahoo.com

INTRODUCTION

As previously outlined several equations are available and have been used for soils and plants. All of them are some form of first Fick's law as given by

$$dQ = -DA(dc/dx)/dt \quad (1)$$

Equation (1) illustrates some important aspects of aeration in waterlogged soils; first, D is a property of the medium and the gas, and is affected by temperature T . Likewise, the amount of diffusing substance dQ in dt is a direct function of the cross sectional area A and inversely proportional to the distance x . In fact, increasing the water content of air-dry soil, drastically decreases A and creates a further resistance for the flow of oxygen through water films around root plants, soil microorganisms and soil aggregates. The solid phase is also limiting the cross-section of surface of the free gaseous diffusion and the length and tortuosity of diffusion path in soil. In most of cases, soil gas porosity and tortuosity of soil voids are expressed in the equations of diffusion as a broad "diffusion coefficient" (apparent coefficient diffusion).

The process of soil respiration is complicated, involves many parameters, and is difficult to realistically quantify. With regard to the oxygen supply, it is convenient to distinguish "macro" and "micromodels" (DeWilligen and NoorDwijk, 1984; Obando, 1990), and hence, the flux of oxygen is assumed to have two steps. The first step is related to oxygen diffusion from the atmosphere and the air-filled porosity. The second step is related to the oxygen diffusion through water-films in and around plant roots, soil microorganisms and aggregates. Because of these models we obtain coefficients of macro or microdiffusion, rates of macro or microdiffusion, etc. (Kowalik, 1985). In the macrodiffusion process oxygen is transferred in the soil profile, mainly from the soil surface to a certain depth of the root zone, while microdiffusion deals with the flux over very short distances. Both processes, macro and microdiffusion are highly influenced by soil water content. Of course, if water is added to the soil, the result is that the air-filled porosity decreases and at the same time the thickness of soil water-films around plant roots and aggregates increases. Consequently, both macro and microdiffusion decrease.

Diffusion coefficients in the macromodel process

During the last 40 years, several investigations have been made on diffusion of gas through porous media. Currie (1960) proposed that the oxygen diffusion in soils can be described by

$$D_g/D_0 = b\epsilon_g^m \quad (2)$$

where D_g is the diffusion coefficient in soil (cm^2/min), D_0 the gas diffusion coefficient in free air (cm^2/min), ε_g the air-filled porosity, b is a coefficient dependent mainly on the total porosity ε_0 , and m a coefficient dependent on the air-filled porosity and the continuity and tortuosity of the flow path. The constant m has a value which depends on the shape of the soil particles, but generally falls between 1 and 2, for dry materials. The constant b , ranges from 0.5 to 1.0 and depends on the value chosen for m . When water is added to the porous material, the cross section for flow is reduced and the tortuosity of the flow path is increased. As water content approaches saturation, dead-end pores may be formed that contribute to air-filled porosity, but do not aid gas diffusion. Theoretically, the parameter m should be a function of ε_g but in the range of $0.1 < \varepsilon_g < 0.4$, the value of m is constant for many soils, making it easier to determine D_g (Sallam et al, 1984).

Commonly proposed macrodiffusion models have been described by several authors (Campbell, 1985; Kowalik, 1985; Sallam et al, 1984; Obando, 1990; Obando 2003). Some of the values for m and b as indicated from the source are given in table 1.

Table 1. Some examples of the models for diffusion coefficients as a function of air-filled porosity ε_g .

Model	D_g/D_0
Currie	$b\varepsilon_g^m$ ($b \leq 1$) and m are functions of the materials investigated.
Bakker and Hidding	ε_g^2 for well structured soils
Bakker and Hidding	$3\varepsilon_g^3$ for heavy and puddle soils
Millington and Quirk	$\varepsilon_g^{3.33}\varepsilon_0^{-2}$ for wet soils (ε_0 = total porosity).
Sallam et al.	$\varepsilon_g^{3.1}\varepsilon_0^{-2}$ soils under relatively low air-filled porosity

Most of the models proposed are reliable at air-filled porosities above 0.30. However, below this level there is a great variation among them. When Sallam et al. (1984) determined gas diffusion at low air filled porosity levels (0.05, 0.10, and 0.15), they obtained better agreement between calculated and measured D_g by reducing the exponent 3.33 in the Millington-Quirk model to 3.1. Therefore, the following formula for soils under relatively low air-filled porosity was proposed: (see table 1).

$$D_g / D_0 = \varepsilon_g^{3.1} \varepsilon_0^{-2} \quad (3)$$

Those models indicate the high influence of soil structure on soil aeration. For example for the Bakker-Hidding models; if one compares the diffusion coefficients for the soils with gas-filled porosity $\varepsilon_g = 0.14$, the puddle soil has D_ε equal to 0.4 of the aggregated soils, but for the soils with air-filled porosity $\varepsilon_g = 0.70$, the puddle soil has a D_ε equal to 0.1 of the aggregated soil, indicating the great influence of the soil structure particularly at low values of ε_g . Thus, for every individual soil sample it is necessary to measure the individual relationship between ε_g and D_ε .

Methods of measurements of values of D_ε as a function of ε_g are described in the literature (e.g. Callebaut, 1987).

Microdiffusion process

As previously stated, the exchange of oxygen and carbon dioxide through the soil is mainly by molecular diffusion in the gas phase. Gaseous diffusion in soil may be expressed by (Currie, 1961)

$$\varepsilon \frac{\partial C}{\partial t} = D_\varepsilon \frac{\partial^2 C}{\partial z^2} - S_r \quad (4)$$

or as:

$$\frac{\partial C}{\partial t} = \frac{D_\varepsilon}{\varepsilon} \frac{\partial^2 C}{\partial z^2} \pm \frac{S_r}{\varepsilon} \quad (5)$$

where the term S_r is the apparent average sink or source expressed as moles of gas produced or consumed per unit time and unit soil volume. S_r represents the rate of respiration, positive for carbon dioxide production, negative for oxygen consumption. Equation (5) may be solved for many appropriate boundary conditions. For example, in a uniform soil, active to a depth L at which there is a layer impermeable to gas exchange, the oxygen concentration at depth $0 < z < L$ is

$$C_z = C_0 - \frac{S_r}{D_\varepsilon} (Lz - z^2 / 2) \quad (6)$$

This and other solutions have two factors in common: The concentration difference ($C_0 - C_z$) is a function of depth, and is proportional to the ratio S_r / D_ε . Any increase in S_r / D_ε , whether arising from an increase in S_r or decreased D_ε , increases the likelihood of oxygen concentration reaching some small and critical value below which some or all of the respiration processes would change from an aerobic to a less desirable anaerobic state.

On a large scale equation (6) is fairly realistic since aeration generally changes slowly and both S_r and D_e often decrease with depth which makes the ratio S_r/D_e relatively depth invariant (Stolzy et al, 1981). However, if the gas phase is discontinuous somewhere within the soil profile, this assumption of constant S_r/D_e will not hold for a soil profile, and the meaning of S_r leads to the microsite concept introduced by Currie (1961). They have shown that most structural soils are bimodal with regard to diffusion. They concluded that the crumbs have their own particular relative diffusion coefficients D_c , which are mainly affected by the oxygen consumption S_r , the spatial distribution of the liquid phase, the pore size distribution and the size of the soil aggregates.

Diffusion within the soil microstructure (microsite concept)

The early mathematical treatments of gas diffusion in soil given in Fick's law equations, deal with soil as a homogeneous porous medium, with a single diffusion coefficient for any set of physical conditions. Currie (1965) pointed out the limitations of this approach. As declared above, he has shown that most structured soils are bimodal with regard to diffusion. "...Most soils show heterogeneity of pore distribution. For example, soil with a highly developed natural ped structure, and cultivate soil with their crumbs and clods, have distinct zones of crumbs pores, separated by more continuous system of intercrumbs pores...measurements of diffusion in packing of soil crumbs show that intercrumbs pores contribute more per unit of their volume to diffusion through the packing than do crumbs pores... Diffusion to depth in heterogeneous soils will thus occur preferentially through intercrumbs pores, but the path to the respiring site will be completed within crumb pores that are partly or even wholly moisture-saturated. Any attempt to describe the aeration pattern in soils possessing such a bimodal pore distribution needs some knowledge of gas diffusion within the crumbs themselves."

Currie (1961) presented expressions to describe the radial diffusion of oxygen towards the centers of waterlogged soil aggregates, which made it possible to estimate what fraction of a spherical aggregate would be anaerobic, if its radius, the external oxygen concentration, the diffusion coefficient, the solubility of oxygen, and the respiration rate were all known. For any given values for these parameters, there is a critical aggregate radius below which no anaerobic zone exists, and above this critical value the radius of the anaerobic zone rises rapidly with the radius of the aggregate. The relationship between these radii is given by (Smith, 1977)

$$r = r_a - 6D_c \left(\frac{C_w S_w}{S_r} \right) \quad (7)$$

where r is the radius of the aggregate, r_a the radius of the anaerobic zone at the center of the aggregate, D_c the diffusion coefficient of oxygen within the aggregate, C_w the

concentration of oxygen in water, S_w the solubility coefficient of the gas in water and S_r the rate of uptake of oxygen by the soil. $r_o = 0$ when $r = r_c = (6D_c C_w S_w / S_r)^{1/2}$, which is the radius of the smallest aggregate which can have an anaerobic zone at the centre for a given value of C_w . Currie (1961) also made the point that the average respiratory activity of the soil is reduced when there are partially anaerobic aggregates within the profile, so the concentration of oxygen between aggregates at a given depth is higher than if the anaerobic zones were absent, even though aeration of the soil as a whole has deteriorated. In fine textured soils with a well-developed structure, water moves mainly in the relatively large interaggregate pores, so while the drainage of a saturated soil leads to a large increase in the rate of diffusion down the profile (macrodiffusion), it does not initially change the diffusion rate within the aggregates (microdiffusion), and the degree of anaerobiosis in the soil will mainly depend on the size of the aggregates (Smith, 1977). Measurements reported in the literature indicate that the smallest aggregate containing an anaerobic center would have a radius of 9mm, assuming $D_c = 10^{-5} \text{ cm}^2 \cdot \text{s}^{-1}$ and a respiration rate of $4.31 \times 10^{-7} \text{ cm}^3 \text{CO}_2 \cdot \text{cm}^{-3} \text{ soil} \cdot \text{s}^{-1}$.

Diffusion Coefficient in soil aggregates

Based on published data Smith (1980) showed that values for diffusion coefficient of gases within soil aggregates range from $10^{-2} \text{ cm}^2 \cdot \text{s}^{-1}$ for very dry aggregates to $10^{-6} \text{ cm}^2 \cdot \text{s}^{-1}$ for completely water saturated aggregates.

Rate of oxygen uptake S_r

In the context of soil microstructure, S_r is defined as the rate of oxygen uptake (when uptake is not limited by lack of oxygen) per unit volume of aggregate, including intra-aggregate pore space, i.e. $\text{cm}^3 \text{O}_2 \cdot \text{cm}^{-3} \cdot \text{s}^{-1}$ aggregate. Thus, the rate of uptake per unit volume of soil, including inter-aggregate pores is $S_r(1-\epsilon_a)$ where ϵ_a is the inter-aggregate porosity (Smith, 1980).

Published values for S_r have generally been in the range from 10^{-7} to $5 \times 10^{-7} \text{ cm}^3 \text{O}_2 \cdot \text{cm}^{-3} \cdot \text{s}^{-1}$ for most of soils (Kowalik, 1985), but the rate of uptake will vary considerably with soil temperature, organic matter content and the presence or absence of living plant roots or fresh crop residues. A reference value has been taken of $2 \times 10^{-7} \text{ cm}^3 \text{O}_2 \cdot \text{cm}^{-3} \cdot \text{s}^{-1}$ at 10°C , which may be varied in either direction (Smith, 1980). Certainly, after increasing the temperature from 5 to 10°C , S_r was increased about 11% for every 1°C ; for changes from 10 to 20°C it was increased about 6.7% per 1°C , and for changes from 20 to 30°C S_r was increased 3.9 to 6.9% for every 1°C . Values of S_r in the range from 10^{-8} up to $10^{-6} \text{ mg} \cdot \text{cm}^{-3} \cdot \text{s}^{-1}$ are true for most of the arable soils in nature (Kowalik, 1985).

Values of S_r are influenced by other environmental factors such as soil water content and oxygen concentration. The influence of the soil water content θ on the S_r was very small for higher values of θ and this range is important in waterlogged soils (Kowalik, 1985). The relation between values of S_r and soil oxygen concentration in the soil air at depth z , C_z , is a bit more clear. In the range of changes of oxygen concentration from 21 to 10% the respiration was decreased by about 15%. For the values of C_z equal to 5 and 2% the respiration was decreased to 40 and 70%, respectively. That is why some authors suggest that if C_z is below 5%, we do not observe a typical aerobic soil respiration.

Diffusion through the water-films

The diffusion of oxygen through the gas phase into the soil profile from the atmosphere can be quick and effective if ϵ_g is relatively large. In the liquid phase the diffusion is about 10^4 times slower than that in the gas phase. It means that resistance to diffusion of 1000mm of the gas phase is the same as the resistance of liquid water-film of depth of 0.1mm. Consequently, thickness of the water-films d create an additional resistance for the flow of oxygen from the gas phase to the surface of plant roots. The value of d is influenced by the soil water content but the quantitative relation between θ and d is unknown. Thus, the general equation of oxygen transfer in soils is

$$J = -D \frac{dC}{dx} \quad (8)$$

For oxygen flow through water-films we have (Kowalik, 1985)

$$J = -D' \frac{\Delta C}{\Delta x} \quad (9)$$

where D' is the “effective” oxygen diffusion coefficient in the liquid phase, taking into account the tortuosity of soil pores and effective cross-section for diffusion. ΔC is the difference of oxygen concentration on the surface with contact with the gas phase and on the surface with contact with the root surface. Δx is the thickness of water film d . For waterlogged soils, and taking into consideration the influence of soil tortuosity and effective cross-section of soil porosity, we have

$$J = -D' \frac{\Delta C}{d} \quad (10)$$

For waterlogged soils, Bolt (cited by Kowalik, 1985) reported a value for D' equal to $2.5 \times 10^{-5} \text{ cm}^2 \cdot \text{s}^{-1}$.

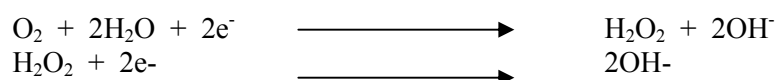
Measurement of Oxygen Diffusion Rate

The polarographic method

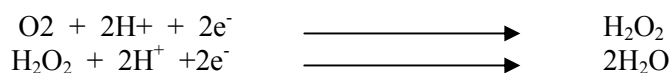
Theory

The polarographic determination of oxygen diffusion rate is based on the characteristic of the current-voltage (I_d -V) curve obtained when oxygen in aqueous solution is electrochemically reduced in a cell in which one electrode, the cathode, consists of a sleeve-insulated thermo-pure platinum wire, while the other is some standard half-cell (e.g. saturated Ag/AgCl reference electrode) the oxygen being replaced by the flow from the surrounding soil. The term polarography was introduced by Herovský and Štichrath in 1925 who developed an apparatus to obtain the graphical representation of the voltage-current curves (Stolzy and Letey, 1964). The curves were called polarograms and the apparatus the polarograph. At present, polarography is a highly developed electrochemical method of analysis. The polarogram shows a step for each reducible species present in solution. This step is the characteristic potential and the height proportional to the concentration of the component. In favorable cases several components may be detected and determined quantitatively from the polarogram. To avoid the residual current due to the dissolved oxygen it is necessary to remove it by bubbling an inert gas (nitrogen or hydrogen) through the solution before the actual measurements. Thus, the limiting current is fixed only by the rate at which the element of interest can reach the electrode surface. It is from this practical principle that the platinum electrode technique was conceived. Oxygen dissolved in electrolytic solutions is easily reduced at both dropping-mercury electrode and platinum electrode and produces a polarogram of two waves of approximately equal height and extending over a considerable range. It has been stated that the first wave is due to the reduction of oxygen to hydrogen peroxide, and the second wave is ascribed to the reduction of hydrogen peroxide either to hydroxyl ion or to water. Thus, the following reactions take place at the surface of the electrodes:

a) In neutral or alkaline solution:



b) In acid solution:



The limiting current I

There are two main mechanisms by which an electroactive substance reaches the surface of an electrode: migration of a charged species caused by the potential difference existing between the electrode surface and the solution, and diffusion of a substance from a region of high concentration to one of lower concentration. Successful polarographic measurements demand that the electroactive species reach the surface of the micro-electrode by diffusion, this being the only process amenable to straight-forward mathematical treatment (Dennis et al., 1974).

In principle, limiting current (total current) that flows in a cell includes contributions from several different processes. It includes the residual current, the migration current and the diffusion current. The current that would flow in the absence of the substance of interest is the residual current; the migration current is the difference between the limiting current actually obtained and the limiting current that would be obtained in the absence of any electrostatic force, and the diffusion current reflects the rate at which the ions or molecules of the substance reach the electrode surface. In practice, the current that actually matters is the difference between the total current and the residual current, which is due to the presence of the substance of interest. This current is the so-called “wave height” (See fig. 1). The total current flowing will in fact be equal to the current carried by the ions undergoing normal electrolytic migration, plus the current due to diffusion of ions

$$I = I_d + I_m \quad (11)$$

where I is the total current, I_d the diffusion current, and I_m the migration current. In practical polarographic work the migration current is eliminated by adding an indifferent electrolyte to the system (e.g. KCl) in concentration so large that its ions carry essentially all the current but does not react with the material under investigation, nor at the electrodes within the potential range studied. Under these conditions the solution is maintained at a low, constant resistance, whilst the migration current of the species under investigation virtually disappears. The residual current is subtracted automatically from the total observed current.

In the determination of oxygen flux in soils the residual current due to impurities is too small to require correction (Lemon, 1962) and as declared earlier, the migration current is controlled by making the reference electrode large in comparison with the small area of the platinum electrode. Under these conditions equation (11) becomes

$$I = I_d \quad (12)$$

The rate of diffusion of the oxygen to the electrode surface is given by Fick's second law equation and the potential of the electrode is controlled by the Nerst equation (Stolzy and Fluhler, 1978) which also applies for the potentiometric method of measurement oxygen in soils. However, this method is out of reach from this

lecture; readers are recommended to review this subject in basic books of soil chemistry, e.g. Bohn et al. (1985).

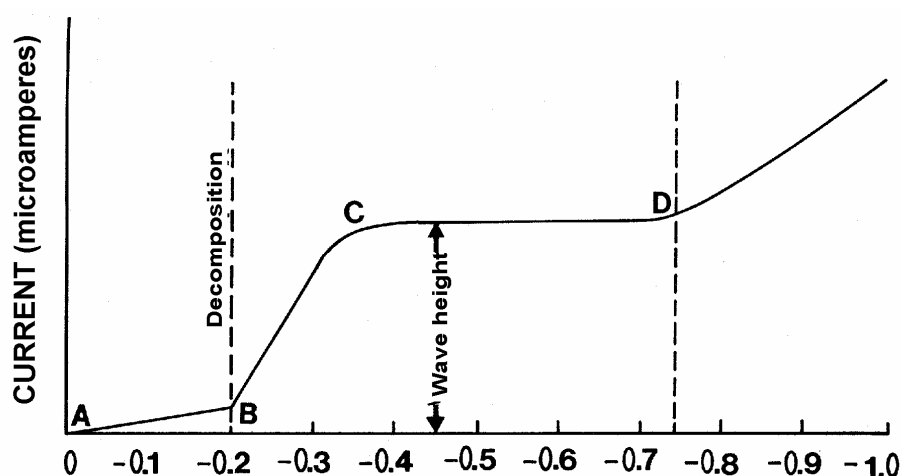


Fig. 1 Typical Oxygen polarographic plateau in a soil suspension.

The diffusion current I_d

Of particular interest in polarography is the diffusion layer, a film of solution perhaps 0.05mm in thickness at the surface of the electrode (Dennis et al, 1974). By referring to the reduction of oxygen in a soil suspension, let us see what happens at the surface of the platinum electrode as its potential is varied (fig. 1). From A to B, at approximately $-0.1V$ versus Ag-AgCl reference electrode, little, if any, oxygen is reduced and the current flow is negligible. At B, where the potential of the platinum electrode is equal to the decomposition potential of the oxygen ions (about $-0.2V$) the current suddenly commences to increase and the platinum electrode becomes depolarized by the oxygen ions which form H_2O_2 , consequently a rapid increase in the current flowing through the cell will be observed. At the point C the current no longer increase linearly with applied potential but approaches a steady limited value at the point D. No increase in current is observed at higher cathode potentials unless a second compound, such as hydrogen depolarize the microelectrode.

At any point on the surface as a result of migration and diffusion from the main bulk of the solution always exceeds the number of oxygen ions which react and are deposited upon the electrode. At the point C the rate of supply of the oxygen ions from the main bulk of the solution to the microelectrode has become equal to the rate of their deposition. Hence at potentials more negative than point D, the concentration of undischarged oxygen ions at the microelectrode surface is negligibly small relative to the oxygen-ion concentration in the bulk of the solution. No further increase in

current passing through the electrolytic cell can be expected, since the limiting current is now fixed by the rate at which oxygen ions can reach the electrode surface. As a consequence of this electrolysis, a concentration gradient is established, causing electrolysis, a concentration gradient is established, causing oxygen to diffuse from the bulk of the bulk of the solution toward the surface of the electrode. If oxygen did not diffuse toward the electrode, the current would fall to zero almost instantaneously because the surface concentration of oxygen would drop to the value governed by the electrode potential and would change no more (Dennis et al, 1974). Nevertheless, the current is sustained by diffusion of additional oxygen toward the electrode under the influence of the concentration gradient. We are now in a position to appreciate the significance of the salient features of a typical current-applied voltage curve with reference to the reduction of oxygen. The minus sign to applied potential signifies that the platinum electrode is made the negative electrode (cathode).

The polarographic principle of platinum electrode

According to the simplest model for a diffusion-controlled process, the observed current is directly related to the difference between the concentration of the oxygen in the bulk of the solution C and at the surface of the electrode C_e . Thus, we may write.

$$I = D(C - C_e) \quad (13)$$

where I is the current and D the diffusion coefficient of oxygen in the porous medium. Fundamentally, it is the potential of the platinum electrode that fixes the surface concentration C_e of the oxygen. At potentials more negative than 0.7v versus Ag-AgCl for the reduction of oxygen, essentially all of the oxygen reaching the electrode surface is immediately reduced. Thus, the surface concentration is so small compared to the bulk concentration that the term $(C - C_e)$ becomes virtually equal to C , and the current attains a limiting value called oxygen diffusion current, which has been denoted by the symbol I_d . Hence,

$$I_d = D \cdot C \quad (14)$$

Analytical applications of polarography to soil oxygen evaluation rely upon the direct proportionality between the diffusion current and the bulk concentration of the oxygen in the liquid and gas phase. For diffusion of an electroactive substance to a stationary platinum electrode under polarographic conditions, in which all the diffusing ions or molecules move in the same direction, the current at an instant t seconds after the electrolysis is begun is given by

$$I_d = nFADt(dC/dx)_0 \quad (15)$$

where n is the number of electrons consumed by each ion or molecule of the electroactive substance ($n = 4$ for oxygen), F the number of coulombs per faraday, A the area of the electrode and $(dC/dx)_0 \cdot t$ is the concentration gradient normal to the electrode surface at time t . Both I_d and n are taken to be positive for cathodic processes and negative for anodic ones, in accordance with the accepted sign convention for the platinum electrode. The factor measured is actually the electric current, which is related to the flux by

$$I_d = nFAF_x \quad (16)$$

Here F_x is the oxygen diffusion rate to the surface of the platinum electrode in soil in $\text{mol}/\text{cm}^2/\text{sec}$. Therefore,

$$F_x = \frac{I_d}{nFA} \quad (17)$$

In order to express results in minutes and grams rather than moles and seconds, the factor 60 and 32 are included, and instead of F_x the symbol ODR can be applied (Letey and Stolzy, 1964). Thus, equation (17) becomes

$$ODR = 32 \cdot 60 \left(\frac{I_d}{nFA} \right) \quad (18)$$

And finally ODR is calculated by

$$ODR = \frac{32 \cdot 60 I_d}{4 \cdot 96500 A} \quad (\text{g} \cdot \text{m}^{-2} \cdot \text{min}^{-1}) \quad (19)$$

where I_d is in amperes.

The physical principle of ODR

Calculating the diffusive resistance offered by the liquid shell (water film of thickness d) surrounding the electrode, it will be shown that at equilibrium, the boundary conditions of the water-film/electrode diffusion-system are those of the simple case for steady-state conditions using cylindrical coordinates. It follows that diffusion must conform with the following equation

$$\frac{Q}{t} = 2\pi h D_\epsilon \left[\frac{C_0 - C_1}{r \ln(b/a)} \right] \quad (20)$$

atmosphere into and through the water-films. This potential gradient can be very strong and have a great effect on C_b (Raats, 1989). For the final segment of the diffusion path to the roots we have

$$J_x = D' \frac{C_b}{R_r \ln(R_w / R_r)} \quad (22)$$

From

$$F_x = \frac{I_d}{nFA} = ODR, \quad (23)$$

we have

$$ODR = 60 \cdot 10^{-3} \cdot D' \frac{C_p / R_r}{\ln(1 + d / R_r)} \quad (24)$$

Equation (24) quantifies the resistance of the water-film thickness d relative to transport in the gas phase of the soil profile, and makes allowance for the fall in oxygen concentration which occurs across the water-film. For polarographical measurements the general equation of oxygen transfer in soil (first Fick's law) can be expressed as

$$J_x = D' \frac{dC}{dx} \quad (25)$$

For oxygen flow through water films we have (Kowalik, 1985)

$$J_x = D' \frac{(C_b - C_a)}{(a - b)} = D' \frac{\Delta C}{\Delta x} \quad (26)$$

where D' is the "effective" oxygen diffusion coefficient in the liquid phase, ΔC the difference of oxygen concentration on the surface in contact with the gas phase and on the surface in contact with the root surface, and Δx the thickness of the path ($b - a$).

Substituting ($b - a$) by the thickness of water film d , we have

$$J_x = D' \frac{\Delta C}{d} \quad \text{mg} \cdot \text{cm}^{-2} \cdot \text{sec}^{-1} \quad (27)$$

Taking a physical unit of rate of flow in $\text{g} \cdot \text{cm}^{-2} \cdot \text{min}^{-1}$ it was proposed by Letey and Stolzy (1964) to introduce a symbol ODR (oxygen diffusion rate) where for one dimensional flow

$$ODR = 60 \cdot 10^{-3} J_x = -60 \cdot 10^{-3} D' (\Delta C / d) \quad \text{g} \cdot \text{cm}^{-2} \cdot \text{min}^{-1} \quad (28)$$

Making the assumption that

$$\Delta C = C - C_e = C_p - C_e \quad (29)$$

and taking $C_e = 0$ for one-dimensional diffusion we obtain

$$ODR = 60 \cdot 10^{-3} D' \frac{C_p}{d} \quad (30)$$

From this notation, it is clear that the measurement of ODR is related at the same time to the measurement of the potential oxygen concentration in soil C_p , the soil water regime related to the thickness of the soil water films d , and the soil structure influencing the coefficient D' (Kowalik, 1985).

References

- Bohn, H.L. Mcleam, B.L. and O'Connor, G.A. 1985. Soil chemistry. Wiley: London.
- Callebaut, F. 1987. Soil aeration. In: College on Soil Physics Internacional Centre for Theoretical Physics, Trieste, Italy.
- Campbell, G.S. 1985. Soil physics with basic, developments in soil science 14, Elsevier, Amsterdam: 12-25.
- Currie, J.A. 1965. Diffusion within soil microstructure: a structural parameter for soils. J. of Soil Sci. 16 (2). 279-289.
- Currie, J.A. 1961. Gaseous diffusion in porous media. III. Wet granular materials. Brit. J. Appl. Phys. 12, 275-281.
- Currie, J.A. 1960. Gaseous diffusion in porous media. Brit. J. Appl. Phys. 11, 314-324.
- Dennis, G.P., Hayes, J.M. and Hieftje, G.M. 1974. Chemical separations and measurements. Theory and practice of analytical chemistry. Indiana University, Saunders Golden Series.
- De Willigen, P. and Van Noordwijk, M. 1984. Mathematical models on diffusion of oxygen to and within plant roots, with special emphasis on effects of soil-root contact. I. Derivation of the models. Plant and Soil 77, 215-231.

- Kowalik, P.J. 1985. Influence of land improvement on soil oxidation. Swedish University of Agricultural Sciences, Department of Ecology and Environmental Research, Energy Forestry project, Report 42, Uppsala.
- Lemon, E.R. 1962. Soil aeration and plant root relations. I theory. *Agronomy Journal* 54: 167-170.
- Letey, J. and Stolzy, L.H. 1964. Measurements of oxygen diffusion rates with the platinum microelectrode. III. correlation of plant response to oxygen diffusion rates. *Hilgardia* 35, 567-576.
- Obando, F.H. 1990. Oxygen transport in tilled clay soils, Ph.D. Thesis, Cranfield Institute of Technology, Silsoe College, U.K. Unpublished.
- Obando, F.H. 2003. El transporte del oxígeno en el suelo. Relaciones agrofísicas básicas. Universidad de Caldas. Manizales, Colombia (In press).
- Raats, P. 1989. Physical aspects of growth and functioning of plant roots. Lecture notes, College on Soil Physics. International Centre for Theoretical Physics, Trieste Italy.
- Sallam, A.; Jury, W.A. and Letey, J. 1984. Measurement of gas diffusion coefficient under relatively low air-filled porosity. *Soil Sci. Soc. Am. J.* 48, 3-6.
- Smith, K.A. 1980. A model of the extent of anaerobic zones in aggregated soils, and its potential application to estimates of denitrification. *Journal of Soil Sci.* 31, 263-277.
- Smith, K.A. 1977. Soil aeration. *Soil Sci.* 123(5), 284-291.
- Stolzy, L.H. Focht, D.D. and Fluhler, H. 1981. Indicators of soil aeration status. *Flora* 171, 236-265.
- Stolzy, L.H. and Fluhler, H. (1978), Measurement and prediction of anaerobiosis in soils. In: Nielsen, D.R. and MacDonald, J.G., *Nitrogen in the environment*. Academic Press, New York: 363-425.
- Stolzy, L.H. and Letey, J. (1964). Characterizing soil oxygen conditions with a platinum microelectrode. *Advances in Agronomy*, 16, 249-279.

Influence of a Compacted Subsurface Layer on Soil Erosion

Svetla Rousseva¹

*N. Poushkarov Research Institute for Soil Science and Agroecology,
Sofia, Bulgaria*

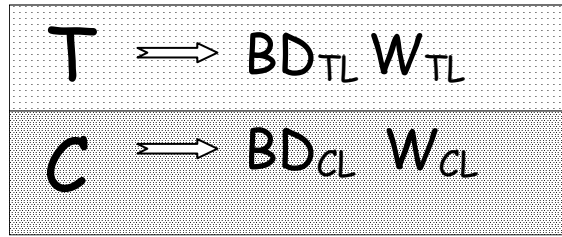
*Lecture given at the
College on Soil Physics
Trieste, 3-21 March 2003*

LNS0418026

¹ svetrou@yahoo.com

It has been recognized that water erosion of soil and soil compaction are among the major soil degradation processes in Europe (Varallyay, 1992; Oldeman et al., 1991; Fraters, 1996). Little is known about the relationships between soil compaction and the soil erosion processes (van den Akker et al., 1999; Froese et al., 1999). Effect of rainfall on soil erosion, i.e. the rainfall erosivity has been related logarithmically to rainfall intensity (Wischmeier and Smith, 1978). Texture, structure, water permeability and humus content are the soil properties, which have been considered as most important for evaluating the effect of soil on water erosion rates (Wischmeier and Mannering, 1969; Wischmeier et al., 1971). I will discuss a mathematical model developed for estimating the influence of compacted subsurface layer formed below a shallow tillage layer on soil erosion.

The mathematical model is developed on the basis of data from field experiments with simulated rainfalls of intensities from 18 to 120 mm h⁻¹ to study the influence of compacted subsurface layer caused by continuous shallow tillage on the soil erosion processes on Haplic Kastanozem (Rousseva and Lozanova, 2000). A soil with a compacted subsurface layer can be represented conceptually as a media consisting of two layers – tilled layer TL and compacted layer CL which differ in their physical properties, such as bulk density BD and water retention W .



Indices of compaction I_{BD} and soil water distribution I_W are defined to characterize the profile variability of the antecedent soil physical conditions. The index of compaction characterizes the degree of compaction by the relative change of soil bulk density in CL with regard to TL while the index of soil water distribution identifies the respective change of soil water content.

$$I_{BD} = \Delta BD = 100 (BD_{CL} - BD_{TL}) / BD_{TL} \quad (1)$$

where I_{BD} ($100 > I_{BD} > 0$) is the index of subsurface compaction, %; ΔBD the relative increase of soil bulk density in CL with regard to TL; BD_{CL} the value of BD in CL, and BD_{TL} the value of BD in TL.

$$I_W = \Delta W = 100 (W_{CL} - W_{TL}) / W_{TL} \quad (2)$$

where I_W ($100 > I_W > -100$) is the index of the soil water distribution profile, %; ΔW the relative change of gravimetric soil water content in CL with regard to TL; W_{CL} the value of W in CL, and W_{TL} the value of W in TL.

Considered characteristics of the soil erosion processes are the minimal rainfall impacting energy needed to initiate runoff E_0 , the sediment load per unit rainfall impacting energy SL and the net sediment load per 50 mm rainfall SL_{net} . The model for estimating the influence of compacted subsurface layer formed below a shallow tillage layer on soil erosion links E_0 , SL and SL_{net} [i.e. $f(I_{\text{BD}}, I_{\text{W}}, I_{\text{R}})$] with the indices of compaction and soil water distribution, and the rainfall intensity. Hence, we have

$$f(I_{\text{BD}}, I_{\text{W}}, I_{\text{R}}) = a_0 + [a_1 (I_{\text{W}})^m + a_2 (I_{\text{BD}})^n] [a_3 + a_4 \log_{10} (I_{\text{R}})] \quad (3)$$

where a_0 , a_1 , a_2 , a_3 , a_4 , m and n are parameters to be evaluated by quasi-Newton non-linear estimation fit of Equation (3) to measured values of E_0 , SL (or SL_{net}), I_{BD} , I_{W} and I_{R} the rainfall intensity, $\text{mm} \cdot \text{h}^{-1}$.

The data shown in Tables 1 and 2 give an idea about the value ranges of the input parameters evaluating the parameters of Equation (3) presented in Table 3.

Table 1. Means and standard deviations of the input (dependent) variables for the left side of Equation (3): the minimal rainfall impact energy needed to initiate runoff E_0 , the sediment load per unit rainfall impact energy SL and the net sediment load per 50 mm rainfall SL_{net} .

Intensity level	E_0 ($\text{MJ} \cdot \text{ha}^{-1}$)		SL ($\text{t} \cdot \text{MJ}^{-1}$)		SL_{net} ($\text{t} \cdot \text{ha}^{-1}$)	
	Mean	Std. Dev.	Mean	Std. Dev.	Mean	Std. Dev.
$I_{\text{R}}1^{\text{a}}$	5.009	6.658	0.205	0.164	2.473	1.973
$I_{\text{R}}2^{\text{a}}$	4.013	5.060	1.511	0.735	17.945	13.200
$I_{\text{R}}3^{\text{a}}$	1.902	2.337	3.889	0.575	48.390	14.423
$I_{\text{R}}4^{\text{a}}$	1.326	1.198	7.294	1.047	94.831	23.475
$I_{\text{R}}1^{\text{b}}$	1.909	2.478	0.209	0.076	2.610	0.987
$I_{\text{R}}2^{\text{b}}$	2.329	3.060	0.523	0.054	6.636	2.250
$I_{\text{R}}3^{\text{b}}$	1.806	2.120	1.098	0.099	13.511	4.036
$I_{\text{R}}4^{\text{b}}$	1.251	1.063	2.779	0.521	36.875	6.321

^a compaction of the layer 10-30 cm; ^b no subsurface compaction of the layer 10-30 cm.

Table 2. Means and standard deviations of the input variables for the right side of Equation (3): rainfall intensity I_R and the indices of subsurface compaction I_{BD} , and soil water profile I_W .

Intensity level	I_{BD} (%)		I_W (%)		I_R (mm·h ⁻¹)	
	Mean	Std. Dev.	Mean	Std. Dev.	Mean	Std. Dev.
I_{R1}^a	16.3	2.6	27.0	60.3	20.1	1.8
I_{R2}^a	14.9	3.2	26.0	61.1	29.1	3.1
I_{R3}^a	14.6	4.2	26.0	61.5	52.8	6.0
I_{R4}^a	13.8	4.0	24.0	62.6	107.3	9.7
I_{R1}^b	8.4	1.1	3.3	8.5	19.7	1.3
I_{R2}^b	9.3	0.5	-1.6	12.3	34.5	5.1
I_{R3}^b	8.9	0.9	-2.2	12.9	57.9	5.5
I_{R4}^b	8.1	1.8	-3.6	13.8	110.2	9.4

^a compaction of the subsurface layer 10-30 cm; ^b no subsurface compaction.

Table 3. Values of the parameters of Equation (3) obtained by non-linear fit to the measured input characteristics.

f	I_W	a_0	a_1	m	a_2	n	a_3	a_4
E_0	≥ 0	4.6	0.08	1	2.8	-0.8	2.9	-1.5
E_0	< 0	0.46	-0.04	1	0.5	1	-0.5	0.4
SL	≥ 0	-0.19	0.07	1	3.58	0.2	-0.7	0.6
SL	< 0	0.0	-0.32	1	0.03	2	-0.9	0.8
SL_{net}	≥ 0	-5.2	0.27	1	13.7	0.6	-1.3	1.03
SL_{net}	< 0	-7.3	-3.3	1	0.03	3	-1.7	1.4

The plots in Figures 1, 2, 3 and 4 illustrate that the model shows good capability of predicting the soil erosion characteristics depending on the degree of compaction and the rainfall intensity. The estimates of E_0 , SL and SL_{net} , predicted by the model for three levels of the index of soil water distribution and four levels of the rainfall intensity, demonstrate the basic trends of soil erosion behaviour under conditions of a compacted subsurface layer. It is established that the type of the relationships between the soil erosion characteristics and the degree of compaction depends considerably on the index of soil water distribution. Generally, a compacted subsurface layer affects soil erosion much more significantly when the water content is higher in TL than in CL. Verification of the model is needed for still broader ranges of the input soil characteristics to confirm its suitability for predictive purposes.

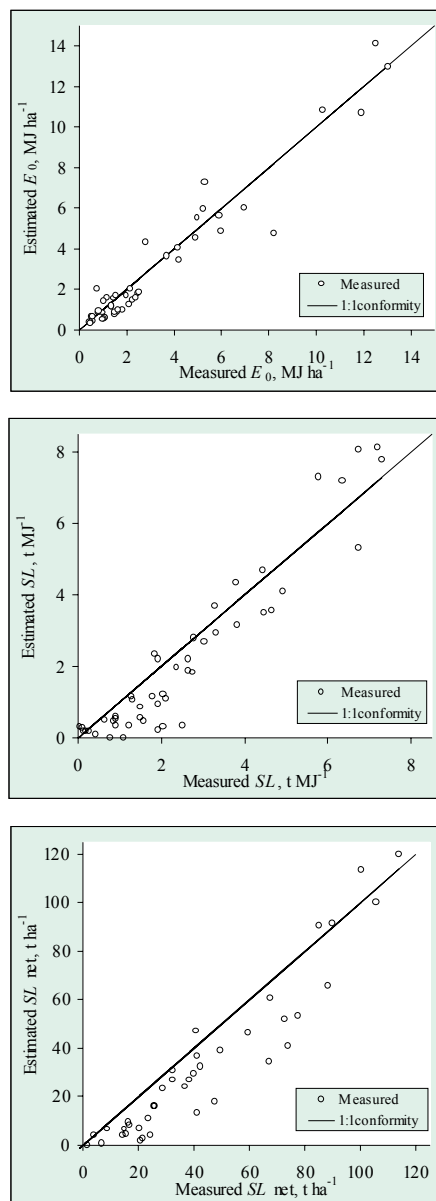


Figure 1. Soil erosion characteristics estimated by Equation (3) versus measured values. The parameters of Equation (3) are as listed in Table 3.

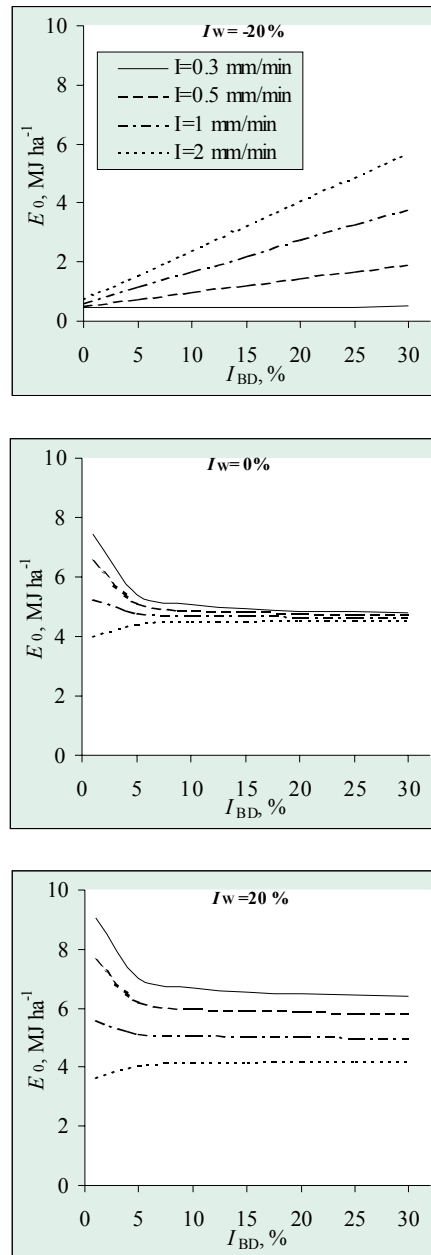


Figure 2. Predicted relationships between the minimal rainfall impact energy needed to initiate runoff E_0 and the index of subsurface compaction I_{BD} for four levels of rainfall intensity I and three levels of the index of soil water distribution I_W .

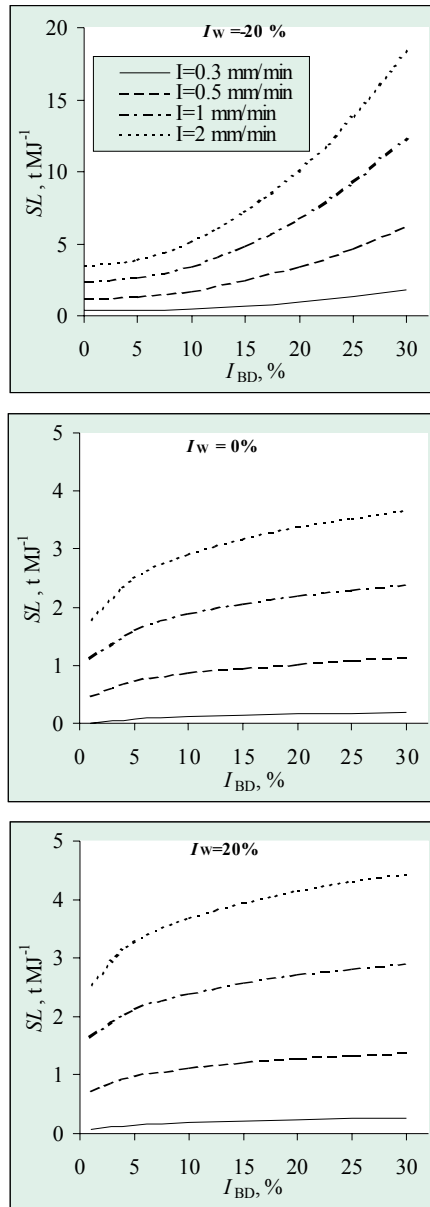


Figure 3. Predicted relationships between the sediment load per unit rainfall, impact energy SL and the index of subsurface compaction I_{BD} for four levels of rainfall intensity I and three levels of the index of soil water distribution I_w .

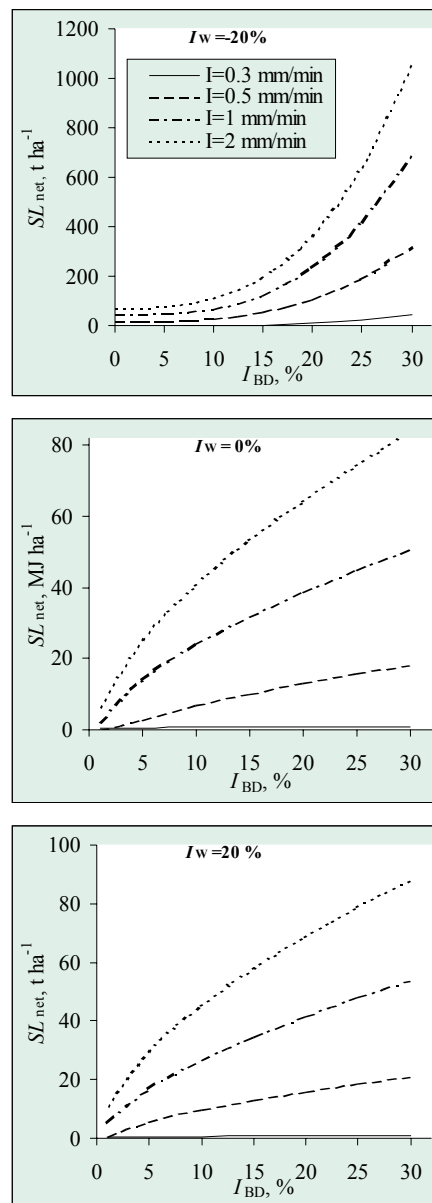


Figure 4. Predicted relationships between the net sediment load SL_{net} caused by 50 mm rainfall and the index of subsurface compaction I_{BD} for four levels of rainfall intensity I and three levels of the index of soil water distribution I_w .

References

- Fraters, B. (1996): *Generalized Soil Map of Europe. Aggregation of the FAO-Unesco soil units based on the characteristics determining the vulnerability to degradation processes*. National Institute of Public Health and the Environment (RIVM), Bilthoven, The Netherlands. RIVM Report no. 481505006. 60 pp.
- Froese, J.C., Cruse, R.M. and Ghaffarzadeh, M. (1999): Erosion mechanics of soils with an impermeable subsurface layer. *Soil Sci. Soc. Am. J.* **63**: 1836-1841.
- Oldeman, R., Hakkeling, R.T.A. and Sombroek, W. (1991): *World Map on the Status of Human-Induced Soil Degradation. An Explanatory Note*. Global Assessment of Soil Degradation. GLASOD. ISRIC – Winand Centre – ISSS – FAO – ITC, Wageningen.
- Rousseva, S. and Lozanova, L. (2000): Influence of subsoil compaction of Kastanozem on the soil erosion processes. In: M. Birkas, C. Gyúicza, C. Farkas and M. Gecse (Eds.) *Proceedings of the 2-nd Workshop and International Conference on Subsoil Compaction*. Gödöllő, Hungary (29-31 May 2000), pp. 73-79.
- Van den Akker, J.J.H., Arvidsson, J. and Horn, R. (Eds.) (1999): *Experiences with the impact and prevention of subsoil compaction in the European Community. Proceedings of the first workshop of the Concerted Action "Experiences with the impact of subsoil compaction on soil, crop growth and environment and ways to prevent subsoil compaction"*, 28-30 May 1998, Wageningen, The Netherlands. Wageningen, DLO-Staring Centrum. Report 168, 344 pp.
- Varallyay, G. (1992): Central and East European erosion overview. In: *Soil erosion prevention and remediation workshop, US-Central and Eastern European Agro-Environmental Program*, April 27 – May 1 1992, Budapest, Hungary. USDA/SCS, pp. 26-37.
- Wischmeier, W.H., Johnson, C.B., Cross, B.V. (1971): A soil erodibility nomograph for farmland and construction sites. *J. Soil and Water Conservation*. **26**: 189-193.
- Wischmeier, W.H. and Smith, D.D. (1978): *Predicting Rainfall Erosion Losses – A Guide to Conservation Planning*. USDA, Agricultural Handbook No. 537. US Government Printing Office, Washington D.C., 58 pp.
- Wischmeier, W.H. and Mannering, J.V. (1969): Relation of soil properties to its erodibility. *Soil Sci. Soc. Am. Proc.* **33**: 131-137.

Ideas for Physical Interpretation of the USLE

Svetla Rousseva¹

*N. Poushkarov Research Institute for Soil Science and Agroecology,
Sofia, Bulgaria*

*Lecture given at the
College on Soil Physics
Trieste, 3-21 March 2003*

LNS0418027

¹ svetrou@yahoo.com

Soil Erosion by Water – Extend, Processes and Model for Conservation Planning

In order to develop sustainable systems of agriculture that satisfy the present and the future needs of the mankind, there must be reliable information on the constraints and potential of the land resource. The UNEP Project GLASOD (GLobal Assessment of SOil Degradation) recognized erosion by water as the most important soil degradation type, representing more than a half of all soil degradation (Oldeman et al., 1991).

Soil erosion by water refers to a series of processes leading to soil depletion and export of sediment. It takes place through three main processes: (i) mechanical disruption, slaking, compaction, dispersion and detachment of soil particles, aggregates and clods from the soil mass due to the impact of raindrops and the overland flow; (ii) movement of detached material by gravity or by overland flow and (iii) deposition.

Planning for soil and water conservation measures requires knowledge of the relations between the driving forces that cause loss of soil (e.g. the erosivity of rainfall, the slope of the land, the erodibility of soil) and the factors that help to reduce such loss (e.g. the plant cover, the conservation practices and measures, the soil resistance). The first developed and one of the most widely-used models for effective conservation planning based on predictions of average annual soil erosion rates and able to estimate soil loss over a wide range of situations is the Universal Soil Loss Equation (USLE). The USLE approach to soil erosion description (Wischmeier and Smith, 1978) is empirical and based on statistical relationships undermining its universal applicability. Further I will discuss ideas for introducing deterministic elements in the USLE approach for estimating the cover and management factor C and the soil erodibility factor K.

Cover and Management Factor C

Concepts

Vegetation, being the most important component of the earth's ecosystems, modifies the impact of raindrops and overland flow. Vegetative canopy influences soil and water losses by changing the impact and intensity of rainfall, the resistance to water flow through the enlarged-by-plants hydraulic roughness, the total amount of water available to transport sediment and the distribution of throughfall (Haynes, 1940; Morgan, 1980; De Ploey, 1982 and 1984). It has been known at least since 1916 (Kiesselbach, 1916) that plants intercept and transmit rainwater down their stems and at least since 1948 that vegetation canopies change the drop-size distribution of rain and that splash detachment under canopies is different from that on a bare soil (Chapman, 1948). For the time being, it has been known that vegetation affects the rainfall impact on soil through storing rainwater on leaves and branches (intercepted store), transmission of rainwater down the leaves, branches and stems to the ground

(steam flow) and transformation of the rainwater to water drops drained from the leaves (leaf drainage).

Considering the present state of knowledge about the role of vegetation during rainfall events, the net volume of the rainfall NR at any moment t after the start of rain can be conceptually presented as a sum of four portions: (i) rainfall directly reaching the soil DR ; (ii) rainwater intercepted by the vegetation IR ; (iii) rainwater reaching the ground through flow down the leaves and stems SF and (iv) rainwater reaching the ground as modified by the vegetation rainfall MR . Hence,

$$NR(t) = DR(t) + IR(t) + SF(t) + MR(t). \quad (1)$$

With respect to soil erosion, IR and SF do not directly contribute to soil detachment. Hence, the net rainfall impact energy on soil with vegetation cover KE_{imp} is considered for DR and MR with

$$KE_{imp}(t) = KE_{DR}(t) + KE_{MR}(t). \quad (2)$$

To resolve Equation (2), we should take into account the following relationships.

- $DR(t)$ is proportional to $NR(t)$ with coefficient of proportionality equal to the portion of the soil that is not protected by the vegetation canopy:

$$DR(t) = (1-c) NR(t); \quad (3)$$

- the model of Van Elewijck (1989a, b), modified by Morgan et al. (1998) for the stemflow:

$$SF(t) = 0.5 (TIF) \cos \alpha; \quad (4)$$

- the sum of $IR(t)$ and $SF(t)$ is actually the temporary intercepted by vegetation rainfall (TIF):

$$TIF(t) = IR(t) + SF(t); \text{ and} \quad (5)$$

- the model of Merriam (1973) for the interception store is:

$$IR(t) = IR_{max} \{1 - \exp[-DR(t)/IR_{max}]\}. \quad (6)$$

Substituting Equations (3) through (6) into Equation (1), solving it for $MR(t)$ and taking into account that

$$EK_{MR}(t) = 0.5 V^2 MR(t) \quad (7)$$

and

$$KE_{DR}(t) = (1-c) KE_{rain}(t), \quad (8)$$

we obtain an equation for estimating the impact energy of rainfall on soil with vegetation cover at any moment t after the start of rain:

$$EK_{\text{imp}}(t) = (1-c)EK_{\text{rain}}(t) + 0.5(1-0.5\cos\alpha)V \int_0^t \{cDR(t') - IR_{\text{max}} \{1 - \exp[-DR(t')/IR_{\text{max}}]\}\} dt' \quad (9)$$

where $EK_{\text{imp}}(t)$ is the impact energy of rainfall on soil with vegetation cover, $\text{J}\cdot\text{m}^{-2}\cdot\text{mm}^{-1}$; $EK_{\text{rain}}(t)$ the impact energy of rainfall on bare soil, $\text{J}\cdot\text{m}^{-2}\cdot\text{mm}^{-1}$; c the canopy cover expressed as a portion of the ground area covered by vegetation canopy ($1 \geq c \geq 0$); α the average acute angle (degrees) of leaves and branches to the plant stem; V the fall velocity of the drops dripping from the vegetation on the soil, $\text{m}\cdot\text{s}^{-1}$; DR the volume of rainfall, mm ; and IR_{max} the maximum volume, mm , of the interception store for particular crop or vegetation cover.

The concept of the USLE cover and management factor C can be presented as:

$$C = \sum_{k=1}^7 (EI_{30} \sum_{j=1}^m \sum_{i=1}^n \frac{A_{cijk}}{A_{ijk}}) \quad (10)$$

$$C \propto \frac{A_c}{A} = F_C \frac{EK_{\text{Cimp}}}{EK_{\text{Rimp}}} \quad (11)$$

where A and EK_{Rimp} are the soil loss and the rainfall impacting energy for bare soil; A_c and EK_{Cimp} are the soil loss and the rainfall impacting energy for a specific vegetation; EI_{30} is the rainfall erosivity factor; F_C is a constant characterizing the specific vegetation.

Considering the average annual number of erosive rainfall events n and the average annual rate of a single rainfall event P , Equation (9) can be rewritten as

$$\frac{EK_{\text{Cimp}}}{EK_{\text{Rimp}}} = 1 - c + \frac{0.5V^2 n (1 - 0.5 \cos\alpha) (cP - IR_{\text{max}})}{EK_{\text{rain}}}. \quad (12)$$

Substituting Equation (12) into Equation (11) results in a formula, which is convenient for calculating the C-factor of a specific vegetation depending on the canopy cover c , the average acute angle of leaves and branches to the plant stem α and maximum volume of the interception store for particular crop or vegetation cover IR_{max} .

Values of the constant F_C have been calculated (Rousseva, 2002) for the main field crops and perennials using a regression analysis of two data sets – calculated proportions of impacting energies according to Equation (12) and values of the C-factor obtained by long-term field plot measurements.

Illustration

Equation (9) is applied to estimate the impacting energy of a 30-mm rainfall of intensity $30 \text{ mm}\cdot\text{h}^{-1}$ on four types of agricultural plants: wheat, maize, alfalfa and apple orchard for the period May – August. The input parameters needed for resolving Equation (9) were set in accordance with data from measurements presented in different literature sources Rousseva et al. (2000), Roshkovan (1988), Laws (1941), Brandt, (1989), Daskalov et al. (1994) and Morgan et al. (1998). Figures 1, 2 and 3 illustrate some results from the application of Equation (9).

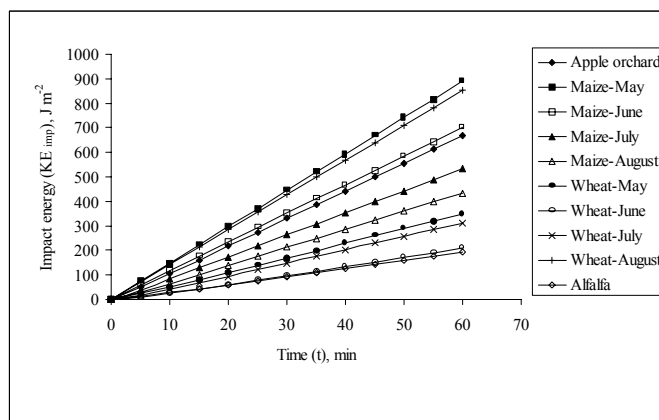


Figure 1. Impacting energy of modified by different plants rainfall with constant intensity of $30 \text{ mm}\cdot\text{h}^{-1}$ calculated according to Equation (9).

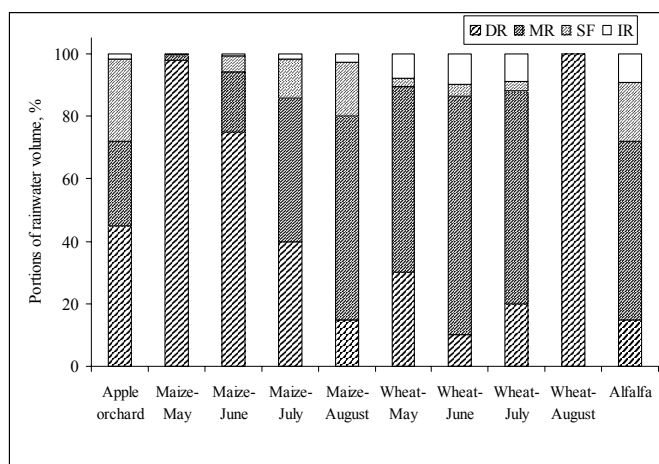


Figure 2. Estimated percentage portions of rainwater: directly reaching the ground (*DR*), reaching the ground as modified by the vegetation (*MR*), reaching the ground through flow down the leaves and stems (*SF*) and intercepted by the vegetation (*IR*), for months with high erosion risk. The amount of rainfall is 30 mm and the intensity is $30 \text{ mm}\cdot\text{h}^{-1}$.

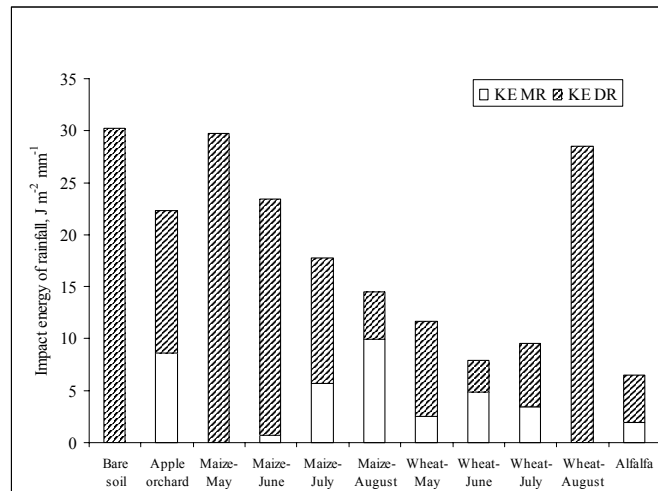


Figure 3. Estimated impacting energy of 30 mm rainfall with constant intensity $30 \text{ mm} \cdot \text{h}^{-1}$ modified by different plants.

Reliability

The reliability of this approach for assessing the rainfall impacting energy on soil with vegetation canopy cover was estimated comparing the KE_{MR} values calculated with Equation (9) for wheat, maize, alfalfa and apple orchard for the period April – August with the respective values calculated according to an already approved model (Morgan et al., 1998) for calculating the kinetic energy of the leaf drainage according to Brandt (1990) is

$$KE_{MR} = 15.8 (H_{\text{eff}})^{0.5} - 5.87 \quad (13)$$

The mean of the differences between the values of KE_{MR} calculated by these two approaches is $0.77 \text{ J} \cdot \text{m}^{-2} \cdot \text{mm}^{-1}$ and was not statistically significant using a t-test ($p = 0.014$). These findings are well visualised in Fig. 4 showing the KE_{MR} estimates according to Equation (13) versus those calculated by Equation (9).

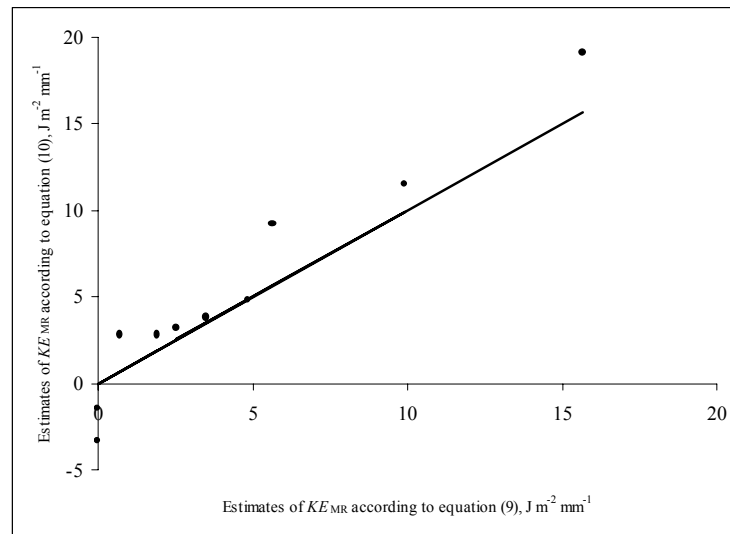


Figure 4. Estimated impact energy (KE_{MR}) of modified-by-vegetation rainfall according to Equation (13) versus respective estimates by Equation (9). Straight line represents 1:1 coincidence.

Fig. 4 also shows well one disadvantage of the estimates of Equation (13), that is that the values of KE_{MR} at effective height of vegetation lower than 0.13 m are negative. Obviously, the Equation proposed in this study does not show such disadvantage, assigning close to zero but still positive values of KE_{MR} .

Application

The approach for estimating cover and management factor was applied for the purposes of a geographic information system for soil erosion risk assessments on the territory of Bulgaria at a scale of 1: 100 000. Values of mean monthly canopy cover c , effective plant height H_{eff} , average acute angle (degrees) of leaves and/or branches to the plant stem α , maximum volume of the interception store IR_{max} , and fall velocity of the drops dripping from the vegetation on the soil V were set for main field crops and perennials in accordance with data from measurements presented in different literature sources. C-factor values were calculated for wheat, maize, sunflower, potatoes, tobacco, beats, alfalfa, vineyards and orchards using Equations (11) and (12) with respect to rainfall erosivity monthly distributions for each of the 47 agro-ecological regions distinguished on the country's territory. The data in tables 1 and 2 show that the approach applied for assessing the cover and management factor has resulted in reasonable estimates of values for the main field crops and perennials grown on the territory of Bulgaria.

Table 1. Mean, minimal and maximal values and standard deviations of the crop and management factor C of the main field crops estimated for 47 agro-ecological regions distinguished on the territory of Bulgaria.

Crop	Wheat	Wheat*	Maize	Maize*	Sunflower	Tobacco	Potatoes	Beats	Alfalfa
Parameter									
Mean	0.22	0.28	0.39	0.50	0.32	0.71	0.69	0.34	0.07
St.Dev.	0.05	0.04	0.06	0.04	0.05	0.08	0.03	0.05	0.02
Minimum	0.12	0.16	0.27	0.42	0.20	0.51	0.62	0.22	0.04
Maximum	0.32	0.34	0.52	0.59	0.44	0.84	0.75	0.44	0.10

* For eroded lands

Table 2. Mean, minimal and maximal values and standard deviations of the crop and management factor C of vineyards and orchards estimated for 47 agro-ecological regions distinguished on the territory of Bulgaria.

Canopy	Orchards			Vineyards	
Parameter	8x8m c*=0.35	8x8m c=0.60	Palmette	c=0.35	c=0.24
Mean	0.42	0.30	0.39	0.64	0.70
St.Dev.	0.08	0.04	0.06	0.05	0.03
Minimum	0.24	0.21	0.26	0.54	0.62
Maximum	0.58	0.39	0.51	0.74	0.77

* Canopy cover

Soil Erodibility Factor K

Index of soil detachability based on laboratory measurements can substitute the USLE soil erodibility factor K . The laboratory test is based on complete orthogonal second order design of two factors with three levels to find the optimal values of the test parameters ensuring minimal standard deviation of the output (Rousseva, 1989).

The soil detachability index I ($\text{g}\cdot\text{J}^{-1}$) is defined as the mass of aggregated soil m detached into micro aggregates and particles finer than 1 mm per unit water drop kinetic energy dispersed into breakdown of the aggregates KE . Hence, we have

$$I = \frac{m}{KE} \quad (14)$$

Statistical analyses have shown that soil detachability indices measured for 11 soils representing wide range of textures were well correlated with respective soil erodibility factor values measured from field plots.

References

- Brandt, C.J. 1989. The Size Distribution of Throughfall Drops Under Vegetation Canopies. *Catena*, **16**, 507-524.
- Brandt, C.J. 1990. Simulation of the Size Distribution and Erosivity of Raindrops and Throughfall Drops. *Earth Surface Processes and Landforms*, **15**, 687-698.
- Chapman, G. 1948. Size of Rain Drops and Their Striking Force at the Soil Surface in a Red Pine Plantation. *Transactions of the American Geophysical Union*, **29**, 664-670.
- Daskalov, Y., L. Lozanova, G. Ruskov, A. Momchev. 1994. Results from Biometric Measurements on Maize and Wheat for Soil Erosion Purposes. *Soil Science, Agrochemistry and Ecology*, **29** (4-6), 132-133.
- De Ploey, J. 1982. A Stemflow Equation for Grasses and Similar Vegetation. *Catena*, **9**, 139-152.
- De Ploey, J. 1984. Stemflow and Colluviation: Modelling and Implications. *Pedologie*, **34**, 135-146.
- Haynes, J.L. 1940. Ground Rainfall Under Vegetative Canopy of Crops. *Journal of the American Society of Agronomy*, **32**, 176-184.
- Kiesselbach, T.A. 1916. Transpiration as a Factor in Crop Production. *University of Nebraska, Agricultural Experimental Station Research Bulletin No 6*.
- Laws, J. O. 1941. Measurements of the Fall-velocity of Water-drops and Raindrops. *Transactions of the American Geophysical Union*, **22**, 709-721.
- Merriam, R.A. 1973. Fog Drip from Artificial Leaves in a Fog Wind Tunnel. *Water Resources Research*, **9**, 1591-1598.
- Morgan, R.P.C. 1980. Implications. – In: M. J. Kirkby and R.P.C Morgan (Eds.) *Soil Erosion*. John Wiley & Sons, New York, 253-301.
- Morgan, R.P.C., J.N. Quinton, R.E. Smith, G. Govers, J.W.A. Poesen, K. Auerswald, G. Chisci, D. Torri, M.E. Styczen, A.J.V. Folly. 1998. *The European Soil Erosion Model (EUROSEM): Documentation and User Guide*. Silsoe College, Cranfield University, U.K.
- Oldeman, R., Hakkeling, R.T.A., Sombroek, W. 1991. *World Map on the Status of Human-Induced Soil Degradation. An Explanatory Note. Global Assessment of Soil Degradation. GLASOD*. ISRIC – Winand Centre – ISSS – FAO – ITC, Wageningen.
- Roshkovan, D.M. 1988. *Dynamics of Vegetation Canopy in Moldavian Agrolandscapes*. “Shtiinca”, Kishinev.
- Rousseva, S.S. 1989. A laboratory index for soil erodibility assessment. *Soil Technology*, **2**: 287-299.
- Rousseva, S. 2000. Assessments of Soil Erosion Impact in Agroecosystems. Part 2. Energy of Simulated Rainfall Impact on Cropped Soil. *Journal of Balkan Ecology*, **3**, (1): 64-70.
- Rousseva S.S. 2002. *Information bases for developing a geographic database for soil erosion risk assessments*. Monograph. N. Poushkarov Institute of Soil Science, Sofia, 198 pp

- Van Elewijck, L. 1989a. Stemflow on Maize: A Stemflow Equation and the Influence of Rainfall Intensity on Stemflow Amount. *Soil Technology*, **2**, 41-48.
- Van Elewijck, L. 1989b. Influence of Leaf and Branch Slope on Stemflow Amount. *Catena*, **16**, 525-533.
- Wischmeier, W. H. & Smith, D. D. 1978. Predicting rainfall-erosion losses – A guide to conservation planning. *Agricultural Handbook No. 537*.

Models for Predicting Water Use and Crop Yields – A Cuban Experience

Maria Elena Ruiz¹ and Angel Utset²

¹*Agrophysics Research Unit, Agrarian University of Havana,
San Jose de las Lajas, La Habana, Cuba*

²*Former member of Agrophysics Research Unit,
Agrarian University of Havana, San Jose de las Lajas
La Habana, Cuba*

*Lecture given at the
College on Soil Physics
Trieste, 3-21 March 2003*

LNS0418028

¹ mruiz80@yahoo.com

Introduction

Modeling has come into agriculture because of several reasons: 1) More comprehension about the processes that take place at the soil water atmosphere continuum SWAC, 2) Specialists from different fields come to work together, 3) Different and more efficient codes for obtaining the solutions of complex equations were introduced, 4) Amazing development of hardware and supporting softwares, 5) Large data banks coming from a lot of years of experimental laboratory and field work (mainly at the developed countries) and 6) Desires to put together as much SWAC processes as possible to get a better comprehension of such a complex system. Here we briefly present some of the results obtained in Cuba using simulation model SWACROP for estimating water use and yields in potato and model SWAP for sugar cane yields.

Materials and Methods

Figure 1 illustrates the processes that model SWAP takes into account according to (Van Dam et al., 1997; Kroes et al., 1998). SWAP is derived from the Feddes et al. (1978) model. The first application of SWAP in Cuba was made for a potato crop in order to determine water use and yields. The first initial version of SWAP devoted to the potato crop was called SWACROP. The first task was to calibrate the model for tropical conditions for a Rhodic Ferralsol. Several field experiments were carried out in order to obtain the soil hydraulic properties as well as the crop functions necessary for using the model. Later a validation procedure was made in the same soil but in another location. Yield, evapotranspiration, and soil moisture data coming from a four-year irrigation field experiment were used to find out how well the model estimated potato production. A detailed explanation is available Ruiz (1998).

The same procedure was followed for sugar cane crop. The leaf area index LAI and root water extraction functions were determined. The crop-dependent coefficient necessary to split evapotranspiration into transpiration and evaporation was also determined. Later and in another location, sugar cane yields obtained for crop seasons between 1991 and 1995 in three soils types and seeded in different months were collected for validation proposes.

Finally, an interface (Garea, 1999) between SWAP and the GIS ILWIS was made in order to more easily facilitate the model input of the data corresponding to small fields and not average values of larger domains.

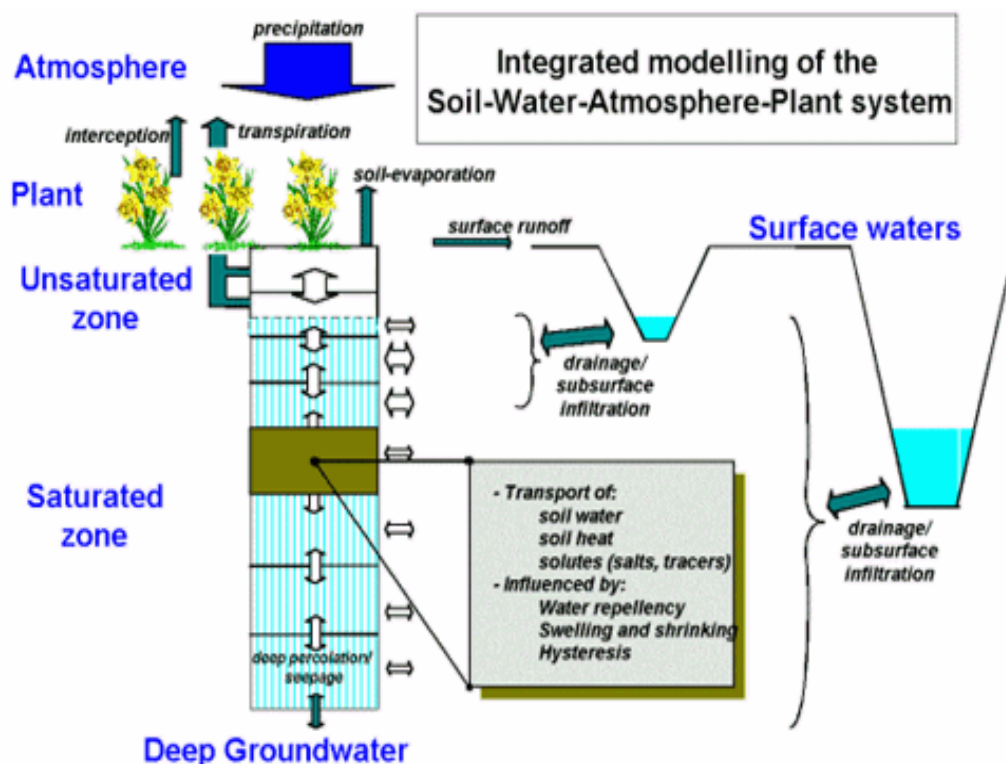


Fig. 1. Conception of model SWAP after Van Dam et al. (1997); Kroes et al. (1999).

Results

Fig. 2 shows the relationship between estimated and measured soil moisture contents for two different irrigation treatments for potato in a Rhodic Ferralsol. The graph to the left shows the results when more water was applied. Simulated values matched better the measured values for the higher water level.

Estimated and measured potato yields are shown in Fig. 3. A determination coefficient of 0.69 was obtained for a 95 % of confidence limit. Although this value could be considered somewhat low, it should be remembered that the soil hydraulic properties used for the simulation were taken from the results of Ruiz and Utset (1992) for this kind of soil, but not determined at the same location where potato yields were measured. Moreover, all the data considering the different irrigation treatments were considered.

For sugar cane, a calibration was made for a Rhodic Ferralsol. Later the model was tested for another location. The data of crop yields, seeding dates

corresponding to three different soils were used for comparing with simulation results. Fig. 4 shows the results A) for each year, B) for the three soils present and C) for different seeding months. In all three cases, the SWAP simulations agree with the measured data. However, when averaged values for the input parameters are used in the model, a determination coefficient between simulated and measured output was only 0.40.

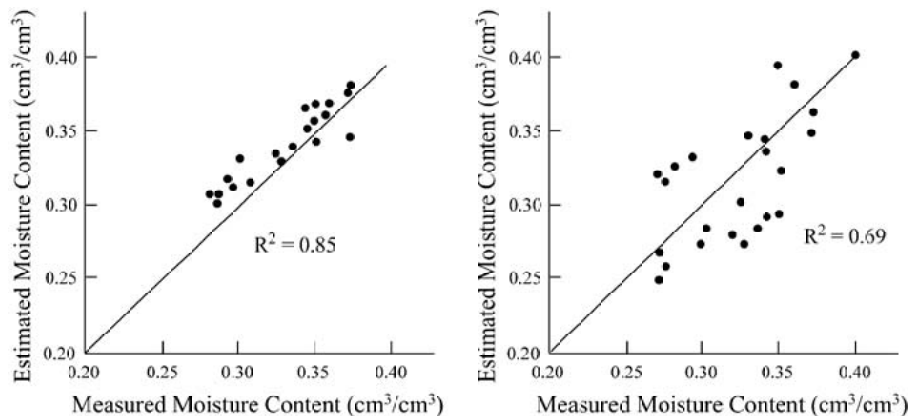


Fig. 2 Estimated and measured moisture content for high (left) and low (right) water irrigation level.

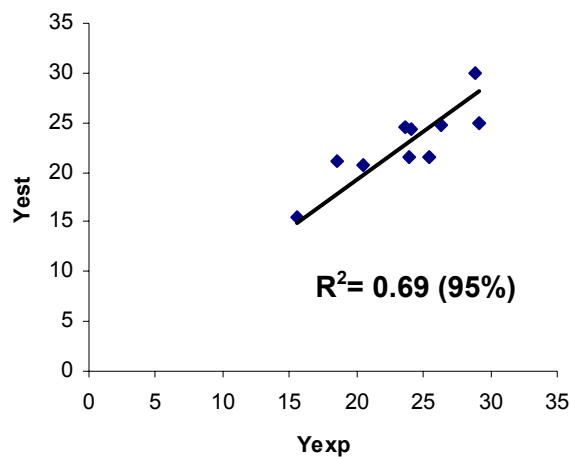


Fig. 3. Estimated and actual potato yields.

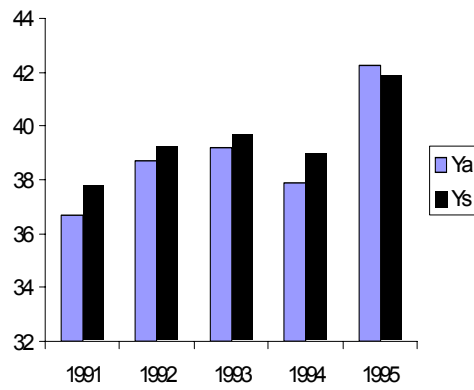
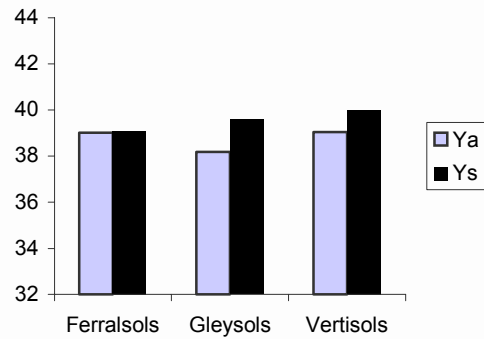
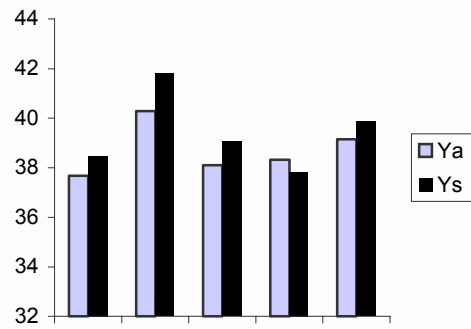
**A-Yearly averaged.****B-Averaged by soil type.****C-Averages by seeding month.**

Fig. 4. Estimated and actual sugar cane yields for different years (A), soil types (B) and seeding months (C)

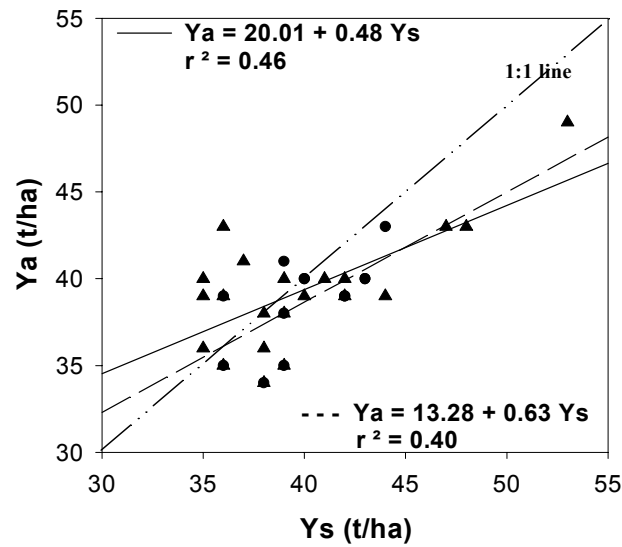


Fig. 5. Sugar cane estimated yields considering seeding dates for small fields ($r^2 = 0.46$) as well as block with seeding date averages ($r^2 = 0.40$)

When the interface was used allowing the input of the individual parameter values for each of the fields, better coefficients of determination were obtained. Nevertheless, because some data came from production areas of a sugar cane factory, some requirements for the model were not adequately fulfilled.

Conclusions

Not only is it necessary to improve estimations of the soil hydraulic properties, but mechanisms should be introduced into the model to take into account sugar cane crop fertilization. Irrigation scheduling for potato crops can be improved by using the SWAP simulation model. Because a sugar cane crop has a very large cycle, it is difficult to model. Problems were found when trying to satisfy the SWAP model assumptions.

All the possibilities of SWAP model have been not explored, and it remains necessary to evaluate the errors involved in SWAP simulations.

References

- Feddes, R. A., P. Kowalik & H. Zaradny, 1978. Simulation of field water use and crop yield. PUDOC, Wageningen, Simulation Monographs, 189 pp.
- Garea, E. 1999. Interface between SWAP model and ILWIS GIS. Technical Report 10. National Scientific Research Project 050130016
- Kroes, J.G., J.C. van Dam, J. Huygen and R.W. Vervoort, 1998. User's Guide of SWAP version 2.0. Simulation of water flow, solute transport and plant growth in the Soil-Water-Atmosphere-Plant *environment*. Technical Document 48, DLO Winand Staring Centre, Report 81, Department Water Resources, Agricultural University, Wageningen. PUDOC, Wageningen, Simulation Monographs, 189 pp.
- Ruiz María y A. Utset. Curva tensión-humedad para algunos agrupamientos de suelos cubanos. *Cienc. Tec. Agrop.* 3(1):11-14, 1992.
- Ruiz, M.E. 1998. Using model SWACROP for potato (v. Desiree) water use and crop yields. PhD thesis, 120 pp. (in Spanish)
- Van Dam, J. C., Huygen, J., Wesseling, J. G., Feddes, R. A., Kabat, P., van Walsum, P. E. V., Groenendijk, P., van Diepen, C. A., 1997. Theory of SWAP version 2.0. Report 71. Technical Document 45, Wageningen, 167 pp.

Soil Hydraulic Properties of Cuban Soils

Maria Elena Ruiz¹ and Hanoi Medina

*Agrophysics Research Unit, Agrarian University of Havana,
San Jose de las Lajas. Habana, Cuba*

*Lecture given at the
College on Soil Physics
Trieste, 3-21 March 2003*

LNS0418029

¹ mruiz80@yahoo.com

Abstract

Because soil hydraulic properties are indispensable for determining soil water retention and soil water movement, their input for deterministic crop simulation models is essential. From these models is possible to access the effect of the weather changes, soil type or different irrigation schedules on crop yields. With these models, possibilities are provided to answer questions regarding virtual “what happen if” experiments with a minimum of fieldwork. Nevertheless, determining soil hydraulic properties can be very difficult owing to unavailability of necessary equipment or the lack of personal with the proper knowledge for those tasks. These deficiencies are a real problem in developing countries, and even more so when there is not enough financial possibilities for research work. This paper briefly presents the way these properties have been accessed for Cuban soils, which methods have been used and the work now in progress.

Introduction

Soil hydraulic properties i.e., soil water retention curve SWRC and hydraulic conductivity function $K[\theta(h)]$, are the main soil properties for determining the water retention and movement in soils. In the literature, different methods are presented to access the hydraulic properties (Klute, 1986). Nevertheless, some these methods require expensive and very specific devices. Others need personnel with special skills while others are very laborious and time consuming. Hence, the same methods are not used in all the countries. Moreover, the soil type will be a reason for selecting one or another method.

SWRC determination in Cuba began in the seventies with the introduction of Richards chamber equipment at the Cuban Institute of Soils. At that time all the SWRCs were determined using disturbed soil samples. In the eighties and in the frame of a research project supported by FAO the first sandbox apparatus was introduced at the Institute of Irrigation and Drainage Research IIRD. It was then when undisturbed soil samples were beginning to be analyzed. Subsequently, many SWRCs were made for soils of the most important agriculture farms of the country and where irrigation systems were installed. A wide range of soils was represented in these determinations. By that time, the first “in situ” SWRCs were determined for Cuban Rhodic Ferralsol and the comparison of several analytical models for fitting the SWRCs data collected (Ruiz et al., 1991; Ruiz and Utset, 1992). It should be noted that Rhodic Ferralsol is the most representative of the agricultural areas in Cuba.

The first determinations of the non-saturated hydraulic conductivity were made in Rhodic Ferralsol using the methodology of calculation appearing in Nielsen et al (1973). The method was used at the experimental station of the IIRD (Utset and Ruiz, 1985) and at the National Institute of Agricultural Science (Ruiz, et al., 1994). This method was followed later in other soils (Villaragut, 1995) and using a neutron probe for moisture content determinations (Lopez, 1996). Because that internal drainage method is time consuming and very laborious, another alternative was used: determining hydraulic conductivity function from the SWRC using the combination Mualem-Van Genuchten theory and analytical model for SWRC (Mualem, 1976; Van Genuchten, 1980). The results were presented in Ruiz, et al. (1994).

After the possibilities of the GIS-simulation model approach for land evaluation, indirect methods for SWRC and $K[\theta(h)]$ have been introduced to extend the results to regional areas. Pedotransfer functions (Bouma and Lanen, 1987) are being used more and more around the world. In Cuba, the first work about pedotransfer functions was related with Ferralsols (Medina et al., 2000). In this paper some of the

results reached in determining SWRC and soil hydraulic conductivity function in Cuba are presented.

Materials and Methods

The methods used for determining SWRC and $K[\theta(h)]$ are shown in Table I.

Table I. Methods used in Cuba for determining SWRC and $K[\theta(h)]$.

SWRC	Direct methods	In “situ” In lab	TDR, tensiometers, neutron probe Using disturbed and undisturbed soil samples
	Indirect methods		Pedotransfer functions
Kns	Direct methods	“in situ”	Internal drainage method
	Indirect methods	From SWRC using Mualem-van Genuchten approach	
Ks	Direct methods	“in situ” In lab	Auger hole, ring infiltrometers, piezometers Permeameter from undisturbed samples

A total of 176 undisturbed SWRCs determined by sandbox apparatus and Richards chamber were collected belonging to different soils. The following models were compared:

$\theta = \theta_r + \frac{\theta_s - \theta_r}{(1 + \alpha h^n)^m}$	$\theta(h) = \theta_r + (\theta_s - \theta_r) \left(\frac{h}{h_b} \right)^{-\lambda}$	$\frac{h}{h_b} \geq 1$	$h = a \cdot \theta^{-b}$
	$\theta(h) = \theta_s$	$\frac{h}{h_b} < 1$	
van Genuchten (1980)	Brooks and Corey (1966)		Gardner (1970)

In these equations θ_r is the residual water content; θ_s the saturated water content; α , n , m are adjustment parameters; λ the soil depending parameter; h_b the soil bubbling pressure and a , b are the adjustment parameters.

The models of Rawls (1982), Vereecken (1988), Batjes (1996) and Tomasella et al. (2000) were used for analyzing the validity of pedotransfer functions for Cuban Ferralsols.

Results

Values of van Genuchten parameters for the soil groups are shown in Table II. Clear physical meanings for the parameter values are not apparent in some cases.

Table II. van Genuchten parameters for some Cuban soils

Soils	θ_r	$\alpha (\text{cm}^{-1})$	n	m	θ_s
Ferralsols	0.176	0.016	1.867	0.375	0.388
Cumbisols	0.184	0.014	1.902	0.430	0.378
Fluvisols	0.179	0.012	1.858	0.427	0.447
Arenosols	0.125	0.016	1.892	0.456	0.390
Vertisols	0.315	0.008	1.795	0.409	0.631

The determined SWRCs appearing in Fig. 1 were used as input for the simulation model SWAP. Because the “in situ” method is excessively laborious and time consuming, undisturbed soil samples were used successfully in the laboratory to determine the van Genuchten parameters (Ruiz, 1998).

The measured SWRC and those estimated with all of the models from pedotransfer functions are shown in Fig. 2. Note that the curve derived from the Tomasella et al. (2000) model is very similar to the experimental data. Although a wider soil database remains to be tested, Medina et al. (2000) concluded that the equations of Tomasella et al. (2000) appear promising for Cuban Ferralsols. Further analysis should also focus on the inclusion of additional variables such as iron and aluminum oxide contents.

The results obtained by the internal drainage method for Rhodic Ferralsols for the years 1988 and 1990 and for all measured depths appear in Fig. 3. The uniformity of these soils is illustrated by most of the data grouping together along a single line. Only a narrow range of K values was obtained because of the very good drainage of these soils.

Finally the indirect method using the Mualem-van Genuchten approach is shown in Fig. 4. In Fig 4a the value of $K_s = 28.4$ m/day was determined using the auger hole method whilst in Fig 6b, the value of $K_s = 57.5$ m/day was obtained from

undisturbed samples analysed in the laboratory. Obviously, values of K_s depended on the method used for its determination.

Conclusions

- Additional studies of hydraulic properties of Cuba soils are needed.
- A data bank of K and SWRC functions for Cuba soils needs to be organized.
- “Simple” methods for determining the hydraulic conductivity need to be introduced,
- Indirect methods for determining K from other soil physical properties or inverse methods need to be explored.

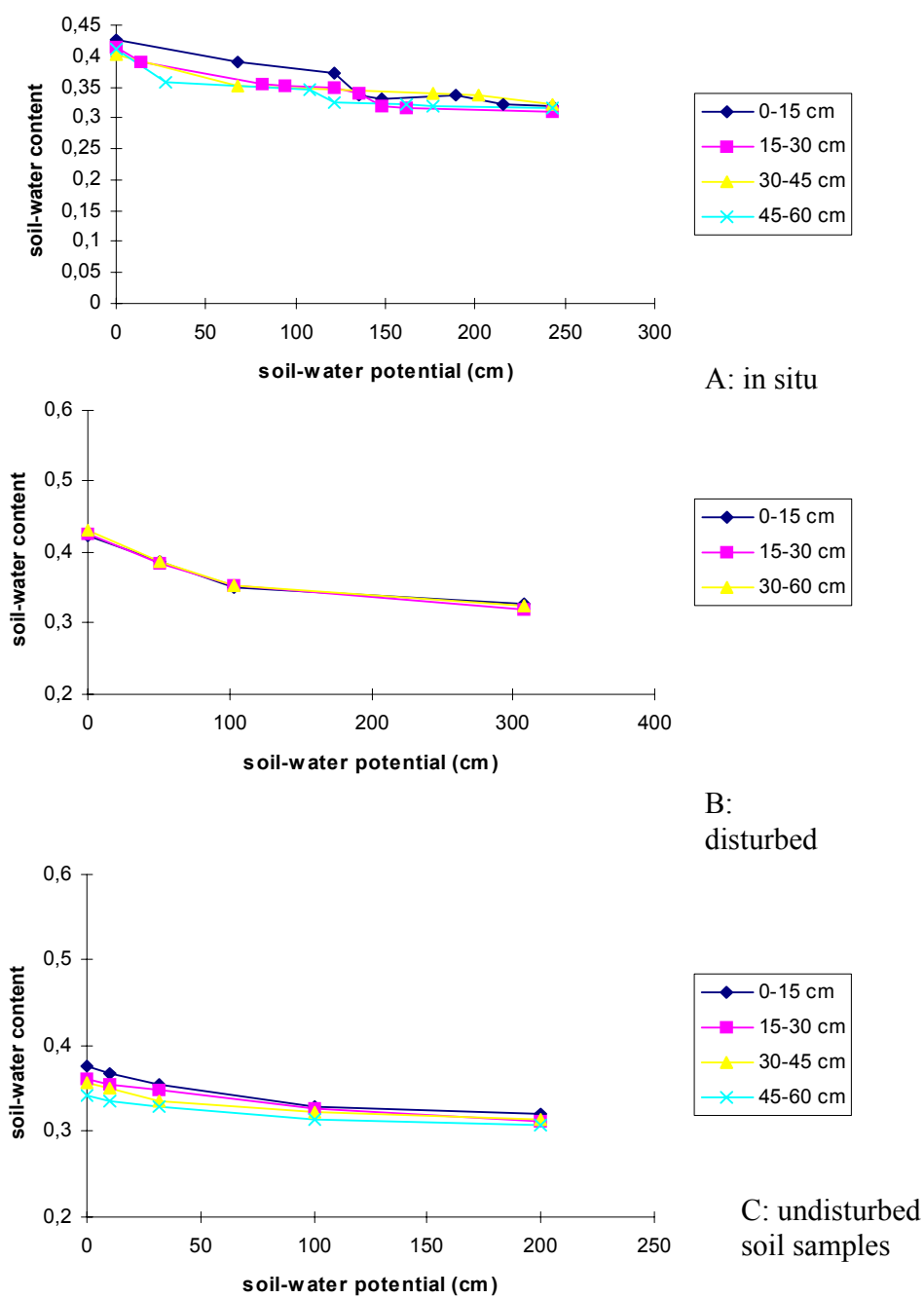


Fig. 1. SWRCs obtained A) “in situ”; B) from disturbed samples and C) for undisturbed samples for a Rhodic Ferralsol.

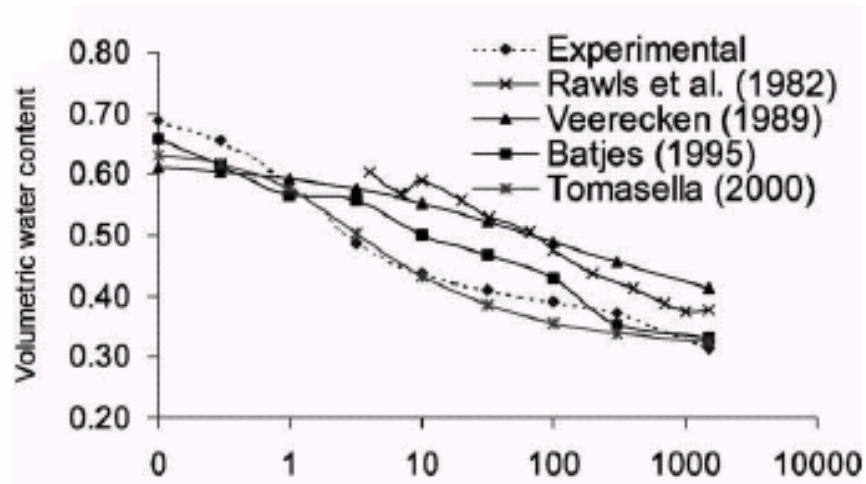


Fig. 2 Estimated and measured soil water retention curves using Rawls (1982), Vereecken (1988), Batjes (1996) and Tomasella et al (2000) after Medina et al (2002).

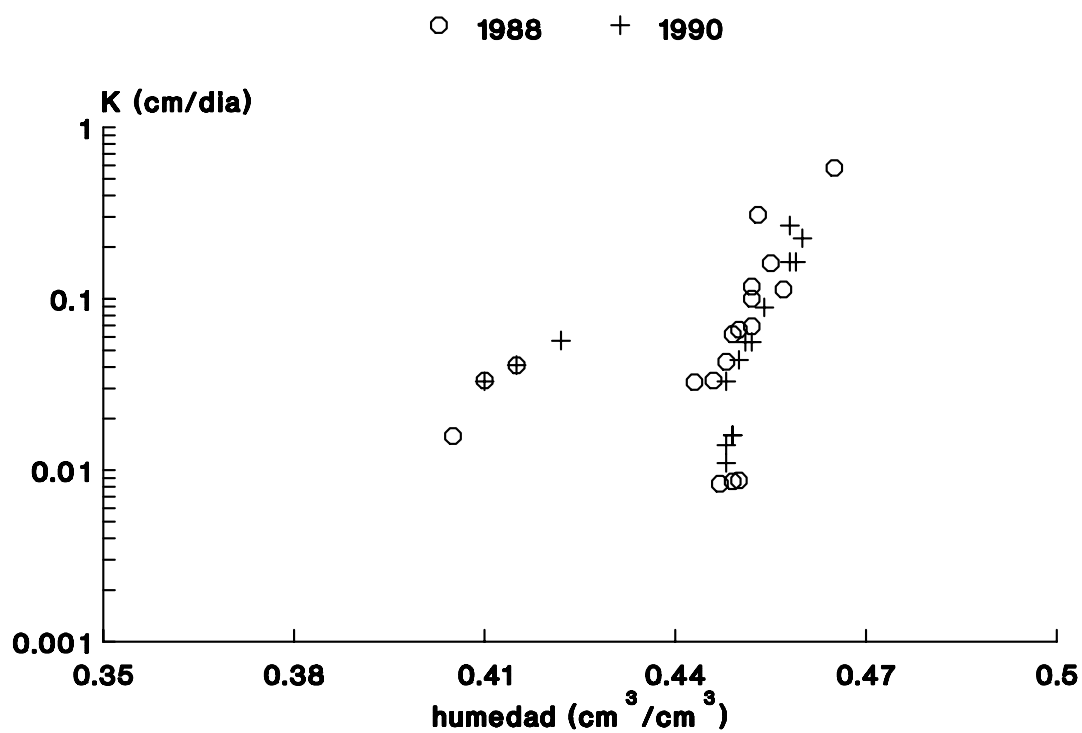


Fig. 3 Results obtained for the internal drainage methods in a Rhodic Ferralsol for years 1988 and 1990 and all the depths studied (0-15; 15-30; 30-45; 45-60 and 60-75 cm)

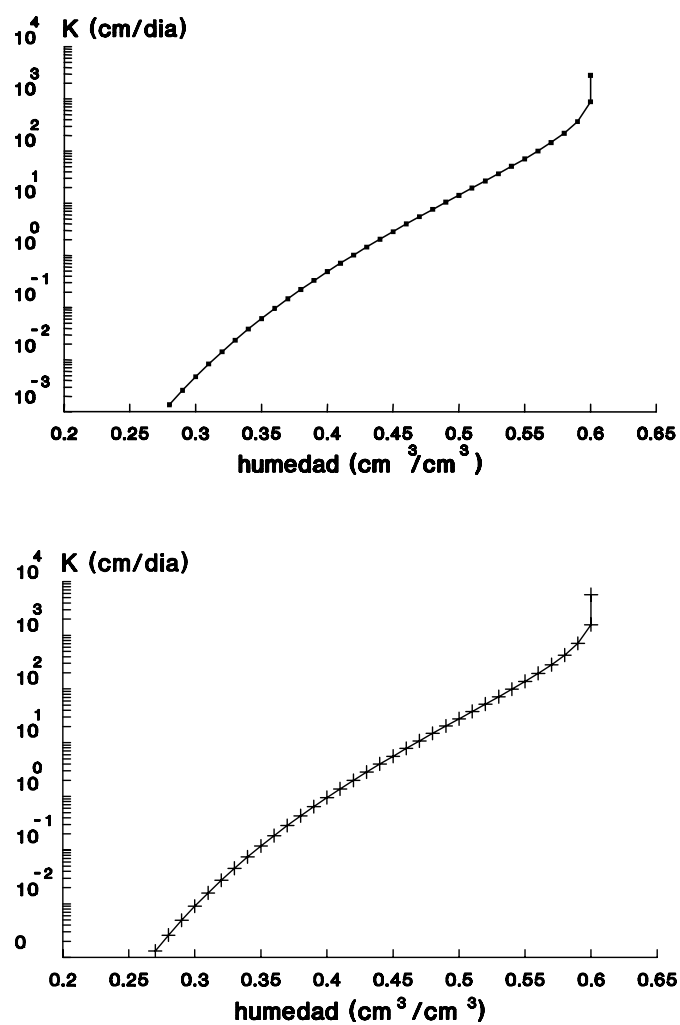


Fig.4 Hydraulic conductivity function obtained from Mualem-van Genuchten using as K_s the values determined by the auger hole method in the field (28.4 m/d) and the permeameter method in the laboratory (57.5 m/d).

References

- Batjes, N.H., 1996. Development of a world data set of soil water retention properties using pedotransfer rules. *Geoderma* 71, 31–52.
- Bouma, J., Van Lanen, H.A.J., 1987. Transfer functions and threshold values: from characteristics to land quality. *Quantified Land Evaluation. Proc. ISSS/SSSA Workshop*. ITC Publication, Enschede, The Netherlands, pp. 106–110.
- Klute, A., 1986. *Methods of Soil Analysis. Part 1. Agronomy Monograph. Series No 9 (2nd Edition)*. ASA and SSSA, Madison, Wisconsin
- López, S.T. 1996. Water dynamic in a Rhodic Ferralsols at the south of Havana province. Thesis presented for MSc title in Irrigation and Drainage. Ciudad de la Habana, 71pp.
- Medina, H., Mohamed T., del Valle, Alicia and Ruiz, Maria E. 2000. Estimating soil water retention curve in Rhodic Ferralsols from basic soil data. *Geoderma* 108:277–285.
- Mualem, Y. 1976 A new model for predicting the hydraulic conductivity of unsaturated porous media. *Water Resour. Res.* 12(3):513–522.
- Nielsen, D., J. Biggar y K. Ehr. 1973. Spatial variability of field-measured soil-water properties. *Hilgardia* 42(7):215–259.
- Rawls, W.J., Brakensiek, D.L., Saxton, K.E., 1982. Estimation of soil water properties. *Trans. ASAE* 108, 1316–1320.
- Ruiz, M.E. 1998. Using model SWACROP for potato (v. Desiree) water use and crop yields. PhD thesis, 120 pp. (in Spanish)
- Ruiz, María, A. Utset and A. Lau. 1991. Three analytical models for the soil water retention curve in some Cuban soils. *Revista Cubana de Física* XII(1):25–30, (in Spanish).
- Ruiz María y A. Utset. 1992. Curva tensión-humedad para algunos agrupamientos de suelos cubanos. *Cienc. Tec. Agrop.* 3(1):11–14.
- Ruiz, María, A. Utset and A. Lau. 1994. Determining the non saturated hydraulic conductivity from internal drainage method and from the soil water retention curve. *Cienc. Tec. Agrop.* Vol 4(2):55–59 (in Spanish).
- Tomasella, J., Hodnett, M.G., Rossato, L., 2000. Pedotransfer functions for the estimation of soil water retention in Brazilian soils. *Soil Sci. Soc. Am. J.* 64, 327–338.

- Utset, A.S. and Ruiz, M.E. 1985. Determining the unsaturated hydraulic conductivity by the internal drainage method. Internal Report. Agrarian University of Havana. 8pp.
- Van Genuchten, M.. 1980. A closed-form equation for predicting the hydraulic conductivity of unsaturated soil. *Soil Sci. Soc. Am.J.* 44:892-898.
- Vereecken, H., 1988. Pedotransfer functions for the generation of hydraulic properties for Belgian soils. Doctoraatsproefschrift Nr. 171 aan de Fakulteit der Lanbouwwetenschappen van de K.U. Leuven.
- Villaragut, A. 1995. The internal drainage method in an alluvial soil. Graduation Thesis, 60 pp. (in Spanish).

Susceptibility of Coarse-textured Soils to Soil Erosion by Water in the Tropics

F.K. Salako¹

*Department of Soil Science and Agricultural Mechanisation,
University of Agriculture, Abeokuta, Nigeria*

*Lecture given at the
College on Soil Physics
Trieste, 3-21 March 2003*

LNS0418030

¹ kolawolesalako@hotmail.com; kfsalako@yahoo.ie

Abstract

The application of soil physics for the evaluation of factors of soil erosion in the tropics received considerable attention in the last four decades. In Nigeria, physical characteristics of rainfall such as drop size and drop-size distribution, rainfall intensity at short intervals and kinetic energy of rainfall were evaluated using different methods. Thus, compound erosivity indices were evaluated which showed a similar trend in annual rainfall erosivity with annual rainfall amounts rainfall amounts. Attempts have also been made to use geostatistical tools and fractal theory to describe temporal variability in rainfall erosivity. High erosivity aggravates the vulnerability of coarse-textured soils to erosion. These soils, high in sand content were poorly aggregated and structurally weak. Thus, they were easily detached and transported by runoff. Long-term data are needed to describe factors of soil erosion in the tropics but quite often, equipment are not available or poorly maintained where available such data useful data are not collected. A greater cooperation of pure physicists, soil physicists and engineers in the developing nations is needed to improve or design equipment and methods for the characterization of factors of soil erosion in the tropics.

Soil erosion in the tropics and application of soil physics

Accelerated soil erosion is a major ecological problem in the tropics. Apart from climatic and edaphic factors which contribute to this menace, socio-economic factors bothering on land misuse are also significant contributors. As Hartemink (2002) noted, in tropical regions, important soil science themes have not changed much in the past decades, and soil science is still closely linked to agriculture and society at large. In other words, provision of food for the ever-increasing population with the highest rate occurring in the tropics, decrease in food production per capita and rapid soil degradation remain major issues for tropical soil scientists. These views were also poignantly expressed by Lal (2000) who stated that the principal issues in the tropics for the 21st century include (i) achieving food security, (ii) curtailing soil degradation and restoring degraded soils; and (iii) improving environmental quality.

The assessment of soil erosion and soil conservation needs has been a major focus in Soil Physics as a sub-discipline of Soil Science. Thus, it can be described as Applied Soil Physics. The development of Soil Physics in the tropics, has understandably been tilted toward Applied Soil Physics for reasons already discussed by Hartemink (2002), although there is a need to be involved in research which focus on non-agricultural use of land now in order to understand the contribution of the tropical environment to global climate change and environmental quality. This paper discusses the assessment of climatic and edaphic factors which influence soil erosion in the tropics, with an emphasis on experiences garnered in Nigeria. The main factors discussed are rainfall and soil characteristics, with attention drawn to methodology and interpretation of results obtained.

Physical characteristics of rainfall in the tropics

Rainfall is the real agent of soil erosion by water in the tropics by virtue of its role as the source of water or the only form of precipitation contributing to the hydrologic cycle. For most of crop production in the tropical Africa, it is also the source of water, as irrigation agriculture is not well developed even in semi-arid and arid regions where such is needed.

The capacity or potential ability of the rain to cause soil erosion is called rainfall erosivity. This attribute of rainfall is linked to its physical characteristics, namely, amount, duration, drop size and drop size distribution, terminal velocity, intensity and kinetic energy.

Rainfall amount and duration

Quantity of rainfall is measured by amount in unit of depth (i.e., mm). In Nigeria, annual in the dry regions is can be less than 500 mm but in the wet coastal regions, it could be greater than 2500 mm. The amount of rainfall and how long it takes to fall influence how much of water infiltrates and runoff the soil. Problems of flooding and soil erosion are basically related to amount and duration of rainfall.

This is done with standard rain gauges which are found in many locations in the tropics. The problem, however, is that standard raingauge records are recorded on daily basis (24 h) and this obscures information on high rainfall intensity because of the long period after which measurements are taken. There are also auto-recording rain gauges (pluviographs) which record on charts which can be resolved to short-intervals of rainfall (e.g. ≤ 15 minutes).

Automatic weather stations exist today in which rainfall can be recorded at intervals of interest, which will be downloaded from data loggers into computers. As will be shown later, attention of meteorological stations need to be drawn to need of soil conservationists for relevant data collection for soil conservation planning or else the benefit of this advanced technique can be reduced or lost in this respect.

Rain drops

Rain falls as drops, which are assumed to have a spherical shape (Carter et al., 1974). The maximum raindrop size at which it can remain stable without breaking into pieces is 5 mm.

Measurement of raindrop size and distribution can be done with a number of methods, among which are:

- Drop-stain method in which an absorbent paper is dusted with powder which form stains as rain drops fall on them
- Flour-pellet method which basically assesses the size of drops from size of pellets (dough-balls) made after exposing baking flour to drops
- Use of pressure transducers or acoustic device or piezoelectric sensors to measure impact of raindrop
- Photographic method in which photographs of falling raindrops were used.

In Nigeria (Table 1), raindrop sizes have been measured by impact made on piezoelectric sensors (Kowal et al., 1973; Kowal and Kassam, 1976; Lal, 1998) and by the flour-pellet method (Aina, 1980; Obi and Salako, 1995; Salako et al., 1995; Akinnifesi and Salako, 1997). Kowal et al. (1973) developed a device which recorded graphically, on a time scale the amplitude of electric pulses originating from the impact of raindrops on the surface of a transducer disc, by making use of the piezo-electric effect.

The flour-pellet method (Carter et al., 1974) consists of calibrating plain baking flour with water drops of known sizes in the laboratory. Pellets formed are air-dried first and later dried further in the oven before weighing. Water drop weight: Pellet weight ratio is calculated. The average pellet weight from rain sample is obtained by exposing the calibrated flour to rainfall in a pan (31 cm diameter x 1.6 cm deep). Raindrop size is obtained by calculation:

$$d = (6W/\pi)^{1/3} \quad (1)$$

where d is raindrop diameter (mm) and W the average drop weight (mg) equal to weight ratio \times average pellet weight. Apart from obtaining the range of drop sizes present in rainfall, the percentage of sample contributed by each drop size is calculated to obtain a cumulative frequency distribution. The median drop size (D_{50}) which is the size at 50% volume is calculated from the cumulative frequency distribution

Table 1. Raindrop size distribution in Nigeria

Agroecological zone	Maximum drop size (mm)	Median drop size (mm)	Source	Method
Northern Guinea Savanna	4.86	3.42	Kowal and Kassam (1976)	Direct with a piezoelectric sensor. Equipment assembled by Kowal et al. (1973)
Derived Savanna Southeastern Nigeria	3.4	1.1-2.9	Obi and Salako (1995)	Flour-pellet method
Derived Savanna Southwestern Nigeria	> 3	2.25-3	Lal (1998)	Direct with a piezoelectric sensor. DISTROMET
Humid forest Southcentral Nigeria	5.1	2.3	Salako et al. (1995)	Flour-pellet method
Humid forest Southwestern Nigeria	4.5	3.0	Aina (1980)	Flour-pellet method

The median drop sizes indicated that large drop sizes played significant role in the erosivity of rainfall in the tropics. Median drop sizes were greater than 3.5 mm at rainfall intensities above 125 mm h⁻¹ in southwestern Nigeria (Aina, 1980). Lal (1998) observed that fogs and gentle rains often account for low drop sizes and energy load. Median drop size generally increases with increases in rainfall intensity up to a certain limit according to the relationship

$$D_{50} = al^b \quad (2)$$

because the constants will vary with rain types. The relationship is also believed to be valid up to 75 mm h⁻¹ rainfall intensity.

Rainfall intensity

Rainfall intensity, which is referred to already in Equation 2, is calculated from rainfall amount relative to duration (amount/duration). The actual duration of rainfall within a day is not discernible from daily rainfall records of standard rain gauges but can be discerned from pluviograph or autoweather station data. Thus, short-interval intensities needed for soil conservation planning and construction of hydrologic structures can only be obtained with gauges whose records can be analyzed at less than 1 h (Figure 1).

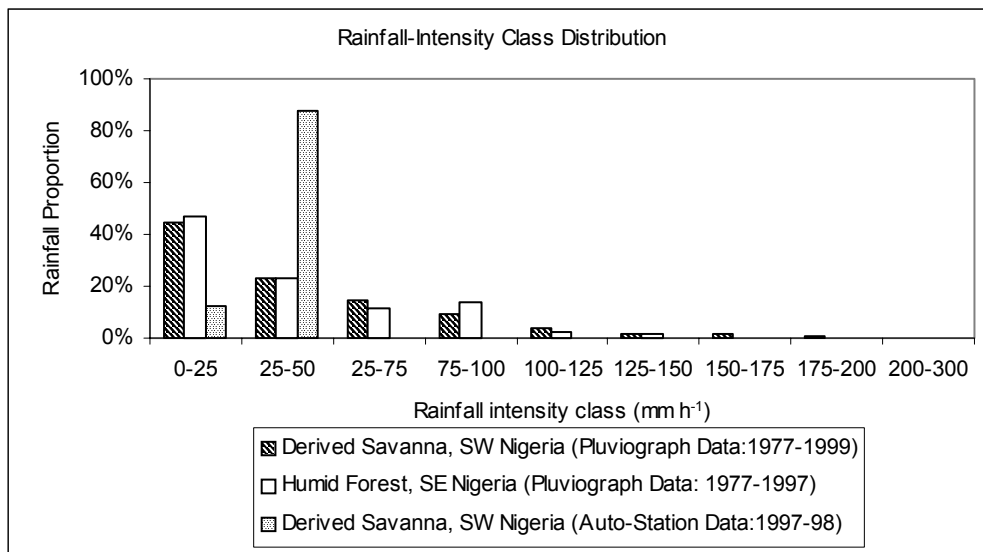


Figure 1: Rainfall-intensity class distribution and comparison of pluviograph data analyzed at 15-minute intervals with automatic-weather station data analyzed at 1-h interval. (Source: Salako, F. K. unpublished)

The pluviograph data in Figure 1 were obtained at 15-minute intervals but those of the auto-weather station which are supposed to be more accurate were obtained at 1-h interval. They suggest the following:

- (i) About 50% of rainfall in the tropics will fall at intensities exceeding 25 mm h^{-1} which is considered the threshold intensity for soil erosion to occur
- (ii) Intensities greater than 75 mm h^{-1} which would hardly occur in temperate regions occur in the tropics. According to Salako F. K. (unpublished), intensities up to 150 mm h^{-1} occur annually.
- (iii) The data suggest that records of rainfall events made at less than 1 hour would obscure exceptional intensities exceeding 50 mm h^{-1} . Definitely, a 24-h measurement with standard rain gauge will quite often show

intensities less than 25 mm h⁻¹ which will cause poor judgment of rainfall erosivity in the region.

Terminal velocity of rainfall and kinetic energy

Terminal velocity refers to the velocity a body falling freely under the force of gravity reaches when frictional resistance of the air is equal to the gravitational force. In physics, kinetic energy and momentum is related to mass and velocity of objects. This has, therefore, generated the argument on which is appropriate for rainfall erosivity; kinetic energy or momentum. However, kinetic energy of rainfall is frequently used for evaluating rainfall erosivity.

Rainfall kinetic energy is related to rainfall drop sizes and intensities. It has, therefore, been possible to evaluate kinetic energy of rainfall directly from piezoelectric sensors which measure drop sizes as those used by Kowal et al. (1976) and Lal (1998) in Nigeria (Table 1). Lal (1998) did not however find a correlation between kinetic energy and momentum of rainfall in Ibadan, southwestern Nigeria in 1980 whereas he found a significant relationship in 1981

$$E = -1018.1 + 996.2D_{50} - 152.3D_{50}^2 \quad r = 0.63 \quad (3)$$

$$MV = -264.6 + 264.0D_{50} - 41.0D_{50}^2 \quad r = 0.66 \quad (4)$$

where E is the kinetic energy (J/m²), D₅₀ the median drop size (mm) and MV the momentum (kg·m/s).

Direct measurement of rainfall kinetic energy or momentum is rare in many locations all over the world. It is common to evaluate rainfall kinetic energy using Wischmeier and Smith (1978) empirical equation proposed for the (Revised) Universal Soil Loss Equation (RUSLE) by Renard et al. (1997):

$$e_m = 0.0119 + 0.0873 \log_{10}(i) \quad i \leq 76 \text{ mm} \cdot \text{h}^{-1} \quad (5)$$

$$e_m = 0.283 \quad i > 76 \text{ mm} \cdot \text{h}^{-1} \quad (6)$$

Another empirical equation which Brown and Foster (1987) suggested for tropical regions and adopted in RUSLE (Renard et al., 1997) is:

$$e_m = 0.29 [1 - 0.72 \exp(-0.05i)] \quad (7)$$

where e_m is kinetic energy of a unit rainfall (MJ·ha⁻¹·mm⁻¹ of rain) and i the corresponding rainfall intensity (mm·h⁻¹). The procedures used for the evaluation of kinetic energy E from e_m have been discussed by Renard et al. (1997). Unless otherwise stated, Equations 5 and 6 are usually used for computation of E or KE.

Application of equations 5 and 6 in the tropics suffered the inherent problem in using empirical equations, which is the fact that they are best suited for similar environment to where they were developed. Unfortunately, these equations had not

taken into consideration the high intensities of tropical rainfall as demonstrated in Figure 1 as it is assumed that intensities above $76 \text{ mm}\cdot\text{h}^{-1}$ would hardly occur. Still, they have been widely used to evaluate rainfall kinetic energy in the tropics, perhaps, because convincing alternatives have not been provided in terms of database used in generating these other empirical equations. For instance, Kowal and Kassam (1976) based on 18 rainstorms proposed the equation:

$$E = 0.414A - 1.2 \quad r = 0.99 \quad (8)$$

where E is the kinetic energy (MJ/ha) and A the rainfall (mm). Salako et al. (1991) found that E computed with Equation 8 was more than E computed with Equation 5. As Lal (1998) reported, the relationships presented in Equations 3 and 4 were valid in 1981 but not in 1980 at the same location. Definitely, there is a need for a large database to account for temporal variability of rainfall and the large database involved in the development of RUSLE has accounted for the confidence often reposed in it for soil conservation planning.

Compound rainfall erosivity

There are three popular indices for rainfall erosivity evaluation:

- (i) EI_{30} index (Wischmeier and Smith, 1978; Renard et al., 1997)
- (ii) $KE \geq 25$ (Hudson, 1995)
- (iii) AI_m index (Lal, 1976)

These are compound erosivity indices because they incorporate more than one rainfall characteristic in their evaluation. The EI_{30} index is a product of rainfall kinetic energy (E) and maximum 30-minute intensity, I_{30} ; the $KE \geq 25$ is a summation of kinetic energy of rainfall exceeding $25 \text{ mm}\cdot\text{h}^{-1}$, based on the premise that such rainfall events are the culprits in the soil erosion problem and the AI_m index is the product of daily rainfall amount and maximum short-term intensity (I_m). Although both the AI_m and $KE \geq 25$ were developed to characterize tropical rainfall, the EI_{30} index had been widely used because it is amenable to RUSLE for soil conservation planning. From published and unpublished data, the magnitude of rainfall in Nigeria follows the distribution and magnitude of annual rainfall amounts (Table 2).

In a recent study with long-term data covering 1977-1999 (Salako, F. K. unpublished; Figure 1), the annual rainfall erosivity for Ibadan with the EI_{30} was $17745 \text{ MJ}\cdot\text{mm}/\text{ha}\cdot\text{h}$ and for Port-Harcourt it was $26829 \text{ MJ}\cdot\text{mm}/\text{ha}\cdot\text{h}$. The AI_m index annual value for this study was $1100 \text{ cm}^2\cdot\text{h}^{-1}$ for Ibadan and $1457 \text{ cm}^2\cdot\text{h}^{-1}$ for Port-Harcourt. The difference in these values, compared with Table 2 for same locations, was due to the use of long-term data and the inclusion of all rainfall events in the analysis. The long-term data caused increase in values because they could capture

rainfall events, especially for some months with infrequent rainfall which might be omitted by short-term data. Problem of underestimation with all-inclusive long-term data is remote and it is better that planning is based on these.

Temporal variability of rainfall erosivity and its prediction from daily rainfall

It is often desirable to evaluate rainfall erosivity with long-term data (≥ 20 years) to account for temporal variability. Unfortunately, such long-term pluviograph data are difficult to obtain in tropical areas. Besides, pluviographs are rare in meteorological stations of many developing nations.

Table 2. Annual rainfall erosivity in southern Nigeria

Rainfall erosivity indices				
Location	Years of observation	EI ₃₀ (MJ·mm/ha·h)	AI _m (cm ² ·h ⁻¹)	KE > 25 (MJ·ha ⁻¹)
Southeastern Nigeria (Annual rainfall between 1500 and 2900 mm) ^{##}				
Nsukka	1976-1983	12814	849	141
Enugu	1977-1980	15776	1055	235
Umudike	1974-1985	15922	1300	210
Owerri	1973-1982	18545	1300	249
Calabar	1976-1980	22168	1468	303
Ikom	1978-1980	19482	1327	297
Port-Harcourt	1973-1981	18611	1400	234
Onitsha	1977-1980	12087	1017	188
Southcentral Nigeria (Mean annual rainfall of 2000 mm) ^{##}				
Okomu, near				
Benin City	1986-1990	18510	1329	216
Southwestern Nigeria (Mean annual rainfall of 1300 mm)				
Ibadan	1996-1999	12137	754	170

^{##} Mean annual rainfall from 1961 to 1990 for different locations are reported by Jagtap (1995), Armon (1984), Salako et al. (1995), and Salako, F.K., Kirchhof G., Tian, G. (Unpublished)

Spatial variability, albeit temporal variability, can be quantitatively assessed with geostatistical tools and fractal theory (Vieira et al., 1983; Webster and Oliver, 1990). This is an area which soil scientists have vigorously explored in the last decade (Burrough, 1993; Anderson et al., 1998) but less so in the tropics due to dearth of data.

Using the regionalized variable theory in geostatistics, an experimental variogram is constructed which is useful for interpolation, optimal sampling and

description of temporal dependence (Figures 2 and 3). A variogram is a plot of variance (Y axis) versus lag (distance or time on X axis).

Variograms are fitted with various theoretical models which take different forms which classified as bounded variograms with finite ranges (e.g., circular and spherical models), bounded variograms with asymptotic ranges (e.g., exponential and gaussian models) and linear variogram (power and linear models) (Vieira et al., 1983; Webster and Oliver, 1990). Below are some variogram models which have been applied to long-term rainfall erosivity data in southern Nigeria (Salako, F. K., unpublished).

The Gaussian model is

$$\gamma(h) = c_0 + c_1[1 - \exp(-h^2/a_0^2)] \quad (9)$$

where $\gamma(h)$ is the semi-variance of erosivity index (units of index)², h the lag distance (years), c_0 the nugget variance, $(c_0 + c_1)$ the sill variance, and $a_0 = (1/\sqrt{3})a$ with a being the range.

The linear model used for the HF zone was of the form

$$\gamma(h) = c_0 + ch \quad (10)$$

where c is the slope. Also, the power model which fitted both the DS and HF zones was used for the calculation of fractal dimensions

$$\gamma(h) = wh^\alpha \quad (11)$$

or

$$\log \gamma(h) = \log w + \alpha \log h \quad (12)$$

which is the linear form of the power model where $\gamma(h)$ is the semi-variance, h the lag distance in years, w the intercept (constant), α the slope = $(4 - 2D)$ with D being the fractal dimension.

Some of these analyses can be carried out with some statistical software like GENSTAT (Lawes Agricultural Trust, 1996). Thus, the burdensomeness of a large body of data is reduced considerably.

As shown in Figures 2 and 3, the typical characteristics of variograms are the sill, the nugget and the range. The sill, which is a horizontal part of the variogram implies a lack of spatial (temporal) dependence as the variances have no defined relationship with the lag. The curve rises to the sill at a lag value called the range. The range is an aspect of the curve which shows data points that are alike or interdependent.

The nugget variance for the EI₃₀ was 86 (MJ·mm/ha·h)², the sill variance was 217 (MJ·mm/ha·h)² and the range was 16.5 years. The nugget variance is an indication of existence of measurement errors or short-term variations with lags less than one year. The range in this situation indicated that within 16.5 years, there was

interdependence of rainfall erosivity by which interpolation could be confidently made. These characteristics have been used to deduce that temporal variations in rainfall erosivity could be adequately accounted for at Ibadan with data spanning 17 years.

Fractal dimensions D are calculated from the sampled data using the exponential model (Burrough, 1993; Anderson et al., 1998). Given the variogram in Figure 3, the fractal dimension D using the AI_m index was 1.927. For EI_{30} , it was 1.88. Fractal dimensions close to 2 such as these indicate the importance of long-range variations (Eghball and Power, 1995; Eghball et al., 1995). Both regionalized and fractal theories have been use to deduce the processes of vegetational and climatic erosivity changes over the years at Ibadan. For about 3 decades, there has been a complex interaction of human, edaphic and climatic factors in the transformation of the forest to savanna. The variograms seemed to suggest that after about two decades of continuous change, the processes became random as a vast area of savanna had been created from the hitherto forest vegetation. Fractal dimensions were large because of the complex interactions of factors which caused these changes.

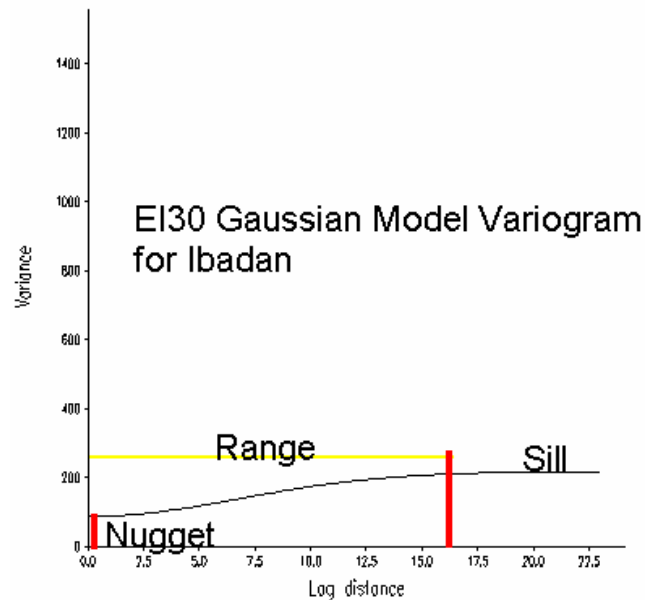


Figure 2: Experimental variogram describing temporal variability of EI_{30} ($MJ \cdot mm/ha \cdot h$) index.

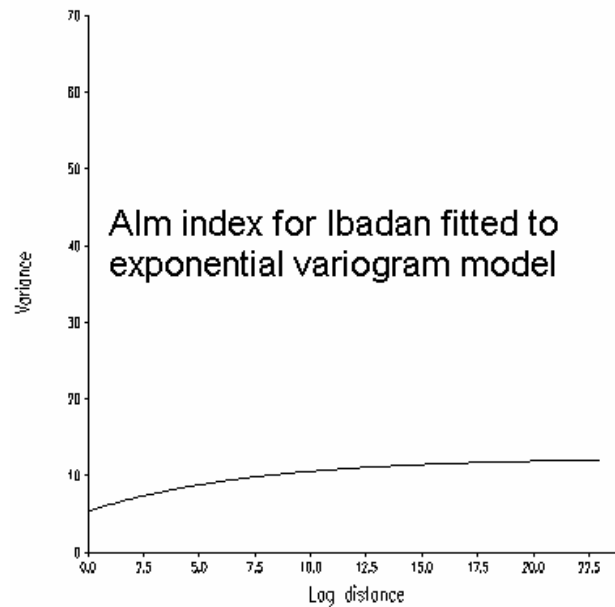


Figure 3: Experimental variogram describing temporal variability of AI_m ($\text{cm}^2\cdot\text{h}^{-1}$) index.

Long-term data of daily rainfall amount are easier to come by than pluviograph or auto-weather station data in the tropics. This has encouraged development of relationships between rainfall erosivity, especially EI_{30} and daily rainfall amount. The relationship of the form below has been found widely applicable (Elsenbeer, 1993; Yu and Rosewell, 1996; Salako, F. K. unpublished) for tropical rainfall:

$$R = aA^b \quad (13)$$

where R is the rainfall erosivity, A the daily rainfall amount, and a and b are constants. Values of a and b calculated for a region in southern Nigeria are given in Table 3.

Table 3. Regression parameters of the model, $R = aA^b$, for the prediction of rainfall erosivity (dependent variable) from daily rainfall amount (mm) (independent variable) in southern Nigeria

Rainfall erosivity index R	Intercept a	Slope b	Coefficient of determination r^2
AI_m ($\text{cm}^2\cdot\text{h}^{-1}$)	0.03	1.76	0.91
$EI_{30}\text{-WS}$ ($\text{MJ}\cdot\text{mm}/\text{ha}\cdot\text{h}$)	0.41	1.85	0.91

Soil characteristics

Susceptibility of soil to erosion is termed soil erodibility. It is strictly a soil attribute while erosivity is a rainfall attribute. Soil susceptibility to erosion is influenced by properties such as texture, aggregate stability, water transmission characteristics, and organic matter content. The process of soil erosion involves detachment, transportation and deposition. Thus, soils which are susceptible to detachment and transportation are can be easily eroded. This explains the reason why characteristics measured in the laboratory or in the field to evaluate soil erodibility focus on splash erosion and transportation of soil materials. Soils, which are weakly aggregated, can be easily detached or dispersed by water while fine materials such as clay are easily transported once detached.

Particle size distribution

Soil texture refers basically to the distribution of sand, silt and clay. These are components of materials less than 2 mm size, called the fine earth fraction. Materials greater than 2 mm in size are called gravel, cobbles and stones. By the United States Department of Agriculture classification, the size ranges are 0.05-2 mm for sand, 0.002-0.05 mm for silt and < 0.002 mm for clay. In southwestern Nigeria, a vast area of the Alfisol formed on basement complex contains particles > 2 mm (i.e., gravel and stones) (Table 4).

Table 4. Particle size distribution, organic carbon, calcium and bulk density values for a forest profile in Ibadan, southwestern Nigeria (Salako F. K., unpublished)

Depth (cm)	Total sand	VCS (1-2 mm)	CS (0.5- 1mm)	MS (0.25- 0.5m)	FS (0.1- 0.25m)	VFS (0.05- 0.10m)	Clay	Silt	Gravel content of field soil (g/kg)	Org. C (g/kg)	Ca (cmol/ kg)	Bulk density (g/cm ³)
0-7	710	90	130	130	280	70	90	210	40	18.6	6.73	1.46
7-15	770	140	220	180	190	40	110	120	120	9.5	2.46	1.54
15-36	420	120	130	80	70	20	220	360	310	6.0	2.79	1.53
36-84	430	130	130	80	60	30	400	160	430	4.2	2.73	1.41
84-132	400	120	120	70	60	30	480	120	150	1.2	3.15	1.36
132-190	460	110	130	80	80	40	410	140	110	2.1	3.09	1.39

Particle size distribution (g kg⁻¹) = 0.1%

Particle size distribution of soil samples ≤ 2 mm is determined by pipet or hydrometer method (Gee and Bauder, 1986). Pre-treatment of samples ensures that samples are properly dispersed before determination. Variations exist from laboratory to laboratory on the pre-treatments. For instance, the removal of organic matter is

skipped when it is known that this is very low in some soils while removal of iron oxides is usually considered optional.

The particle size distribution in Table 4 was determined by pipet method although it is often determined by hydrometer method in most laboratories. It is often not a common practice to separate sand in many laboratories but this is highly desirable for the evaluation of soil erodibility (Renard et al., 1997) and the application of fractal theory (Tyler and Wheatcraft, 1992; Anderson et al., 1998; Salako et al., 1999).

Particle size distribution is basic to the behavior of soils in terms of their chemical and physical properties. In spite of the higher clay content of the subsoil in Table 4, gravel concentration is higher. Thus when the topsoil is eroded, it is not just the chemical fertility that is reduced, there are more grave consequences with stones exposed which would make cultivation either with hand hoe or machinery difficult. Besides, the subsoils often exhibit more hardsetting properties (Mullins et al., 1990).

Aggregate stability and soil structure

In soils, the particles are aggregated and arranged in various forms. Soil aggregation is as a result of flocculation of clay and cementation of the particles through some chemical, biological and physical mechanisms. The arrangement of these particles into peds or aggregates is referred to as soil structure. Kay (1990) stated that soil structural form is the heterogeneous arrangement of solid and void space that exist at a given time while the stability is the ability to retain its arrangement of solid and void spaces when exposed to different stresses.

Aggregate stability is a measure of the resistance of the aggregates so formed to disruptive forces such as impact of rainfall. Aggregate stability with regard to water erosion can be measured by measuring resistance of aggregates wet-sieving (Yoder, 1936; Angers and Mehuys, 1993). In this method, aggregates placed on sieves are oscillated in a cylinder of water to disrupt the bonds cementing the soil particles. This is to simulate aggregates vulnerability to breakdown under the influence of runoff. Also, resistance of aggregates to water drops are measured by bombarding the aggregates with water drops from a drop former (Bruce-Okine and Lal, 1975), which could be as simple as a buret.

Aggregates occur in soils in hierarchical size orders (Dexter, 1988). Soil aggregates can be broadly classified as macroaggregates ($> 250 \mu\text{m}$) and microaggregates ($< 250 \mu\text{m}$). Wet-sieving and water drop impacts are carried out to test macroaggregate ($> 250 \mu\text{m}$). Microaggregates ($< 250 \mu\text{m}$) are tested for stability usually by dispersion techniques, which in the simple form involves comparison of water-dispersible clay (and silt) with clay (and silt) dispersed in a dispersing agent like calgon. There are variations from laboratory to laboratory on pre-treatment of aggregates, period of wet-sieving, nest of sieves selected, method of dispersion, etc.

Wet-sieving can be done by a single sieve or multiple sieves. When multiple sieves are used, the data are amenable to calculation of aggregate stability indices such as the mean-weight diameter MWD and geometric diameter GMD. For instance

in some studies carried out in southwestern Nigeria (Salako et al., 1999; Salako and Hauser, 2001), wet sieving of 4-10 mm aggregate samples was carried out in a nest of sieves with 4, 2, 1, 0.25, 0.125 and < 0.125 mm openings. To calculate MWD and GMD,

$$\text{MWD} = \sum x_i \text{WSA} \quad (14)$$

where WSA is the proportion of water stable aggregates retained on sieves, and x_i the mean aggregate size obtained from mean sieve size (e.g., the mean sieve or aggregate size for aggregates retained on the 2 mm sieve is $(4+2)/2$ which is 3).

The geometric mean diameter GMD is another index based on the observation that distribution of aggregates after wet-sieving follows a log-normal distribution (Gardner, 1956).

$$\text{GMD} = \exp[\sum (w_1 - w_2) \log (x_i/W)] \quad (15)$$

where w_2 is the water stable aggregates after wet-sieving, w_1 the coarse materials in aggregates and W the initial sample mass

The time period soil aggregates are subjected to sieving vary as many other pre-treatments from laboratory to laboratory. In order to improve efficiency in laboratories, it is necessary to understand the adequacy of period used for sieving. Salako and Hauser (2001) found that there was no significant relationship in aggregate stability of coarse-textured Alfisols and Ultisols of southern Nigeria when sieved between 5 and 35 minutes (Table 5) because of the inherently weak aggregation due to the dominance of sand. This was consistent with the position of Raine and So (1997) who showed that unstable soils might not be sensitive to increases in the amount of energy applied to break down their aggregates

Table 5. Variations of soil aggregate stability with we-sieving period for Alfisols and Ultisols in southern Nigeria*

Wet-sieving period (min)	Alfisol (0-30 cm depth)			Ultisol (0-15 cm depth)		
	MWD (mm)	GMD (mm)	WSA > 0.25 mm	MWD (mm)	GMD (mm)	WSA > 0.25 mm
5	3.55	1.20	57	3.55	1.09	57
10	5.09	1.21	76	3.80	1.11	63
15	3.05	1.12	51	4.11	1.23	64
20	5.10	1.20	76	3.81	1.11	61
25	2.98	1.10	46	3.08	1.05	55
30	3.59	1.19	58	2.34	1.08	43
35	3.82	1.06	61	3.11	1.04	51

* Source: Salako and Hauser (2001).

The study by Salako and Hauser (2001) showed that prolonged wet-sieving analysis (> 10 minutes) was not necessary for coarse-textured soils. Therefore, it was recommended that wet-sieving analyses for such soils be carried out within 10 minutes (5-minute wetting by immersion followed by 5-minute wet sieving). The study further showed that soil aggregate stability differed between soil types, land uses and soil management and its characterization should therefore be site specific.

Soil aggregate stability varied with season for the coarse-textured soils of southwestern Nigeria (Figure 4; Salako et al., 1999). The MWD was higher in the dry season (January) than the wet season (July and September) due to closer association of the soil particles in the dry season and their dispersion in the wet season. The intermediate period (March) between the dry and wet seasons had similar MWD to both seasons.

Dispersion ratio, which is the ratio of (silt + clay) in water to (silt + clay) in a dispersant such as calgon is an index of structural stability inasmuch as its magnitude is related to the stability the soil microaggregates. If the ratio is higher than 50% and could be up to 87% for the coarse textured Alfisol of southwestern Nigeria (Salako, 2001), the soils are structurally weak.

Describing particle size distribution and aggregate stability with fractal theory

There is a review of the application of fractal theory to soil studies by Anderson et al. (1998). Fractal theory has been applied to a wide range of topics in natural and physical sciences but appear to be used more by soil physicists among soil scientists, especially with regards to particle soil distribution and soil structural characterization.

Salako et al. (1999) and Salako (2001) used the number-size distributions of soil aggregates as described by a power law relationship to obtain fractal dimensions:

$$N_{>x} = k X^{-D}$$

where X is the mean sieve size obtained by finding the average value of successive sieve sizes, $N_{>x}$ the cumulative number of aggregates and D the fractal dimension. A log-log regression analysis between N and X provides values of k and D. Salako et al. (1999) reported that fractal dimensions D for 4-10 mm ranged from 2.29-2.72 with low D values associated with more stable aggregates under fallow and high D values associated with unstable aggregates under cultivation. Furthermore, the coarseness of soil influenced the D values with higher D values being observed for fine-textured soils. The increase in D after the removal of coarse fragments indicates the higher irregularity of aggregate shapes. Such separation of coarse and fine materials in soils occurs with soil erosion, and the implications can be described using the fractal theory.

Water transmission characteristics

Water entry into the soil by infiltration is a major determinant of how much rain will runoff and cause soil erosion. Coarse-textured soils have high water infiltration rates and hydraulic conductivity. For soils in southwestern Nigeria, saturated hydraulic conductivity could be as high as $525 \text{ cm}\cdot\text{h}^{-1}$, and after 2 hours, water infiltration rate may still exceed $72 \text{ cm}\cdot\text{h}^{-1}$ (Salako, 2002). Water infiltration rate is usually measured with a double-ring infiltrometer having an outer ring of 60 cm diameter and an inner ring of 30 cm diameter, both having a depth of 25 cm. The water head maintained in such a method is usually between 5 and 12 cm.

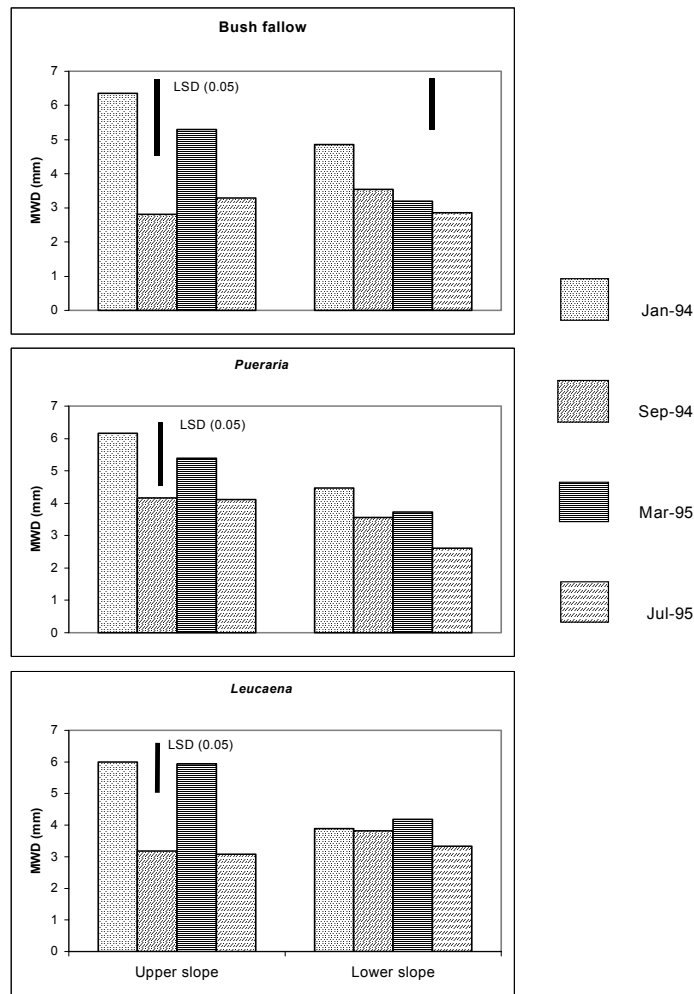


Figure 4. Temporal and spatial variations of soil aggregates in southwestern Nigeria (Source: Salako et al., 1999)

There have been recent advances in which both saturated and unsaturated flow characteristics can be measured with less strenuous equipment such as the disc permeameter. Preliminary studies using the disc permeameter in southwestern Nigeria showed that the sorptivity values may not actually be different from those obtained by double-ring infiltrometer (Table 6) but the equations for calculating parameters such as the hydraulic conductivity would need to be revised for coarse-textured and heterogeneous tropical soils because unreasonable negative values were obtained for the hydraulic conductivity (Salako F. K. and Kirchhof, G., unpublished).

Table 6. A preliminary study comparing of sorptivity ($\text{cm}\cdot\text{h}^{-0.5}$) measured with double-ring and disc-permeameter on a coarse surface soil at Ibadan, southwestern Nigeria (Salako F. K. and Kirchhof G., unpublished)

Method	Sorptivity
Double-ring	135
Disc permeameter	104
LSD	NS

Evaluating soil erodibility and soil loss

Soil erodibility is actually defined as the susceptibility of soils to erosion. Particle size distribution, soil dispersion and aggregate stability have been used for many years as indices of soil erodibility (Bryan, 1968). Therefore, the foregoing discussion on soil characteristics are relevant to this sub-topic, which however, will be discussed in the context of the (Revised) Universal Soil Loss Equation, RUSLE (Renard et al., 1997).

Average annual soil erosion expected from field slopes is computed from the USELE or RUSLE as follows:

$$A = RKLSCP \quad (16)$$

where A is the computed spatial average soil loss and temporal average soil loss per unit of area ($\text{t}\cdot\text{ha}^{-1}\cdot\text{yr}^{-1}$), R the rainfall-runoff erosivity factor, K the soil erodibility factor which is the soil loss rate per erosion index unit for a specified soil as measured on a standard plot, which is defined as a 22.1 m length of uniform 9% slope in continuous clean fallow, L the slope length factor - the ratio of soil loss from the field slope length to soil loss from a 22.1 m length under identical condition, S the slope steepness factor - the ratio of soil loss from the field slope gradient to soil loss from a 9% slope under otherwise identical conditions, C the cover-management factor - the ratio of soil loss from an area with specified cover and management to soil loss from an identical area in tilled continuous fallow, and P the support practice factor - the ratio of soil loss with a support practice like contouring, strip cropping or terracing to soil loss with straight-row farming up and down the slope.

The USLE or RUSLE has been widely criticized (e.g., Hudson, 1993) for the fact that an empirical equation cannot be universally applicable. The review of USLE leading to RUSLE is an obvious attestation to this fact. Nonetheless, the RUSLE has proven to be a useful tool in many developing nations where there have been major constraints in establishing long-term experiments.

Soil erodibility can be evaluated using (i) runoff plots, (ii) rainfall simulators in laboratory or field plots and/or (iii) nomograph (Hudson, 1993; Lal, 1994). Runoff plots are very expensive to establish and maintain, and may not yield meaningful results for watershed management as the plots are often unrepresentative of watersheds (Hudson, 1993). Rainfall simulators vary in sophistication, and this would determine the cost involved in their use. The nomograph requires data on (i) percent silt + very fine sand, (ii) percent sand (0.10-2 mm), (iii) percent organic matter, (iv) soil structural class and (v) permeability. These properties have earlier been discussed. Comparison of soil erodibility values from runoff plots in southeastern Nigeria with the nomograph for its evaluation in the USLE showed that significant differences existed between the two methods (Vaneslande et al., 1984; Obi et al., 1989), suggesting some inadequacies in the nomograph. Such inadequacies could be due to the dominance of medium to coarse sand in the tropical soils whereas the nomograph was developed with soils having substantial fine particles. Obi et al. (1989) found that actual measurement of soil erodibility was 0.007 t·h/MJ·mm compared with 0.012 t·h/MJ·mm using the nomograph and 0.03 t·h/MJ·mm using rainfall simulator for a sandy loam soil in southeastern Nigeria. Table 7 gives a comparison of the nomograph with rainfall simulator estimates for different parent materials.

Table 7. Soil erodibility measured with erodibility nomograph and under rainfall simulator for soils from different parent materials in southeastern Nigeria

Parent material	Erodibility (t·h/MJ·mm)	
	Nomograph	Simulated rainfall
Sandstone	0.008	0.09
	0.002	0.02
	0.008	0.006
	0.03	0.08
	0.012	0.03
	0.058	0.05
Shale	0.013	0.006
Shale/Sandstone	0.042	0.03

Source: Obi et al. (1989)

Soil loss tolerance T is the maximum rate of annual soil loss that will permit plant productivity to be maintained economically and indefinitely. In the USA, upper limit T is $11.2 \text{ t·ha}^{-1}\cdot\text{y}^{-1}$ (Hudson, 1995; Renard et al., 1997) but for major soils in the

humid and subhumid tropics it is less than $2 \text{ t} \cdot \text{ha}^{-1} \cdot \text{y}^{-1}$ (Lal, 1985; Igwe, 1999). Either by estimation using USLE or by field plot measurements, soil loss or soil erosion from the coarse textured soils exceed a tolerance limit of about $2 \text{ t} \cdot \text{ha}^{-1} \cdot \text{y}^{-1}$ for tropical soils. Obi et al. (1989) reported that soil loss from bare soils with very poor aggregation and tilled up and down the slope could be up to $59 \text{ t} \cdot \text{ha}^{-1} \cdot \text{y}^{-1}$. Lal (1997) reported annual soil losses in relation to slope length under conventional tillage in Ibadan southwestern Nigeria as 9.59 t/ha for 60 m long slope, 9.88 t/ha for 50 m, 6.84 t/ha for 40 m, 5.69 t/ha for 30 m, 1.27 t/ha for 20 m and 2.19 t/ha for 10m slopes. The slope length L and erosion Y relationship fitted a polynomial function:

$$Y = c + aL + bL^2 \quad (17)$$

where a , b and c depend on soil, slope, rainfall regime, and management practices.

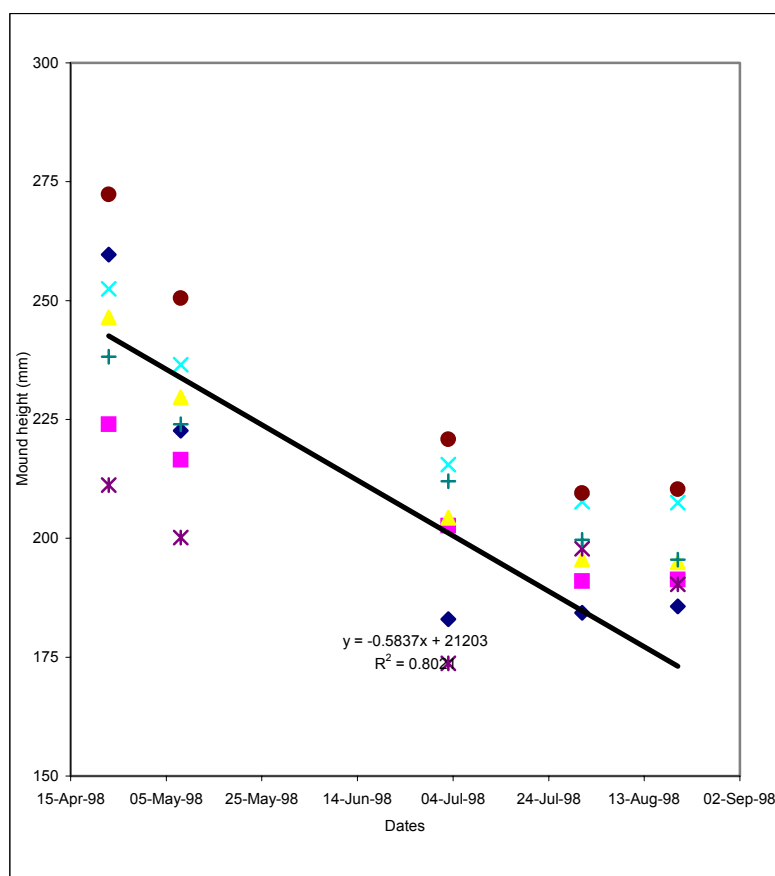


Figure 5. Changes in mound height as a measure of soil erosion, monitored during the rainy season with a profile meter in Ibadan, southwestern Nigeria in 1998 (Salako, F. K. and Kirchhof, G. unpublished data)

Profilemeters measure small changes in surface level along a cross section (Hudson, 1995) and can be found useful in detecting problems of sheet erosion, which can go unnoticed by ordinary visual observation. Soil erosion from mounds has been observed for the coarse-textured Alfisols in southwestern Nigeria (Figure 5, Salako, F. K. and Kirchhof G., unpublished). Mound tillage is a common practice for cultivation of tuber and root crops in the tropics and soil erosion studies have not focused adequately on this particular tillage practice. When depth of an area eroded is known with a profile meter, the volume of soil eroded can be calculated for a given area, and the mass of soil eroded obtained from the bulk density of the soil.

Other models and their application in the tropics

There are some other empirical models like the Soil Loss Estimation of Southern Africa (SLEMSA) (Elwell, 1977):

$$A = KCX \quad (18)$$

where A is the predicted mean annual soil loss, K the mean annual soil loss from a standard field plot on a 4.5% slope, C the crop management factor and X the slope length factor.

Process-based models now exist, requiring mathematical analyses to explain the physical processes involved in soil erosion. They are usually run with computing aids. The application of such models is rare in the tropics because of expertise and availability of data.

General discussion and recommendations

The various studies reported in this paper indicated a few areas where physics can be applied in Soil Science. Basic soil physics needs to grow along with applied soil physics but emphasis is currently on the latter because soil science is still strongly linked with food production and inter or multidisciplinary approach to research is not encouraged in many national institutions. Multi-disciplinary researches involving physicists, soil physicists and engineers like those of Kowal et al. (1973), Kowal and Kassam (1976), Lal (1976) and Lal (1992) have always led to simultaneous fabrication or design of equipment and use of the equipment for data collection. Very high rainfall intensities falling on coarse-textured soils in the tropics still cause considerable soil erosion in spite of high water infiltration rates. Often, this is due to weak soil structure. The processes involved are not yet adequately explained.

References

- Aina, P. O. 1980. Drop characteristics and erosivity of rainfall in southwestern Nigeria. *Ife Journal of Agriculture* 2: 35-43.
- Akinnifesi, F. K. and Salako, F. K. 1997. Growth of *Gmelina arborea* and *Senna siamea* and their effects on microclimate in southern Nigeria. *Tropical Ecology* 38: 55-63.
- Anderson, A. N., McBratney, A. B. and Crawford, J. W. 1998. Applications of fractals to soil studies. *Advances In Agronomy* 63: 1-76.
- Angers, D. A. and Mehuys, G. R. 1993. Aggregate stability to water. In: M. R. Carter (ed.) *Soil Sampling and methods of analysis*. Canadian Society of Soil Science/Lewis Publishers, Boca Raton, Florida, USA. pp. 651-657.
- Armon, M.N. 1984. Soil erosion and degradation in southeastern Nigeria in relation to biophysical and socio-economic factors. Ph.D. Thesis, Department of Agronomy, University of Ibadan, Ibadan, Nigeria
- Brown L.C. and Foster G.R., 1987. Storm erosivity using idealized intensity distributions. *Trans. ASAE* 30: 379-386.
- Bruce-Okine, E. and Lal, R. 1975. Soil erodibility as determined by raindrop technique. *Soil Science* 119: 149-157.
- Bryan, R. B. 1968. The development, use and efficiency of indices of soil erodibility. *Geoderma* 2: 5-26.
- Burrough, P.A., 1993. Soil variability: a late 20th century view. *Soils and Fertilizer* 56: 529-562.
- Carter C. E., Greer, J. D., Braud, H. J. and Floyd, J. M. 1974. Raindrop characteristics in south central United States. *Transactions of the ASAE* 6: 1033-1037.
- Dexter, A. R. 1988. Advances in characterization of soil structure. *Soil & Tillage Research* 11: 199-238.
- Eghball, B. and Power, J.F., 1995. Fractal description of temporal yield variability of 10 crops in the United States. *Agronomy Journal* 87: 152-156.
- Eghball, B., Binford, G.D., Power, J.F., Baltensperger, D.D. and Anderson, F.N., 1995. Maize temporal yield variability under long-term and fertilizer application: Fractal analysis. *Soil Science Society American Journal* 59: 1360-1364.
- Elseenbeer, H., Cassel, D.K. and Tinner, W., 1993. A daily rainfall erosivity model for western Amazonia. *Journal of Soil & Water Conservation* 48: 439-444.
- Elwell, H. A. 1977. Soil loss estimation for southern Africa. Research Bulletin 22. Department of Conservation and Extension: Harare, Zimbabwe.
- Gardner, W. R. 1956. Representation of soil aggregate-size distribution by a logarithmic-normal distribution. *Soil Science Society of America Proceedings* 20: 151-153.
- Gee, G. W. and Bauder, J. W. 1986. Particle-size analysis. In: Klute A. (ed.) *Methods of soil analysis*. Part 1. Physical and mineralogical methods. 2nd edition ASA-SSSA, Madison, WI, USA. pp. 383-411.
- Hartemink, A. E. 2002. Soil science in tropical and temperate regions-Some differences and similarities. *Advances in Agronomy* 77: 269-292.

- Hudson, N. W. 1993. Field measurement of soil erosion and runoff. *FAO Soils Bulletin* 68:139 pp.
- Hudson, N., 1995. Soil conservation. 3rd edition. Iowa State University Press, Ames, 391 pp.
- Igwe, C.A. 1999. Land use and soil conservation strategies for potentially highly erodible soils of central-eastern Nigeria. *Land Degradation and Development* 10: 425-434.
- Jagtap, S.S., 1995. Changes in annual, seasonal and monthly rainfall in Nigeria during 1961-1990 and consequences to agriculture. *Discovery and Innovation* 7: 337-348.
- Kay, B. D. 1990. Rates of change of soil structure under different cropping systems. *Advances in Soil Science* 12; 1-52.
- Kowal, J. M., Kijewski, W. and Kassam, A. H. 1973. A simple device for analyzing the energy load and intensity of rainstorms. *Agricultural Meteorology* 12: 271-280.
- Kowal, J. M. and Kassam, A. H. 1976. Energy load and instantaneous intensity of rainstorms at Samaru, Northern Nigeria. *Tropical Agriculture* 53:185-197.
- Lal, R. 1976. Soil erosion problems on Alfisols in western Nigeria and their control. Monograph No. 1. IITA, Ibadan.
- Lal, R. 1985. A soil suitability guide for different tillage systems in the tropics. *Soil & Tillage Research* 5: 179-196.
- Lal, R., 1992. Tropical agricultural hydrology and sustainability of agricultural systems. The West Bank project (1978-1988). Ohio State University/International Institute of Tropical Agriculture, 303 pp.
- Lal, R. (editor) 1994. Soil erosion research methods. 2nd edition. 339 pp.
- Lal, R. 1997. Soil degradative effects of slope length and tillage methods on Alfisols in western Nigeria. I. Runoff, erosion and crop response. *Land Degradation & Development* 8: 201-219.
- Lal, R. 1998. Drop size distribution and energy load of rain storms at Ibadan, western Nigeria. *Soil & Tillage Research* 48: 103-114.
- Lal, R. 2000. Physical management of soils of the tropics: Priorities for the 21st Century. *Soil Science* 165: 191-207.
- Lawes Agricultural Trust, 1996. GENSTAT 5 Release 3.2, Rothamsted, UK
- Mullins, C. E., MacLeod, D. A., Northcote, K. H., Tisdall, J. M. and Young, I. M. 1990. Hardsetting soils: Behavior, occurrence and management. *Advances in Soil Science* 11: 37-108.
- Obi, M. E., Salako, F. K. and Lal, R. 1989. Relative susceptibility of some southeastern Nigeria soils to erosion. *CATENA* 16: 215-225.
- Raine, S. R. and So, H. B. 1997. An investigation of the relationships between dispersion, power and mechanical energy using the end-over-end shaking and ultrasonic methods of aggregate stability assessment. *Australian Journal of Soil Research* 35: 41-53.
- Renard, K.G., Foster, G.R., Weesies, G.A., McCool, D.K., and Yoder, D.C., 1997. Predicting soil erosion by water: A guide to conservation planning with the

- revised universal soil loss equation (RUSLE). USDA, Agriculture Handbook No. 703, Washington DC, 404 pp.
- Salako, F. K. 2001. Structural stability of an Alfisol under various fallow management practices in southwestern Nigeria. *Land Degradation & Development* 12: 319-328.
- Salako, F. K. 2002. Ponded water flow in an Alfisol under different intensities and fallow systems in southwestern Nigeria. *Asset Series A* 2:156
- Salako, F. K., Obi, M. E. and Lal, R. 1991. Comparative assessment of several rainfall erosivity indices in southern Nigeria. *Soil Technology* 4: 93-97.
- Salako, F. K., Ghuman, B. S. and Lal, R. 1995. Rainfall erosivity in south-central Nigeria. *Soil Technology* 7: 279-290
- Salako, F. K., Babalola, O., Hauser, S. and Kang, B. T. 1999. Soil macroaggregate stability under different fallow management systems and cropping intensities in southwestern Nigeria. *Geoderma* 91: 103-123.
- Salako, F. K. and Hauser, 2001. Influence of different fallow management systems on stability of soil aggregates in southern Nigeria. *Communications in Soil Science and Plant Analysis* 32: 1483-1498
- Tyler, S. W. and Wheatcraft, S. W. 1992. Fractal scaling of soil particle-size distributions: Analysis and limitations. *Soil Science Society of America Journal* 56: 362-369.
- Vanelslande, A., Rousseau P., Lal, R., Gabriels, D. and Ghuman, B. S. 1984. Testing the applicability of a soil erodibility nomograph: In: Challenges in African Hydrology and Water Resources. Proceedings of Harare Symposium. July 1984. International Association of Hydrological Sciences Publication 144: 463-473.
- Vieira, S. R., Hartfield, J. L., Nielsen, D. R. and Biggar, J. W., 1983. Geostatistical theory and application to variability of some agronomical properties. *Hilgardia* 51: 1-51.
- Webster, R. and Oliver, M. A. 1990. Statistical methods in soil and land resource survey. Oxford University Press, New York, USA. 316 pp.
- Wischmeier, W. H. and Smith, D.D., 1978. Predicting rainfall erosion losses: a guide to conservation planning. USDA Handbook No. 537. Washington DC, 58 pp.
- Yoder, R. E. 1936. A direct method of aggregate analysis of soils and a study of the physical nature of erosion losses. *Journal of American Society of Agronomy* 28: 337-351.
- Yu, B. and Rosewell, C.J., 1996. An assessment of a daily rainfall erosivity model for New South Wales. *Australian Journal of Soil Research* 34: 139-152.

Soil Physical Conditions in Nigerian Savannas and Biomass Production

F.K. Salako¹

*Department of Soil Science and Agricultural Mechanisation,
University of Agriculture, Abeokuta, Nigeria*

*Lecture given at the
College on Soil Physics
Trieste, 3-21 March 2003*

LNS0418031

¹ kolawolesalako@hotmail.com; kfsalako@yahoo.ie

The Savannas of Nigeria and Agricultural Production

Nigeria is located in the tropical zone (between latitude 4° and 14°N, and longitude 2°E), with a vast area having savanna vegetation (Figure 1). This is a region that is itself diverse, necessitating a classification into derived savanna, southern Guinea savanna and northern Guinea savanna. These classifications reflect environmental characteristics such as length of growing period, which for instance is 151-180 days for the northern Guinea savanna, 181-210 days for the southern Guinea savanna and 211-270 days for the derived savanna/coastal savanna (Jagtap, 1995). The major soils found in the various agroecological zones have coarse-textured surface soil, and are low in organic matter and chemical fertility (Tables 1-3). Although, yields can be improved by addition of inorganic and organic fertilizer, this can only be sustained and assured with high soil physical qualities. Soil physical qualities can be sustained at a high level with conservation tillage and soil conservation measures

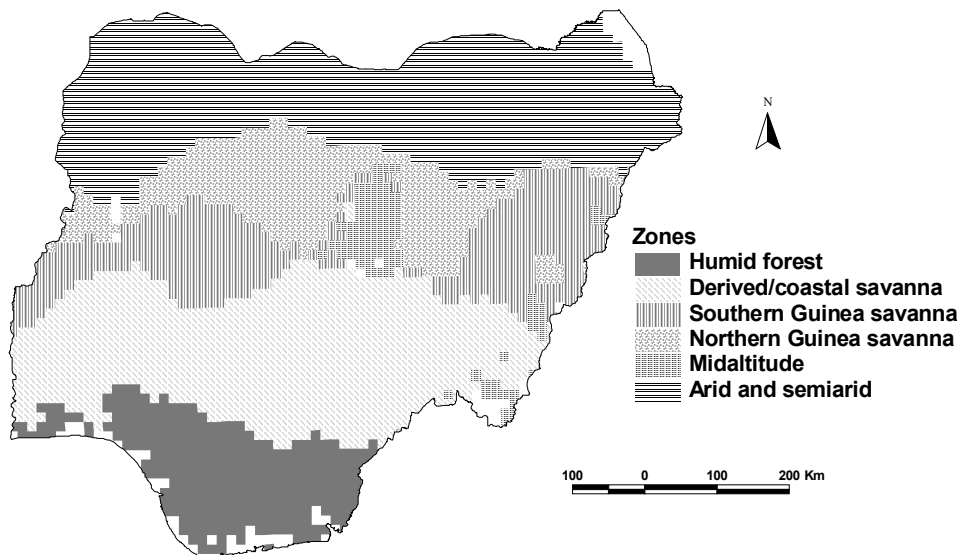


Fig. 1: Agroecological zones of Nigeria (Source: IITA GIS Unit, Ibadan, Nigeria)

Table 1. Some characteristics of agroecological zones of Nigeria (Source: Crop Modeling Unit, IITA, Ibadan, Nigeria).

Agroecological zone	Major soils (FAO classification)
Humid forest	Ferralsols, Nitosols and Gleysols
Derived/Coastal savanna (Moist savanna)	Ferralsols, Luvisols, Nitosols, Arenosols, Acrisols, Lithosols
Southern Guinea savanna (Moist savanna)	Luvisols, Acrisols, Ferralsols and Lithosols
Northern Guinea savanna (Moist savanna)	Luvisols
Mildaltitude savanna	Ferralsols, Nitosols

Table 2. Soil characteristics of soil in various agroecological zones of Nigeria Northern Guinea Savanna: Samaru, Zaria, Nigeria (Source: Oikeh et al., 1998)

Soil characteristics	Soil depth (cm)			
	0-17	17-31	31-82	>82
pH (H ₂ O)	5.2	4.9	5.4	5.3
Bulk density (Mg·m ⁻³)	1.39	1.47	1.45	1.67
Water retention at -0.01 MPa (g·kg ⁻¹)	310	359	343	344
Water retention at -1.5 MPa (g·kg ⁻¹)	61	147	206	253
Sand (g·kg ⁻¹)	44	36	29	36
Clay (g·kg ⁻¹)	15	28	38	35

Derived savanna: Nsukka, southeastern Nigeria (Source: Igwe et al., 1995)				
Soil characteristics	Soil depth (cm)			
	0-18	18-35	35-77	77-122
pH (H ₂ O)	5.77	5.02	5.35	5.01
Bulk density (Mg·m ⁻³)	1.54	1.56	1.34	1.50
Sand (g·kg ⁻¹)	760	740	800	580
Clay (g·kg ⁻¹)	220	240	180	380

Table 3. Particle and gravel distribution ($\text{g}\cdot\text{kg}^{-1}$) in the forest/savanna transition zone: Ibadan, southwestern Nigeria (Source: Salako et al., 1999).

Soil depth (cm)	Sand	Silt	Clay	Air-dried soil gravel content
0-15	834	94	72	124
15-30	745	95	160	120
30-45	706	105	190	128
45-60	658	97	245	172
60-90	646	83	271	232
90-120	616	109	275	125
120-150	618	128	254	156
150-200	644	175	181	144

Concepts of soil quality, degradation and sustainability

In one of the plethora of definitions, soil quality is defined as the capacity of a specific soil to function, within natural or managed ecosystem boundaries, to sustain plant and animal productivity, maintain or enhance water and air quality, and support human health and habitation (Brady and Weil, 1999). Thus, soil quality assessment reflects biological, chemical and physical properties, processes, and their interactions within each resource unit (Karlen et al., 2001). Lal (2001) stated that soil supports terrestrial life through five processes: (1) biomass production, (2) restoration and resilience of ecosystems, (3) purification of water, (4) detoxification of pollutants and (5) cycling of C, B, P, S and H_2O . Soil quality is depleted as the soil is degraded through individual or combined processes of soil degradation which in the savanna region is mainly by soil erosion and compaction. When a soil is degraded, its capacity to produce biomass is reduced. Recovery of the soil through efforts to rehabilitate it depends on the inherent capacity of the soil and the level of degradation reached before rehabilitation efforts; soil resilience.

The soils of the savanna region are physically fragile (Tables 1-3) because the topsoil contains a large proportion of sand, causing weak aggregation given the low level of organic matter in this layer. The physical constraints are further compounded in gravelly soils (Table 3) or soils with shallow depth overlying plinthic or hardpan layers (Adeoye and Mohammed-Saleem, 1990; Salako et al., 2002).

The erosion of the 0-15 cm of the soil in Table 3 will lead to exposure of more gravel which will make working of the soil difficult. Also, the particle size distribution indicates that water retention is low while infiltration rate will be high. It is therefore imperative that appropriate soil management options for sustainable crop production and improved soil and environmental quality be found for the tropics.

Tillage, soil physical properties and crop production

Tillage is physical manipulation of the soil. Thus, the most profound effect of tillage is in relation to soil physical properties. For socio-economic and cultural reasons, manual tillage is still widely practiced in Africa as farming is largely at subsistence level. However, there are now a number of commercial farms especially for cash crop production in many parts of Africa. Many of these are located in locations which were hitherto reserved as forest and a need for sustainable production is pertinent to maintain ecological balance.

Soil physical properties which are altered by tillage are bulk density, water content, penetration resistance, soil temperature and aggregate stability. Tilled plots are more susceptible to soil erosion as soil aggregates will be loosened which leads to alteration of soil texture (Table 4; Lal, 1997a). Since the surface of the soil was low in clay content, silt was more eroded causing increase in sand content of tilled compared with no tillage plots as cultivation progressed from 1982 to 1986. Available water content and water infiltration were highest under no tillage and both were particularly low for ridge-tilled plots. Less erosion of particles enhanced water retention in the no till while the high infiltration rates were due to high macroporosity.

Mound tillage was also found to improve soil bulk density significantly compared to flat tillage in compacted soil ameliorated with planted fallows in southwestern Nigeria (Table 5). Such improvements in bulk density encourage root growth either for cereals, tuber crops or root crops in ridge tillage, mound tillage and deep tillage in different agroecological zones (Adeoye and Mohamed-Saleem, 1990; Salako *et al.*, 2001). Rapid drying and increase in soil temperature on ridges and mounds occur if they are not mulched. Lal (1997b) advocated management of gravelly Alfisols in southwestern Nigeria with no tillage on short slopes (less than 100 m length) as the rate of increase in bulk density was higher for conventionally tilled plots compared with no tillage.

An interesting observation by Kirchhoff and Salako (2000) showed that after fallowing a degraded Alfisol caused by tillage and soil erosion in southwestern Nigeria for 6 years, the previously tilled plots under bare fallow (tilled up and down slope without crop cover) and conventional tillage still recorded more soil losses (1.78-2.83 t/ha) than the previous no tillage plots (1.34 t/ha). These results indicate that soil degradation caused by tillage cannot be easily obliterated. A land user should carefully weigh the options for tillage and no tillage before embarking on tillage. Conventional tillage should be avoided while conservation tillage should be practiced when tillage is adopted.

Table 4. Changes in soil particle size distribution of the 0-10 cm soil depth due to tillage between 1982 and 1986 on a Luvisol (Alfisol) in Ibadan, southwestern Nigeria (Lal, 1997b)

Tillage treatment [#]	Particle size distribution (g/kg)			AWC (%)	Equilibrium infiltration rate (cm/h)
	Sand	Silt	Clay	4.8	40
No till + mulch	738	86	177	4.3	30
No till + chisel	759	83	159	4.4	22
Ploughing	758	78	164	4.7	25
Disking	746	80	174	4.8	32
No till-mulch	748	82	168	5.4	24
Dry season ploughing	757	78	165	3.7	27
Ploughing + mulch	778	71	151	3.8	16
Ridge till	780	62	158	4.5	27
LSD (0.05)	23	12	NS	1.8	20

[#] No till + mulch = no till + crop residue mulch, No till + chisel = no till + crop residue mulch and chiseling in the row to about 50 cm depth once a year, Ploughing = Mouldboard ploughing and two harrowings, Disking = Disc ploughing and rotovation, No till – mulch = No till – crop residue, Dry season ploughing = Mouldboard ploughing in the dry season and two harrowings just before seeding, Ploughing + mulch = Mouldboard ploughing and two harrowings + mulch, Ridging = Moldboard ploughing and two harrowings with contour ridging

Table 5. Improvement of soil bulk density by tillage after fallowing a compacted/hardsetting soil in southwestern Nigeria in 1995 (Salako et al., 2001)

Fallow species	Tillage	
	Level tillage	Mound tillage
<i>P. phaseoloides</i>	1.44	1.22
<i>L. leucocephala</i>	1.39	1.15
Natural fallow	1.35	1.17
Continuous cropping	1.45	1.35
Effect	P < 0.0001	

Soils which were naturally hardened or which had been compacted by machinery will probably need to be tilled to restore their productivity (Tables 6 and 7). Furthermore, Table 7 shows that there is an enhancement of fertilizer usage by tillage.

Table 6. Effect of deep tillage on maize grain and *Stylosanthes hamata* yields in Kurmin Biri grazing reserve, sub-humid northern Nigeria (Adeoye and Mohammed-Saleem, 1990)

Tillage system	Tillage depth or height of ridge (cm)	Maize grain (t/ha)	Dry matter of 'Stylo' (t/ha)
Disc harrowing	10- 15	4.00	5.48
Disc harrowing + subsoiling	40	4.93	6.87
Disc harrowing + ridging	25-30	4.21	5.04
LSD ($P < 0.05$)		0.84	0.84

Table 7. Tillage effects on yield of intercropped maize and cassava in southwestern Nigeria (Salako and Tian, 2003)

7a. Maize yield as affected by tillage and fertilization after 2 years of cultivating a degraded Alfisol

Nitrogen level (kg ha ⁻¹)	Stover yield			Grain yield		
	Mound	Level	Mean	Mound	Level	Mean
0 N	2.11	0.68	1.39	0.75	0.2	0.49
30 N	1.33	0.91	1.12	0.83	0.63	0.73
60 N	3.01	2.12	2.57	1.60	1.11	1.36
Continuous cropping	0.62	0.09	1.69	0.24	0.06	0.15
Mean	1.77	0.95		0.86	0.51	
Treatment means	LSD	P		LSD	P	
N level	1.042	0.0127		0.625	0.0091	
Manual tillage	0.817	0.0065		0.348	0.0343	
Tillage x N level	1.199	0.0379		0.69	0.0358	

Table 7b. Effects of tillage and different levels of N on intercropped cassava yields (t·ha⁻¹) on the degraded Alfisol in southwestern Nigeria in 1995/1996 crop year

Nitrogen level (kg ha ⁻¹)	Cassava root yield		
	Mound	Level	Mean
0 N	19.9	15.7	17.8
30 N	17.1	15.2	16.2
60 N	19.8	16.3	18.1
Continuous cropping	13.7	9.0	11.4
Mean	17.6	14.1	
Treatment means	LSD	P	
N level	6.4	0.0002	
Manual tillage	3.55	0.0034	
Tillage x N level	4.54	0.0432	

Fallow management, physical properties and crop production

Soils with coarse texture are not often sensitive to some physical parameters while some physical parameters are more relevant in a given study than others. Sustainable crop production researches in the tropics have focused on the role of planted fallows and their spatial arrangement (e.g., as in alley cropping) for many decades.

In some studies carried out in Nigeria, physical properties measured were water content by gravimetric and volumetric methods, bulk density by core method, aggregate stability by wet-sieving and drop method, penetrometer resistance, water retention characteristics using tension table and pressure-plate apparatus. Water infiltration rates were measured using double-ring infiltrometer. These methods are discussed by various authors in Klute (1986) and Carter (1993). There have been advances in many these methods but experiences are limited by availability of equipment. One of such is the use of less cumbersome equipment such as tension infiltrometers to measure saturated and unsaturated flow in the field (Topp et al., 1992) and the improvements in penetrometers which make dynamic measurements with soil depth possible. These equipments are often equipped with dataloggers that facilitate data management.

The effects of fallow management systems on soil physical properties and intercropped maize (*Zea mays* L.) grain were studied in Ibadan, southwestern Nigeria between 1994 and 1995 (Table 8). The A-horizon of the Alfisol at the site had a coarse texture which was rapidly degraded by continuous cropping. Soil physical properties improved with decrease in cropping intensities but the trend shown by aggregate stability under impact of water drops was not as discernible as other characteristics when compared to crop yield. Also, soil water retention was generally similar. The effects of fallow were obscured by the coarse-textured surface soil, and might not be noticed at all if the topmost layer (0-5 cm) of soil was not sampled. Thus, it is often difficult to detect changes in soil physical properties in coarse textured soils.

Table 8. Effects of various cropping intensities on soil physical properties and maize yield in Ibadan, southwestern Nigeria.

Parameters	Cropping intensities (%)				LSD (0.05)
	25	33	50	100	
Bulk density (0-10 cm depth)(g·cm ⁻³)	1.18	1.21	1.25	1.31	0.05
Soil resistance within <i>Leucaena</i> hedgerow (kPa)	51	58	62	66	13
Soil resistance in <i>Leucaena</i> alley (kPa)	52	66	73	74	15
Number of water drops (0-5 cm depth)	108	117	109	86	22
Number of water drops (5-10 cm depth)	102	75	81	63	23
Grain yield in 1994 (t/ha)	3.11	-	-	1.19	0.36
Grain yield in 1995 (t/ha)	-	1.85	1.47	0.86	0.24

Experiences with advanced equipment

Disc permeameter: In-situ techniques of measuring soil hydraulic properties constitute one of the major advances in soil physics in the last three decades (Topp et al., 1992). Prior to the development of such techniques, unsaturated water flow had in particular been determined largely with models or inferred from other soil physical properties such as texture. However, the advent of tension infiltrometers or disk permeameters had made it possible to evaluate such flows directly on the field (White et al., 1992).

Water transmission characteristics under different fallow management systems shown in Figure 2 were measured with the CSIRO disc permeameter in southwestern Nigeria in 1996. The equipment can be used to generate data on cumulative infiltration, infiltration rate, sorptivity, steady-state flow rate, hydraulic conductivity, macroscopic capillary length and mean pore size (CSIRO, 1988). These parameters are calculated from infiltration theories, particularly those proposed by Philip (1957). Sorptivity, which is water uptake by the soil when there is no gravitational effect (Philip, 1957), is a good index of how these fallow management systems have influenced soil structure. It provides information on the soil's absorption rate and varies with initial water content and structural stability (Hamblin, 1985).

Using the CSIRO (1988) manual as guide, cumulative infiltration, infiltration rates and difference d between final (volumetric water content at measurement potential or θ_m) and initial soil water (θ_i) content ($\text{m}^3 \cdot \text{m}^{-3}$) were calculated from the data collected from fallow management plots at Ibadan southwestern Nigeria. Sorptivity s , steady-state flow rates, hydraulic conductivity K ($\text{cm} \cdot \text{h}^{-1}$), macroscopic capillary length λ_c (cm) and characteristic mean pore size λ_m (cm) were calculated.

Sorptivity s ($\text{cm} \cdot \text{h}^{-0.5}$) was obtained as the slope of the cumulative infiltration (cm) plotted against the square root of time ($t^{0.5}$ where t is in h). The steady state flow rate SF was found from the plot of cumulative infiltration as a function of time during the last part. The calculation of hydraulic conductivity at each water supply head was based on steady state flow rate and sorptivity:

$$K = SF - 4bs^2 \cdot (\pi r d)^{-1} \quad (1)$$

where r is the radius of the disc permeameter ring and $b = 0.55$ (shape factor).

Steady-state infiltration was actually assumed to occur during the last part of the saturated flow (at 10 mm water supply head) because flow was very rapid and water in the calibrated reservoir was usually exhausted in less than 6 minutes.

The macroscopic capillary length was calculated from

$$\lambda_c = bs^2 / dK \quad (2)$$

and the characteristic mean pore size λ_m was calculated from

$$\lambda_m = 7.4 / \lambda_c. \quad (3)$$

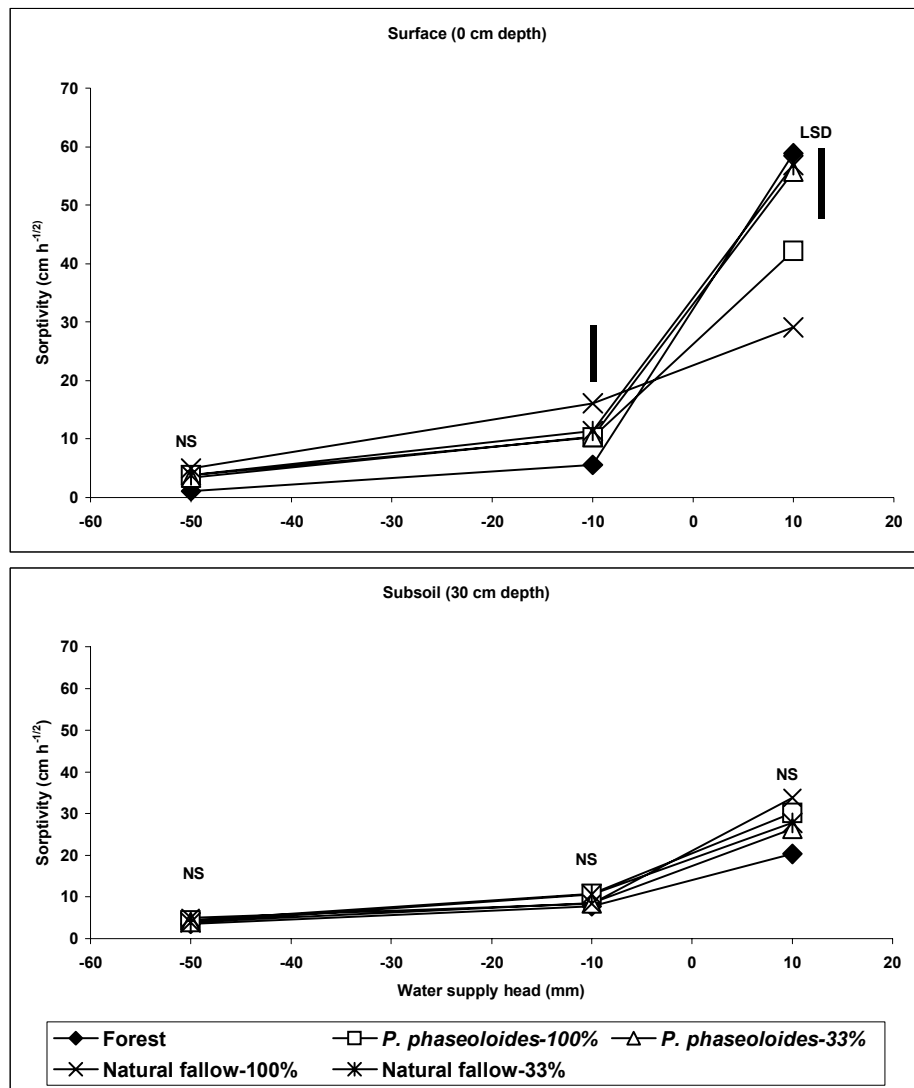


Figure 2. Water transmission characteristics under different fallow management systems measured with a disc permeameter in Ibadan, southwestern Nigeria

Although the sorptivity values appeared reasonable when compared with data obtained with the traditional double-ring infiltrometer for saturated flow, many negative values of hydraulic conductivity K were obtained. Positive values of K were obtained in all observations made on the soil surface (0 cm depth) at -10 mm water supply head. Also, the hydraulic conductivity for 0 cm depth at -50 mm water supply head was generally positive, and was left out because the observation implied the use of the shape factor. Thus, the negative values were usually under the following conditions: saturated water flow ($+10$ mm water supply head) irrespective of depth, and subsoil (30 cm soil depth) irrespective of water supply potential. Mean pore sizes could not be evaluated reasonably because of the various negative hydraulic conductivity values.

It was assumed that the observations of unrealistic negative values of hydraulic conductivity were due to soil heterogeneity and/or change in soil structure during measurements, i.e. collapse of macropores. Soil physical heterogeneity was accentuated at the site by the gravel interspersing soil particles. Thus, it appears the simplifying assumptions in calculating hydraulic parameters with the disc permeameter have to be modified for applicability in heterogeneous tropical soils.

Penetrometer: Penetrometers can be broadly classified as static or dynamic (Herrick and Jones, 2002). Most static penetrometers consist of a rigid, cone-tipped rod attached to a pressure-measuring device while dynamic penetrometers supply a known amount of kinetic energy to the penetrometer and are not subject to operators' variability. In the gravely soils of University of Agriculture, Abeokuta, Nigeria a cone penetrometer in the dynamic category called RIMIK CP20 penetrometer had been used to evaluate variability of soil strength with depth (Figure 3). This penetrometer uses an ultrasonic method for measuring depth (AGRIDRY RIMK PTY Ltd (1994). In Figure 3, changes in penetrometer resistance in the gravely coarse-textured soils with depth in the dry season were affected by gravel concentration. The measurements were taken in a field which had a vegetation biomass of 32 t/ha for trees and 18 t/ha for grasses and herbaceous plants. Field water content within 0-50 cm depth was less than 20 g/kg. A maximum value of 5000 kPa was not actually recorded but assumed for the impenetrable depths of some points which were penetrated at others. Overall, penetrometer could only reach a depth of 325 mm at some points although it was configured to read up to 500 mm depth. The value of 5000 kPa is the maximum possible measurement by the cone penetrometer. A reading of 3628 kPa was recorded at the 0-25 mm soil depth, indicating that the gravel in the soil can constitute impediment to root growth. Soil water content was very low as these measurements of penetrometer resistance were carried out in February. The soil strength data indicated that roots can easily be deformed at this site in the bid to grow in soil interspersing gravel, since they cannot penetrate gravel. It was also indicated that impediment to root growth can be encountered from the surface as it was possible to record penetrometer resistance existing 3600 kPa. Roots may meet lesser resistance in the wet season when most crops are grown but this expectation may be dashed due

to presence of the stones and gravel. Crop root growth may be drastically impeded at soil strength values exceeding 2500 kPa, depending on management practices.

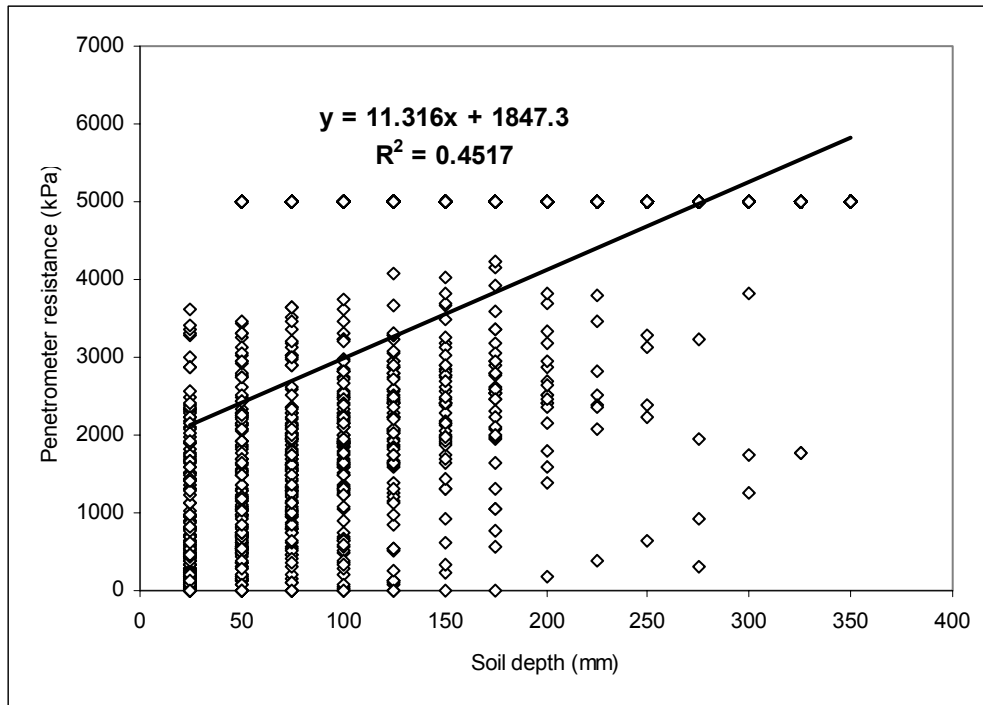


Figure 3. Penetrometer resistance (kPa) on a field under fallow at Abeokuta, southwestern Nigeria in February 2001. Gravel and stones constituted impediments to penetrometer as they would to plant roots even in topsoil (Salako F. K. unpublished).

Concluding remarks

Application of soil physics in the area of food production and environmental management still lags behind other sub-disciplines of soil science, particularly soil fertility in the tropics. A great challenge is posed by the vast area of upland soils which are made up of coarse-textured soils and in some cases gravel and stones. Aggregates of such soils are weak, they loose productivity fast and do not retain adequate water and nutrients for sustainable production. These characteristics imply that even with the best of soil fertility amendments, soil physical conditions must be managed to achieve sustainable crop production. Plant growth had to be encouraged in the soils, such that enough biomass is produced for food and soil management. Another area which requires attention in the tropics is with regard adaptability of equipment for accurate evaluation of soil physical properties. Most commercially available equipment in the field of soil physics needs to be modified to suit the tropical environment.

References

- Adeoye, K. B., and Mohamed-Saleem, M. A. 1990. Comparison of effects of tillage methods on soil physical properties and yield of maize and stylo in a degraded ferruginous tropical soil. *Soil & Tillage Research* 18: 63-72
- Brady, N.C. and Weil, R.R. 1999. The nature and properties of soil. 12th edition. Prentice Hall, New Jersey, USA. 881 pp.
- Carter, M. R. (editor) 1993. Soil sampling and methods of analysis. Canadian Society of Soil Science/Lewis Publishers, Boca Raton, Florida, USA.
- CSIRO, 1988. CSIRO disc permeameter instruction manual. CSIRO Center for Environmental Mathematics, Canberra, Australia.
- Hamblin AP 1985. The influence of soil structure on water movement, crop root growth, and water uptake. *Advances in Agronomy* 38, 95-157.
- Herrick, J. E. and Jones, T. L. 2002. A dynamic cone penetrometer for measuring soil penetration resistance. *Soil Science Society of America Journal* 66: 1320-1324.
- Igwe, C. A., Akamigbo, F. O. R. and Mbagwu, J. S. C. 1995. Physical properties of soils of southeastern Nigeria and the role of some aggregating agents in their stability. *Soil Science* 160: 431-440.
- Jagtap, S. S. 1995. Environmental characterization of the moist lowland savanna of Africa. In: Kang, B. T., Akobundu, I. O., Manyong, V. M., Carsky, R. J., Sanginga, N. and Kueneman, E. A. (editors), *Moist savannas of Africa: Potentials and constraints for crop production. Proceedings of an IITA/FAO Workshop held from 19-23 September 1994, Cotonou, Republic of Benin*, pp. 13-30.
- Karlen, D. L., Andrews, S. S. and Doran J. W. 2001. Soil quality: Current concepts and applications. *Advances in Agronomy* 74: 1-40.
- Klute, A. (editor). 1986. Methods of soil analysis. Part 1. Physical and mineralogical methods. 2nd edition. American Society of Agronomy-Soil Science Society of America, Madison, Wisconsin, USA.
- Kirchhof, G. and Salako, F. K. 2000. Residual tillage and bush-fallow effects on soil properties and maize intercropped with legumes on a tropical Alfisol. *Soil Use and Management*. 16: 183-188.
- Lal, R. 1997a Long-term tillage and maize monoculture effects on a tropical Alfisol in western Nigeria. I. Crop yield and soil physical properties. *Soil & Tillage* 42: 145-160.
- Lal, R. 1997b. Soil degradative effects of slope length and tillage methods on Alfisols in western Nigeria. 3. Soil Physical properties. *Land Degradation and Development* 8: 325-342.
- Lal, R. 2001. Managing world soils for food security and environmental quality. *Advances in Agronomy* 74: 155-192.
- Oikeh, S. O., Chude, V. O., Carsky, R. J., Weber, G. K. and Horst, W. J. 1998. Legume rotation in the moist tropical savanna: Managing soil nitrogen dynamics and cereal yields in farmers' fields. *Experimental Agriculture* 34: 73-83.

- Philip JR 1957. The theory of infiltration: Sorptivity and algebraic equations. *Soil Science* 84, 257-264.
- Salako, F. K., Babalola, O., Hauser, S. and Kang, B. T. 1999. Soil macroaggregate stability under different fallow systems and cropping intensities in southwestern Nigeria. *Geoderma* 91: 103-123.
- Salako, F. K., Hauser, S., Babalola, O. and Tian, G. 2001. Improvement of the physical fertility of a degraded Alfisol with planted and natural fallows under humid tropical conditions. *Soil Use and Management* 17: 41-47.
- Salako, F. K., Tian, G. and Kang, B. T. 2002. Indices of root and canopy growth of leguminous cover crops in the savanna zone of Nigeria. *Tropical Grasslands* 36: 33-46.
- Salako, F. K. and Tian, G. 2003. Management of a degraded Alfisol for crop production in southwestern Nigeria: Effects of fallow, mounding and nitrogen. *Journal of Sustainable Agriculture* (In press).
- Topp, G. C., Reynolds, W. D. and Green, R. E. (editors) 1992. Advances in measurement of soil physical properties: Bringing theory into practice. Proceedings of a symposium sponsored by Division S-1 of the Soil Science Society of America in San Antonio, Texas 21-26 Oct 1990. Soil Science Society of America Publication 30.
- White, I., Sully, M. J. and Perroux, K. M. 1992. Measurement of surface-soil hydraulic properties: Disk permeameters, tension infiltrometers, and other techniques. In: Topp, G. C., Reynolds, W. D. and Green, R. E. (editors) 1992. Advances in measurement of soil physical properties: Bringing theory into practice. Proceedings of a symposium sponsored by Division S-1 of the Soil Science Society of America in San Antonio, Texas 21-26 Oct 1990. Soil Science Society of America Publication 30. pp. 69-103.

Boundary Layer Theory for Solute Transport in Soils

Mingan Shao¹

*Ministry of Water Resources,
Yangling, People's Republic of China*

*Lecture given at the
College on Soil Physics
Trieste, 3-21 March 2003*

LNS0418032

¹ mashao@ms.iswc.ac.cn

This presentation is available in the following publication:

Shao, Mingan, R. Horton and R.K. Miller. 1998. Approximate solution to the convection-dispersion equation of solute transport in soil. *Soil Sci.* 163: 339-345.

General Similarity Theory and Integral Method for Water Flow in Soils

Mingan Shao¹

*Ministry of Water Resources
Yangling, People's Republic of China*

Lecture given at the
College on Soil Physics
Trieste, 3-21 March 2003

LNS0418033

¹ mashao@ms.iswc.ac.cn

This presentation is available in the following publications:

- Shao, Mingan, and R. Horton. 1996. Soil water diffusivity determination by general similarity theory. *Soil Sci.* 161: 727-734.
- Shao, Mingan, and R. Horton. 1998. Integral method for estimating soil hydraulic properties. *Soil Sci. Soc. Am. J.* 62: 585-592.
- Shao, Mingan, and R. Horton. 2000. Exact solution for horizontal water redistribution by general similarity. *Soil Sci. Soc. Am. J.* 64: 561-564.

State-Space Approach for Evaluating the Soil-Plant-Atmosphere System

L.C. Timm^{1,*}, K. Reichardt¹, J.C.M. Oliveira², F.A.M. Cassaro¹,
T.T. Tominaga¹, O.O.S. Bacchi¹ and D. Dourado-Neto³

¹*Soil Physics Laboratory, CENA/USP, Piracicaba, SP, Brazil*

²*Municipal University of Piracicaba, EEP, Piracicaba, SP, Brazil*

³*Crop Production Department, ESALQ/USP, Piracicaba, SP, Brazil*

*Lectures given at the
College on Soil Physics
Trieste, 3-21 March 2003*

LNS0418034

* lctimm@carpa.ciagri.usp.br

Abstract

Using as examples one sugarcane and one forage oat experiment, both carried out in the State of Sao Paulo, Brazil, this chapter presents recent state-space approaches used to evaluate the relation between soil and plant properties. A contrast is made between classical statistics methodologies that do not take into account the sampling position coordinates, and the more recently used methodologies which include the position coordinates, and allow a better interpretation of the field-sampled data. Classical concepts are first introduced, followed by spatially referenced methodologies like the autocorrelation function, the crosscorrelation function, and the state-space approach. Two variations of the state-space approach are given: one emphasizes the evolution of the state system while the other based on the bayesian formulation emphasizes the evolution of the estimated observations. It is concluded that these state-space analyses using dynamic regression models improve data analyses and are therefore recommended for analyzing time and space data series related to the performance of a given soil-plant-atmosphere system.

Introduction

There is a great class of physical, chemical and biological phenomena that, when observed and numerically quantified, result in a sequence of data distributed along time and/or space. Time data sequences are called time series. Examples are: a) monthly average values of air temperature at a given location, b) yearly average values of rainfall for a given location, c) yearly sugarcane yield data for a given field and d) yearly soil organic matter contents for a given site. Similarly, space data sequences are called space series. Examples are: a) soil temperature values collected across a landscape at the same time, b) soil water content values collected across a corn field on the same day, c) sugarcane yield values measured across a field during a single harvest and d) soil pH values collected across a pasture in a given year.

Because these kinds of series were first analyzed in terms of a time series, we introduce the subject through sequences of data collected along time t at a given location. For a space series of data x observed at a given time, the concepts introduced here are also valid if x is substituted for t .

A discrete time or temporal series can be considered as a set of observations Y described by

$$Y(t_i) \quad i = 1, 2, 3, \dots, n \quad (1)$$

evaluated at equidistant times t

$$t_i - t_{i-1} = \alpha \quad (2)$$

and manifest a serial dependence among themselves. Series collected continuously during a given time interval have to be transformed into a discrete series through a “sampling” procedure at equidistant time intervals. The interval α between observations is, in general, chosen by the scientist, however in several situations, it is defined by the available data set. For a given time interval, the smaller α the greater the number of observations n , allowing for a more detailed analysis of the phenomenon. According to Tukey (1980), the basic objectives for analyzing a time series are: a) modeling of the process under consideration, b) obtaining conclusions in statistical terms and c) evaluation of model’s ability in terms of forecast.

When planning an investigation involving statistical methodologies, special care must be taken with sampling procedures and data preparation. Depending on the objectives of the investigation, several potential problems regarding the measurements should be avoided, or at least minimized. Among them are the stationarity of the set, transformations of data, lost or “irregular” observations, outliers and short amplitudes.

The models used to describe temporal series are stochastic processes controlled by probabilistic laws. The choice of these models depends on several factors such as the behavior of the phenomenon or the “a priori” knowledge we have about its nature, and the objective of the analysis. From a practical point of view, the

choice also depends on the existence of good estimation methods and on the availability of adequate software.

A temporal (spatial) series can be analyzed in two ways: 1) in the time (space) domain and 2) in the frequency domain. In both cases we wish to construct models for the series based on known concepts. For the time (space) domain models, the analysis should identify the stationary components (aleatory or purely random variables) and the nonstationary components that define the mean function of the process. In the time (space) domain the models are parametric with a finite number of parameters. Among the parametric models we find are, for example, autoregressive models AR, moving average models MA, autoregressive moving average models ARMA, autoregressive integrated moving average models ARIMA and state-space models. For the frequency domain, the models are non-parametric, and the procedures involve the decomposition of the series into frequency components with the existence of a spectrum being a fundamental characteristic. Among these models in which periodic phenomena of the data are analyzed, spectral and cospectral analyses have several applications in the soil-plant-atmosphere system.

When interested in the analysis of a series in the time (or space) domain, one of the most frequent assumptions is that the series is stationary, which means that the series develops in an aleatory or purely random way along time (or space) with their statistical properties (mean and variance) being constant reflecting some sort of a stable equilibrium. Most of the series we come across in practice, however, manifest some sort of non-stationarity. Hence, whenever a statistical procedure relies on the assumption of stationarity, it is usually necessary to transform the original data in order to satisfy the stationarity assumption.

With the simple definition of time series given above, "Time Series Analysis" becomes a well-defined area within statistics, since data that are independent and identically distributed are clearly discarded, but that are commonly used in classical statistics models. Hence, classical statistics and the statistical analysis of data that present serial dependence complement each other, one not excluding the other, and questions answered by one cannot be necessarily answered by the other.

Until recently, research in agronomic relied on classical statistics (analysis of variance, mean, coefficient of variation, regression analysis, etc), which presupposes the independence of observations among themselves and ignores the sampling locations in the field. Commonly, agronomic experiments are carried out ignoring the fact that observations might be spatially or temporally dependent. More recently it has been emphasized that adjacent observations of a given variable are not necessarily independent, and that the variability has to be taken into consideration in their statistical analysis. Nielsen & Alemi (1989) comment that observations within and among treatments might not, in fact, be independent among themselves, rendering the experimental design inadequate.

Soil spatial variability occurs at different scales and is related to variations of the parent material, climate, relief, organisms and time, i.e., related to the processes of soil formation and/or effects of management practices adopted for each agricultural use (McGraw, 1994). Statistical tools like autocorrelograms, crosscorrelograms,

semivariograms, spectral analysis, kriging, co-kriging, autoregressive models, ARIMA models, state-space models, etc, are now frequently used to study the spatial variability of soil attributes, and can potentially lead to management practices that allow a better understanding of the interactive processes within the soil-plant-atmosphere system (Vieira et al., 1981; Vauclin et al., 1982; Nielsen et al., 1983; Morkoc et al., 1985; Shumway, 1988; Nielsen & Alemi, 1989; Wendroth et al., 1992; Katul et al., 1993; Wendroth et al., 1997; Hui et al., 1998; Dourado-Neto et al., 1999; Nielsen et al., 1999; Timm et al., 2000; Wendroth et al., 2001; Timm et al., 2001). This chapter intends to introduce them to the reader, presenting recent examples of application.

The concern about the spatial variability of soil properties is expressed in several reports related to agronomy. Until recently, the most detailed studies of this variability indicated limitations of the classical methods of Fisher's statistics. In general, normality and independence of observations are not tested, even knowing that the independence must be assumed a priori, i.e., before sampling. All variability is assumed to be residual, being due to uncontrolled factors. Recently applied statistical tools now take into consideration the structure of the spatial dependence of the observations. This approach has lead to an improvement in the understanding of physical, chemical and biological processes that control the soil-plant-atmosphere system and, therefore, to the adoption of better management practices with less environmental impact. Having this in mind, we now present and illustrate the basic principles of concepts and tools most commonly used to analyze and characterize the spatial variability of agronomic data sets.

Autocorrelation Function ACF

After sampling a variable Y , its mean and variance are calculated to reflect the sampled population, assuming that the set is representative and obtained randomly. In many cases the observations are not independent of each other, and it is possible to calculate an autocorrelation coefficient, which plotted as a function of the distance between observations will indicate their level of auto-dependence. For stationary processes (those in which the static properties are independent of space or time), the covariance between observations is a function of the number of lags h between their sampling points. Time series are collected along time at intervals of α (equation 2) minutes, hours, months, etc, and space series along transects (or grids) at spacings of α ($x_i - x_{i-1} = \alpha$), in cm, m, km, etc. The covariance between such variables given by Salas et al. (1988) is

$$C(h) = \frac{1}{n-h} \sum_{i=1}^{n-h} [Y(x_{i+h}) - \bar{Y}][Y(x_i) - \bar{Y}] \quad (3)$$

If $C(h)$ is normalized dividing it by the variance s^2 of the population, we obtain the coefficient $r(h)$ of the autocorrelation function

$$r(h) = \frac{C(h)}{s^2} \quad (4)$$

which manifests values between +1 and -1. It is important to note that for the calculation of $r(h)$, the observations Y have to be collected at regularly spaced intervals. The values of $r(h)$ for $h = 0$, which represents the correlation between $Y(x_i)$ and $Y(x_i)$ is obviously equal to 1. For the first neighbor pairs $Y(x_i)$ and $Y(x_{i+1})$ for a distance of one lag α ($h = 1$), a value of $r(1)$ can be obtained using equations (3) and (4). The same procedure is used for second neighbor pairs [$Y(x_i)$ and $Y(x_{i+2})$], and further neighbors ($h = 3, 4, \dots$) obtaining a $r(h)$ value for each h . Plotting r as a function of h we obtain the autocorrelogram of the variable Y .

The next step is the calculation of the fiducial intervals of r , to recognize if they are significant or not, and in this way define the length interval αh in which the spatial dependence of the variable is significant. One way to measure the autocorrelation confidence interval CI is using the accumulated probability function (e.g., ± 1.96 for a 95% probability level) for the normalized distribution function (Davis, 1986), and the number of observations ($n-h$). Therefore,

$$CI = \pm \frac{p}{\sqrt{n-h}} \quad (5)$$

Crosscorrelation function CCF

Having two sets of variables $Y(x_i)$ and $W(x_i)$ observed at the same locations x_i (or same times t_i), their spatial crosscorrelation structure can be analyzed calculating coefficients of crosscorrelation. Although each variable has its own autocorrelogram, an analysis of their crosscorrelation indicates to which distance (or time interval) one is related to the other. The coefficient r_c of the crosscorrelation function will be also a function of h , and describes the degree of linear association between both variables (Davis, 1986; Shumway, 1988; Wendroth et al., 1997).

The coefficients of the crosscorrelation function $r_c(h)$, between the variables Y and W , separated by distances αh , or by a lag number h , are calculated with

$$r_c(h) = \frac{\text{cov}_{YW}(h)}{s_Y \times s_W} \quad (6)$$

where

$$\text{cov}_{YW}(h) = \frac{1}{n-h} \sum_{i=1}^{n-h} [Y(x_{i+h} - \bar{Y})][W(x_i - \bar{W})] \quad (7)$$

and s_Y^2 is the variance

$$s_Y^2 = \frac{1}{n} \sum_{i=1}^n [Y(x_{i+h}) - \bar{Y}]^2 \quad (8)$$

and s_W^2 is the variance

$$s_W^2 = \frac{1}{n} \sum_{i=1}^n [W(x_{i+h}) - \bar{W}]^2 \quad (9)$$

A plot of r_c as a function of h represents the crosscorrelogram. For $h = 0$ (observations taken at the same position x_i), the value $r_c(0)$ given by equation (6) is the linear regression coefficient obtained through classical statistics. For the first neighbor pairs $[Y(x_i), W(x_{i+1})]$ collected at a distance α in one direction ($h = 1$), we obtain the coefficient $r_c(1)$, and for the other direction ($h = -1$) the coefficient $r_c(-1)$. This is because in the case of two variables, each of them has different neighbors for each direction, i.e., we have two pairs – (Y_i, W_{i+1}) and (Y_i, W_{i-1}) . The same procedure is used for more distant neighbors, obtaining values of $r_c(h)$ and $r_c(-h)$. A crosscorrelogram indicates how far two different observations are spatially related (Wendroth et al., 1997).

According to Nielsen & Wendroth (2003), it is more difficult to estimate the significance of $r_c(h)$ as compared to $r(h)$. Significance tests like the t test are usually based on the assumption that the observed values of $Y(x_i)$ and $W(x_i)$ are normally distributed and independent among themselves. Taking this into consideration, the significance level of r_c is, in general, given by

$$t = \sqrt{\frac{(n-h)-2}{1-r_c^2}} \quad (10)$$

where $(n-h)$ is the number of pairs used for the calculation of r_c . The level of significance of the test is obtained by comparing the value of t in equation (10) with critical values of t for $(n-2)$ degrees of freedom. The crosscorrelation function is, in general, not symmetric, i.e., $r_c(h) \neq r_c(-h)$. Note that in the case of the autocorrelation there is symmetry, $r(h) = r(-h)$. According to Nielsen & Wendroth (2003), when there is a physical relation between Y and W , the crosscorrelogram will tend to symmetry.

The State-Space Approach

The state-space model of a stochastic process involving j data sets $Y_j(x_i)$, all collected at the same locations is based on the property of Markovian systems that establish the independence of the future of the process in relation to its past, once given the present state. In these systems, the state of the process condenses all information of the past needed to forecast the future.

The state-space model is a combination of two systems of equations. The first is the observation equation

$$\mathbf{Y}_j(\mathbf{x}_i) = \mathbf{M}_{jj}(\mathbf{x}_i) \mathbf{Z}_j(\mathbf{x}_i) + \mathbf{v}_{Y_j}(\mathbf{x}_i) \quad (11)$$

where observation vector $\mathbf{Y}_j(\mathbf{x}_i)$ of the process is generated as a function of the state vector $\mathbf{Z}_j(\mathbf{x}_i)$. The second is the state equation

$$\mathbf{Z}_j(\mathbf{x}_i) = \phi_{jj} \mathbf{Z}_j(\mathbf{x}_{i-1}) + \mathbf{u}_{Z_j}(\mathbf{x}_i) \quad (12)$$

where the non observed state vector $\mathbf{Z}_j(\mathbf{x}_i)$ is dynamically evolved.

The matrix \mathbf{M}_{jj} in equation (11) comes from the following set of linear observation equations

$$\begin{aligned} Y_1(x_i) &= m_{11}Z_1(x_i) + m_{12}Z_2(x_i) + \dots + m_{1j}Z_j(x_i) + v_{Y_1}(x_i) \\ Y_2(x_i) &= m_{21}Z_1(x_i) + m_{22}Z_2(x_i) + \dots + m_{2j}Z_j(x_i) + v_{Y_2}(x_i) \\ &\vdots \quad \quad \quad \vdots \quad \quad \quad \vdots \quad \quad \quad \vdots \quad \quad \quad \vdots \\ Y_j(x_i) &= m_{j1}Z_1(x_i) + m_{j2}Z_2(x_i) + \dots + m_{jj}Z_j(x_i) + v_{Y_j}(x_i) \end{aligned}$$

which can be written in the matrix form

$$\begin{bmatrix} Y_1(x_i) \\ Y_2(x_i) \\ \vdots \\ Y_j(x_i) \end{bmatrix} = \begin{bmatrix} m_{11} & m_{12} & \dots & m_{1j} \\ m_{21} & m_{22} & \dots & m_{2j} \\ \vdots & \vdots & & \vdots \\ m_{j1} & m_{j2} & \dots & m_{jj} \end{bmatrix} \times \begin{bmatrix} Z_1(x_i) \\ Z_2(x_i) \\ \vdots \\ Z_j(x_i) \end{bmatrix} + \begin{bmatrix} v_{Y_1}(x_i) \\ v_{Y_2}(x_i) \\ \vdots \\ v_{Y_j}(x_i) \end{bmatrix}$$

The matrix ϕ_{jj} in equation (12) comes from the following set of state equations

$$\begin{aligned} Z_1(x_i) &= \phi_{11}Z_1(x_{i-1}) + \phi_{12}Z_2(x_{i-1}) + \dots + \phi_{1j}Z_j(x_{i-1}) + u_{Z_1}(x_i) \\ Z_2(x_i) &= \phi_{21}Z_1(x_{i-1}) + \phi_{22}Z_2(x_{i-1}) + \dots + \phi_{2j}Z_j(x_{i-1}) + u_{Z_2}(x_i) \\ &\vdots \quad \quad \quad \vdots \quad \quad \quad \vdots \quad \quad \quad \vdots \quad \quad \quad \vdots \\ Z_j(x_i) &= \phi_{j1}Z_1(x_{i-1}) + \phi_{j2}Z_2(x_{i-1}) + \dots + \phi_{jj}Z_j(x_{i-1}) + u_{Z_j}(x_i) \end{aligned}$$

or in the matrix form:

$$\begin{bmatrix} Z_1(x_i) \\ Z_2(x_i) \\ \vdots \\ Z_j(x_i) \end{bmatrix} = \begin{bmatrix} \phi_{11} & \phi_{12} & \dots & \phi_{1j} \\ \phi_{21} & \phi_{22} & \dots & \phi_{2j} \\ \vdots & \vdots & & \vdots \\ \phi_{j1} & \phi_{j2} & \dots & \phi_{jj} \end{bmatrix} \times \begin{bmatrix} Z_1(x_{i-1}) \\ Z_2(x_{i-1}) \\ \vdots \\ Z_j(x_{i-1}) \end{bmatrix} + \begin{bmatrix} u_{Z_1}(x_i) \\ u_{Z_2}(x_i) \\ \vdots \\ u_{Z_j}(x_i) \end{bmatrix}$$

The observation vector $\mathbf{Y}_j(\mathbf{x}_i)$ is related to the state vector $\mathbf{Z}_j(\mathbf{x}_i)$ through the observation matrix $\mathbf{M}_{jj}(\mathbf{x}_i)$ and by the observation error $\mathbf{v}_{Yj}(\mathbf{x}_i)$ (equation 11). On the other hand, the state vector $\mathbf{Z}_j(\mathbf{x}_i)$ at position i is related to the same vector at position $i-1$ through the state coefficient matrix $\phi_{jj}(\mathbf{x}_i)$ (transition matrix) and an error associated to the state $\mathbf{u}_{Zj}(\mathbf{x}_i)$ with the structure of a first order autoregressive model. It is assumed that $\mathbf{v}_j(x_i)$ and $\mathbf{u}_j(x_i)$ are normally distributed and independent as well as being non correlated among themselves for both lags.

The above equations contain distinct perturbations or noises, one associated with observations $\mathbf{v}_{Yj}(x_i)$ and the other with state $\mathbf{u}_{Zj}(x_i)$. According to Gelb (1974), the development of methods to process noise-contaminated observations can be credited to the work carried out by Gauss and Legendre (around 1800) who both independently developed the method of the minimum squares for the linear models. More recently, Plackett (1950) developed a recursive solution for the minimum square method in linear models. Kalman (1960) using a state-space formulation, developed a very good recursive filter for estimations in stochastic, dynamic linear systems, being well known today as the Kalman Filter KF. According to Gelb (1974), a good estimator is a computational algorithm that processes observations in order to find a minimum estimate (following some sort of optimization criterion) of the state error of a system, using: a) the knowledge of the dynamics of the observations and of the system, b) assuming statistical inferences for the noises associated to observations and to states and c) knowledge of the initial condition of the information. In summary, given a dynamic system of equations that describes the behavior of the vectors of state and of observations, the statistic models that characterize the observational and state errors, and an initial condition of the information, the KF performs the sequential actualization of the state vector at time (or space) $i-1$ to time (or space) i . It can therefore be said, that the KF is essentially a recursive solution that permits a sequential processing of the observations, within the original method of the minimum squares of Gauss. It should be noted however, that another algorithm has to be used [for example, the algorithm of maximum likelihood (EM) thoroughly discussed in Shumway & Stoffer (2000)] so that, together with the KF, the problem of noise-contaminated observations can be solved (Gelb, 1974).

Depending on the objectives of a study involving the state-space methodology, one can have three different types of estimates: a) when the time (or space) at which an estimate is wished coincides with the last observed value, the problem is said to be one of filtering; b) when the time (or space) of interest is inside the set of observations, i.e., the complete set of data is used to estimate the point of

interest, the problem is said to be one of smoothing; and c) when the time (or space) of interest is after the last observation, the problem is said to be one of forecasting.

From this it can be seen that any linear or non-linear model (Katul et al., 1993) can be represented in the state-space formulation, i.e., by a system of two equations: one for the observations vector and another for the evolution of the state vector.

The state-space approach can also be used like the kriging and co-kriging (Alemi et al., 1988; Deutsch & Journel, 1992) to interpolate data spatially (or temporally). However, the philosophy behind these tools is different. For kriging and co-kriging the condition of stationarity of the data is required, which is not the case in state-space (Shumway, 1985).

The linear system of dynamic equations (11 and 12) has been presented here in a generalized form of the state-space approach. Now we shall present two different ways of using this approach, the first presented by Shumway (1988) which has been used by several researchers in agronomy, giving emphasis to the equation of the evolution of the state of the system (equation 12); and the second, introduced by West & Harrison (1989, 1997) which is still not so frequently used in agronomy, giving greater emphasis to the observation equation (11). The presentation of these two different procedures will be made using space data series, one using data from a sugarcane field experiment established in Piracicaba, and the other using data from an oat field experiment established in São Carlos, both in SP, Brazil.

Shumway's State-Space Approach

This approach, presented by Shumway (1988) and more recently by Shumway & Stoffer (2000), gives more attention to the equation of the evolution of the state of the system, where the matrix of the transition coefficients ϕ in equation (12) is a matrix of dimension $j \times j$ that indicates the spatial measure of the linear association among the variables of interest. These coefficients are optimized through a recursive procedure, using an algorithm of the KF type (Shumway & Stoffer, 1982) in which the method of maximum likelihood is used together with the mean maximization algorithm of Dempster et al. (1977). In this case, equations (11 and 12) are solved assuming initial values for the mean and the variance of each variable in the covariance matrix \mathbf{R} of the noise of the observations, for the covariance matrix \mathbf{Q} of the noise associated with the state vector, for the matrix ϕ of the transition coefficients, and for the observation matrix \mathbf{M} . Because Shumway (1988) considers the matrix \mathbf{M} as being a unit matrix (identity), equation (11) becomes

$$\mathbf{Y}_j(\mathbf{x}_i) = \mathbf{Z}_j(\mathbf{x}_i) + \mathbf{v}_{Y_j}(\mathbf{x}_i) \quad (11a)$$

During the development of the software ASTSA (Applied Statistical Time Series Analysis) which is used for the analysis of time (space) series, the unit matrix \mathbf{M} is fixed during all steps of variable estimation. This shows the greater emphasis of

this approach in being referenced to the equation of state evolution, and not to the observation equation. More specific details can be found in Shumway (1988) and Shumway & Stoffer (2000).

We now illustrate the application of equations (11a and 12) on data collected in the above-mentioned sugarcane field.

Sugarcane is a semi-perennial crop, once planted being harvested for canes to extract sugar after every year, up to 5-7 years. After harvest, crops grown from sprouted rhizomes are called ratoons. The crop was planted on a 15 x 100m area, with a spacing of 1.4m between rows, using a randomized block design with four treatments and four replicates each. All treatments with borders were disposed along crop lines, so that a transect of 84 sampling points could be obtained to measure several variables of interest. Figure 1 shows schematically this experimental design.

Treatment T_1 corresponds to a mulched crop (trash residues from previous harvest) that received ^{15}N -labeled ammonium sulfate at planting, receiving in the following year non-labeled mulch from T_2 . The treatment T_2 is similar to T_1 but received non-labeled ammonium sulfate and labeled mulch from T_1 . T_3 corresponds to a bare inter-row treatment and T_4 received the same labeled fertilizer but its straw is burned before each harvest. These treatments are based on a recent trend of changing sugarcane management practices in Brazil, substituting the traditional trash burning by mulching.

Soil Water Content and Soil Temperature

This example has as an objective illustrating the use of the state-space methodology to better understand the behavior of soil temperature and water content in relation to the sugarcane experiment described above. Soil water content data from the 0-0.15m soil surface layer were collected along the 84 point transect with a surface gamma/neutron probe. Simultaneously, soil temperature data were collected with digital thermometers at depths 0.03, 0.06 and 0.09m, the average of all three depths being used here to represent the same soil layer. The analysis was performed using the software ASTSA (Shumway, 1988).

From equation (12) it can be seen that the transition coefficients ϕ relate the variable Z_j at position i to its value at position $i-1$. When data are normalized using

$$z_j(x_i) = \frac{Z_j(x_i) - (\bar{Z}_j - 2s)}{4s} \quad (13)$$

before the application of the state-space methodology, the magnitude of the coefficients ϕ become directly proportional to the contribution of each variable in the estimation of $Z_j(x_i)$. Original values of $Z_j(x_i)$ for soil water content SWC and soil temperature T used in this example are shown in Figure 2. Both variables manifest large variations along the transect, clearly showing treatment effects. Analyzing Figures 1 and 2 in conjunction, one can clearly recognize the effects of mulching (T_1

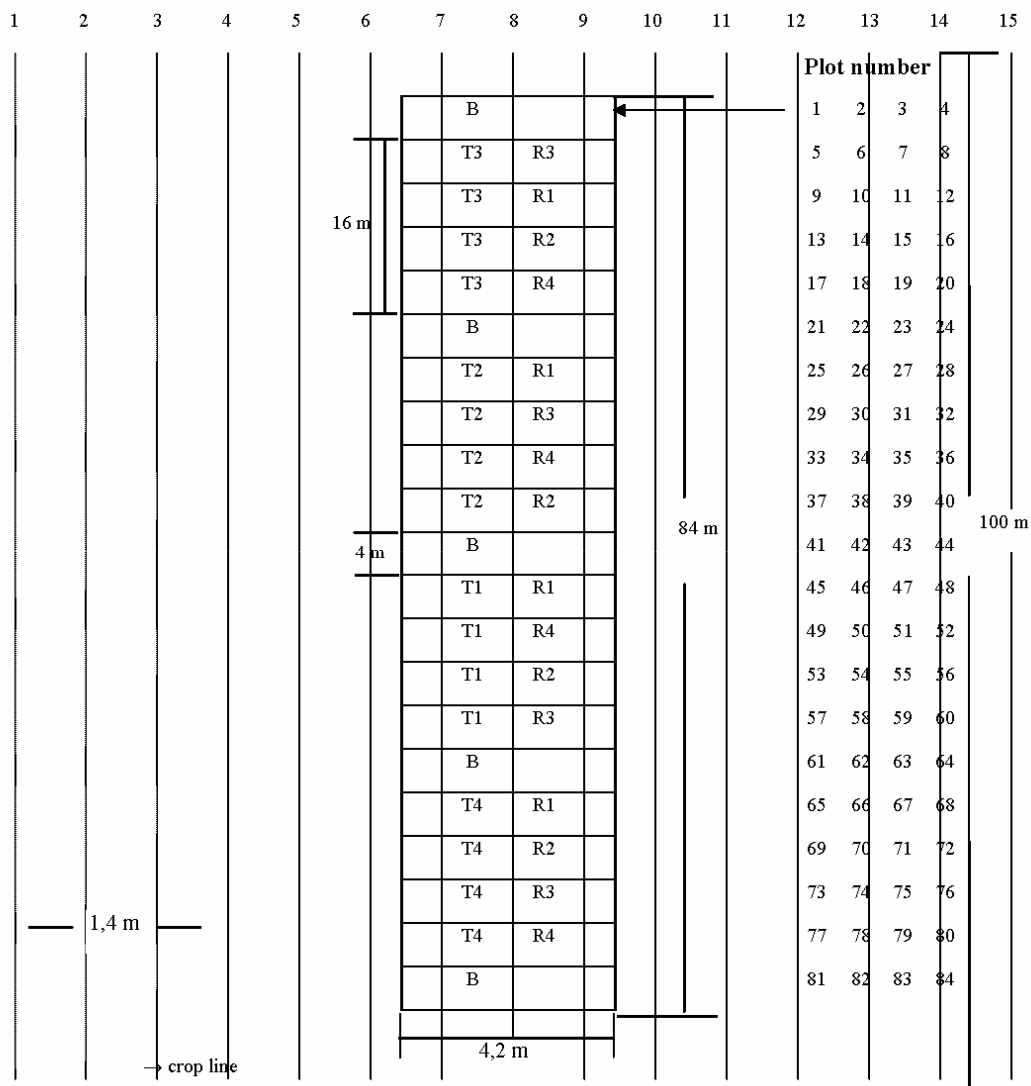


Figure 1. Schematic experimental design of the sugarcane crop, showing the 15 cane lines, 100 m long, indicating the 3 central lines (7, 8 and 9) used to measure physical and chemical soil properties. B = border; T = treatment; R = replicate.

and T_2) with higher soil water contents and lower soil temperatures. This distinct variation is due to the fact that the measurements were made shortly after harvest (November 20, 1998), a late spring day of the southern hemisphere when ratoon sprouts were very small, not covering much of the soil surface. The linear regression shown in Figure 3 ($R^2 = 0.4493$) demonstrates that soil water content is inversely related to soil temperature. Their crosscorrelogram given in Figure 4 indicates a significant (5%) spatial dependence up to 6-8 lags.

The results of the state-space approach applied on $z_j(x_i)$ data (scaled by equation 13) of soil water content and temperature are shown in Figures 5 and 6, respectively. For this particular example, equation (12) becomes

$$(SWC)_i = 0.8810 (SWC)_{i-1} + 0.1148 T_{i-1} + u_{(SWC)i} \quad (12a)$$

and

$$T_i = 0.0615 (SWC)_{i-1} + 0.9272 T_{i-1} + u_{Ti} \quad (12b)$$

or in the matrix form

$$\begin{pmatrix} (SWC)_i \\ T_i \end{pmatrix} = \begin{pmatrix} 0.8810 & 0.1148 \\ 0.0615 & 0.9272 \end{pmatrix} \times \begin{pmatrix} (SWC)_{i-1} \\ T_{i-1} \end{pmatrix} + \begin{pmatrix} u_{(SWC)i} \\ u_{Ti} \end{pmatrix} \quad (12c)$$

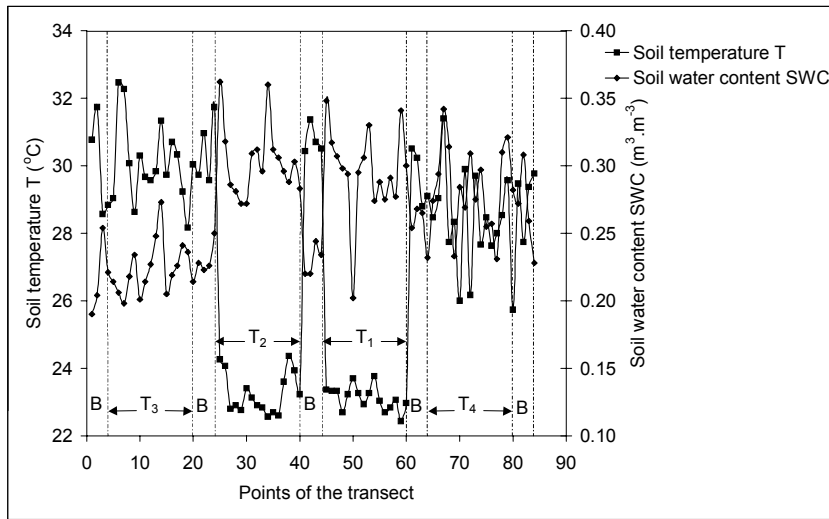


Figure 2. Soil temperature and soil water content distributions, meter by meter, along the 84 point transect, at noon (11:00 – 12:00) on Nov. 20, 1998. B= border; T₁ and T₂= trash mulching; T₃= bare soil; T₄= burned trash.

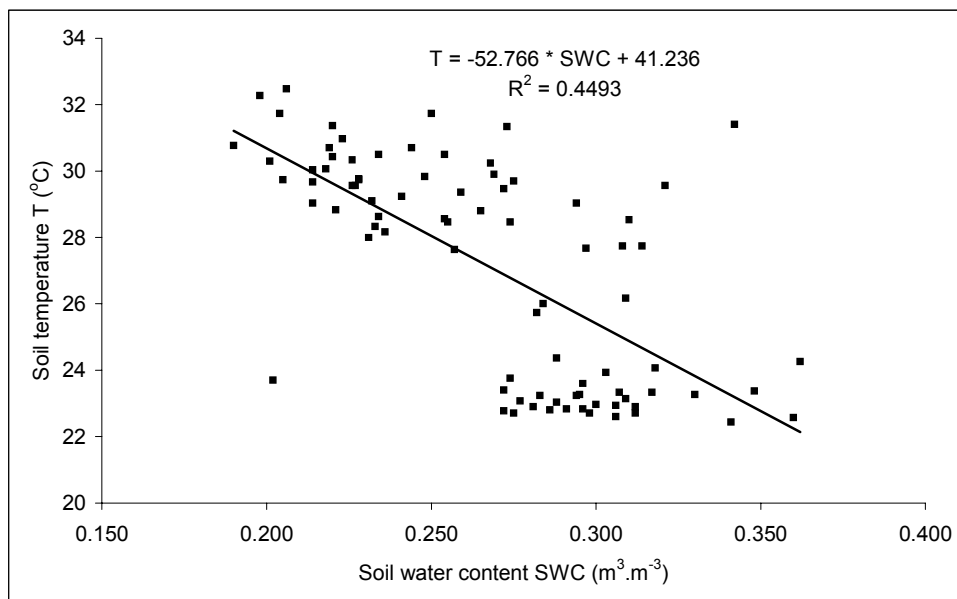


Figure 3. Correlation between soil temperature and soil water content data of Figure 2.

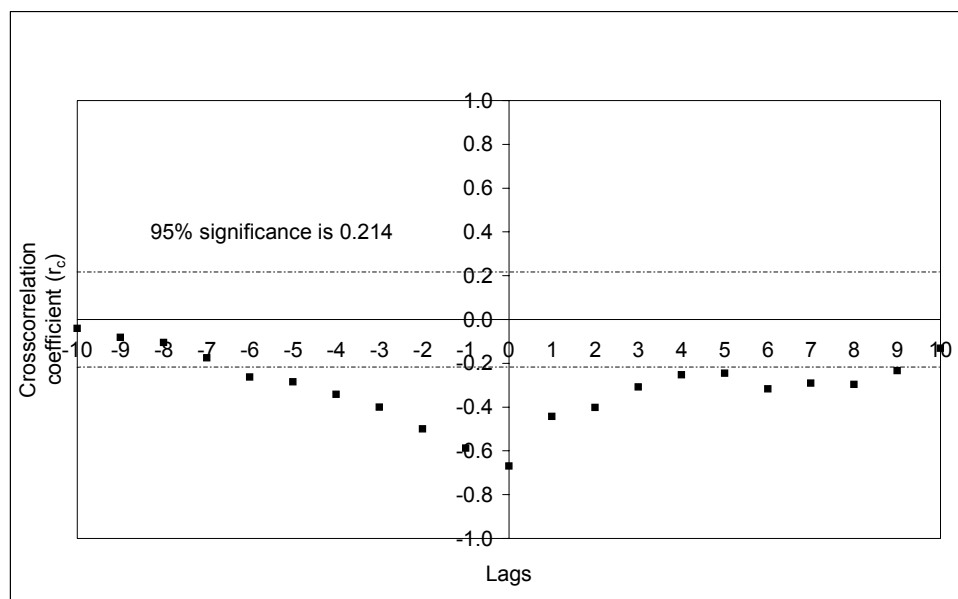


Figure 4. Crosscorrelogram between soil temperature and soil water content data of Figure 2.

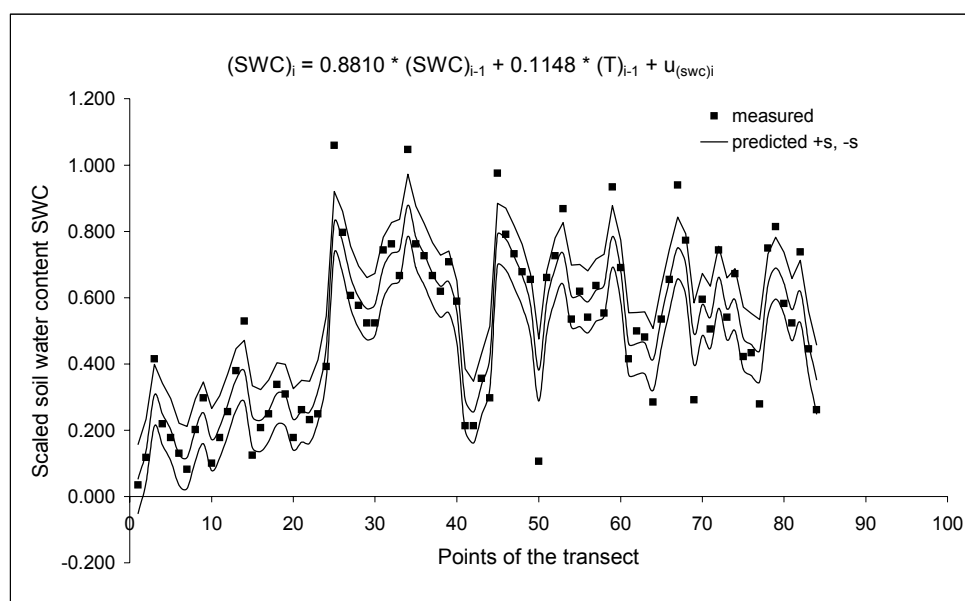


Figure 5. State-space analysis of scaled (equation 13) soil water content SWC data of Figure 2.

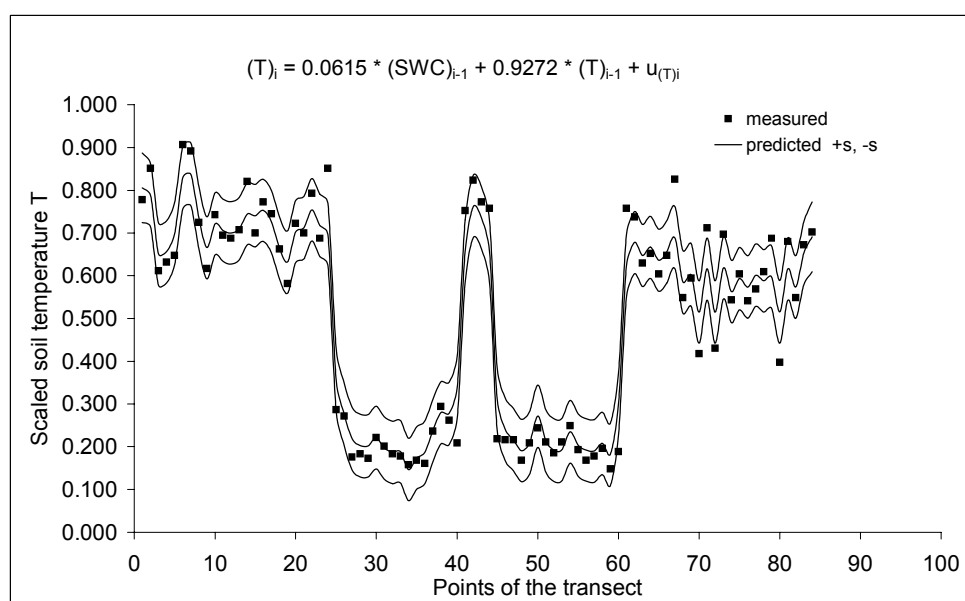


Figure 6. State-space analysis of scaled (equation 13) soil temperature T data of Figure 2.

The 95% fiducial limit area represents the interval $\pm s$ for each estimated value at positions i . The mean value of s is 0.0937. Examining equation (12a) we can see that the SWC at position $i-1$ contributes 88.1% to the estimate of SWC at location i , while T_{i-1} contributes only 11.5%. Figure 6 similar to Figure 5, shows the state-space estimate for soil temperature.

The mean value of s for the soil temperature estimates was 0.0732, which is smaller compared to that for soil water content (Note, because we are working with reduced variables, we can compare means!), and we can say that temperature was better estimated along the transect than soil water content. This statement is also confirmed by the relations between observed and estimated values, which yielded coefficients R^2 of 0.9063 for SWC and 0.9587 for T .

Analyzing equation (12b) we can see that the soil water content at position $i-1$ contributes 6.15% to the estimate of the temperature at location i , which means that the contribution of the first neighbor is much larger in the case of temperature compared to that of soil water content.

It is important to mention that this example, analyzed with a first order model, could also have been carried out with models of higher order. Hui et al. (1998) used a second order model when relating water infiltration rate at location i with itself and soil-water electrical conductivity at location $i-1$, and with the infiltration rate of the second neighbor ($i-2$). We could also have used more than two related variables, as for example, soil clay content, soil bulk density, incident solar radiation, or mineralogy and micro-topography of the soil surface.

This example, more completely reported in Dourado-Neto et al. (1999), is the first application of the state-space methodology in Brazil using space series, having the objective of introducing this approach into the soil science Latin American literature, as a tool for the better understanding of variables of the soil-plant-atmosphere system.

Evaluation of the Relation between Physical and Chemical Soil Properties

This second example illustrates the state-space approach applied to four space series (soil water content SWC, soil organic matter SOM, clay content CC and aggregate stability AS) sampled along the same 84 point transect of the sugarcane field. Soil water content was measured as described above, during a dry season day (September 6, 1999). Soil samples taken from the 0-0.15m surface layer were used to evaluate SOM, CC and AS. After a long time without rainfall it would be expected that there would be a relation between the “residual” SWC and the other chosen variables. Data were also normalized according to equation (13) before submission to the ASTSA software.

Soil water content data presented in Figure 7 have a CV of 13.4%, indicating that the variability of the data in relation to the mean is relatively small, although the fluctuation from point to point seems large in comparison to the total variation along the transect. Although treatment effects cannot visually be recognized, it is obvious that there is an increasing trend along the transect. The autocorrelation function given

by equation (4) for soil water content is presented in Figure 8. There is a large correlation structure up to 14 lags (in this case 14m), at a 5% probability level using the t test of equation (5). This large spatial structure is a expected result owing to the spatial trend in the data.

Figures 9 and 10 show the same features for SOM. The CV is only 7.8%, yet the spatial dependence reaches 10 lags. Here, the SOM data manifest a decreasing trend along the transect.

The spatial variation of CC and its ACF shown in Figures 11 and 12, respectively, also reflect the presence of a spatial trend along the transect. Point to point variations are also large in comparison to the total variation along the transect. This behavior, according to Wendroth et al. (1999), is better identified when we use statistical tools that consider local behavior tendencies.

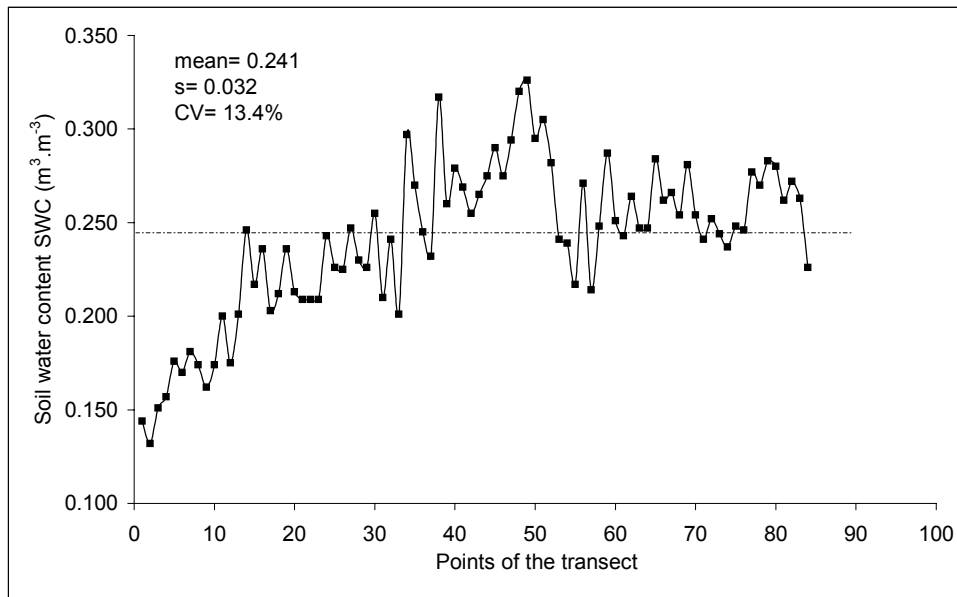


Figure 7. Soil water content distribution, meter by meter, along the 84 point transect, on September 06, 1999.

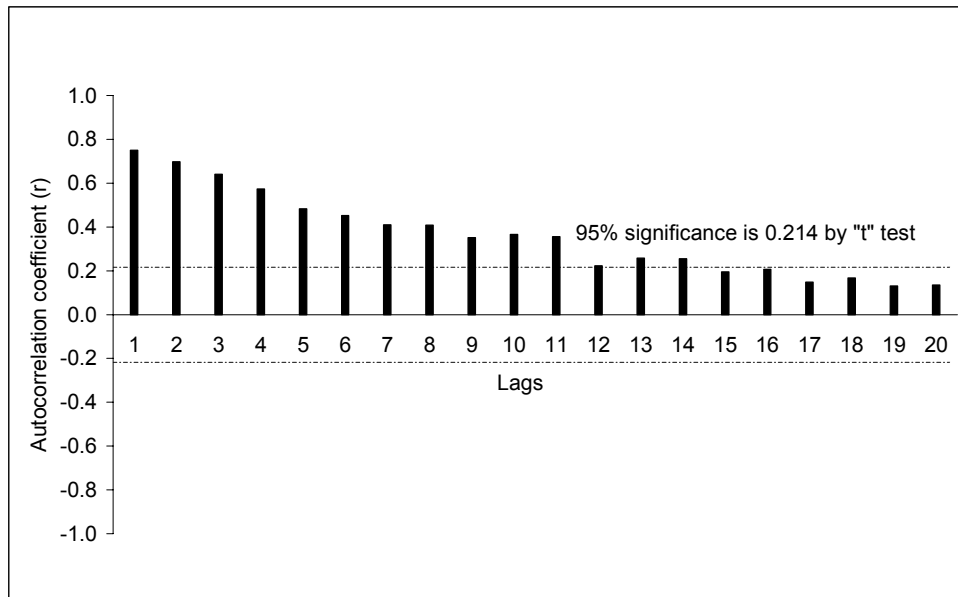


Figure 8. Calculated autocorrelation function (ACF) for soil water content data of Figure 7.

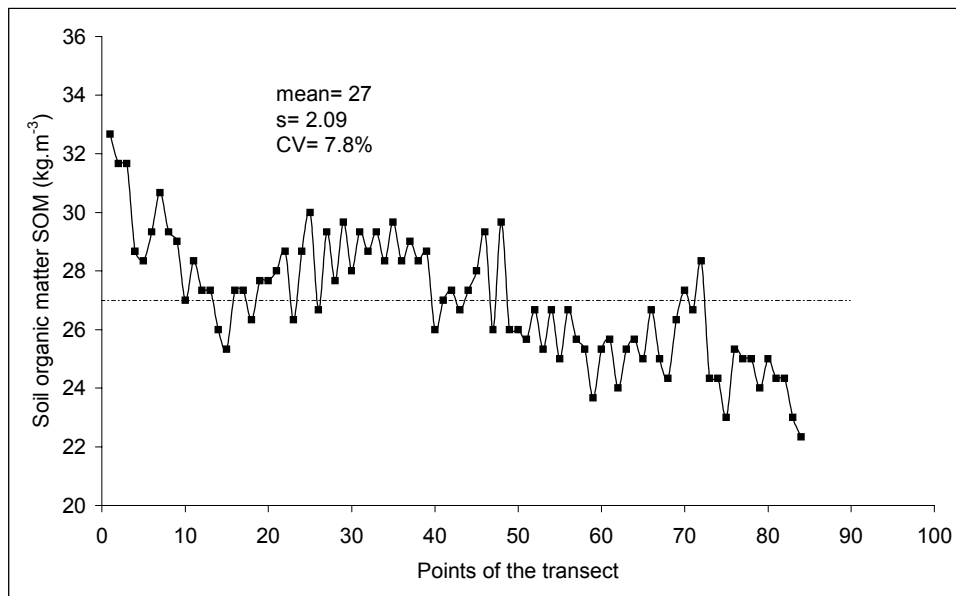


Figure 9. Soil organic matter distribution, meter by meter, along the 84 point transect.

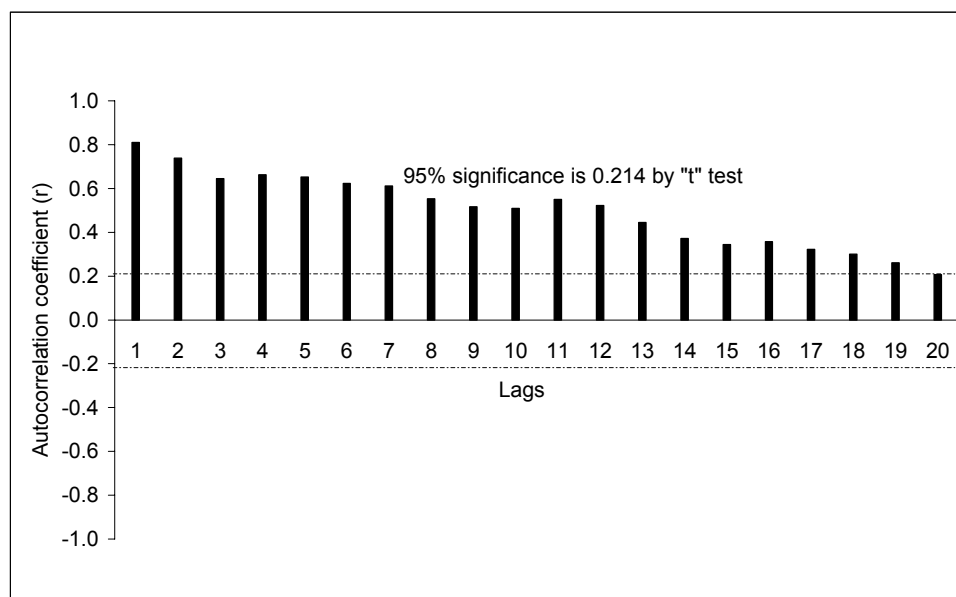


Figure 10. Calculated autocorrelation function (ACF) for soil organic matter data of Figure 9.

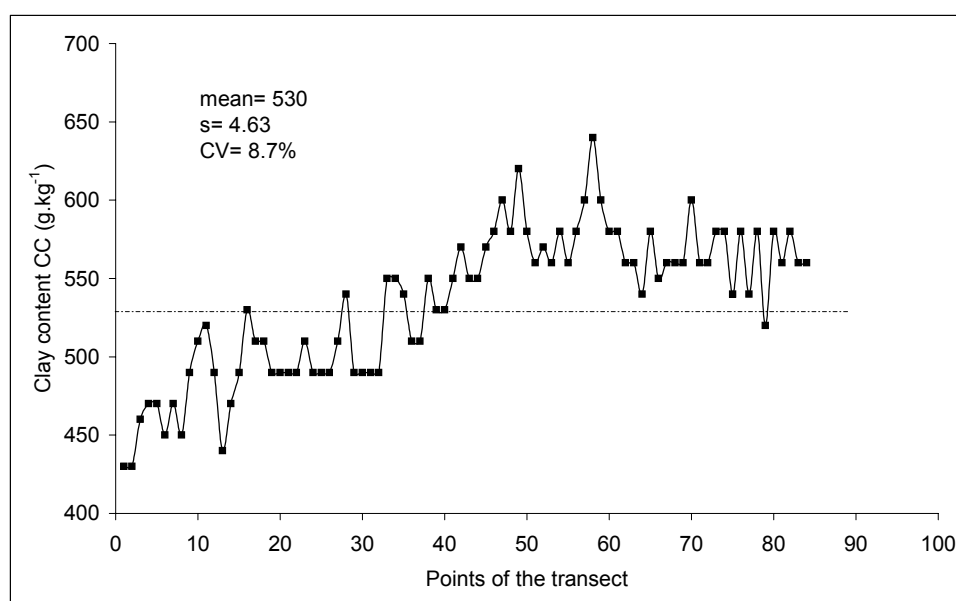


Figure 11. Clay content distribution, meter by meter, along the 84 point transect.

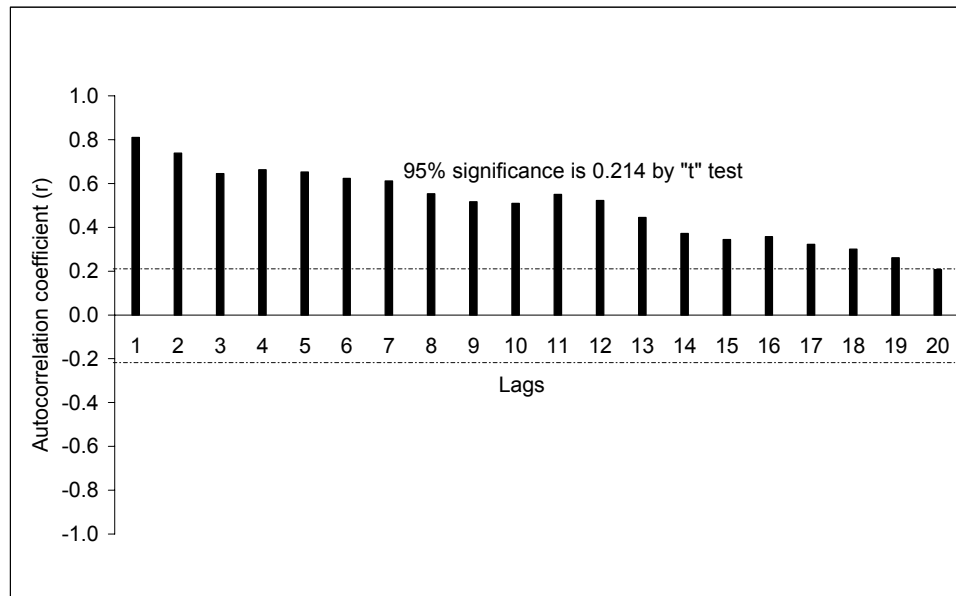


Figure 12. Calculated autocorrelation function (ACF) for clay content data of Figure 11.

Such is not the case in traditional agronomic experiments using classical statistics [variance analysis (ANOVA) and regression analysis] assuming independence of the data. In such cases when observations within and among treatments are not independent, Nielsen & Alemi (1989) state that the experimental field design does not provide a legitimate opportunity for applying classical statistical analysis.

In the absence of a spatial trend, the data for AS yield a CV of 14.6% (Figure 13), and a spatial autocorrelation reaching to only 3 lags (Figure 14).

Crosscorrelograms show strong spatial dependence structures between SWC and a) SOM, and b) CC, and a very weak crosscorrelation structure between SWC and AS. The crosscorrelogram for SWC and SOM is given in Figure 15. Crosscorrelation coefficients (equation 6) which describe the degree of linear association between two variables can be used to learn if the application of the state-space approach that requires a first order autoregressive model is justified.

Several combinations among the variables were analyzed with equations (11a and 12) to compare estimated versus observed values. The best state-space estimate of SWC, was obtained using the variables SWC, CC and. For this case (Figures 16 and 17, $R^2 = 0.9069$), $(SWC)_{i-1}$ contributed 76.8% of the estimate of $(SWC)_i$. On the other hand, $(CC)_{i-1}$ and $(AS)_{i-1}$ contributed 14.6% and 9.6%, respectively. The flexible state-space approach allows the study of dynamic processes involving several variables with local behavioral tendencies, and can provide a better understanding of the impact of soil spatial variability on crop productivity.

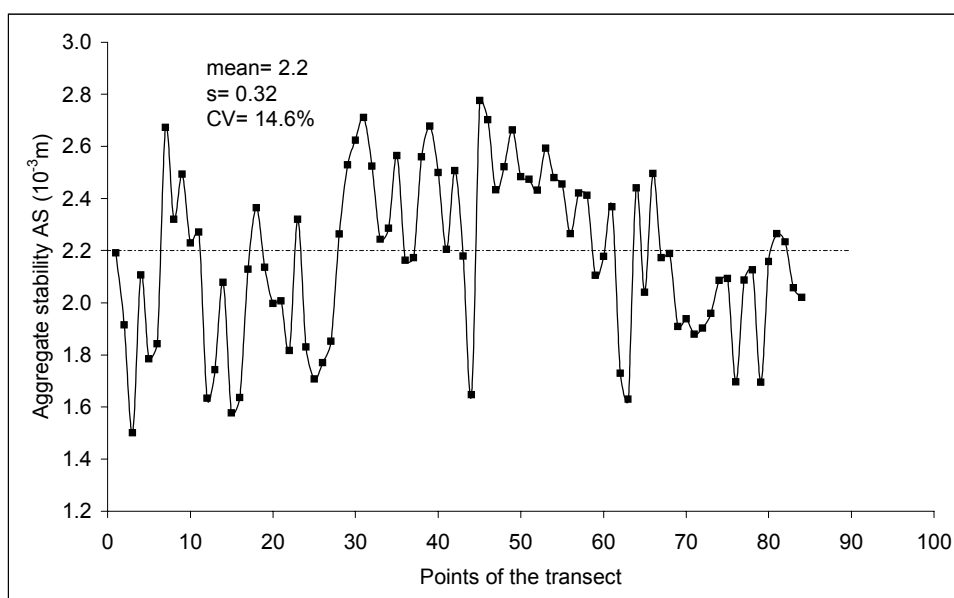


Figure 13. Aggregate stability distribution, meter by meter, along the 84 point transect.

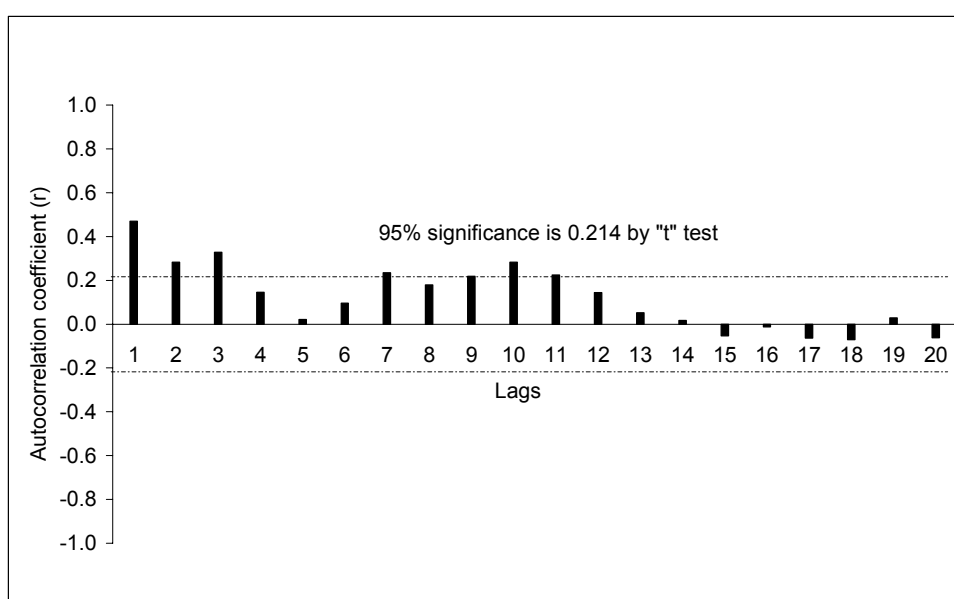


Figure 14. Calculated autocorrelation function (ACF) for aggregate stability data of Figure 13.

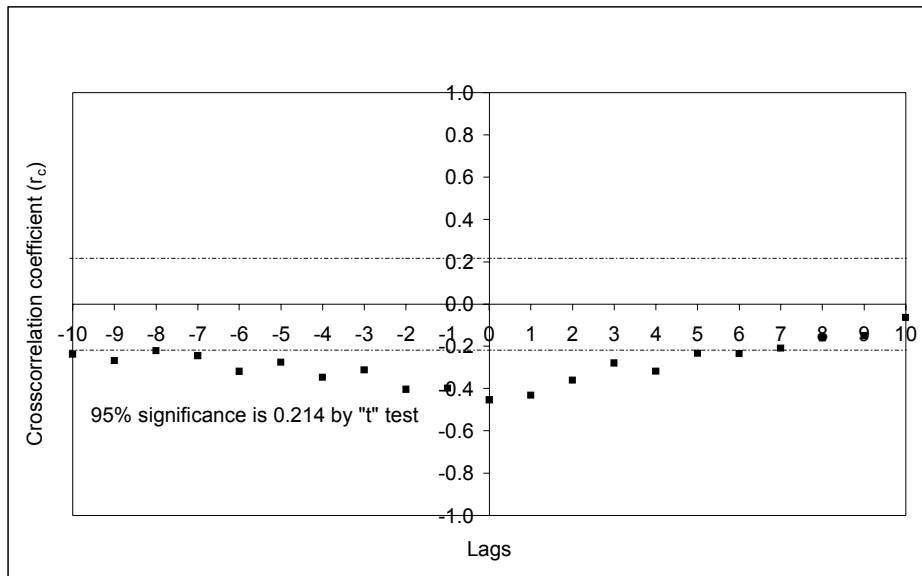


Figure 15. Calculated crosscorrelogram function (CCF) between soil water content and soil organic matter data.

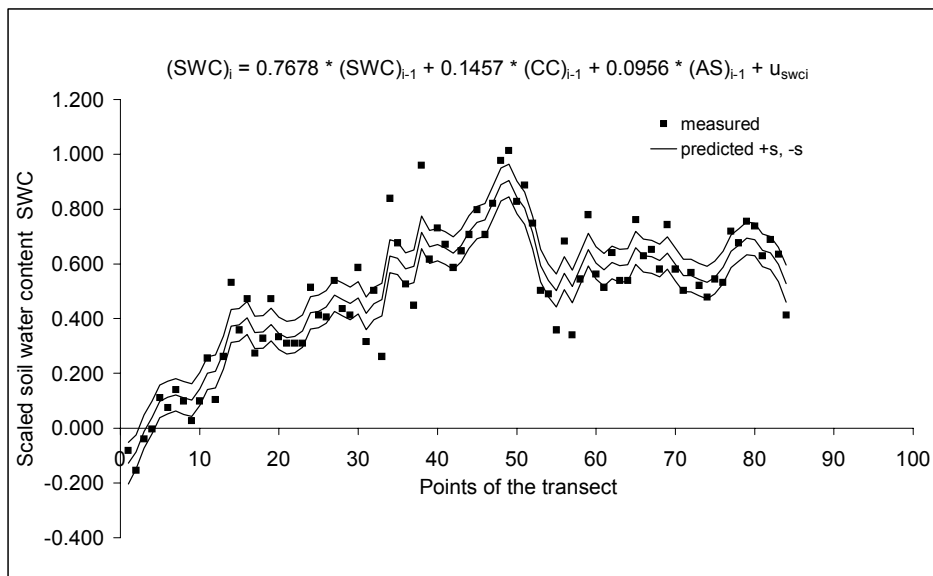


Figure 16. State-space analysis of scaled soil water content data as a function of scaled soil water content, scaled clay content and scaled aggregate stability, all at location $i-1$. The standard deviation s is estimated point by point.

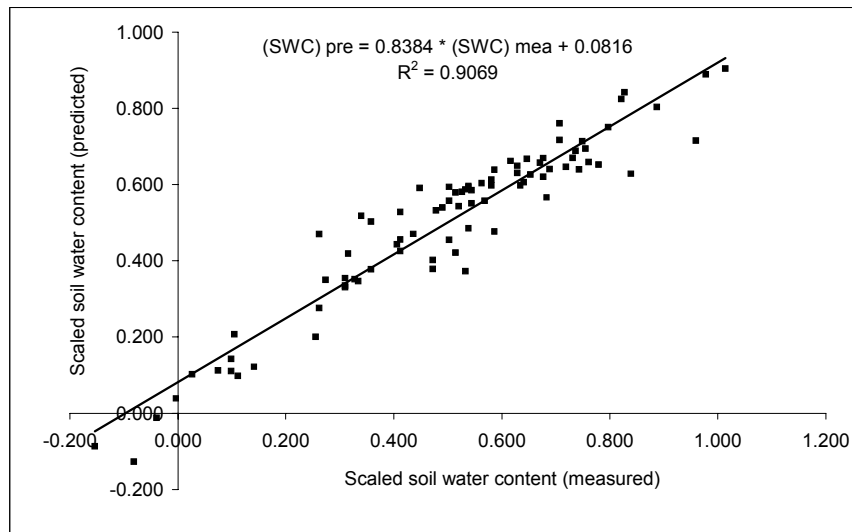


Figure 17. Correlation between predicted and measured scaled soil water content data of Figure 16.

a) Evaluation of the Soil-Plant System

This third example illustrates the application of the state-space methodology to evaluate the same sugarcane soil-plant system, using six variables measured along the 84 point transect. The crop variable number of cane stalks NCS per meter of row (Figure 18) is related to soil chemical properties - availability of phosphorus (P, Figure 19), calcium (Ca, Figure 20), and magnesium (Mg, Figure 21), and to soil physical properties - clay content (CC, Figure 11) and aggregate stability (AS, Figure 13).

In Figure 22 we note that the autocorrelation structure of NCS exceeds 10 lags associated with its spatial trend shown in Figure 18. We also found that all of the above soil chemical and physical properties were each spatially crosscorrelated with NCS. Figure 23 for NCS and Mg provides an example of such crosscorrelation. Therefore, we used 31 different combinations of these variables to yield state-space equations and evaluated the behavior of the model with respect to the estimates of the observed values.

The number of cane stalks NCS estimated with all six sets of variables used in the state-space analysis is given in Figure 24. The general trend of NCS is captured by the analysis, but not the local variation of the data. Note that many of the measured values of NCS fall outside the area of the 95% fiducial limits, and the value of R^2 obtained from a regression of estimated and measured values of NCS is only 0.502. Neighboring values of NCS at location $i-1$ contribute 86% of the estimate while the remaining neighboring variables each contribute between ± 10 and 20%. As a result, the KF excludes many measured values of NCS from the narrow fiducial limits derived from the use of all six variables.

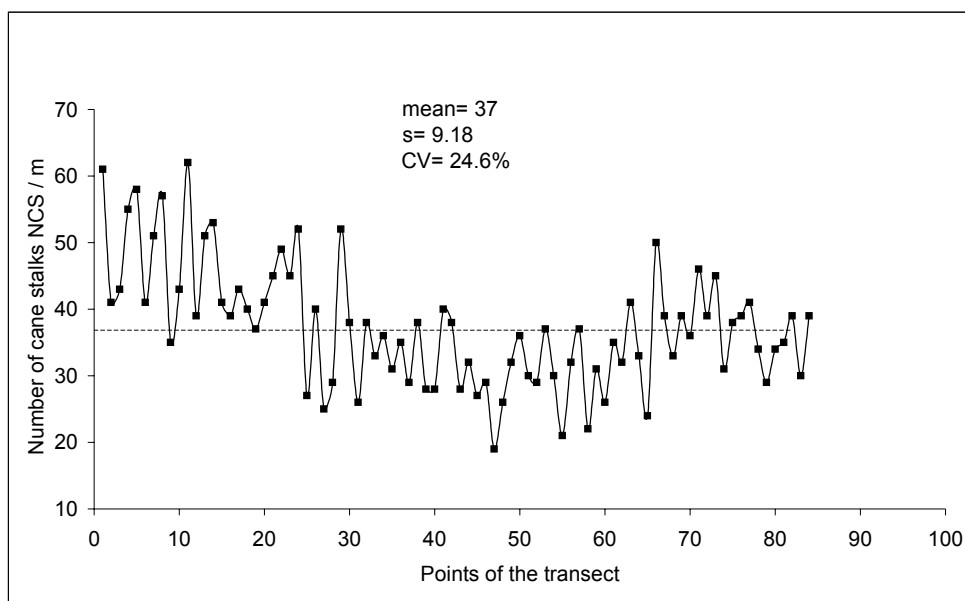


Figure 18. Number of cane stalks per meter of row (NCS) distribution, meter by meter, along 84 point transect.

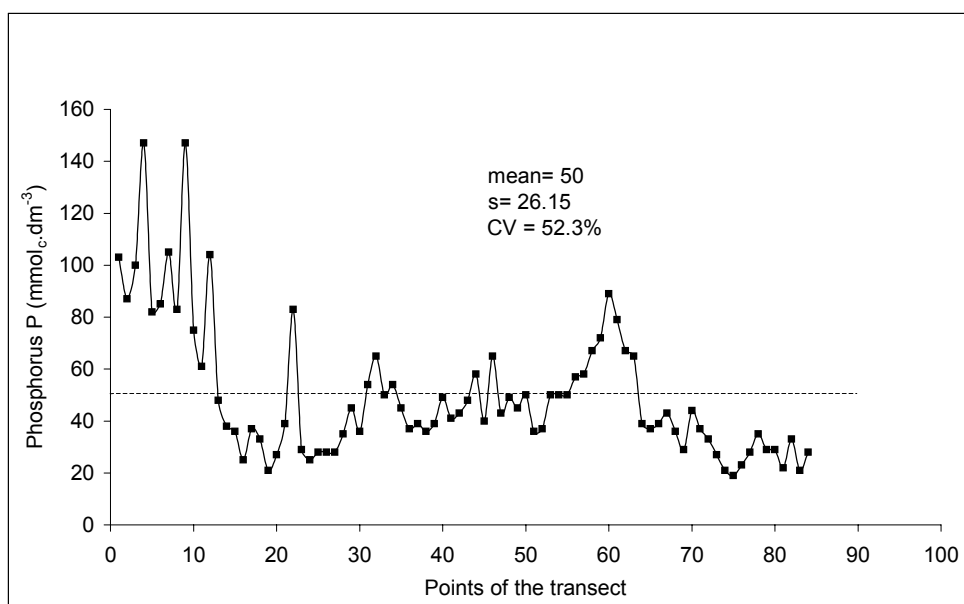


Figure 19. Available soil phosphorus (P) distribution, meter by meter, along 84 point transect.

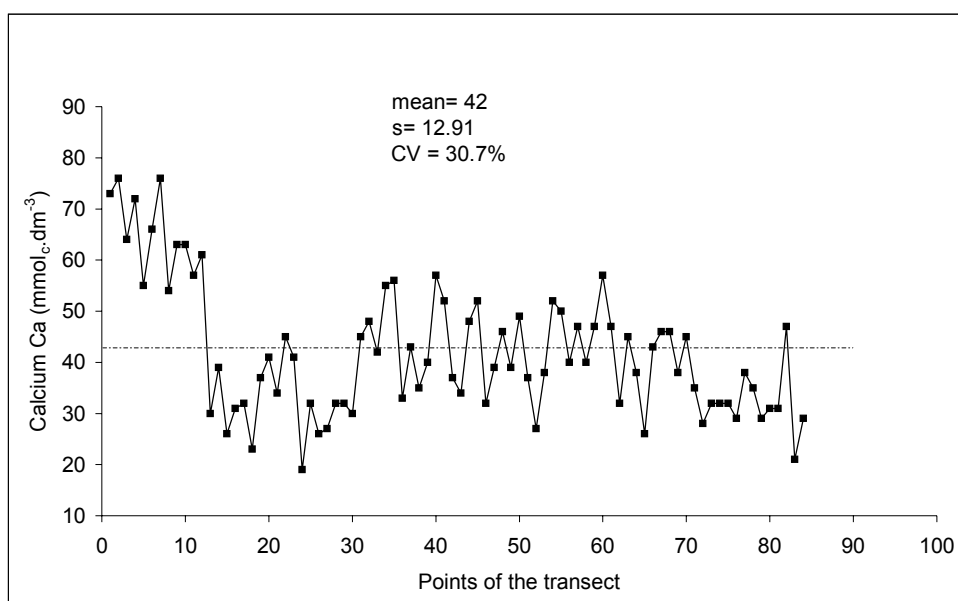


Figure 20. Available soil calcium (Ca) distribution, meter by meter, along 84 point transect.

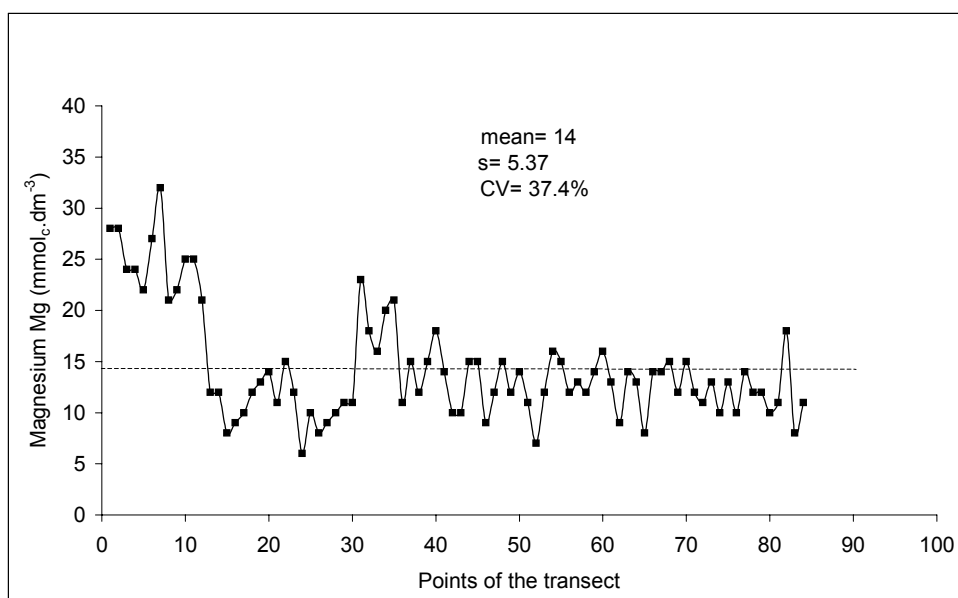


Figure 21. Available soil magnesium (Mg) distribution, meter by meter, along 84 point transect.

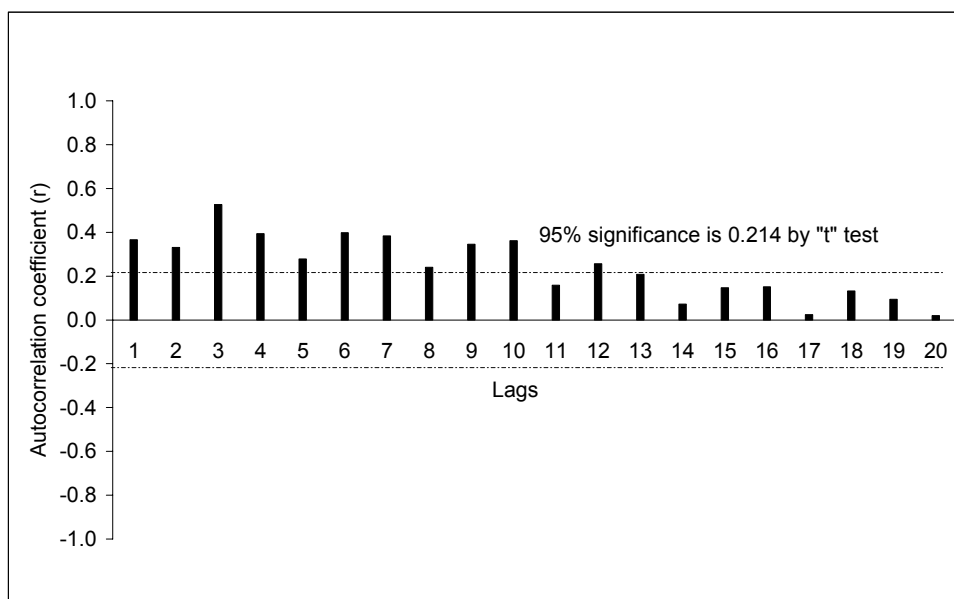


Figure 22. Calculated autocorrelation function (r) for number of cane stalks per meter of row (NCS).

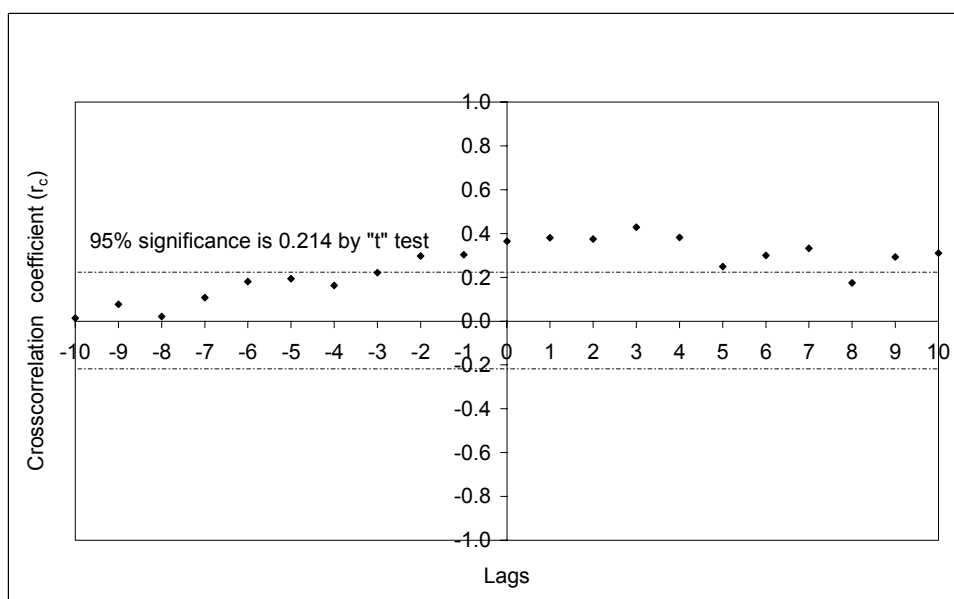


Figure 23. Calculated crosscorrelogram function (r_c) between number of cane stalks per meter of row (NCS) and magnesium (Mg) data.

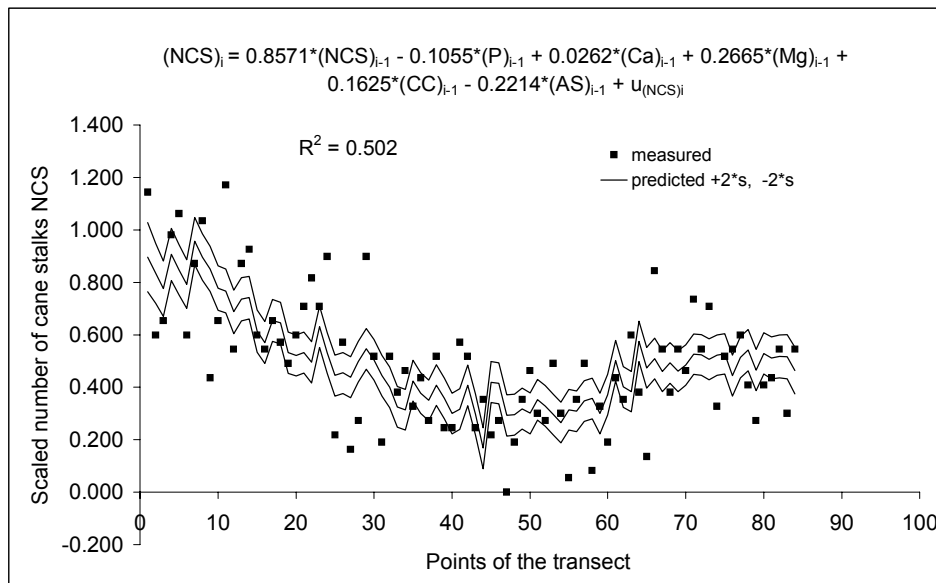


Figure 24. State-space analysis of scaled number of cane stalks data as a function of scaled number of cane stalks, scaled phosphorus content, scaled calcium content, scaled magnesium content, scaled clay content, and scaled aggregate stability, all at location i-1. The solid line in the middle of the 95% confidence interval area represents the state-space estimate. The standard deviation s is estimated point by point.

Because our initial classical regression analysis of the data showed that Ca was related to P, and P was related to Mg, and that both Ca and P manifested small crosscorrelation distances with NCS, variables Ca and P were omitted from the state-space analysis shown in Figure 25. Although the area of the fiducial limits is slightly larger than that in Figure 24, the results of the state-space analysis remains about the same – the general trend of NCS is captured, but not the local variation.

The largest crosscorrelation distance between NCS and the other five variables was manifested by clay content. The results of using only clay content in conjunction with NCS in the state-space analysis is given in Figure 26. The value of R^2 increased very little, with only 5% of the estimate of NCS coming from the neighboring value of the clay content.

In summary, with the local variations in number of cane stalks not being adequately described by the state-space analysis using any combination of the measured variables, we conclude that the cause of the NCS variation remains unknown, and it would have to be determined by the measurement of still other variables and perhaps the selection of a different model.

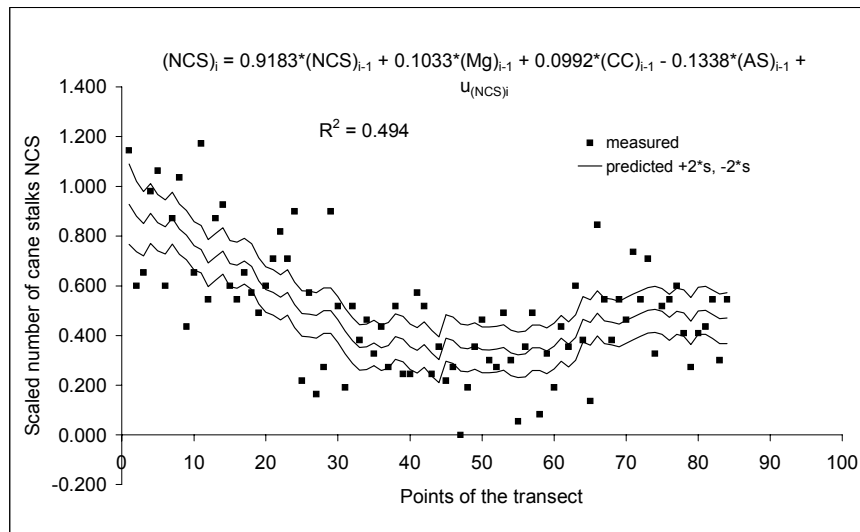


Figure 25. State-space analysis of scaled number of cane stalks data as a function of scaled number of cane stalks, scaled magnesium content, scaled clay content, and scaled aggregate stability, all at location $i-1$. The solid line in the middle of the 95% confidence interval area represents the state-space estimate. The standard deviation s is estimated point by point.

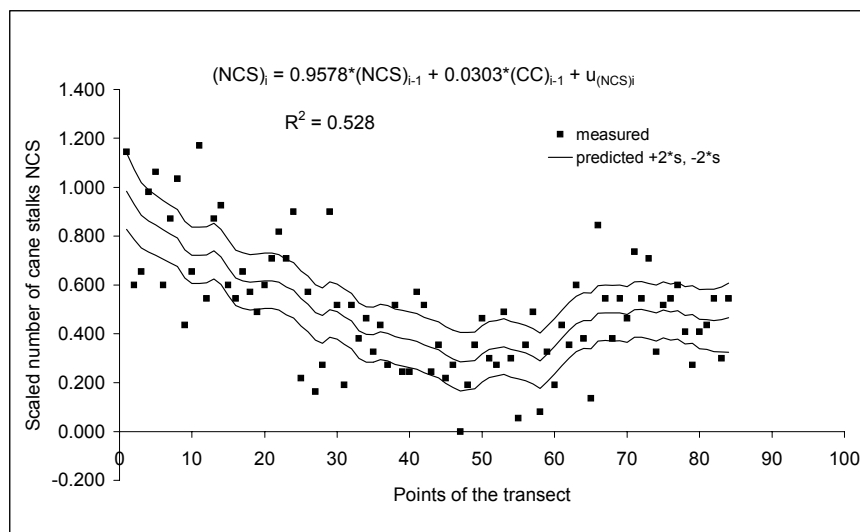


Figure 26. State-space analysis of scaled number of cane stalks data as a function of scaled number of cane stalks and scaled clay content, all at location $i-1$. The solid line in the middle of the 95% confidence interval area represents the state-space estimate. The standard deviation s is estimated point by point.

West & Harrison (1989, 1997) State-Space Approach

The bayesian formulation presented by West & Harrison (1989, 1997) and originally published by Harrison & Stevens (1976) has not yet been used in agronomy. In this case a general parametric formulation is used by which the observations are linearly related to parameters (equation 11), that have a dynamic evolution according to a random walk (equation 12), with the possibility of the incorporation of uncertainties associated to the model itself and to the parameters of the model. The probabilities of the model and its parameters are continuously updated in time/space using the Bayes theorem (Cantarelis, 1980). The acceptance and use of this approach was not as quick as expected, particularly by those without a deep knowledge in statistics, due to the difficulties in establishing values (or their law of variation) for the parameters " $v_j(x_i)$ " and " $u_j(x_i)$ ". To make this approach more accessible, Ameen & Harrison (1984) used discount factors to calculate the covariance matrix of the noise parameters $u_j(x_i)$. Discount factors relate to the relevance of the observations during the evolution of time/space – with the most recent information usually being more relevant in the modeling process. The smaller the discount factor, the less importance is given to previous information. Hence, the use of these factors assures that the stochastic influence on the evolution of the parameters (equation 12) is not directly made explicit through the noise $u_j(x_i)$. The stochastic influence is derived by the combination of a relation that establishes only the deterministic evolution of $Z_j(x_i)$ and the random process guaranteed by the discount matrix.

To illustrate this approach not yet commonly used in agronomy, we present an application related to the characterization of the root distribution of an agricultural crop, a fundamental study of the evaluation of the efficiency of management systems. We view the optimization of agricultural productivity in a context of sustainability and conservation of the resources of the soil-plant-atmosphere system. The crop root distribution reflects a series of complex, dynamic processes related to soil physical, chemical and biological attributes. According to Brown & Scott (1984), the conditions that define root growth, form and distribution, are found in the explored soil layer, among them soil density and porosity, water movement, nutrient distribution, pH, and the presence of toxic elements.

Although several studies give emphasis to soil density and porosity as the main factors responsible of the soil-root interaction (Hatano et al., 1988; Salih et al., 1998; Merotto Jr. & Mundstock, 1999). In their studies, presence of roots was negatively correlated with soil density and positively correlated with soil porosity.

There are several methods used to investigate plant root distributions (e.g., Bohm, 1979; Crestana et al., 1994) the evaluation of roots in terms of explored soil volume, dry mass or length is not an easy task with great difficulties being encountered in most techniques. For the time and work spent, very little information is obtained and oftentimes the sparse data manifest extreme variability. This variability might be a limiting factor for crop yield (Hui et al., 1998; Fante Jr. et al., 1999) and, therefore, the analysis and interpretation of root architecture and its

relation to soil characteristics, has lead to the development of new techniques, new ideas and approaches that open more possibilities for a detailed and broader understanding of the soil-root interface (Longsdon & Linden, 1992).

In this context, with the dynamic regression model of West & Harrison (1989, 1997) we use the state-space analysis to identify possible significant relations between the root system distribution of an agricultural crop and soil physical attributes. We also show that these dynamic state-space models have advantages over more conventional static models to better explain interrelations between soil-plant attributes.

We analyze the data from Fante Jr. *et al.* (1999) taken from an experiment carried out in São Carlos (SP), Brazil, on a Dark Red Latosol planted to forage oats. To evaluate root distribution, soil density and porosity, the authors used the volumetric ring method (Bohm, 1979; Kiehl, 1979; EMBRAPA, 1997). Cylindrical samples (0.046m diameter and 0.03m height) were extracted from the soil profile, corresponding to 25 samples separated by 0.1m (2.5m of plant row), and in three depths: 0-0.1, 0.1-0.2, and 0.2-0.3m. The samples were water saturated, weighed and immediately placed on a tension table at a negative pressure head of 0.6m of water (60kPa) for 48 hours. After weighing they were dried in an oven at 105 °C until at constant weight. This procedure allowed the calculation of soil bulk density, and macro-, micro- and total porosity.

Thereafter, roots were separated desegregating the soil in water using mechanical agitation and a 0.2mm sieve. Separated, water-saturated roots were spread on a surface and scanned to obtain digital images. These images were processed using the program SIARCS (Crestana *et al.*, 1994) which yielded values of root length per unit of soil volume DRC - the primary variable of interest. We initially calculated the linear correlation coefficients between DRC and each of the other variables soil bulk density, total porosity, macroporosity and microporosity. The correlation coefficients were, respectively, -0.62, 0.70, 0.63 and 0.61. With DRC being correlated the least with soil microporosity, we ignored any further analysis of soil microporosity. Further linear analysis between DRC and the remaining three variables (soil bulk density, total porosity and macroporosity) revealed that only total porosity at the first neighbor (one lag distance at a position $i-1$) was correlated with DRC (Figure 27). Hence, the only variable that could be used in the state-space analysis was total porosity.

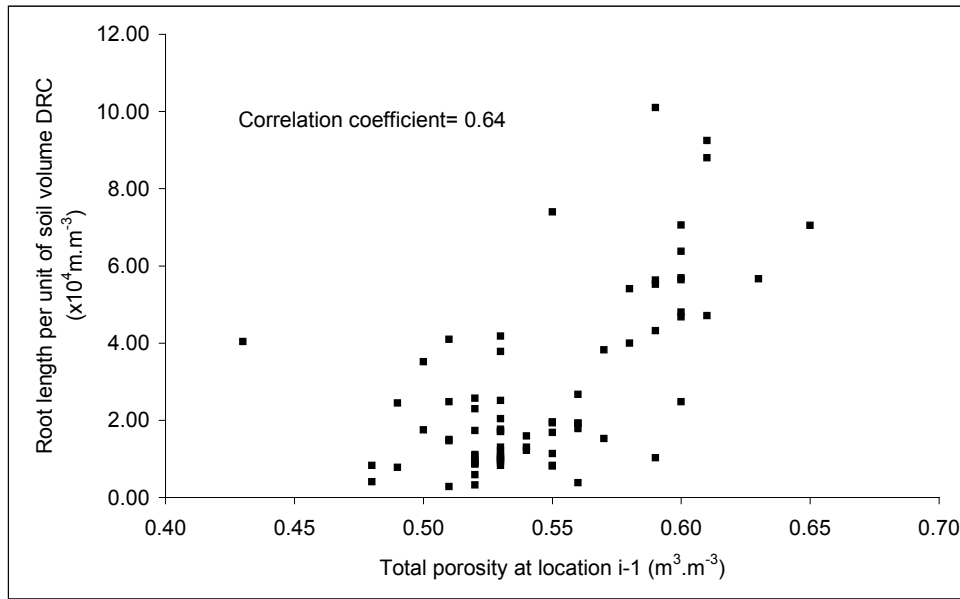


Figure 27. Correlation between root length per unit of soil volume DRC and total porosity at location i-1.

Because one of the equations used in the state-space approach of West & Harrison (1989, 1997) requires variables to be normally distributed, a normality analysis of the DRC data was performed using a histogram and a normal plot to verify its probability function. Taking the logarithm of each DRC value transformed the set of measurements into a nearly normal distribution. In order to have a better appreciation of the characteristics and advantages of the dynamic regression within the state-space approach in studying soil-plant relations, we compare two methods for calculating classical static regression equations for DRC versus total porosity. Here we have

$$(\text{LDRC})_i = \beta_0 + \beta_1 (\text{Poro})_i + \beta_2 (\text{Poro})_{i-1} + (\text{Error})_i \quad i = 1, 2, 3, \dots, n \quad (14)$$

where $(\text{LDRC})_i$ is the logarithm of DRC at location i , $(\text{Poro})_i$ and $(\text{Poro})_{i-1}$ are total porosity at locations i and $i-1$, respectively, $\beta_0, \beta_1, \beta_2$ are the regression coefficients of the model and $(\text{Error})_i$ are the random observation errors at locations i having zero mean, constant variance v and a normal distribution. The covariance between errors at locations i is assumed to be zero.

For this static model the regression coefficients β_0, β_1 and β_2 are considered fixed and constant along space, and can be estimated in two ways: 1) using the conventional ordinary minimum squares estimator MSE in its standard form with all

of the data being analyzed at once, and 2) an alternative sequential version of MSE with the data being processed in sequence beginning with data from only the first two locations used in equation (14). The next calculation includes data from the third location, and so on continuing to increase the number of locations in the sequential analysis until data from all n locations has been included. The MSE presents standard presuppositions (non correlated errors with constant variance, etc.) which according to the known Gauss-Markov theorem (theory of linear regression models) guarantees optimal properties to this estimator. Estimates of the coefficients β_0 , β_1 and β_2 in equation (14) calculated using the conventional MSE and the sequential MSE are given in Figure 28. Values of β_0 , β_1 and β_2 from the conventional MSE remain constant at all locations along the transect, while those from the sequential MSE differ at each location. Note that the estimates for β_0 , β_1 and β_2 from the last sequential MSE are identical to those from the conventional MSE.

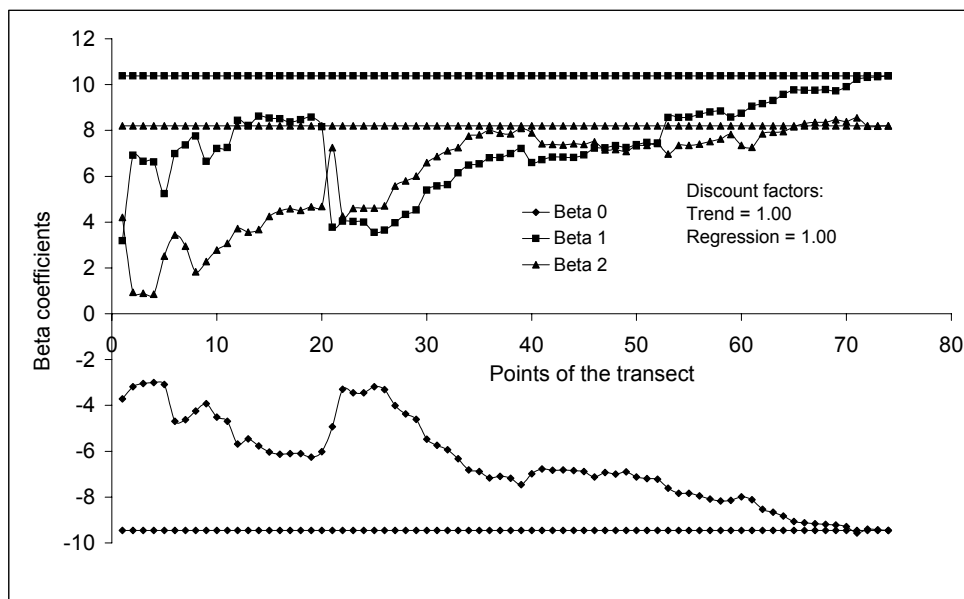


Figure 28. Static regression model: sequential estimates versus constant coefficient estimates.

We now consider the dynamic regression model which is local and not global, and contains variable β coefficients having the subscript i . These coefficients vary along space according to a Markovian evolution (first order autoregressive process, not having to be stationary), being therefore called “state variables of the system” (West & Harrison, 1989, 1997; Pole et al., 1994).

Hence, we have a basic regression equation (observation equation), and a second equation (evolution equation) which characterizes the form of the variation of these state parameters along space. Parameters are estimated in an optimal way through algorithms of the type KF (extensions of the basic KF). The equations of

estimation are sequential, comprising the observational equations of actualization (via Bayes theorem and observation equation) and the spatial actualization equations (consequence of the evolution equation). We apply these algorithms here in both versions, the ordinary (forward) filter and the smoothing (backward) filter.

Using the software BATS (Bayesian Analysis of Time Series) (West & Harrison, 1989, 1997; Pole et al., 1994), we performed the analysis of the data according to the observation equation

$$(\text{LDRC})_i = \beta_{0i} + \beta_{1i}(\text{Poro})_i + \beta_{2i}(\text{Poro})_{i-1} + (\text{Error})_i \quad (15)$$

and the state evolution equation

$$\begin{pmatrix} \beta_{0i} \\ \beta_{1i} \\ \beta_{2i} \end{pmatrix} = \begin{pmatrix} \beta_{0(i-1)} \\ \beta_{1(i-1)} \\ \beta_{2(i-1)} \end{pmatrix} + \begin{pmatrix} u_{0i} \\ u_{1i} \\ u_{2i} \end{pmatrix} \quad (16)$$

where β_{0i} is the process level component at location i , β_{1i} the dynamic regression coefficient at location i , β_{2i} the dynamic regression coefficient at location $(i-1)$, $(\text{Error})_i$ the observational random error component at location i , having zero mean, variance v_i and normally distributed and $(u_{0i} \ u_{1i} \ u_{2i})$ the system perturbation vector having zero mean, constant variance and normally distributed.

Note that the static model corresponds to a particular case of the dynamic model, in which the variances of the perturbations $u_j(x_i)$ are zero when the stochastic beta coefficients are fixed. In this case more emphasis is given to equation (11). In the dynamic regression, the beta coefficients are considered as a state vector (equation 12) following a random walk process. The transition matrix ϕ is unity and the observation matrix \mathbf{M} that relates the state vector with the observation vectors, being formed of the regression coefficients.

Figures 29a and 29b show static model estimates of DRC with constant and sequential coefficient estimates, respectively. As expected, for the last observation ($i = n$) the coefficients of both approaches coincide (Figure 28). These sequential estimates, besides including fixed estimates with one of the locations (the last one) are obtained using the algorithm of sequential square minimum SSM, which is a particular case of the KF algorithm implemented via discount factors, which make these factors equal to unity, corresponding to zero variances of $u_j(x_i)$. An important difference between the sequential and static versions is the fact that the sequential version yields different adjusted values and, as a consequence, has the greater coefficient R^2 of 0.708 compared with 0.566 when comparing estimated LDRC with measured LDRC (Figure 29).

Figures 30a and 30b show coefficient estimates obtained by a dynamic regression model in which a variability of 2% is permitted for the regression coefficients between each two consecutive locations (corresponding to a discount factor of 0.98 in the KF). With this imposed variability, the regression model became

dynamic in the ordinary KF version of Figure 30a, as well as in the smoothed KF version of Figure 30b.

For the process level coefficient β_0 we considered a more dynamic procedure (discount factor 0.90), which represents an improvement in relation to the static model considered in its sequential version.

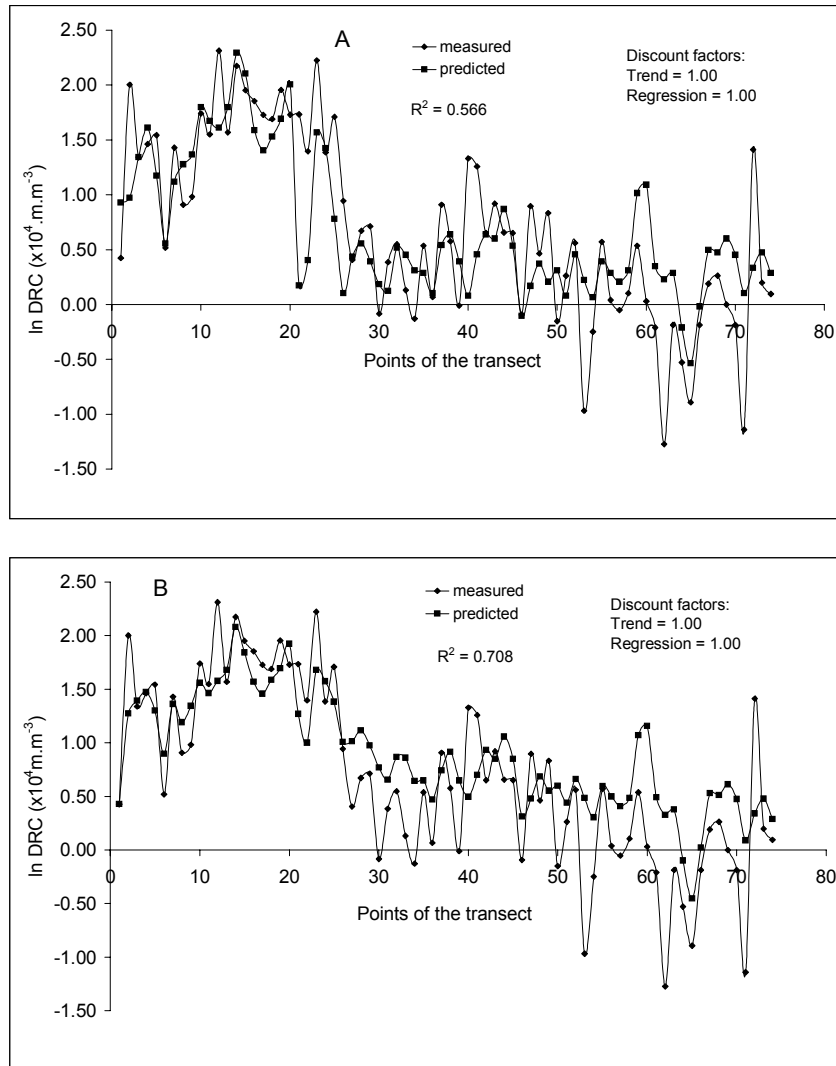


Figure 29. Root length per unit of soil volume DRC distribution along the transect: (A) \ln (DRC) measured versus \ln (DRC) predicted by static regression model using constant coefficient estimates; and (B) \ln (DRC) measured versus \ln (DRC) predicted by static regression model using sequential coefficient estimates.

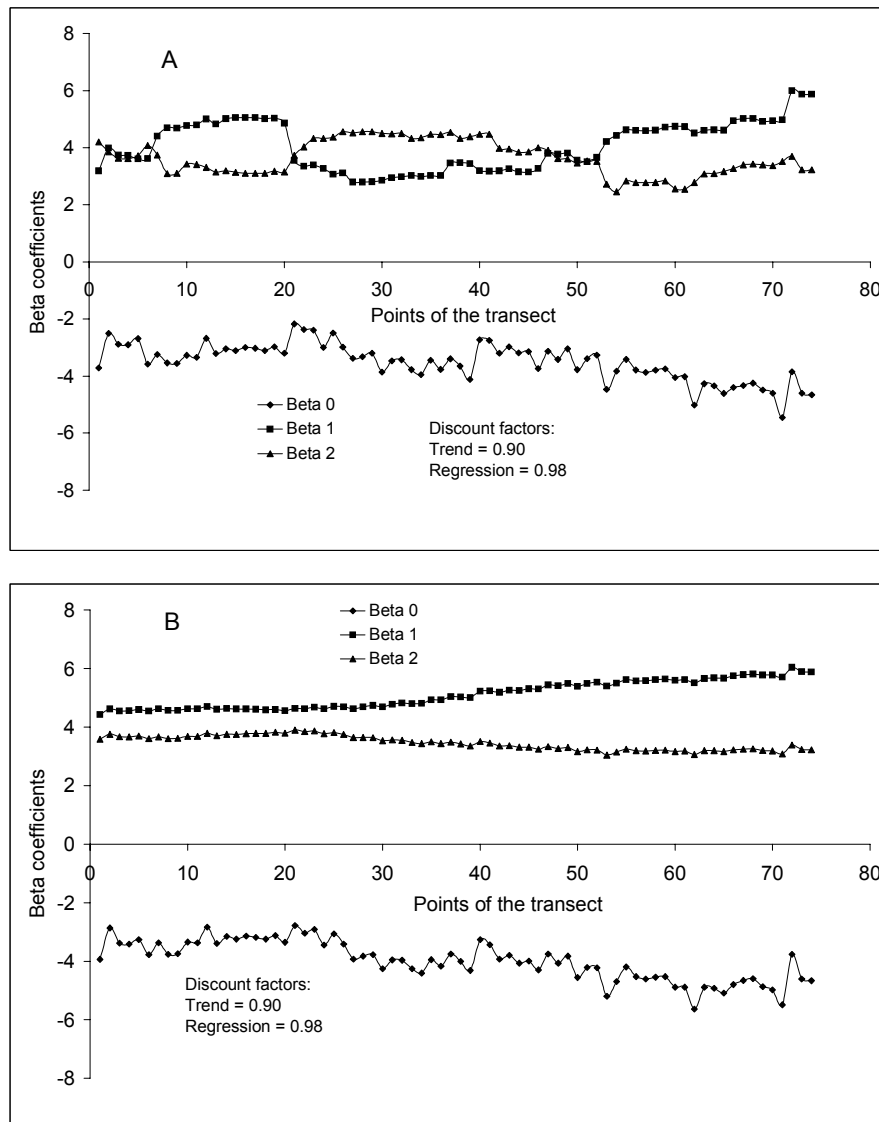


Figure 30. Dynamic regression model (state-space model): (A) sequential coefficient estimates; and (B) smoothed sequential coefficient estimates.

Here we point out the advantage of the smoothed version in relation to the ordinary version of the dynamic model. Notice that even with a small reduction in the degree of explanation of the data (from R^2 decreasing from 0.998 to 0.994), we have a much better interpretation of the coefficients estimated in the smoothed version due to the fact that they are much less variable as can be seen in Figures 30a and 30b.

Last, we mention that the precise choice of the dynamic model can be automated, allowing the use of adequate software for their implementation. For example, the software BATS used here, reference or “default” values of 0.98 and 0.90 are taken for the discount value of the regression coefficients and the process level (called tendency) which yielded the results of Figures 30 and 31. Hence, it is easy to implement these models that have major advantages over the static conventional models.

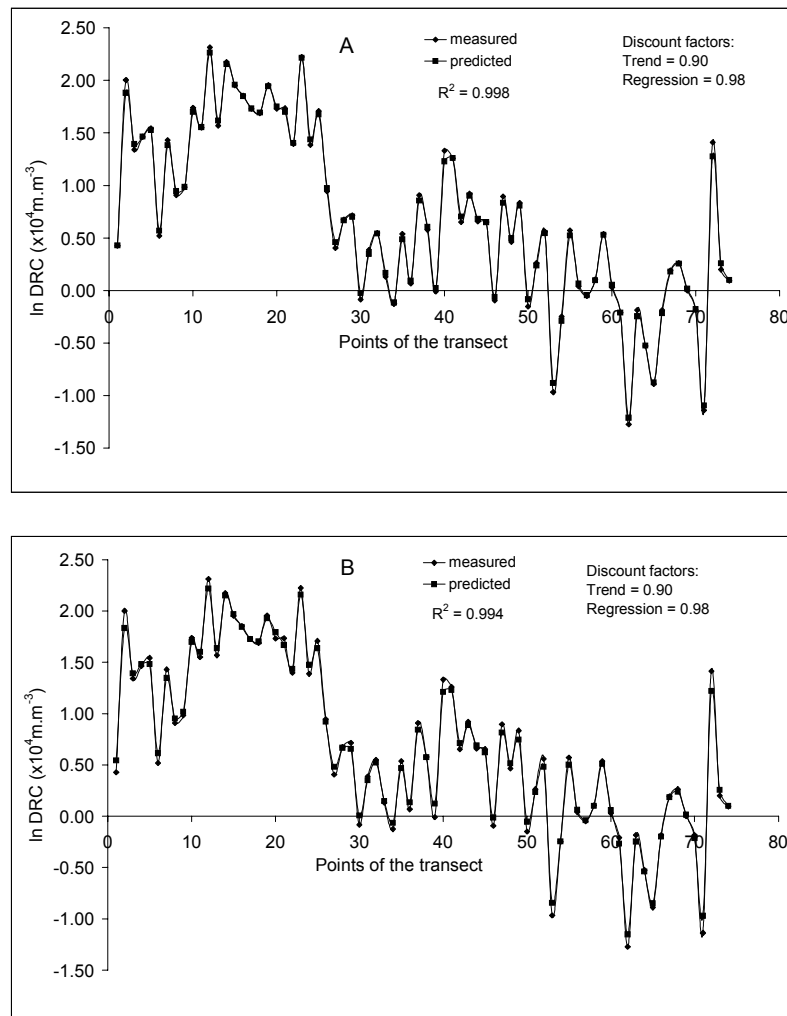


Figure 31. Root length per unit of soil volume DRC distribution along the transect: (A) $\ln(\text{DRC})$ measured versus $\ln(\text{DRC})$ predicted by dynamic regression model (state-space model) using sequential coefficient estimates; and (B) $\ln(\text{DRC})$ measured versus $\ln(\text{DRC})$ predicted by dynamic regression model (state-space model) using smoothed sequential coefficient estimates.

Because dynamic regression models represented in the state-space form are relatively recent tools, they have not yet been frequently used to quantify soil-plant relations. Having been introduced in the sixties, their greater implementation occurred only since the late eighties (West & Harrison, 1989, 1997). Being models of local adjustment, it is possible to precisely estimate regression coefficients for each sampled location. This possibility tends to alleviate the problem of spatial variability encountered in precision agriculture. Today, the more commonly used static models are models of global behavior with their regression coefficients being average values not varying along space. They provide an opportunity to describe the spatial association among different variables measured across a field and can, therefore, provide a better understanding of the complex relations between plant and soil variables. Inasmuch as the response of one variable is not unique in a field, the application of statistical multiple regressions oftentimes yield low coefficients of determination.

Because these kinds of analyses give only a global estimate of coefficients that do not represent point to point variations, and their use can lead to interpretations that induce inadequate management procedures. We conclude that dynamic regression models of state-space form are more adequate for the study of soil-plant relationships mainly because they account for the local spatial and temporal character of agronomic processes.

Summary

In this chapter we presented two types of representations of the state-space models. One gives emphasis to the state equation (Shumway, 1988 and Shumway & Stoffer, 2000) and the other gives emphasis to the observation equation (West & Harrison, 1989, 1997). Both are presented as dynamic systems composed of two equations, differing only in the way they are solved and implemented. The first does not allow the user to interfere in the estimation routine of the software ASTSA with the system being treated as a multidimensional spatial process in which there is no hierarchy among variables - all being treated in the same way. The second representation, implemented with software BATS, allows 1) the construction of a statistical model based on the user's judgement to best represent the dynamic system of interest, and 2) allows making local adjustments of the regression coefficients to follow the variations of the response variable, point by point, along the experimental transect.

In this chapter, soil and plant attributes thought to be correlated with each other were selected and sampled at different locations and times, and then with state-space formulations, they were empirically examined solely on the basis of their field-measured values. We anticipate that these kinds of models will become even more valuable as physically based deterministic equations are used in combination with observations that are correlated in space or time (See e.g. Wendroth et al., 1993). Processes may be physical, chemical and/or biological in nature (e.g., infiltration, cation exchange, plant root absorption of soil minerals, etc.). An equation describing a physical process occurring in the topsoil of a farmer's field is derived and

transformed into a state-space formulation. The parameters in the equation are theoretically well-known and relate to coefficients of diffusion, hydraulic conductivity, solute precipitation and dissolution, enzyme kinetics, plant growth, etc. These kinds of state-space models provide a simultaneous examination of the theoretically based equation and its parameters as well as the observations embracing the uncertainties of soil heterogeneity and instrument calibration.

The representation of models in terms of state-space in the area of agronomy is relatively recent, and from what is known today, such models are potentially valuable tools to study the relations among several variables linked to the dynamic system comprised by the soil, the plant, and the atmosphere.

References

- Alemi, M.H., Shahriari, M.R., Nielsen, D.R. 1988. Kriging and cokriging of soil water properties. *Soil Tech.* 1: 117-132.
- Ameen, J.R.M., Harrison, P.J. 1984. Discount weighted estimation. *Journal of Forecasting*, 3: 285-296.
- Bohm, W. 1979. *Methods of studying root systems*. New York: Springer-Verlag, 189p.
- Brown, D.A., Scott, H. don. 1984. Dependence of crop growth and yield on root development and activity. In: BARBER, S.A.; BOULDIN, D.R., ed. *Roots and water influx, and plant growth*. Madison: Soil Science Society of America, 1984. cap. 6, p.101-36.
- Cantarelis, N.S. 1980. *An investigation into the properties of Bayesian forecasting models*. Ph.D. Thesis, School of Industrial and Business Studies, Warwick University, England.
- Crestana, S., Guimarães, M.F., Jorge, L.A.C., Ralish, R.; Tozzi, C.L.; Torre, A.; Vaz, C.M.P. 1994. Evaluation of soil root distribution aided by digital image processing. *Brazilian Journal of Soil Science*, 18 (3): 365-371.
- Davis, J.C. 1986. *Statistics and data analysis in geology*. 2nd ed. Wiley and Sons, New York, NY, USA.
- Dempster, A.P., Laird, N.M., Rubin, D.B. 1977. Maximum likelihood from incomplete data via the EM algorithm. *J. Roy. Stat. Soc., Ser. B.*, 39: 1-38.
- Deutsch, C.V., Journel, A.G. 1992. *GSLIB. Geostatistical software library and user's guide*. Oxford University Press, New York, NY, USA.
- Dourado-Neto, D., Timm, L.C., Oliveira, J.C.M., Reichardt, K., Bacchi, O.O.S., Tominaga, T.T., Cassaro, F.A.M. 1999. State-space approach for the analysis of soil water content and temperature in a sugarcane crop. *Scientia Agricola*, 56: 1215-1221.
- EMBRAPA: Brazilian Agricultural Research Corporation – Embrapa. *Embrapa Soils*. 1997. *Manual of soil analyses methods*. 2.ed. Rio de janeiro, Brazil. 212p.
- Fante Júnior, L., Reichardt, K., Jorge, L.A.C.; Bacchi, O.O.S. 1999. Root system distribution of a forage oat crop. *Scientia Agricola*, 56 (4): 1091-1100.

- Gelb, A. 1974. Applied optimal estimation. Massachusetts Institute of Technology Press, Cambridge, MA.
- Harrison, P.J., Stevens, C.F. 1976. Bayesian forecasting (with discussion). JRSS, Series B, 38, 3, 205-267.
- Hatano, R., Iwanaga, K., Okajima, H., Sakuma, T. 1988. Relationship between the distribution of soil macropores and root elongation. Soil Sci. Plant Nutr., 34: 535-546.
- Hui, S., Wendroth, O., Parlange, M. B., Nielsen, D. R. 1998. Soil variability – Infiltration relationships of agroecosystems. Journal of Balkan Ecology, 1: 21-40.
- Kalman, R. E. 1960. A new approach to linear filtering and prediction theory. Trans. ASME J. Basic Eng., 8: 35-45.
- Katul, G.G., Wendroth, O., Parlange, M.B., Puente, C.E., Folegatti, M.V., Nielsen, D.R. 1993. Estimation of in situ hydraulic conductivity function from nonlinear filtering theory. Water Resources Research, 29: 1063-1070.
- Kiehl, E.J. 1979. Manual of edaphology: soil-plant relationships. São Paulo - SP, Agronômica Ceres, 246p.
- Longsdon, S.D., Linden, D.R. 1992. Interactions of earthworms with soil physical conditions influencing plant growth. Soil Sci., v.154,n.4,p.330-337.
- McGraw, T. 1994. Soil test level variability in Southern Minnesota. Better crops, Potash & Phosphate Institute, Norcross, 78(4): 24-25.
- Merotto Júnior, A., Mundstock, C.M. 1999. Wheat root growth as affected by soil strength. Rev. Bras. Ci. Solo, 23 (2): 197-202.
- Morkoc, F., Biggar, J. W., Nielsen, D. R., Rolston, D. E. 1985. Analysis of soil water content and temperature using State-space approach. Soil Sci. Soc. Am. J., 49: 798-803.
- Nielsen, D.R., Tillotson, P.M., Vieira, S.R. 1983. Analyzing field-measured soil water properties. Agric. Water Man., 6: 93-109.
- Nielsen, D. R., Alemi, M. H. 1989. Statistical opportunities for analyzing spatial and temporal heterogeneity of field soils. Plant and Soil, 115: 285-296.
- Nielsen, D.R., Wendroth, O., Pierce, F.J. 1999. Emerging concepts for solving the enigma of precision farm research. In: Robert, P.C., Rust, R.H., Larson, W.E. (Eds.), Proceedings of the Fourth International Conference on Precision Agriculture, ASA-SSSA-CSSA, Madison, WI, USA, p.303-318.
- Nielsen, D.R., Wendroth, O. 2003. Spatial and temporal statistics: sampling field soils and their vegetation. Catena-Verlag, Reiskirchen, Germany, 398 p.
- Plackett, R.L. 1950. Some theorems in least squares. Biometrika, 37: 149-157.
- Pole, A., West, M., Harrison, J. 1994. Applied Bayesian Forecasting and Time Series Analysis. Chapman & Hall, London. 409p.
- Salas, J.D., Delleur, J.W., Yevjevich, V., Lane, W.L. 1988. Applied modeling of hydrologic time series. Water Resources Publications, Littleton, CO., USA.
- Salih, A.A., Babikir, H.M., Ali, S.A.M. 1998. Preliminary observations on affects of tillage systems on soil physical properties, cotton root growth and yield in Gezira Scheme, Sudan. Soil & Tillage Research, 46: 187-191.

- Shumway, R. H. 1988. Applied statistical time series analyses. Prentice Hall, Englewood Cliffs, New York.
- Shumway, R. H. 1985. Time series in soil science: is there life after kriging? **In:** D.R. Nielsen & J. Bouma, eds. Soil spatial variability. Proc. Workshop ISSS/SSSA, Las Vegas, Nev., USA.
- Shumway, R. H., Stoffer, D. S. 1982. An approach to time series smoothing and forecasting using the EM algorithm. *J. Time Ser. Anal.*, 3: 253-264.
- Shumway, R.H., Stoffer, D. S. 2000. Time Series Analysis and Its Applications. New York: Springer, New York, USA.
- Timm, L.C., Fante Junior, L., Barbosa, E.P., Reichardt, K., Bacchi, O.O.S. 2000. A study of the interaction soil – plant using state-space approach. *Scientia Agricola*, 57:751-760.
- Timm, L.C., Reichardt, K., Oliveira, J.C.M., Cassaro, F.A.M., Tominaga, T.T., Bacchi, O.O.S., Dourado-Neto, D., Nielsen, D.R. 2001. State-space approach to evaluate the relation between soil physical and chemical properties. **In:** Joint Meeting of the Czech Society of Soil Science and the Soil Science Society of America and International Conference of the Czech Society of Soil Science. Prague, Czech Republic, September 16-20, 2001.
- Tukey, J.W. 1980. “Can we predict where ‘Time Series’ should go next?”. **In:** Directions in Time Series (eds. D.R. Brillinger & G.C. Tiao), *Inst. Math. Statist.*, Hayward, 1-31.
- Vaughan, M., Vieira, S. R., Bernard, R., Hatfield, J. L. 1982. Spatial variability of surface temperature along two transects of a soil. *Water Resour. Res.*, 18: 1677-1686.
- Vieira, S.R., Nielsen, D.R., Biggar, J.W. 1981. Spatial variability of field-measured infiltration rate. *Soil Sci. Soc. Am. J.*, 45: 1040-1048.
- Wendroth, O.; Al Omran, A. M.; Kirda, K.; Reichardt, K. & Nielsen, D. R. 1992. State-space approach to spatial variability of crop yield. *Soil Sci. Soc. Am. J.*, 56: 801-807.
- Wendroth, O., Katul, G.G., Parlange, M.B., Puente, C.E., Nielsen, D.R. 1993. A nonlinear filtering approach for determining hydraulic conductivity functions. *Soil Sci.*, 156: 293-301.
- Wendroth, O., Reynolds, W. D., Vieira, S. R., Reichardt, K., Wirth, S. 1997. Statistical approaches to the analysis of soil quality data. **In:** Soil quality for crop production and ecosystem health, Gregorich, E.G. & Carter, M. R. (ed.). 448 p.
- Wendroth, O., Jürschik, P., Giebel, A., Nielsen, D.R. 1999. Spatial statistical analysis of on-site-crop yield and soil observations for site-specific management. **In:** Robert, P.C., Rust, R.H., Larson, W.E. (Eds.), Proceedings of the Fourth International Conference on Precision Agriculture, ASA-SSSA-CSSA, Madison, WI, USA, p. 159-170.
- Wendroth, O., Jürschik, P., Kersebaum, K.C., Reuter, H., van Kessel, C., Nielsen, D.R. 2001. Identifying, understanding, and describing spatial processes in agricultural landscapes – four case studies. *Soil & Tillage Research*, 58: 113-127.

- West, M., Harrison, J. 1989. Bayesian Forecasting and Dynamic Models. Springer-Verlag, London, 1^a edição. 704p.
- West, M., Harrison, J. 1997. Bayesian Forecasting and Dynamic Models. Springer-Verlag, London, 2^a edição. 681p.

Dimensional Analysis, Scaling and Fractals

Luís Carlos Timm, Klaus Reichardt¹ and Osny Oliveira Santos Bacchi

Soil Physics Laboratory, CENA, USP, Piracicaba, Brazil

*Lecture given at the
College on Soil Physics
Trieste, 3-21 March 2003*

LNS0418035

¹ klaus@cena.usp.br

Introduction

Dimensional analysis refers to the study of the dimensions that characterize physical entities, like mass, force and energy. Classical mechanics is based on three fundamental entities, with dimensions MLT, the mass M, the length L and the time T. The combination of these entities gives rise to derived entities, like volume, speed and force, of dimensions L^3 , LT^{-1} , MLT^{-2} , respectively. In other areas of physics, four other fundamental entities are defined, among them the temperature θ and the electrical current I.

To introduce the topic of Dimensional Analysis, let us look at a classical example of the romantic literature, in which Dean Swift, in “The Adventures of Gulliver” describes the imaginary voyages of Lemuel Gulliver to the kingdoms of Liliput and Brobdingnag. In these two places life was identical to that of normal humans, their geometric dimensions were, however, different. In Liliput, man, houses, dogs, trees were twelve times smaller than in the country of Gulliver, and in Brobdingnag, everything was twelve times taller. The man of Liliput was a geometric model of Gulliver in a scale 1:12, and that of Brobdingnag a model in a scale of 12:1.

One can come to interesting observations of these two kingdoms through dimensional analysis. Much time before Dean Swift, Galileus already found out that amplified or reduced models of man could not be like we are. The human body is built of columns, stretchers, bones and muscles. The weight of the body that the structure has to support is proportional to its volume, that is, L^3 , and the resistance of a bone to compression or of a muscle for fraction, is proportional to L^2 .

Let's compare Gulliver with the giant of Brobdingnag, which has all of his linear dimensions twelve times larger. The resistance of his legs would be 144 times larger than that of Gulliver, and his weight 1728 times larger. The ratio resistance/weight of the giant would be 12 times less than ours. In order to sustain its own weight, he would have to make an equivalent effort to that we would have to make to carry eleven other men.

Galileus treated this subject very clearly, using arguments that deny the possibility of the existence of giants of normal aspect. If we wanted to have a giant with the same leg/arm proportions of a normal human, we would have to use a stronger and harder material to make the bones, or we would have to admit a lower resistance in comparison to a man of normal stature. On the other hand, if the size of the body would be diminished, the resistance would not diminish in the same proportion. The smaller the body, the greater its relative resistance. In this way, a very small dog could, probably, carry two or three other small dogs of his size on his back; on the other hand, an elephant could not carry even another elephant of his own size!

Let's analyze the problem of the liliputans. The heat that a body loses to the environment goes through the skin, being proportional to the area covered by the skin, that is, L^2 , maintaining constant the body temperature and skin characteristics. This energy comes from the ingestion of food. Therefore, the minimum amount of food to be ingested would be proportional to L^2 . If Gulliver would be happy with a broiler, a bread and a fruit per day, a liliputan would need a $(1/12)^2$ smaller food

volume. But a broiler, a bread, a fruit when reduced to the scale of his world, would have volumes $(1/12)^3$ smaller. He would, therefore, need twelve broilers, twelve breads and twelve fruits to be as happy as Gulliver.

The Liliputans should be famine and restless people. These qualities are found in small mammals, like mice. It is interesting to note that there are not many hot blooded animals smaller than mice, probably in light of the scale laws discussed above. These animals would have to eat such a large quantity of food, that would be difficult to obtain or, that could not be digested over a feasible time.

From all we saw, it is important to recognize that, although being geometric models of our world, Brobdingnag and Liliput could never be our physical models, since they would not have the necessary physical similarity which is found in natural phenomena. In the case of Brobdingnag, for example, the giant would be able to support his own weight having the stature of humans, only if he would be living on a planet having a gravitational force of $(1/12)g$.

Physical Entities and Dimensional Analysis

The parameters that characterize physical phenomena are related among themselves by laws, in general of quantitative nature, in which they appear as measures of the considered physical entities. The measure of an entity is the result of its comparison with another one, of the same type, called unit. In this way, an entity (G) is given by two factors, one being the measure (M) and the other the unit (U). When we write $V = 50 \text{ m}^3$, V is the entity G, 50 is the ratio between the measures (M), and the unit U is m^3 . Therefore:

$$G = M(G) \cdot U(G)$$

$M(G)$ being the measure of G and $U(G)$ the unit of G. In addition, the entity G has a dimensional symbol, which is the combination of the fundamental units that comprise the entity. Some examples are given below:

Entity	Dimensional symbol
Area	L^2
Speed	LT^{-1}
Force	MLT^{-2}
Pressure	$ML^{-1}T^{-2}$
Flow	L^3T^{-1}

The International Units System has seven fundamental entities:

- Mass (M): quilogram (kg);
- Length (L): meter (m);
- Time (T): second (s);
- Electrical current (I): Ampere (A);
- Thermodynamic temperature (θ): Kelvin (K);

- f) Light intensity (Iv): candela (cd);
- g) Quantity of matter (N): mol (mol).

Physical entities are, in general, expressed by a relation involving the entities X, Y, Z, ... which make part of the definition:

$$G = kX^a \cdot Y^b \cdot Z^c \dots$$

where k is a non dimensional constant, and a, b, c, ... are constant exponents.

If, for example, we would have doubts on the formula $F = m \cdot a$, we could make a check but have to admit, at least, that F is a function of m and a:

$$G = kX^a \cdot Y^b \quad \text{or} \quad F = km^a \cdot a^b$$

since F has dimensions MLT^{-2} , the right hand side member must also have dimensions MLT^{-2} , that is:

$$MLT^{-2} = kM^a \cdot (LT^{-2})^b$$

remembering that the dimensions of a are LT^{-2} . Hence, $MLT^{-2} = kM^a \cdot L^b \cdot T^{-2b}$, and we can see that the only possibility is $k = 1$, $a = 1$ and $b = 1$, thus confirming $F = m \cdot a$.

Products of variables P are any products of the variables that involve a phenomenon. The fall of bodies in a vacuum involves the variables space S, acceleration of gravity g and time t, according to:

$$S = \frac{1}{2} g \cdot t^2$$

For this phenomenon we can write an infinite number of products P, as for example:

$$P_1 = S^2 \cdot t^{-2} \cdot g, \text{ with dimensions } L^2 \cdot T^{-2} \cdot L \cdot T^{-2} = L^3 \cdot T^{-5}$$

$$P_2 = S^0 \cdot t^2 \cdot g, \text{ with dimensions } 1 \cdot T^2 \cdot L \cdot T^{-2} = L$$

$$P_3 = S^{-3} \cdot t^4 \cdot g, \text{ with dimensions } L^{-3} \cdot T^4 \cdot L \cdot T^{-2} = L^{-2} \cdot T^2$$

$$P_4 = S^{-2} \cdot t^4 \cdot g^2, \text{ with dimensions } L^{-2} \cdot T^4 \cdot (L \cdot T^{-2})^2 = L^0 \cdot T^0 = 1$$

When a chosen product is non-dimensional, as is P_4 , it is called a non-dimensional product and is symbolized by the Greek letter π , in this case $P_4 = \pi_4$. The Buckingham Pi Theorem states that: "given n dimensional entities G_1, G_2, \dots, G_n generated through products of k fundamental entities, if a phenomenon can be expressed by $F(G_1, G_2, \dots,$

$G_n) = 0$, it can also be fully described by $\phi(\pi_1, \pi_2, \dots, \pi_{n-k}) = 0$, a function with less variables.

The problem mentioned in the introduction about the Kingdoms of Liliput and Brobdingnag, is of physical similarity. Every time we work with models of objects in different scales it is necessary that there is a physical similarity between the model (a prototype, which is generally smaller) and the real object of study. Depending on the case, we talk about kinematic similarity, which involves relations of velocity and acceleration between model and object; or about dynamic similarity, which involves relations between the forces that act on the model and on the object. In the similarity analysis we use the π products, like the known “numbers” of Euler, Reynolds, Froude and Mach. In this analysis we have:

OBJECT:

$$F(G_1, G_2, \dots, G_n) = 0 \longrightarrow \phi(\pi_1, \pi_2, \dots, \pi_{n-k}) = 0$$

PROTOTYPE:

$$F(G'_1, G'_2, \dots, G'_n) = 0 \longrightarrow \phi(\pi'_1, \pi'_2, \dots, \pi'_{n-k}) = 0$$

where the G_i 's can be different from the G'_i 's. There will be physical similarity between object and prototype, only if $\pi_1 = \pi'_1$; $\pi_2 = \pi'_2$; \dots ; $\pi_{n-k} = \pi'_{n-k}$.

Although this analysis is frequently used in hydrodynamics, studies of machines, engineering, etc., it has rarely been applied in soil-plant-atmosphere systems. The study of Shukla et al. (2002) which utilizes the non dimensional products π to describe miscible displacement, is an exception. Texts of Maia (1960), Fox & McDonald (1995) and Carneiro (1996) are good references on this subject.

Non dimensional entities, like the π products, have a numerical value k of dimension 1:

$$M^o L^o T^o K^o = 1$$

It is also common to produce non-dimensional variables through the ratio of two entities G_1 and G_2 of the same dimension: $G_1/G_2 = \pi$. This is the case of the number $\pi = 3.1416\dots$ which is the result of the ratio of the length of any circle (πD , of dimension L) and the respective diameter (D , also dimension L).

In the soil-plant-atmosphere system, several variables are non dimensional by nature (or definition), and are represented in % or parts per million (ppm). Soil water content u (on mass basis), θ (on volume basis), porosities, etc., are examples of π products. The procedure of turning dimensional variables into non dimensional variables is important. The simplest case is dividing the variable by itself, in two different conditions. For instance, in experiments using soil columns, each researcher uses a different column length L . How can we compare results? If the space coordinate x or z (along the column) is divided by its maximum value L , we have a new variable: $X = x/L$, with the advantage that, for any L , at $x = 0$, $X = 0$; at $x = L$, $X = 1$, and varying, therefore, within the interval 0 to 1.

This procedure can also be used for variables which already are dimensionless, like the soil water content θ . If we divide $(\theta - \theta_s)$ by its largest interval $(\theta_o - \theta_s)$, where θ_s and θ_o are, respectively, initial and saturation values, we obtain a new variable $\Theta = (\theta - \theta_s)/(\theta_o - \theta_s)$, for which $\Theta = 0$ for $\theta = \theta_s$ (dry soil) and $\Theta = 1$ for $\theta = \theta_o$ (saturated soil). In this way, for any type of soil, Θ varies from 0 to 1 and comparisons can be made more adequately.

Scales and Scaling

We already mentioned scales when presenting the “Adventures of Gulliver” and discussing physical similarity between object and prototype. Maps are also drawn in scale, for example, in a scale of 1:10,000, 1 cm² of paper can represent 10,000 m² in the field. Entities that differ in scale cannot be compared in a simple way. As we have seen, there is the problem of physical similarity, and hence, how can we make a comparison without changing the scale of each entity? One technique to do this is called “scaling”, frequently used in soil physics. It was introduced into soil science by Miller & Miller (1956) through the concept of similar media applied to “capillary flow” of fluids in porous media. According to these authors, two media M_1 and M_2 are similar when the variables that describe the physical phenomena that occur within them, differ by a linear factor λ , called microscopic characteristic length, which relates their physical characteristics. The best way to visualize this concept is to consider M_2 as an amplified (or reduced) photograph of M_1 by a factor λ . For these media, the particle diameter of one is related to the other by: $D_2 = \lambda D_1$. The surface of this particle by: $S_2 = \lambda^2 S_1$, and its volume by $V_2 = \lambda^3 V_1$ (Figure 1). Under these conditions, if we know the flow of water through M_1 , would it be possible to estimate the flow through M_2 , based only on λ ? Using artificial porous media (glass beads), Klute & Wilkinson (1958) and Wilkinson & Klute (1959) obtained results on water retention and hydraulic conductivity that validated the similar media concept.

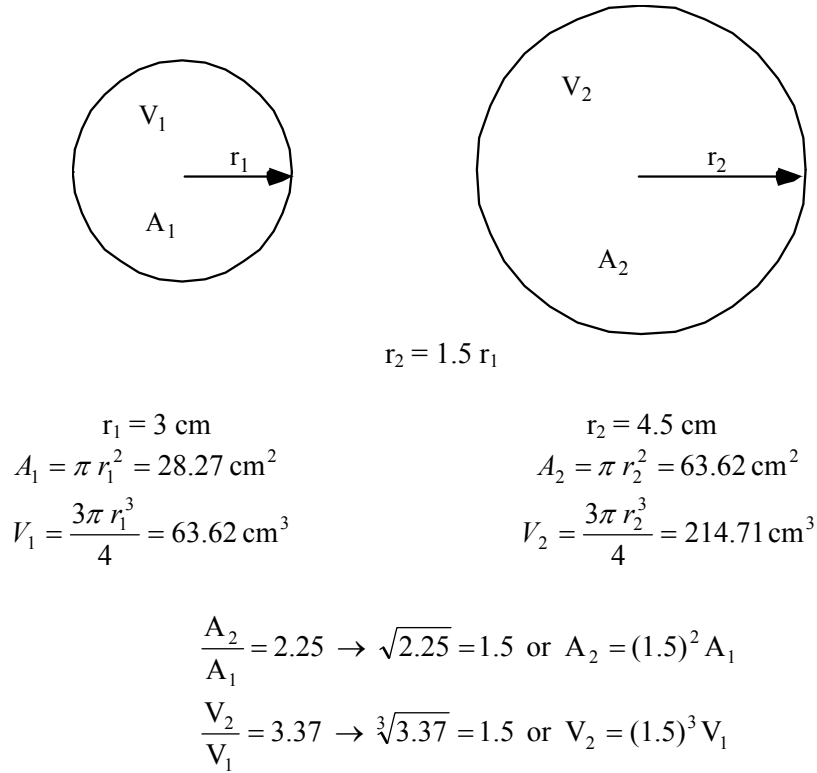


Figure 1 – Spheres seen under the similar media concept.

Subsequent contributions that appeared in the literature did not significantly improve this concept. More than 10 years later, Reichardt et al. (1972) continuing with the subject, had success even with natural porous media, i.e., soils of a wide range in texture. They assumed that soils can be considered similar media, each one characterized by its factor λ which, they initially did not know how to measure. They tested the concept on horizontal soil water infiltration tests, using homogeneous soil columns of initial soil water content θ_i , applying free water at the entrance ($x = 0$) so that at this point the saturation water content θ_0 was maintained thereafter:

$$\theta = \theta_i, \quad x > 0, \quad t = 0 \quad (1)$$

$$\theta = \theta_0, \quad x = 0, \quad t > 0 \quad (2)$$

$$\frac{\partial \theta}{\partial t} = \frac{\partial}{\partial x} \left[D(\theta) \frac{\partial \theta}{\partial x} \right] \quad (3)$$

where $D(\theta) = K(\theta) \cdot dh/d\theta$; $K(\theta)$ is the soil hydraulic conductivity and h the soil water matric potential.

Since for any soil the solution of this boundary value problem is of the same type: $x = \phi(\theta) \cdot t^{1/2}$, in which $\phi(\theta)$ depends on the characteristics of each porous media, would it not be possible to find a generalized solution for all media (considered similar) if λ of each would be known? The procedure they used included the non-dimensionalization of all involved variables, using the similar media theory applied to the i soils, each with its $\lambda_1, \lambda_2, \dots, \lambda_i$. The soil water content θ and the space coordinate x were transformed as indicated above:

$$\Theta = \frac{(\theta - \theta_i)}{(\theta_o - \theta_i)} \quad (4)$$

$$X = \frac{x}{x_{\max}} \quad (5)$$

In relation to the matric soil water potential h , it was considered to be the result of only capillary forces: $h = 2\sigma/\rho g r$ or $hr = 2\sigma/\rho g = \text{constant}$. If each soil I would have only capillaries of radius r_i , and if the characteristic length λ_i would be proportional to r_i , we would have:

$$h_1 r_1 = h_2 r_2 = \dots = h_i r_i = \text{constant}$$

If, among the i soils, we choose one as a standard, for which $\lambda^* = r^* = 1$ (one μm , or any other value), the constant above becomes $h^* r^* = h^*$, which is the matric potential h^* of the standard soil (Figure 2). Through dimensional analysis we can also make h^* non-dimensional:

$$h^* = \frac{\lambda_1 \rho g h_1}{\sigma} = \frac{\lambda_2 \rho g h_2}{\sigma} = \dots = \frac{\lambda_i \rho g h_i}{\sigma} \quad (6)$$

In relation to the hydraulic conductivity K , since it is proportional to the area (λ^2) available for water flow (k = intrinsic permeability, L^2), and using the known relation $K = k\rho g/\eta$ or $K/k = \rho g/\eta = \text{constant}$, we have:

$$\begin{aligned} \frac{K_1}{k_1} &= \frac{K_2}{k_2} = \dots = \frac{K_i}{k_i} = \text{constant} \\ K^* &= \frac{\eta K_1}{\lambda_1^2 \rho g} = \frac{\eta K_2}{\lambda_2^2 \rho g} = \dots = \frac{\eta K_i}{\lambda_i^2 \rho g} \end{aligned} \quad (7)$$

where K^* is the hydraulic conductivity of the standard soil, assuming $\lambda^* = r^* = k^* = 1$ (Figure 3).

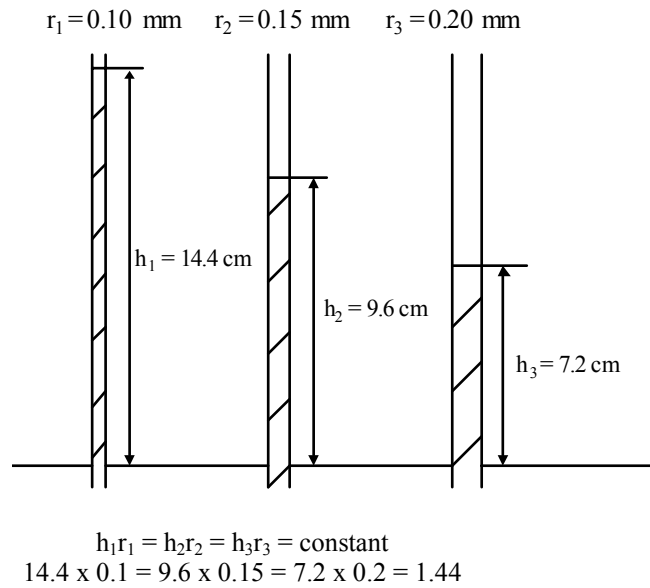
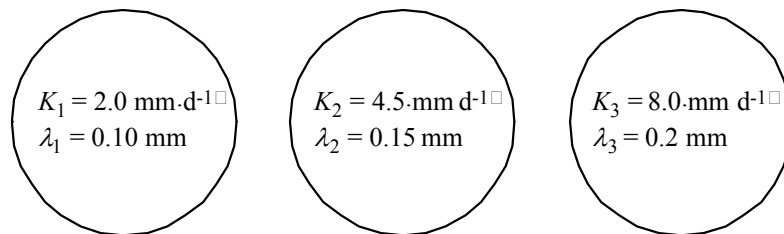


Figure 2 – Similar capillaries in water.



$$\frac{K_1}{\lambda_1^2} = \frac{K_2}{\lambda_2^2} = \frac{K_3}{\lambda_3^2} = \text{constant}$$

$$\frac{2}{(0.10)^2} = \frac{4.5}{(0.15)^2} = \frac{8}{(0.20)^2} = 200$$

Figure 3 – Cross-sections of soil columns with their respective conductivities.

Through the definition of $D = K.dh/d\theta$, it is possible to verify that the soil water diffusivity D^* is given by:

$$D^* = \frac{\eta D_1}{\lambda_1 \sigma} = \frac{\eta D_2}{\lambda_2 \sigma} = \dots = \frac{\eta D_i}{\lambda_i \sigma} \quad (8)$$

To make equation 3 dimensionless it is now needed to make the time t dimensionless. In accordance to all other variables, we can have a time t^* for the standard soil, as follows:

$$t^* = \frac{\lambda_1 \sigma t_1}{\eta (x_{1\max})^2} = \frac{\lambda_2 \sigma t_2}{\eta (x_{2\max})^2} = \dots = \frac{\lambda_i \sigma t_i}{\eta (x_{i\max})^2} \quad (9)$$

It can now be seen that if we substitute θ by Θ , x by X , t by t_i and D by D_i in equation (3), we obtain the differential equation for the standard soil, which differs from the equations of all other soils only by factors λ_i , not seen in equation (10), but built-in the definitions of t^* and D^* :

$$\frac{\partial \Theta}{\partial t^*} = \frac{\partial}{\partial X} \left[D^*(\Theta) \frac{\partial \Theta}{\partial X} \right] \quad (10)$$

subject to conditions:

$$\Theta = 0, \quad X \geq 0, \quad t^* = 0 \quad (11)$$

$$\Theta = 1, \quad X = 0, \quad t^* > 0 \quad (12)$$

with a solution of the form:

$$X = \phi^*(\Theta) \cdot (t^*)^{1/2} \quad (13)$$

It is interesting to analyze equation (9), of the non dimensional infiltration time t^* , in light of the physical similarity of the kingdoms of Liliput and Brobdingnag, which shows that to compare different soils (considered similar media), their times have to be different and dependent of λ which is a length! We could even suggest that this fact contributes to explain how the time t is considered the fourth coordinate, together with x , y and z , in modern physics.

By analogy with what was made with h and K , we can write:

$$t_1 \lambda_1 = t_2 \lambda_2 = \dots = t_i \lambda_i = \frac{t^* \eta (x_{\max})^2}{\sigma} = \text{constant}$$

Once the theory was established, Reichardt et al. (1972) looked for ways to measure λ for the different soils. They were surprised when they realized that if the linear regressions of x_i versus $t_i^{1/2}$ for the position of the wetting front for each soil, should overlap to one single curve for the standard soil (X versus $t^{*1/2}$), and that the factors used to rotate the line of each soil to the position of the line of the standard soil, could be used as characteristic lengths λ_i . We know that straight lines passing through the origin: $y = a_i x$ can be rotated over each other using the relation a_i/a_j of their slopes. Since in our case the lines involve a square root, the relation to be used is:

$$\frac{\lambda_i}{\lambda^*} = \left(\frac{a_i}{a^*} \right)^2 \quad (14)$$

With this relation Reichardt et al. (1972) found the values λ_i for each soil, taking arbitrarily as a standard the soil of fastest infiltration, for which they postulated $\lambda^* = 1$. In this way, the slower the infiltration rate of soil i , the slower its λ_i . This way of determining λ as a scaling factor and not as a physical soil characteristic like the microscopic characteristic length of Miller & Miller (1956), facilitated the experimental part of the study and, more than that, opened the door for a much wider concept of scaling applied in other areas of soil physics. Because soils are truly not similar media, Reichardt et al. (1972) had success scaling $D(\theta)$, but only a partial success scaling $h(\theta)$ and $K(\theta)$. The success of scaling $D(\theta)$ lead Reichardt & Libardi (1973) to establish a general equation to estimate $D(\theta)$ of a given soil, by measuring only the slope a_i of the wetting front advance x versus $t^{1/2}$:

$$D(\Theta) = 1.462 \cdot 10^{-5} a_i^2 \exp(8.087\Theta) \quad (15)$$

Reichardt et al. (1975) also presented a method to estimate $K(\Theta)$ through a_i ; Bacchi & Reichardt (1988) used scaling techniques to evaluate $K(\theta)$ measurement methods, and Shukla et al. (2002) used scaling to analyze miscible displacement experiments. Scaling has also widely been used in studies of soil spatial distribution, assuming characteristic values of λ for each point of a transect, making particular curves to coalesce into a single one. An excellent review of scaling was made by Tillotson & Nielsen (1984), and, more recently, by Kutilek & Nielsen (1994) and Nielsen et al. (1998).

Fractals and Fractal Geometry

Fractal geometry, in contrast to the Euclidean geometry, admits fractional dimensions. The term fractal is defined in Mandelbrot (1982) as coming from the Latin *fractus*, derived from *frangere* which signifies to break, to form irregular fragments. The term fractal is opposite to the term algebra (from the Arabic: *jabara*) which means to join, to put together the parts. For Mandelbrot, fractals are non

topologic objects, that is, objects which have as their dimension a real, non integer number, which exceeds the topologic dimension. For the topologic objects, or Euclidean forms, the dimension is an integer (0 for the point, 1 for a line, 2 for a surface, and 3 for a volume). The fractal dimension of Mandelbrot is a measure of the degree of irregularity of the object under consideration. It is related to the “speed” by which the estimate of the measure of an object increases as the measurement scale decreases. An object normally taken as uni-dimensional, like a piece of a straight line, can be divided into N identical parts, so that each part is a new straight line segment represented in a scale $r = 1/N$ of the original segment. Therefore, $Nr^1 = 1$.

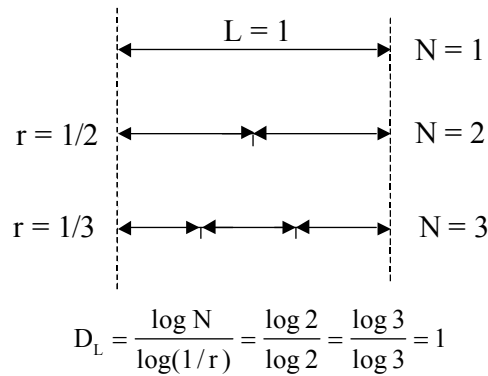


Figure 4 – Generalization of the relation $N \cdot r^D = 1$, for the case $D=1$, i.e., $N \cdot r^1 = 1$

In a similar way, a bi-dimensional object like a square, can be divided into N identical squares of scale $r = 1/\sqrt{N}$ of the original area, so that $N \cdot r^2 = 1$ (see Figure 5). For a cube we can write $N \cdot r^3 = 1$, and for any dimension D we can say that $N \cdot r^D = 1$ (see Figure 6).

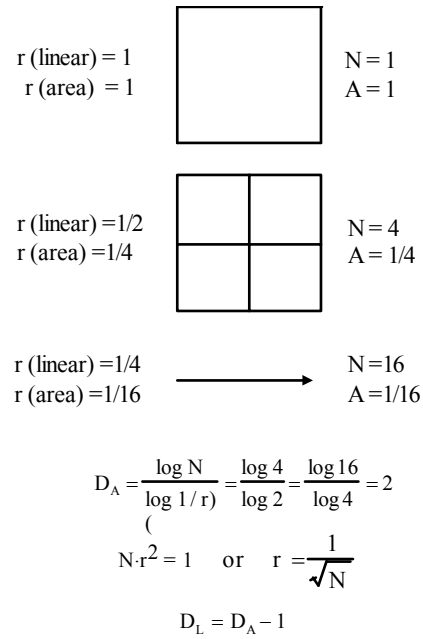


Figure 5 – Bi-dimensional objects

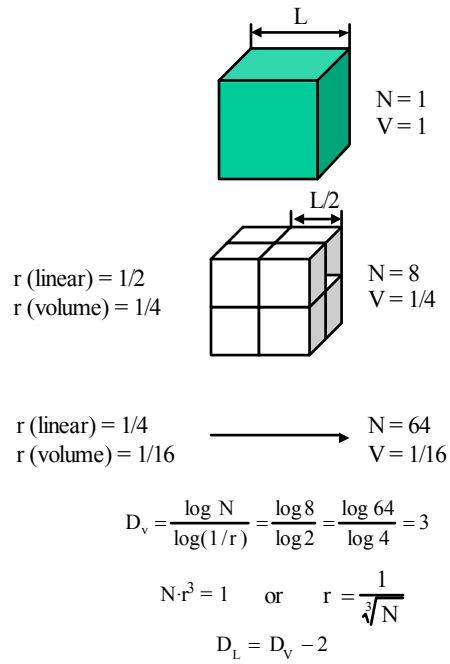
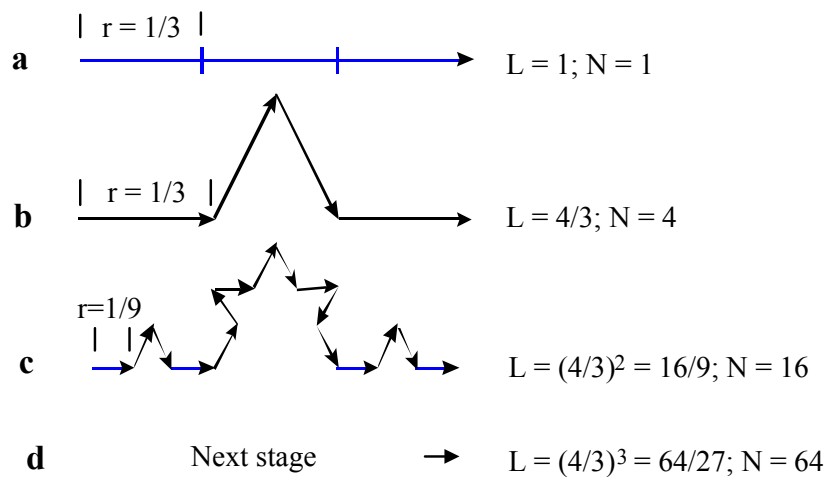


Figure 6 – Tri-dimensional objects

Therefore, the Euclidean dimensions 0, 1, 2 and 3, can be seen as particular cases of a variety of forms and dimensions found in nature. Figure 7, adapted from Barnsley et al. (1988), known as the curve of von Koch, is considered in an interactive or recursive way, starting from a segment (a), divided in 3 equal parts, where the central one is substituted by 2 segments forming an equilateral triangle (b). In the next step, each of the 4 segments is again divided in 3 parts, the central one replaced by two, and so on. After stage (b), in each change of stage, the total length L of the figure increases by a factor $4/3$, the number N of similar elements increases by a factor 4, and its dimensions are in a scale $r = 1/3$ of the previous stage. At each stage the figure can be divided into N similar segments, so that $N \cdot r^D = 1$, D being the fractal dimension of the object. In this case, $D = 1.26$, which is larger than 1 and smaller than 2, indicating that Koch's curve covers a greater space than a simple line ($D = 1$), and less area than an Euclidean area ($D = 2$).

Very complex and irregular forms and structures found in nature can be reproduced in much detail through similar procedures using fractal dimensions, indicating that behind of an apparent disorder of these forms, structures and dynamic processes, there is some regularity that can be better understood. During the last two decades, scientists of several fields like physics, astronomy and biology, have been developing a new approach to deal with the complexity of nature, called the "Theory of Chaos", which mathematically defines the casually generated by simple deterministic dynamic systems. This approach allows the description of a certain degree of order in dynamic processes that in the past were seen as completely random.

With the indispensable aid of computers, fractal geometry is developing very fast in several areas of knowledge, including arts, as a new tool to better understand nature. In agronomic research it is used to study the dynamic processes that occur in soils (water, solute, heat and gas movements), soil structure, plant architecture and development, drainage of watersheds, etc.



Solving $(N \cdot r^D = 1)$ for D we have: \square

$$D = \frac{\log N \square}{\log(1/r) \square} = \frac{\log 4 \square}{\log 3 \square} = \frac{\log 16 \square}{\log 9 \square} = \frac{\log 64 \square}{\log 27 \square} = 1.26$$

Figure 7. von Koch's curve

Figure 8, extracted from Barnsley et al. (1988), shows a graphic computational image, generated through iterative function systems (IFS), which simulates a plant in a very realistic form. The possibilities of object simulation are enormous, being widely used for morphological and functional characterization of these objects.

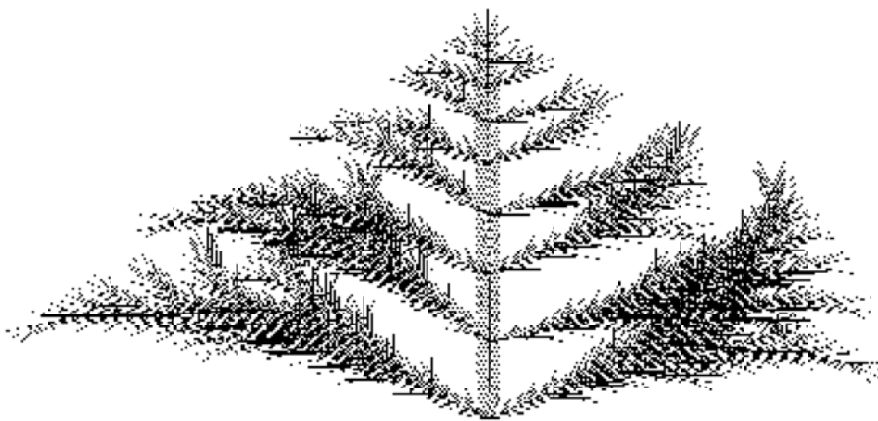


Figure 8 – Plant image simulation through graphic computation, using the iterative function system (IFS), adapted from Barnsley et al. (1988)

Fractal models that simulate soil structure (Figure 9) are also used to better understand soil behavior. The fractal characteristic of several soil attributes has led to the use of these new technologies in substitution to several empirical procedures.

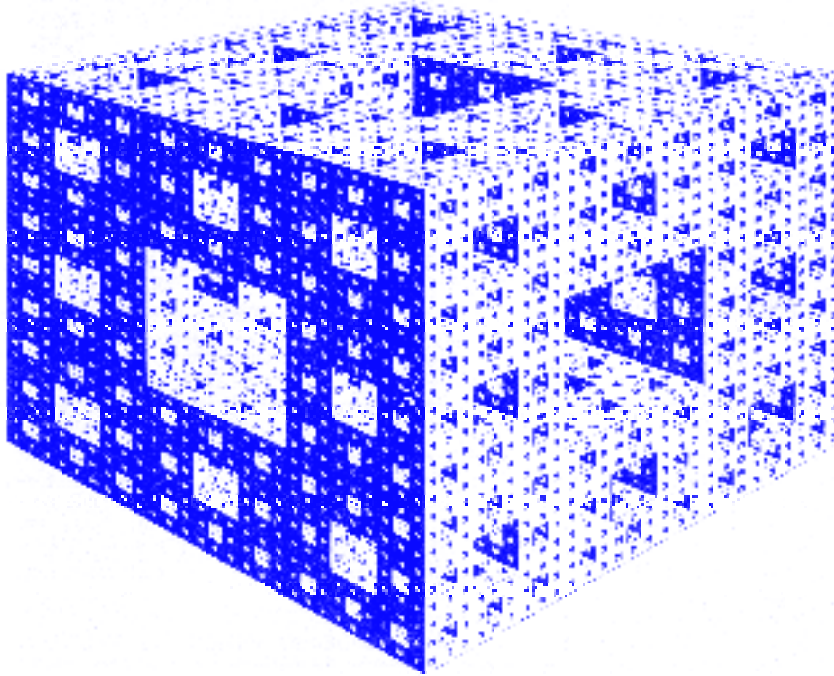


Figure 9 – Soil matrix simulations

Let's now clarify in more detail what was said about Figures 4 to 7. When measuring a length L , which can be a straight line segment, a curve or the contour line of a map, we use as unit a linear ruler of "size" ϵ , smaller than L . If ϵ fits N times into L , we have

$$L(r) = N(r) r$$

where $r = (\epsilon / L)$. We write $L(r)$ since it is a tortuous length L measured with a straight ruler and, therefore, the measure depends on the size of the ruler, since arcs or curves are measured linearly. The smaller the ruler, the better the measure. In Figure 4, L is a straight line, and nothing is lost by tortuosity. For the first case $L=1$, $N=1$ and $r=1$, the ruler is the length to be measured. If the ruler is half of L , we have $N=2$ and $r=1/2$. If the ruler is one third of L , $N=3$ and $r=1/3$. In a general way:

$$N \cdot r^D = 1 \quad \text{or} \quad N = r^{-D} \quad (16)$$

where D is the geometric dimension [$D=1$ (line); $D=2$ (plane); $D=3$ (volume)]. Applying logarithm to both members of equation (16), we have:

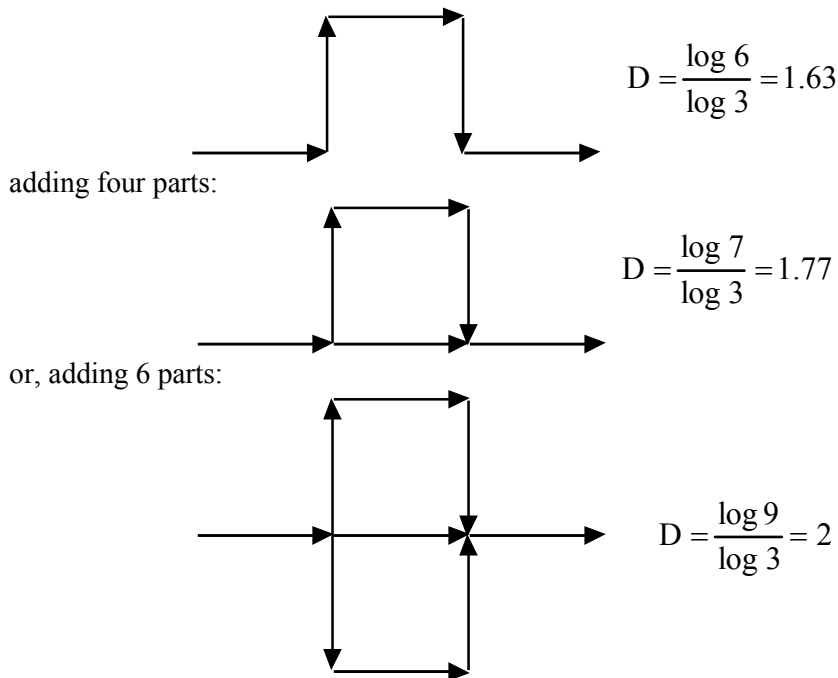
$$\log N = -D \cdot \log r \quad \text{or} \quad \log N = D \cdot \log (1/r)$$

Hence,

$$D = \frac{\log N}{\log(1/r)} \quad (17)$$

In Figure 4 we use the symbol D_L for the linear dimension, and it can be seen, through equation (17) that for a linear measurement $D_L = 1$, in agreement with the Euclidean geometry. Figure 5 presents bi-dimensional objects, for which the Euclidean dimension $D_A = 2$, and $D_A = (D_L - 1)$. For tri-dimensional objects, $D_V = 3$, and $D_L = (D_V - 2)$ (See Figure 6). Equation (16) also allows fractional dimensions. In Figure 7, the tortuosity is shown in a progressive way, in a) a basic length L_0 is given; in b) one third of L_0 is added in such a way that it fits in the same space, as shown. If the ruler is L_0 , it does not measure L , which is $4/3 L_0$. In c) for each part of b, the same procedure is repeated in each part, yielding $L_2 = 16/9 L_0$. From equation (17), the dimension of this example is $D = 1.26$, greater than 1 and less than 2. It is not a straight line, nor an area, it is a “tortuous line”.

In Figure 7, if we add two parts, we have:



and $D = D_A = 2$, which means that the tortuosity is so large that the curve tends to an area !

In Soil Physics, since the pathway of water, ions and gases; the particle distribution and the pore distribution, are all tortuous, the fractal concepts might be a good choice for modeling. Tyler & Wheatcraft (1989) recognized the difficulty of measuring the number of particles N and replaced this by the mass of particles, in a non-dimensional form $M(R < R_i)/M_t$. Radia were also transformed to become non-dimensional: R_i/R_t .

Bacchi & Reichardt (1993) used these concepts to model soil water retention curves, estimating pore length L_i which correspond to a given texture class, using the empirical expression of Arya & Paris (1981): $L_i = 2R_i N_i^\alpha$, where $2R_i$ is the diameter of the particles within class i , and N_i the number of particles of the same class. They did not have success, and this theme is open for further research. Bacchi et al. (1996) compared the use of particle or pore distributions to estimate D_v , and studied their effects on hydraulic conductivity data. Other important contributions are those of Guerrini (1992, 2000), which applied fractal concepts with success in agronomy. As a basic text we recommend Mandelbrot (1982) and besides the cited papers, Puckett et al. (1985), Turcotte (1986), Tyler & Wheatcraft (1990, 1992), Guerrini & Swartzendruber (1994, 1997) and Perfect & Kay (1995), are interesting papers.

References

- Arya, L.M., Paris, J.F. 1981. A physicoempirical model to predict the soil moisture characteristic from particle-size distribution and bulk density data. *Soil Sci. Soc. Am. J.* 45: 1023-1030.
- Bacchi, O.O.S., Reichardt, K. 1988. Escalonamento de propriedades hídricas na avaliação de métodos de determinação da condutividade hidráulica. *Revista Brasileira de Ciência do Solo* 12 (3):217-223.
- Bacchi, O.O.S., Reichardt, K. 1993. Geometria fractal em física de solo. *Scientia Agricola*, 50 (2): 321-325.
- Bacchi, O.O.S., Reichardt, K., Villa Nova, N.A. 1996. Fractal scaling of particle and pore size distributions and its relation to soil hydraulic conductivity. *Scientia Agricola*, 53: 356-361.
- Barnsley, M.F., Devaney, R.L., Mandelbrot, B.B., Peitgen, H.O., Saupe, D., Voss, R.F. 1988. The science of fractal images. New York: Springer-Verlag, 312 p.
- Carneiro, F.L. 1996. Análise dimensional e teoria da semelhança e dos modelos físicos. 2. ed. Rio de Janeiro: Editora Universidade Federal do Rio de Janeiro, 258 p.
- Fox, R.W., McDonald, A.T. 1995. Introdução à mecânica dos fluídos. 4. ed. Rio de Janeiro: Editora Guanabara Koogan S.A., 662 p.
- Guerrini, I.A. 2000. Caos e fractais: apostila didática. 4. ed. Botucatu: UNESP, 86 p.
- Guerrini, I.A. 1992. Uma abordagem não-convencional para a infiltração da água no solo. Botucatu, 158 p. Tese (Livre-Docência) – Instituto de Biociências, Universidade de São Paulo.

- Guerrini, I.A., Swartzendruber, D. 1994. Fractal characteristics of the horizontal movement of water in soil. *Fractal*, 2 (3): 465-468.
- Guerrini, I.A., Swartzendruber, D. 1997. Fractal concepts in relation to soil-water diffusivity. *Soil Sci.* 162 (11): 778-784.
- Klute, A., Wilkinson, G.E. 1958. Some tests of the similar media concept of capillary flow: I. Reduced capillary conductivity and moisture characteristic data. *Soil Sci. Soc. Am. Proc.* 22: 278-281.
- Kutilek, M., Nielsen, D.R. *Soil hydrology*. 1994. Cremlingen-Destedt: Catena Verlag, 370 p.
- Maia, L.P.M. 1960. *Análise dimensional*. Rio de Janeiro: Editora Nacionalista, 110 p.
- Mandelbrot, B.B. 1982. *The fractal geometry of nature*. New York: W.H. Freeman and Company, 468 p.
- Miller, E.E., Miller, R.D. 1956. Physical theory of capillary flow phenomena. *J. Appl. Physics*, 27: 324-332.
- Nielsen, D.R., Hopmans, J., Reichardt, K. 1998. An emerging technology for scaling field soil water behavior. In: Sposito, G. (ed.). *Scale dependence and scale invariance in hydrology*. 1. ed. New York: Cambridge University Press, p. 136-166.
- Perfect, E., Kay, B.D. 1995. Applications of fractals in soil and tillage research: a review. *Soil & Tillage Research*, 36: 1-20.
- Puckett, W.E., Dane, J.H., Hajek, B.F. 1985. Physical and mineralogical data to determine soil hydraulic properties. *Soil Sci. Soc. Am. J.* 49 (4): 831-836.
- Reichardt, K., Libardi, P.L., Nielsen, D.R. 1975. Unsaturated hydraulic conductivity determination by a scaling technique. *Soil Science*, 120 (3):165-168.
- Reichardt, K., Libardi, P.L. 1973. A new equation for the estimation of soil water diffusivity. In: *FAO/IAEA Symposium on Isotopes and Radiation Techniques in Studies of Soil Physics, Irrigation and Drainage in Relation to Crop Production*. Vienna, Austria, p. 45-51.
- Reichardt, K., Nielsen, D.R., Biggar, J.W. 1972. Scaling of horizontal infiltration into homogeneous soils. *Soil Sci. Soc. Am. Proc.*, 36: 241-245.
- Shukla, M.K., Kastanek, F.J., Nielsen, D.R. 2002. Inspectional analysis of convective-dispersion equation and application on measured break-through curves. *Soil Sci. Soc. Am. J.* 66, (4): 1087-1094.
- Tillotson, P.M., Nielsen, D.R. 1984. Scale factors in soil science. *Soil Sci. Soc. Am. J.* 48: 953-959.
- Turcotte, D.L. 1986. Fractals and fragmentation. *J. of Geophys. Res.*, 91: 1921-1926.
- Tyler, W.S., Wheatcraft, S.W. 1989. Application of fractal mathematics to soil water retention estimation. *Soil Sci. Soc. Am. Journal*, 53: 987-996.
- Tyler, W.S., Wheatcraft, S.W. 1990. Fractal Processes in soil water retention. *Water Resources Research*, 26 (5): 1047-1054.
- Tyler, W.S., Wheatcraft, S.W. 1992. Fractal Scaling of Soil Particle-Size Distributions: Analysis and Limitations, *Soil Sci. Soc. Am. J.*, 56: 362-369.
- Wilkinson, G.E., Klute, A. 1959. Some tests of the similar media concept of capillary flow: II. Flow systems data. *Soil Sci. Soc. Am. Proc.*, 23: 434-437.

Use of a Combined Penetrometer-TDR Moisture Probe for Soil Compaction Studies

Carlos Manoel Pedro Vaz¹

Embrapa Agricultural Instrumentation, São Carlos, Brazil

*Lecture given at the
College on Soil Physics
Trieste, 3-21 March 2003*

LNS0418036

¹ vaz@cnpdia.embrapa.br

Introduction

Soil mechanical strength is an important soil parameter that affects root growth and water movement, and controls nutrient and contaminant transport below the rooting zone. The most common way to assess soil strength is by using a soil penetrometer, which characterizes the force needed to drive a cone of specific size into the soil (Bradford, 1986). The measured penetration resistance (PR) depends on such soil properties as bulk density, water content and potential, texture, aggregation, cementation and mineralogy.

Soil scientists have related changes in PR as caused by tillage, traffic or soil genetic pans to root growth, crop yields and soil physical properties. For example, correlation between PR and crop root growth and water and nutrient exploration have been obtained (Stelluti et al. 1998), and cone penetrometers have been used extensively in soil science studies to identify natural and induced compacted layers (Henderson, 1989) or to predict related soil properties (Ayers and Bowen, 1987).

Many studies have been conducted to understand the influence of bulk density (ρ) and water content (θ) on PR in the laboratory (Taylor and Gardner, 1963; Mirreh and Ketcheson, 1972; Ayers and Perumpal, 1982; Ayers and Bowen, 1987; Ohu et al. 1988) and field (Simmons and Cassel, 1989; Vasquez et al. 1991, Busscher et al. 1997), from which both empirical and theoretical relationships were obtained. From the many different models that have been introduced to test these relationships (polynomial, exponential, power and linear equations), Busscher et al. (1997) suggested that either the power or exponential equations are the most adequate. Using dimensional analysis techniques, Upadhyaya et al. (1982) suggested a power-exponential equation for prediction of the PR as a function of ρ and θ for a silt loam soil, but also suggested additional experimental work for its validation.

However, many referenced studies lack accurate and representative data, because PR is a highly variable soil property, whereas it is usually determined from local small-scale measurements. Hence, difficulties in relating PR with other soil parameters can be attributed mostly to soil spatial variability, because available measurement techniques prevent determination of the different soil attributes (PR, ρ , θ , organic matter, texture) at the same spatial location.

To improve on the measurement technique, we have developed a combined cone penetrometer-TDR moisture probe by wrapping two TDR wires around the penetrometer rod (combined rod TDR) as a double helix, so that both soil water content and penetration resistance can be measured simultaneously and at approximately the same location within the soil profile (Vaz and Hopmans, 2001). The main advantage of the coiled design is that relative long travel times can be obtained, allowing accurate water content measurements for small-sized TDR probes.

The objective of this lecture is to present the combined penetrometer-TDR probe as a new tool to study soil compaction. The presentation will cover the following topics:

- Theory of the dynamic cone penetrometer;
- Laboratory calibration of a coiled TDR moisture probe and application of the mixing model;
- Field calibration and use of the combined penetrometer-coiled TDR moisture probe;
- Penetration resistance, bulk density, water content and potential relationships;
- Practical applications of the combined penetrometer-coiled TDR moisture probe.

Coiled TDR probe design

The basic configuration of the combined penetrometer coiled TDR moisture probe is shown in Figure 1. The coiled TDR probe consists of 2 parallel copper wires (ground and conductor wire), each 0.8 mm diameter and 30 cm long, coiled around a 5 cm long PVC core, with a 3 mm separation distance between the two wires. The coil is constructed at the bottom of the penetrometer rod, immediately above the cone of the penetrometer. A 2.5 m long 50 Ω coaxial cable is passed through the hollow steel shaft of the penetrometer probe and connected to a cable tester (Tektronix 1502C).

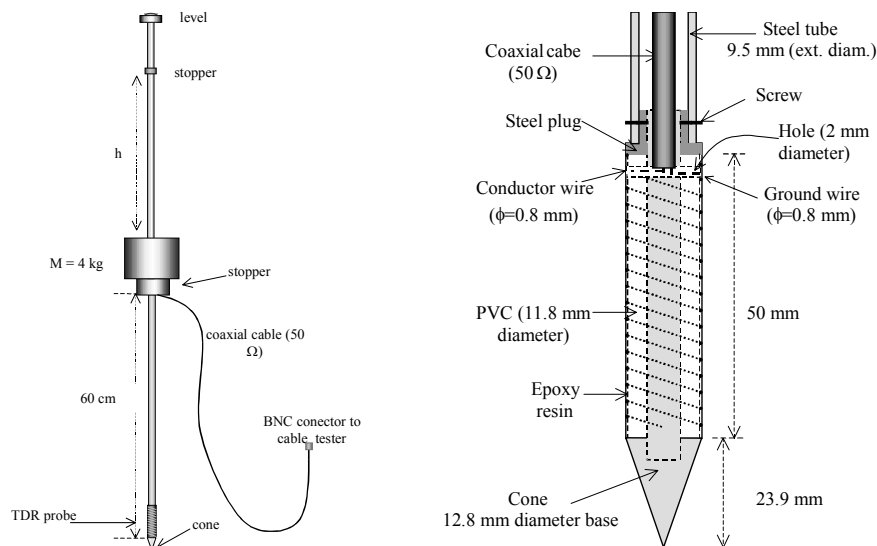


Figure 1. Combined penetrometer – coiled TDR moisture probe.

Laboratory calibration

The waveform or trace is transferred from the cable tester to a personal computer through the RS232 serial port and analyzed. The trace (Figure 2) is a visualization of the amplitude of a reflected pulsed electromagnetic wave as a function of propagation or travel time along the TDR probe. The trace can be

regarded as a signature of the physical status of the soil, and it can be shown that knowledge of the travel time is sufficient to determine the bulk material dielectric constant of the soil (Topp et al., 1980).

Using a mixing model approach, the dielectric constant measured by the coiled TDR probe (ϵ_{coil}) can be related to the soil dielectric constant as determined by the conventional probe (ϵ_{soil}):

$$\epsilon_{\text{coil}} = \left[w \epsilon_{\text{probe}}^n + (1 - w) \epsilon_{\text{soil}}^n \right]^{1/n} \quad [1]$$

In Eq. [1], w is a weighting factor that partitions the measured dielectric by the coiled TDR probe between contributions by the epoxy and PVC of the probe (ϵ_{probe}) and the bulk soil (ϵ_{soil}) and the parameter n defines the probe's geometry and ϵ_{probe} is the dielectric constant of the PVC and epoxy material in which the wire coils are imbedded. The dielectric constant of the soil (ϵ_{soil}) as determined by a conventional probe is written in terms of the fractional bulk volume of each of the 3 soil phases ($1-\phi$, $\phi-\theta$, and θ , for the solid, gas and water phase, respectively). Hence,

$$\epsilon_{\text{soil}} = \left[(1 - \phi) \epsilon_s^\alpha + (\phi - \theta) \epsilon_a^\alpha + \theta \epsilon_w^\alpha \right]^{1/\alpha} \quad [2]$$

where ϕ ($\text{cm}^3 \text{cm}^{-3}$) and θ ($\text{cm}^3 \text{cm}^{-3}$) denote the soil porosity and volumetric water content, respectively, and ϵ_s , ϵ_a and ϵ_w are the dielectric constant of the soil solid material, air and water, respectively, with assumed values of $\epsilon_a = 1.0$; $\epsilon_w = 80$ and $\epsilon_s = 3.9$ (Dasberg and Hopmans, 1992).

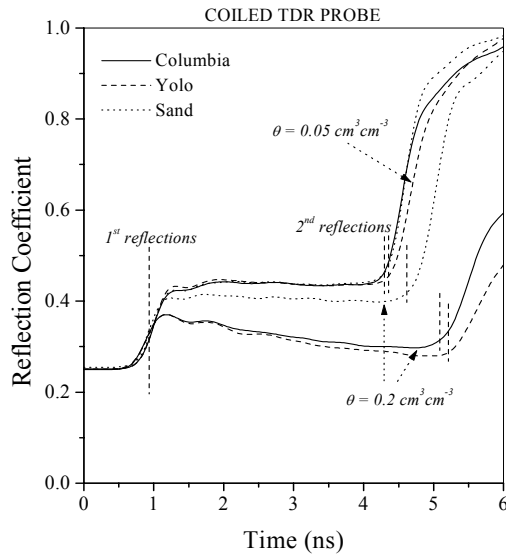


Figure 2. Waveforms for the coiled TDR probe designs for three soils at water contents values of 0.05 and 0.20 $\text{cm}^3 \text{cm}^{-3}$.

The ϵ_s -value varies slightly with mineralogical composition of the soil solid material (Yu et al. 1999). For instance, the dielectric constant of quartz can vary between 3.75 and 4.1 (Lide, 1996), whereas an aluminum silicate has a dielectric constant of 4.8 (Fink, 1978). Also, the presence of organic matter increases the dielectric constant of organic soils to values as high as 5.0. For the mineral soils studied here, an ϵ_s -value of 3.9 appears to be a good estimation for the investigated mineral soils. The exponent α depends on the geometry of the soil solid phase and the soil's orientation with respect to the applied electric field and must be $-1 < \alpha < 1$ (Roth et al. 1990).

After substitution of Eq. [2] into [1], the dielectric constant as measured with the coiled TDR probe (ϵ_{coil}) can be written as:

$$\epsilon_{\text{coil}} = \left\{ w \epsilon_{\text{probe}}^n + (1 - w) \left[(1 - \phi) \epsilon_s^\alpha + (\phi - \theta) \epsilon_a^\alpha + \theta \epsilon_w^\alpha \right]^{n/\alpha} \right\}^{1/n} \quad [3]$$

The presented mixing model approach is preferred to allow for a meaningful physical interpretation of the calibration results (Roth et al., 1990), rather than the model fitting of an arbitrary empirical functional relationship. Moreover, the application of Eq. [3] inherently corrects for the influence of bulk soil density on the bulk soil dielectric constant. Alternatively, one can simply use a polynomial to substitute for Eq. [3], writing ϵ_{coil} as a function of water content, and fit the data to estimate the regression coefficients as was done in Topp et al. (1980), and later for the field calibration results.

The calibration data of the coiled TDR probe for three soils are presented in Figure 3. Calibration curves (lines in Figure 3) for the coiled probe were obtained substituting the fitted parameters n , w and α in Eq. [3] and using average values of bulk density and porosity.

Influence of soil water content and bulk density on penetration resistance

The combined penetrometer-cone TDR data are averaged and presented in Figure 5 for both the dry and wet soil treatments. PR is presented as a function of θ , with different symbols indicating ranges in magnitude of depth-averaged dry bulk soil density (ρ). As expected, there is a tendency of PR to increase as ρ increases at equal θ values. Moreover, the fitted curves demonstrate the intuitive-correct results that (1) the bulk density effect on PR decreases as the water content increases and (2) PR increases exponentially with decreasing water content.

Depth distribution of penetration resistance (a) and volumetric water content (b) as determined from measurements with the combined penetrometer-coiled cone TDR probe are presented in Figure 4 for a dry (before irrigation) and wet soil condition.

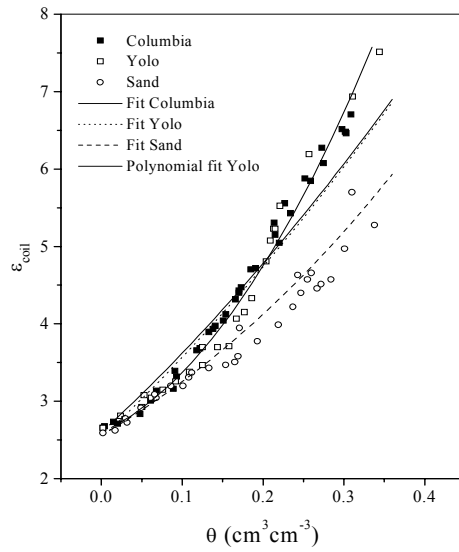


Figure 3. Calibration data for the coiled TDR probe using Eq. [3] for 3 soils, using parameters n , w , ϵ_{probe} fitted to Eq. [1] and soil specific α -values fitted to Eq. [2].

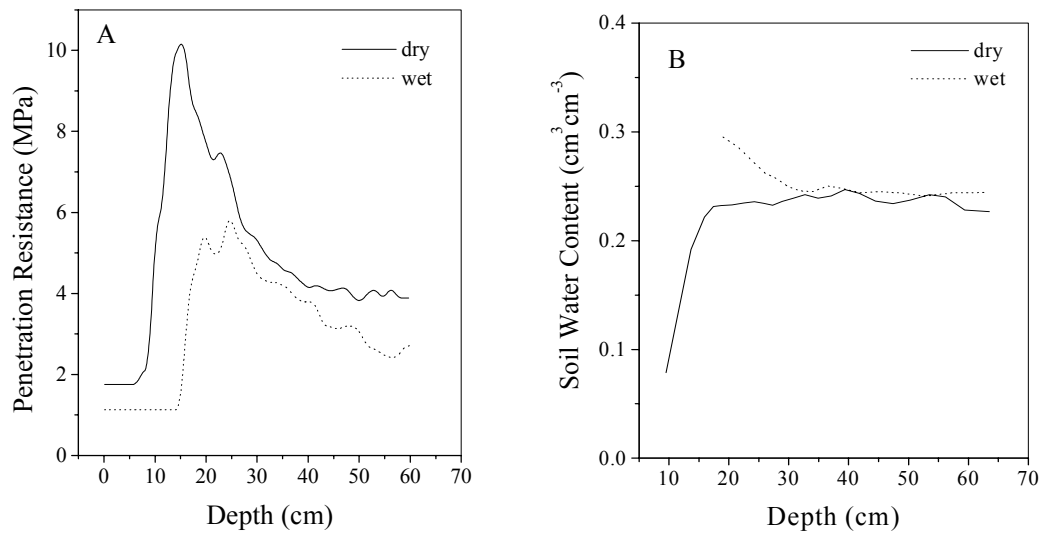


Figure 4. Combined field measurement results of penetration resistance (PR) and water content (θ) obtained with the combined coiled TDR-cone penetrometer probe

Using the model-fitting software of Wraith and Or (1998), the PR, θ , and ρ data in Figure 5 were fitted to Equation [3], yielding soil-specific parameter values of $a = 170.15$, $n = 3.22$, and $b = 5.99$, and a r^2 -value of 0.72 and RMSE = 0.98. We conclude that Eq. [3] of Upadhyaya et al. (1982) described the experimental data fairly well within the water content range of $0.15 - 0.30 \text{ cm}^3 \text{ cm}^{-3}$. Scattering of data

presented in Figure 5 was caused by a combination of factors such as the relatively narrow range of water content; different sampling locations of combined probe

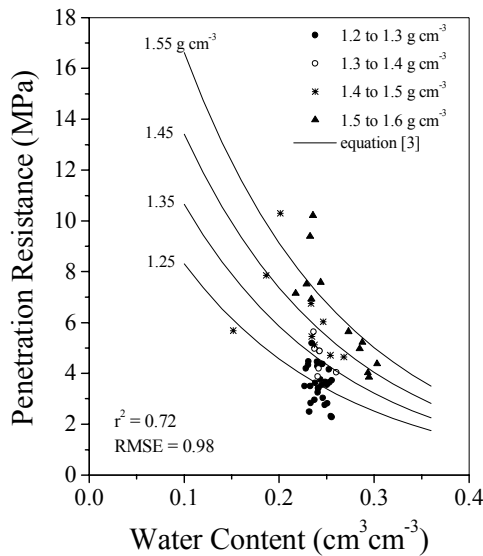


Figure 5. Correlation between water content measured by the coiled TDR probe (ϵ_{coil}) and gravimetric data from collected soil cores

References

- Ayers, P.D. and J.V. Perumpral. 1982. Moisture and density effects on cone index. *ASAE Trans.*, 25(5):1169-1172.
- Ayers, P.D., H.D. Bowen. 1987. Predicting soil density using cone penetration resistance and moisture profile. *ASAE Trans.*, 30: 1331-1336.
- Bradford, J. L. 1986. Penetrability. In: *Methods of Soil Analysis*, Madison, ASA-SSSA Inc. Publisher, 463-477.
- Busscher, W.J., P.J. Bauer, C.R. Camp, R.E. Sojka. 1997. Correction of cone index for soil water content differences in a coastal plain soil. *Soil Till. Res.*, 43:205-217.
- Dasberg, S., J.W. Hopmans. 1992. Time domain reflectometry calibration for uniformly and nonuniformly wetted sandy and clayey loam soils. *Soil Sci. Soc. Am. J.*, 56:1341-1345.
- Fink, D.G. 1978. *Standard handbook for electrical engineers*. 11th Edition. Mc Graw Hill Inc.
- Henderson, C.W.L. 1989. Using a penetrometer to predict the effects of soil compaction on the growth and yield of wheat on uniform, sandy soils. *Aust. J. Agric. Res.*, 40:498-508.
- Lide, D.R. 1996. *CRC Handbook of Chemistry and Physics*. 77th Edition, CRC Press Inc.
- Mirreh, H.F., J.W. Ketcheson. 1972. Influence of bulk density and matric pressure to soil resistance to penetration. *Can. J. Soil Sci.* 52:477-483.

- Ohu, J.O, G.S.V. Raghavan, E. McKyes.1988. Cone index prediction of compacted soils. *ASAE Trans.*, 31(2):306-310.
- Roth, K., R. Schulin, H. Fluehler, W. Attinger. 1990. Calibration of TDR for water content measurement using a composite dielectric approach . *Water Resour. Res.* 26:2267-2273.
- Simmons, F.W. and D.K. Cassel. 1989. Cone index and soil physical properties relationships on sloping paleudult complex. *Soil Sci.* 147:40-46.
- Stelluti, M., M. Maiorana, D. DeGiorgio. 1998. Multivariate approach to evaluate the penetrometer resistance in different tillage systems. *Soil & Tillage Research*, 46:145-151.
- Taylor, H.M. and H.R Gardner. 1963. Penetration of cotton seedling taproot as influenced by bulk density, moisture content, and strength of the soil. *Soil Sci.* 96:153-156.
- Topp, G.C., J.L. Davis and A.P. Annan. 1980. Eletromagnetic determination of soil water content: measurements in coaxial transmission lines. *Water Resour. Res.*, 16:574-582.
- Upadhyaya, S.K., L.J. Kemble, N.E. Collins. 1982. Cone index prediction equations for Delaware soils. *ASAE Paper*, 82:1452-1456.
- Vaz, C.M.P., J.W. Hopmans. Simultaneous measurement of soil strength and water content with a combined penetrometer-moisture probe. *Soil Science Society of America Journal*, 65(1):4-12, 2001.
- Vasquez, L., D.L. Myhre, E.A. Hanlon, R.N. Gallaher. 1991. Soil penetrometer resistance and bulk density relationships after long-term no tillage. *Commun. Soil Plant Anal.*, 22:2101-2117.
- Wraith, J.M. and D. Or. 1998. Nonlinear parameter estimation using spreadsheet software. *J. Nat. Resour. Life Sci. Educ.* 27:13-19.
- Yu, C., W. Warrick and M.H. Conklin. 1999. Derived functions of time domain reflectometry for soil moisture measurements. *Water Resources Research*. 35(6): 1789-1796.

Automatic Gamma-Ray Equipment for Multiple Soil Physical Properties Measurements

Carlos Manoel Pedro Vaz¹

Embrapa Agricultural Instrumentation, São Carlos, Brazil

*Lecture given at the
College on Soil Physics
Trieste, 3-21 March 2003*

LNS0418037

¹ vaz@cnpdia.embrapa.br

Introduction

Determination of soil physical parameters is sometimes very laborious and time consuming. For instance, the soil water retention curve takes several weeks. Particle density by picnometer and granulometry (texture) by pipette method are laborious methods. Other parameters, such as bulk density and total porosity, are determined by gravimetric methods and depends on oven drying the samples for 24 hours.

In order to help in the soil physical parameters determination we have developed automatic equipment based on the attenuation of a gamma-ray beam by soil samples (see Figure 1). Two types of samples are analyzed: solid (undisturbed) and dispersed soil particles in water (see Figure 2), allowing the measurement and estimation of the following parameters:

- Particle size distribution (measured);
- Retention curve (estimated by Arya and Paris (1981) method);
- Particle density (estimated from measured mass attenuation coefficient of the soil sample);
- Bulk density (measured);
- Total porosity (estimated);
- Water content (measured).

Here we focus on the explanation of gamma-ray attenuation method to measure and estimate the soil physical parameters mentioned above. Each method will be presented in detail together with calibrations and practical applications.

Material and Methods

Automatic gamma-ray attenuation equipment



Figure 1. Equipment for multiple soil physical parameters determination.

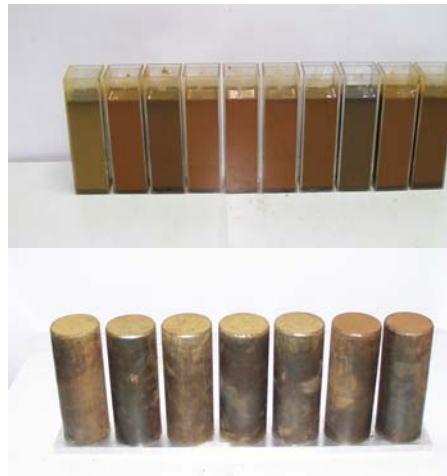


Figure 2. Soil particles samples dispersed in water and undisturbed samples in steel cylinders.

The equipment has the following characteristics:

- Am-241 gamma-ray source (300 mCi);
- Platform for 10 samples;
- Vertical movement to scan the sample;
- Horizontal movement for sample positioning;
- Controlled by a PC computer;
- Electronic based on micro-controller 80535;
- Runs under Windows® 95 or later;
- Software developed in Microsoft Visual Basic® 4.0 32 bits.

Particle size distribution analysis

Dispersed particles falling in water are measured for several heights (h) and times (t) and the particle size distribution is determined according to the method introduced by Vaz et al. (1992), Oliveira et al. (1997) and Naime et al. (2001).

Results of soil particle size distribution of 24 samples (6 soils, 4 depths) and a comparison between the gamma-ray and the densimeter method are presented for 236 soil samples.

Soil Particle Density

A linear experimental correlation between the particle density determined by pycnometer method and the mass attenuation coefficient measured with the equipment allows the particle density estimation (Vaz et al. 1992).

This experimental correlation is presented for 27 soil samples. Also, particle density of about 535 Brazilian soil samples estimated with this procedure, are presented.

Soil Water Retention Curves

Using a modification of Arya and Paris (1981) model, the soil water retention curves are determined with the particle size distribution curve measured with the automatic gamma-ray attenuation equipment.

This modification includes a dependence of the fitting parameter α with the soil water content similarly to the ones suggested by Basile and D'Urso (1997) and Arya et al. (1999).

Results are presented for 24 soil samples (6 soils, 4 depths) and compared with the experimental retention curves measured in laboratory for undisturbed samples.

Soil bulk density and water content profile

Undisturbed soil samples collected in steel cylinders (diameter = 7.8 cm, height = 18 cm) are vertically scanned in increment of 2 mm or longer. Wet samples

are initially measured, then, it is oven dried at 100° C for 24h and again measured at the same points of the wet sample, allowing the determination of both bulk density and water content soil profile.

Results of 5 collected soil samples, 18 cm long, are presented, with bulk density and water content determined each 5 mm along the samples.

Results

Particle size distribution curves

Figure 3 presents the complete particle size distribution curves of 24 Brazilian soil samples. Figure 4 presents a validation of the equipment and the methodology with the densimeter method. A good linear correlation coefficient was obtained ($r^2 = 0.94$) and RMSE = 5.03) for all fractions.

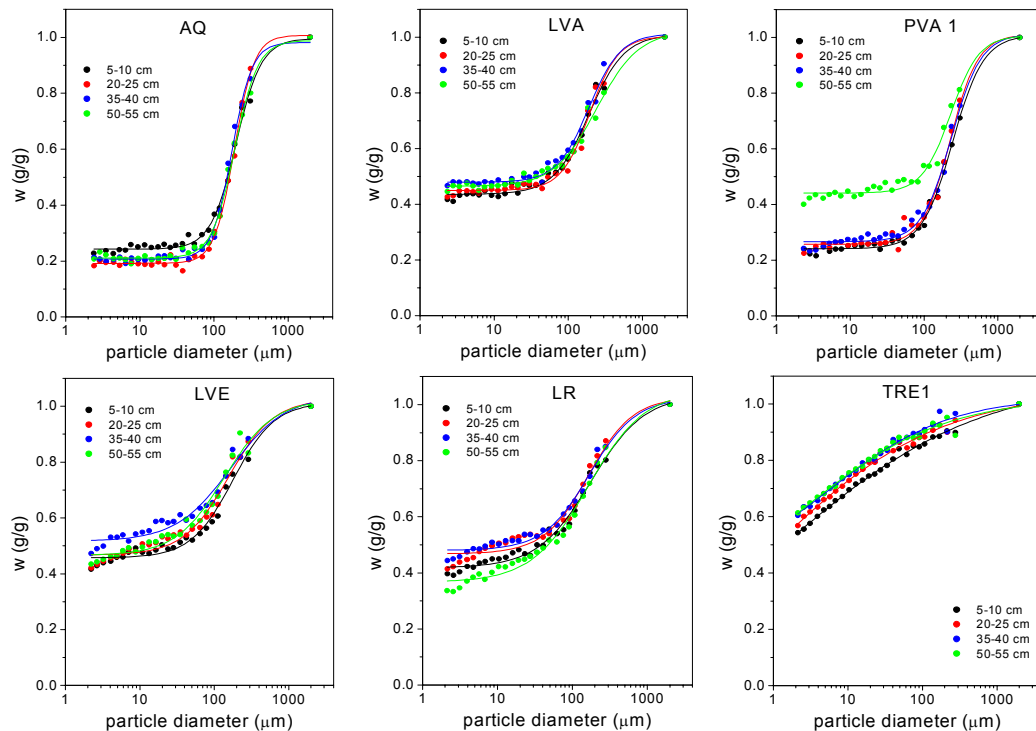


Figure 3. Particle size distribution of 6 Brazilian soil at 4 depths each, measured with the automatic gamma-ray attenuation equipment. AQ, LVA, LR, LVE and TRE are Oxisols and PVA is an Ultisol.

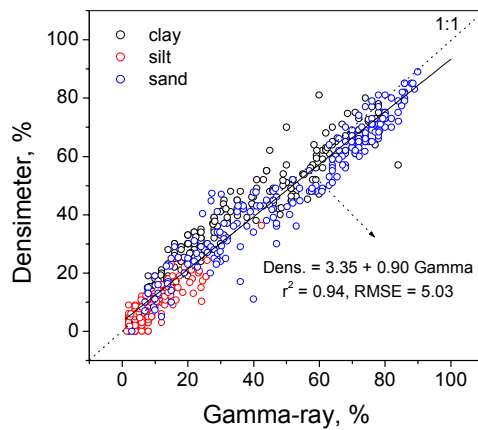


Figure 4. Granulometric fractions of 236 Brazilian soil samples, measured by densimeter and gamma ray-attenuation methods.

Soil Particle Density

Figure 5 shows the empirical correlation obtained between the mass attenuation coefficient and the soil particle density. The good linear correlation allows good estimation of the ρ_p parameter. A distribution of ρ_p for 535 Brazilian soils are presented in Figure 6. Basically, 3 groups of ρ_p can be identified.

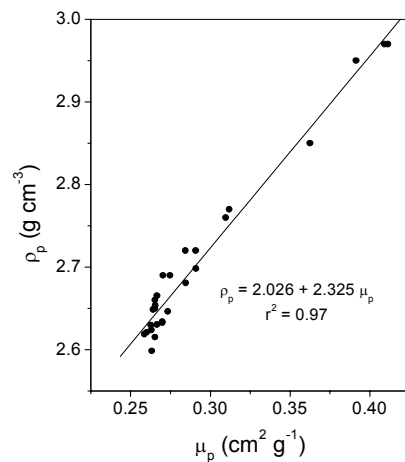


Figure 5. Correlation between the soil mass attenuation coefficient (μ_p) and the soil particle density (ρ_p) for 27 Brazilian soil samples.

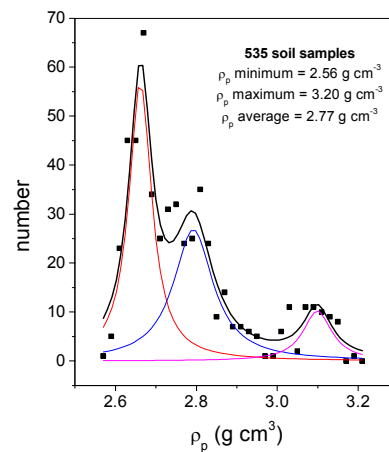


Figure 6. Histogram of particle density for 535 Brazilian soil samples, estimated by the mass attenuation coefficient.

Soil Water Retention Curves

Figure 7 shows estimated and measured water retention curves of 6 different soils (AQ, LVA, LVE, LR and TRE are Oxisols and PV is Ultisol). The fitting parameter α (Arya and Paris, 1981) was assumed as h and θ dependent, as suggested by Basile and D'Urso, 1997) and its dependence is showed in Figure 8 for 24 soil samples.

The performances of the α variable procedure and the α constant procedure (0.938, Arya and Dierolf, 1992) are compared in Figure 9. The estimate of θ improves when using the α variable procedure is used.

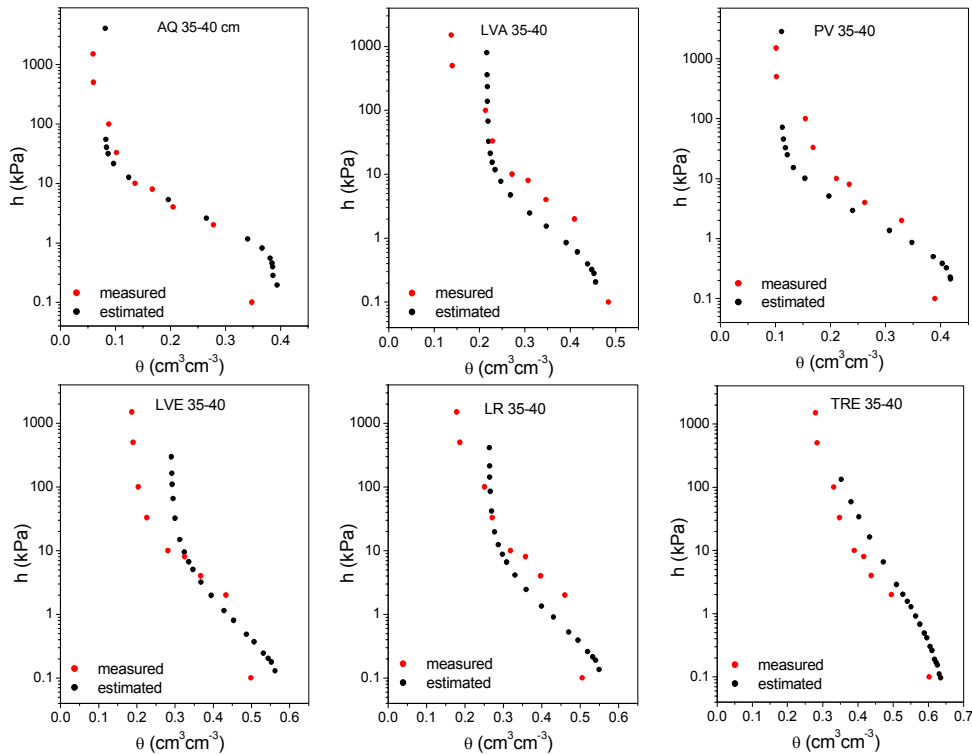


Figure 7. Retention curves measured and estimated by the Arya and Paris method modified for the fitting parameter α as a function of the soil water content and potential (Basile and D'Urso, 1997).

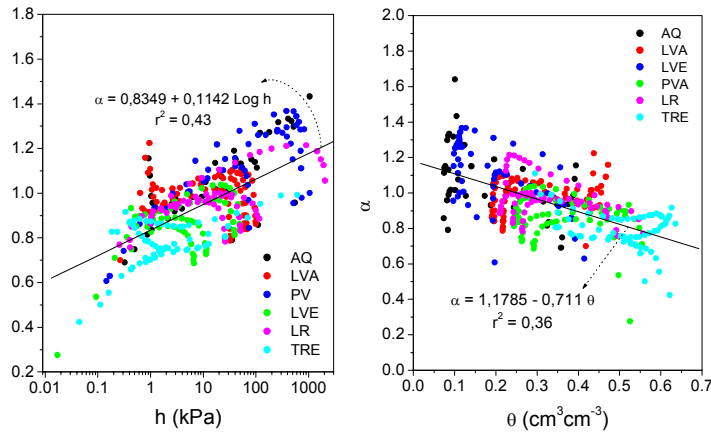


Figure 8. Dependence of the fitting parameter α with the soil water content and potential, for 24 Brazilian soil samples.

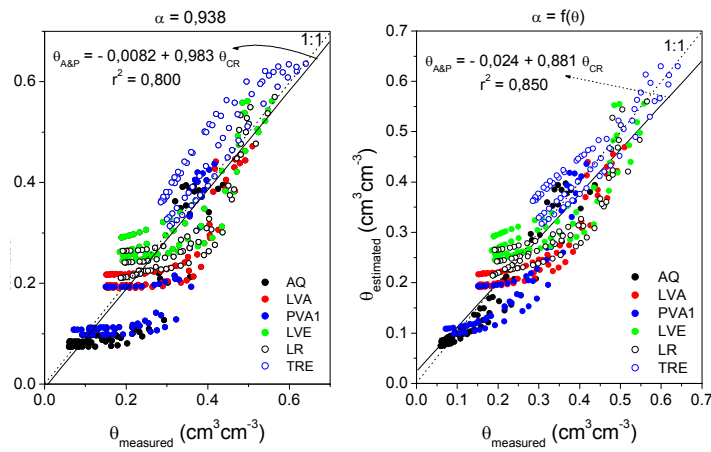


Figure 9. Water content estimated by the modified Arya and Paris method for the fitting parameter $\alpha = 0.938$ (Arya and Dierolf, 1992) and $\alpha = f(\alpha)$ (Figure 7).

Soil bulk density and water content profile

Bulk density and water content variation of 5 soil samples (Oxisol-LVA), 18 cm long, are presented in Figure 10. The equipment allows determination of detailed profile of both parameters.

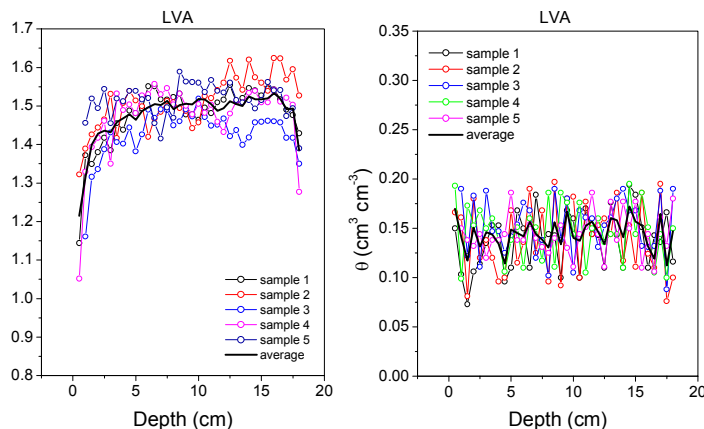


Figure 10. Soil bulk density and water content profile measured for the LVA soil with a spatial resolution of 5mm.

Conclusions

The automatic gamma-ray attenuation equipment allows determination of several soil physical parameters with good accuracy. Best advantages are the possibility of easily estimating some parameters like particle density and water retention curves, and determining precisely and fast the soil particle size distribution or granulometry, bulk density, porosity and water content.

Measurement of other physical parameters as hydraulic conductivity and even chemical parameters as pH, electrical conductivity, ion concentration and others (using convenient sensors) can be, in principle measured or estimated, with the automated equipment and is now being investigated.

References

- Arya, L.M., F.J. Leij, M.T. vanGenuchten and P.J. Shouse. Scaling parameter to predict the soil water characteristic from particle-size distribution data. *Soil Sci. Soc. Am. J.* 63:1063-1070, 1999.
- Arya, L.M., J.F. Paris. A physicoempirical model to predict soil moisture characteristics from particle-size distribution and bulk density data. *Soil Sci. Soc. Am. J.* 45:1023-1030, 1981.
- Arya, L.M., T.S. Dierolf. Predicting soil moisture characteristics from particle-size distribution: an improved method to calculate pore radii from particle radii. In: ed. Van Genuchten, M. Th. Lij, F.J. and Lund, L.J. Proc. Int. Workshop on Indirect Meth. For Estimating the Hydraulic Properties of Unsaturated Soils, Riverside, CA., pp. 115-125, 1992.
- Basile, A., G. D'Urso. Experimental corrections of simplified methods for predicting water retention curves in clay-loamy soils from particle-size determination. *Soil Technology*.10:261-272, 1997.

- Naime, J.M., C.M.P. Vaz, A. Macedo. Automated soil particle size analyzer based on gamma-ray attenuation. *Computers and Electronics in Agriculture*. 31(3):295-304, 2001.
- Oliveira, J.C.M.; Vaz, C.M.P.; Reichardt, K.; Swartzendruber, D. Improved soil particle-size analysis through gamma-ray attenuation. *Soil Sci. Soc. Am. J.*, 60(7):23-26, 1997.
- Vaz, C.M.P., J.C.M. Oliveira, K. Reichardt, S. Crestana, P.E. Cruvinel, O.O.S. Bacchi. Soil mechanical analysis through gamma ray attenuation. *Soil Technology*, 5:319-325, 1992.

Soil Shrinkage Characteristics in Swelling Soils

Miguel A. Taboada¹

*Departamento de Ingeniería Agrícola y Uso de la Tierra,
Facultad de Agronomía UBA, Buenos Aires, Argentina*

*Lecture given at the
College on Soil Physics
Trieste, 3-21 March 2003*

LNS0418038

¹ mtaboada@agro.uba.ar

The objectives of this presentation are to:

- understand soil swelling and shrinkage mechanisms, and the development of desiccation cracks;
- distinguish between soils having different magnitude of swelling, as well as the consequences on soil structural behaviour;
- know methods to characterize soil swell/shrink potential;
- construct soil shrinkage curves, and derive shrinkage indices, as well to apply them to assess soil management effects.

The “physics” of soil physics traditionally assumes that soils have rigid behavior; that means relatively stable relations between their solid and pore volume. In the well-known schematic diagram of the three phase system, the solid phase remains stable while the volumes of water and air vary conversely within pore space (Figure 1).

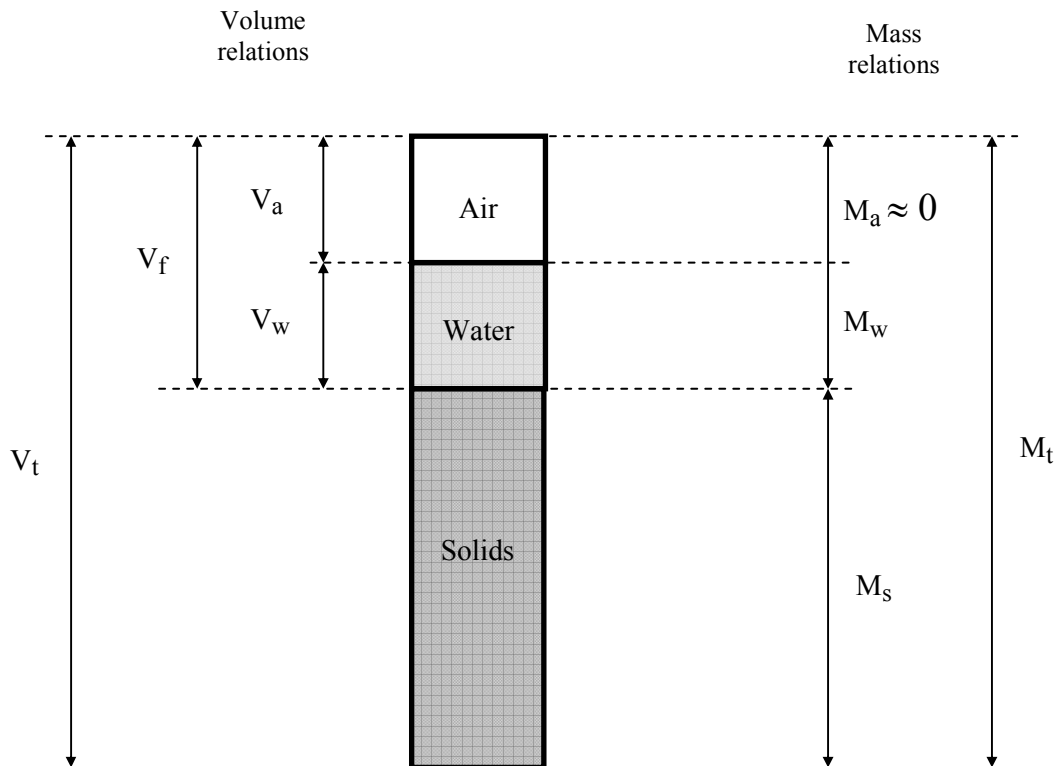


Figure 1. Schematic diagram of the soil as a three phase system

When a rigid soil dries, a given volume of air enters to the pore space in replacement of an equivalent volume of water. On the basis of this theoretical

approach several methodologies have been developed. For instance, the determination of pore size distribution using the water desorption method (Burke et al. 1986).

$$\delta V_w = \delta V_a \quad [1]$$

Therefore, air-filled porosity increases as a rigid soil dries. As can be observed in Figure 2, rigid or non swelling soils do not change their specific volume, v , and hence, their bulk density ρ_b during their water content θ variation range. Rigid or non swelling soils are usually coarse – textured, organic matter – poor, and hard to till. They also have low aggregate stability, high module of rupture, and low resilience after a given damage (e.g. compaction by agricultural traffic). They are considered to have hard-set behavior. Figure 3 shows a non swelling sandy loam (Haplic Phaeozem) of the Argentine Pampas. After several years of disc plowing, a hard plow pan is developed in the subsoil.

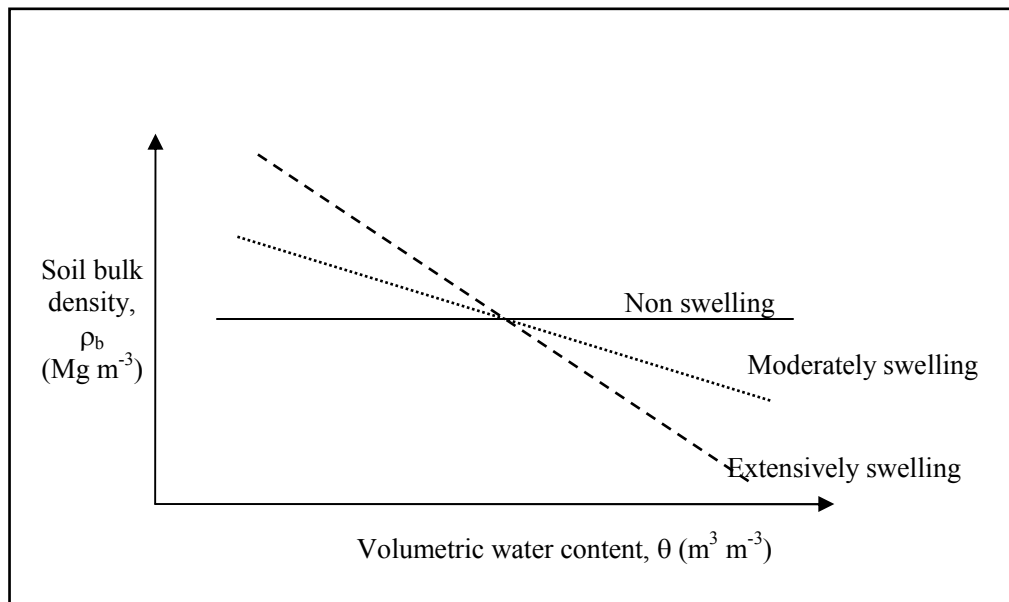


Figure 2. Schematic variation of soil bulk density in non swelling (rigid), moderately swelling and extensively swelling soils.

In contrast, extensively swelling soils undergo significant bulk density, ρ_b , variations during their water content, θ , variation range. They are usually fine – textured, with smectitic type of clays. They develop desiccation cracks on drying, which confers them high resilience, and little tillage requirement. They are considered to have self-mulch behavior. Figure 4 shows an extensively swelling soil, a Vertisol cropped to soybean in the Argentine Mesopotamia. Their self mulching facilitates their management under continuous zero tillage.



Figure 3. A hard plow pan developed in the subsoil of a sandy loam (Haplic Phaeozem) of the Argentine Pampas.



Figure 4. Extensively swelling Vertisol of the Argentine Mesopotamia, cropped to soybean using zero tillage.

Generally, most agricultural soils in the world develop only moderate volumetric changes during wetting and drying. This occurs provided the soil has less 8 % swelling clays (Dexter 1988). Although moderate, this swelling is highly important to the regeneration of soil structure after a given damage.

Processes taking place in swelling soils during drying and wetting

Different processes take place when a swelling soil dries or swells. On drying the soil decreases its volume by shrinkage, and desiccation cracks appear because of internal stresses in the shrunken and dried soil mass. These cracks are created in pre-existing planes of weakness within soil clods. As a result of shrinkage, soil decreases its height by subsidence. On wetting the soil increases its volume by swelling, the cracks are closed, and soil level rises. The process of swelling is mainly caused by the intercalation of water molecules entering to the inter-plane space of smectitic clay minerals (after Low and Margheim 1979, Schafer and Singer 1976, Parker et al. 1982). An schematic visualization of this process is depicted by Figure 5.

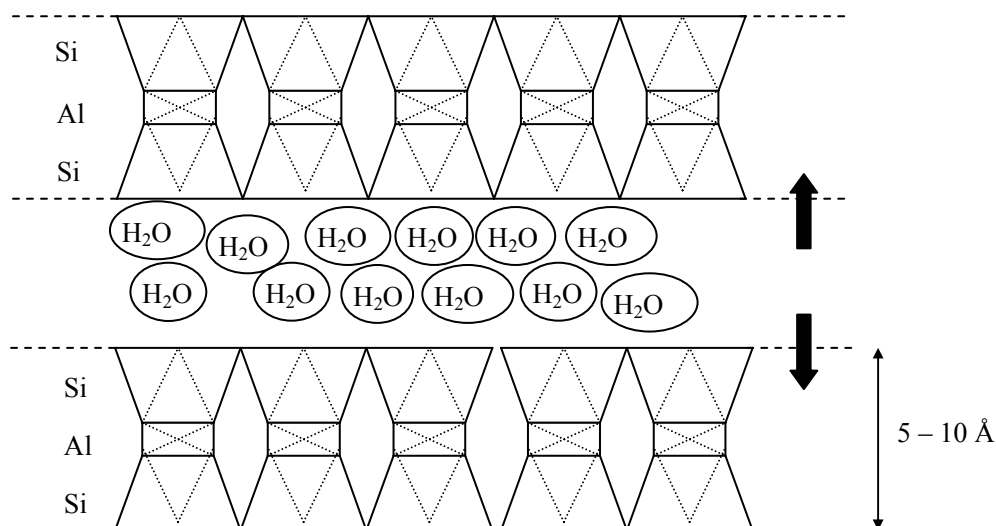


Figure 5. A diagram showing the intercalation of water molecules in the inter-plane space of clay smectites.

The expansive characteristics of smectites are affected by the nature of adsorbed ions and molecules. Smectite increases its plane spacing as a result of the loss of adsorbed cations.

Types of soil swelling

When a dry soil wets, during the first stage it undergoes three dimensional (3-D) volumetric expansions, because its desiccation cracks are still opened (Figure 6). In a second stage, after desiccation cracks were closed, soil volumetric expansion is only 1-D, causing the rising of soil level (Figure 7).

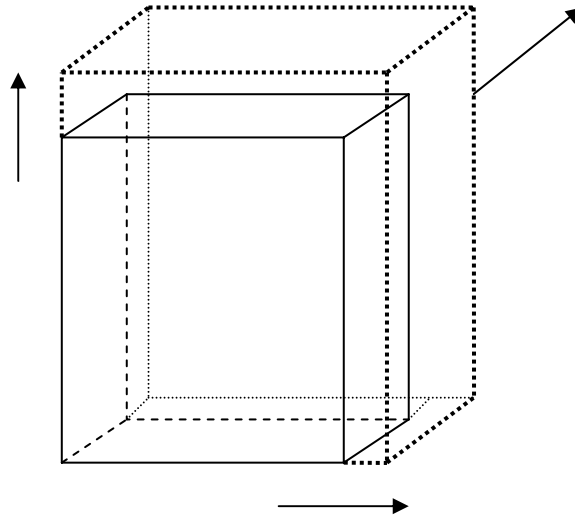


Figure 6. Schematic diagram of 3-D soil swelling

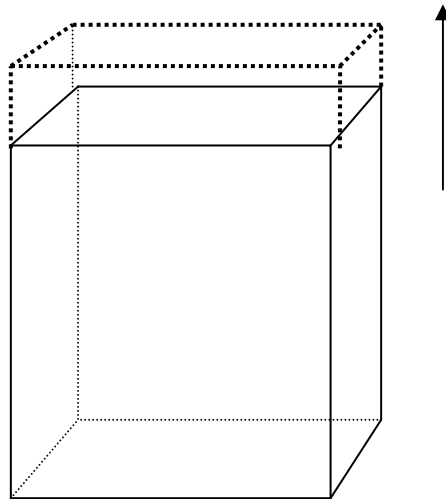


Figure 7. Schematic diagram of 1-D soil swelling

Consequences of soil swelling

Soil volumetric changes may cause both unfavorable and favorable effects on human activities. Unfavorable effects are the destruction of buildings, roads and pipelines in uncropped soils, and the leaching of fertilizers and chemicals below the root zone through desiccation cracks (by pass flow). In these soils horizontal cracks break capillary flux of water. On the other hand, swelling clays can be used to seal landfills storing hazardous wastes. This sealing avoids the downward migration of contaminants to groundwater. In cropped soils, the development of a dense pattern of cracks on drying improves water drainage and soil aeration, and decreases surface runoff in sloped areas. Soil cracking is closely related to the recovery of porosity damages by compaction. For a complete revision of these topics, the lecture of a review by A. R. Dexter (1988) is recommended. Here in, a conceptual model describing the sequence of paths leading to the development of desiccation cracks is provided (Figure 8). Tensile stresses are developed on drying, which to the creation of primary, secondary and tertiary cracks. The cracks are, at the same time, future void spaces, and represent the walls of the future aggregates. This sequence of paths is believed to recover soil porosity in a previously compacted soil layer.

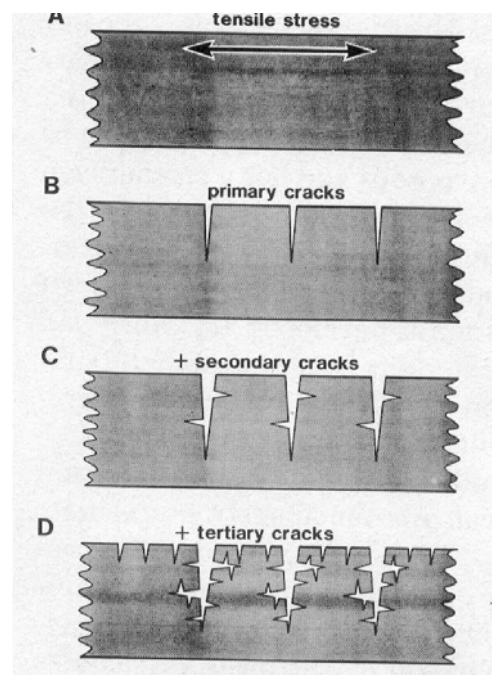


Figure 8. Conceptual model describing the development of primary, secondary and tertiary cracks, resulting from the build up of tensile stresses on drying (taken from Dexter 1988).

Methods for assessing soil swell-shrink potential

a) Coefficient of linear extensibility, COLE

It characterizes the variation of soil volume from 1/3 atm water retention (i.e. field capacity) to oven dry conditions:

$$\text{COLE} = (v_{1/3 \text{ atm}} - v_{\text{dry}})^{1/3} - 1 \quad [2]$$

where $v_{1/3 \text{ atm}}$ is the soil volume at 1/3 atm water retention and v_{dry} the soil volume at oven dry conditions. According to their COLE, a range of soil swell-shrink potential can be distinguished:

<u>Soil swell – shrink potential</u>	<u>COLE</u>
Low	< 0.03
Moderate	0.03 – 0.06
High	0.06 – 0.09
Very high	> 0.09

The COLE index was found to be closely related to a number of soil variables (Parker et al. 1982). The higher determination coefficients correspond to the contents of total and swelling clays.

<u>Independent variables</u>	<u>R²</u>
Clay < 2 μm	0.87***
Clay 2 - 0.2 μm	0.41**
Clay < 0.2 μm	0.43**
Smectites < 0.2 μm	0.61***
Interstratified swelling clay < 0.2 μm	0.2
Swelling clay < 0.2 μm	0.91***
Porosity	0.33*
organic C	0.08
Sodium Adsorption Ratio	0.01

b) The shrinkage characteristic or shrinkage curve (Mc Garry and Daniells 1987)

Each soil has a characteristic water retention curve, which relates its water content to the energy at which water is retained by the solid phase (soil matric potential). Likewise, swelling soils may be also characterized by its shrinkage curve. This shows the variation of soil specific volume, v , with water content, θ , during the air – drying of water saturated natural clods.

To construct a shrinkage curve, the volume of natural soil clods must be determined by hydrostatic up thrust in a non polar liquid (kerosene) during air drying (Figure 9). The corresponding water content is also measured at different times of drying. Another option is to coat the clods with SARAN resin, and then, submerge them in water (Coughlan et al. 1991; Mc Garry and Daniells 1987; Mc Garry and Malafant 1987).

In a shrinkage curve the inverse of bulk density (i.e. soil specific volume, v) is plotted to the volumetric water content θ of the soil (Figure 10). In this graphic two theoretical lines are depicted: a) the solid phase line (from the converse of soil particle density) that represents the lowest soil volume of a soil having zero pore space; and b) the 1:1 saturation line that represents soil swelling with zero air within pore space.

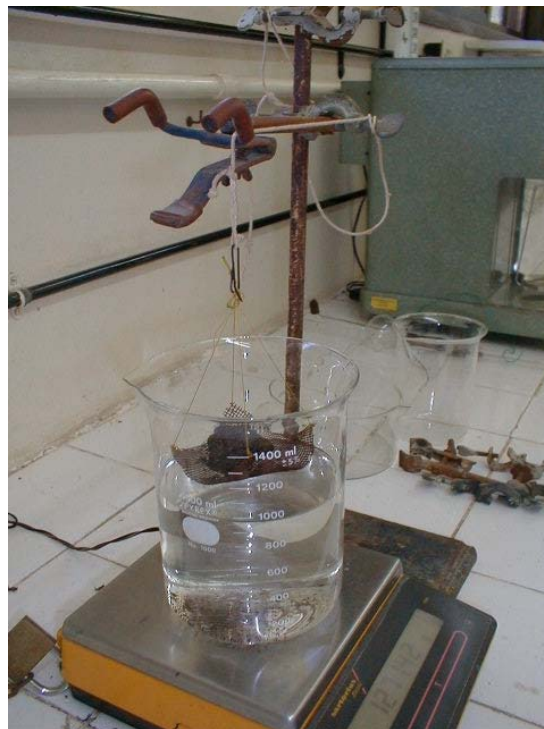


Figure 9. Experimental device to measure the volume of natural clods, by hydrostatic up thrust in a non polar liquid (kerosene)

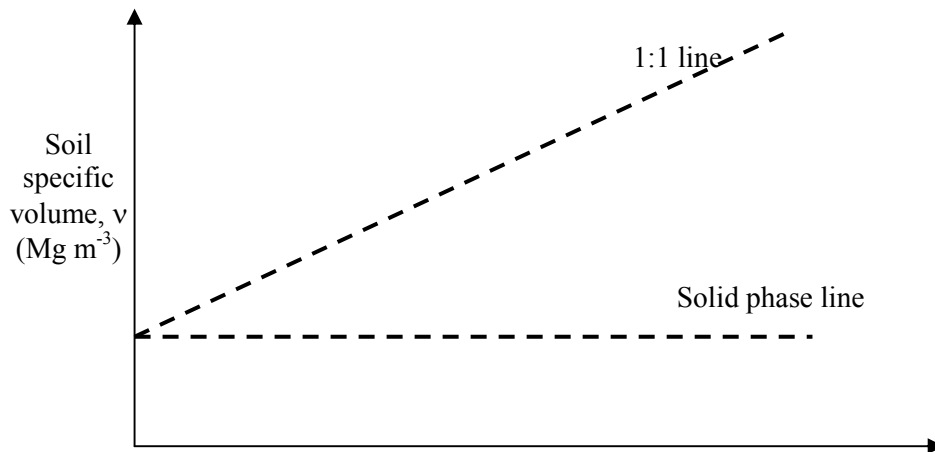


Figure 10. Initial plot to construct a soil shrinkage curve

After introducing $v - \theta$ pairs of data, straight lines can be fitted. This allows the identification of different shrinkage zones (Figure 11). Normal shrinkage ($B \rightarrow A$) is characterised by equivalent decreases in both v and θ on drying, and thus, no air enters into soil pores (Coughlan et al., 1991; Mc Garry and Daniells, 1987). In the drier range of the θ variation, soil v decreases during drying are lower or even null. Residual shrinkage ($A \rightarrow \alpha$) allows air entrance into soil pores, and hence the creation of air-filled porosity. Swelling soils are considered to have normal, or equivalent v and θ variations throughout their water variation range. Moderately swelling soils, in turn, develop residual shrinkage during the drier range of soil moisture variation. This allows air entry to soil pore space, and the process is also recognized as irreversible shrinkage. The location of the air entry point θ_A is considered a index of soil quality in swelling soils, the higher θ_A , the better the soil aeration (Coughlan et al. 1991).

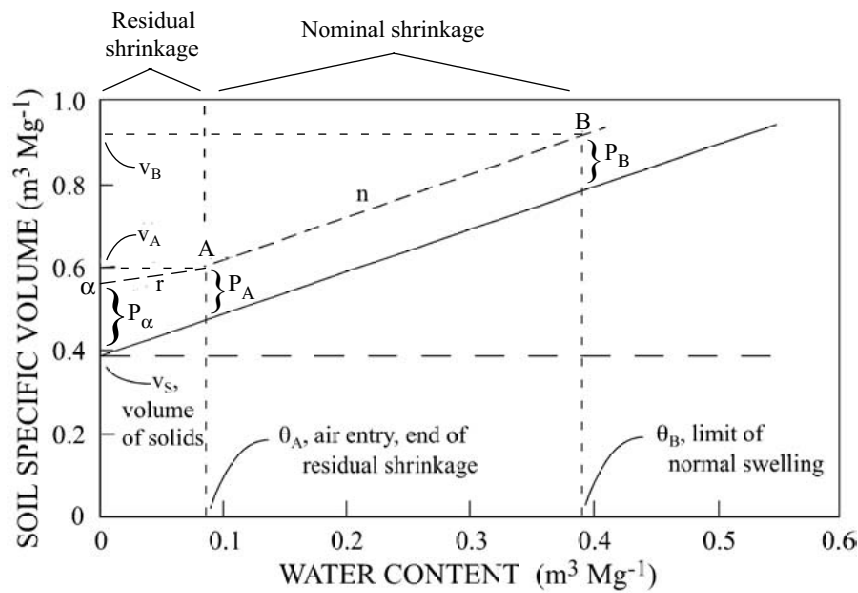


Figure 11. Theoretical shrinkage curve of a swelling soil.

Table 1: indices and related variables from the shrink data of natural soil clods (Mc Garry and Daniells, 1987).

θ_B	θ at the limit of normal swelling
θ_A	θ at the air entry point, i.e. the end of residual shrinkage
n	slope of the line $B \rightarrow A$ (normal shrinkage)
r	slope of the line $A \rightarrow \alpha$ (residual shrinkage)
v_B	specific volume at the limit of normal swelling
v_A	specific volume at the air entry point
α	specific volume at zero water content
P_B	specific volume of air filled pores at B
P_A	specific volume of air filled pores at A
P_α	specific volume of air filled pores at α
$\theta_B - \theta_A$	difference between θ at the limit of normal swelling and θ at the air entry point, i.e. range of θ in the normal shrinkage zone

Mc Garry and Daniells (1987) derived several indices and related variables from the shrink data of natural soil clods (Figure 11; Table 1). These are derived from the mathematical expression of two or three straight lines, fitted to the data. The figure shows the different soil shrinkage lines and indices of interest. We applied this approach to study soil volumetric variations in the Pampean soils of Argentina (Figure 12).

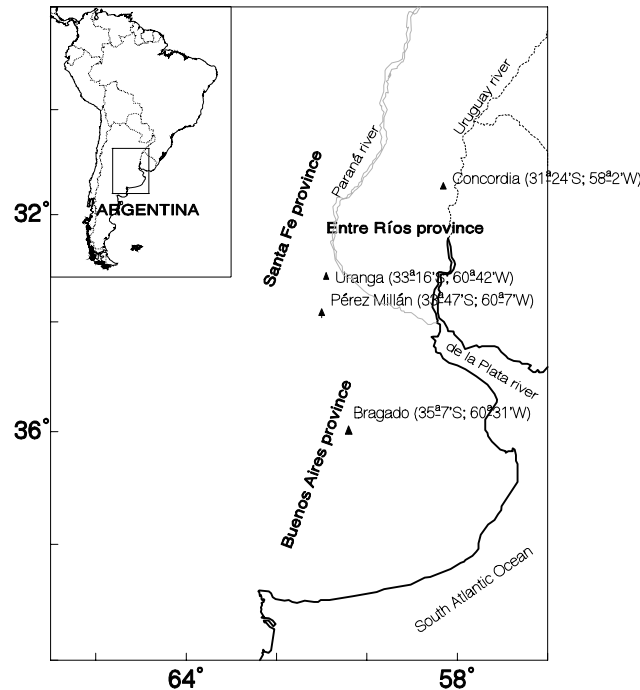


Figure 12. Geographical location of the main Argentine cropland area. Vertisols are highly conspicuous in Entre Ríos province, while silty loams covered thousand hectares in Santa Fe and Buenos Aires provinces.

a) Shrinkage characteristic of pampean silty clay loams affected by water erosion (Barbosa et al., 1999)

Silty loams (Argillic Phaeozems) are highly conspicuous in the north of the Pampean region. These soils are affected –to a different degree- by degradation, which can be classified in moderate and severe. Figure 13 graphically describes how degradation changed soil properties in the moderate and severe levels. Because of their high content of fine silt (2-20 μm), these soils have low structural regeneration capacity after degradation. We hypothesized whether this could be improved, or not, by the enrichment of topsoil with swelling clays. This situation can be found in severely degraded soils, in which the shallow A horizon was previously mixed with the below lying B horizon.

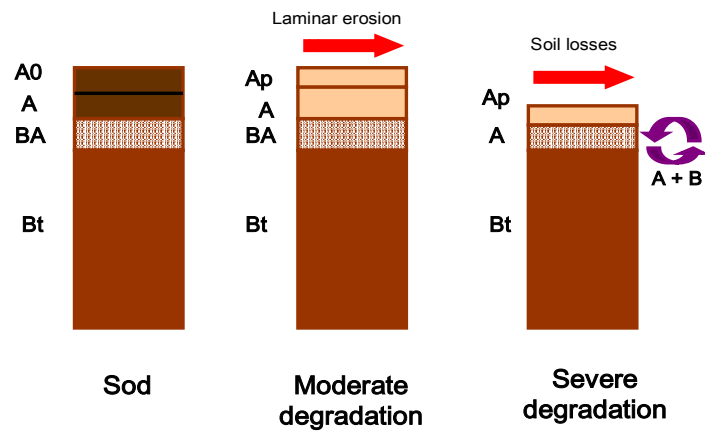


Figure 13. Idealization of soil profiles in non degraded (sod), moderately and severely degraded situations.

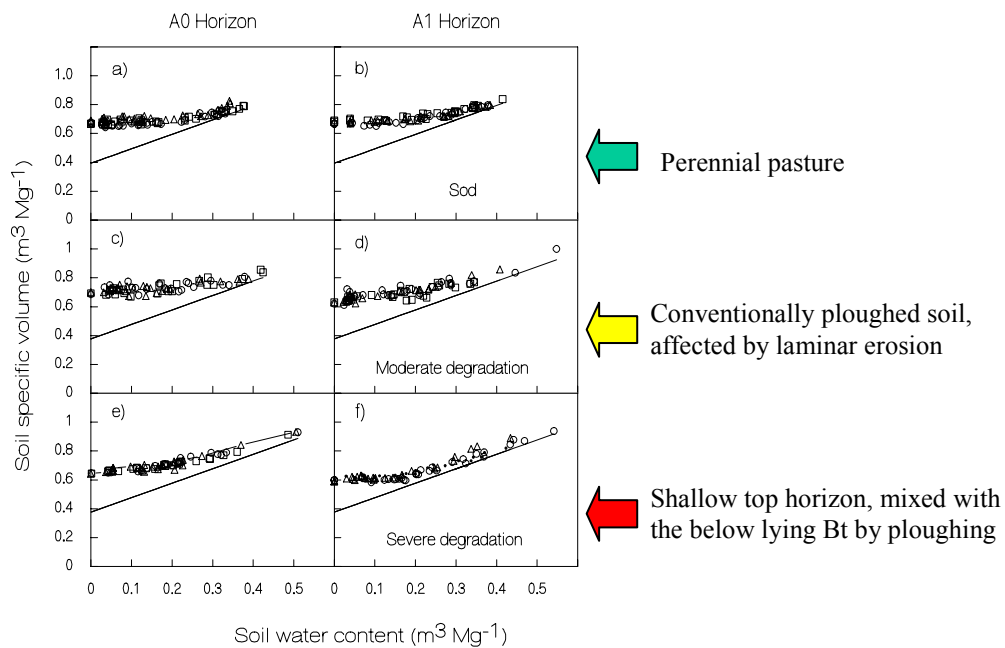


Figure 14. Soil shrinkage curves in the A0 and A1 horizons of a Peyrano silty clay loam (Argillic Phaeozem), under different degradation levels.

Soil shrinkage curves differed because of the different degradation levels (Figure 14). At first sight it becomes evident the wider volumetric variation range of the severely degraded soils. Soil volume at zero water content, α , and the air entry point θ_A showed no significant differences between the sod and moderately degraded soils, and were significantly lower in the severely degraded soil (Figure 15a). The slope, n , increased significantly from the sod to the severely degraded soil. The same happened with the normalcy range (Figures 15c and d). The severely degraded soil reached significantly higher volume, v_B , and water content θ_B when swollen at maximum.

It can be concluded that clay enrichment (severe degradation) accentuated soil swelling ($> v_B$ and θ_B and normalcy range), but did not improve air filled porosity. Soil horizons mixture can not be recommended to the farmers, as a practice suitable to improve topsoil structure in Pampean silty loams.

b) Shrinkage characteristic of natric soils in the Flooding Pampa (Taboada et al., 2001)

In the flooding Pampa there are different kinds of Solonchets, that are periodically flooded. The region is characterized by water table rises and surface ponding during winter-spring periods. Figure 16 (a through d) shows soil specific volume – water content relations in two different Solonchets of the region. It can be observed that the fitted straight lines departed from the 1:1 line, showing air – filled porosity increases as soil wets.

The soils have no definite expansible clay mineralogy. Water table rises and surface ponding promote the build up of trapped air pressures in top horizons. This shows abnormal soil swelling caused by air entrapment.

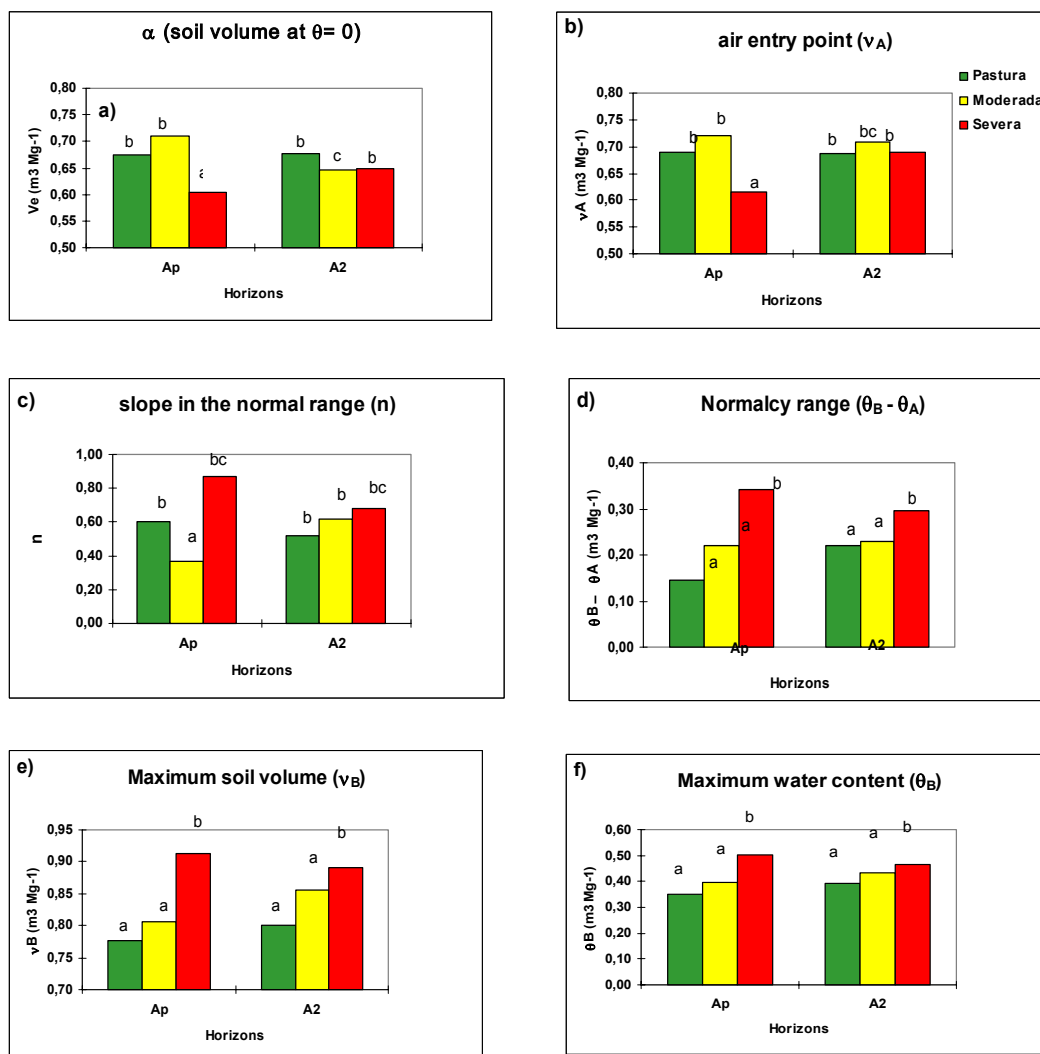


Figure 15. a) soil volume at zero water content, α ; and b) air entry point θ_A in the sod, and moderately and severely degraded soils. c) slope in the normal range, n, and d) the normalcy range, $\theta_B - \theta_A$, in the sod, and moderately and severely degraded soils. e) maximum soil volume, v_B , and d) maximum water content, θ_B , in the sod, and moderately and severely degraded soils.

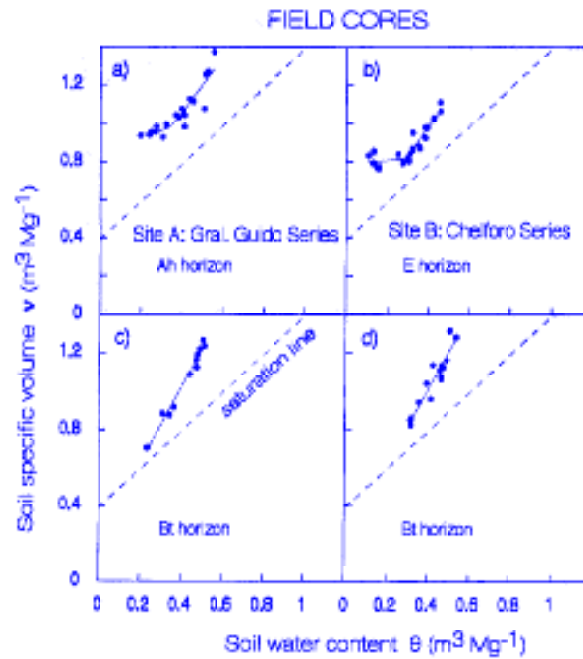


Figure 16. Soil specific volume, v , - water content relationships from repeated core sampling of surface (a, b) and Bt (c, d) horizons of two Solonchets.

In the environmental conditions of the flooding Pampa of Argentina, trapped air is responsible for most of the swelling of soils having little expansible mineralogy of clays. Results show that trapped may an important soil swelling factor in soils.

Recommended bibliography

- Barbosa O.A., Taboada M.A., Cosentino D.J. 1999. Contracción al secado de agregados en diferentes fases de degradación de un suelo limoso de la pampa Ondulada (Soil shrinkage characteristic of soil aggregates in different degradation phases in the rolling Pampa, Argentina). *Ciencia del Suelo* 17: 1-7.
- Burke W., Gabriels D., Bouma J. (Eds.). 1986. Soil structure assessment. A.A. Balkema, Rotterdam. 92 pages.
- Coughlan K.J., Mc Garry D., Loch R. J., Bridge B., Smith G. D. 1991. The measurement of soil structure - Some practical initiatives. *Australian Journal of Soil Research* 29: 869-889.
- Dexter A.R., 1988. Advances in characterization of soil structure. *Soil and Tillage Research*, 199-238.
- Low, P.F., Margheim, J.F. 1979. The swelling of clay: I. Basic concepts and empirical equations. *Soil Science Society of America Journal* 43: 473-481.
- Mc Garry D., Daniells I. G. 1987. Shrinkage curves indices to quantify cultivation effects on soil structure of a Vertisol. *Soil Science Society of America Journal* 51:1575-1580.
- Mc Garry D., Malafant K.W. J. 1987. The analysis of volume change in unconfined units of soil. *Soil Science Society of America Journal* 51: 290-297.
- Parker J.C., Amos D. F., Zelazny L. W. 1982. Water adsorption and swelling of clay minerals in soil systems. *Soil Science Society of America Journal* 46: 450-456.
- Schafer W.M., Singer M.J., 1976. Influence of physical and mineralogical properties on swelling of soils in Yolo County, California. *Soil Science Society of America Journal* 40: 557-562.
- Taboada, M. A., Lavado R. S., Rubio G., Cosentino D. J. 2001. Soil volumetric changes in natric soils caused by air entrapment following seasonal ponding and water table. *Geoderma* 101,:49 - 64.

Soil Structural Behaviour of Flooded Soils

Miguel A. Taboada¹

*Departamento de Ingeniería Agrícola y Uso de la Tierra,
Facultad de Agronomía UBA, Buenos Aires, Argentina*

*Lecture given at the
College on Soil Physics
Trieste, 3-21 March 2003*

LNS0418039

¹ mtaboada@agro.uba.ar

The objectives of this presentation are to:

- identify factors determining of the structural behaviour of flooded soils, as compared to those acting in upland soils;
- analyse the influence of reductive processes on aggregate stabilising agents;
- discuss mechanisms of structural deterioration and recovery during the flooding-drying cycle, on the basis of a case study: cattle trampling effects in the flooding Pampa of Argentina.

Flooded soils: where do they occur?

Flooded soils, now known as Hydric soils, are characteristic of wetlands and irrigated fields cropped to rice (paddy soils). In them, water covers the soil, or is present either at or near the surface of the soil all year or for varying periods of time during the year. Hydric soils belong to different taxa of the FAO-UNESCO Soil Map (2000). Figure 1 (a, b, c) shows the geographical distribution of Fluvisols, Planosols and Gleysols in the World.

As can be observed, they are widespread distributed in the globe. The generation of redoximorphic features is due to different causes in each of them. Fluvisols are covered part of the year by surface water from river overflows; Planosols are soils having an impervious Bt horizon, supporting perched water during short periods; and Gleysols are soils affected by stagnant water tables during long periods.

Key factors determining the structural behavior of flooded soils

The structural behavior of flooded soils received in general terms little attention by published literature. This behavior is affected by these characteristics:

- a) the development of anaerobiosis and reductive processes, and whether they affect, or not, soil organic matter (SOM);
- b) the quality of flooding water, as strongly depending on its origin (where does flooding water come from?);
- c) the response of soil to ponding – drying cycles (when soil is susceptible to structural damage? and how fast soil damages are recovered?).

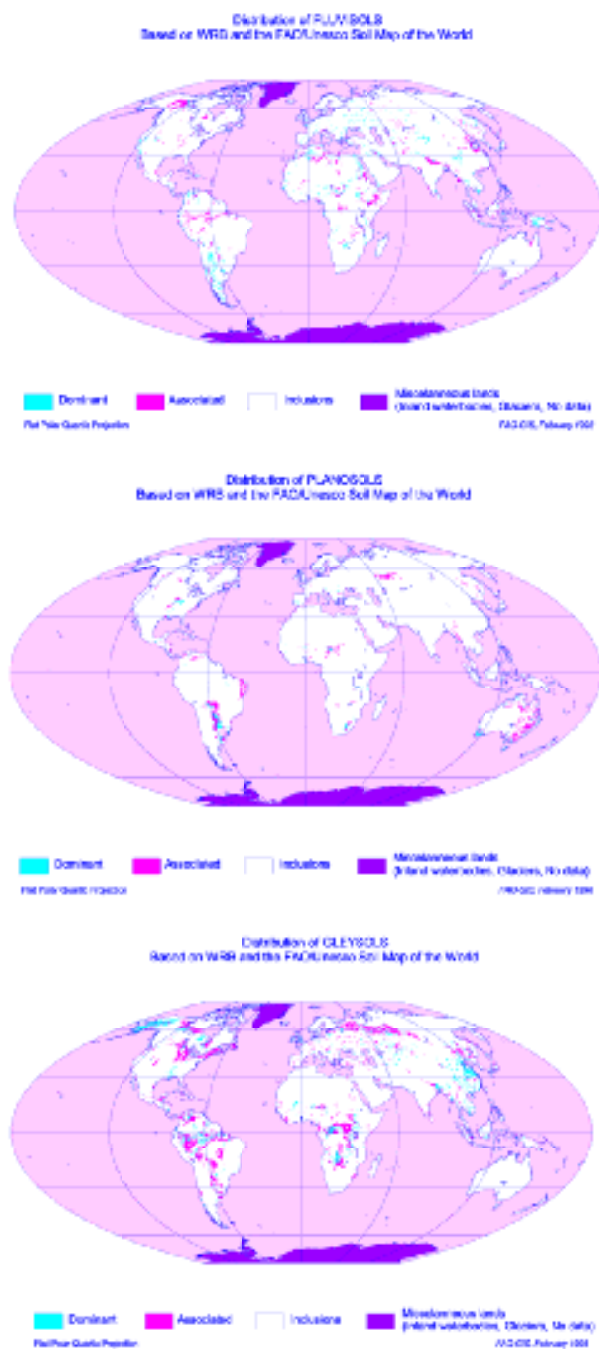


Figure 1. Geographical distribution of Fluvisols (a), Planosols (b) and Gleysols (c) in the World (FAO-UNESCO 2000)

Reductive processes in flooded soils

Hydric soil identification is normally done by looking for these redoximorphic features:

- Grey colours (chromas < 2 in Munsell Soil Color Chart)
- Red mottles
- Concretions of Fe-Mn
- Sesquioxidic glebules
- Gley horizons with yellow and olivaceous colours (hues < 10).

There is a sequence of reductive processes in flooded soils, as a function of the decrease in soil redox potential (Eh) and the prevailing redox couple taking part in each stage of reduction (Patrick and Mahapatra, 1968). This sequence is described in Table 1.

Table 1. Sequence of reductive processes (after Patrick and Mahapatra, 1968)

range of Eh (mV)	redox condition
> 600	highly oxidated
600 to 300	oxidated
300 to 100	moderately reduced
100 to - 100	reduced
< - 100	highly reduced

Oxidated soils (non flooded) have most time high Eh values (> 300 mV), and in them oxygen (O₂) is the main acceptor of electrons in soil respiration processes. In periods when O₂ disappears from soil atmosphere, typically when soil is flooded, ponded or waterlogged, the electron donated by soil organic matter are then accepted by soil nitrates (NO₃⁻) that, in this way, are reduced to molecular nitrogen (N₂) and nitrous oxides (NO_x). This process is known as denitrification, it means a loss of nitrogen evolving to the atmosphere. Soil nitrates disappear only in some days, thus allowing that other redox couples take place. They are those composed by FeIII – FeII, and MnIV, III – MnII compounds. Mineral soils usually have high contents of several iron and manganese oxides and hydroxides, so that Eh values seldom decrease below about -100 mV in seasonally flooded soils. Only those soils that remain submerged for long periods, such as some estuarine soils and permanent ponds can reach high reduction. In them Eh values may reach highly negative values, and as a result, sulphide and methane gases are emitted from these soils.

Due to their low mineralization rate under reduced conditions, flooded soils tend to accumulate high organic carbon contents. These high organic matter contents have strong influence on soil structural behavior.

Figure 2 shows results obtained by Lavado and Taboada (1986) in the flooding Pampa of Argentina. We measured water table depth and topsoil redox potential during about three years, during which the soil was ponded during winter – spring periods. The topsoil was most time under moderately - reduced conditions, according to its condition of grassland soil. Only during ponding periods became the topsoil highly reduced.

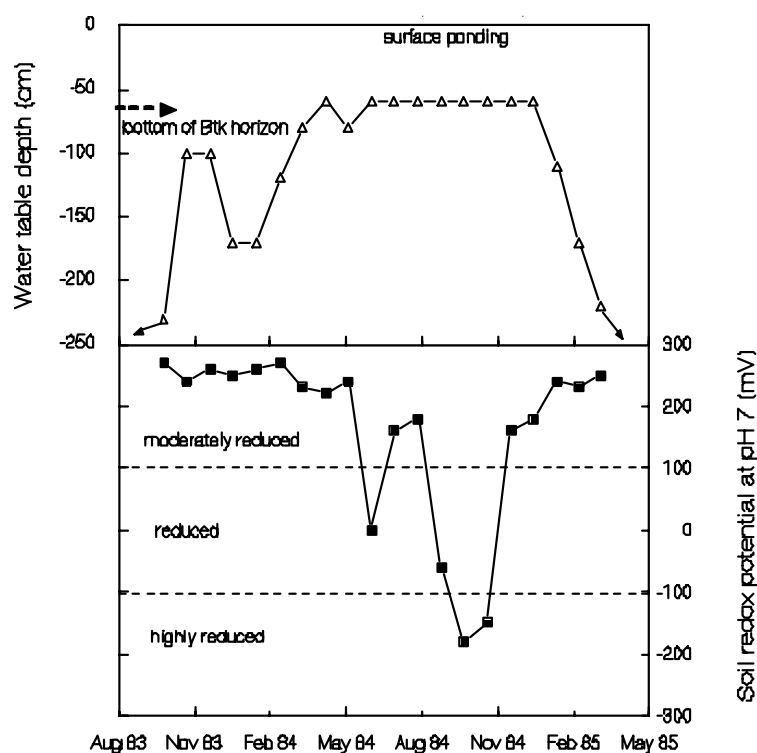


Figure 2. Water table depth and topsoil redox potential in a Solonchak of the flooding Pampa of Argentina (after Taboada and Lavado, 1986).

Quality of flooding water

Soil profile characteristics determine whether groundwater reaches soil surface, or not. The evolution of soil structure after flooding mainly depends on the quality of flooding water (e.g. salinity, sodicity, type of sodium salt, etc.) (after Lavado and Taboada, 1988). It is important to determine the origin of flooding water, which in about 90 % of cases comes from groundwater. The diagram in Figure 3 shows the

possible consequences of different kind of water qualities on soil structure. Soil ponding or flooding by fresh water does not cause severe consequences; only those related to the loss of soil bearing capacity. In change, soil flooding by salty or brackish water may lead to irreversible consequences, such as those caused by alkali excesses on soil structure.

Whether the soil will be ponded by fresh or salty water it will depend on soil profile characteristics. Figure 4 illustrates two cases. Those soils not having a tough Bt horizon allow free down- and upward water movements throughout the profile. So, in them groundwater rises may reach the topsoil, causing eventually (if groundwater has high salt contents) saline deposits in surface horizons. This situation mainly concerns to most Fluvisols.

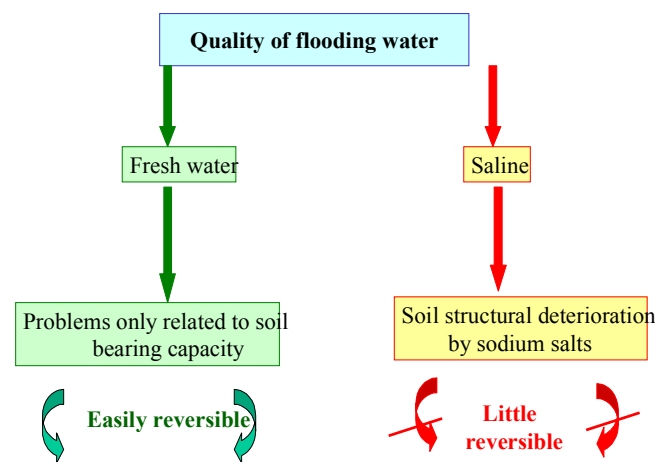


Figure 3. Schematic diagram showing the consequences of flooding water quality on soil structure

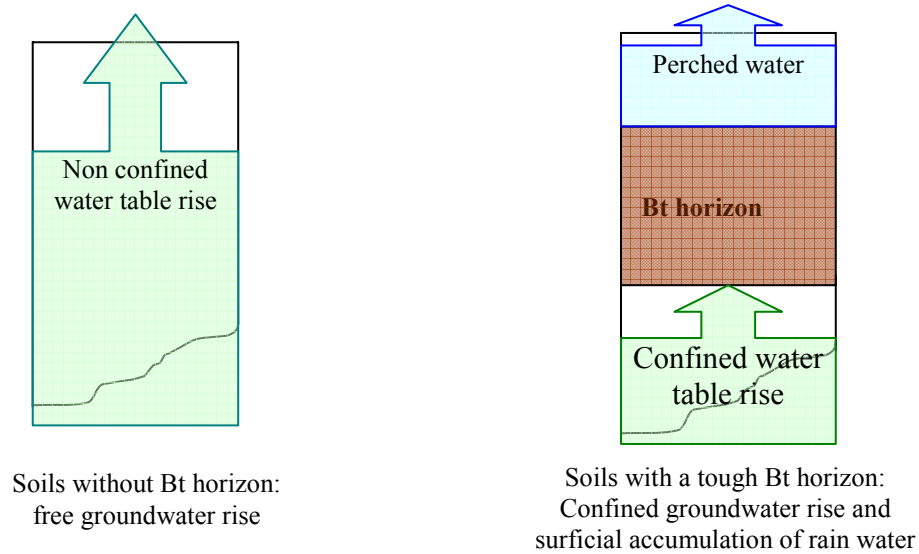


Figure 4. Schematic diagram describing unconfined and confined groundwater rises in soils not having and having a tough Bt horizon.

Figure 5 shows the profile of Solonetz of the flooding Pampa of Argentina. It can be observed a columnar Bt horizon, above which a perched water table is seasonally accumulated. In these kind of soils, floods are largely caused by the accumulation of rain water from the perched water table. Calcium carbonates are precipitated at the bottom the Bt horizon, showing the zone of maximum groundwater rise.

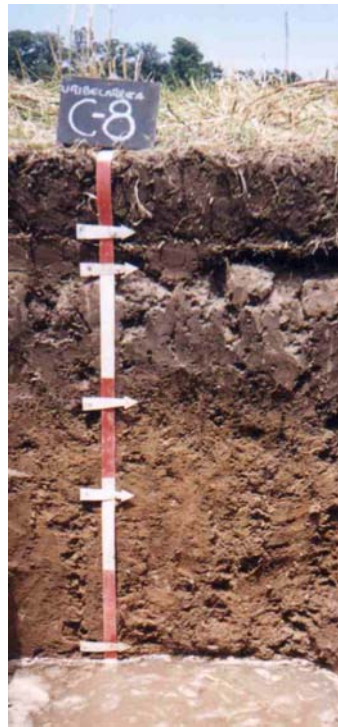


Figure 5. Mollic Solonetz in the northern flooding Pampa of Argentina, having a tough natric horizon with columnar structure. Groundwater can be observed at the bottom.

The case of fresh water flooding: when soil is susceptible to structural damage?

In these soils ponding periods correspond to losses in soil bearing capacity. The “Proctor Curve” constructed from a compactability test can predict the probability of bulk density increases caused by impact stresses upon soil (Figure 6). This curve indicates that a given soil reaches a maximum density at a critic water content. This critic water content is always lower than saturation.

According to the prediction provided by a Proctor test, a given soil will be resistant to support structural damages when dry. At this condition it will have high bearing capacity, and low susceptibility to structural damage by trampling or agricultural traffic. When soil is wet, in change, its bearing capacity is low, and it becomes prone to undergo structural damage. We tested the case of trampling damages by cattle trampling in the flooding Pampa of Argentina, in which the soils are periodically flooded as shows the picture in Figure 7.

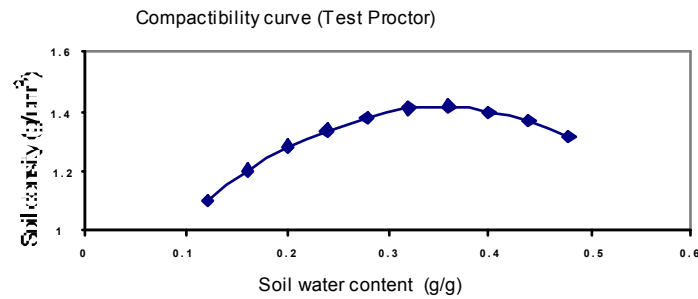
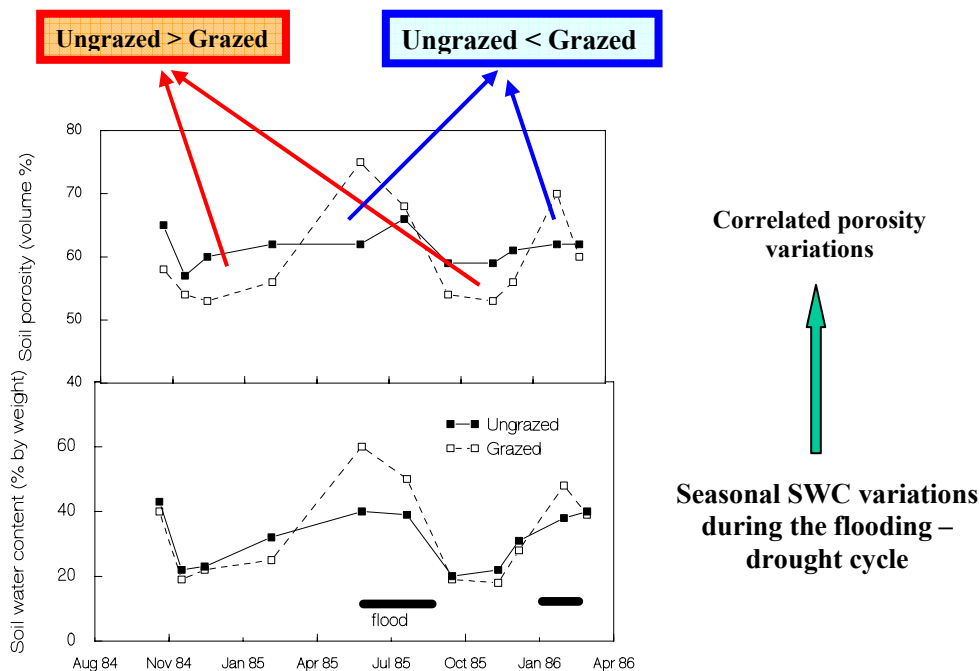


Figure 6. Theoretical soil density – water content relation obtained from a compactibility test (Proctor test).



Figure 7. Landscape view of flooding in the flooding Pampa of Argentina.

In this region structural damage by poaching when a flooded soil is trampled by large herbivores is expected. Poaching is caused by the repeated impact of animal hooves, which weakens topsoil structure. This results in large and massive soil clods, which become very hard when dry. What did we find when studied cattle trampling effects in the center of the flooding Pampa of Argentina?



(after Taboada and Lavado
1993)

Figure 8. Variations of soil water content and total porosity in a Solonetz of the flooding Pampa of Argentina, in grazed and ungrazed enclosure situations.

Figure 8 shows the variation soil water content, which followed as expected the seasonal ponding-drying cycle. Total soil porosity followed the variations in water content, because of the occurrence of swelling and shrinking. Trampling effects were investigated by comparing grazed to ungrazed situation. The latter corresponded to a 4 ha enclosure deferred from grazing for several years. In the figure, it can be observed that soil porosity was significantly higher in ungrazed than in grazed situations in summer periods, when soil was somewhat dry. The opposite occurred during winter- spring periods, showing the recovery of porosity damages during floods. Results show that structural damages by poaching did not occur under our study conditions (continuous grazing by about 1 stock per ha).

Cattle trampling effects are expected to affect mainly the larger soil pores. Figure 9 shows the response of these pores in summer and winter. In agreement with the effects on total porosity, trampling caused the destruction of topsoil pores $> 60 \mu\text{m}$, in summer when soil is dry. This damage was fastly recovered some months later, during winter ponding when soil macroporosity was higher under grazing.

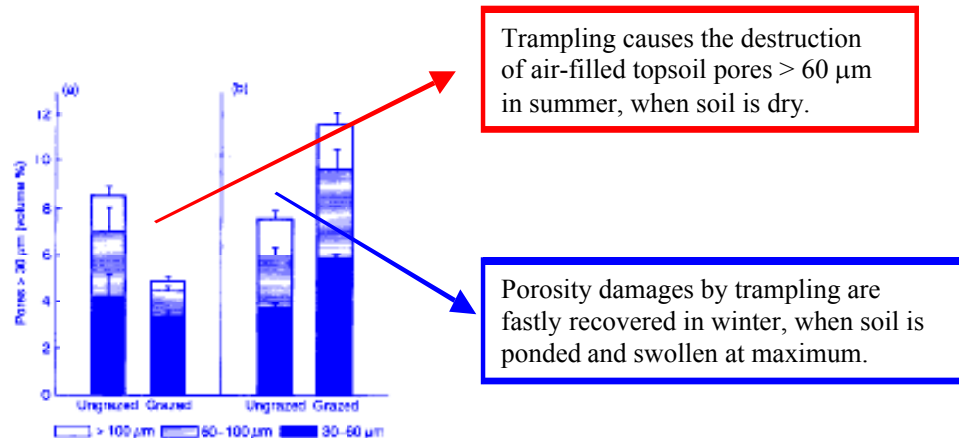


Figure 9. Soil macroporosity in the 30 – 60 µm, 60 – 100 µm, and > 100 µm pore size ranges in summer and winter.

Aggregate stability variations followed the same pattern of soil porosity (Figure 10). They showed higher stability values in the ungrazed enclosure during summer, and stability recoveries during winter, when soil is flooded.

The periods when trampling affects topsoil porosity and aggregate stability agree well. They are in summer when soil is dry. The same happens with the periods for porosity and stability recovery. They are in winter when the soil is flooded. This structural behavior is opposite to expectation, as trampling did not cause structural damage by poaching. We propose a conceptual model showing the process of soil structural destabilisation when the soil dries, and the process of structural recovery when the soil wets (Taboada et al. 1999). This conceptual model is depicted in Figure 11.

The conceptual model that postulates decreases in structural stability resulting from crushing air-filled pores by cattle hooves. This yields smaller water-stable aggregates, as shown by the higher proportion of aggregates < 0.3 mm usually found in the soil of the grazed area compared to the soil in the enclosure area. Only at low water contents was the structure of the topsoil destabilized by grazing. The recovery of structural stability began in the fall and was completed in the winter, when the soil was ponded. The structural recovery results from swelling, when the smaller aggregates created by trampling of dry soil are bound again into larger structural units.

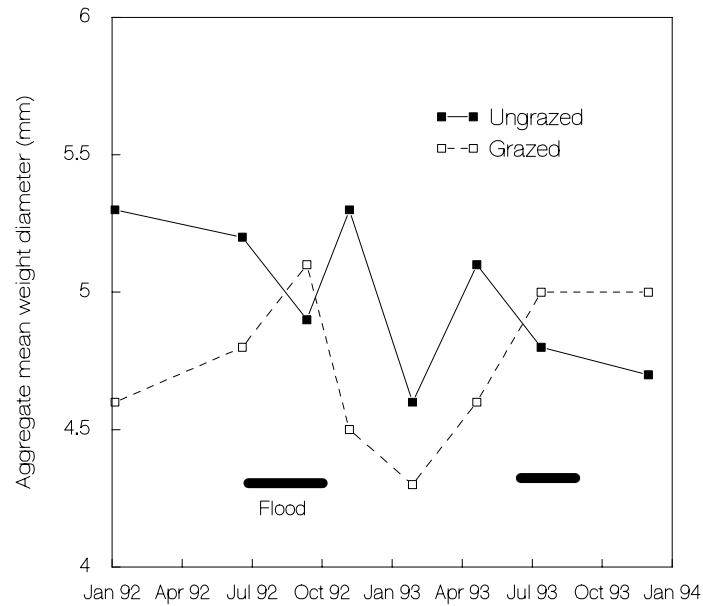


Figure 10. Aggregate stability variations in ungrazed and grazed situation in the flooding Pampa of Argentina.

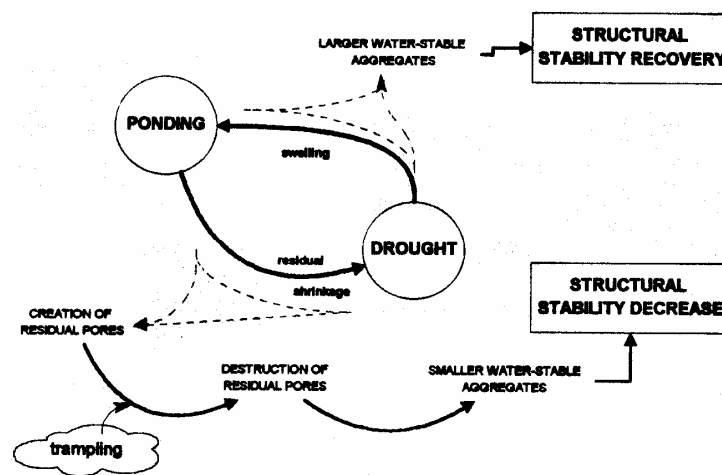


Figure 11. Conceptual model showing the variations in soil aggregate stability in the flooding Pampa of Argentina.

Upland soils tend to decrease their stability when sampled wet, and to increase it when sampled dry. This stability regime is commonly known as the “antecedent soil moisture content effect”, and it depends on the build up of soil cohesion forces. The studied flooded soils showed an opposed response to the antecedent soil moisture effect. It can be concluded that in flooded soils their structural behavior is mainly determined by their volumetric response to the ponding – drying cycle.

Recommended bibliography

- FAO-UNESCO, 2000. The FAO/UNESCO Digital Soil Map of the World and Derived Soil Properties on CD-Rom. FAO-AGL, Roma.
- Lavado R.S., Taboada M.A., 1988. Soil water, salts, and sodium dynamics in a Natraquoll of Argentina. *Catena* 15, 577 - 594.
- Patrick, W.H., Jr., and Mahapatra, I.C. 1968. Transformation and availability to rice of nitrogen and phosphorus in waterlogged soils. *Adv. Agron.* 20:323-359.
- Taboada, M.A., Lavado, R.S., 1986. Características del régimen ácuico de un Natracuol de la Pampa Deprimida (Characterization of the aquic regime of Natraquoll of the flooding Pampa). *Ciencia del Suelo* 4, 66 - 71.
- Taboada M.A., Lavado R.S., 1993. Influence of trampling on soil porosity under alternate dry and ponded conditions. *Soil Use and Management* 9, 139-143.
- Taboada M.A., Lavado R.S., Svartz H., Segat A.M.L. 1999. Structural stability changes in a grazed grassland Natraquoll of the Flooding Pampa of Argentina. *Wetlands* 19, 50 – 55.